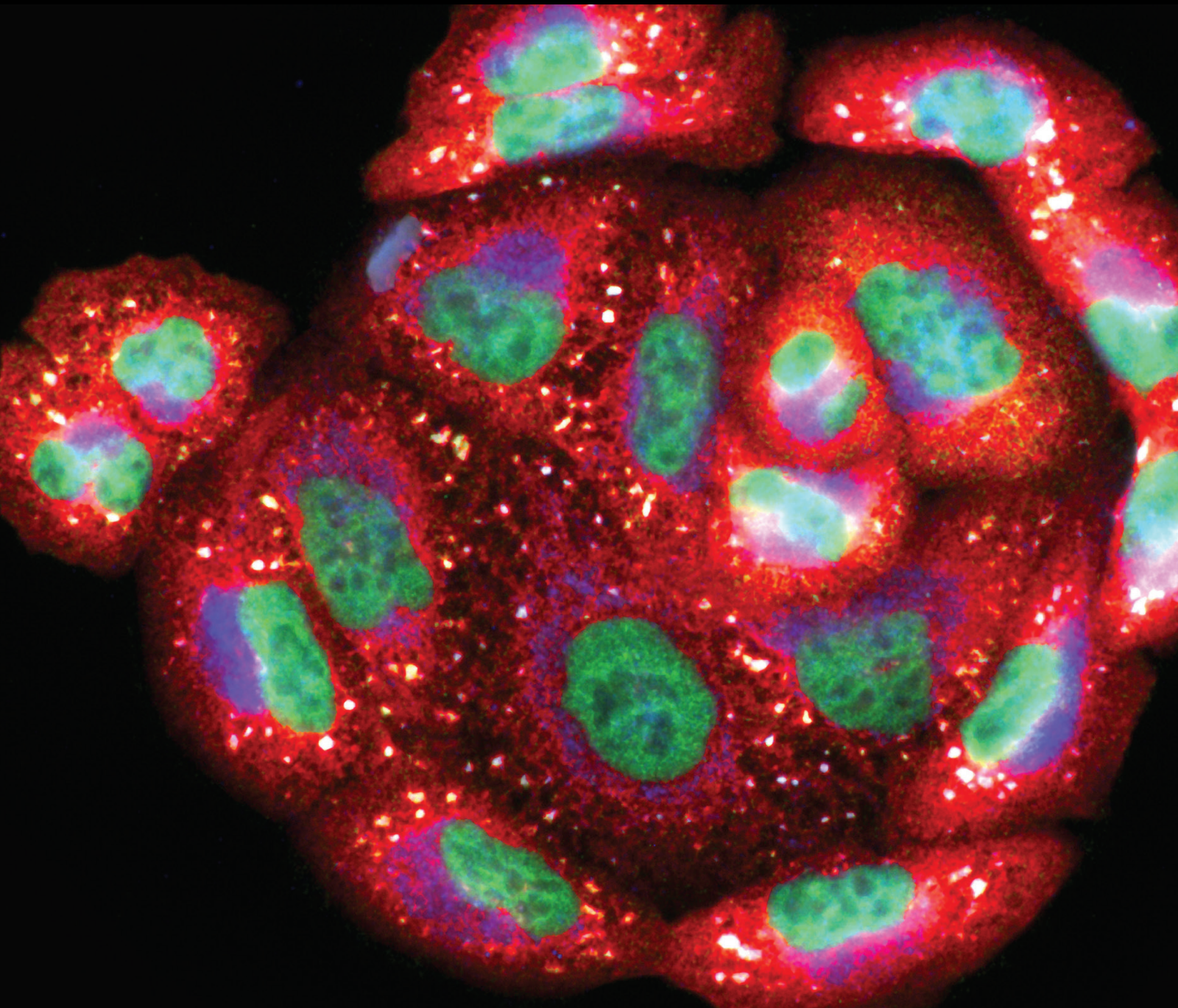# Molecular Basis of Redox Signalling 2020

Lead Guest Editor: Maria C. Franco
Guest Editors: Luciana Hannibal and Jesús Tejero

Molecular Basis of Redox Signalling 2020

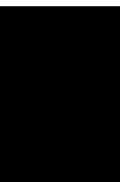# Molecular Basis of Redox Signalling 2020

Lead Guest Editor: Maria C. Franco
Guest Editors: Luciana Hannibal and Jesús Tejero

Chief Editor

Jeannette Vasquez-Vivar, USA

Tim Hofer, Norway
John D. Horowitz, Australia
Silvana Hrelia, Italy
Dragan Hrncic, Serbia
Zebo Huang, China
Zhao Huang, China
Tarique Hussain, Pakistan
Stephan Immenschuh, Germany
Norsharina Ismail, Malaysia
Franco J. L, Brazil
Sedat Kacar, USA
Andleeb Khan, Saudi Arabia
Kum Kum Khanna, Australia
Neelam Khaper, Canada
Ramoji Kosuru, USA
Demetrios Kouretas, Greece
Andrey V. Kozlov, Austria
Chan-Yen Kuo, Taiwan
Gaocai Li, China
Guoping Li, USA
Jin-Long Li, China
Qiangqiang Li, China
Xin-Feng Li, China
Jialiang Liang, China
Adam Lightfoot, United Kingdom
Christopher Horst Lillig, Germany
Paloma B. Liton, USA
Ana Lloret, Spain
Lorenzo Loffredo, Italy
Camilo López-Alarcón, Chile
Daniel Lopez-Malo, Spain
Massimo Lucarini, Italy
Hai-Chun Ma, China
Nageswara Madamanchi, USA
Kenneth Maiese, USA
Marco Malaguti, Italy
Steven McAnulty, USA
Antonio Desmond McCarthy, Argentina
Sonia Medina-Escudero, Spain
Pedro Mena, Italy
Víctor M. Mendoza-Núñez, Mexico
Lidija Milkovic, Croatia
Alexandra Miller, USA
Sara Missaglia, Italy

Premysl Mladenka, Czech Republic
Sandra Moreno, Italy
Trevor A. Mori, Australia
Fabiana Morroni, Italy
Ange Mouithys-Mickalad, Belgium
Iordanis Mourouzis, Greece
Ryoji Nagai, Japan
Amit Kumar Nayak, India
Abderrahim Nemmar, United Arab Emirates
Xing Niu, China
Cristina Nocella, Italy
Susana Novella, Spain
Hassan Obied, Australia
Pál Pacher, USA
Pasquale Pagliaro, Italy
Dilipkumar Pal, India
Valentina Pallottini, Italy
Swapnil Pandey, USA
Mayur Parmar, USA
Vassilis Paschalis, Greece
Keshav Raj Paudel, Australia
Ilaria Peluso, Italy
Tiziana Persichini, Italy
Shazib Pervaiz, Singapore
Abdul Rehman Phull, Republic of Korea
Vincent Pialoux, France
Alessandro Poggi, Italy
Zsolt Radak, Hungary
Dario C. Ramirez, Argentina
Erika Ramos-Tovar, Mexico
Sid D. Ray, USA
Muneeb Rehman, Saudi Arabia
Hamid Reza Rezvani, France
Alessandra Ricelli, Italy
Francisco J. Romero, Spain
Joan Roselló-Catafau, Spain
Subhadeep Roy, India
Josep V. Rubert, The Netherlands
Sumbal Saba, Brazil
Kunihiro Sakuma, Japan
Gabriele Saretzki, United Kingdom
Luciano Saso, Italy
Nadja Schroder, Brazil

Anwen Shao (ID), China
Iman Sherif, Egypt
Salah A Sheweita, Saudi Arabia
Xiaolei Shi, China
Manjari Singh, India
Giulia Sita (ID), Italy
Ramachandran Srinivasan (ID), India
Adrian Sturza (ID), Romania
Kuo-hui Su (ID), United Kingdom
Eisa Tahmasbpour Marzouni (ID), Iran
Hailiang Tang, China
Carla Tatone (ID), Italy
Shane Thomas (ID), Australia
Carlo Gabriele Tocchetti (ID), Italy
Angela Trovato Salinaro, Italy
Rosa Tundis (ID), Italy
Kai Wang (ID), China
Min-qi Wang (ID), China
Natalie Ward (ID), Australia
Grzegorz Wegrzyn, Poland
Philip Wenzel (ID), Germany
Guangzhen Wu (ID), China
Jianbo Xiao (ID), Spain
Qiongming Xu (ID), China
Liang-Jun Yan (ID), USA
Guillermo Zalba (ID), Spain
Jia Zhang (ID), China
Junmin Zhang (ID), China
Junli Zhao (ID), USA
Chen-he Zhou (ID), China
Yong Zhou (ID), China
Mario Zoratti (ID), Italy

Contents

Research Article

MICAL2 Contributes to Gastric Cancer Cell Proliferation by Promoting YAP Dephosphorylation and Nuclear Translocation

Chenxiang Qi [1], **Pengxiang Min** [2], **Qianwen Wang** [1], **Yueyuan Wang** [3], **Yixuan Song** [1], **Yujie Zhang** [1], **Maria Bibi** [1], and **Jun Du** [1]

[1]*Department of Physiology, Nanjing Medical University, Nanjing, Jiangsu 211166, China*
[2]*Key Laboratory of Cardio Vascular & Cerebrovascular Medicine, School of Pharmacy, Nanjing Medical University, Nanjing, Jiangsu 211166, China*
[3]*The Laboratory Center for Basic Medical Sciences, Nanjing Medical University, Nanjing, Jiangsu 211166, China*

Correspondence should be addressed to Jun Du; dujun@njmu.edu.cn

Dynamic cytoskeletal rearrangements underlie the changes that occur during cell division in proliferating cells. MICAL2 has been reported to possess reactive oxygen species- (ROS-) generating properties and act as an important regulator of cytoskeletal dynamics. However, whether it plays a role in gastric cancer cell proliferation is not known. In the present study, we found that MICAL2 was highly expressed in gastric cancer tissues, and this high expression level was associated with carcinogenesis and poor overall survival in gastric cancer patients. The knockdown of MICAL2 led to cell cycle arrest in the S phase and attenuated cell proliferation. Concomitant with S-phase arrest, a decrease in CDK6 and cyclin D protein levels was observed. Furthermore, MICAL2 knockdown attenuated intracellular ROS generation, while MICAL2 overexpression led to a decrease in the p-YAP/YAP ratio and promoted YAP nuclear localization and cell proliferation, effects that were reversed by pretreatment with the ROS scavenger N-acetyl-L-cysteine (NAC) and SOD-mimetic drug tempol. We further found that MICAL2 induced Cdc42 activation, and activated Cdc42 mediated the effect of MICAL2 on YAP dephosphorylation and nuclear translocation. Collectively, our results showed that MICAL2 has a promotive effect on gastric cancer cell proliferation through ROS generation and Cdc42 activation, both of which independently contribute to YAP dephosphorylation and its nuclear translocation.

1. Introduction

Gastric cancer is one of the most commonly diagnosed malignancies worldwide [1, 2]. The malignancy of gastric cancer cells is strongly associated with their high proliferative ability. The Hippo pathway-related kinase cascade is a critical contributor to the balance among cell proliferation, differentiation, and apoptosis. Yes-associated protein (YAP), an effector of the Hippo signaling pathway, is a transcriptional coactivator for several key transcription factors that regulate the expression of a wide variety of cell proliferation-related genes [3–5]. A recent study revealed that YAP knockdown could inhibit tumor growth in a gastric cancer xenograft mouse model [6], suggesting that YAP has an important role in the development of gastric

cancer and may be a novel target for attenuating gastric cancer cell proliferation.

The Hippo signaling pathway is highly associated with cell growth regulation. The core Hippo pathway signaling cascade is comprised of molecules such as MST1/2, SAV1, LATS1/2, YAP, and its paralog TAZ. Following the detection of an extracellular growth-inhibitory signal, a series of kinase cascade phosphorylation reactions are activated, leading to YAP phosphorylation. Cytoskeleton proteins then bind to phosphorylated YAP and sequester it in the cytoplasm, thereby reducing its nuclear activity and limiting cell proliferation. In contrast, unphosphorylated YAP can translocate into the nucleus, where it primarily interacts with the transcription factors TEAD1–4, thereby inducing the transcription of multiple oncogenes and promoting cell proliferation. Impaired Hippo

signaling was reported to induce YAP- or TAZ-dependent oncogene addiction for cancer cells [7, 8]. Furthermore, YAP is localized to the nucleus in various types of human cancer, including breast, lung, and pancreatic cancers [9–11]. Although elevated YAP expression and its nuclear accumulation are known to be associated with poor disease-specific survival in gastric cancer patients [12], the precise molecular mechanisms underlying the regulatory effects of YAP in gastric carcinogenesis remain poorly understood.

A recent report indicated that YAP nuclear translocation could be induced *via* cytoskeleton tension and that this regulation required Rho GTPase activity and was independent of the canonical Hippo kinase cascade [13]. Rho GTPases are central regulators of actin reorganization, with Cdc42, Rac1, and Rho being the most prominent members. Cdc42 deficiency was reported to attenuate the Nwasp/stress fibers/YAP signaling pathway, leading to podocyte apoptosis [14]. Specifically, reduced Cdc42 levels lead to decreased F-actin content, which, in turn, frees up LATS1, allowing it to bind to and phosphorylate YAP, thereby inactivating it and reducing its nuclear accumulation, finally leading to attenuated cancer cell proliferation [15]. Although Cdc42 is known to exert its function by switching between an inactive GDP-bound state and an active GTP-bound form [16], the mechanisms involved in activating Cdc42 in gastric cancer cells are largely unknown.

Molecule interacting with CasL2 (MICAL2) is a microtubule-associated monooxygenase with a role in regulating cellular cytoskeletal dynamics through the induction of reactive oxygen species (ROS) production [17, 18]. MICAL2 is highly expressed in primary human epithelial tumors as well as in neoangiogenic endothelial cells in human solid tumors [19] and is thought to accelerate tumor progression [20–22]. MICAL2 has been reported to activate ERK1/2 signaling and promote vascular smooth muscle cell proliferation [23]. MICAL2-deficient breast cancer cells develop marked migration defects through the inhibition of P38/HSP27/cytoskeleton signaling [22]. We have recently shown that MICAL-L2, a member of the MICAL protein family, enhances the migratory ability of gastric cancer cells *via* regulating EGFR stability in a Cdc42-dependent manner. We further demonstrated that MICAL-L2 can activate Cdc42 [24]. As MICAL family members have a similar structure [25], we hypothesized that MICAL2 might promote YAP nuclear translocation *via* ROS generation and/or Cdc42 activation, thereby promoting gastric cancer cell proliferation. In the present study, we investigated whether MICAL2 regulates YAP activation and explored the underlying mechanism.

2. Materials and Methods

2.1. Ethics Statement. All immunohistochemistry assays with human tumors specimens were conducted under the institutional guidelines of Jiangsu Province.

2.2. Cell Culture. Human gastric cancer cell lines (BGC-823 and SGC-7901) and normal gastric epithelial cell line GES-1 were purchased from the Typical Culture Preservation Commission Cell Bank, Chinese Academy of Sciences (Shanghai, China). All cells were maintained in Dulbecco's modified Eagle's medium (DMEM; high glucose) (HyClone, Waltham, Massachusetts, USA) supplemented with 10% fetal bovine serum (FBS, Gibco, Carlsbad, California, USA), 100 U/ml penicillin, and 100 μg/ml streptomycin (Invitrogen, Carlsbad, CA). The cells were cultured in a humid, constant temperature incubator (Thermo, Waltham, Massachusetts, USA) with 5% CO_2 at 37°C. Cells were grown on coverslips for immunofluorescence staining and on 6-well plates (Thermo, Waltham, Massachusetts, USA) for protein extraction.

2.3. Plasmids and siRNAs. The pEGFP-N1 vector containing the full-length Cdc42-Q61L (CA) or Cdc42-T17N (DN) insert was kept in this laboratory. The empty vector control pcDNA-3.1-HA-C and the full-length human MICAL2 cDNA were purchased from YouBio (Hunan, China). The empty vector control pEGFP-N1 and the full-length human YAP1 cDNA were also purchased from YouBio (Hunan, China). The transfection procedure followed manufacturer's protocol, using Lipofectamine 2000 (Invitrogen, Carlsbad, California, USA).

The siRNAs were synthesized and purified by Gene-Pharma (Shanghai, China). The transfection of MICAL2 siRNA or control siRNA with Lipofectamine 2000 was performed according to manufacturer's instruction. The siRNAs specifically targeting MICAL2 were as follows: #1, 5′-GAGAACGUGAACCAAGACATT-3′; #2, 5′-GCAUAG AUCUUGAGAACAUTT-3′; #3, 5′-GCAGCGACACG UGUUACUUTT-3′. The siRNAs specifically targeting YAP were as follows: #1, 5′-GCAUCUUCGACAGUCU UCUTT-3′; #2, 5′-GGUCAGAGAUACUUCUUAUTT-3′; #3, 5′-GGUAGCGCUUUGUAUGCAUTT-3′. After transfected with plasmid or siRNA for 24 h, the cells were cultured and then treated with N-acetyl-L-cysteine (NAC, scavenger of ROS) and tempol (SOD-mimetic drug) at the indicated time points.

2.4. CCK8 Assay. Cell viability was determined by the CCK-8 assay. In short, cells were seeded into 96-well plates at a density of 5×10^3 cells per well and transfected with siRNA or plasmids according to the groups. After incubated for 0, 24, 48, and 72 h, 10 μl of CCK-8 reagent (Bimake, Houston, Texas) was added per well. Then, the 96-well plate was incubated in the dark for 40 min and then measured at 450 nm using a microplate reader (Bio-Tek, Elx800, USA).

2.5. Flow Cytometry Analysis. Cell cycle analysis was performed by flow cytometry. In short, the cells were collected and fixed in 75% ethanol overnight at -20°C. The cells were then incubated with RNase A and propidium iodide staining solution at 37°C for 30 min in the dark. Subsequently, the stained cells were analyzed using a flow cytometer.

2.6. 5-Ethynyl-2-Deoxyuridine (EdU) Incorporation Assay. The cell proliferation was measured using EdU staining kit (RiboBio, Guangzhou, China) according to manufacturer's instructions. Three replicas were made for each group. In

short, the cells were seeded on a 96-well plate (Thermo, Waltham, Massachusetts, USA) and cultured until 70% confluence was reached, and then, EdU reagent was added to the culture medium and incubated for 2 h. After labeled, the cells were washed 3 times with PBS and fixed with 4% paraformaldehyde. Then, the cells were incubated with 0.2% glycine and washed 3 times with 0.5% Triton X-100 in PBS. Finally, the cells were counterstained with DAPI and then imaged by a fluorescence microscope (Olympus BX 51, Tokyo, Japan) combined with an Olympus DP70 digital camera.

2.7. Western Blotting. The total protein sample was prepared using the cell lysate (Beyotime, Shanghai, China), and the protein concentration was measured using the BCA protein assay kit (Thermo, Waltham, Massachusetts, USA). By SDS-PAGE electrophoresis, an equal amount of cellular protein fragments were separated and transferred to a pure nitrocellulose membrane. Then, after blocking with 5% skimmed milk, the membrane was incubated with different specific primary antibodies overnight at 4°C and then incubated with secondary antibodies (Jackson, Lancaster, Pennsylvania, USA) for 1.5 h at room temperature for detection. The following antibodies were used: MICAL2 (ProteinTech, Wuhan, China), GAPDH (Bioworld, Nanjing, China), p-YAP (Cell Signaling, Danvers, MA and Affinity Biosciences, Cincinnati, OH, USA), YAP (Cell Signaling), Cdc42 (Cell Signaling), HA-tag (Cell Signaling), CDK2 (ProteinTech), CDK4 (ProteinTech), CDK6 (ProteinTech), cyclin D (Cell Signaling), cyclin E (Cell Signaling), cyclin H (Cell Signaling), NF-κB (Cell Signaling), ERK (Cell Signaling), and p-ERK (Cell Signaling). After using an appropriate amount of secondary antibody at a dilution of 1 : 10000, ECL (FuDe-Bio, Hangzhou, China) reagent was used to detect bands, and positive bands were analyzed with Quantity One (Bio-Rad, Hercules, CA).

2.8. Cytoplasmic and Nuclear Protein Extraction. Cytoplasmic and nuclear proteins were extracted using the nuclear protein and cytoplasmic protein extraction kit (Beyotime, Shanghai, China). In short, the cells were collected and resuspended in cytoplasmic extractant A. The suspension was vortexed and incubated on ice for 15 min. Then, the cytoplasmic extractant B was added to the cell pellet. The pellet was resuspended and incubated on ice for 1 min. The pellet was vortexed again and centrifuged at 12,500 g for 5 min. The collected supernatant is the cytoplasmic protein extract. Then, the pellet was resuspended by adding a nuclear extraction reagent. After several times of vortex, the mixture was centrifuged at 12,000 rpm for 10 min. The collected supernatant was the nuclear protein extract.

2.9. Immunofluorescence Microscopy. The cells planted on the glass cover slip were washed 3 times with precooled PBS, then were fixed with 4% paraformaldehyde solution for 20 min. After treated with 0.2% Triton X-100 for 5 min and blocked with 1% BSA at room temperature for 1.5 h, the cells were incubated with specific primary antibody overnight. Then, Alexa-conjugated species-matched secondary

antibody was used to incubate cells at room temperature for 1 h. DAPI (Southern Biotech, Birmingham, AL) staining was used to determine the position of nuclei. The immunofluorescence image was taken with Olympus DP70 digital camera and Olympus BX51 microscope (Olympus, Tokyo, Japan).

2.10. Pulldown Assay. Cdc42 activity was measured by pulldown assay as described previously [24]. The PAK-CRIB with GST tag is purified and extracted from BL21 bacteria, and the active Cdc42-GTP could be pulled down by PAK-CRIB magnetic beads. In short, the cells were lysed, and protein was collected in a new tube. 300 μg of protein was mixed with PAK-CRIB precoupled beads by rotation at 4°C for 2 h. The beads were then washed, and the proteins bound to the beads were separated by SDS-PAGE gel electrophoresis. Active Cdc42 was determined by analysis of its specific bands by Western blotting.

2.11. Measurement of ROS. ROS measurement was carried out by kit as described previously [26]. For intracellular ROS staining, individual cells were inoculated in 6-well plate and treated with interfering strands, plasmids, or NAC (5 mM, 4 h) (Beyotime, Shanghai, China) and tempol (3 mM, 4 h) (MCE, New Jersey, USA), and then, 10 μM 2$'$,7$'$-dichlorodihydrofluorescein diacetate (DCFH-DA) (Beyotime) or 10 μM DHE (Beyotime) was used to stain the cells at 37°C for 30 min. The immunofluorescence image was taken with Olympus DP70 digital camera and Olympus BX51 microscope (Olympus, Tokyo, Japan). Green fluorescence (DCF) intensity was quantitated using the microscope with 488 nm excitation and 525 nm emission settings, respectively. Red fluorescence (HE) was measured with 300 nm excitation and 610 nm emission settings.

2.12. Immunohistochemistry. Gastric cancer tissue microarrays were purchased from Outdo Biotech (Shanghai, China). In this study, 30 samples of gastric adenocarcinoma and their corresponding precancerous tissue samples were subjected to immunohistological examination. After dewax and hydration, the microarray was incubated with 3% H_2O_2 for 30 min to inactivate endogenous peroxidase and then was incubated with citric acid antigen retrieval solution at 95°C for 20 min. The microarray was then blocked with goat serum for 2 h at room temperature. After incubated with MICAL2 antibody at 4°C overnight, the microarray incubated with species matched secondary antibodies (Maxim Biotechnologies, Fuzhou, China) for 2 h at room temperature. DAB solution was used to detect the expression of MICAL2. Sections were counterstained with hematoxylin. The photo was taken by Olympus BX51 microscope. By evaluating the percentage of the number of stained cells and the staining intensity on the staining scores of MICAL2, the immune response score (IRS) was evaluated as described previously [27].

2.13. Statistical Analysis. All experiments were repeated at least three times independently. Statistical differences between two groups were tested using Student's t-test. Comparisons among three or more groups were conducted using

one-way ANOVA with a posttest to correct for multiple comparisons. The chi-squared test was used to evaluate the significance of correlation. $P < 0.05$ indicates statistical significance, and $P < 0.01$ and $P < 0.001$ indicate sufficiently statistical significance (two tailed). Error bars represent standard error of the mean. All calculations were performed with SPSS Version 20.0 (IBM Corp., Armonk, NY, USA).

3. Results

3.1. MICAL2 Is Highly Expressed in Human Gastric Cancer Samples and Is Associated with Poor Clinical Outcome.
Gastric cancer-related information obtained from the TCGA database (http://gepia.cancer-pku.cn/) and GTEx data indicated that MICAL2 or YAP mRNA levels were significantly higher in gastric cancer samples compared with those in precancerous tissues (Figures 1(a) and 1(b)). Kaplan–Meier plotter (https://kmplot.com/analysis/)-based analysis also showed that elevated MICAL2 or YAP expression was correlated with shorter overall survival in gastric cancer patients (Figures 1(a) and 1(b)). Next, MICAL2 protein levels were further analyzed by immunoblotting in the gastric cancer cell lines BGC-823 and SGC-7901 and the nonmalignant gastric epithelial cell line GES-1. As shown in Figure 1(c), MICAL2 levels were higher in BGC-823 cells than in SGC-7901 cells and were lowest in GES-1 cells (Figure 1(c)). In addition, YAP levels were higher in both gastric cancer cell lines than in the GES-1 line. MICAL2 protein levels were also analyzed in a tissue microarray containing 30 paired gastric cancer and adjacent nontumor tissues. The immunohistochemical analysis showed that MICAL2 protein levels were significantly higher in gastric cancer tissues than in adjacent normal tissues ($P < 0.05$) (Figures 1(d) and 1(e)). Overall, the *in vitro* and *in vivo* data strongly suggested that MICAL2 is highly expressed in human gastric cancer samples and is associated with poor clinical outcome.

3.2. The Effect of MICAL2 on Gastric Cancer Cell Proliferation.
Next, we used both gain- and loss-of-function assays to alter MICAL2 contents and confirm its role in the regulation of gastric cancer cell proliferation. First, we silenced MICAL2 in BGC-823 and SGC-7901 cells using siRNA targeting MICAL2. The knockdown efficiency was determined by Western blotting. As shown in Figures 2(a) and 2(b), siMICAL2 #2 and #3 significantly depleted MICAL2 levels in both BGC-823 and SGC-7901 cells. Additionally, as expected, MICAL2 overexpression markedly increased the MICAL2 protein content (Figure 2(c)). We then also evaluated the effect of MICAL2 on gastric cancer cell proliferation using CCK-8 and EdU staining assays. The results showed that MICAL2 silencing effectively impaired the growth kinetics of BGC-823 and SGC-7901 cells (Figures 2(d), 2(e), and 2(g)), whereas its overexpression enhanced the proliferative ability of SGC-7901 cells (Figures 2(f) and 2(h)). These data indicated that MICAL2 may exert an oncogenic function in gastric cancer.

To further understand the potential underlying mechanisms, we examined the effect of MICAL2 on cell cycle progression. For this, BGC-823 cells transfected with siMICAL2 #3 for 48 h, followed by staining with PI, were harvested for analysis of DNA content using flow cytometry. The results showed that the percentage of cells in the S phase was lower in BGC-823 cells than in the controls (Figure 3(a)). In contrast, the percentage of S-phase cells in MICAL2-overexpressing SGC-7901 cells was markedly higher than that of control cells (Figure 3(b)). These findings suggested that MICAL2 plays a role in promoting G1-to-S phase cell cycle progression.

To further confirm that MICAL2 indeed regulates the G1/S-phase transition, gastric cancer cells were treated with siMICAL2 after which the effects on the protein levels of cyclin D and CDK6 were determined by Western blotting analysis. In addition to their roles in regulating G1-to-S-phase progression, cyclin D and CDK6 are also regarded as key targets of the Hippo signaling pathway [28]. The results showed that, compared with the control condition, MICAL2 depletion resulted in a significant decrease in cyclin D and CDK6 protein levels, while MICAL2 overexpression elicited the opposite effect (Figures 3(c) and 3(d)).

3.3. MICAL2 Regulates YAP Nuclear Translocation.
We next tested whether MICAL2 modulates YAP expression and subcellular localization in gastric cancer cells. To determine whether MICAL2 regulates YAP expression, we silenced MICAL2 in BGC-823 cells using siMICAL2. As shown in Figure 4(a), the transfection of both siMICAL2 #2 and #3 led to a significant decrease in YAP protein levels. siMICAL2 treatment also increased the p-YAP/YAP ratio in BGC-823 cells. Western blotting analysis further showed significant levels of MICAL2 translocation from the nucleus to the cytoplasm in these cells (Figure 4(c)). As expected, YAP immunofluorescence staining revealed that YAP nuclear content was decreased in MICAL2-silenced BGC-823 cells when compared with that in control cells (Figure 4(e) and Figure S1a). Notably, MICAL2 overexpression only reduced YAP phosphorylation levels and not total YAP content (Figure 4(b)). In contrast, cells overexpressing MICAL2 displayed increased YAP nuclear accumulation as determined by Western blotting and immunofluorescence assays (Figures 4(d) and 4(f) and Figure S1b). These results suggested that the inhibitory effects of MICAL2 on Hippo signaling pathway activation may depend on the promotion of YAP nuclear translocation.

Next, we examined whether YAP mediates MICAL2-induced cell proliferation using both gain- and loss-of-function assays to alter YAP contents (Figures S1c and S1d). We found that MICAL2 overexpression-stimulated gastric cancer cell proliferation was attenuated in siYAP-transfected cells, while YAP overexpression reversed the inhibitory effect of siMICAL2 on cell proliferation (Figures 4(g) and 4(h)). This result indicated that YAP is indeed an effector of MICAL2-mediated regulation of gastric cancer cell proliferation.

3.4. MICAL2-Mediated Cell Proliferation Is Independent of the NF-κB and ERK Pathways.
Activated NF-κB and ERK signaling pathways play a central role in cell survival and proliferation, and both pathways are involved in G1/S-phase

(a)

(b)

(c)

(d)

(e)
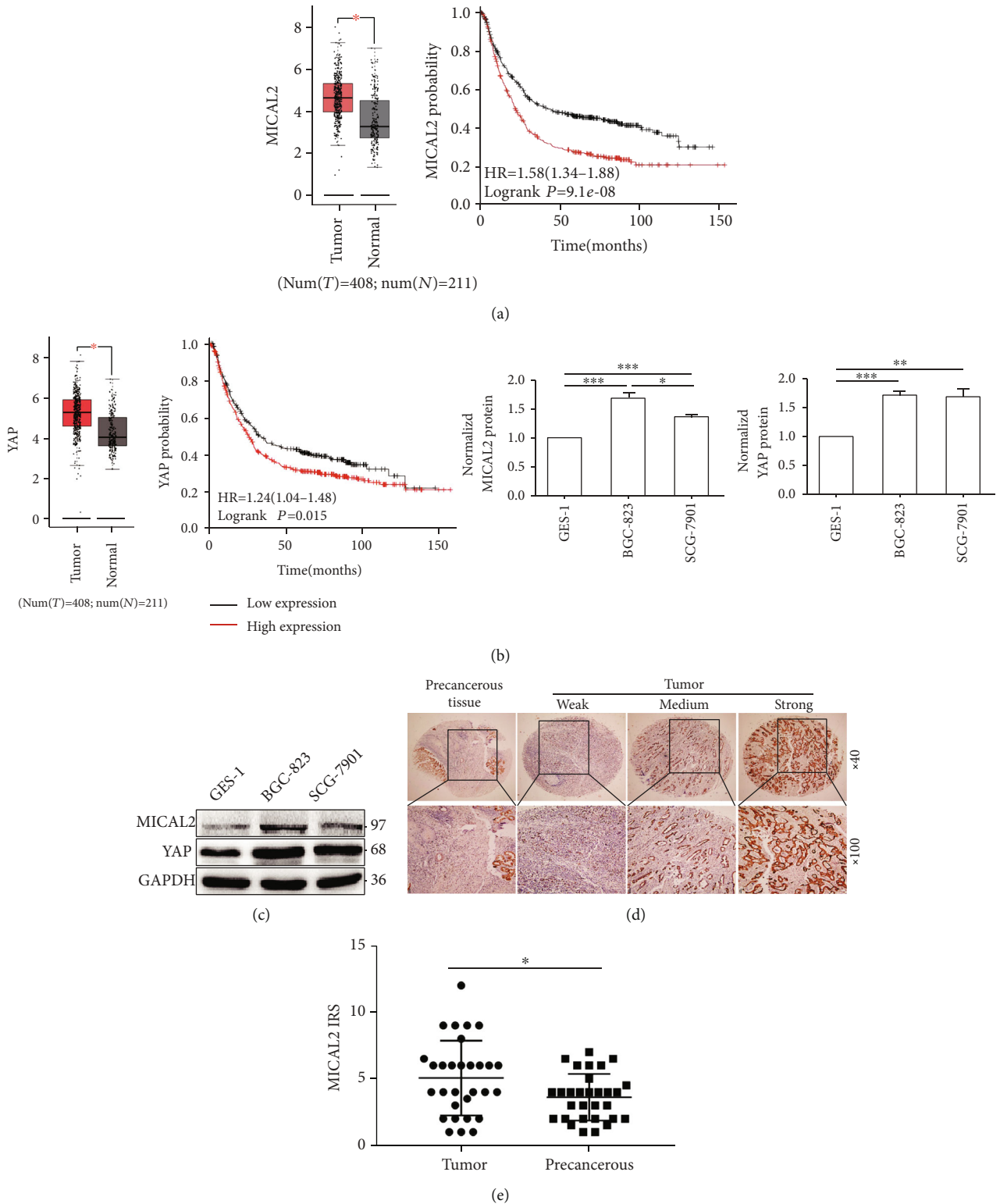
Figure 1: Analysis of MICAL2 levels in gastric cancer tissues. (a) MICAL2 mRNA expression levels are higher in gastric cancer tissues than that in precancerous tissues based on information retrieved from The Cancer Genome Atlas (TCGA) database and the overall survival of patients with gastric cancer showing low or high MICAL2 levels. (b) YAP mRNA expression levels are higher in gastric cancer tissues than that in precancerous tissues and the overall survival of patients with gastric cancer showing low or high YAP levels. (c) MICAL2 and YAP protein levels in GES-1, BGC-823, and SGC-7901 cells. Data in (c) are presented as mean ± SEM of 3 determinations. (d) Representative images of MICAL2 staining in gastric cancer tissues. MICAL2-positive staining is shown in brown, and the nuclei are counterstained with hematoxylin. (e) A scatterplot showing correlations with protein levels in gastric cancer tissue ($n = 30$) and precancerous tissue ($n = 30$) as determined by immunoreactivity scores (IRS). $^{*}P < 0.05$, $^{**}P < 0.01$, $^{***}P < 0.001$.

(a)

(b)

(c)

(d)

(e)

(f)

FIGURE 2: Continued.

(g)

(h)
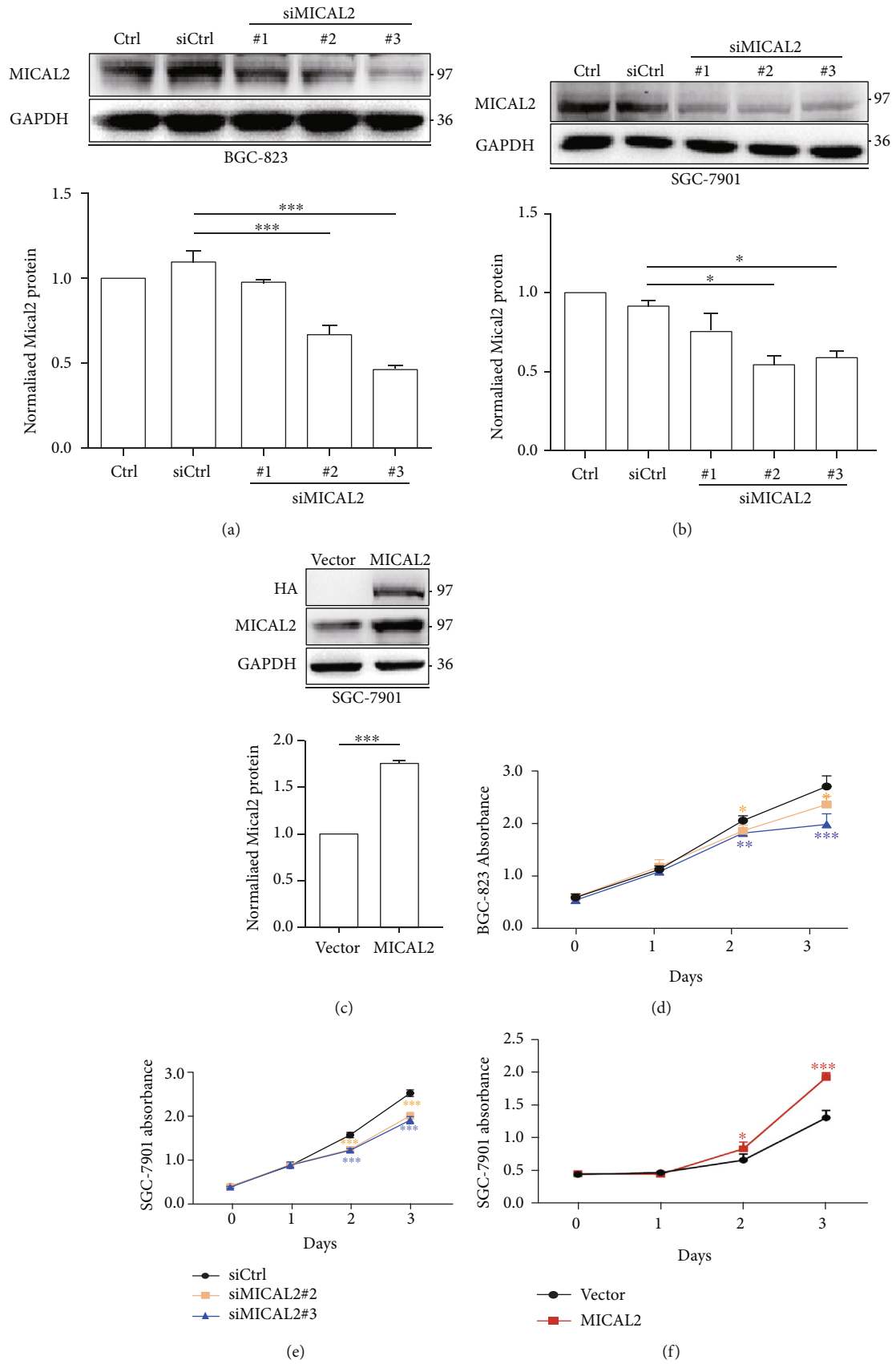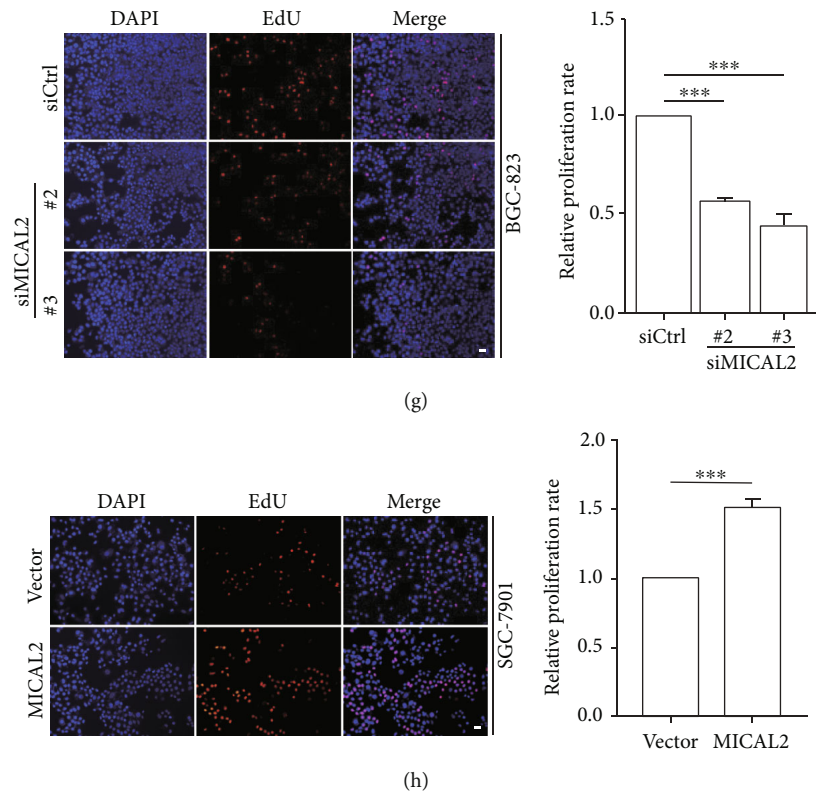
FIGURE 2: The effect of MICAL2 on the proliferation of gastric cancer cells. (a, b) BGC-823 (a) and SGC-7901 cells (b) were transfected with control siRNA or siRNA specifically targeting MICAL2 (siMICAL2). After 48 h, total protein extracts from cells were analyzed for MICAL2 protein expression. Western blot bands corresponding to MICAL2 were quantified and normalized against GAPDH levels. (c) SGC-7901 cells were transfected with empty vector or MICAL2 overexpression plasmids, and total cellular proteins were extracted and analyzed for MICAL2 expression by Western blotting. Data in (a–c) are presented as mean ± SEM of 3 determinations. $^{*}P < 0.05$, $^{***}P < 0.001$. (d–f) The viability of BGC-823 and SGC-7901 cells transfected with siMICAL2 (d, e) and SGC-7901 cells transfected with MICAL2 overexpression plasmids (f) was assessed by cell counting kit-8 (CCK-8) assay. Data are presented as mean ± SEM of 5 determinations. (d, e) $^{*}P < 0.05$, $^{**}P < 0.01$, $^{***}P < 0.001$ vs. siCtrl. (f) $^{*}P < 0.05$, $^{***}P < 0.001$ vs. the empty vector. (g, h) Representative images of EdU staining in BGC-823 cells transfected with siMICAL2 (g) and SGC-7901 cells transfected with MICAL2 overexpression plasmids (h), and the cell proliferation rate was quantified. Data are presented as mean ± SEM of 5 determinations. Scale bar, 5 μm. $^{***}P < 0.001$.

cell cycle transition. To determine whether the effects of MICAL2 on cell proliferation are associated with either the ERK or NF-κB pathway, we assessed the changes in the protein levels of key markers of both pathways in MICAL2-depleted cells. Compared with control cells, neither NF-κB nor p-ERK protein levels were markedly altered with MICAL2 knockdown (Figures S2a and S2c). Furthermore, no significant changes in NF-κB and p-ERK subcellular localization were detected in MICAL2-depleted BGC-823 cells (Figures S2b and S2d). These findings suggested that the effects of MICAL2 on cell proliferation were likely not mediated *via* the NF-κB and ERK signaling pathways.

3.5. MICAL2 Promotes YAP Nuclear Translocation through ROS Generation. Previous study reported that YAP-targeted gene transcription can be regulated by ROS [29]. As MICAL2 participates in ROS production and contributes to YAP nuclear localization, we speculated that MICAL2 might promote YAP nuclear translocation by regulating ROS generation. To test this possibility, we first transfected BGC-823 cells with siMICAL2 (#2 and #3) and examined the effects on ROS generation. As shown in Figure 5(a), ROS levels were

suppressed in these cancer cells when compared with those of control cells; a similar effect on cell proliferation was observed when cells were treated with the ROS scavenger NAC and tempol (Figure 5(b) and Figures S3a and S3b).

MICAL2 depletion led to an increase in p-YAP levels and a decrease in those of CDK6 and cyclin D in BGC-823 cells (Figures 5(c) and 5(d) and Figures S3c and S3d). Additionally, NAC and tempol pretreatment did not aggravate these changes greatly, suggesting that ROS production is likely to mediate the effect of MICAL2 on YAP nuclear translocation. Moreover, MICAL2 overexpression in BGC-823 cells resulted in a decrease in p-YAP content and an increase in that of CDK6 and cyclin D, while all these effects were reversed with NAC and tempol pretreatment (Figures 5(e) and 5(f) and Figures S3e and S3f). Next, we treated BGC-823 cells with NAC, tempol, and examined whether YAP subcellular localization was affected. As shown in Figure 5(g) and Figure S3g, NAC and tempol pretreatment prevented YAP nuclear accumulation in MICAL2-overexpressing cells. These results suggested that MICAL2 promotes YAP nuclear localization in a ROS-dependent manner.

(a)

(b)

(c)

(d)
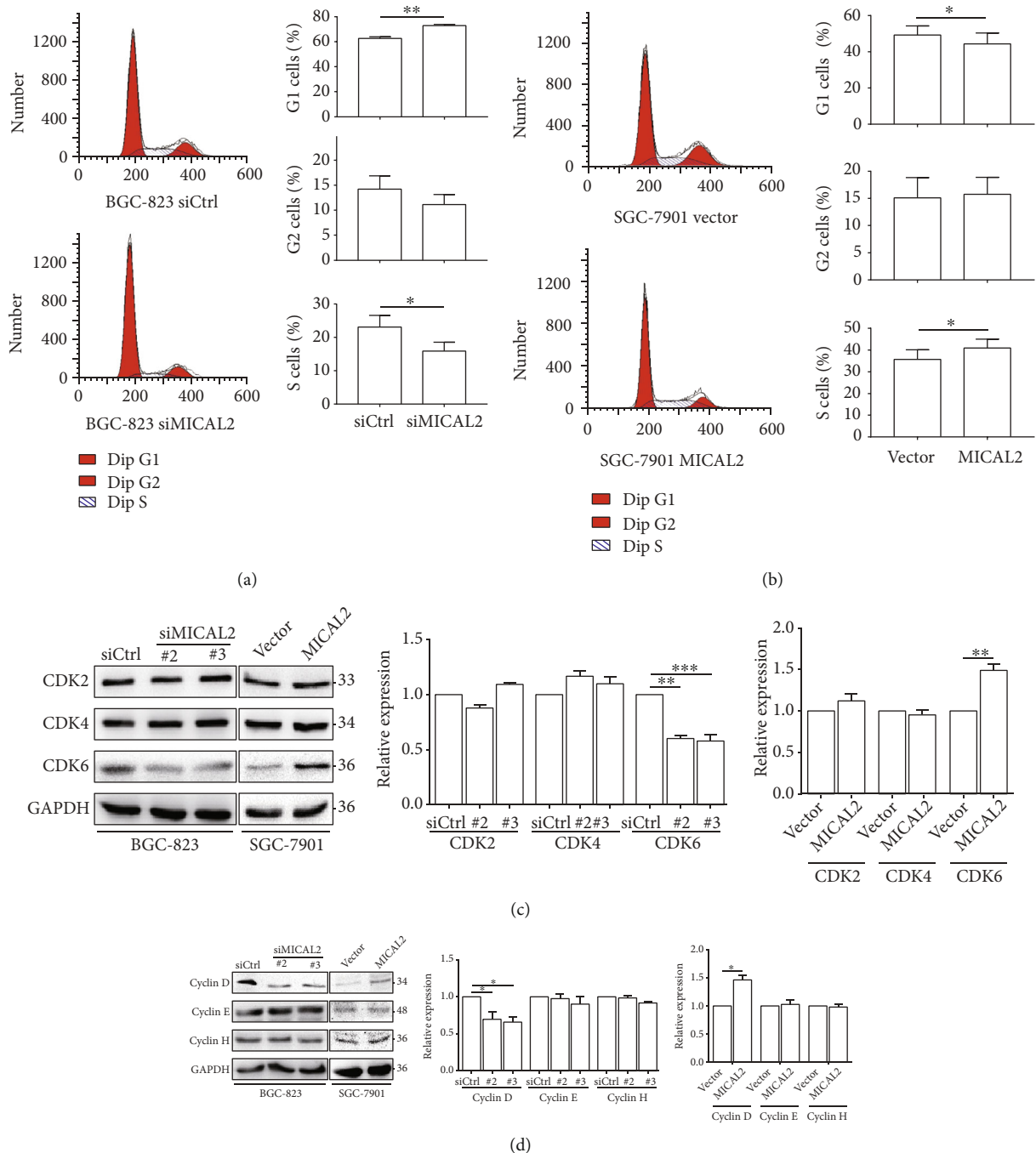
FIGURE 3: The effect of MICAL2 on the cell cycle. (a, b) Cell cycle progression in BGC-823 (a) and SGC-7901 cells (b) transfected with the indicated siRNA or plasmids was analyzed by flow cytometry. Cell cycle data are shown in histograms. (c, d) MICAL2-depleted BGC-823 cells and MICAL2-overexpressing SGC-7901 cells were subjected to Western blotting analysis for CDK2, CDK4, CDK6 (c), and cyclin D–H (d). Data are presented as mean ± SEM of 3 determinations. $^*P < 0.05$, $^{**}P < 0.01$, $^{***}P < 0.001$.

3.6. MICAL2 Regulates YAP Nuclear Translocation via Cdc42 Activation.

Finally, we explored whether MICAL2 can promote YAP nuclear translocation by means other than ROS production. Because Cdc42 is known to also increase YAP accumulation in the nucleus and play an important role in the regulation of cell proliferation [5], we assessed whether MICAL2 influenced Cdc42 activation. First, pull-down assays were performed to detect Cdc42 activity in BGC-823 cells transfected with siMICAL2 (#2, #3) and SGC-7901 cells transfected with MICAL2 overexpression plasmids. We found that MICAL2 depletion reduced Cdc42 activation (Figure 6(a)), while the opposite effect was observed when MICAL2 was overexpressed (Figure 6(b)). We further found that treatment with the ROS scavenger NAC and tempol led to only a small increase in Cdc42 activation levels (Figure 6(c) and Figure S4a),

(a)

(b)
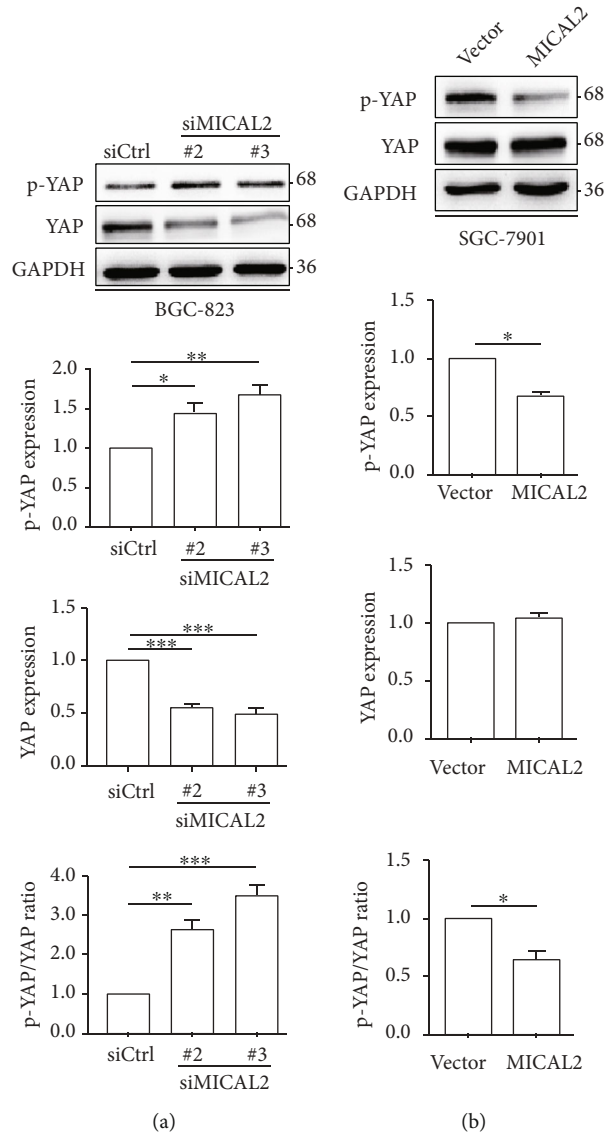
FIGURE 4: Continued.

(c)   (d)

(e)
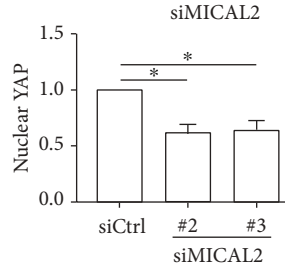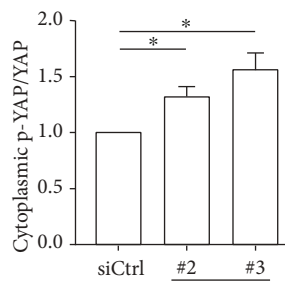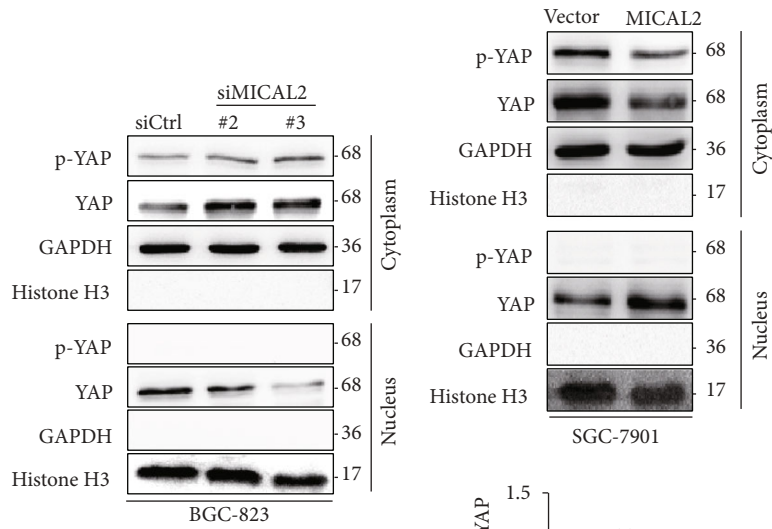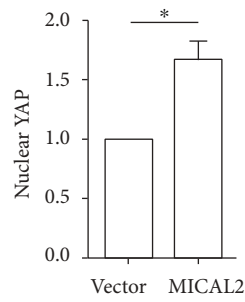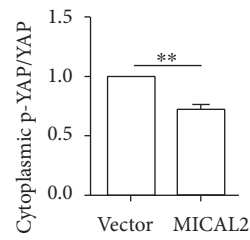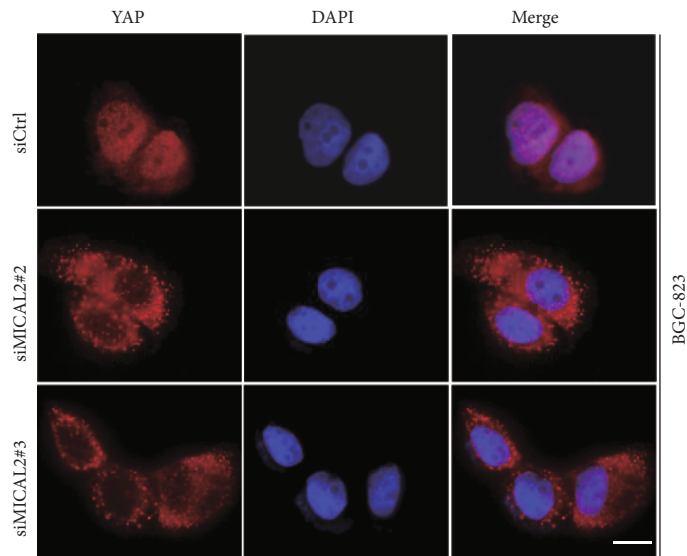
Figure 4: Continued.
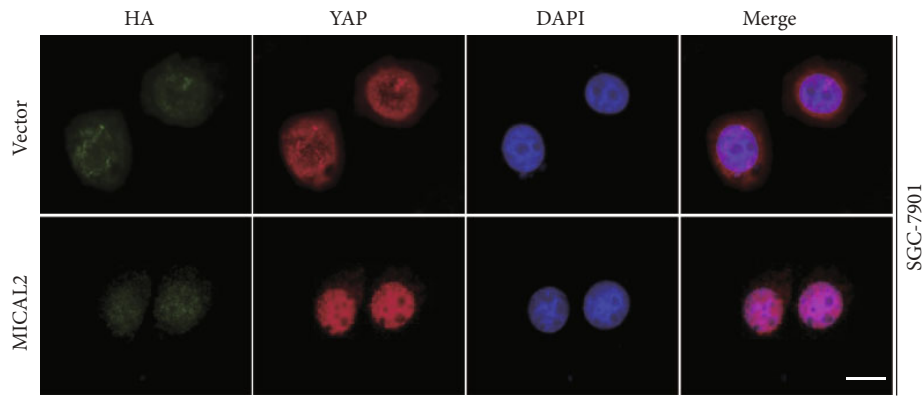
(f)
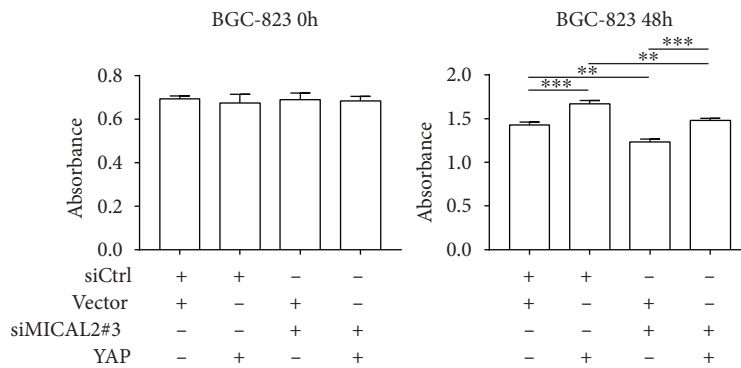
(g)
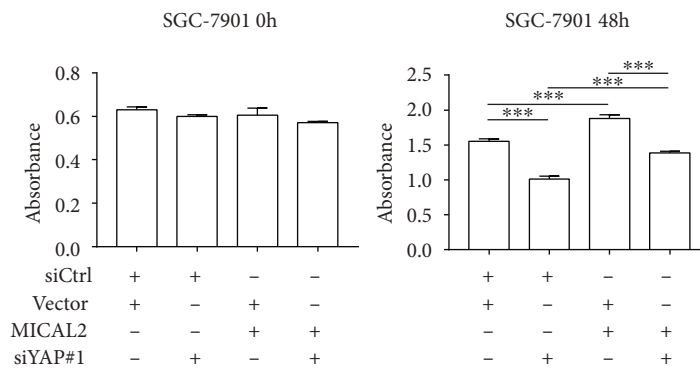
(h)

Figure 4: MICAL2 positively regulates YAP protein levels and reduces YAP phosphorylation. (a, b) The protein levels of YAP and p-YAP were detected by Western blotting analysis in BGC-823 cells transfected with siMICAL2 (a) and SGC-7901 cells transfected with MICAL2 overexpression plasmids (b). (c, d) p-YAP/YAP protein levels in cytoplasmic and nuclear extracts of BGC-823 or SGC-7901 cells separately transfected with siMICAL2 (c) or MICAL2 overexpression plasmids (d) were examined. GAPDH served as the cytoplasmic control and histone H3 as the nuclear control. $^{*}P < 0.05$, $^{**}P < 0.01$, $^{***}P < 0.001$. Data are presented as mean ± SEM of 3 determinations. (e, f) Representative immunofluorescence images of YAP staining in BGC-823 cells transfected with siMICAL2 (e) or SGC-7901 cells transfected with MICAL2 overexpression plasmids (f). Scale bar, 5 μm. (g) The viability of MICAL2-silenced BGC-823 cells cotransfected with YAP expression plasmids and (h) MICAL2-overexpressing SGC-7901 cells cotransfected with siYAP#1 was evaluated by cell counting kit-8 (CCK-8) assay. Data are presented as mean ± SEM of 5 determinations. $^{**}P < 0.01$, $^{***}P < 0.001$.

suggesting the ROS and Cdc42 independently modulate YAP nuclear translocation. When the Cdc42-T17N (inactive mutant) plasmid was cotransfected with the MICAL2 overexpression plasmid into SGC-7901 cells, the reduced p-YAP/YAP level was reversed (Figure 6(d)). In contrast, the increased p-YAP/YAP level was attenuated when Cdc42-Q61L (active mutant) plasmids were transfected into the MICAL2-depleted BGC-823 cells (Figure 6(e)). In addition, Cdc42-Q61L transfection not only attenuated the upregulation of p-YAP/YAP in the cytoplasm but also reversed the downregulation of YAP in the nucleus of those MICAL2-depleted BGC-823 cells (Figure 6(f)). On the contrary, Cdc42-T17N transfection reversed the downregulation of p-YAP/YAP in the
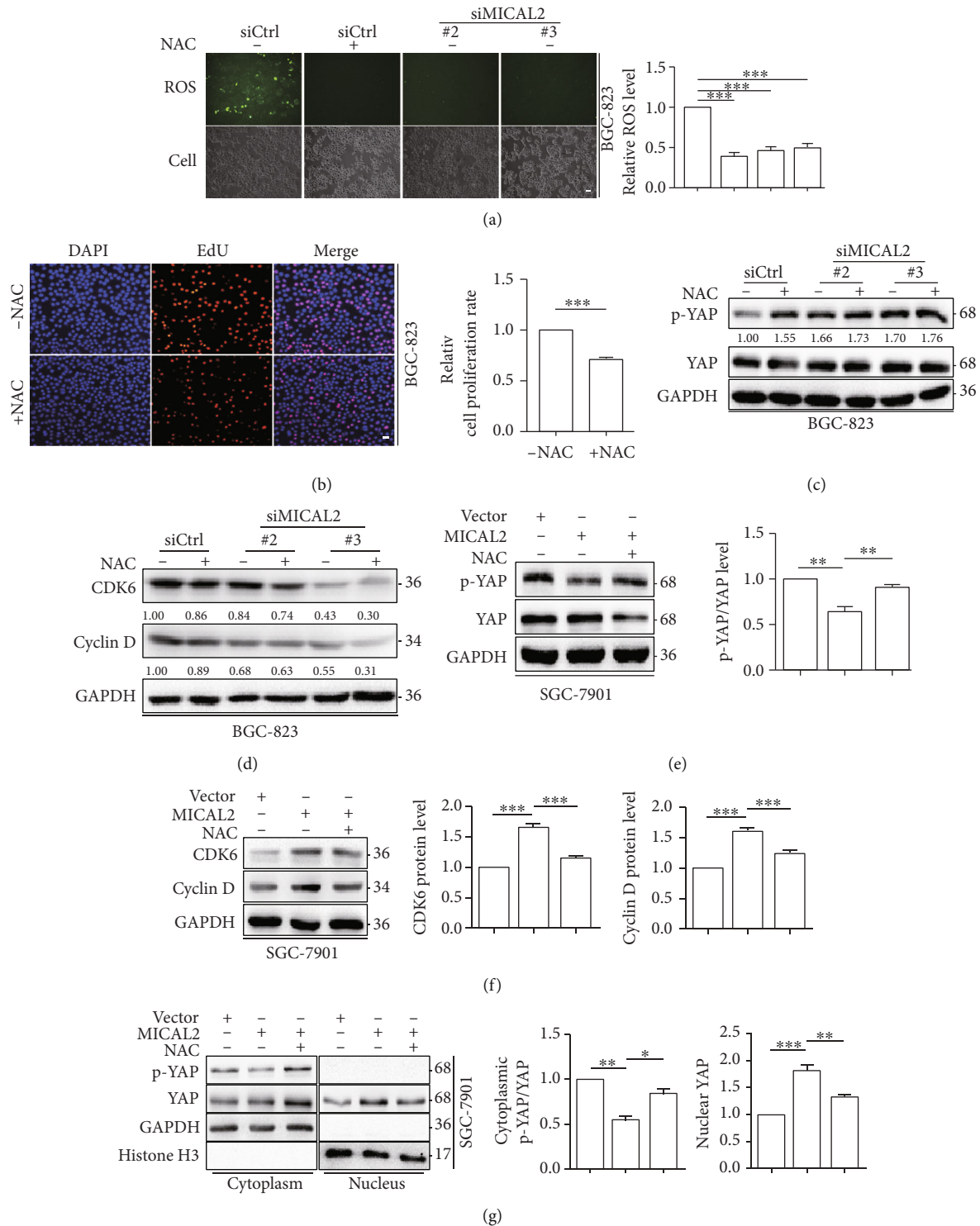
Figure 5: MICAL2 promotes YAP nuclear translocation *via* reactive oxygen species (ROS) generation. (a) The effect of MICAL2 on ROS generation was detected using DCFH-DA in BGC-823 cells transfected with siMICAL2. (b) The effect of N-acetyl-L-cysteine (NAC) on cell proliferation in BGC-823 cells. Scale bar, $5\,\mu$m. Data are presented as mean ± SEM of 5 determinations. (c, d) MICAL2-depleted BGC-823 cells were pretreated with NAC, following which the protein levels of p-YAP, YAP (c), CDK6, and cyclin D (d) were detected by Western blotting analysis. (e, f) MICAL2-overexpressing SGC-7901cells were pretreated with NAC, following which the protein levels of p-YAP, YAP (e), CDK6, and cyclin D (f) were quantified. (g) MICAL2-overexpressing SGC-7901 cells were pretreated with NAC after which the protein levels of p-YAP/YAP in cytoplasmic extracts and YAP in nuclear extracts were examined. GAPDH served as the cytoplasmic control and histone H3 as the nuclear control. $^{*}P < 0.05$, $^{**}P < 0.01$, $^{***}P < 0.001$. Data are presented as mean ± SEM of 3 determinations.
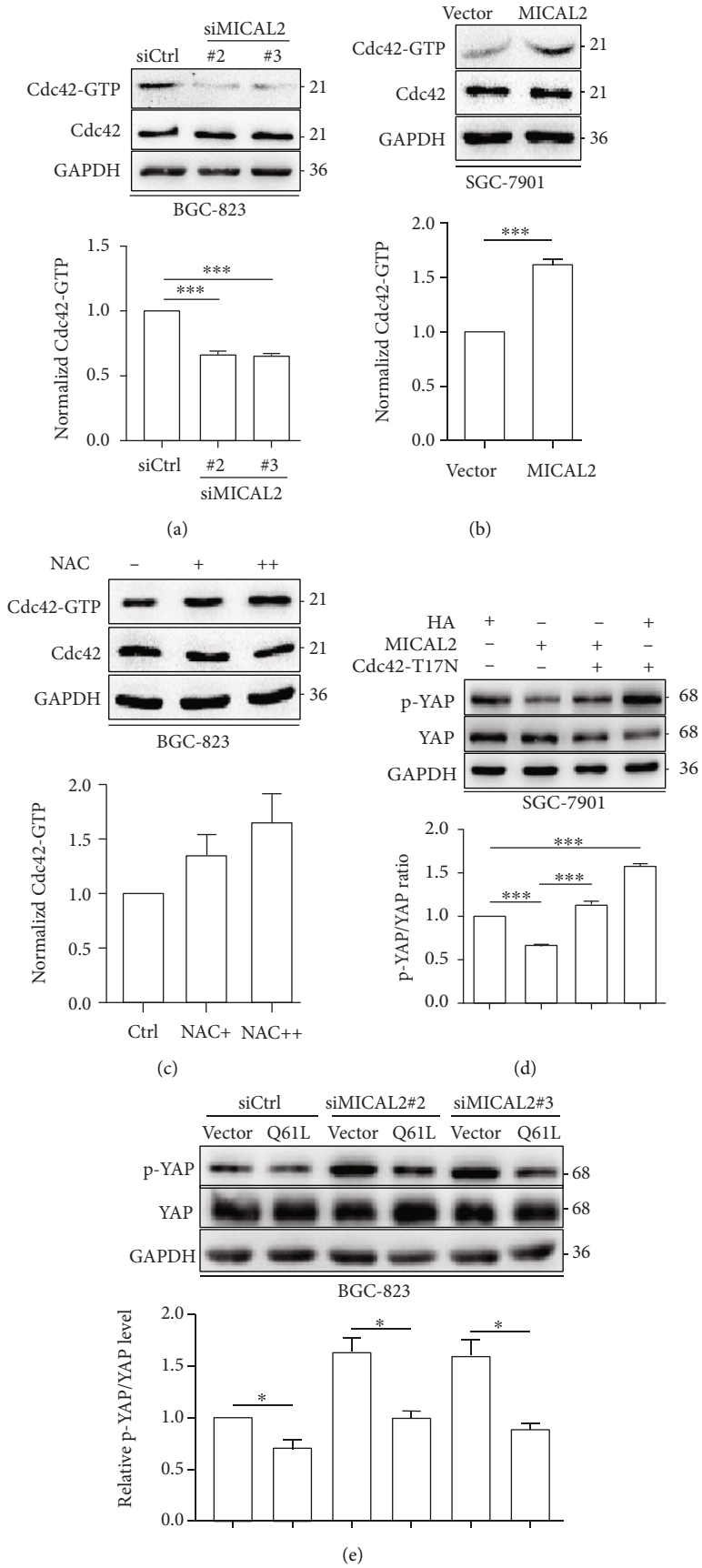
Figure 6: Continued.

(f)

(g)
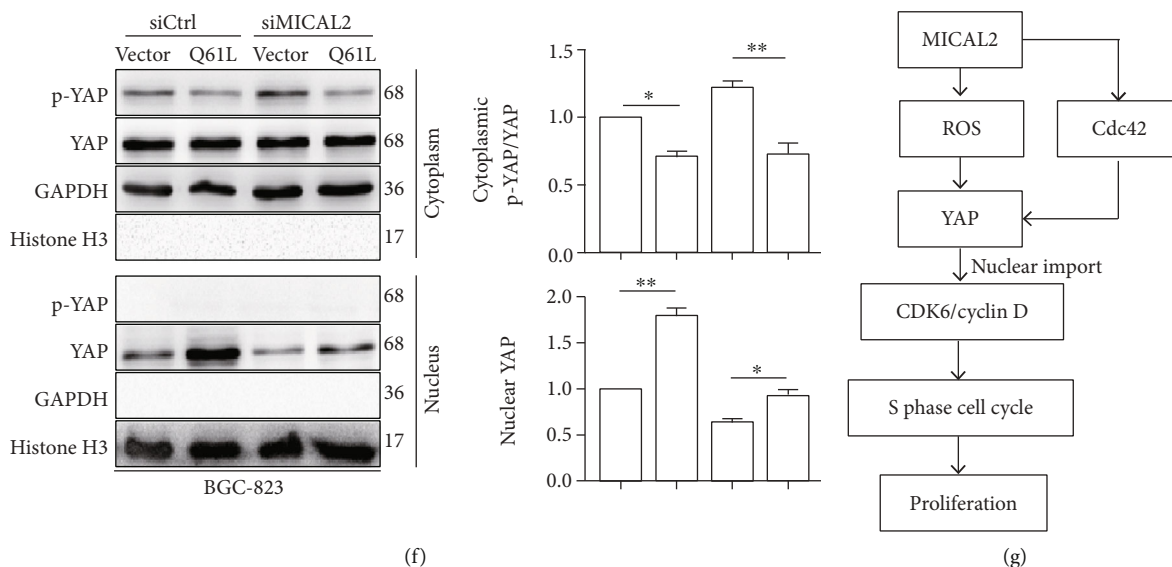
Figure 6: MICAL2 promotes YAP nuclear translocation through Cdc42 activation. (a, b) BGC-823 or SGC-7901 cells were separately transfected with siMICAL2 or MICAL2 overexpression plasmids, following which the levels of the activated form of Cdc42 were measured by pulldown assays. (c) BGC-823 cells were pretreated with 5 mM or 10 mM N-acetyl-L-cysteine (NAC) for 4 h after which the protein levels of GTP-Cdc42 were assessed. (d) MICAL2-depleted BGC-823 cells were transfected with Cdc42-Q61L expression plasmids and analyzed for p-YAP/YAP levels by Western blotting. (e) Cells overexpressing MICAL2 were transfected with Cdc42-T17N and analyzed for p-YAP/YAP levels. (f) MICAL2-depleted BGC-823 cells were transfected with Cdc42-Q61L following which p-YAP/YAP levels in cytoplasmic extracts and YAP levels in nuclear extracts were examined. GAPDH served as the cytoplasmic control and histone H3 as the nuclear control. $^*P < 0.05$, $^{**}P < 0.01$, $^{***}P < 0.001$. Data are presented as mean ± SEM of 3 determinations. (g) Schematic model for how MICAL2 regulates YAP nuclear translocation and proliferation in gastric cancer cells.

cytoplasm and upregulation of YAP in the nucleus of those MICAL2-overexpressed SGC-7901 cells (Figure S4b). Combined, these findings demonstrated that Cdc42 activation is required for MICAL2-mediated YAP nuclear translocation in gastric cancer cells. A schematic model showing how MICAL2 regulates YAP nuclear translocation and proliferation in gastric cancer cells is shown in Figure 6(g).

4. Discussion

It is increasingly clear that cytoskeletal rearrangements can activate oncogenes and induce changes in cell proliferation [30–32]. MICALs are multidomain flavoprotein monooxygenases that catalyze actin redox reactions and destabilize F-actin in cytoskeletal structures [33]. However, to date, relatively few studies have explored the roles of these proteins in the proliferation of human cancer cells. In mammals, the MICAL family of proteins comprises both MICAL (1–3) and MICAL-like (-L1, -L2) forms [34]. In contrast to previous findings indicating that MICAL2 is highly expressed in several other types of cancer [20, 21, 35], in the present study, we found that MICAL2 is highly expressed in gastric cancer cells and is associated with gastric cancer cell proliferation. Subsequently, we investigated the mechanisms by which MICAL2 exerts its proliferative effects in these cancer cells.

Cyclins are cell cycle regulators and function in association with cyclin-dependent kinases (CDKs). Cyclin D, a putative protooncogene, forms a complex with CDK6,

thereby accelerating the G1/S cell cycle transition. We showed that CDK6 and cyclin D protein levels were markedly downregulated in MICAL2-knockdown gastric cancer cells, whereas MICAL2 overexpression elicited the opposite effect. Additionally, compared with control cells, the percentage of cells at the S phase of the cell cycle was decreased when MICAL2 was silenced and increased when MICAL2 was overexpressed. Together, these data revealed that MICAL2 promotes cell proliferation via stimulating the G1-to-S-phase cell cycle transition, presumably by modulating the levels of CDK6 and cyclin D.

Cyclin D and CDK6 are regulated by several pathways, including the ERK/MAPK, NF-κB, and Hippo signaling pathways. The ERK/MAPK pathway is at the core of the signaling network involved in regulating G1/S-phase progression [36] and both cyclin D and CDK6 are important target genes of this pathway [37, 38]. Although MICAL1, another MICAL family member, was shown to promote ERK phosphorylation and nuclear translocation, a key mechanism mediating breast cancer cell proliferation [39], our results revealed that the knockdown of MICAL2 did not induce significant changes either in p-ERK content or in its nuclear distribution. The NF-κB pathway is also reported to exert its functions in cell cycle progression through the induction of cyclin D during the G1/S-phase transition [40], and the NF-κB subunit p65 has been observed to physically and functionally interact with CDK6 [41]. However, our results showed that MICAL2 depletion did not significantly alter the protein level or subcellular localization of p65. Meanwhile, the Hippo pathway is known

to limit organ size, which is associated with its capacity to regulate cell proliferation, apoptosis, and stem cell self-renewal [42, 43]. In this study, we uncovered that YAP is a target of MICAL2, as evidenced by the findings that the knockdown of MICAL2 increased the p-YAP/YAP ratio and inhibited YAP protein levels and its nuclear translocation, opposite to that seen with MICAL2 overexpression. Our results suggested that the function of MICAL2 in gastric cancer cell proliferation is mediated through YAP rather than an ERK- or NF-κB-dependent mechanism.

MICAL family members normally contain an N-terminal flavoprotein monooxygenase (MO) domain; a Lin11, Isl-1, and Mec-3 (LIM) domain; a calponin homology (CH) domain; and a C-terminal coiled-coil (CC) domain [44]. The latter is responsible for an autoinhibitory mechanism that prevents ROS generation [44]. As MICAL2 lacks a CC domain, its MO domain is constitutively active and generates ROS directly. Additionally, MICAL2 oxidizes and promotes depolymerization of F-actin through its MO domain [45]. Consistent with these findings, we showed that ROS contents were markedly reduced in MICAL2-knockdown cells, suggesting that MICAL2 is a primary source of ROS production in gastric cancer cells. The Hippo signaling pathway is particularly sensitive to redox reactions [46, 47]. There is increasing evidence indicating that Hippo signaling activation is critically regulated by oxidative stress. For example, ROS production has been reported to lead to increased YAP mRNA and protein levels in hepatocellular carcinoma cells [48], while Ras activation- and mitochondrial dysfunction-stimulated ROS production can inactivate the Hippo pathway and induce metastatic behavior in benign tumors [49]. Here, we found that the ROS scavenger NAC and antioxidant Tempol prevented MICAL2 overexpression-induced increases in YAP nuclear translocation, CDK6 and cyclin D levels, and cell proliferation and decreases in p-YAP content. These findings provide solid evidence that MICAL2 promotes gastric cancer cell proliferation via ROS-dependent YAP signaling.

It is noteworthy that Cdc42 also associated with YAP nuclear translocation in cancer cells. For example, activated Cdc42 suppresses YAP phosphorylation, resulting in its nuclear localization and, consequently, the growth of, and development of drug resistance in, colorectal cancer cells [50]. Meanwhile, Cdc42 deficiency was shown to induce podocyte apoptosis by inhibiting the activation of the Nwasp/stress fibers/YAP signaling pathway [14]. Studies have demonstrated that ROS can suppress the activation of Cdc42GAP (GTPase-activating protein), a protein that is required for Cdc42-mediated GTP hydrolysis [51], which suggests that ROS might stimulate YAP nuclear translocation via Cdc42 activation. In contrast, our results showed that MICAL2 overexpression resulted in a significant increase in Cdc42 activation in gastric cancer cells. Cdc42 activation reduced YAP phosphorylation levels and increased its nuclear translocation in MICAL2-silenced cells, initially suggestive of a dependency of Cdc42 on MICAL2/YAP signaling; however, our results further revealed that treatment with NAC or tempol resulted in a moderate stimulation of Cdc42 activity, which implied that ROS and

Cdc42 activation might serve as independent mediators of MICAL2-induced YAP nuclear translocation. ROS levels can reportedly regulate the expression of MST1, which acts upstream of the Hippo pathway [52], as well as upregulate YAP mRNA and protein levels through the c-Myc pathway in hepatocellular carcinoma cells [48]. The mechanism involved in ROS-mediated regulation of YAP nuclear translocation requires further investigation.

5. Conclusion

The present study was a continuation of our previous work in which we demonstrated that the P38/HSP27/cytoskeleton signaling pathway is selectively responsible for MICAL2-induced breast cancer cell invasion [17]. In this study, we have identified a pathway that contributes to MICAL2-mediated gastric cancer cell proliferation involving YAP nuclear translocation. We have also found that MICAL2-mediated cellular ROS generation and Cdc42 activation may independently serve as important mediators of MICAL2-stimulated YAP nuclear translocation. Our results are of importance for understanding the pathophysiological role of MICAL2 in cancer cell proliferation and highlight that targeting MICAL2 may represent a novel intervention strategy for inhibiting gastric cancer progression.

Data Availability

The data used to support the findings of this study are available from the corresponding author upon request.

Conflicts of Interest

The authors confirm that there are no conflicts of interest.

Authors' Contributions

JD designed the study. CQ, PM, and QW performed the experiments. CQ, YW, YS, MB, and YZ performed the statistical analysis. JD and CQ drafted the manuscript. JD supervised the experimental work. All authors read and approved the final manuscript.

Acknowledgments

Supplementary Materials

Figure S1: the effect of MICAL2 on YAP distribution. (a, b) The effects of MICAL2 on YAP distribution in BGC-823 cells transfected with siMICAL2 (a) or SGC-7901 cells transfected with MICAL2 plasmids (b) were quantified. (c) SGC-7901 cells were transfected with empty vector or YAP overexpression plasmids, and total cellular proteins were extracted and analyzed for YAP expression by Western

blotting. (d) BGC-823 cells were transfected with control siRNA or siRNA specifically targeting YAP (siYAP). After 48 h, total protein extracts from cells were analyzed for YAP protein expression. Western blot bands corresponding to YAP, p-YAP, and MICAL2 were quantified and normalized against GAPDH levels. $^*P < 0.05$, $^{**}P < 0.01$. Data are presented as mean ± SEM of 3 determinations. Figure S2: MICAL2 induces cell proliferation independently of the NF-κB and ERK pathways. (a, b) The effects of MICAL2 on NF-κB expression and distribution in BGC-823 cells transfected with siMICAL2 were examined by Western blotting and immunofluorescence assays. (c, d) The effects of MICAL2 on ERK signaling in BGC-823 cells transfected with siMICAL2 were examined by Western blotting and immunofluorescence assays. Scale bar, 5 μm. Figure S3: the effect of tempol on YAP distribution. (a) The effect of tempol on ROS generation was detected using DHE in BGC-823 cells transfected with siMICAL2. (b) The effect of tempol on cell proliferation in BGC-823 cells. Scale bar, 5 μm. Data are presented as mean ± SEM of 5 determinations. (c, d) MICAL2-depleted BGC-823 cells were pretreated with tempol, following which the protein levels of p-YAP, YAP (c), CDK6, and cyclin D (d) were detected by western blotting analysis. (e, f) MICAL2-overexpressing SGC-7901 cells were pretreated with tempol, following which the protein levels of p-YAP, YAP (e), CDK6, and cyclin D (f) were quantified. (g) MICAL2-overexpressing SGC-7901 cells were pretreated with tempol after which the protein levels of p-YAP/YAP in cytoplasmic extracts and YAP in nuclear extracts were examined. GAPDH served as the cytoplasmic control and histone H3 as the nuclear control. Data are presented as mean ± SEM of 3 determinations. $^*P < 0.05$, $^{**}P < 0.01$, $^{***}P < 0.001$. Figure S4: Cdc42 inactivation prevents MICAL2-induced YAP nuclear translocation. (a) BGC-823 cells were pretreated with 3 mM or 6 mM tempol for 4 h after which the protein levels of GTP-Cdc42 were assessed. (b) MICAL2-overexpressed SGC-7901 cells were transfected with Cdc42-T17N following which p-YAP/YAP levels in cytoplasmic extracts and YAP levels in nuclear extracts were examined. GAPDH served as the cytoplasmic control and histone H3 as the nuclear control. $^*P < 0.05$, $^{**}P < 0.01$. Data are presented as mean ± SEM of 3 determinations. (Supplementary Materials)

References

[1] S. McGuire, *World Cancer Report 2014*, vol. 7, no. 2, 2015, Switzerland: World Health Organization, International Agency for Research on Cancer, WHO Press, Geneva, 2015, Adv Nutr 2016.

[2] A. Digklia and A. D. Wagner, "Advanced gastric cancer: current treatment landscape and future perspectives," *World Journal of Gastroenterology*, vol. 22, no. 8, pp. 2403–2414, 2016.

[3] V. Rausch and C. G. Hansen, "The Hippo pathway, YAP/TAZ, and the plasma membrane," *Trends in Cell Biology*, vol. 30, no. 1, pp. 32–48, 2020.

[4] S. A. Manning, B. Kroeger, and K. F. Harvey, "The regulation of Yorkie, YAP and TAZ: new insights into the Hippo pathway," *Development*, vol. 147, no. 8, 2020.

[5] J. W. Jang, M. K. Kim, and S. C. Bae, "Reciprocal regulation of YAP/TAZ by the Hippo pathway and the Small GTPase pathway," *Small GTPases*, vol. 11, no. 4, pp. 280–288, 2020.

[6] C. Huang, W. Yuan, C. Lai et al., "EphA2-to-YAP pathway drives gastric cancer growth and therapy resistance," *International Journal of Cancer*, vol. 146, no. 7, pp. 1937–1949, 2020.

[7] K. Snigdha, K. S. Gangwani, G. V. Lapalikar, A. Singh, and M. Kango-Singh, "Hippo signaling in cancer: lessons from Drosophila models," *Frontiers in Cell and Development Biology*, vol. 7, p. 85, 2019.

[8] N. Raj and R. Bam, "Reciprocal crosstalk between YAP1/hippo pathway and the p53 family proteins: mechanisms and outcomes in cancer," *Frontiers in Cell and Development Biology*, vol. 7, p. 159, 2019.

[9] E. J. Vlug, R. A. van de Ven, J. F. Vermeulen, P. Bult, P. J. van Diest, and P. W. Derksen, "Nuclear localization of the transcriptional coactivator YAP is associated with invasive lobular breast cancer," *Cellular Oncology (Dordrecht)*, vol. 36, no. 5, pp. 375–384, 2013.

[10] M. McGowan, L. Kleinberg, A. R. Halvorsen, A. Helland, and O. T. Brustugun, "NSCLC depend upon YAP expression and nuclear localization after acquiring resistance to EGFR inhibitors," *Genes & Cancer*, vol. 8, no. 3-4, pp. 497–504, 2017.

[11] F. Hao, Q. Xu, J. Wang et al., "Lipophilic statins inhibit YAP nuclear localization, co-activator activity and colony formation in pancreatic cancer cells and prevent the initial stages of pancreatic ductal adenocarcinoma in KrasG12D mice," *PLoS One*, vol. 14, no. 5, article e0216603, 2019.

[12] W. Kang, J. H. Tong, A. W. Chan et al., "Yes-associated protein 1 exhibits oncogenic property in gastric cancer and its nuclear accumulation associates with poor prognosis," *Clinical Cancer Research*, vol. 17, no. 8, pp. 2130–2139, 2011.

[13] S. Dupont, L. Morsut, M. Aragona et al., "Role of YAP/TAZ in mechanotransduction," *Nature*, vol. 474, no. 7350, pp. 179–183, 2011.

[14] Z. Huang, L. Zhang, Y. Chen et al., "Cdc42 deficiency induces podocyte apoptosis by inhibiting the Nwasp/stress fibers/YAP pathway," *Cell Death & Disease*, vol. 7, no. 3, article e2142, 2016.

[15] Q. Jia, W. Zhou, W. Yao et al., "Downregulation of YAP-dependent Nupr1 promotes tumor-repopulating cell growth in soft matrices," *Oncogene*, vol. 5, no. 4, article e220, 2016.

[16] R. B. Haga and A. J. Ridley, "Rho GTPases: regulation and roles in cancer cell biology," *Small GTPases*, vol. 7, no. 4, pp. 207–221, 2016.

[17] Y. Cai, J. Lu, and F. Tang, "Overexpression of MICAL2, a novel tumor-promoting factor, accelerates tumor progression through regulating cell proliferation and EMT," *Journal of Cancer*, vol. 9, no. 3, pp. 521–527, 2018.

[18] C. Ortegon Salas, K. Schneider, C. H. Lillig, and M. Gellert, "Signal-regulated oxidation of proteins via MICAL," *Biochemical Society Transactions*, vol. 48, no. 2, pp. 613–620, 2020.

[19] I. Barravecchia, S. Mariotti, A. Pucci et al., "MICAL2 is expressed in cancer associated neo-angiogenic capillary endothelia and it is required for endothelial cell viability, motility and VEGF response," *Biochimica et Biophysica Acta - Molecular Basis of Disease*, vol. 1865, no. 9, pp. 2111–2124, 2019.

[20] W. Zhou, Y. Liu, Y. Gao et al., "MICAL2 is a novel nucleocytoplasmic shuttling protein promoting cancer invasion and growth of lung adenocarcinoma," *Cancer Letters*, vol. 483, pp. 75–86, 2020.

[21] S. Mariotti, I. Barravecchia, C. Vindigni et al., "MICAL2 is a novel human cancer gene controlling mesenchymal to epithelial transition involved in cancer growth and invasion," *Oncotarget*, vol. 7, no. 2, pp. 1808–1825, 2016.

[22] Y. Wang, W. Deng, Y. Zhang et al., "MICAL2 promotes breast cancer cell migration by maintaining epidermal growth factor receptor (EGFR) stability and EGFR/P38 signalling activation," *Acta Physiologica (Oxford, England)*, vol. 222, no. 2, 2018.

[23] W. Tao, W. Sun, H. Zhu, and J. Zhang, "miR-205-5p suppresses pulmonary vascular smooth muscle cell proliferation by targeting MICAL2-mediated Erk1/2 signaling," *Microvascular Research*, vol. 124, pp. 43–50, 2019.

[24] P. Min, S. Zhao, L. Liu et al., "MICAL-L2 potentiates Cdc42-dependent EGFR stability and promotes gastric cancer cell migration," *Journal of Cellular and Molecular Medicine*, vol. 23, no. 6, pp. 4475–4488, 2019.

[25] S. Fremont, G. Romet-Lemonne, A. Houdusse, and A. Echard, "Emerging roles of MICAL family proteins - from actin oxidation to membrane trafficking during cytokinesis," *Journal of Cell Science*, vol. 130, no. 9, pp. 1509–1517, 2017.

[26] J. Du, C. Sun, Z. Hu et al., "Lysophosphatidic acid induces MDA-MB-231 breast cancer cells migration through activation of PI3K/PAK1/ERK signaling," *PLoS One*, vol. 5, no. 12, article e15940, 2010.

[27] W. Deng, L. Gu, X. Li et al., "CD24 associates with EGFR and supports EGF/EGFR signaling via RhoA in gastric cancer cells," *Journal of Translational Medicine*, vol. 14, no. 1, p. 32, 2016.

[28] E. Rozengurt, J. Sinnett-Smith, and G. Eibl, "Yes-associated protein (YAP) in pancreatic cancer: at the epicenter of a targetable signaling network associated with patient survival," *Signal Transduction and Targeted Therapy*, vol. 3, no. 1, p. ???, 2018.

[29] L. Wang, C. Wang, Z. Tao et al., "Curcumin derivative WZ35 inhibits tumor cell growth via ROS-YAP-JNK signaling pathway in breast cancer," *Journal of Experimental & Clinical Cancer Research*, vol. 38, no. 1, p. 460, 2019.

[30] P. P. Provenzano and P. J. Keely, "Mechanical signaling through the cytoskeleton regulates cell proliferation by coordinated focal adhesion and rho GTPase signaling," *Journal of Cell Science*, vol. 124, no. 8, pp. 1195–1205, 2011.

[31] Q. Xu, L. P. Huff, M. Fujii, and K. K. Griendling, "Redox regulation of the actin cytoskeleton and its role in the vascular system," *Free Radical Biology & Medicine*, vol. 109, pp. 84–107, 2017.

[32] A. Hall, "The cytoskeleton and cancer," *Cancer Metastasis Reviews*, vol. 28, no. 1-2, pp. 5–14, 2009.

[33] S. S. Giridharan and S. Caplan, "MICAL-family proteins: complex regulators of the actin cytoskeleton," *Antioxidants & Redox Signaling*, vol. 20, no. 13, pp. 2059–2073, 2014.

[34] M. A. Vanoni, T. Vitali, and D. Zucchini, "MICAL, the flavoenzyme participating in cytoskeleton dynamics," *International Journal of Molecular Sciences*, vol. 14, no. 4, pp. 6920–6959, 2013.

[35] J. Lu, Y. Li, Y. Wu et al., "MICAL2 mediates p53 ubiquitin degradation through oxidating p53 methionine 40 and 160 and promotes colorectal cancer malignance," *Theranostics*, vol. 8, no. 19, pp. 5289–5306, 2018.

[36] S. Meloche and J. Pouyssegur, "The ERK1/2 mitogen-activated protein kinase pathway as a master regulator of the G1- to S-phase transition," *Oncogene*, vol. 26, no. 22, pp. 3227–3239, 2007.

[37] C. H. Lee, H. J. Yun, H. S. Kang, and H. D. Kim, "ERK/MAPK pathway is required for changes of cyclin D1 and B1 during phorbol 12-myristate 13-acetate-induced differentiation of K562 cells," *IUBMB Life*, vol. 48, no. 6, pp. 585–591, 1999.

[38] L. Scheiblecker, K. Kollmann, and V. Sexl, "CDK4/6 and MAPK-crosstalk as opportunity for cancer treatment," *Pharmaceuticals (Basel)*, vol. 13, no. 12, p. 418, 2020.

[39] W. Deng, Y. Wang, S. Zhao et al., "MICAL1 facilitates breast cancer cell proliferation via ROS-sensitive ERK/cyclin D pathway," *Journal of Cellular and Molecular Medicine*, vol. 22, no. 6, pp. 3108–3118, 2018.

[40] Z. Q. Liang, X. Wang, L. Y. Li et al., "Nuclear factor-kappaB-dependent cyclin D1 induction and DNA replication associated with N-methyl-D-aspartate receptor-mediated apoptosis in rat striatum," *Journal of Neuroscience Research*, vol. 85, no. 6, pp. 1295–1309, 2007.

[41] K. Handschick, K. Beuerlein, L. Jurida et al., "Cyclin-Dependent Kinase 6 Is a Chromatin-Bound Cofactor for NF-κB-Dependent Gene Expression," *Molecular Cell*, vol. 53, no. 2, pp. 193–208, 2014.

[42] U. Ehmer and J. Sage, "Control of proliferation and cancer growth by the hippo signaling pathway," *Molecular Cancer Research*, vol. 14, no. 2, pp. 127–140, 2016.

[43] J. S. Mo, H. W. Park, and K. L. Guan, "The Hippo signaling pathway in stem cell biology and cancer," *EMBO Reports*, vol. 15, no. 6, pp. 642–656, 2014.

[44] S. S. Giridharan, J. L. Rohn, N. Naslavsky, and S. Caplan, "Differential regulation of actin microfilaments by human MICAL proteins," *Journal of Cell Science*, vol. 125, no. 3, pp. 614–624, 2012.

[45] B. C. Lee, Z. Péterfi, F. W. Hoffmann et al., "MsrB1 and MICALs regulate actin assembly and macrophage function via reversible stereoselective methionine oxidation," *Molecular Cell*, vol. 51, no. 3, pp. 397–404, 2013.

[46] A. Ashraf and S. Pervaiz, "Hippo circuitry and the redox modulation of hippo components in cancer cell fate decisions," *The International Journal of Biochemistry & Cell Biology*, vol. 69, pp. 20–28, 2015.

[47] B. Mao, Y. Gao, Y. Bai, and Z. Yuan, "Hippo signaling in stress response and homeostasis maintenance," *Acta Biochimica et Biophysica Sinica*, vol. 47, no. 1, pp. 2–9, 2015.

[48] Y. Cho, M. J. Park, K. Kim et al., "Reactive oxygen species-induced activation of Yes-associated protein-1 through the c-Myc pathway is a therapeutic target in hepatocellular carcinoma," *World Journal of Gastroenterology*, vol. 26, no. 42, pp. 6599–6613, 2020.

[49] S. Ohsawa, Y. Sato, M. Enomoto, M. Nakamura, A. Betsumiya, and T. Igaki, "Mitochondrial defect drives non-autonomous tumour progression through Hippo signalling in _Drosophila_," *Nature*, vol. 490, no. 7421, pp. 547–551, 2012.

[50] Y. Ye, R. Zhang, and H. Feng, "Fibronectin promotes tumor cells growth and drugs resistance through a CDC42-YAP-dependent signaling pathway in colorectal cancer," *Cell Biology International*, vol. 44, no. 9, pp. 1840–1849, 2020.

[51] Q. F. Li, A. M. Spinelli, and D. D. Tang, "Cdc42GAP, reactive oxygen species, and the vimentin network," *American Journal of Physiology. Cell Physiology*, vol. 297, no. 2, pp. C299–C309, 2009.

[52] F. Qin, J. Tian, D. Zhou, and L. Chen, "Mst1 and Mst2 kinases: regulations and diseases," *Cell & Bioscience*, vol. 3, no. 1, p. 31, 2013.

Review Article

Reactive Oxygen Species (ROS) Regulates Different Types of Cell Death by Acting as a Rheostat

Gloria E. Villalpando-Rodriguez[1,2] **and Spencer B. Gibson** [1,2]

[1]*Research Institute in Oncology and Hematology, CancerCare Manitoba, University of Manitoba, Winnipeg, Manitoba, Canada*
[2]*Department of Biochemistry and Medical Genetics, University of Manitoba, Winnipeg, Manitoba, Canada*

Correspondence should be addressed to Spencer B. Gibson; spencer.gibson@umanitoba.ca

Reactive oxygen species (ROS) are essential for cellular signaling and response to stress. The level of ROS and the type of ROS determine the ability of cells to undergo cell death. Furthermore, dysregulation of the antioxidant pathways is associated with many diseases. It has become apparent that cell death can occur through different mechanisms leading to the classifications of different types of cell death such as apoptosis, ferroptosis, and necroptosis. ROS play essential roles in all forms of cell death, but it is only now coming into focus that ROS control and determine the type of cell death that occurs in any given cell. Indeed, ROS may act as a rheostat allowing different cell death mechanisms to be engaged and crosstalk with different cell death types. In this review, we will describe the ROS regulatory pathways and how they control different types of cell death under normal and disease states. We will also propose how ROS could provide a mechanism of crosstalk between cell death mechanisms and act as a rheostat determining the type of cell death.

1. Introduction

Cellular reactive oxygen species (ROS) are tightly controlled to dictate different cell fates, such as differentiation or cell survival. When ROS are produced in excess, such as in cells under metabolic stress, this leads to cell death. This suggests that a "ROS rheostat" exists in cells controlling cellular survival. This rheostat controls ROS levels in the context of cellular microenvironmental signals ensuring that appropriate cellular functions are conducted. This is accomplished by ROS participating in cell signaling pathways, for example, during cell adhesion, host defense, or gene expression. When in excess, ROS may have deleterious effects on signaling and cellular damage leading to cell death.

Cell death was considered a passive event when cells become damaged or injured to a point that they disintegrate into cellular debris often termed necrotic cell death. It was not until genetic studies on *C. elegans* showed that many genes could control the amount of cell death, and physiological changes in cells undergoing cell death were reproducible and distinct [1, 2]. Apoptosis was the first cell death type to

be described in this way, where cell membranes become blebbed and chromatin becomes condensed. This form of cell death was implicated in many physiological and pathological conditions such as immune system development and cellular homestasis [3, 4]. Over time, other forms of cell death were described under different physiological conditions such as iron-mediated cell death, ferroptosis, and autophagy- (self-eating-) induced cell death. Similar to apoptosis, they are regulated by distinct genes; for instance, some of the key genes involved in apoptosis regulation are caspases, TP53, FAS, BCL-2, and BAX. Genes that regulate ferroptosis include GPx4, Nrf2, LSH, TFR1, and SLC7A11. Necroptosis is regulated by LEF1, RIP1, and RIP3, and finally, autophagy regulations are regulated by genes ATG5, ATG7, DRAM3, and TFEB [5, 6].

The different types of cell death induce specific cell signaling pathways. Nevertheless, there are common features among these cell death pathways. One predominant feature is the reliance on ROS signaling and control. ROS produced by cells under stress, or cells with reduced antioxidant capacity, can determine whether the cell survives or dies,

and the type of cell death mechanism engaged. This ability of ROS to act as a rheostat determining not only cell death but the type of cell death is only now coming into focus under pathological or physiological conditions. This review will explore the importance of ROS and its signalling on different types of cell death and how ROS acts a rheostat to determine different types of cell death.

2. Regulation of ROS Production and Antioxidants

Reactive oxygen species (ROS) is a type of unstable molecule that contains oxygen and easily reacts with other molecules in a cell [7]. ROS include reactive molecule derivatives of oxygen (nonradicals) and also oxygen-centered radicals (free radicals). Free radicals and nonradicals can react with each other to produce more free radicals and nonradicals; for instance, two superoxide anions ($O_2^{\bullet-}$) can react to form hydrogen peroxide (H_2O_2), a nonradical ($2O_2^{\bullet-} + 2H_2 \longrightarrow H_2O_2 + O_2$). In turn, hydrogen peroxide can break down in the presence of transition metal ions to produce hydroxyl radical HO^-, the most reactive and damaging of all oxygen free radicals [4, 8, 9]. Other oxygen-derived free radicals are peroxide ion ($O_2^{\bullet 2-}$), perhydroxyl radical ($HO_2^{\bullet}$), alkoxyl radical ($RO^{\bullet}$), and peroxyl radical ($ROO^{\bullet}$). Singlet oxygen ($^1O_2$) and hypochlorous acid (HOCL) are other nonradical derivatives of oxygen [10, 11].

Under physiological conditions, ROS are generated by numerous sources including mitochondria respiratory chain (the major source), NADPH oxidases, xanthine oxidases, lipoxygenases, nitric oxide synthases, and cyclooxygenases (Figure 1). Ninety percent of ROS are generated when electrons escape from the mitochondrial electron transport chain (ETC). The ETC is composed of transmembrane protein complexes (I-IV) and ubiquinone and cytochrome c (electron transfer carriers); when these complexes are assembled, together with complex V (F_1F_0ATP synthase), the oxidative phosphorylation occurs resulting in ATP production. There are two electron transport pathways in the ETC: complex I/III/IV, with NADH as substrate and complex II/III/IV, with succinic acid as substrate. The electrons in the ETC leak out and interact with oxygen to produce superoxide or hydrogen peroxide. CI and CIII, especially CI, are considered to be the main sites of ROS production in mitochondria. There are 11 sites within the ETC where superoxide or hydrogen peroxide are produced. In the matrix, at sites I_F (FMN site) and I_Q (CoQ binding site), ROS are produced during the transfer of electrons from NADH to CoQ in CI. CII produces ROS at site II_F associated with succinate dehydrogenase. CIII transfers electrons through the Q-cycle; in this process, ubisemiquinone (QH^-) of the Q_o site carrying a single electron can move freely in CIII, directly leaking the single electron to O_2, forming ROS through a nonenzymatic reaction. Then, the formed ROS can be released into both the matrix and the intermembrane space; here, superoxide dismutase converts superoxide into hydrogen peroxide, which freely disperses through the outer membrane of mitochondria. It has been found that superoxide can also translocate to the cytosol

through anion channels [8, 9, 12, 13]. Interestingly, ROS production by the mitochondria ETC causes oxidation of cysteine residues in mitochondrial proteins, modifying their function. For instance, cysteine residues in the 51 and 75 kDa subunits of the hydrophilic arm of complex I are sites of S-oxidation (oxidation on thioether moieties of cysteine to form sulfoxides), resulting in decreased complex I activity by limiting proton-motive force reduction and electron flow through the respiratory chain, which could become irreversible upon further oxidation [14]. The electron transport chain from other membranes in the cell (endoplasmic reticulum and plasmatic and nuclear membranes) also produce ROS but at a small scale compared to mitochondria [15–17]. ETC and proton-motive force regulates ROS accumulation, but how this controls the ROS rheostat remains unclear.

As mentioned before, several enzymes are responsible for ROS production. The most important, NADPH oxidase (NOX), catalyzes the process called respiratory burst. There are seven NOX family members: NOX 1-5 and dual oxidases 1 and 2 (DUOX 1 and 2); upon activation, they reduce dioxygen to superoxide anion using NADPH or NADH as an electron donor. Despite the fact that NOX members have a similar structure and enzymatic activity, they differ in their activation mechanism. For instance, NOX 1-4 require p22^{phox}, NOX 1 and 3 need NOXO1, and the small GTPase Rac subunit is associated with NOX 1 and 2. In addition, NOX5 and DUOX 1-2 are activated by calcium and do not require any other subunit [18]. The DUOX enzymes have a double function; they are ROS-generating enzymes and use H_2O_2 to carry out oxidations of other substrates using their peroxidase domain [19]. In neutrophils, NOX activity results in the release of superoxide that plays a bactericidal role. In nonimmune cells, NOX activity plays a role in proliferation, migration, cell adhesion, and growth, and in the nucleus, it plays a role in gene expression [7, 20–24]. Here, GSH donates a hydrogen atom from water oxidizing GSSG. Another scavenger vitamin is ascorbic acid (vitamin C).

Antioxidants are responsible for ROS elimination or prevention of ROS formation to avoid damaging oxidative stress. The antioxidant systems can be divided as enzymatic and nonenzymatic (Table 1). The first one consists mainly in superoxide dismutases, catalase, glutathione peroxidases, peroxiredoxins, and thioredoxins. Nonenzymatic antioxidants are molecules that act by directly quenching free radicals or by radical scavenging; this include but are not limited to vitamins E, C, and A; glutathione; and uric acid [8, 10, 25].

2.1. Enzymatic Antioxidants. Superoxide dismutase (SOD) enzyme is the most important one that protects the cells against superoxide anion. According to cation type and cellular localization, there are three SODs: SOD1 or copper/zinc Cu/ZnSOD, localized mainly in the cytoplasm (but also found in mitochondria and nucleus); SOD2 or manganese MnSOD, localized in the mitochondrial matrix; and extracellular SOD3 or copper/zinc SOD. SODs catalyze superoxide dismutation into hydrogen peroxide using copper/zinc or manganese as cofactors that continuously shift between reduced and oxidized forms in the active site of the enzymes.
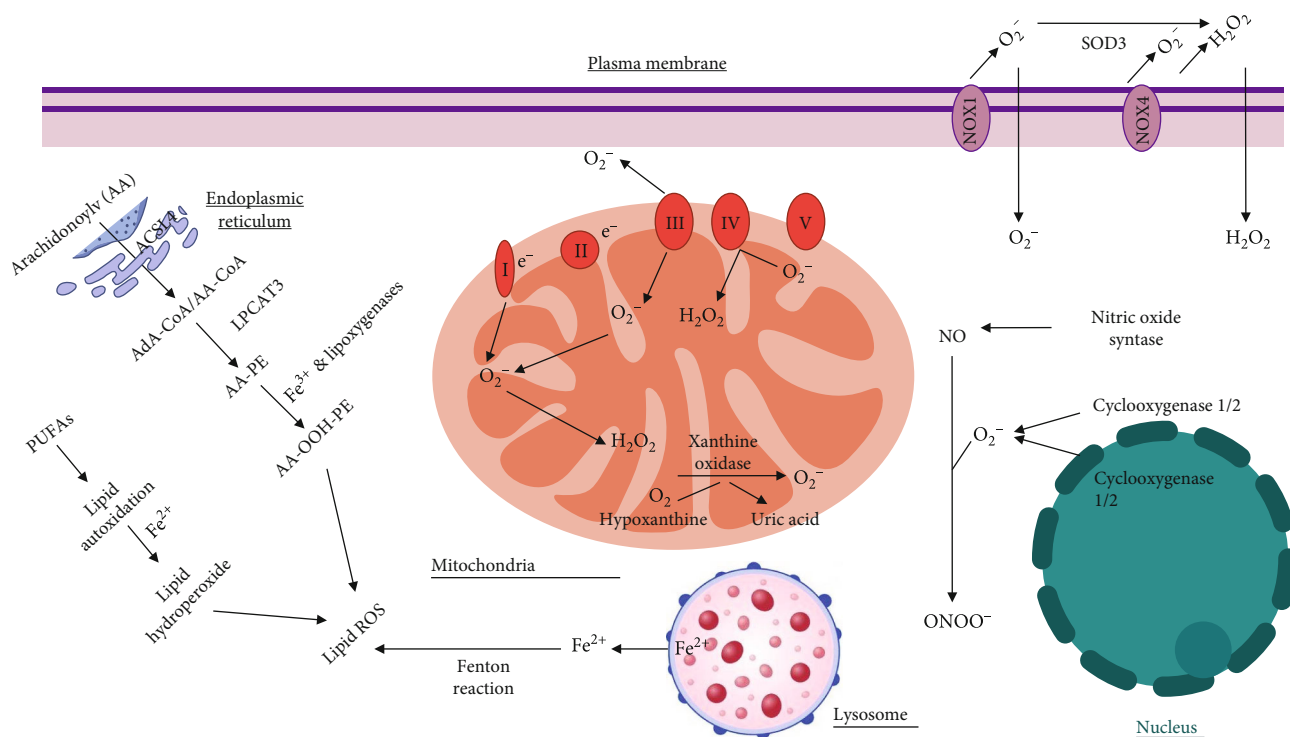
FIGURE 1: Subcellular localization of reactive oxygen species (ROS). The plasma membrane contains NOX enzymes that generate superoxide and hydrogen peroxide. The mitochondrial electron transport chain generates superoxide and hydrogen peroxide at several locations within the mitochondria. Lysosome releases reactive iron that generates lipid ROS. The nucleus generates superoxide through cyclooxygenases. Finally, the endoplasmic reticulum generates lipid ROS.

TABLE 1: Antioxidants and their targets.

Enzymatic antioxidants		
Antioxidant	ROS	Reaction
Superoxide dismutases	Superoxide	$O_2^{\bullet-} + e^- + 2H^+ \longrightarrow H_2O_2$
Catalase	Hydrogen peroxide	$2H_2O_2 \longrightarrow 2H_2O + O_2$
Glutathione peroxidase	Hydrogen peroxide	$H_2O_2 + 2GSH \longrightarrow 2H_2O + GSSG$
Thioredoxins	Oxidized proteins	$R\text{-}S_2 + Trx\text{-}(SH)_2 \longrightarrow R\text{-}(SH)_2 + Trx\text{-}S_2$
Peroxiredoxin	Hydrogen peroxide	$H_2O_2 + Prx\text{-}S^\bullet \longrightarrow H_2O + Prx\text{-}SOH$ $H_2O_2 + Prx\text{-}SOH \longrightarrow H_2O + Prx\text{-}SO_2H$
Nonenzymatic antioxidants		
Antioxidant	ROS	Reaction
GSH	Hydrogen peroxide Oxygen radicals	$2GSH + H_2O_2 \longrightarrow GSSG + 2H_2O$ $GSSG + NADPH + H^\bullet \longrightarrow 2GSH + NADP^+$
$\alpha^\bullet$-Tocopherol (vitamin E)	Lipid peroxyl radicals	$\alpha\text{-}TOH + LOO^\bullet \longrightarrow \alpha\text{-}TO^\bullet + LOOH$ $\alpha\text{-}TO^\bullet + AscH^{-\bullet} \longrightarrow \alpha\text{-}TOH + Asc^{\bullet-}$
Ascorbic acid (vitamin C)	Free radicals, iron, and copper	$AscH^{-\bullet} \rightarrow Asc^{\bullet-} + 2H^+ + 2e$

SOD activity is important not only because it prevents the accumulation of superoxide anion but also because it prevents its reaction to nitric oxide (NO). When these two molecules react, there is not only the production of peroxynitrite, a strong oxidant, but also the inactivation of NO which has anti-inflammatory and anticoagulant properties. Finally, superoxide dismutation by SODs produces hydrogen peroxide which, as mentioned before, is an important signaling molecule [10, 26, 27]. SODs catalyze transformation of superoxide anion by dismutation into hydrogen peroxide. In turn, catalase decomposes hydrogen peroxide into water and oxygen. Catalase contains four identical subunits of 62 kDa, each subunit containing four distinct domains and one prosthetic heme group. One domain has a distal histidine essential for catalase reaction, the second domain has a hydrophobic core that confers its tridimensional structure,

the third domain has a tyrosine residue for heme group binding, and the last domain is an α-helical domain for NADPH binding. Catalase has a nuclear origin and contains a peroxisome-targeting signal sequence KANL (lysine-ala-nine-asparagine-leucine) that imports catalase monomers to the perixosomes where tetramerization and heme addition occur. The hydrogen peroxide decomposition occurs in two reactions: in the first reaction, the catalase heme group is oxidized by one molecule of hydrogen peroxide into a hypervalent iron intermediate compound I (an oxoferryl porphyrin cation radical) with concomitant production of water, and in the second reaction, compound I is reduced by a second hydrogen peroxide molecule to its resting state generating two molecules of water and oxygen [28, 29].

Catalase is not the only antioxidant enzyme that decomposes hydrogen peroxide into water. Glutathione peroxidases (GPxs) belong to a family of enzymes that catalyze the reduction of hydrogen peroxide into water and organic hydroperoxides into alcohols using glutathione as reductant. There are eight human GPxs. GPx1-4 and GPx6 are selenoproteins, whereas GPx5, GPx7, and GPx8 have a cysteine in the catalytic site [30, 31]. GPx4 is widely expressed and differs in its structure and substrate specificity compared to the other family members. This monomer, can react not only with hydrogen peroxide but also with a wide range of lipid hydroperoxides, including those derived from cholesterol and cholesteryl esters using GSH as reducing substrate, though it can also use protein thiols as reductants [32].

Thioredoxins are enzymes that reduce oxidized proteins through the TXR active site that contains a specific and highly conserved motif with two residues of cysteine. There are two isoforms: TRX1, which is localized in the cytosol and nucleus, and TRX, which is found in mitochondria. Thioredoxin reductase enzymes continuously reconvert the oxidized TXR form into the reduced form. Peroxiredoxins reduce hydrogen peroxide by cycling between oxidation and reduction reactions thanks to their enzymatic active site constituted by cysteine amino acids that metabolize H_2O_2. During these redox reactions, the cysteine recycling is mediated by GSH, ascorbic acid, or sulfiredoxins [22].

2.2. Nonenzymatic Antioxidant. GSH is a nonenzymatic antioxidant, the most abundant nonprotein thiol GSH. Its reduced form is tripeptide g-glutamil-cysteinyl-glycine, and its second form is the disulfide-oxidized GSSG. It localizes in the cytoplasm, in the outer mitochondrial membrane, within the endoplasmic reticulum, and in bile and plasma. GSH is synthesized in the cytosol in two reactions. The first one is the rate-limiting reaction that generates γ-glutamyl-cysteine (γ-Glu-Cys) from cysteine and glutamate by the enzyme glutamate cysteine ligase. In the second reaction, glycine is added to the C-terminus of γ-Glu-Cys to generate reduced glutathione (GSH) by the enzyme glutathione synthetase. GSH has several functions, but when acting as an antioxidant, its function is accomplished by glutathione peroxidase (see above) catalyzed reactions. Here, GSH donates a hydrogen atom from water and the oxidized GSSG. GSSG in turn is reduced back to GSH by GSSG reductase at the expense of NADPH, forming a redox cycle. GSH can also

react directly to oxygen radicals by a radical transfer process giving place to the GSH thiol radical and eventually to GSSG [33–35]. Other nonenzymatic antioxidants include vitamins. For instance, the scavenger α-tocopherol (vitamin E) is a lipophilic compound known as a "chain-breaking antioxidant" that protects membranes from oxidation by intercepting lipid peroxyl radicals, preventing the propagation step in the lipid peroxidation process. By doing so, α-tocopherol becomes a tocopheroxyl radical, a stable radical insufficiently reactive to participate in lipid peroxidation reactions [8, 36, 37]. Another scavenger vitamin include ascorbic acid (vitamin C). This hydrophilic molecule acts as an antioxidant by donating electrons, thus acting as a reducing agent that prevents the oxidation of other molecules. By donating electrons, ascorbic acid is oxidized, transforming itself into a free radical called ascorbyl radical; however, this radical is stable and almost unreactive. Also, ascorbic acid can regenerate a tocopheroxyl radical by reducing it back to α-tocopherol [9, 38].

The balance between prooxidant and antioxidant regulatory mechanisms within a cell determines whether it survive or dies. Under physiological conditions, the production of reactive oxygen species (ROS) is counterbalanced by their elimination and/or prevention of formation to maintain a steady-state (stationary) ROS level. This maintains cellular homeostasis, allowing ROS to act as signaling molecules to accomplish physiological functions. When this balance is lost, favouring enhanced ROS levels (through increased ROS production or decreased antioxidants), oxidative damage can occur on proteins, lipids, DNA, nucleic acids, and other macromolecules, leading to functional disturbances and eventually to cell death [11, 39, 38].

Oxidative stress can be classified depending on its intensity. Under physiological conditions, oxidative stress is called oxidative eustress, while the exposure to supraphysiological oxidative challenge is called oxidative distress [38]. Another classification of oxidative stress also based on its intensity has been proposed. In this classification, there are four zones: (1) basal oxidative stress (BOS), (2) low-intensity oxidative stress (LOS), (3) intermediate intensity oxidative stress (IOS), and (4) high-intensity oxidative stress (HOS) [9]. By setting a ROS rheostat level, cellular functions can adapt to microenvironmental signals in favour of cell survival or in favour of a specific cell death pathway as described in the following sections.

3. ROS Signaling

Beyond regulating the level of ROS within the cell using antioxidant or oxidative pathways, ROS induces a wide range of signals within the cell. One of these major signals is the ability of ROS to activate transcription factors. A study reported that production of hydrogen peroxide by xanthine oxidase regulates gene expression of c-jun and c-myc [7]. Hydrogen peroxide, acting as a signaling molecule, has been shown to induce gene expression, through activation of transcription factors c-jun, egr-1, and JE [40, 41]. ROS, in particular hydrogen peroxide, also activates transcription factor NF-κB. Degradation of the NF-κB inhibitory subunit (IκB) is

necessary for NF-κB activation. IKK phosphorylates IκB leading to its ubiquitination and degradation. It has been shown that IKK is S-glutathionylated by ROS inactivating its kinase activity [42, 43]. The kinase upstream of IKK, MEKK1, is also regulated by ROS. MEKK1 is a redox-sensitive kinase that can also be glutathionylated leading to its inactivation. Finally, ROS can block the ubiquitination and degradation of IκB through inhibition of UBcl2 [44, 45]. This activation of NF-κB leads to upregulation of genes associated with cell survival and activation of a negative feedback loop where antioxidant genes such as SOD family members are upregulated (for more detailed information on NF-κB in oxidative stress, refer to Lingappan) [46].

Besides transcription factors, ROS can regulate several signaling pathways affecting many cellular functions and ultimately influencing cell survival or cell death. The MAPK signaling pathway can be activated by ROS. This pathway that includes MAPKs Erk, JNK, and p38 play important roles in cell growth, differentiation, development, cell cycle, and cell survival. The MAPK pathways are often activated by growth factor activation of receptor tyrosine kinases. This leads to the activation of small G proteins such as RAS that leads to MAPK pathway activation. ROS has been shown to activate receptor tyrosine kinases without binding of the ligand and inactivate dual-specificity phosphatase that negatively regulates MAPKs [47]. The JAK/STAT pathway can be activated by ROS oxidation of glutathione [48]. In addition, ROS can allow ASK1 oligomerization and autophosphorylation through oxidizing thioredoxin which inhibits the activation of ASK1. Similar to Erks, phosphatases may be inactivated by ROS leading to prolonged activation of JNK. MAPK p38 is also activated by ROS mediated by MAPK kinase kinase such as ASK1 or MEKK1-4 [49, 50]. The PI3K-Akt signaling pathway, which participates in functions such as protein synthesis, cell cycle progression, proliferation, and cell death, can also be regulated by ROS. On one hand, ROS directly activate PI3K, amplifying its downstream signaling. On the other hand, ROS can inactivate PTEN, which negatively regulates the synthesis of PIP3, inhibiting the activation of Akt, via oxidizing cysteine residues within the active center [51].

Finally, there are regulatory systems responsible for adaptation in response to oxidative stress. The nuclear factor erythroid 2-related factor 2 (Nrf2) pathway is one of them. The Nrf2 protein is ubiquitously expressed, and it is found in the cytosol interacting with its suppressor E3 ligase adapter Kelch-like ECH-associated protein 1 (KEAP1). This interaction happens by binding between the kelch domain of KEAP1 and the Nrf2 second domain (Neh2) (seven domains in total) at two amino acid sequences DLG and ETGE [52–54]. In normal conditions, KEAP1 presents NRF2 for ubiquitination by the E3 ligase complex formed by Cullin3 and RBX1 proteins (CUL3/RBX1), resulting in subsequent NRF2 proteasomal degradation. Additionally, Nrf2 can be degraded by ubiquitination, independent of Keap1, and by phosphorylation of the Nrf2 Neh6 domain [55, 56]. Under redox-challenging conditions, where high levels of ROS induce glutathionylation and alkylation of macromolecules, Nrf2-KEAP1 is dissociated and Nrf2 is translocated to the nucleus. Alteration in KEAP1 cysteine residues leads to the activation of Nrf2. The Nrf2 Neh5 domain has a redox-sensitive nuclear export signal, and once in the nucleus, Nrf2 functions as a transcription factor, and the Neh1 domain enables Nrf2 binding to the antioxidant region elements (AREs: enhancer sequences in the regulatory region of Nrf2 target genes) leading to the expression of antioxidant genes like glutathione peroxidases and stress response iron genes, like for instance, heme-oxygenase 1 [57–59].

Based upon the transcriptional signatures that ROS generates, this could lead to (1) execution of physiological functions such as cell adhesion, migration, and growth; (2) cell survival and proliferation; or (3) cell arrest and cell death. Many ROS-mediated signaling pathways activate cell survival mechanisms such as upregulation of anticell death BCL-2 family members (via NF-κB) or increased expression of antioxidant enzymes that prevents buildup of ROS-generated cell damage, for instance, through the Nrf2 pathway. Conversely, ROS-mediated signaling could activate procell death pathways such a JNK signaling [13, 43, 53]. The balance between this competing ROS signaling pathways will set the rheostat for cellular homeostasis and will determine how a cell will survive or which type of cell death a cell undergoes.

4. ROS in Different Types of Cell Death

When cells die, there is a corresponding increase in ROS from different sources within a cell. During an increase in ROS, damage to cellular organelles such as the mitochondria occurs. Also, ROS produced by nitroxide synthase causes damage to the plasma membrane contributing to cell death. In addition, antioxidant pathways can also be inhibited leading to increased levels of ROS and cell death. At the same time, ROS triggers signaling pathways that contribute to cell survival such as transcription factor NF-κB that increases the expression of antiapoptotic proteins. This balance will determine whether the cell dies or survives. However, how ROS regulate the different types of cell death is only recently coming into focus. For the purpose of this review, four types of cell death will be described (apoptosis, ferroptosis, autophagy, and necroptosis) and the role of ROS in these types of cell death (Figure 2) will be discussed:

4.1. Apoptosis. Apoptosis was the type of programmed cell death that was first described. During apoptosis, three major events take place: activation of protease, degradation of DNA, and phagocytization of apoptotic bodies by neighbour cells. Depending on the proteases activated, we can distinguish two different types of apoptosis: caspase dependent and caspase independent. Caspase-dependent apoptosis can be triggered by two pathways depending on the nature of the inducer agent, that is, by extracellular (extrinsic pathway) or intracellular (intrinsic pathway) perturbations.

The apoptotic extrinsic pathway is initiated by a death receptor and its ligand or by a dependence receptor and the drop on the levels of its ligand. Death receptors contain in their intracellular region a domain called death domain that
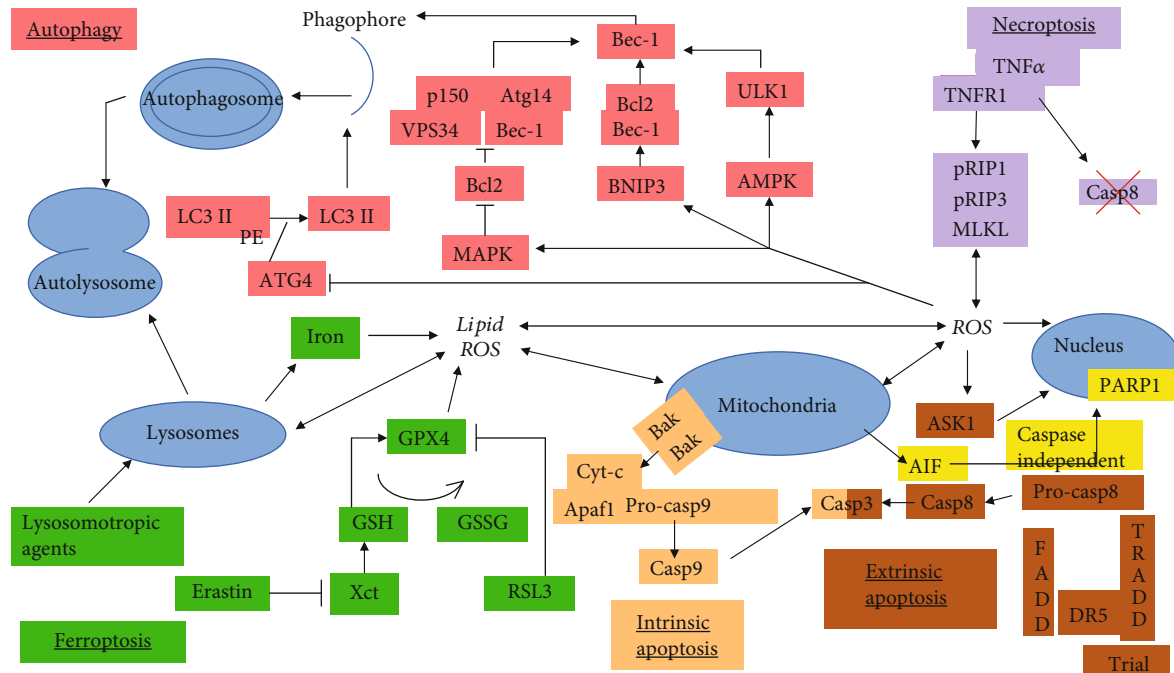
FIGURE 2: Role of reactive oxygen species (ROS) in different types of cell death signaling. ROS contributes to autophagy-induced cell death through activation of BNIP3, AMPK, and MAPK and inactivation of ATG4. ROS also induces apoptosis through mitochondrial damage, ASK1 activation, and PARP activation. Ferroptosis is regulated by lipid ROS leading to lysosome disruption, mitochondrial damage, and increased ROS. Finally, RPS contributes to necroptosis through activation of the MLK1 complex.

allows the formation of the death-inducing signaling complex (DISC). The best studied death domains are Fas, TNFR1, and DR4-5, and the ligands involved in this pathway are Fas ligand, TNF-α, and TNF-related apoptosis-inducing ligand (TRAIL). DISC is composed of the death receptor, an adaptor protein like the Fas-associated death domain (FADD) or the TNF receptor 1-associated protein (TRADD), and procaspase 8. This last element suffers autoproteolitic cleavage that results in the activation of caspase 8 which in turn will activate executioner caspase 3 [60–63]. Even though intracellular ROS have been shown to activate intrinsic apoptosis (described below), there is evidence that ROS also participate in the execution of extrinsic apoptosis; even more, it has been found that ROS can induce both extrinsic and intrinsic pathways at the same time. In a study, HL-7702 cells treated with matrine showed an increase in ROS levels and lipid peroxidation as well as a decrease in SOD and GSH activity in a dose-dependent manner. Matrine also induced upregulation of Keap1 expression and downregulation of cytosolic and nuclear Nrf2, and it also inhibited the expression of Nrf2 downstream targets, heme-oxygenase and quinone reductase NQO1, and promoted the KEAP1/Nrf2 complex formation. Mitochondrial membrane potential was decreased, and cytochrome c was released from the mitochondria to the cytosol. Besides the intrinsic pathway, matrine also increased Fas death receptor expression and caspase 8 activation. In addition, antioxidant N-acetylcysteine (NAC) partially reduced matrine-induced apoptosis [64]. It was also shown that TNF-α-sensitive mesangial cells stimulated by the death receptor ligand TNF-α undergo apoptosis through increased superoxide anion, whereas its downstream

compounds hydrogen peroxide and peroxynitrite remained unchanged. This was demonstrated by using the superoxide anion scavenger Tiron, the hydrogen peroxide scavengers GSH and catalase, and the peroxynitrite scavenger uric acid. Results showed no effect from pretreatment with GSH, catalase, or uric acid on cell death; only Tiron was able to reduce all apoptotic markers. This was further confirmed by transient transfection with SOD2 plasmid that significantly reduced the percentage of apoptotic cells, whereas catalase transfection had no effect on cell death. Pretreatment with both catalase and uric acid had no effect on TNF-α induced cell death [65]. Thus, ROS is involved in the extrinsic apoptotic pathway.

As mentioned before, the apoptotic intrinsic pathway is initiated by intracellular stress such as DNA damage, endoplasmic reticulum stress, and oxidative stress. These stress signals generally activate proapoptotic proteins BAK and BAX, belonging to the BCL-2 family of proteins. These two proteins mediate mitochondrial outer membrane permeabilization by forming pores across the outer mitochondrial membrane. Oxidative stress is a factor that enhances the opening of the mitochondrial permeability transition pore (mPTP). A transient opening may occur under physiological conditions; however, sustained opening of mPTP induces cell death by increasing oxidant stress, causing ATP depletion, and/or by triggering matrix swelling and subsequent rupture of the outer mitochondrial membrane. This permeabilization leads to the release of apoptotic molecules like apoptosis-inducing factor (AIF), SMAC/DIABLO, or cytochrome c. Cytosolic cytochrome c binds to the apoptotic protease-activating factor-1 (APAF-1) that undergoes oligomerization

and recruits procaspase 9 forming the apoptosome. Procaspase 9 within the apoptosome is activated and liberated from the complex; caspase 9 then activates the executioner caspases 3 and/or caspase 7 [62, 66–68]. The intrinsic apoptotic pathway is the most studied form of cell death that requires increased mitochondrial ROS. This mitochondrial ROS is generated by dysfunctional oxidative phosphorylation mediated in part by NOX. It has been shown, in an *in vivo* model, that angiotensin II induced sustained activation of calcium/calmodulin- (Ca^{2+}/CaM-) dependent protein kinase II due to NOX oxidation, resulting in myocardial apoptosis. Moreover, transgenic mice $p47^{-/-}$ (unable to assemble the ROS-producing complex NADPH oxidase) did not show apoptotic markers after angiotensin II treatment; however, direct addition of hydrogen peroxide caused apoptosis, showing that the resistance to induce apoptosis is due to NOX inability to produce ROS [69]. In addition, inhibition of thioredoxin reductase leads to increased ROS and apoptosis [70]. Another source of ROS comes from the deregulation of the antioxidant pathways leading to apoptosis. In thymocytes, glucocorticoid methylprednisolone induced production of peroxides and depletion of GSH prior to an increase of intracellular calcium and later DNA fragmentation, as shown by the oligonucleosomal-length fragments [71]. Another study found that artesunate treatment of doxorubicin-resistant T leukemia cells resulted in an accumulation of hydrogen peroxide followed by caspase-dependent apoptosis via the intrinsic pathway as confirmed by the release of cytochrome c from mitochondria, the activation of caspase 9 and caspase 3, and DNA fragmentation. Moreover, pretreatment with NAC not only decreased hydrogen peroxide levels but also significantly blocked artesunate-induced apoptotic cell death [65]. Accumulation of superoxide anion in vascular endothelial ECV304, treated with *Vibrio vulnificus* cytolysin, induced release of cytochrome c, caspase 3 activation, and DNA fragmentation. In addition, the superoxide anion scavenger TEMPO successfully blocked its production, totally blocked cytochrome c release, abolished caspase 3 activation, and completely inhibited apoptosis [66]. Finally, lysosome-disrupting agents lead to lysosomal membrane permeabilization (LMP), causing increased ROS production followed by mitochondrial dysfunction and apoptosis [72]. This indicates a central role of ROS in the intrinsic apoptotic pathway.

Mitochondrial dysfunction due to ROS can induce the release of mitochondrial AIF resulting in its translocation to the nucleus where it causes DNA condensation and apoptosis through caspase-independent mechanisms [73]. The effect of oxidized alpha-linolenic acid-rich oils was analyzed in neuronal SH-SY5Y cells. After 3 hours of treatment with oxidized perilla and linseed oil (oxidized by heat), cells presented increased ROS levels followed by loss in mitochondrial membrane potential. Annexin V and PI staining showed that the oxidized oil treatment induced apoptosis, and pretreatment with antioxidant drug N-acetylcysteine (NAC) decreased apoptosis. Even more, oxidized oil treatment also induced release of mitochondrial AIF and an increase in nuclear truncated AIF (tAIF) expression, showing activation of caspase-independent apoptosis. Blocking ROS accumulations with NAC results in restoring mitochondrial

AIF levels but had no effect on caspase-3-activated levels [74]. This suggest that ROS plays a role in both caspase-dependent and independent apoptosis.

4.2. *Ferroptosis.* The cell death mechanism called ferroptosis is a newly described regulated cell death characterized by the iron-dependent intracellular accumulation of ROS and lipid peroxidation products. From a biochemical, morphological, and genetic perspective, ferroptosis is different from other regulated cell death types. During ferroptosis, cells are rounded-up and detached and mitochondria size is smaller than the normal, with increased mitochondrial membrane density and reduction/vanishing of mitochondria crista and outer mitochondrial membrane rupture, similar to apoptosis. Unlike apoptosis, normal nuclear size and nonchromatin condensation is observed [75, 76].

Ferroptosis was first characterized by treatment of cells with two small molecules, Ras Selective Lethal (RSL) and erastin that were developed to be selectively lethal to cells expressing oncogenic mutant Ras. Erastin was shown to inhibit the mitochondrial voltage-dependent anion channel 2 and 3 (VDAC2 and VDAC3) and cysteine/glutamate antiporter or system xCT. The xCT system is an antiporter composed of the transmembrane transporter protein SLC7A11 and the single-pass transmembrane regulatory protein SLC3A2, both linked by a disulfide bridge. It imports extracellular cysteine and exports intracellular glutamate. Cysteine import is necessary for GSH synthesis, and it has been found that erastin treatment depletes intracellular GSH [77–79]. GPx4 inhibits lipid peroxidation by catalyzing the transformation of lipid hydroperoxides into lipid alcohols, utilizing glutathione downstream of the xCT system. RLS3 induces ferroptosis by directly inhibiting GPx4 [80].

Iron is an essential component for ferroptosis, and it is thought that iron chelators block ferroptosis because iron plays the role of electron donor to oxygen for ROS formation. For this, iron must be free and in its reactive form (labile iron pool). A labile iron pool is distributed mainly in lysosomes and the cytoplasm, and it is supplied by circulating iron through the following steps. Protein transferrin receptor 1 (TFR1) imports ferric iron Fe^{+3} (carried by transferrin). It is located in the endosome where it is reduced to ferrous iron Fe^{+2} by the STEAP3 enzyme and released by divalent metal transporter 1 (DMT1) into the cytoplasm iron labile pool. Iron is stored by ferritin, and ferroportin exports it. Ferroptosis-sensitive cells bearing a Ras mutation have increased TFR1 and decreased ferritin; this is an example of iron transport protein deregulation that leads to iron overload. Under this circumstance, excessive Fe^{+2} will produce ROS by the Fenton reaction generating hydroperoxides or lipid hydroperoxides which damage intracellular structures such as membranes [81–83]. This lipid oxidation is inhibited by iron chelator deferoxamine; antioxidants like α-tocopherol, GSH, and NAC; and specific ferroptosis inhibitors like ferrostatin-1 (Fer-1), Liproxstatin-1, and Zileuton. Studies with these inhibitors showed that iron-dependent ROS and lipid peroxidation are necessary for ferroptosis induction [84].

Besides iron, ferroptosis also relies on disruption of the antioxidant pathways, for instance, through inhibition of

GPx4, the xCT system, and heme-oxygenase-1. One study showed that hemin treatment in human monocytic THP-1 cells induced ROS generation and cell death in a dose-dependent manner. Pretreatment with antioxidants NAC and diphenyleneiodonium chloride (NADPH oxidase inhibitor) as well as the iron chelator deferoxamine (DFO) decreased ROS generation and cell death. Fer-1 decreased hemin-induced cell death, and a combination of hemin and erastin further increased cell death. In addition, neither necroptosis inhibitors nor pan-caspase zVAD-fmk affect cell death rates of hemin-treated cells [85]. Another study also showed the involvement of NADPH oxidase in ferroptosis. SH-SY5Y dopaminergic cells were treated with two pesticides, paraquat and maneb, and results showed induction of ferroptosis associated with NOX. Furthermore, an increase in lipid peroxidation and reductions in GSH and GPx4 were found. Inhibition of NOX with apocynin or diphenyleneiodonium reduced lipid peroxidation, restored GSH and GPx4, and reduced ferroptotic cell death. In addition, NOX activation with phorbol myristate acetate or addition of hydrogen peroxide amplified the effects of both pesticides on ferroptosis [86]. A study in carbon tetrachloride- (CCl4-) induced mouse liver fibrosis showed the presence of ferroptosis biomarkers in fibrotic cells when treated with artesunate. It also showed that artesunate, in human hepatic stellate cell line LX2, induced cell death after 24 hr. Iron accumulation, an increase in ROS production, an increase in lipid peroxidation, and a decrease in GSH content and GPx4 activity, were also observed in these cells, indicating that artesunate triggered ferroptosis *in vitro* and *in vivo*. Furthermore, cotreatment with DFO inhibited iron release, lipid peroxidation, and ROS and increased cell viability compared with artesunate alone in the cell line [87]. Taken together, ROS play a central role in ferroptosis.

4.3. Autophagy-Mediated Cell Death. Autophagy is a double-edged sword providing cell survival but under certain conditions, it induces cell death. Autophagy is activated in the context of nutrient and growth factor deprivation, endoplasmic reticulum stress, bacteria infection, and protein aggregate and damaged organelle elimination. It also has a role in cell differentiation, development, growth control, remodelling tissue, among others [88, 89].

There are at least three types of autophagy: chaperon-mediated autophagy, microautophagy, and macroautophagy (hereafter referred to as autophagy, which is the best studied among the three forms). The genes involved in the execution and regulation of autophagy are called autophagy-related genes (ATG), and the resultant proteins form complexes that regulate the different stages of autophagy such as nucleation, autophagosome membrane elongation, autophagosome closure, autophagosome-lysosome fusion, and autolysosome content degradation. The nucleation complex is the structure that forms the membrane autophagosome. The endoplasmic reticulum, mitochondria, Golgi, and plasma membrane are sources for the autophagosome formation, but they also recruit and assemble the complex of vsp34, beclin1, vsp15, and ATG9 in the autophagosome membrane formation. ATG7, the ATG5/12 complex, conjugation of the light chain

protein 3 (LC3), and phosphatidyethanolamine are responsible for the autophagosome membrane elongation, and finally, the autophagosome fuse with a lysosome to form the autolysosome. Once in the autolysosome, the cargo will be degraded by hydrolases and the acidification of autolysosome lumen by the proton pump. The constituent components of the degraded cargo exit the lysosome through permeases at the lysosomal membrane into the cytosol. During selective autophagy, proteins like p62 or neighbour of BRACA1 gene 1 (NBRI) act as receptors and adaptors of ubiquitinated substrates to be degraded; hence, they act as bridges between the specific cargo to be degraded and the autophagic machinery [90–93].

Autophagy-mediated cell death is induced through this machinery degrading essential cellular structures to a point where the cell cannot recover. In addition, autophagy could lead to apoptosis through the intrinsic pathway. Under severe stress or injury, cells undergo a form of autophagy-induced cell death called autosis. This autophagy-dependent nonapoptotic form of cell death is characterized by enhanced cell substrate adhesion, focal ballooning of the perinuclear space, and dilation and fragmentation of the endoplasmic reticulum. Autosis is mediated by the Na/K+ ATPase and has been associated with neonatal cerebral hypoxia ischemia [94].

Autophagy is regulated by several negative regulatory pathways. The best characterized mechanism of autophagy regulation is mTOR dependent. Protein kinase mammalian target of rapamycin (mTOR) is an autophagy negative regulator and responds to nitrogen levels in the cell. When nutrients are sufficient, mTOR is activated and autophagy is inhibited. There are several mTOR downstream targets that regulate autophagy. For instance, mTOR complex 1 phosphorylates and actively sequesters the mammalian homolog of Atg1, ULK1, in a complex with Atg13 and FIP200 in an inactive state inhibiting autophagy. AMP-activated protein kinase (AMPK) inhibits mTOR activity, reducing ULK1 phosphorylation and promoting its release from mTORC1, during nutrient deprivation. AMPK can also phosphorylate and activate Tuberous sclerosis complex 2 (TSC2) and Raptor inhibiting of mTOR activity. This in turn activates autophagy [90]. Further downstream, the antiapoptotic protein BCL-2 binds to Beclin-1 preventing the formation of autophagosomes. Under starvation conditions, BCL-2 dissociates from Beclin-1 through JNK phosphorylation of BCL-2 allowing autophagy activation. The growth factor receptor EGFR also binds to Beclin-1 also preventing the induction autophagy. Under cellular stresses such as hypoxia, EGFR is degraded allowing Beclin-1 to induce autophagy. When this negative regulation is eliminated, cells die through an autophagy mechanism [95–97].

Autophagy-mediated cell death also requires ROS. For example, a study showed that macrophages treated with lipopolysaccharides and the pan-caspase inhibitor zVAD induced PARP activation downstream of ROS accumulation inducing autophagic cell death. Another study in our laboratory showed that mitochondrial complex I inhibitor rotenone and complex II inhibitor TTFA induced autophagic cell death mediated by ROS production in HEK 293, U87, and HeLa cells but not in nontransformed cells [98, 99]. Bufaline

treatment in colorectal cancer cell lines induced ROS generation, JNK activation, autophagy, and cell death. The NAC antioxidant inhibited JNK activation and decreased autophagic cells and cell death. Also, inhibition of JNK partially decreased autophagic cells and cell death. This study concluded that ROS were responsible for JNK activation which in turn induced autophagic cell death [100]. It has been shown that treatment with amyloid-β peptide $A\beta_{1-42}$ in human neuroblastoma cell line SH-SY5Y induced both apoptosis and autophagy, but in the human glioma cell line, U87 induced only autophagy. In both cell lines, $A\beta_{1-42}$ induced production of ROS; however, ROS levels were higher in U87 cells. The NAC antioxidant inhibited autophagy, and autophagy inhibitor 3-MA and NAC inhibited cell death. In contrast, although pan-caspase inhibitor zVAD-fmk prevented the apoptosis induced by $A\beta_{1-42}$ in SH-SY5Y cells, it failed to rescue cells from death. Finally, downregulation of beclin-1 inhibited $A\beta_{1-42}$-induced autophagic cell death, demonstrating that $A\beta_{1-42}$ induced autophagic cell death mediated by ROS [101]. One more study in the U87 cell line showed that treatment with β-lapachone-induced autophagy and cell death. Furthermore, neither pan-caspase inhibitor zVAD-fmk nor necrosis inhibitor Necrostatin-1 were able to block cell death; however, autophagy inhibitors 3-MA and bafilomycin as well as siRNA-mediated knockdown of ATG6 or ATG7 expression inhibited cell death. β-Lapachone treatment also induced ROS production, and treatment with NAC, α-tocopherol, or trolox decreased cell death and autophagy, suggesting that ROS-mediated β-lapachone-induced autophagic cell death [102]. Taken together, ROS play a role in autophagy-induced cell death.

4.4. Necroptosis.

Necrosis has been considered an accidental, passive, nonprogrammed, and uncontrolled form of cell death. Necroptosis is at the crossroads between apoptosis and necrosis and is characterized (like necrosis) by cell swelling, nuclear membrane dilation, chromatin condensation, and membrane permeabilization and subsequent release of cell damage-associated molecular patterns and production of inflammatory cytokines triggering inflammation in surrounding tissue. This regulated cell death type is triggered by perturbations of the extracellular or intracellular environment and is detected by death receptors like FAS and TNFR1 [103, 104]. Necroptosis depends on MLKL, RIPK3, and on the kinase activity of RIPK1. Once initiated by TNFR1, RIPK3 is activated by RIPK1 (as long as caspase 8 is inactivated), then RIPK3 and RIPK1 form an amyloid-like signaling complex called necrosome at which point both proteins undergo a series of trans- and autophosphorylations required for MLKL recruitment and necroptosis activation [105–107].

Negative regulators of necroptosis include CHIP, which promotes RIPK1 and RIPK2 ubiquitination; A20, which promotes deubiquitination of RIPK3; PPM1B, which induces dephosphorylation of RIPK3; and AURKA, which inhibits phosphorylation of MLKL; these four regulators act at the necrosome level [108–111]. Finally, some necroptosis inhibitors are necrostatin-1, 3, and 5 (Nec-1, Nec-3, and Nec-5, respectively); the three of them inhibit RIP1 kinase activity [112, 113].

ROS participate in necroptosis regulation. One of studies reported that selenium nanoparticle (SeNP) treatment induced mitochondrial ROS, mitochondrial damage, TNF and IRF1 necroptotic gene overexpression, increase in RIP1 protein expression, and decrease of cell viability. Necroptosis inhibitor necrostatin-1 increased cell viability [114]. Interestingly selenite has been reported to induce apoptotic cell death in the PC3 cell line accompanied by superoxide generation [115]. Other studies on the colorectal adenocarcinoma Caco-2 cell line treated with an alkynyl gold (I) complex showed antiproliferative effects in a dose- and time-dependent manner with the absence of apoptosis markers. It was also found that this treatment causes loss of mitochondrial membrane potential, ROS generation, and increased RIP1 expression levels. Pretreatment with NAC, necrostatin-1, TNFR1 analog, and NF-κB inhibitor SN50 increased cell survival [116]. TNF-α treatment with RelA KO and cIAP1/2 DKO MEF cells induced cell death; however, pretreatment with necrostatin-1 blocked TNF-α-induced cell death and pretreatment with the antioxidant, butylated hydroxyanisole (BHA), blocked both induced cell death and ROS accumulation, suggesting that TNF-α-induced necroptotic cell death is dependent on ROS. In this study, it is also shown that necrostatin-1 but not BHA inhibited phosphorylation of RIPK1, which suggests that ROS act downstream of RIPK1 activation regulating necroptois [117].

4.5. Interplay between ROS and Cell Death.

In the studies presented above, the increase in ROS levels is not simply a consequence of cell death but rather a key player in the induction of cell death. These examples showed that the use of antioxidants (scavengers) not only decreased levels of ROS but also rescued cells, and even more, the use of selective ROS inhibitors enlightened us on the particular type of ROS that triggered cell death as shown in Moreno-Manzano et al. In addition to ROS inhibitors, other strategies were used (siRNA, overexpression, transgenic mice) in order to prove that increased ROS or dysfunctional antioxidant systems were directly responsible for cell death induction. These examples, with the use of a combination of ROS inhibitors and cell death inhibitors, also showed the relationship between ROS and cell death. For example, some studies used NAC which promoted not only the decrease in ROS levels but also a decrease in dell death, and then the different cell death inhibitors like zVAD, Fer-1, 3MA, and/or Nec-1 were tested in order to determine the type of cell death induced by ROS. These studies also showed how increased levels of ROS can be caused by either a decrease in antioxidant levels, such as a decrease in GSH or SOD activity [64] or by enhanced ROS production, for instance, by NOX [69] or both [87]. It is worth noting that even though the types of ROS that induce ferroptosis are well defined (iron-dependent ROS and lipid peroxidation), the source of these ROS is not specific for ferroptosis and, it can be shared between different types of cell death; for example, NOX produced ROS that can induce apoptosis [69] or ferroptosis [86]. Another important concept presented in the previous studies is how one stimulus can increase ROS, which in turn will activate two or more different cell death pathways within the cell, but in some

cases only one of those two pathways is responsible for causing cell death [101], and in other cases, both or more cell death mechanisms are responsible for cell demise [118] (see below).

4.6. ROS and Cell Death Crosstalk. For a long time, the different cell death types (apoptosis, autophagy, ferroptosis, and necroptosis) were studied as independent processes; however, a huge amount of evidence shows that these different types of cell death often share, for example, signaling pathways or initiator molecules and this promotes an interplay between pathways. Since ROS plays a critical role in different forms of programmed cell death, it is not surprising that it could also play a role in crosstalk between these types of cell death. For instance, a study in pancreatic cell lines showed that TRAIL treatment increased ROS and induced apoptosis in the TRAIL-sensitive pancreatic cancer cell lines MiaPaCa-2 and BxPC-3. Inhibition of peroxide decreased apoptotic cell death in MiaPaCa-2 cells but had no effect on BxPC-3 apoptotic cells. On the contrary, superoxide anion inhibition increased apoptosis levels on BxPC-3 cells but had no effect on MiaPaCa-2 apoptosis. In addition, peroxide inhibition increased the necrotic-like population in both cell lines while superoxide inhibition had the same effect but only in BxPC-3 cells. Moreover, addition of necrostatin 1 decreased the necrotic population in both cell lines. To further confirm these results, RIP3 siRNA in combination with TRAIL and peroxide inhibitor in BxPC-3 cells decreased the necroptotic population and increased the apoptotic population. Interestingly, MiaPaCa-2 cells do not express RIP3, only RIP1. These results suggested that TRAIL treatment of MiaPaCa-2 and BxPC-3 cells under inhibition of peroxide promotes RIP1-dependent necroptosis, and that TRAIL treatment under inhibition of ROS (peroxide and superoxide) promotes RIP3-dependent necroptosis in BxPC-3 cells [119].

Combined lysosomotropic agents (siramesine and clemastine) and tyrosine kinase inhibitors (lapatinib and ibrutinib) induced synergistic cell death; however, the type of ROS produced and the type of cell death induced were different depending on the cell type. In breast and lung cancers and in glioblastoma, the combination induced ferroptotic cell death, while in CLL cells, it induced apoptosis. In glioblastoma, LMP leads to an increase in reactive iron, and this leads to iron-dependent oxidation and lipid peroxidation accompanied by a decrease in HO-1 and its antioxidant properties, thus leading to ferroptosis [120, 121]. In contrast, in CLL, LMP leads to an increase in ROS and a loss of mitochondrial membrane potential accompanied by a decrease in antiapoptotic MCL-1, which results in apoptotic cell death [72]. In another study mentioned above, selenium nanoparticles (SeNPs) induced necroptosis in prostate cancer PC3 cells. Interestingly, glucose-decorated selenium nanoparticles induced apoptosis in the hepatocellular carcinoma cell line HepG2. In both cases, the treatment caused mitochondrial damage mediated by ROS [114, 122]. While these studies show how ROS function as a rheostat, the regulatory features of this crosstalk and how ROS controls it remains unclear.

5. ROS and Cell Death in Disease

The setting of the ROS rheostat can maintain cellular homeostasis through balancing cell survival with different types of cell death. When this ROS rheostat balance is altered, it can contribute to the development and progression of disease. The link between ROS and cell death and its connection to several diseases is discussed below.

5.1. Alzheimer's Disease. Analysis of *post mortem* tissue from Alzheimer's disease (AD) patients and AD models have shown, on one hand, increased ROS and elevated markers of oxidative stress, and on the other hand, the activation of caspase 3, caspase 8, and caspase 9 in sporadic AD [123–127]. One characteristic of AD is the presence of amyloid beta (Aβ) plaques composed of Aβ peptide. Protein and lipid oxidation in brain regions rich in Aβ in early stages of the disease has been found [128]. Aβ peptides produce ROS in the presence of metal ions; similarly, mitochondria also generate ROS causing mitochondrial dysfunction which has been involved in AD pathogenesis [129–131]. The idea that mitochondrial ROS induce mitochondrial dysfunction comes from the "mitochondrial cascade hypothesis" proposed by Swerdlow and Khan. Briefly, it proposes that mitochondrial function and its ability to counteract and recover from stress mediated, among others, by ROS comes from inherited mutations in mtDNA. When oxidative damage amplifies ROS production, three events are triggered: (1) a reset response in which cells respond to elevated ROS by generating Aβ which further perturbs mitochondrial function, (2) a removal response in which compromised cells are purged via programmed cell death mechanisms, and (3) a replace response in which neuronal progenitors unsuccessfully attempt to reenter the cell cycle, thus giving place to Aβ plaques and neurofibrillary tangles [126]. This indicates that ROS regulation is a key feature in AD and may play an important role in future treatments for this disease.

5.2. Kidney Failure. Kidney failure is a serious chronic condition. One study showed that acyl-CoA synthetase long-chain family member 4 (*Acsl4*) is a predictive and pharmacodynamic biomarker of ferroptosis *in vivo* in acute kidney failure. In addition, *in vitro* experiments showed that deletion of *Acsl4* caused resistance to erastin and RSL3 induced ferroptosis; however, cells underwent necroptosis when treated with a combination of TNF-α and zVAD-fmk. Inversely, *Mlkl*-knockout cells were protected against necroptosis induced by the combination but died by ferroptosis when treated with erastin and RSL3. These observations were confirmed in an *in vivo* model of ischemia-reperfusion injury. ACSL4 protein expression significantly increased during the first 24 hours after reperfusion in *Mlkl*-knockout animals, suggesting a switch toward ferroptosis signaling when necroptosis signaling fails. Even more, an increase in ACSL4 expression in kidney biopsies from patients with acute tubular injury (ATI) was observed following kidney transplantation and severe thrombotic microangiopathy of native kidney [132]. This suggests that limiting lipid peroxidation can inhibit ferroptotic cell death in kidney failure, and

crosstalk between ferroptosis and necroptosis in a disease context occurs.

5.3. Cancer. One of the hallmarks of cancer is the avoidance of cell death. This occurs through overexpression of anti-poptotic BCL-2 family members and mutations in tumor suppressor genes. In addition, the antioxidant pathways are overexpressed. Collectively, these changes in cancer cells block ROS production in cancer cells to levels that will damage cellular structures leading to cell death. Many chemotherapies selectively increased ROS beyond this limit to induce different types of cell death. Radiation therapy also generates free radicals that damage cellular membranes and DNA leading to apoptosis. Drug resistance prevents apoptosis by protecting the mitochondria from inducing ROS and releasing mitochondrial proteins. Cells also upregulate antioxidant defences limiting ROS levels after cells are treated with chemotherapy or radiation. Immunotherapy for cancer also allows cancer cells to die from ferroptosis where iron-generated ROS plays a critical role [133, 134].

There are several examples where increased ROS induce two or more different types of cell death in different cancer in vivo models. For instance, it has been shown that the immunosuppressant FTY720 can induce autophagy, extrinsic apoptosis, and necroptosis in glioblastoma cells. It was also found that autophagy was the promoter of apoptosis and necroptosis and that upstream autophagy, FTY720, inhibited the PI3K/Akt/mTOR/p70S6K signaling pathway by dephosphorylation of Akt, mTOR, and p70S6K. Furthermore, an increase in ROS and the activation of p53 and JNK were found. Conversely, inhibition of p53 and JNK reduces ROS generation, and antioxidant NAC inhibited both p53 and JNK. This suggests the existence of a ROS-JNK-p53 feedback loop. It was also found that this loop participated in the activation of autophagy, apoptosis, and necroptosis. Finally, it was found that FTY720 induced autophagy, apoptosis, and necrosis in xenograft mouse models of human U251 or U87 glioblastoma cells; treatment also inhibited tumor growth, and the high-dose group resulted in smaller tumors compared to the low-dose group [118].

There are few studies in vivo showing ROS as a rheostat for one cell death type or another. One exception is studies involving BAY 87-2243, a mitochondrial complex I inhibitor. It was shown that in melanoma cell lines, the inhibitor induced mitochondrial membrane depolarization and increased ROS reduced ATP levels and cell death, which was reversed by vitamin B and glucose. Moreover BAY 87-2243 was able to reduce tumor growth in both BRAF mutant melanoma mouse xenografts and patient-derived melanoma mouse models [135]. It was later found that in melanoma cell lines G361 and SK-MEL-28, BAY 87-2243 induced a combination of ferroptotic/necroptotic cell death due to an opening of the mitochondrial permeability and a decrease in the mitochondrial membrane potential which in turn induced autophagosome formation, mitophagy, and an increase in ROS. zVAD-FMK, a caspase inhibitor failed to prevent cell death; however, necrostatin-1 and ferrostatin-1 both decreased cell death induced by BAY 87-2243. Furthermore RIPK1, MLKL, and GPx4 knockdown prevented loss of cell viability; in con-

trast, GPx4 overexpression inhibited the BAY-induced increase in intracellular ROS and lipid peroxidation and inhibited reduction in cell viability [136]. Interestingly, in hepatoma cell line Hep3B, treatment with BAY 87-2243 had antiproliferative effects and induced cell death by apoptosis; it was also observed that both effects were enhanced when BAY 87-2243 was combined with histone deacetylase inhibitors [137]. This mitochondrial complex-1 inhibitor was the object of a phase I clinical trial (NCT01297530).

Taken together, cancer cells have the capacity to adapt to toxic ROS levels and different ROS types and to overcome apoptosis through altering the ROS rheostat. In addition, cancer cells can switch from one cell death mechanism to another using ROS as a rheostat. This could be a valuable therapeutic strategy that should be explored. Thus, more in vivo studies need to be done in order to confirm the findings presented in vitro (Table 2) in which ROS function as a rheostat between two different cell death types.

6. Perspective and Future Questions

ROS play major roles in inducing different types of cell death. One reason ROS induce different types of cell death is the different types of ROS being produced within cells. Ferroptosis is induced through iron-generated ROS, whereas induction of apoptosis happens through hydrogen peroxide and superoxide. We have published that oxidative stress-induced autophagy-mediated cell death is driven by a superoxide. Another reason is the ability of cells to remove ROS through antioxidant pathways. This could be through inhibition of GPx4 in ferroptosis or reduced expression of SOD or catalase during apoptosis. This, however, cannot explain all the variations in cell death observed in cells. For example, mitochondrial-derived ROS is detected in many forms of cell death. Another variable is the cell type undergoing cell death. Leukemia cells will undergo apoptosis, but under the same treatment conditions, a glioma cell line will undergo ferroptotic cell death.

Cell organelles play another important role in regulating ROS induction of different types of cell death. Mitochondria damage precedes cell death often caused by ROS but leads to different types of cell death. For example, glucose-coated selenium nanoparticle (SeNP) treatment of prostate cancer leads to necroptosis, whereas SeNP treatment in HepG2 cells induce apoptosis. This could be due to the degree of mitochondrial damage mediated by ROS. Limited damage will release mitochondrial protein leading to activation of the intrinsic pathway, whereas widespread mitochondrial damage will lead to high levels of ROS and lipid oxidation causing plasma membrane damage and necroptosis. Lysosomes are also a source of ROS associated with apoptosis and ferroptosis. Lysosomes are known as a major iron source. Upon lysosome disruption, iron-mediated lipid oxidation and ferroptosis may occur. The same lysosome disruption in other cell types leads to apoptosis not ferroptosis. One possible difference could be differing levels of antioxidant activation allowing for apoptosis before ferroptosis could be induced. Further investigation is warranted to understand how ROS regulates different types of cell death.

TABLE 2: Drugs and type of cell death.

Drug	Model of study	ROS/antioxidant	Cell death type	Ref.
Methylprednisolone	Thymocytes0	Peroxides and decreased GSH	Apoptosis	[71]
Artesunate	Doxorubicin-resistant T leukemia cells	Hydrogen peroxide	Intrinsic apoptosis	[65]
Vibrio vulnificus cytolysin	Vascular endothelial ECV304 cells	Superoxide anion	Intrinsic apoptosis	[66]
Angiotensin II	Myocardial ischemia	Superoxide anion and/or hydrogen peroxide	Intrinsic apoptosis	[69]
TNF-α	Mesangial cells	Superoxide anion	Extrinsic apoptosis	[65]
Matrine	Liver HL-7702 cells	Hydrogen peroxide and lipid peroxidation Decreased SOD and GSH activity, KEAP1 upregulation, Nrf2 downregulation and inhibition of HO-1 and NQO1	Intrinsic and extrinsic apoptosis	[64]
Oxidized perilla and linseed oil	Neuronal SH-SY5Y cells	Hydrogen peroxide	Caspase-independent apoptosis (AIF) and intrinsic apoptosis	[74]
Clemastine and ibrutinib combination	CLL cells	Superoxide anion and/or hydrogen peroxide	Apoptosis	[72]
Sodium selenite	Prostate cancer PC3	Superoxide anion	Apoptosis	[115]
Glucose-decorated selenium nanoparticles	Hepatocellular carcinoma HepG2 cells	Superoxide anion and/or hydrogen peroxide	Apoptosis	[122]
BAY 87-2243	Hepatoma cell line Hep3B	ROS	Apoptosis	[137]
Siramesine and lapatinib combination	Breast cancer MDA MB 231cells, adenocarcinoma A549 cells, and glioblastoma U87 cells	Iron-mediated ROS and lipid peroxidation	Ferroptosis	[120, 121]
Paraquat and maneb	Neuronal SH-SY5Y cells	Lipid peroxidation NADPH-mediated ROS Decreased GSH and GPx4	Ferroptosis	[86]
Hemin	Monocytic THP-1 cells	Iron-mediated ROS and NADPH-mediated ROS	Ferroptosis	[85]
Artesunate	Hepatic stellate LX2 cells	Iron mediate ROS and lipid peroxidation Decreased GSH and GPx4 activity	Ferroptosis	[87]
Deletion of *Acsl4* and RSL3	Acute kidney failure	Oxidation of fatty acids	Ferroptosis	[132]
Deletion of *Acsl4* and TNF-α and zVAD-fmk	Acute kidney failure	Oxidation of fatty acids	Necroptosis	[132]
Rotenone	HEK 293, U87, and HeLa cells	Superoxide anion and/or hydrogen peroxide	Autophagic cell death	[99]
Bufaline	Colon cancer HT-29 and Caco-2 cells	Hydrogen peroxide	Autophagic cell death	[100]
Amyloid-β_{1-42}	Glioblastoma U87 and SH-SY5Y cells	Hydrogen peroxide	Autophagic cell death	[101]
β-Lapachone	Glioblastoma U87 cells	Hydrogen peroxide	Autophagic cell death	[102]
Selenium nanoparticles	Prostate cancer PC3 cells	Superoxide anion and/or hydrogen peroxide	Necroptosis	[114]
Alkynyl gold(I) complex	Colorectal adenocarcinoma Caco-2 cells	ROS	Necroptosis	[116]
TNF-α	Mouse embryonic fibroblast RelA KO and cIAP1/2 DKO cells	Hydrogen peroxide	Necroptosis	[117]
FTY720	U87 and U251MG xenograft mouse model	ROS	Autophagy and ferroptosis and necroptosis	[118]
BAY 87-2243	BRAF mutant melanoma mouse xenografts and patient-derived melanoma mouse models	ROS and lipid peroxidation	Ferroptosis and necroptosis	[135]

There is crosstalk between different types of cell death where players responsible for one type of cell death may play another role in other cell death types. ROS is one of these important players. Indeed, ROS drive different cell death pathways in disease and under treatments. Even though this is not a new concept and several studies have shown this, there are still some questions that cannot be answered with what we know about crosstalk between different cell death types: why the same treatment strategy can induce different types of ROS and in turn different cell death types? And why ROS from the same source induce different cell death types? One way to describe the role of ROS is as a rheostat that allows different types of cell death to be induced under different conditions and with different cell types. How this ROS rheostat is controlled is still not well understood and need to be investigated in this context to predict how cells die and used to develop better treatment strategies for diseases.

7. Conclusion

In conclusion, the role of ROS as a rheostat is evident in *in vitro* studies, but its role needs to be further studied *in vivo* to confirm that ROS can act as a rheostat under pathological conditions. Finally, if this phenomenon is proven in different *in vivo* disease models, then the therapeutic potential of this ROS rheostat should be explored.

Conflicts of Interest

The authors declare that they have no conflicts of interest.

References

[1] P. G. Clarke, "Developmental cell death: morphological diversity and multiple mechanisms," *Anatomy and Embryology*, vol. 181, no. 3, pp. 195–213, 1990.

[2] G. Lettre and M. O. Hengartner, "Developmental apoptosis in *C. elegans*: a complex CEDnario," *Nature Reviews Molecular Cell Biology*, vol. 7, no. 2, pp. 97–108, 2006.

[3] P. G. H. Clarke and S. Clarke, "Nineteenth century research on naturally occurring cell death and related phenomena," *Anatomy and Embryology*, vol. 193, no. 2, 1996.

[4] *Programmed cell death in cancer progression and therapy*, Springer, 2008.

[5] L. Galluzzi, I. Vitale, S. A. Aaronson et al., "Molecular mechanisms of cell death: recommendations of the Nomenclature Committee on Cell Death 2018," *Cell Death and Differentiation*, vol. 25, no. 3, pp. 486–541, 2018.

[6] Y. Mou, J. Wang, J. Wu et al., "Ferroptosis, a new form of cell death: opportunities and challenges in cancer," *Journal of Hematology and Oncology*, vol. 12, no. 1, p. 34, 2019.

[7] J. T. Hancock, R. Desikan, and S. J. Neill, "Role of reactive oxygen species in cell signalling pathways," *Biochemical Society Transactions*, vol. 29, no. 2, pp. 345–349, 2001.

[8] K. H. Cheeseman and T. F. Slater, "An introduction to free radical biochemistry," *British Medical Bulletin*, vol. 49, no. 3, pp. 481–493, 1993.

[9] V. I. Lushchak, "Classification of oxidative stress based on its intensity," *EXCLI Journal*, vol. 13, pp. 922–937, 2014.

[10] *Oxygen Radicals and the Disease Process*, Harwood Academic Publ, 1997.

[11] *Encyclopedia of Stress*, Academic Press, 2007.

[12] H. Sies, "Role of Metabolic H_2O_2 Generation:," *The Journal of Biological Chemistry*, vol. 289, no. 13, pp. 8735–8741, 2014.

[13] R. Zhao, S. Jiang, L. Zhang, and Z.-. B. Yu, "Mitochondrial electron transport chain, ROS generation and uncoupling (review)," *International Journal of Molecular Medicine*, 2019.

[14] D. W. Bak and E. Weerapana, "Cysteine-mediated redox signalling in the mitochondria," *Molecular BioSystems*, vol. 11, no. 3, pp. 678–697, 2015.

[15] L. Brignac-Huber, J. R. Reed, and W. L. Backes, "Organization of NADPH-cytochrome P 450 reductase and CYP1A2 in the endoplasmic reticulum—microdomain localization affects monooxygenase function," *Molecular Pharmacology*, vol. 79, no. 3, pp. 549–557, 2011.

[16] S. Lüthje, B. Möller, F. C. Perrineau, and K. Wöltje, "Plasma membrane electron pathways and oxidative stress," *Antioxidants & Redox Signaling*, vol. 18, no. 16, pp. 2163–2183, 2013.

[17] L. S. Vartanian and S. M. Gurevich, "NADH- and NADPH-dependent formation of superoxide radicals in liver nuclei," *Biokhimiia (Moscow, Russia)*, vol. 54, pp. 1020–1025, 1989.

[18] K. Bedard and K. H. Krause, "The NOX family of ROS-generating NADPH oxidases: physiology and pathophysiology," *Physiological Reviews*, vol. 87, no. 1, pp. 245–313, 2007.

[19] J. D. Lambeth, "NOX enzymes and the biology of reactive oxygen," *Nature Reviews. Immunology*, vol. 4, no. 3, pp. 181–189, 2004.

[20] B. M. Babior, R. S. Kipnes, and J. T. Curnutte, "Biological defense mechanisms. The production by leukocytes of superoxide, a potential bactericidal agent," *J. Clin. Invest*, vol. 52, no. 3, pp. 741–744, 1973.

[21] R. F. Wu, Y. C. Xu, Z. Ma, F. E. Nwariaku, G. A. Sarosi Jr., and L. S. Terada, "Subcellular targeting of oxidants during endothelial cell migration," *The Journal of Cell Biology*, vol. 171, no. 5, pp. 893–904, 2005.

[22] A. Y. Zhang, F. Yi, G. Zhang, E. Gulbins, and P. L. Li, "Lipid raft clustering and redox signaling platform formation in coronary arterial endothelial cells," *Hypertension*, vol. 47, no. 1, pp. 74–80, 2006.

[23] J. Kuroda, K. Nakagawa, T. Yamasaki et al., "The superoxide-producing NAD(P)H oxidase Nox 4 in the nucleus of human vascular endothelial cells," *Genes to Cells*, vol. 10, no. 12, pp. 1139–1151, 2005.

[24] E. Dubois-Deruy, V. Peugnet, A. Turkieh, and F. Pinet, "Oxidative stress in cardiovascular diseases," *Antioxidants*, vol. 9, no. 9, p. 864, 2020.

[25] V. Mugoni and M. Mattia, "Manipulating redox signaling to block tumor angiogenesis," in *Research Directions in Tumor Angiogenesis*, J. Chai, Ed., InTech, 2013.

[26] M. Che, R. Wang, X. Li, H. Y. Wang, and X. F. S. Zheng, "Expanding roles of superoxide dismutases in cell regulation and cancer," *Drug Discovery Today*, vol. 21, no. 1, pp. 143–149, 2016.

[27] T. Fukai and M. Ushio-Fukai, "Superoxide dismutases: role in redox signaling, vascular function, and diseases," *Antioxidants & Redox Signaling*, vol. 15, no. 6, pp. 1583–1606, 2011.

[28] C. Glorieux and P. B. Calderon, "Catalase, a remarkable enzyme: targeting the oldest antioxidant enzyme to find a new cancer treatment approach," *Biological Chemistry*, vol. 398, no. 10, pp. 1095–1108, 2017.

[29] M. M. Goyal and A. Basak, "Human catalase: looking for complete identity," *Protein & Cell*, vol. 1, no. 10, pp. 888–897, 2010.

[30] R. Brigelius-Flohé and M. Maiorino, "Glutathione peroxidases," *Biochimica et Biophysica Acta Reviews on Cancer*, vol. 1830, no. 5, pp. 3289–3303, 2013.

[31] Y. Chen, K. Wang, D. Zhang et al., "GPx6 is involved in the in vitro induced capacitation and acrosome reaction in porcine sperm," *Theriogenology*, vol. 156, pp. 107–115, 2020.

[32] *Glutathione*, CRC Press, Taylor & Francis Group, 2019.

[33] S. C. Lu, "Glutathione synthesis," *Biochimica et Biophysica Acta*, vol. 1830, no. 5, pp. 3143–3153, 2013.

[34] S. C. Lu, "Regulation of glutathione synthesis," *Molecular Aspects of Medicine*, vol. 30, no. 1-2, pp. 42–59, 2009.

[35] T. Nauser, W. H. Koppenol, and J. M. Gebicki, "The kinetics of oxidation of GSH by protein radicals," *The Biochemical Journal*, vol. 392, no. 3, pp. 693–701, 2005.

[36] G. W. Burton and M. G. Traber, "Vitamin E: antioxidant activity, biokinetics, and bioavailability," *Annual Review of Nutrition*, vol. 10, no. 1, pp. 357–382, 1990.

[37] M. G. Traber and J. Atkinson, "Vitamin E, antioxidant and nothing more," *Free Radical Biology & Medicine*, vol. 43, no. 1, pp. 4–15, 2007.

[38] H. Sies, "On the history of oxidative stress: concept and some aspects of current development," *Current Opinion in Toxicology*, vol. 7, pp. 122–126, 2018.

[39] *Oxidative stress*, Academic Press, Orlando, 1985.

[40] K. NOSE, M. SHIBANUMA, K. KIKUCHI, H. KAGEYAMA, S. SAKIYAMA, and T. KUROKI, "Transcriptional activation of early-response genes by hydrogen peroxide in a mouse osteoblastic cell line," *European Journal of Biochemistry*, vol. 201, no. 1, pp. 99–106, 1991.

[41] Y. Devary, R. A. Gottlieb, L. F. Lau, and M. Karin, "Rapid and preferential activation of the c-Jun gene during the mammalian UV response," *Molecular and Cellular Biology*, vol. 11, no. 5, pp. 2804–2811, 1991.

[42] R. Schreck, P. Rieber, and P. A. Baeuerle, "Reactive oxygen intermediates as apparently widely used messengers in the activation of the NF-kappa B transcription factor and HIV-1," *The EMBO Journal*, vol. 10, no. 8, pp. 2247–2258, 1991.

[43] N. L. Reynaert, A. van der Vliet, A. S. Guala et al., "Dynamic redox control of NF-kappaB through glutaredoxin-regulated S-glutathionylation of inhibitory kappaB kinase beta," *Proceedings of the National Academy of Sciences*, vol. 103, no. 35, pp. 13086–13091, 2006.

[44] J. V. Cross and D. J. Templeton, "Oxidative stress inhibits MEKK1 by site-specific glutathionylation in the ATP-binding domain," *The Biochemical Journal*, vol. 381, no. 3, pp. 675–683, 2004.

[45] N. Kumar Rajendran, B. P. George, R. Chandran, I. M. Tynga, N. Houreld, and H. Abrahamse, "The influence of light on reactive oxygen species and NF-κB in disease progression," *Antioxidants*, vol. 8, no. 12, p. 640, 2019.

[46] K. Lingappan, "NF-κB in oxidative stress," *Current Opinion in Toxicology*, vol. 7, pp. 81–86, 2018.

[47] L. Fialkow, C. K. Chan, D. Rotin, S. Grinstein, and G. P. Downey, "Activation of the mitogen-activated protein kinase signaling pathway in neutrophils. Role of oxidants.," *Journal of Biological Chemistry*, vol. 269, no. 49, pp. 31234–31242, 1994.

[48] A. R. Simon, U. Rai, B. L. Fanburg, and B. H. Cochran, "Activation of the JAK-STAT pathway by reactive oxygen species," *American Journal of Physiology-Cell Physiology*, vol. 275, no. 6, pp. C1640–C1652, 1998.

[49] K. Z. Guyton, Y. Liu, M. Gorospe, Q. Xu, and N. J. Holbrook, "Activation of Mitogen-activated Protein Kinase by H_2O_2:," *Journal of Biological Chemistry*, vol. 271, no. 8, pp. 4138–4142, 1996.

[50] H. Nagai, T. Noguchi, K. Takeda, and H. Ichijo, "Pathophysiological roles of ASK1-MAP kinase signaling pathways," *Journal of Biochemistry and Molecular Biology*, vol. 40, no. 1, pp. 1–6, 2007.

[51] J. Zhang, X. Wang, V. Vikash et al., "ROS and ROS-mediated cellular signaling," *Oxidative Medicine and Cellular Longevity*, vol. 2016, Article ID 4350965, 18 pages, 2016.

[52] K. Itoh, J. Mimura, and M. Yamamoto, "Discovery of the negative regulator of Nrf 2, Keap 1: a historical overview," *Antioxidants & Redox Signaling*, vol. 13, no. 11, pp. 1665–1678, 2010.

[53] K. I. Tong, Y. Katoh, H. Kusunoki, K. Itoh, T. Tanaka, and M. Yamamoto, "Keap 1 recruits Neh 2 through binding to ETGE and DLG motifs: characterization of the two-site molecular recognition model," *Molecular and Cellular Biology*, vol. 26, no. 8, pp. 2887–2900, 2006.

[54] K. I. Tong, B. Padmanabhan, A. Kobayashi et al., "Different electrostatic potentials define ETGE and DLG motifs as hinge and latch in oxidative stress response," *Molecular and Cellular Biology*, vol. 27, no. 21, pp. 7511–7521, 2007.

[55] A. Cuadrado, "Structural and functional characterization of Nrf2 degradation by glycogen synthase kinase 3/β-TrCP," *Free Radical Biology & Medicine*, vol. 88, Pt B, pp. 147–157, 2015.

[56] A. T. Dinkova-Kostova, W. D. Holtzclaw, R. N. Cole et al., "Direct evidence that sulfhydryl groups of Keap 1 are the sensors regulating induction of phase 2 enzymes that protect against carcinogens and oxidants," *Proceedings of the National Academy of Sciences of the United States of America*, vol. 99, no. 18, pp. 11908–11913, 2002.

[57] W. Li, S. W. Yu, and A. N. T. Kong, "Nrf2 Possesses a Redox-sensitive Nuclear Exporting Signal in the Neh5 Transactivation Domain," *The Journal of Biological Chemistry*, vol. 281, no. 37, pp. 27251–27263, 2006.

[58] Y.-S. Keum and B. Choi, "Molecular and chemical regulation of the Keap1-Nrf2 signaling pathway," *Molecules*, vol. 19, no. 7, pp. 10074–10089, 2014.

[59] K.-A. Jung and M. K. Kwak, "The Nrf2 system as a potential target for the development of indirect antioxidants," *Molecules*, vol. 15, no. 10, pp. 7266–7291, 2010.

[60] G. V. Putcha, C. A. Harris, K. L. Moulder, R. M. Easton, C. B. Thompson, and E. M. Johnson Jr., "Intrinsic and extrinsic pathway signaling during neuronal apoptosis: lessons from the analysis of mutant mice," *The Journal of Cell Biology*, vol. 157, no. 3, pp. 441–453, 2002.

[61] J. P. Sheridan, S. A. Marsters, R. M. Pitti et al., "Control of TRAIL-induced apoptosis by a family of signaling and decoy receptors," *Science*, vol. 277, no. 5327, pp. 818–821, 1997.

[62] N. Yan and Y. Shi, "Mechanisms of apoptosis through structural biology," *Annual Review of Cell and Developmental Biology*, vol. 21, no. 1, pp. 35–56, 2005.

[63] A. Ashkenazi and V. M. Dixit, "Death receptors: signaling and modulation," *Science*, vol. 281, no. 5381, pp. 1305–1308, 1998.

[64] L. You, C. Yang, Y. Du et al., "Matrine exerts hepatotoxic effects via the ROS-dependent mitochondrial apoptosis pathway and inhibition of Nrf2-mediated antioxidant response," *Oxidative Medicine and Cellular Longevity*, vol. 2019, no. 1045345, 15 pages, 2019.

[65] V. Moreno-Manzano, Y. Ishikawa, J. Lucio-Cazana, and M. Kitamura, "Selective Involvement of Superoxide Anion, but Not Downstream Compounds Hydrogen Peroxide and Peroxynitrite, in Tumor Necrosis Factor-α-induced Apoptosis of Rat Mesangial Cells," *The Journal of Biological Chemistry*, vol. 275, no. 17, pp. 12684–12691, 2000.

[66] Q. Hu, D. Wu, W. Chen et al., "Molecular determinants of caspase-9 activation by the Apaf-1 apoptosome," *Proceedings of the National Academy of Sciences of the United States of America*, vol. 111, no. 46, pp. 16254–16261, 2014.

[67] S. J. Riedl and G. S. Salvesen, "The apoptosome: signalling platform of cell death," *Nature Reviews. Molecular Cell Biology*, vol. 8, no. 5, pp. 405–413, 2007.

[68] J. M. Schriewer, C. B. Peek, J. Bass, and P. T. Schumacker, "ROS-mediated PARP activity undermines mitochondrial function after permeability transition pore opening during myocardial ischemia-reperfusion," *Journal of the American Heart Association*, vol. 2, no. 2, article e000159, 2013.

[69] J. R. Erickson, M. L. A. Joiner, X. Guan et al., "A dynamic pathway for calcium-independent activation of CaMKII by methionine oxidation," *Cell*, vol. 133, no. 3, pp. 462–474, 2008.

[70] C. Marzano, V. Gandin, A. Folda, G. Scutari, A. Bindoli, and M. P. Rigobello, "Inhibition of thioredoxin reductase by auranofin induces apoptosis in cisplatin-resistant human ovarian cancer cells," *Free Radical Biology & Medicine*, vol. 42, no. 6, pp. 872–881, 2007.

[71] A. Fernandez, J. Kiefer, L. Fosdick, and D. J. McConkey, "Oxygen radical production and thiol depletion are required for Ca(2+)-mediated endogenous endonuclease activation in apoptotic thymocytes," *Journal of Immunology*, vol. 1950, no. 155, pp. 5133–5139, 1995.

[72] A. Chanas-Larue, G. E. Villalpando-Rodriguez, E. S. Henson, J. B. Johnston, and S. B. Gibson, "Antihistamines are synergistic with Bruton's tyrosine kinase inhibitor ibrutinib mediated by lysosome disruption in chronic lymphocytic leukemia (CLL) cells," *Leukemia Research*, vol. 96, p. 106423, 2020.

[73] H. K. Lorenzo, S. A. Susin, J. Penninger, and G. Kroemer, "Apoptosis inducing factor (AIF): a phylogenetically old, caspase-independent effector of cell death," *Cell Death and Differentiation*, vol. 6, no. 6, pp. 516–524, 1999.

[74] Y. Ueno, Y. Kawamoto, Y. Nakane et al., "Oxidized perilla and linseed oils induce neuronal apoptosis by caspase-dependent and -independent pathways," *Foods*, vol. 9, no. 5, p. 538, 2020.

[75] S. J. Dixon, K. M. Lemberg, M. R. Lamprecht et al., "Ferroptosis: an iron-dependent form of nonapoptotic cell death," *Cell*, vol. 149, no. 5, pp. 1060–1072, 2012.

[76] W. S. Yang and B. R. Stockwell, "Ferroptosis: death by lipid peroxidation," *Trends in Cell Biology*, vol. 26, no. 3, pp. 165–176, 2016.

[77] S. Dolma, S. L. Lessnick, W. C. Hahn, and B. R. Stockwell, "Identification of genotype-selective antitumor agents using synthetic lethal chemical screening in engineered human tumor cells," *Cancer Cell*, vol. 3, no. 3, pp. 285–296, 2003.

[78] N. Yagoda, M. von Rechenberg, E. Zaganjor et al., "RAS-RAF-MEK-dependent oxidative cell death involving voltage-dependent anion channels," *Nature*, vol. 447, no. 7146, pp. 864–868, 2007.

[79] H. Sato, M. Tamba, T. Ishii, and S. Bannai, "Cloning and Expression of a Plasma Membrane Cystine/Glutamate Exchange Transporter Composed of Two Distinct Proteins," *The Journal of Biological Chemistry*, vol. 274, no. 17, pp. 11455–11458, 1999.

[80] W. S. Yang, R. SriRamaratnam, M. E. Welsch et al., "Regulation of ferroptotic cancer cell death by GPX4," *Cell*, vol. 156, no. 1-2, pp. 317–331, 2014.

[81] S. J. Dixon and B. R. Stockwell, "The role of iron and reactive oxygen species in cell death," *Nature Chemical Biology*, vol. 10, no. 1, pp. 9–17, 2014.

[82] F. Petrat, H. de Groot, and U. Rauen, "Subcellular distribution of chelatable iron: a laser scanning microscopic study in isolated hepatocytes and liver endothelial cells," *The Biochemical Journal*, vol. 356, no. 1, pp. 61–69, 2001.

[83] W. S. Yang and B. R. Stockwell, "Synthetic lethal screening identifies compounds activating iron-dependent, nonapoptotic cell death in oncogenic-RAS-harboring cancer cells," *Chemistry & Biology*, vol. 15, no. 3, pp. 234–245, 2008.

[84] Y. Xie, W. Hou, X. Song et al., "Ferroptosis: process and function," *Cell Death and Differentiation*, vol. 23, no. 3, pp. 369–379, 2016.

[85] S. Imoto, M. Kono, T. Suzuki et al., "Haemin-induced cell death in human monocytic cells is consistent with ferroptosis," *Transfusion and Apheresis Science*, vol. 57, no. 4, pp. 524–531, 2018.

[86] L. Hou, R. Huang, F. Sun, L. Zhang, and Q. Wang, "NADPH oxidase regulates paraquat and maneb-induced dopaminergic neurodegeneration through ferroptosis," *Toxicology*, vol. 417, pp. 64–73, 2019.

[87] Z. Kong, R. Liu, and Y. Cheng, "Artesunate alleviates liver fibrosis by regulating ferroptosis signaling pathway," *Biomedicine Express*, vol. 109, pp. 2043–2053, 2019.

[88] N. Mizushima, B. Levine, A. M. Cuervo, and D. J. Klionsky, "Autophagy fights disease through cellular self-digestion," *Nature*, vol. 451, no. 7182, pp. 1069–1075, 2008.

[89] F. Cecconi and B. Levine, "The role of autophagy in mammalian development: cell makeover rather than cell death," *Developmental Cell*, vol. 15, no. 3, pp. 344–357, 2008.

[90] R. Singh and A. M. Cuervo, "Autophagy in the cellular energetic balance," *Cell Metabolism*, vol. 13, no. 5, pp. 495–504, 2011.

[91] S. Sridhar, Y. Botbol, F. Macian, and A. M. Cuervo, "Autophagy and disease: always two sides to a problem," *The Journal of Pathology*, vol. 226, no. 2, pp. 255–273, 2012.

[92] A. M. Cuervo, "The plasma membrane brings autophagosomes to life," *Nature Cell Biology*, vol. 12, no. 8, pp. 735–737, 2010.

[93] T. Lamark, V. Kirkin, I. Dikic, and T. Johansen, "NBR1 and p 62 as cargo receptors for selective autophagy of ubiquitinated targets," *Cell Cycle*, vol. 8, no. 13, pp. 1986–1990, 2009.

[94] Y. Liu and B. Levine, "Autosis and autophagic cell death: the dark side of autophagy," *Cell Death and Differentiation*, vol. 22, no. 3, pp. 367–376, 2015.

[95] Y. Wei, S. Pattingre, S. Sinha, M. Bassik, and B. Levine, "JNK1-mediated phosphorylation of Bcl-2 regulates starvation-induced autophagy," *Molecular Cell*, vol. 30, no. 6, pp. 678–688, 2008.

[96] J. Cui, Y. F. Hu, X. M. Feng et al., "EGFR inhibitors and autophagy in cancer treatment," *Tumor Biology*, vol. 35, no. 12, pp. 11701–11709, 2014.

[97] Y. Wei, Z. Zou, N. Becker et al., "EGFR-mediated Beclin 1 phosphorylation in autophagy suppression, tumor progression, and tumor chemoresistance," *Cell*, vol. 154, no. 6, pp. 1269–1284, 2013.

[98] Y. Xu, S. O. Kim, Y. Li, and J. Han, "Autophagy Contributes to Caspase-independent Macrophage Cell Death," *The Journal of Biological Chemistry*, vol. 281, no. 28, pp. 19179–19187, 2006.

[99] Y. Chen, E. McMillan-Ward, J. Kong, S. J. Israels, and S. B. Gibson, "Mitochondrial electron-transport-chain inhibitors of complexes I and II induce autophagic cell death mediated by reactive oxygen species," *Journal of Cell Science*, vol. 120, no. 23, pp. 4155–4166, 2007.

[100] C.-M. Xie, W. Y. Chan, S. Yu, J. Zhao, and C. H. K. Cheng, "Bufalin induces autophagy-mediated cell death in human colon cancer cells through reactive oxygen species generation and JNK activation," *Free Radical Biology & Medicine*, vol. 51, no. 7, pp. 1365–1375, 2011.

[101] H. Wang, J. Ma, Y. Tan et al., "Amyloid-β1-42 induces reactive oxygen species-mediated autophagic cell death in U87 and SH-SY5Y cells," *Journal of Alzheimer's Disease*, vol. 21, no. 2, pp. 597–610, 2010.

[102] E. J. Park, K. S. Choi, and T. K. Kwon, "β-Lapachone-induced reactive oxygen species (ROS) generation mediates autophagic cell death in glioma U87 MG cells," *Chemico-Biological Interactions*, vol. 189, no. 1-2, pp. 37–44, 2011.

[103] D. Vercammen, P. Vandenabeele, R. Beyaert, W. Declercq, and W. Fiers, "Tumour necrosis factor-induced necrosis versus anti-Fas-induced apoptosis in L929 cells," *Cytokine*, vol. 9, no. 11, pp. 801–808, 1997.

[104] D. Vercammen, G. Brouckaert, G. Denecker et al., "Dual signaling of the Fas receptor: initiation of both apoptotic and necrotic cell death pathways," *The Journal of Experimental Medicine*, vol. 188, no. 5, pp. 919–930, 1998.

[105] P. Vandenabeele, W. Declercq, F. van Herreweghe, and T. vanden Berghe, "The role of the kinases RIP1 and RIP3 in TNF-induced necrosis," *Science Signaling*, vol. 3, no. 115, article re4, 2010.

[106] J. Li, T. McQuade, A. B. Siemer et al., "The RIP1/RIP3 necrosome forms a functional amyloid signaling complex required for programmed necrosis," *Cell*, vol. 150, no. 2, pp. 339–350, 2012.

[107] Y. Cho, S. Challa, D. Moquin et al., "Phosphorylation-driven assembly of the RIP1-RIP3 complex regulates programmed necrosis and virus-induced inflammation," *Cell*, vol. 137, no. 6, pp. 1112–1123, 2009.

[108] M. Gyrd-Hansen, "All roads lead to ubiquitin," *Cell Death and Differentiation*, vol. 24, no. 7, pp. 1135-1136, 2017.

[109] M. Onizawa, S. Oshima, U. Schulze-Topphoff et al., "The ubiquitin-modifying enzyme A20 restricts ubiquitination of the kinase RIPK3 and protects cells from necroptosis," *Nature Immunology*, vol. 16, no. 6, pp. 618–627, 2015.

[110] W. Chen, J. Wu, L. Li et al., "Ppm1b negatively regulates necroptosis through dephosphorylating Rip3," *Nature Cell Biology*, vol. 17, no. 4, pp. 434–444, 2015.

[111] Y. Xie, S. Zhu, M. Zhong et al., "Inhibition of aurora kinase A induces necroptosis in pancreatic carcinoma," *Gastroenterology*, vol. 153, no. 5, pp. 1429–1443.e5, 2017.

[112] A. Degterev, Z. Huang, M. Boyce et al., "Chemical inhibitor of nonapoptotic cell death with therapeutic potential for ische-

[113] A. Degterev, J. Hitomi, M. Germscheid et al., "Identification of RIP1 kinase as a specific cellular target of necrostatins," *Nature Chemical Biology*, vol. 4, no. 5, pp. 313–321, 2008.

[114] P. Sonkusre and S. S. Cameotra, "Biogenic selenium nanoparticles induce ROS-mediated necroptosis in PC-3 cancer cells through TNF activation," *Journal of Nanobiotechnology*, vol. 15, no. 1, p. 43, 2017.

[115] N. Xiang, R. Zhao, and W. Zhong, "Sodium selenite induces apoptosis by generation of superoxide via the mitochondrial-dependent pathway in human prostate cancer cells," *Cancer Chemotherapy and Pharmacology*, vol. 63, no. 2, pp. 351–362, 2009.

[116] I. Mármol, M. Virumbrales-Muñoz, J. Quero et al., "Alkynyl gold(I) complex triggers necroptosis *via* ROS generation in colorectal carcinoma cells," *Journal of Inorganic Biochemistry*, vol. 176, pp. 123–133, 2017.

[117] R. Shindo, H. Kakehashi, K. Okumura, Y. Kumagai, and H. Nakano, "Critical contribution of oxidative stress to TNFα-induced necroptosis downstream of RIPK1 activation," *Biochemical and Biophysical Research Communications*, vol. 436, no. 2, pp. 212–216, 2013.

[118] L. Zhang, H. Wang, K. Ding, and J. Xu, "FTY720 induces autophagy-related apoptosis and necroptosis in human glioblastoma cells," *Toxicology Letters*, vol. 236, no. 1, pp. 43–59, 2015.

[119] M. Zhang, N. Harashima, T. Moritani, W. Huang, and M. Harada, "The roles of ROS and caspases in TRAIL-induced apoptosis and necroptosis in human pancreatic cancer cells," *PLoS One*, vol. 10, no. 5, article e0127386, 2015.

[120] G. E. Villalpando-Rodriguez, A. R. Blankstein, C. Konzelman, and S. B. Gibson, "Lysosomal destabilizing drug siramesine and the dual tyrosine kinase inhibitor lapatinib induce a synergistic ferroptosis through reduced heme oxygenase-1 (HO-1) levels," *Oxidative Medicine and Cellular Longevity*, vol. 2019, Article ID 9561281, 14 pages, 2019.

[121] S. Ma, R. F. Dielschneider, E. S. Henson et al., "Ferroptosis and autophagy induced cell death occur independently after siramesine and lapatinib treatment in breast cancer cells," *PLoS One*, vol. 12, no. 8, article e0182921, 2017.

[122] T. Nie, H. Wu, K. H. Wong, and T. Chen, "Facile synthesis of highly uniform selenium nanoparticles using glucose as the reductant and surface decorator to induce cancer cell apoptosis," *Journal of Materials Chemistry B*, vol. 4, no. 13, pp. 2351–2358, 2016.

[123] A. Aliyev, S. G. Chen, D. Seyidova et al., "Mitochondria DNA deletions in atherosclerotic hypoperfused brain microvessels as a primary target for the development of Alzheimer's disease," *Journal of the Neurological Sciences*, vol. 229-230, pp. 285–292, 2005.

[124] S. M. Khan, D. S. Cassarino, N. N. Abramova et al., "Alzheimer's disease cybrids replicate beta-amyloid abnormalities through cell death pathways," *Annals of Neurology*, vol. 48, no. 2, pp. 148–155, 2000.

[125] J. Wang, W. R. Markesbery, and M. A. Lovell, "Increased oxidative damage in nuclear and mitochondrial DNA in mild cognitive impairment," *Journal of Neurochemistry*, vol. 96, no. 3, pp. 825–832, 2006.

[126] T. T. Rohn, E. Head, W. H. Nesse, C. W. Cotman, and D. H. Cribbs, "Activation of Caspase-8 in the Alzheimer's Disease

Brain," *Neurobiology of Disease*, vol. 8, no. 6, pp. 1006–1016, 2001.

[127] T. T. Rohn, R. A. Rissman, M. C. Davis, Y. E. Kim, C. W. Cotman, and E. Head, "Caspase-9 Activation and Caspase Cleavage of tau in the Alzheimer's Disease Brain," *Neurobiology of Disease*, vol. 11, no. 2, pp. 341–354, 2002.

[128] D. A. Butterfield, "The 2013 SFRBM discovery award: Selected discoveries from the butterfield laboratory of oxidative stress and its sequela in brain in cognitive disorders exemplified by Alzheimer disease and chemotherapy induced cognitive impairment," *Free Radical Biology & Medicine*, vol. 74, pp. 157–174, 2014.

[129] C. Opazo, X. Huang, R. A. Cherny et al., "Metalloenzyme-like Activity of Alzheimer's Disease β-Amyloid:," *The Journal of Biological Chemistry*, vol. 277, no. 43, pp. 40302–40308, 2002.

[130] C. A. Rottkamp, A. K. Raina, X. Zhu et al., "Redox-active iron mediates amyloid-β toxicity," *Free Radical Biology & Medicine*, vol. 30, no. 4, pp. 447–450, 2001.

[131] R. H. Swerdlow and S. M. Khan, "A "mitochondrial cascade hypothesis" for sporadic Alzheimer's disease," *Medical Hypotheses*, vol. 63, no. 1, pp. 8–20, 2004.

[132] T. Müller, C. Dewitz, J. Schmitz et al., "Necroptosis and ferroptosis are alternative cell death pathways that operate in acute kidney failure," *Cellular and Molecular Life Sciences*, vol. 74, no. 19, pp. 3631–3645, 2017.

[133] D. Hanahan and R. A. Weinberg, "Hallmarks of cancer: the next generation," *Cell*, vol. 144, no. 5, pp. 646–674, 2011.

[134] P. L. de Sá Junior, D. A. D. Câmara, A. S. Porcacchia et al., "The roles of ROS in cancer heterogeneity and therapy," *Oxidative Medicine and Cellular Longevity*, vol. 2017, Article ID 2467940, 12 pages, 2017.

[135] L. Schöckel, A. Glasauer, F. Basit et al., "Targeting mitochondrial complex I using BAY 87-2243 reduces melanoma tumor growth," *Cancer & Metabolism*, vol. 3, no. 1, p. 11, 2015.

[136] F. Basit, L. M. P. E. van Oppen, L. Schöckel et al., "Mitochondrial complex I inhibition triggers a mitophagy-dependent ROS increase leading to necroptosis and ferroptosis in melanoma cells," *Cell Death & Disease*, vol. 8, no. 3, pp. e2716–e2716, 2017.

[137] Y. Li, M.-. J. Rao, N.-. Y. Zhang, L.-. W. Wu, N.-. M. Lin, and C. Zhang, "BAY 87-2243 sensitizes hepatocellular carcinoma Hep3B cells to histone deacetylase inhibitors treatment via GSK-3β activation," *Experimental and Therapeutic Medicine*, 2019.

Review Article

Redox Homeostasis and Prospects for Therapeutic Targeting in Neurodegenerative Disorders

Musbau Adewumi Akanji [1], **Damilare Emmanuel Rotimi,** [2,3] **Tobiloba Christiana Elebiyo,** [3] **Oluwakemi Josephine Awakan** [2,3] **and Oluyomi Stephen Adeyemi** [2,3]

[1]*Department of Biochemistry, University of Ilorin, Ilorin, Nigeria*
[2]*Landmark University SDG 3 (Good Health and Well-being Research Group), PMB 1001, Omu-Aran 251101, Nigeria*
[3]*Department of Biochemistry, Medicinal Biochemistry, Nanomedicine & Toxicology Laboratory, Landmark University, KM 4 Ipetu Road, Omu-Aran 251101, Kwara State, Nigeria*

Correspondence should be addressed to Musbau Adewumi Akanji; akanjima@yahoo.com,
Oluwakemi Josephine Awakan; amira.oluwakemi@lmu.edu.ng, and Oluyomi Stephen Adeyemi; yomibowa@yahoo.com

Reactive species, such as those of oxygen, nitrogen, and sulfur, are considered part of normal cellular metabolism and play significant roles that can impact several signaling processes in ways that lead to either cellular sustenance, protection, or damage. Cellular redox processes involve a balance in the production of reactive species (RS) and their removal because redox imbalance may facilitate oxidative damage. Physiologically, redox homeostasis is essential for the maintenance of many cellular processes. RS may serve as signaling molecules or cause oxidative cellular damage depending on the delicate equilibrium between RS production and their efficient removal through the use of enzymatic or nonenzymatic cellular mechanisms. Moreover, accumulating evidence suggests that redox imbalance plays a significant role in the progression of several neurodegenerative diseases. For example, studies have shown that redox imbalance in the brain mediates neurodegeneration and alters normal cytoprotective responses to stress. Therefore, this review describes redox homeostasis in neurodegenerative diseases with a focus on Alzheimer's and Parkinson's disease. A clearer understanding of the redox-regulated processes in neurodegenerative disorders may afford opportunities for newer therapeutic strategies.

1. Introduction

Neurodegeneration, which is characterized by gradual neuronal and synaptic degradation, glial focal proliferation, neuroinflammation, vascular abnormalities in specific brain regions, and modifications of proteins such as α-synuclein, amyloid-β, and tau proteins [1–3], contributes significantly to the global health burden. The major groups of neurodegenerative diseases include Alzheimer's disease (AD), Parkinson's disease (PD), spinal muscular atrophy (SMA), prion diseases, spinocerebellar ataxia (SCA), motor neuron disease (MND), and Huntington's disease (HD). Different neurodegenerative diseases have a variety of pathophysiologies, which include cognitive and memory impairments or the inability to move, speak, or breathe [4].

In the brain, a concomitant low activity of antioxidant defense mechanisms and the presence of highly redox-active metals (copper and iron) allow for greater sensitivity to reactive oxygen species (ROS) than other organs [5]. Although oxygen is necessary for life, an imbalance between the number of ROS produced and the antioxidant system causes neural disorders. Although there is no unified etiology for neurodegenerative diseases, strong evidence has implicated oxidative stress in the pathogenesis of all forms of neurodegeneration [6, 7]. Overproduction of reactive oxygen species in neuronal cells induces oxidative stress, which

destroys neural mitochondrial defense mechanisms, causes mitochondrial DNA mutations, affects Ca^{2+} homeostasis, alters membrane permeability, and damages the mitochondrial respiratory chain. These modifications are thought to play a role in the progression of neurodegenerative disorders by mediating or amplifying neuronal dysfunction and causing neurodegeneration [5].

A series of events, such as oxidative stress, protein modification, and mtDNA damage, eventually results in impaired neuronal proteins, further resulting in neuroinflammation and neurological disorders, which manifest as cognitive function loss [8]. However, numerous antioxidant therapeutic targets have been identified that can protect neurons against oxidative stress by preventing free radical formation and modulating normal metal homeostasis [7]. Antioxidants are now being developed to treat neuronal inflammation and scavenge free radicals. The disruption of the redox potential in neurons often results in the oxidative modification of proteins, leading to aberrant peptide oligomerization and eventually neuronal death. Research efforts have focused on discovering agents that can protect against oxidative damage to neurons [9]. In this paper, we reviewed scientific reports on the pathogenesis and prospects for therapeutically targeting oxidative stress in neurodegenerative diseases, especially Alzheimer's and Parkinson's disease.

2. Reactive Oxygen Species and Oxidative Stress

Oxidative stress arises as a result of an imbalance in the oxidant/antioxidant ratio and can create a hazardous state that contributes to cellular damage due to a disequilibrium in the number of ROS molecules generated and the level of the antioxidant enzyme system that detoxifies the reactive intermediates in the biological system [10]. The majority of free radicals (hydrogen peroxide, superoxide anion radical, and hydroxyl radical) are produced by molecular oxygen activation (Figure 1). Superoxide anion ($O_2^{\cdot-}$) is highly reactive and generated in the electron transport chain (ETC) through mitochondrial complexes I and III. $O_2^{\cdot-}$ can be reduced to hydrogen peroxide (H_2O_2) as it crosses the inner mitochondrial membrane [11]. Peroxisomes can also generate H_2O_2 in addition to what is produced by the mitochondria. However, catalase is present in the peroxisomes and is responsible for converting H_2O_2 to water, thereby preventing its buildup. However, if there is damage to the peroxisomes or the enzyme is downregulated, the release of H_2O_2 into the cytosol increases oxidative stress [12]. Direct pathways involving Fenton and Haber-Weiss reactions that occur between redox-active metals and oxygen species or indirect interactions involving enzyme activation (NADPH oxidase or nitric oxide synthase) are examples of pathways that generate ROS [13, 14]. The Fenton reaction in the presence of ferrous iron (Fe^{2+}) converts H_2O_2 into the most harmful ROS, the hydroxyl radical ($\cdot OH$) (Figure 1) [13].

ROS can also interact with nitric oxide to generate reactive nitrogen species resulting in nitrosative stress. NO is produced by one of the three synthase isoforms, inducible NO synthase (iNOS), endothelial NO synthase (eNOS), and neuronal NO synthase (nNOS), and is found in cells and in the extracellular space surrounding dopaminergic neurons. nNOS is expressed mainly in neurons, eNOS is expressed in the vascular endothelium, and iNOS is expressed in glial cells. These NOSs have been implicated in pathological conditions. Damaged mitochondria and activated microglia produce large amounts of iNOS and serve as the main sources of ROS in the inflammatory process, which is a hallmark of neurodegenerative diseases [15–18]. For instance, the production of NO by iNOS or nNOS in the extracellular space surrounding dopaminergic neurons and its subsequent reaction could involve interaction with superoxide to produce large quantities of peroxynitrite ($ONOO^-$) (Figure 1) [19]. Compared to NO, peroxynitrite is a more potent oxidizing agent and is an oxidatively more active molecule which can induce lipid peroxidation and DNA fragmentation [20]. The generated $ONOO^-$ and NO can also modify proteins via nitration [21]. NO can also react with thiolate ions to form S-nitrosothiols, which may form adducts with protein or lipids. Another cellular mechanism implicated in neurodegenerative conditions that involve the production of ROS occurs in the endoplasmic reticulum (ER). Ca^{2+} release from the ER leads to the promotion of ROS generation when the Ca^{2+} enters the mitochondria and can also trigger mitochondrial-mediated apoptosis. Additionally, abnormal protein degradation and ER stress are considered to contribute to PD pathogenesis [22].

3. Neuronal ROS Generation

Cellular ROS can be generated via exogenous and endogenous sources. Exogenous sources include metabolism of xenobiotics and exposure to ultraviolet and ionizing radiation, whereas endogenous generation is mediated by enzymes such as NADH, coenzyme Q oxidoreductase (complex 1), ubiquinol cytochrome C reductase (complex III), NADPH oxidase (NOX), lipoxygenase (LOX), cyclooxygenase (COX), xanthine oxidase (XO), the cytochrome p450 family of enzymes, and flavin oxidase. The majority of these enzymes are localized in the mitochondria, and as such, the mitochondria are the primary source for the endogenous generation of ROS [23].

Neurons are energy-demanding cells; as such, they are extremely sensitive to changes in mitochondrial function. They depend on the mitochondria for ATP generation and calcium regulation, processes required for synaptic transmission, vesicle recycling, neuronal electrical activity, and axonal transport [6]. Thus, deficiencies in mitochondrial function ultimately result in the degradation of neurons. Neurodegeneration is an age-related disease; it is associated with mitochondria, DNA damage, mutations, and deletions, which increase in an age-dependent manner. Based on evidence, the levels of mutated or deleted mtDNA are the highest in the substantia nigra (SN) and cerebral cortex (CC) of adult humans in normal aging, and these damages are often 1% higher in patients with neurodegenerative diseases [24]. The neurons in the brain regions of subjects with neurodegenerative diseases often show alterations in the ETC, intracellular ROS levels, and calcium homeostasis. The processes of mitochondrial fusion and fission are deregulated in most
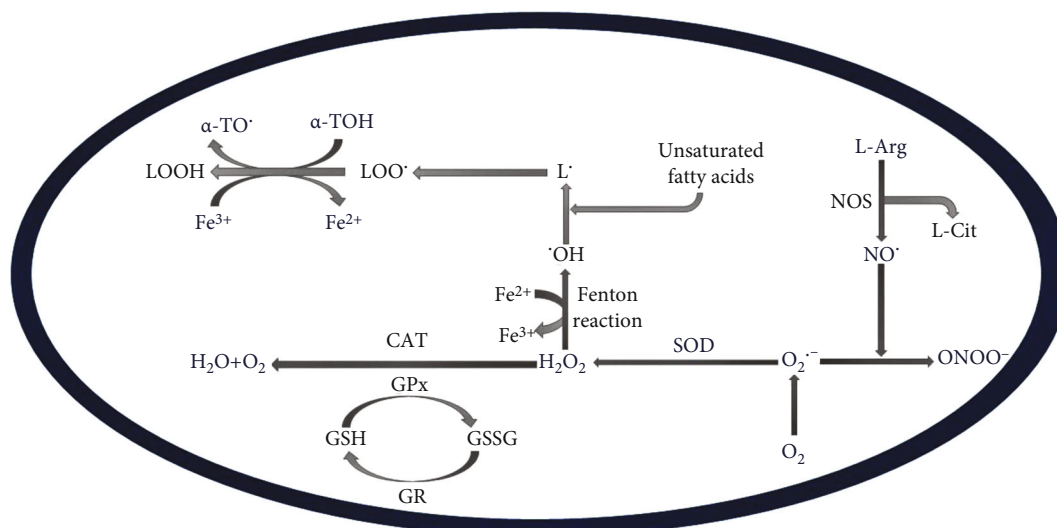
FIGURE 1: Generation of reactive oxygen species and reactive nitrogen species. H_2O: water; O_2: oxygen; $O_2^{\cdot-}$: superoxide anion; H_2O_2: hydrogen peroxide; CAT: catalase; SOD: superoxide dismutase; $ONOO^-$: peroxynitrite; GSH: reduced glutathione; GSSG: glutathione disulfide; Fe^{2+}: ferrous iron; $^{\cdot}OH$: hydroxyl radical; NOS: nitric oxide synthase; L-Arg: L-arginine; L-Cit: L-citrulline; $NO^{\cdot}$: nitric oxide radical; LOOH: lipid hydroperoxides; $LOO^{\cdot}$: lipid peroxy radical; α-TOH: α-tocopherol; α-$TO^{\cdot}$: α-tocopheroxyl radical.

neurodegenerative diseases, leading to impaired neuronal plasticity and development [6].

Mitochondrial dysfunction and the increased generation of ROS alter dopamine metabolism and calcium and iron homeostasis, resulting in the death of dopaminergic neurons in the substantia nigra pars compacta (SNpc). The eventual depletion of antioxidants such as glutathione (GSH) also leads to the generation and accumulation of lipid peroxides as ROS interacts with abundant polyunsaturated fatty acids (PUFA) in the brain [25–27]. Reports also show that aging is accompanied by an increased level of iron and copper in the brain tissue; such alterations in ion homeostasis could initiate excitotoxicity via the overactivation of neuronal receptors such as N-methyl-D-aspartate (NMDA) receptors [28]. The aberrant activation of NMDA receptors produces high levels of NO, which could interact with superoxide and induce nitrosative stress [29].

4. Sources of ROS Generation in Neurons

4.1. Iron.
Ions such as iron and calcium are involved in the generation of ROS. Postmortem evaluation of the brains of patients with ND (neuronal disease) indicates that alterations in the levels of certain ions are present in the specific brain regions of ND patients compared with non-ND [30]. Iron is an indispensable cofactor for the synthesis of catecholamine neurotransmitters, but neuronal iron overload is a characteristic feature of neurodegenerative diseases [31]. In dysfunctional neurons, iron is transported from the extracellular matrix around the neurons via mechanisms such as transport via transferrin lactoferrin and hemopexin receptors and divalent metal transporter 1 as well as by heme degradation by heme oxygenase 2 [31–33]. Since iron is abundant in dysfunctional neurons, free iron interacts with the reaction between superoxide and hydrogen peroxide with ferrous iron (Fe^{2+}) and ferric iron (Fe^{3+}) resulting in the formation of a highly reactive hydroxyl free radical. Neuronal iron overload in ND is often accompanied by depleted iron concentration in the extracellular matrix; this results in poor iron incorporation into protein structures, premature protein degradation, and loss of protein function [31, 34–36]. Lewy's SN bodies of PD patients are characterized by nitrosylated iron-regulated protein 2 (IRP), which promotes the possibility of oxidative stress and iron dysfunction [37].

The human brain is heavily endowed with PUFAs, such as docosahexaenoic acid and arachidonic acid, which are required to fortify the blood-brain barrier (BBB). This makes the cell membrane of brain tissues susceptible to lipid peroxidation and oxidative damage [38]. Interaction between iron and lipid hydroperoxides results in the production of alkoxyl radicals, which further react in the presence of free reactive iron with polyunsaturated fatty acids to generate more lipid peroxides. 4-Hydroxy-2-nonenal (HNE), which is a lipid peroxide associated with PD and AD, forms stable adducts with amine or thiol groups in proteins and may, in turn, result in the aberrant activation of caspases, leading to neuronal death [39, 40]. HNE reactivity with sulfhydryl groups also depletes the GSH level, making the brain tissue more susceptible to oxidative stress. High HNE levels have been detected in the cerebrospinal fluid of patients with PD and AD [41].

4.2. Zinc and ROS Generation.
Experiment carried out on mouse cortical cultures showed mitochondrial ROS production induced by zinc, possibly via inhibition of the lipoamide dehydrogenase (LADH) component of alpha-ketoglutarate dehydrogenase complex (KGDHC) in the TCA cycle [42, 43]. LADH catalyses NAD^+ reduction to NADH, but zinc inhibits this process and favours NADH oxidation in the mitochondrial matrix. This reaction produces superoxide, which is converted to H_2O_2. Complex III inhibition by zinc also generates ROS in rat brain mitochondria which is also similar to that reported in mitochondria isolated from rat

hearts [44, 45]. ROS generation via zinc may be a result of its inhibition of ETC components and TCA cycle. Some other sources of zinc-induced ROS generation include nicotinamide adenine dinucleotide phosphate (NAPDH) oxidase (NOX) upregulation. NOX converts NADPH and oxygen to NADP+, superoxide and a hydrogen ion [46, 47].

4.3. Aluminium and ROS Generation. Aluminium (Al) generates highly reactive oxy and hydroxy free radicals which result in mitochondrial damage. Al increases oxidative stress via mediated Fenton reactions which increase the concentration of iron and it can also lead to H_2O_2 accumulation [48]. Al also activates SOD and inhibits CAT. Increase in H_2O_2 pool increases redox-active iron present either by modulating the electron transport chain or from loosely bound Fe. Studies have shown that oxidative stress and Aβ are closely linked and Al increases the production of Aβ, leading to aggregation [49]. Another study also revealed that Al initially enhances oxidative stress, redox-active iron, and Aβ immunoreactivity [50, 51]. The Fenton reaction helps Al to cause a lot of havoc via increasing the redox active iron concentration in the brain. Thus, Al significantly plays a role in neurodegeneration through oxidative stress.

5. Parkinson's Disease and Oxidative Stress

Parkinson's disease (PD) is a major neurological disease common among the aged (>60 years); it is characterized by a progressive loss of motor control [52]. PD has become the second most reported neurodegenerative disease with around 10 million people having the condition worldwide [53]. PD is more predominant among men than women and seems to be strongly attributable to exposure to environmental toxins, illness, and head trauma [54]. Some of the clinical features of PD are impaired balance, tremor, rigidity, and bradykinesia, which progress to cognitive, sensory, psychiatric, and autonomic impairments [55]. Other manifestations of PD include memory loss, depression, anxiety, insecurity, stress, constipation, diminished sense of smell, difficulty in swallowing and excessive salivation, skin problems, confusion, erectile dysfunction, increased sweating, and a monotone voice [56].

The main risk factor for Parkinson's disease is age, with the disease's occurrence increasing exponentially after 60 years. Apart from the years it takes for pathogenic proteins to misfold to the point where they cause neuronal damage, age-related mitochondrial dysfunction and high generation of ROS are vital factors in neurodegenerative disorders [57]. Elevated deletions in mtDNA are reported in SN pigmented neurons in aged and PD-affected brains [58]. mtDNA damage results in the expression of mutant forms of ETC subunits and mitochondrial tRNAs, both of which contribute to aberrant ROS production, leading to a vicious cycle of mtDNA damage and other mitochondrial dysfunction, which also increase the development of ROS (Figure 2).

Sustained exposure to pesticides and insecticides has been identified as a risk factor for PD. According to Marras et al. [54], higher levels of pesticides and organochlorine insecticides and their metabolites can be detected in the serum and SN of PD patients than of non-PD subjects. Silver

et al. [59] also suggested that the utilization of well-water contaminated with pesticides could increase the PD risk. Paraquat and rotenone, active ingredients in herbicides and pesticides, have been linked to PD-associated oxidative stress upon entry into a biological system; they are metabolized to generate reactive species, which could damage mtDNA and inhibit enzymes involved in the ETC [60–62].

The pathogenesis of PD has shown that the disease involves the gradual and selective degradation of neurons in the SN, an area responsible for movement. The SN contains numerous neurons that release dopamine and then communicate with both the basal ganglia and the frontal lobe responsible for the movement [63]. The oxidation of dopamine to produce dopamine quinones results in a generation of a highly reactive aminochrome that generates superoxides and depletes NADPH pools [64]. Aminochrome in turn forms an adduct with α-synuclein, and this stimulates disease progression. Postmortem brain analysis in the SN of PD patients has revealed a significant increase in dopamine cysteinyl adducts [65, 66]. Dopamine cysteinyl adducts become a precursor for the synthesis of neuromelanin, a molecule responsible for inflammation and degeneration in catecholaminergic neurons (Figure 2) [65, 67].

Postmortem examination of the SN brain regions of PD patients indicates a significant reduction in reduced glutathione (GSH) levels relative to glutathione disulfide (GSSG) level ratio (GSH/GSSG ratio) compared to non-PD patients [68]. The decreased GSH levels could be indicative of glutathione reductase inhibition in the SN of PD subjects as studies have shown that progressive nigral dopaminergic neurodegeneration leads to a downregulation of GSH production [25, 69].

Interestingly, mitochondrial anomalies have also long been considered as a major factor underlying PD pathogenesis, and studies have revealed the huge part played by mitochondrial dynamics and quality control in PD. In brief, implications of the involvement of mitochondrial dysfunction in PD stem from findings that (1) substantia nigra neurons from PD patients exhibit accumulations of mtDNA deletions; (2) significant deficits occur in the activity of mitochondrial respiratory chain complex I; and mutants of PINK-1, DJ-1, and Parkin, which are involved in mitochondrial functioning [70, 71], are found in PD.

6. Alzheimer's Disease and Oxidative Stress

Alzheimer's disease (AD) is an irreversible neurodegenerative disease, characterized by neuronal degradation in brain regions that control cognitive, memory, and emotional functions [72]. AD is age-related, progressive in nature, and can only be managed but not cured. The global prevalence of AD is estimated to rise from 26 million cases to 100 million cases by 2050 [73, 74].

The hallmarks of Alzheimer's disease are the formation of neurofibrillary tangles and senile plaques, neuronal and synaptic loss, severe neuroinflammation, and a global decrease in brain volume [72, 75]. Although the complex nature of AD makes it difficult to accurately diagnose in living patients, advances in biomedical engineering have
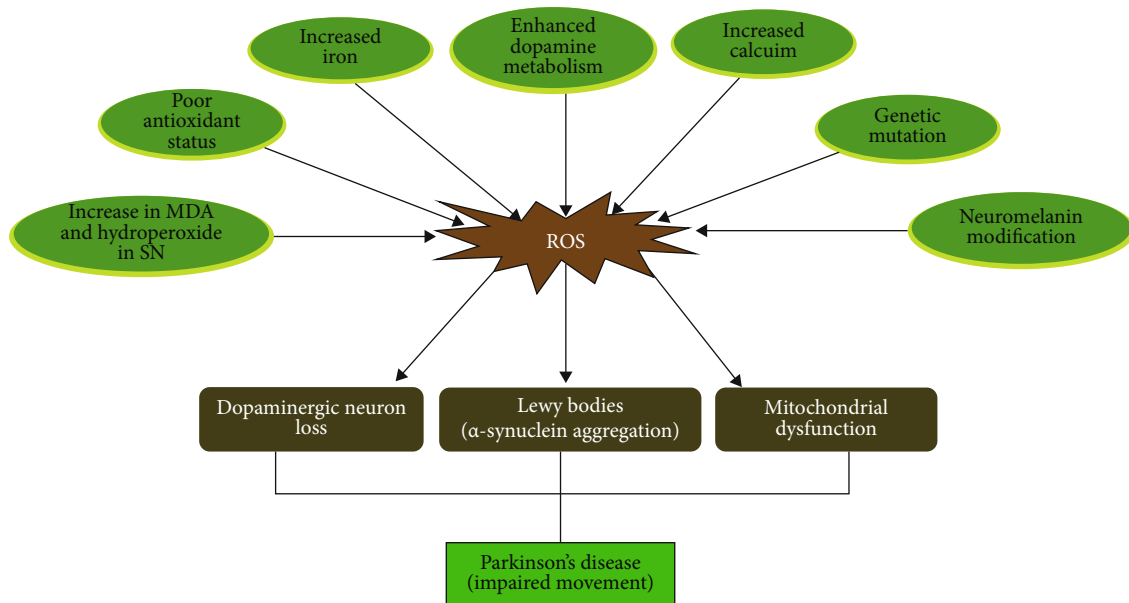
FIGURE 2: The role of oxidative stress in the pathology of Parkinson's disease.

provided a wide array of tools that can diagnose AD in living patients with at least 95% accuracy. These tools include clinical tests to rule out other disease states, such as deficiencies in certain vitamins, infections, cancers, depression; neuropsychological tests for the evaluation of cognitive function; the use of cerebrospinal fluid protein analysis to differentiate AD from other dementias, especially, Creutzfeldt-Jakob disease, Lewy body dementia, or frontotemporal dementia; magnetic resonance imaging to check for shrinkage of brain regions responsible for learning and memory; and the detection of abnormal protein deposits using positron emission tomography scans [74, 76].

The etiology of AD is sporadic, and there is no single generally accepted cause of AD. However, about 5% of known cases are caused by a germline mutation in presenilin 1 or 2 (PSEN 1 or 2) and/or amyloid precursor protein (APP) [77]. After translation of the APP gene to about 11 different isoforms, the protein undergoes amyloidogenic or nonamyloidogenic posttranslational modifications into various proteins, one of which is the amyloid-β (Aβ) protein, a prominent culprit in the pathology and progression of AD [78]. Mutations in the APP gene produce misfolded Aβ peptides/proteins. The resultant formation of senile plaques fosters neurofibrillary tangle synthesis via tau protein hyperphosphorylation, a second protein culprit in the pathogenesis of AD [79, 80]. The neurofibrillary tangles and senile plaque accumulation may occur decades before cognitive and memory deficits are observed in AD patients [81].

Mitochondrial morphology has become a major factor in AD pathogenesis. For instance, compared with age-matched controls, AD neurons contain a large number of mitochondria with broken cristae. Also, the size and number of the neuronal mitochondria, especially those of the CA1/CA3 regions of the hippocampus, dentate gyrus, and the entorhinal cortex, differ from those in normal participants [82, 83]. Furthermore, fibroblasts from AD patients demonstrate abnormal mitochondrial dynamics [82]. The overall expression levels of the fission/fusion proteins DLP-1, OPA-1, Mfn1 and 2, and Fis1 are altered in AD (Figure 3).

Extensive research on the pathology of AD indicates that Aβ hastens the synthesis of neurofibrillary tangles via the activation of specific kinases involved in tau protein phosphorylation [84, 85]. Normal tau proteins are "natively unfolded" and have an extremely low tendency towards misfolding, aggregation, and accumulation (Figure 3). They are involved in microtubule assembly and stability. Microtubules are the structural and functional backbone of neurons and are involved in intracellular trafficking and transport and in the maintenance of cell polarity and microtubules [86, 87], so normal tau proteins are also indirectly involved in these roles. Upon hyperphosphorylation, tau proteins lose their charge and conformation, which causes them to self-aggregate and oligomerize [88, 89]. These aggregates are eventually converted to intracellular neurofibrillary tangles, which result in microtubule disassembly, leading to the cessation of intracellular transduction and to neuroinflammation and neuronal degradation [90, 91].

AD progresses in three stages. First, there is the gradual buildup of extracellular senile plaques and intracellular neurofibrillary tangles, followed by mild cognitive impairment (MCI), which is linked with the buildup of plaques and tangles, and ending with early AD [72]. Several in vitro studies suggest that mitochondrial dysfunctions resulting from the production of reactive oxygen species (ROS) and reactive nitrogen species (RNS) [72, 92–94] play a detrimental role in the progression of AD. Oxidative-associated modifications in membrane-associated macromolecules and nucleic acids have been noted in the brains of AD subjects [95]. According to Haluska et al. [96], increased levels of lipid peroxides and aldehyde-4-hydroxynonenal (HNE) were detected in the brain during the early stages of AD models. Oxidation of nuclear and mitochondrial DNA/RNA molecules, especially
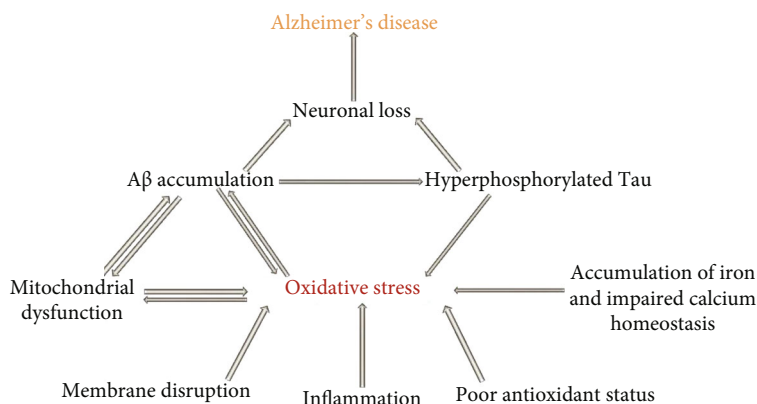
FIGURE 3: The role of oxidative stress in Alzheimer's disease.

of guanosine bases to 8-hydroxyguanosine, in brain regions that coordinate cognitive and emotional functions has also been documented [95].

Redox proteomics is essential for identifying specific proteins that are differentially oxidized in specific brain regions of AD patients. Specifically, several analyses have shown that the levels of protein nitration, protein carbonyls, and 4-hydroxynonenal-modified proteins increase significantly in the brains of MCI AD patients [97, 98]. The identified oxidatively modified proteins involved in regulating energy metabolism, cellular communication, and tau hyperphosphorylation include phosphoglycerate, enolase 1, pyruvate kinase, lactate dehydrogenase, peroxiredoxin, creatine kinase B, glucose-regulated protein precursor, glutamine synthetase, actin, α-tubulin, neuropolypeptide, and prolyl isomerase [72].

AD-associated oxidative stress is mediated by $A\beta$, which fosters disease progression. For instance, Giraldo et al. [99] stated that $A\beta$-mediated oxidative stress triggers the oxidation of both NADPH oxidase and p38; the aberrant activation of p38, in turn, triggers the hyperphosphorylation of tau proteins. $A\beta$-mediated oxidative stress also plays an important role in the activation of calcineurin, sometimes known as a death molecule, which activates Bcl-2 death-associated proteins and fosters cytochrome c release from the mitochondria resulting in the apoptotic death of neurons [100]. $A\beta$ deposits contain elevated levels of copper, zinc, and iron ions, which could interact with $A\beta$ to produce ROS via the Fenton reaction [101]. These ions could also bind to tyrosine and histidine residues of $A\beta$, resulting in the oligomerization of $A\beta$ proteins to form senile plaques [102, 103].

7. Therapeutic Intervention in Parkinson and Alzheimer's Disease

Over the last few years, intense study on multiple fronts has advanced the understanding of the genetics and mechanisms of neuronal pathogenesis and has contributed greatly to our understanding of neurodegenerative diseases, creating a basis for innovative technologies and therapeutic interventions against neurodegenerative diseases [4]. However, there are no available drugs for delaying the progression of PD or

AD although some drugs have been approved for the relief of PD and AD symptoms. Available therapeutic agents for PD often work by inhibiting striatal cholinergic effects or enhancing the activity of dopaminergic neurons [104]. Inhibitors of N-methyl-D-aspartic acid (NMDA), such as memantine and acetylcholinesterase (AChE), which include donepezil, rivastigmine, and galantamine, are also currently used to alleviate AD-related symptoms. Although these agents have succeeded in stimulating mild improvements in cognitive and memory functions, they do not reverse or delay PD and AD progression [101]. Since oxidative stress has been implicated in the pathology and progression of AD, current research trends are shifting focus to the use of antioxidative agents in PD and AD treatment.

The molecules that have displayed great antioxidant activity when treating neurodegenerative diseases in *in vitro* and *in vivo* models are present in pure natural products or plant extracts. However, clinical outcomes in human patients have had limited success and are still inconclusive. This could be linked to the use of single compounds in most clinical trials. In contrast, preclinical studies have used plant extracts that contain several secondary metabolites. The synergistic effects of several active ingredients may provide better antioxidant/disease-modifying activity (Figures 4 and 5) [105–108].

8. Targeting Oxidative Stress in Parkinson's Disease

Antioxidants protected against PD pathogenesis in several in vitro and in vivo studies. However, the defense was only partial, leaving an open window for identifying more appropriate antioxidants for use as PD therapeutics [9]. Endogenous antioxidants, such as coenzyme Q10 (CoQ10), protect cells from oxidative stress (Figure 4). Coenzyme Q10, which is expressed in the mitochondria, acts as a free radical scavenger and electron carrier and accepts electrons released by complexes I and II. Coenzyme Q10 functions as a cofactor and may reduce free radical formation by activating the mitochondrial uncoupling protein. CoQ10 and creatine have shown great promise and are undergoing clinical trials for Parkinson's disease [109, 110].CoQ10 is involved in α-
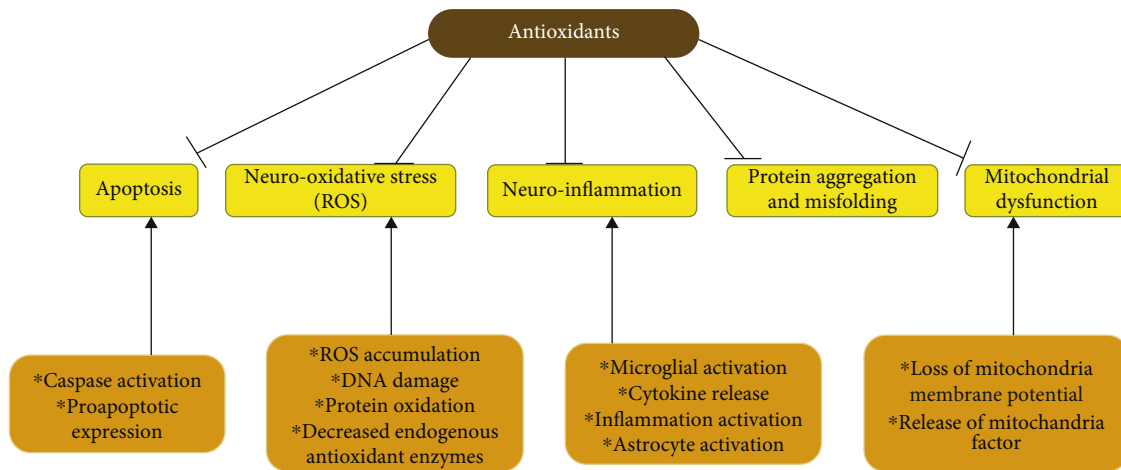
FIGURE 4: Antioxidant intervention at the cellular and molecular levels in neurodegeneration.
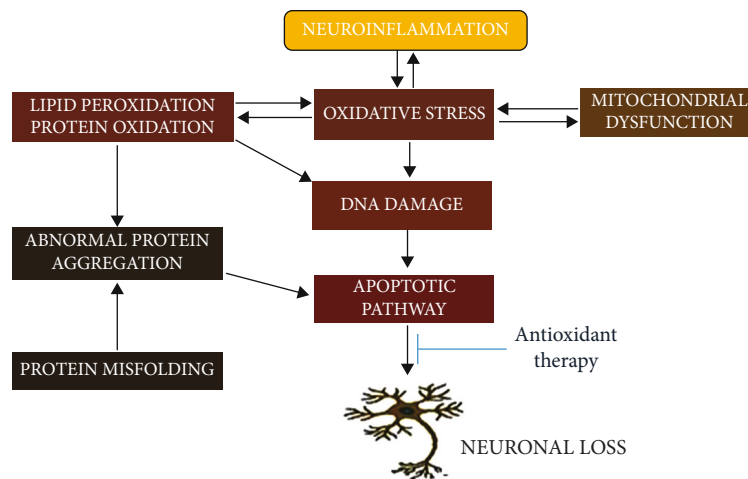
FIGURE 5: Schematic diagram on the effects of antioxidant on neuronal damage.

tocopheroxyl radical reduction and the regeneration of α-tocopherol, making it a powerful free radical scavenger. CoQ10, which reduces the generation of free radicals and regulates the production of ATP, is also a required cofactor for mitochondrial uncoupling proteins [111].

Curiously, CoQ10 levels are reduced in platelets of PD patients, and this may correspond to mitochondrial complex I activity deficiency [112]. CoQ10 has also been shown to prevent death from oxidative stress, apoptosis, and cell death by inhibiting the mitochondrial permeability transfer pore (MPTP), which causes cell death by increasing mitochondrial calcium retention. Because of the decreased level of CoQ10 in PD patients, ATP synthesis is altered and mitochondrial membrane disruption occurs. Significantly improved mitochondrial dysfunction, depletion of dopamine, and axonal degeneration of dopamine neurons following oral CoQ10 were also found in experimental models of PD and in PD patients [113]. CoQ10's underlying protective mechanism is still not clearly defined. CoQ10 may reduce apoptosis by decreasing the Bl-2 antiapoptotic factor level, inhibits cytochrome c release to maintain the integrity of the membrane,

and stops caspase 3 and caspase 9 activation to protect cells against apoptosis [96]. Other naturally occurring cellular molecules, such as creatine, have shown antioxidative properties [114].

The use of creatine in PD treatment is not well established, so further investigation is required. Exogenous polyphenolic compounds such as curcumin, resveratrol, quercetin, puerarin, luteolin, genistein, epigallocatechin gallate, baicalein, and citrus flavonoids (naringenin and hesperidin) can cross the blood-brain barrier and may be neuroprotective during the progression of Parkinson's disease. Extensive research has shown that diets supplemented with polyphenols are beneficial to health. Polyphenols provide neuroprotection against a variety of neuropathological and neurodegenerative conditions [115, 116].

Studies of the pathways of the Nrf2/antioxidant response element (ARE) indicate that it protects neurons from the PD insult of oxidative stress (OS). Two novel drug categories involving this signaling pathway have been developed. These are pathologically activated therapeutics and proelectrophilic drugs, both of which activate the Nrf2/ARE pathway through

TABLE 1: Natural compounds with therapeutic action against neurodegeneration disorders.

Compounds	Therapeutic target	Mechanism of action	Reference
Coenzyme q10	PD	α-Tocopheroxyl radical reduction and regeneration of α-tocopherol Suppression of nigrostriatal dopaminergic cell death	[9, 110, 113]
Luteolin	PD	Increases dopamine uptake	[139]
Resveratrol	PD, AD	Nrf2 activation	[115, 116, 123, 135]
Curcumin	PD	Nrf2 activation	[123]
Epigallocatechin gallate	PD	Nrf2 activation	[123]
α-Tocopherol	AD	Proteolytic degradation of Aβ plaques	[130–133]
Quercetin	PD	Scavenges hydroxyl radicals	[140]
Selenium	AD	Proteolytic degradation of Aβ plaques	[130–133]
8-Hydroxyquinoline derivative	AD	Inhibit Aβ fibril formation and aggregation	[82]
N-(4-Phenoxybenzyl) aniline derivative	AD	Inhibition of acetylcholinesterase	[137]

powerful cellular defense systems against OS [117]. In SH-SY5Y cell models of PD, high Nrf2 protein levels and gene activation of the ARE pathway were induced by naringenin, a natural flavonoid compound [118]. Lou and colleagues demonstrated that 6-OHDA-induced oxidation in SH-SY5Y cells was ameliorated by naringenin via Nrf2/ARE signaling [118]. Additionally, an antioxidant effect of a small catechol, 3,4-dihydroxybenzalacetone, is also involved in the AKT/Nrf2/glutathione pathway [119]. Wei et al. found that Wnt3a could reduce 6-OHDA-induced neurotoxicity through the activation of the Wnt/b-catenin pathway, implying that the mechanism underlying OS inhibition is related to mitochondrial functional maintenance [120].

Moreover, several antioxidants have been studied to determine if they can improve the damage caused by OS in Parkinson's disease. For example, behavioral studies indicated that sulforaphane reduced 6-OHDA-induced rotation and motor coordination deficits in mice [121]. Standardized extracts of *Hypericum perforatum*, gallic acid, and *Sida cordifolia* had potent antioxidant activities in a 6-OHDA rotenone-induced rat model of Parkinson's disease [122]. Several drugs, heavy metals, carotenoids, oxathiolene oxides, dimercaptans, dithiocarbamates, trivalent arsenicals, 1,2-dithiole-3-thiones, isothiocyanates, and quinones, have been reported to interact with specific redox-sensitive cysteines in Keap1 to dissociate Nrf2 from Keap1. There is strong evidence that these Nrf2 inducers may help slow down PD progression [123]. Similar results have been reported for dietary polyphenols, such as resveratrol, curcumin, or certain catechols. In addition, dopamine agonist (DA) and its derivatives as well as levodopa may hold prospects for PD treatment. These compounds are not electrophilic, but become electrophilic by oxidative conversion, which leads to increased expression and activity of GSK-3β (glycogen synthase kinase–3 beta). Besides aging, the major risk factor for PD has been identified as being a steady increase in GSK-3β activity and a decline in Nrf2 transcriptional activity. GSK-3β inhibitors including antioxidative phytochemicals have been shown to protect against

the death of oxidative neuronal cells induced by stress [124, 125]. Overall, phytochemicals appear to be a promising treatment option for current neurodegenerative diseases.

Finally, understanding the link between oxidative stress and impaired mitochondrial function could indicate that targeting oxidative stress by using antioxidants may also confer protection for mitochondria. Preclinical studies have shown that mitochondria-targeted antioxidants (such as CoQ10, vitamin E, MitoQ, or urate) improve mitochondrial activity, but creatine, MitoQ, and coenzyme Q10 did not demonstrate disease-modifying benefits in PD patients in clinical trials. Taking these results together indicates that oxidative stress is a downstream effect of mitochondrial dysfunction rather than a direct cause of PD-related neurodegeneration [126–129].

9. Targeting Oxidative Stress in Alzheimer's Disease

Some experiments in transgenic mouse models and some human clinical trials demonstrated that α-tocopherol- and selenium-supplemented diets promote the proteolytic degradation of Aβ plaques, ameliorate the aggregation of tau proteins, and improve cognitive function [130–133]. These findings were, however, contradicted by a 5-year clinical trial that revealed that the supplemental use of α-tocopherol and selenium only treated AD symptoms but did not prevent the progression of AD [134]. According to Yang et al. [135], the little or no improvement in cognitive function in response to antioxidant supplements during clinical trials could have resulted from ineffective delivery of the antioxidant to the mitochondria of neurons. With that in mind, some researchers now focus on the targeted delivery of antioxidants to the mitochondria of neurons. Gao et al. [136] reported that the biomimetic nanosystem designed for their study effectively crossed the blood-brain barrier and delivered curcumin to the mitochondria of neurons. Based on the findings reported by Yang et al. [135], the resveratrol-

encapsulated neuronal mitochondria-targeted micelle designed for their study was able to facilitate the delivery of high levels of resveratrol into the brain mitochondria; this efficiently reduced oxidative stress, decreased $A\beta$ plaque formation, and ameliorated tau hyperphosphorylation, neuroinflammation, and declined memory function in an aged AD mice model.

Another strategy that has been adopted for targeting oxidative stress in AD patients involves the use of AChE inhibitors with strong antioxidant potential and good blood-brain barrier-permeating abilities. According to Yang et al. [101], a series of newly synthesized 8-hydroxyquinoline derivatives with good brain barrier permeating ability, strong antioxidative activity, and significant metal-chelating ability was able to inhibit the generation of $A\beta$ fibrils and aggregates in AD mouse models. Srivastava et al. [137] also reported that a new class of N-(4-phenoxybenzyl) aniline derivatives designed for their study improved learning and memory functions in transgenic mice via mechanisms that involve the inhibition of acetylcholinesterase, the formation of $A\beta$ aggregates, and the reduction of oxidative stress.

Recently, the pharmacologically developed compound diethyl(3,4-dihydroxyphenethylamino) (quinolin-4-yl) methylphosphonate (DDQ) demonstrated positive effects on mRNA and protein levels related to mitochondrial dysfunction and synaptic dysregulation. DDQ also had an effect on mitochondrial dynamics related to $A\beta$ interactions, fusion proteins (Mfn1 and 2), and fission proteins (Lis1 and DRP1) [138]. The table below shows a summary of natural antioxidative compounds that have been reported for therapeutic effects against AD and PD (Table 1).

10. Future Directions

The intervention of a single or few antioxidants to treat neuronal dysfunction may be termed as too simple to combat the complex ROS metabolism due to their results seen in clinical trials. An effective approach to antioxidant therapy would be to decrease ROS generation and upregulate the various intracellular and mitochondrial antioxidant defense system. For example, Nrf2 activates the antioxidant enzyme network and is termed as the master regulator of redox homeostasis. Therefore, therapeutic target of Nrf2 in the neuron offers a reliable means of regulating oxidative stress. Although, however, controlling oxidative stress alone may not be enough to target neurodegenerative diseases, the restoration of the neuronal function may depend also on targeting some other cell survival pathways. A considerable understanding of ROS biology will also provide insights into what can be targeted than what we have at present.

11. Conclusion

The underlying mechanisms of neurodegenerative disorders are not fully understood; however, there is strong evidence that redox imbalance not only plays a key role but mostly precedes neurodegenerative manifestations. Redox control in physiologic processes is important for maintaining the redox balance and for achieving redox homeostasis. Cells counteract redox imbalance by harnessing an array of both endogenous and exogenous redox-active substances through multiple cellular processes or pathways. Identifying and targeting these redox-regulated pathways in neurodegeneration may provide an avenue for newer treatment strategies. Moreover, as our understanding of the role of redox-regulated events in neurodegeneration becomes clearer, compounds such as phytochemicals that have antioxidative, anti-inflammatory, and anticholinesterase properties may be explored as a source of new treatments for neurodegenerative disorders in the future.

Abbreviations

ND: Neurodegenerative disease
PD: Parkinson's disease
AD: Alzheimer's disease
EAD: Early Alzheimer's disease
MCI: Mild cognitive impairment
SNpc: Substantia nigra pars compacta
BBB: Blood-brain barrier
SN: Substantia nigra
CC: Cerebral cortex
mtDNA: Mitochondrial DNA
nNOS: Neuronal nitric oxide synthase
eNOS: Endothelial nitric oxide synthase
iNOS: Inducible nitric oxide synthase
NADPH: Nicotinamide adenine dinucleotide phosphate
NOX: NADPH oxidase
LOX: Lipoxygenase
COX: Cyclooxygenase
XO: Xanthine oxidase
H_2O_2: Hydrogen peroxide
$O_2^{\cdot-}$: Superoxide anion
ETC: Electron transport chain
$\cdot OH$: Hydroxyl radical
GSH: Glutathione
NMDA: N-Methyl-D-aspartate
HNE: Hydroxynonenal
AChE: Acetylcholinesterase
CoQ10: Coenzyme Q10.

Data Availability

All data are included in the manuscript.

Conflicts of Interest

The authors declare that they have no conflicts of interest.

References

[1] P. Villoslada, R. Baeza-Yates, and J. C. Masdeu, "Reclassifying neurodegenerative diseases," *Nature Biomedical Engineering*, vol. 4, no. 8, pp. 759-760, 2020.

[2] S. Karanth, P. T. Nelson, Y. Katsumata et al., "Prevalence and clinical phenotype of quadruple misfolded proteins in older adults," *JAMA Neurology*, vol. 77, no. 10, pp. 1299–1307, 2020.

[3] C. Peng, J. Q. Trojanowski, and V. M. Y. Lee, "Protein transmission in neurodegenerative disease," *Nature Reviews. Neurology*, vol. 16, no. 4, pp. 199–212, 2020.

[4] R. V. Badhe, D. R. Chejara, P. Kumar, Y. E. Choonara, and V. Pillay, "Neurodegenerative disease conditions and genomic treatment for better health," in *Genomics-Driven Healthcare*, Y. Pathak, Ed., Adis, Singapore, 2018.

[5] A. Singh, R. Kukreti, L. Saso, and S. Kukreti, "Oxidative stress: a key modulator in neurodegenerative diseases," *Molecules*, vol. 24, no. 8, p. 1583, 2019.

[6] C. Cid-Castro, D. R. Hernandez-Espinosa, and J. Moran, "ROS as regulators of mitochondrial dynamics in neurons," *Cellular and Molecular Neurobiology*, vol. 38, no. 5, pp. 995–1007, 2018.

[7] H. Yaribeygi, Y. Panahi, B. Javadi, and A. Sahebkar, "The underlying role of oxidative stress in neurodegeneration: a mechanistic review," *CNS & Neurological Disorders Drug Targets*, vol. 17, no. 3, pp. 207–215, 2018.

[8] A. Haque, R. Polcyn, D. Matzelle, and N. L. Banik, "New insights into the role of neuron-specific enolase in neuro-inflammation, neurodegeneration, and neuroprotection," *Brain Sciences*, vol. 8, no. 2, p. 33, 2018.

[9] A. Sarrafchi, M. Bahmani, H. Shirzad, and M. Rafieian-Kopaei, "Oxidative stress and Parkinson's disease: new hopes in treatment with herbal antioxidants," *Current Pharmaceutical Design*, vol. 22, no. 2, pp. 238–246, 2016.

[10] M. Redza-Dutordoir and D. A. Averill-Bates, "Activation of apoptosis signalling pathways by reactive oxygen species," *Biochimica et Biophysica Acta*, vol. 1863, no. 12, pp. 2977–2992, 2016.

[11] P. R. Angelova and A. Y. Abramov, "Functional role of mitochondrial reactive oxygen species in physiology," *Free Radical Biology & Medicine*, vol. 100, pp. 81–85, 2016.

[12] A. V. Snezhkina, A. V. Kudryavtseva, O. L. Kardymon et al., "ROS generation and antioxidant defense systems in normal and malignant cells," *Oxidative Medicine and Cellular Longevity*, vol. 2019, Article ID 6175804, 17 pages, 2019.

[13] F. Collin, "Chemical basis of reactive oxygen species reactivity and involvement in neurodegenerative diseases," *International Journal of Molecular Sciences*, vol. 20, no. 10, p. 2407, 2019.

[14] M. Valko, K. Jomova, C. J. Rhodes, K. Kuca, and K. Musilek, "Redox- and non-redox-metal-induced formation of free radicals and their role in human disease," *Archives of Toxicology*, vol. 90, no. 1, pp. 1–37, 2016.

[15] N. Asiimwe, S. G. Yeo, M. S. Kim, J. Jung, and N. Y. Jeong, "Nitric oxide: exploring the contextual link with Alzheimer's disease," *Oxidative Medicine and Cellular Longevity*, vol. 2016, Article ID 7205747, 10 pages, 2016.

[16] T. Nakamura and S. A. Lipton, "Aberrant nitric oxide signaling contributes to protein misfolding in neurodegenerative diseases via S-nitrosylation and tyrosine nitration," *Nitric Oxide*, L. J. Ignarro and B. A. Freeman, Eds., pp. 373–384, 2017.

[17] M. Ramalingam and S. J. Kim, "Reactive oxygen/nitrogen species and their functional correlations in neurodegenerative diseases," *Journal of Neural Transmission (Vienna)*, vol. 119, no. 8, pp. 891–910, 2012.

[18] M. Virarkar, L. Alappat, P. G. Bradford, and A. B. Awad, "L-arginine and nitric oxide in CNS function and neurodegener-

[19] ative diseases," *Critical Reviews in Food Science and Nutrition*, vol. 53, no. 11, pp. 1157–1167, 2013.

[19] U. Forstermann and W. C. Sessa, "Nitric oxide synthases: regulation and function," *European Heart Journal*, vol. 33, no. 7, pp. 829–837, 2012.

[20] O. Ifeanyi, "A review on free radicals and antioxidants," *Ifeanional Journal of Research in Medical Sciences*, vol. 4, no. 2, pp. 123–133, 2018.

[21] C. Guo, L. Sun, X. Chen, and D. Zhang, "Oxidative stress, mitochondrial damage and neurodegenerative diseases," *Neural Regeneration Research*, vol. 8, no. 21, pp. 2003–2014, 2013.

[22] T. Cali, D. Ottolini, and M. Brini, "Mitochondria, calcium, and endoplasmic reticulum stress in Parkinson's disease," *BioFactors*, vol. 37, no. 3, pp. 228–240, 2011.

[23] G. H. Kim, J. E. Kim, S. J. Rhie, and S. Yoon, "The role of oxidative stress in neurodegenerative diseases," *Exp Neurobiol*, vol. 24, no. 4, pp. 325–340, 2015.

[24] N. Nissanka and C. T. Moraes, "Mitochondrial DNA damage and reactive oxygen species in neurodegenerative disease," *FEBS Letters*, vol. 592, no. 5, pp. 728–742, 2018.

[25] M. al Shahrani, S. Heales, I. Hargreaves, and M. Orford, "Oxidative Stress: Mechanistic Insights into Inherited Mitochondrial Disorders and Parkinson's Disease," *Journal of Clinical Medicine*, vol. 6, no. 11, p. 100, 2017.

[26] I. Badillo-Ramirez, J. M. Saniger, and S. Rivas-Arancibia, "5-S-Cysteinyl-dopamine, a neurotoxic endogenous metabolite of dopamine: implications for Parkinson's disease," *Neurochemistry International*, vol. 129, p. 104514, 2019.

[27] P. Pradhan, O. Majhi, A. Biswas, V. K. Joshi, and D. Sinha, "Enhanced accumulation of reduced glutathione by scopoletin improves survivability of dopaminergic neurons in Parkinson's model," *Cell Death & Disease*, vol. 11, no. 9, p. 739, 2020.

[28] L. Mezzaroba, D. F. Alfieri, A. N. Colado Simao, and E. M. Vissoci Reiche, "The role of zinc, copper, manganese and iron in neurodegenerative diseases," *Neurotoxicology*, vol. 74, pp. 230–241, 2019.

[29] S. Hu, H. Hu, S. Mak et al., "A novel tetramethylpyrazine derivative prophylactically protects against glutamate-induced excitotoxicity in primary neurons through the blockage of N-methyl-D-aspartate receptor," *Frontiers in Pharmacology*, vol. 9, p. 73, 2018.

[30] A. Martin-Bastida, B. S. Tilley, S. Bansal, S. M. Gentleman, D. T. Dexter, and R. J. Ward, "Iron and inflammation: in vivo and post-mortem studies in Parkinson's disease," *Journal of Neural Transmission (Vienna)*, vol. 128, no. 1, pp. 15–25, 2021.

[31] G. A. Salvador, "Iron in neuronal function and dysfunction," *BioFactors*, vol. 36, no. 2, pp. 103–110, 2010.

[32] T. Moos and E. H. Morgan, "The significance of the mutated divalent metal transporter (DMT1) on iron transport into the Belgrade rat brain," *Journal of Neurochemistry*, vol. 88, no. 1, pp. 233–245, 2004.

[33] T. Moos and E. H. Morgan, "The metabolism of neuronal iron and its pathogenic role in neurological disease: review," *Annals of the New York Academy of Sciences*, vol. 1012, no. 1, pp. 14–26, 2004.

[34] M. I. Flydal, T. A. Kråkenes, M. D. S. Tai, M. P. A. Tran, K. Teigen, and A. Martinez, "Levalbuterol lowers the feedback inhibition by dopamine and delays misfolding and

aggregation in tyrosine hydroxylase," *Biochimie*, vol. 183, pp. 126–132, 2020.

[35] B. Lozoff and M. K. Georgieff, "Iron deficiency and brain development," *Seminars in Pediatric Neurology*, vol. 13, no. 3, pp. 158–165, 2006.

[36] Y. E. Yoo, J. H. Hong, K. C. Hur, E. S. Oh, and J. M. Chung, "Iron enhances NGF-induced neurite outgrowth in PC12 cells," *Molecules and Cells*, vol. 17, no. 2, pp. 340–346, 2004.

[37] H. Jiang, N. Song, Q. Jiao, L. Shi, and X. Du, "Iron pathophysiology in Parkinson diseases," *Advances in Experimental Medicine and Biology*, vol. 1173, pp. 45–66, 2019.

[38] A. Gegotek and E. Skrzydlewska, "Biological effect of protein modifications by lipid peroxidation products," *Chemistry and Physics of Lipids*, vol. 221, pp. 46–52, 2019.

[39] G. Barrera, S. Pizzimenti, M. Daga et al., "Lipid peroxidation-derived aldehydes, 4-hydroxynonenal and malondialdehyde in aging-related disorders," *Antioxidants (Basel)*, vol. 7, no. 8, p. 102, 2018.

[40] M. M. Gaschler and B. R. Stockwell, "Lipid peroxidation in cell death," *Biochemical and Biophysical Research Communications*, vol. 482, no. 3, pp. 419–425, 2017.

[41] O. V. Taso, A. Philippou, A. Moustogiannis, E. Zevolis, and M. Koutsilieris, "Lipid peroxidation products and their role in neurodegenerative diseases," *Annals of Research Hospitals*, vol. 3, p. 2, 2019.

[42] H. Y. Liu, J. R. Gale, I. J. Reynolds, J. H. Weiss, and E. Aizenman, "The Multifaceted Roles of Zinc in Neuronal Mitochondrial Dysfunction," *Biomedicine*, vol. 9, no. 5, p. 489, 2021.

[43] K. M. Noh and J. Y. Koh, "Induction and activation by zinc of NADPH oxidase in cultured cortical neurons and astrocytes," *The Journal of Neuroscience*, vol. 20, no. 23, p. RC111, 2000.

[44] K. E. Dineley, T. V. Votyakova, and I. J. Reynolds, "Zinc inhibition of cellular energy production: implications for mitochondria and neurodegeneration," *Journal of Neurochemistry*, vol. 85, no. 3, pp. 563–570, 2003.

[45] D. Malinska, B. Kulawiak, A. P. Kudin et al., "Complex III-dependent superoxide production of brain mitochondria contributes to seizure-related ROS formation," *Biochimica et Biophysica Acta*, vol. 1797, no. 6-7, pp. 1163–1170, 2010.

[46] K. Bedard and K. H. Krause, "The NOX family of ROS-generating NADPH oxidases: physiology and pathophysiology," *Physiological Reviews*, vol. 87, no. 1, pp. 245–313, 2007.

[47] G. Salazar, J. Huang, R. G. Feresin, Y. Zhao, and K. K. Griendling, "Zinc regulates Nox1 expression through a NF-κB and mitochondrial ROS dependent mechanism to induce senescence of vascular smooth muscle cells," *Free Radical Biology & Medicine*, vol. 108, pp. 225–235, 2017.

[48] V. P. Bharathi, M. Govindaraju, A. P. Palanisamy, K. Sambamurti, and K. S. Rao, "Molecular toxicity of aluminium in relation to neurodegeneration," *The Indian Journal of Medical Research*, vol. 128, no. 4, pp. 545–556, 2008.

[49] C. Exley, "The aluminium-amyloid cascade hypothesis and Alzheimer's disease," *Sub-Cellular Biochemistry*, vol. 38, pp. 225–234, 2005.

[50] R. J. Castellani, P. I. Moreira, G. Liu et al., "Iron: the redox-active center of oxidative stress in Alzheimer disease," *Neurochemical Research*, vol. 32, no. 10, pp. 1640–1645, 2007.

[51] C. A. Rottkamp, A. Nunomura, A. K. Raina, L. M. Sayre, G. Perry, and M. A. Smith, "Oxidative stress, antioxidants, and Alzheimer disease," *Alzheimer Disease and Associated Disorders*, vol. 14, Supplement, pp. S62–S66, 2000.

[52] O. B. Tysnes and A. Storstein, "Epidemiology of Parkinson's disease," *Journal of Neural Transmission (Vienna)*, vol. 124, no. 8, pp. 901–905, 2017.

[53] Z. Li, Z. Zheng, J. Ruan, Z. Li, and C. M. Tzeng, "Chronic inflammation links cancer and Parkinson's disease," *Frontiers in Aging Neuroscience*, vol. 8, p. 126, 2016.

[54] C. Marras, C. G. Canning, and S. M. Goldman, "Environment, lifestyle, and Parkinson's disease: implications for prevention in the next decade," *Movement Disorders*, vol. 34, no. 6, pp. 801–811, 2019.

[55] M. T. Hayes, "Parkinson's disease and parkinsonism," *The American Journal of Medicine*, vol. 132, no. 7, pp. 802–807, 2019.

[56] S. Manoharan, G. J. Guillemin, R. S. Abiramasundari, M. M. Essa, M. Akbar, and M. D. Akbar, "The role of reactive oxygen species in the pathogenesis of Alzheimer's disease, Parkinson's disease, and Huntington's disease: a mini review," *Oxidative Medicine and Cellular Longevity*, vol. 2016, Article ID 8590578, 15 pages, 2016.

[57] S. Y. Pang, P. W. L. Ho, H. F. Liu et al., "The interplay of aging, genetics and environmental factors in the pathogenesis of Parkinson's disease," *Translational Neurodegeneration*, vol. 8, no. 1, p. 23, 2019.

[58] E. S. Chocron, E. Munkacsy, and A. M. Pickering, "Cause or casualty: the role of mitochondrial DNA in aging and age-associated disease," *Biochimica et Biophysica Acta - Molecular Basis of Disease*, vol. 1865, no. 2, pp. 285–297, 2019.

[59] M. R. Silver, B. A. Racette, U. Dube, I. M. Faust, and S. Searles Nielsen, "Well water and Parkinson's disease in Medicare beneficiaries: a nationwide case-control study," *Journal of Parkinson's Disease*, vol. 10, no. 2, pp. 693–705, 2020.

[60] B. Doktór, M. Damulewicz, and E. Pyza, "Overexpression of mitochondrial ligases reverses rotenone-induced effects in a Drosophila model of Parkinson's disease," *Frontiers in Neuroscience*, vol. 13, p. 94, 2019.

[61] V. Lawana and J. R. Cannon, "Rotenone neurotoxicity: relevance to Parkinson's disease," in *Advances in Neurotoxicolog*, M. Aschner and L. G. Costa, Eds., pp. 209–254, Academic Press, 2020.

[62] C. Vaccari, R. El Dib, and J. L. V. de Camargo, "Paraquat and Parkinson's disease: a systematic review protocol according to the OHAT approach for hazard identification," *Systematic Reviews*, vol. 6, no. 1, p. 98, 2017.

[63] B. G. Trist, D. J. Hare, and K. L. Double, "Oxidative stress in the aging substantia nigra and the etiology of Parkinson's disease," *Aging Cell*, vol. 18, no. 6, article e13031, 2019.

[64] E. Monzani, S. Nicolis, S. Dell'Acqua et al., "Dopamine, oxidative stress and protein-quinone modifications in Parkinson's and other neurodegenerative diseases," *Angewandte Chemie (International Ed. in English)*, vol. 58, no. 20, pp. 6512–6527, 2019.

[65] A. R. Carta, G. Mulas, M. Bortolanza et al., "l-DOPA-induced dyskinesia and neuroinflammation: do microglia and astrocytes play a role?," *The European Journal of Neuroscience*, vol. 45, no. 1, pp. 73–91, 2017.

[66] R. A. Maki, M. Holzer, K. Motamedchaboki et al., "Human myeloperoxidase (hMPO) is expressed in neurons in the substantia nigra in Parkinson's disease and in the hMPO-α-synuclein-A53T mouse model, correlating with increased

nitration and aggregation of α-synuclein and exacerbation of motor impairment," *Free Radical Biology & Medicine*, vol. 141, pp. 115–140, 2019.

[67] O. Karlsson and N. G. Lindquist, "Melanin and neuromelanin binding of drugs and chemicals: toxicological implications," *Archives of Toxicology*, vol. 90, no. 8, pp. 1883–1891, 2016.

[68] L. D. Coles, P. J. Tuite, G. Öz et al., "Repeated-dose oral N-acetylcysteine in Parkinson's disease: pharmacokinetics and effect on brain glutathione and oxidative stress," *Journal of Clinical Pharmacology*, vol. 58, no. 2, pp. 158–167, 2018.

[69] R. Kaur, S. Mehan, and S. Singh, "Understanding multifactorial architecture of Parkinson's disease: pathophysiology to management," *Neurological Sciences*, vol. 40, no. 1, pp. 13–23, 2019.

[70] X. Jiang, T. Jin, H. Zhang et al., "Current progress of mitochondrial quality control pathways underlying the pathogenesis of Parkinson's disease," *Oxidative Medicine and Cellular Longevity*, vol. 2019, Article ID 4578462, 11 pages, 2019.

[71] S. R. Subramaniam and M. F. Chesselet, "Mitochondrial dysfunction and oxidative stress in Parkinson's disease," *Progress in Neurobiology*, vol. 106-107, pp. 17–32, 2013.

[72] A. Tramutola, C. Lanzillotta, M. Perluigi, and D. A. Butterfield, "Oxidative stress, protein modification and Alzheimer disease," *Brain Research Bulletin*, vol. 133, pp. 88–96, 2017.

[73] Alzehimer's association, "2020 Alzheimer's disease facts and figures," *Alzheimers Dement*, vol. 16, no. 3, pp. 391–460, 2020.

[74] L. Mucke, "Alzheimer's disease," *Nature*, vol. 461, no. 7266, pp. 895–897, 2009.

[75] Y. W. Wan, R. al-Ouran, C. G. Mangleburg et al., "Meta-Analysis of the Alzheimer's Disease Human Brain Transcriptome and Functional Dissection in Mouse Models," *Cell Reports*, vol. 32, no. 2, p. 107908, 2020.

[76] R. J. Bateman, N. R. Barthelemy, and K. Horie, "Another step forward in blood-based diagnostics for Alzheimer's disease," *Nature Medicine*, vol. 26, no. 3, pp. 314–316, 2020.

[77] A. F. Shah, J. A. Morris, and M. Wray, "Pathogenesis of Alzheimer's disease: multiple interacting causes against which amyloid precursor protein protects," *Medical Hypotheses*, vol. 143, p. 110035, 2020.

[78] R. J. O'Brien and P. C. Wong, "Amyloid precursor protein processing and Alzheimer's disease," *Annual Review of Neuroscience*, vol. 34, no. 1, pp. 185–204, 2011.

[79] S. Hunter and C. Brayne, "Understanding the roles of mutations in the amyloid precursor protein in Alzheimer disease," *Molecular Psychiatry*, vol. 23, no. 1, pp. 81–93, 2018.

[80] A. Tsatsanis, B. X. Wong, A. P. Gunn et al., "Amyloidogenic processing of Alzheimer's disease β-amyloid precursor protein induces cellular iron retention," *Molecular Psychiatry*, vol. 25, no. 9, pp. 1958–1966, 2020.

[81] W. H. Habig, M. J. Pabst, and W. B. Jakoby, "Glutathione S-transferases: the first enzymatic step in mercapturic acid formation," *The Journal of Biological Chemistry*, vol. 249, no. 22, pp. 7130–7139, 1974.

[82] X. Wang, B. Su, L. Zheng, G. Perry, M. A. Smith, and X. Zhu, "The role of abnormal mitochondrial dynamics in the pathogenesis of Alzheimer's disease," *Journal of Neurochemistry*, vol. 109, Supplement 1, pp. 153–159, 2009.

[83] M. H. Yan, X. Wang, and X. Zhu, "Mitochondrial defects and oxidative stress in Alzheimer disease and Parkinson disease," *Free Radical Biology & Medicine*, vol. 62, pp. 90–101, 2013.

[84] M. Blurton-Jones and F. LaFerla, "Pathways by which Abeta facilitates tau pathology," *Current Alzheimer Research*, vol. 3, no. 5, pp. 437–448, 2006.

[85] S. Oddo, A. Caccamo, J. D. Shepherd et al., "Triple-transgenic model of Alzheimer's disease with plaques and tangles: intracellular Aβ and synaptic dysfunction," *Neuron*, vol. 39, no. 3, pp. 409–421, 2003.

[86] S. Muralidar, S. V. Ambi, S. Sekaran, D. Thirumalai, and B. Palaniappan, "Role of tau protein in Alzheimer's disease: the prime pathological player," *International Journal of Biological Macromolecules*, vol. 163, pp. 1599–1617, 2020.

[87] M. Amir Mishan, M. Rezaei Kanavi, K. Shahpasand, and H. Ahmadieh, "Pathogenic tau protein species: promising therapeutic targets for ocular neurodegenerative diseases," *Journal of Ophthalmic and Vision Research*, vol. 14, no. 4, pp. 491–505, 2019.

[88] A. D. Alonso, L. S. Cohen, C. Corbo et al., "Hyperphosphorylation of tau associates with changes in its function beyond microtubule stability," *Frontiers in Cellular Neuroscience*, vol. 12, p. 338, 2018.

[89] J. Neddens, M. Temmel, S. Flunkert et al., "Phosphorylation of different tau sites during progression of Alzheimer's disease," *Acta Neuropathologica Communications*, vol. 6, no. 1, p. 52, 2018.

[90] A. J. Moszczynski, M. Gohar, K. Volkening, C. Leystra-Lantz, W. Strong, and M. J. Strong, "Thr^{175}-phosphorylated tau induces pathologic fibril formation via GSK3β-mediated phosphorylation of Thr^{231} in vitro," *Neurobiology of Aging*, vol. 36, no. 3, pp. 1590–1599, 2015.

[91] H. Zhao, R. Chang, H. Che et al., "Hyperphosphorylation of tau protein by calpain regulation in retina of Alzheimer's disease transgenic mouse," *Neuroscience Letters*, vol. 551, pp. 12–16, 2013.

[92] D. A. Butterfield, M. L. Bader Lange, and R. Sultana, "Involvements of the lipid peroxidation product, HNE, in the pathogenesis and progression of Alzheimer's disease," *Biochimica et Biophysica Acta*, vol. 1801, no. 8, pp. 924–929, 2010.

[93] Y. Zhao and B. Zhao, "Oxidative stress and the pathogenesis of Alzheimer's disease," *Oxidative Medicine and Cellular Longevity*, vol. 2013, Article ID 316523, 10 pages, 2013.

[94] J. E. Selfridge, L. E, J. Lu, and R. H. Swerdlow, "Role of mitochondrial homeostasis and dynamics in Alzheimer's disease," *Neurobiology of Disease*, vol. 51, pp. 3–12, 2013.

[95] F. Cioffi, R. H. I. Adam, and K. Broersen, "Molecular mechanisms and genetics of oxidative stress in Alzheimer's disease," *Journal of Alzheimer's Disease*, vol. 72, no. 4, pp. 981–1017, 2019.

[96] C. K. Haluska, M. S. Baptista, A. U. Fernandes, A. P. Schroder, C. M. Marques, and R. Itri, "Photo-activated phase separation in giant vesicles made from different lipid mixtures," *Biochimica et Biophysica Acta*, vol. 1818, no. 3, pp. 666–672, 2012.

[97] C. D. Aluise, R. A. S. Robinson, T. L. Beckett et al., "Preclinical Alzheimer disease: brain oxidative stress, Aβ peptide and proteomics," *Neurobiology of Disease*, vol. 39, no. 2, pp. 221–228, 2010.

[98] C. D. Aluise, R. A. S. Robinson, J. Cai, W. M. Pierce, W. R. Markesbery, and D. A. Butterfield, "Redox proteomics analysis of brains from subjects with amnestic mild cognitive impairment compared to brains from subjects with

preclinical Alzheimer's disease: insights into memory loss in MCI," *Journal of Alzheimer's Disease*, vol. 23, no. 2, pp. 257–269, 2011.

[99] E. Giraldo, A. Lloret, T. Fuchsberger, and J. Vina, "Aβ and tau toxicities in Alzheimer's are linked _via_ oxidative stress-induced p38 activation: protective role of vitamin E," *Redox Biology*, vol. 2, pp. 873–877, 2014.

[100] N. Bulat and C. Widmann, "Caspase substrates and neurodegenerative diseases," *Brain Research Bulletin*, vol. 80, no. 4-5, pp. 251–267, 2009.

[101] X. Yang, P. Cai, Q. Liu et al., "Novel 8-hydroxyquinoline derivatives targeting _β_ -amyloid aggregation, metal chelation and oxidative stress against Alzheimer's disease," *Bioorganic & Medicinal Chemistry*, vol. 26, no. 12, pp. 3191–3201, 2018.

[102] K. P. Kepp, "Bioinorganic chemistry of Alzheimer's disease," *Chemical Reviews*, vol. 112, no. 10, pp. 5193–5239, 2012.

[103] P. Zatta, D. Drago, S. Bolognin, and S. L. Sensi, "Alzheimer's disease, metal ions and metal homeostatic therapy," *Trends in Pharmacological Sciences*, vol. 30, no. 7, pp. 346–355, 2009.

[104] S. Hernando, O. Gartziandia, E. Herran, J. L. Pedraz, M. Igartua, and R. M. Hernandez, "Advances in nanomedicine for the treatment of Alzheimer's and Parkinson's diseases," *Nanomedicine (London, England)*, vol. 11, no. 10, pp. 1267–1285, 2016.

[105] F. Pohl and P. Kong Thoo Lin, "The potential use of plant natural products and plant extracts with antioxidant properties for the prevention/treatment of neurodegenerative diseases: in vitro, in vivo and clinical trials," *Molecules*, vol. 23, no. 12, p. 3283, 2018.

[106] I. H. Cho, "Effects of Panax ginseng in neurodegenerative diseases," *Journal of Ginseng Research*, vol. 36, no. 4, pp. 342–353, 2012.

[107] M. di Paolo, L. Papi, F. Gori, and E. Turillazzi, "Natural products in neurodegenerative diseases: a great promise but an ethical challenge," *International Journal of Molecular Sciences*, vol. 20, no. 20, p. 5170, 2019.

[108] N. S. Mohd Sairazi and K. N. S. Sirajudeen, "Natural products and their bioactive compounds: neuroprotective potentials against neurodegenerative diseases," *Evidence-based Complementary and Alternative Medicine*, vol. 2020, Article ID 6565396, 30 pages, 2020.

[109] A. Negida, A. Menshawy, G. el Ashal et al., "Coenzyme Q10 for patients with Parkinson's disease: a systematic review and meta-analysis," *CNS & Neurological Disorders Drug Targets*, vol. 15, no. 1, pp. 45–53, 2016.

[110] H. W. Park, C. G. Park, M. Park et al., "Intrastriatal administration of coenzyme Q10 enhances neuroprotection in a Parkinson's disease rat model," *Scientific Reports*, vol. 10, no. 1, p. 9572, 2020.

[111] Z. G. Zhu, M. X. Sun, W. L. Zhang, W. W. Wang, Y. M. Jin, and C. L. Xie, "The efficacy and safety of coenzyme Q10 in Parkinson's disease: a meta-analysis of randomized controlled trials," *Neurological Sciences*, vol. 38, no. 2, pp. 215–224, 2017.

[112] J. S. Park, R. L. Davis, and C. M. Sue, "Mitochondrial dysfunction in Parkinson's disease: new mechanistic insights and therapeutic perspectives," *Current Neurology and Neuroscience Reports*, vol. 18, no. 5, p. 21, 2018.

[113] D. Charvin, R. Medori, R. A. Hauser, and O. Rascol, "Therapeutic strategies for Parkinson disease: beyond dopaminergic drugs," *Nature Reviews. Drug Discovery*, vol. 17, no. 11, pp. 804–822, 2018.

[114] A. Bender and T. Klopstock, "Creatine for neuroprotection in neurodegenerative disease: end of story?," *Amino Acids*, vol. 48, no. 8, pp. 1929–1940, 2016.

[115] S. L. Hor, S. L. Teoh, and W. L. Lim, "Plant polyphenols as neuroprotective agents in Parkinson's disease targeting oxidative stress," *Current Drug Targets*, vol. 21, no. 5, pp. 458–476, 2020.

[116] A. Singh, P. Tripathi, A. K. Yadawa, and S. Singh, "Promising polyphenols in Parkinson's disease therapeutics," *Neurochemical Research*, vol. 45, no. 8, pp. 1731–1745, 2020.

[117] T. Satoh, S. R. McKercher, and S. A. Lipton, "Nrf2/ARE-mediated antioxidant actions of pro-electrophilic drugs," *Free Radical Biology & Medicine*, vol. 65, pp. 645–657, 2013.

[118] H. Lou, X. Jing, X. Wei, H. Shi, D. Ren, and X. Zhang, "Naringenin protects against 6-OHDA-induced neurotoxicity via activation of the Nrf2/ARE signaling pathway," *Neuropharmacology*, vol. 79, pp. 380–388, 2014.

[119] K. Gunjima, R. Tomiyama, K. Takakura et al., "3,4-Dihydroxybenzalacetone protects against Parkinson's disease-related neurotoxin 6-OHDA through Akt/Nrf2/glutathione pathway," *Journal of Cellular Biochemistry*, vol. 115, no. 1, pp. 151–160, 2014.

[120] L. Wei, L. Ding, M. S. Mo et al., "Wnt3a protects SH-SY5Y cells against 6-hydroxydopamine toxicity by restoration of mitochondria function," *Translational Neurodegeneration*, vol. 4, no. 1, p. 11, 2015.

[121] F. Morroni, A. Tarozzi, G. Sita et al., "Neuroprotective effect of sulforaphane in 6-hydroxydopamine-lesioned mouse model of Parkinson's disease," *Neurotoxicology*, vol. 36, pp. 63–71, 2013.

[122] T. Sengupta, J. Vinayagam, R. Singh, P. Jaisankar, and K. P. Mohanakumar, "Plant-derived natural products for Parkinson's disease therapy," *Advances in Neurobiology*, vol. 12, pp. 415–496, 2016.

[123] A. Cuadrado, P. Moreno-Murciano, and J. Pedraza-Chaverri, "The transcription factor Nrf2 as a new therapeutic target in Parkinson's disease," *Expert Opinion on Therapeutic Targets*, vol. 13, no. 3, pp. 319–329, 2009.

[124] H. Kumar, H. W. Lim, S. V. More et al., "The role of free radicals in the aging brain and Parkinson's disease: convergence and parallelism," *International Journal of Molecular Sciences*, vol. 13, no. 8, pp. 10478–10504, 2012.

[125] A. Silva-Palacios, M. Ostolga-Chavarria, C. Zazueta, and M. Konigsberg, "Nrf2: molecular and epigenetic regulation during aging," *Ageing Research Reviews*, vol. 47, pp. 31–40, 2018.

[126] H. Jin, A. Kanthasamy, A. Ghosh, V. Anantharam, B. Kalyanaraman, and A. G. Kanthasamy, "Mitochondria-targeted antioxidants for treatment of Parkinson's disease: preclinical and clinical outcomes," *Biochimica et Biophysica Acta*, vol. 1842, no. 8, pp. 1282–1294, 2014.

[127] A. Camilleri and N. Vassallo, "The centrality of mitochondria in the pathogenesis and treatment of Parkinson's disease," *CNS Neuroscience & Therapeutics*, vol. 20, no. 7, pp. 591–602, 2014.

[128] K. H. Chang and C. M. Chen, "The role of oxidative stress in Parkinson's disease," *Antioxidants (Basel)*, vol. 9, no. 7, p. 597, 2020.

[129] A. P. Duarte-Jurado, Y. Gopar-Cuevas, O. Saucedo-Cardenas et al., "Antioxidant Therapeutics in Parkinson's Disease:

Current Challenges and Opportunities," *Antioxidants (Basel)*, vol. 10, no. 3, p. 453, 2021.

[130] T. Jiang, Q. Sun, and S. Chen, "Oxidative stress: a major pathogenesis and potential therapeutic target of antioxidative agents in Parkinson's disease and Alzheimer's disease," *Progress in Neurobiology*, vol. 147, pp. 1–19, 2016.

[131] V. Conte, K. Uryu, S. Fujimoto et al., "Vitamin E reduces amyloidosis and improves cognitive function in Tg2576 mice following repetitive concussive brain injury," *Journal of Neurochemistry*, vol. 90, no. 3, pp. 758–764, 2004.

[132] H. Nakashima, T. Ishihara, O. Yokota et al., "Effects of α-tocopherol on an animal model of tauopathies," *Free Radical Biology & Medicine*, vol. 37, no. 2, pp. 176–186, 2004.

[133] S. Sung, Y. Yao, K. Uryu et al., "Early vitamin E supplementation in young but not aged mice reduces Aβ levels and amyloid deposition in a transgenic model of Alzheimer's disease," *The FASEB Journal*, vol. 18, no. 2, pp. 323–325, 2004.

[134] R. J. Kryscio, E. L. Abner, A. Caban-Holt et al., "Association of antioxidant supplement use and dementia in the prevention of Alzheimer's disease by vitamin E and selenium trial (PREADViSE)," *JAMA Neurology*, vol. 74, no. 5, pp. 567–573, 2017.

[135] P. Yang, D. Sheng, Q. Guo et al., "Neuronal mitochondria-targeted micelles relieving oxidative stress for delayed progression of Alzheimer's disease," *Biomaterials*, vol. 238, p. 119844, 2020.

[136] C. Gao, Y. Wang, J. Sun et al., "Neuronal mitochondria-targeted delivery of curcumin by biomimetic engineered nanosystems in Alzheimer's disease mice," *Acta Biomaterialia*, vol. 108, pp. 285–299, 2020.

[137] P. Srivastava, P. N. Tripathi, P. Sharma, and S. K. Shrivastava, "Design, synthesis, and evaluation of novel _N_ -(4-phenoxybenzyl)aniline derivatives targeting acetylcholinesterase, β-amyloid aggregation and oxidative stress to treat Alzheimer's disease," *Bioorganic & Medicinal Chemistry*, vol. 27, no. 16, pp. 3650–3662, 2019.

[138] M. van Bulck, A. Sierra-Magro, J. Alarcon-Gil, A. Perez-Castillo, and J. Morales-Garcia, "Novel Approaches for the Treatment of Alzheimer's and Parkinson's Disease," *International Journal of Molecular Sciences*, vol. 20, no. 3, p. 719, 2019.

[139] H. Q. Chen, Z. Y. Jin, X. J. Wang, X. M. Xu, L. Deng, and J. W. Zhao, "Luteolin protects dopaminergic neurons from inflammation-induced injury through inhibition of microglial activation," *Neuroscience Letters*, vol. 448, no. 2, pp. 175–179, 2008.

[140] S. S. Karuppagounder, S. K. Madathil, M. Pandey, R. Haobam, U. Rajamma, and K. P. Mohanakumar, "Quercetin up-regulates mitochondrial complex-I activity to protect against programmed cell death in rotenone model of Parkinson's disease in rats," *Neuroscience*, vol. 236, pp. 136–148, 2013.

Review Article

Reactive Oxygen Species as a Link between Antioxidant Pathways and Autophagy

Dan Li [iD], **Zongxian Ding, Kaili Du** [iD]**, Xiangshi Ye** [iD]**, and Shixue Cheng** [iD]

Collaborative Innovation Center of Yangtze River Delta Region Green Pharmaceuticals, College of Pharmaceutical Sciences, Zhejiang University of Technology, Hangzhou, China

Correspondence should be addressed to Dan Li; lidan@zjut.edu.cn

Reactive oxygen species (ROS) are highly reactive molecules that can oxidize proteins, lipids, and DNA. Under physiological conditions, ROS are mainly generated in the mitochondria during aerobic metabolism. Under pathological conditions, excessive ROS disrupt cellular homeostasis. High levels of ROS result in severe oxidative damage to the cellular machinery. However, a low/mild level of ROS could serve as a signal to trigger cell survival mechanisms. To prevent and cope with oxidative damage to biomolecules, cells have developed various antioxidant and detoxifying mechanisms. Meanwhile, ROS can initiate autophagy, a process of self-clearance, which helps to reduce oxidative damage by engulfing and degrading oxidized substance. This review summarizes the interactions among ROS, autophagy, and antioxidant pathways. The effects of natural phytochemicals on autophagy induction, antioxidation, and dual-function are also discussed.

1. Introduction

Reactive oxygen species (ROS) are generally small, short-lived, and highly reactive molecules that are formed by incomplete one-electron reduction of oxygen. ROS are generated by multiple cellular organelles, including mitochondria, peroxisomes, and endoplasmic reticulum [1–3]. ROS can also be produced in Fenton and Haber-Weiss reactions, thymidine catabolism, and polyamine catabolism. Mitochondria are the major source of ROS generation, as a by-product of respiration [4].

Under pathological conditions, dysfunctional mitochondria produced excessive ROS, breaking cellular homeostasis. The process of removal of damaged mitochondria through autophagy is called mitophagy, which is thus critical for maintaining cellular functions [5, 6]. Autophagy and mitophagy are important cellular processes that are responsible for removing excessive ROS and damaged organelles. Cells have also developed various antioxidant and detoxifying mechanisms. So far, there are over 20 redox-sensitive transcription factors, found in human cells [7–9]. In addition,

ROS have been identified as a signal molecule in various pathways regulating cell survival and cell death [10, 11].

In response to oxidative stress, autophagy is found to contribute to antioxidant function [12, 13]. Recent studies have shown that ROS play a crucial role in autophagy initiation [14]. On the one hand, stimulating factors such as starvation, pathogens, or death receptors initiate autophagy via ROS [15]. On the other hand, oxidized biomaterials such as damaged mitochondria are targeted by autophagy for lysosomal degradation [6, 16]. Hence, ROS and autophagy constitute a negative feedback mechanism that mitigates oxidative stress and promotes cell survival [17]. However, single treatment with antioxidant or autophagy activator has defects on treating diseases with autophagy dysfunction and antioxidative stress. Studies have been conducted to investigate dual-target treatments that can regulate both antioxidant pathways and autophagy [18].

The purpose of this review is to summarize the molecular mechanisms of ROS signals, autophagy, and redox regulation in health and disease. Furthermore, dual-target phytochemicals

based on autophagy and antioxidant regulation are exemplified and discussed.

2. ROS and Oxidative Stress

ROS are single-electron reduction products of oxygen that include superoxide anion (O_2^-), hydrogen peroxide (H_2O_2), and hydroxyl radical ($HO^\bullet$), but also diverse peroxides, such as lipid peroxides, peroxides of proteins, and nucleic acids [4, 19, 20]. ROS attack amino acid residues of proteins, specifically Tyr, Phe, Trp, Met, and Cys, to form carbonyl derivatives and promote intra- and intermolecular crosslinking through the formation of disulfide bonds. Superoxide generates hydroxyl free radicals, which initiate peroxidation of phospholipids [21]. The majority of ROS produced in mitochondria are dependent on the respiratory chain complexes I and III and a variety of enzymes [22]. Complex I (NADH-ubiquinone oxidoreductase, C-I), an integral inner membrane polyprotein complex, is considered to be the most significant source of ROS in mitochondria. But the exact site within the C-I is not clear [23]. Another pathway of ROS generation is the Q cycle in complex III, an enzyme complex of the oxidase coenzyme Q with cytochrome c as the electron acceptor [24]. Mitochondrial membrane potential, reflecting the functional status of the mitochondrion, is found to be highly related to ROS levels [25, 26].

Cells have developed an antioxidant system to remove the excessive ROS. When the balance between the formation of ROS and antioxidant defense is damaged, oxidative stress occurs [18]. Oxidative stress can be caused by the following: (i) The level of endogenous and exogenous oxidants entering the body is increased, (ii) The reserve of antioxidants is consumed, (iii) The antioxidant enzymes are inactive, (iv) the production of antioxidant enzymes is reduced, and (v) Certain combination of the above two or more factors affects. Of course, redox imbalance may affect many other physiological and pathological processes [27]. Oxidative stress causes DNA damage, lipid peroxidation, protein modification, and other effects [28]. Oxidative stress is associated with numerous chronic pathological processes, including diabetes, cardiovascular diseases, atherosclerosis, thalassemia, cancers, chronic kidney disease, and neurodegenerative diseases such as Alzheimer's disease (AD) and Parkinson's disease (PD) [28–30]. Natural antioxidants derived from plants and other living organisms have been widely discussed as potential drugs in diseases caused by redox imbalance [31].

3. ROS and Antioxidant Pathways

Antioxidant defense is an important part for organisms to adapt to environmental stresses. Cells have developed different antioxidant responses to maintain redox homeostasis including endogenous antioxidant and redox-dependent transcriptional regulation pathways.

Antioxidant molecules are nucleophilic and react with oxidants, which are generally electrophiles. Glutathione (GSH), a ubiquitous low molecular weight thiol, is considered the most abundant endogenous antioxidant molecule [32]. GSH is a reduced peptide consisting of three-residues

(γ-l-glutamyl-l-cysteinyl glycine), which can donate an electron to form oxidized GSSG. Alterations in the ratio of the redox pair 2GSH/GSSG towards a more oxidized status form the biochemical basis of targeting redox-sensitive cysteine residues in proteins. As an antioxidant, GSH removes ROS directly or indirectly and limits the lifetime of the oxidative signal [33]. GSH is also a substrate of several antioxidant enzymes. The indirect ROS-scavenging functions of GSH by revitalizing other antioxidant enzymes are also very important [34].

Multiple ROS sensors and pathways are triggered to converge in the regulation of transcription factors. So far, more than 20 redox-sensitive transcription factors have been reported [9, 35, 36]. These transcriptional factors induce the expression of multiple genes that are required for the detoxification and for the repair and maintenance of cellular homeostasis. In this review, we will discuss two well-studied ROS-sensitive transcriptional factors in detail as follows.

3.1. Nrf2 Pathway. Nuclear factor E2-related factor 2 (Nrf2), a redox-sensitive transcription factor, regulates multiple antioxidant gene expression and plays a crucial role in antioxidant pathways. Kelch-like ECH-associated protein 1 (Keap1) is the main regulator of Nrf2 [37]. Under normal conditions, Nrf2 binds to Keap1 and stays in the cytosol. Keap1 homodimer and cullin 3 (CUL3) combine to form a Keap1-CUL3 ubiquitin ligase complex, which catalyzes the polyubiquitination of Nrf2 to induce its degradation [38]. Under stress conditions, such as exposure to ROS, Nrf2 dissociates from Keap1 and transfers into the nucleus [9, 39]. Nrf2 then binds to the antioxidant response element (ARE) and increases the expression of downstream cytoprotective genes [40]. The Keap1/Nrf2/ARE system is the most crucial cytoprotective defense to oxidative stress (Figure 1) [41, 42].

3.2. FoxO Pathway. FoxOs are divergent members of the Fox/winged-helix transcription factor superfamily [43], which has various biological functions, including stopping the cell cycle at the G1-S and G2-M checkpoints, reduction of ROS, and repairing damaged DNA and apoptosis [7]. FoxO family members usually exist in the cytoplasm in an inactive form. Once activated, it will transfer to the nucleus to initiate transcriptional activity (Figure 1). FoxOs, composed of FoxO 1, 3, 4, and 6, coordinate gene expressions in cellular processes such as apoptosis and oxidative stress. For example, as a target of class III histone/protein deacetylase sirtuin 1 (SIRT1), FoxO1 forms a complex with SIRT1 under oxidative stress, resulting in activation of cell cycle arrest/anti-stress-related genes, thereby promoting cellular survival [44]. Several studies have shown that FoxOs and p53 have overlapping functions in cell cycle regulation and tumor suppression [45, 46]. In addition, p53 can directly target the FoxO3a gene, leading to an increase in FoxO3a in the nucleus, which causes apoptosis. FoxOs induce the expression of a number of autophagy-related genes (such as *Atg4*, *Atg7*, and *Atg14*), suggesting its role in autophagy regulation [47]. These evidences reveal that the FoxO-autophagy axis plays a crucial role in health and disease [48, 49].
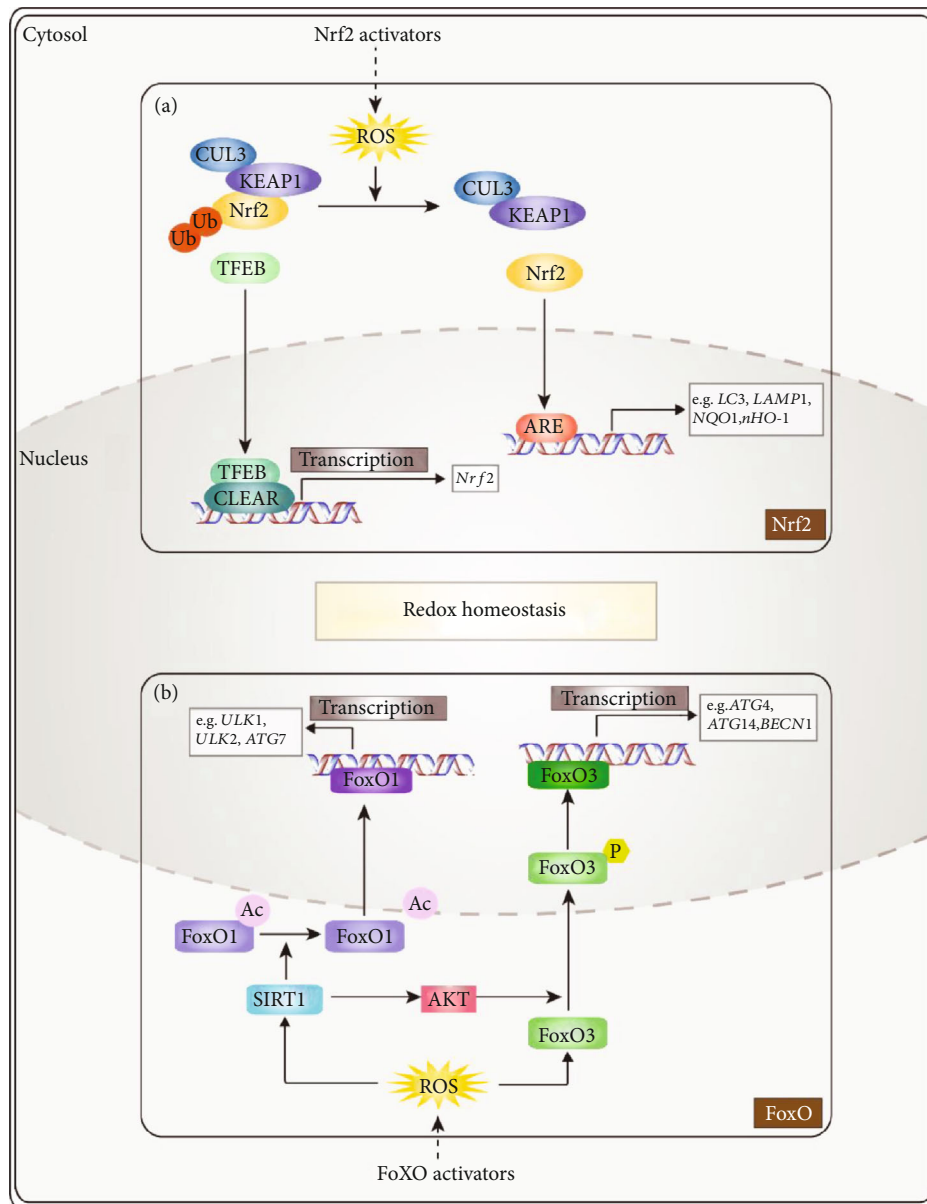
FIGURE 1: Schematic representation of redox-sensitive transcription factor-related antioxidant pathways. (a) Nrf2 pathway: when cells are exposed to ROS, Nrf2 dissociates from Keap1 and transfers into the nucleus, binding to ARE and regulating transcriptions of various antioxidant and lysosomal and autophagic genes [42]. Nrf2 activators, i.e., sulforaphane, show their protective effect against oxidative stress based on the Nrf2 signaling cascade [72]. (b) FoxO pathway: once activated by ROS, FoxO (mainly FoxO1 and FoxO3) transfers to the nucleus to initiate transcriptional activity [48]. Under oxidative stress, FoxO1 forms a complex with SIRT1 and deacetylates, resulting in preferential activation of autophagic and lysosomal genes [124]. Meanwhile, AKT, regulated by SIRT1, can phosphorylate FoxO3 proteins, thereby promoting the transcriptional activity of antioxidant-related genes. Resveratrol, gossypol acetic acid, etc., as FoxO activators, are reported to prevent chronic diseases by preventing oxidative stress and upregulate level of autophagy [125, 126].

3.3. The Effects of Single Antioxidant Treatment. Antioxidants including beta- carotene, lycopene, quercetin, resveratrol, and vitamin C have shown preventive effects in various diseases. However, poor biopharmaceutical properties and variable pharmacokinetics limit their application as therapeutic agents. For example, N-acetylcysteine (NAC), a powerful antioxidant that impacts GSH levels via cysteine, is approved by FDA [50, 51]. NAC is the precursor of GSH synthesis, which can scavenge free radicals and increase the content of GSH. Administration of NAC has shown protec-tive effects against oxidative stress [52, 53]. However, the clinical effect of NAC is controversial [54, 55]. NAC's antioxidant effect lies in its ability to restore the cytosolic level of GSH, which is transported to mitochondria to exert its detoxification function. One example is the effect of NAC on Niemann-Pick disease type C (NPC). Reduced GSH levels have been detected in the liver of NPC mice with NAC treatment; however, the transport of GSH is delayed in NPC mouse hepatocytes [56, 57]. Thus, NAC is not effective in NPC treatment, although GSH increase in the cytoplasm.
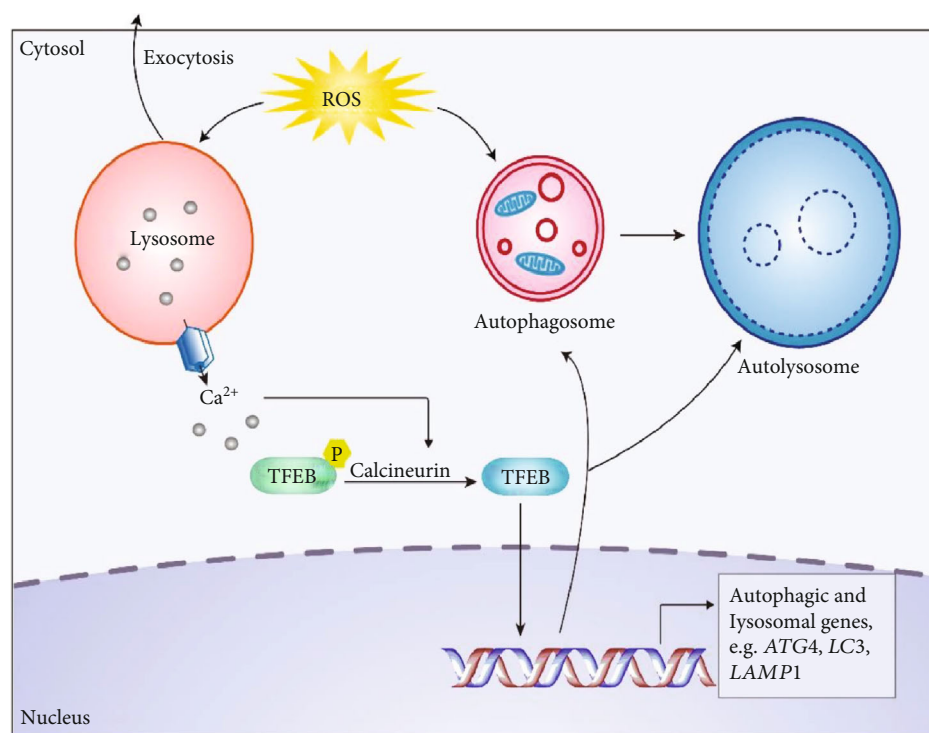
FIGURE 2: ROS regulates TFEB-dependent autophagy promotion. Lysosomes are activated by mitochondrial ROS, followed by lysosomal Ca^{2+} release and calcineurin activation. Calcineurin bound to Ca^{2+} dephosphorylates TFEB. Then, nuclear-localized TFEB causes the transcription of a series of genes, including autophagy induction, autophagosome biogenesis, lysosomal biogenesis, and autolysosome biogenesis [60, 69]. Autophagy is enhanced to promote the removal of damaged mitochondria and excess ROS [127]. Among them, a low level of oxidative stress will stimulate lysosomal exocytosis, but at a high level, it will inhibit lysosomal exocytosis [128].

The transport of GSH to mitochondria is still defective. So far, single antioxidant treatment is not efficient, and more therapeutic approaches need to be explored.

4. ROS and Autophagy

Autophagy is a cellular self-eating phenomenon. It degrades and digests damaged, denatured, senescent, and loss-function cells, organelles, proteins, nucleic acids, and other biological macromolecules and participates in various processes such as biological development and growth. Autophagy is regulated by ROS and redox signaling including oxidized macromolecules and organelles, and mild oxidative stress [58]. Activated autophagy then removes damaged organelles and excessive ROS [59, 60]. ROS can oxidize cysteine residues of autophagy-associated proteins and modify their functions, facilitating the formation of the autophagosome [61] such as cysteine protease Atg4 [12].

ROS increase in the mitochondrial matrix can lead to mitochondrial damage and depolarization. The depolarized mitochondria are then fragmented, and PARK2 (mitochondrial E3 ubiquitin ligase) is recruited, leading to ubiquitination of damaged mitochondria [62], which are then phagocytosed by LC3-positive autophagosomes and directed to lysosomes for degradation [63]. This process is called mitophagy. Under starvation, mitophagy is triggered by mitochondrial ROS to remove damaged mitochondria and other organelles [14]. In turn, damaged mitochondria will produce more ROS. Mitochondrial dysfunction has been

considered as a key factor in neurodegenerative diseases, which contains a high level of ROS in the brain [64]. Thus, autophagy promotion has been considered as a potential treatment for neurodegenerative diseases.

4.1. TFEB as a Drug Target. Transcription factor EB (TFEB), a master regulator of the autophagic and lysosomal biogenesis, acts as a critical mediator of the cellular response to stress (Figure 2) [65, 66]. TFEB binds to the "coordinated lysosomal expression and regulation (CLEAR)" element located in the promoter region of many lysosomal and autophagic genes [67]. TFEB is responsive to multiple types of intracellular stress including mitochondrial damage and oxidative stress [68]. Increased ROS levels can lead to activation of transient receptor potential mucolipin 1 and lysosomal calcium release, which induces nuclear translocation of TFEB and then promotes autophagic and lysosomal biogenesis [69]. TFEB activity is controlled by its phosphorylation status. In nutrient-rich conditions, TFEB is phosphorylated and retained in the cytoplasm. Upon starvation, TFEB is dephosphorylated and translocated from the cytoplasm to the nucleus, regulating the expression of target genes [70]. According to its important role in promoting autophagy and lysosome, TFEB has become an important therapeutic target for diseases involving excess ROS and autophagy dysfunction, such as AD, PD, and atherosclerosis (see Figure 2 for details about TFEB and autophagy). Recently, several TFEB agonists have been identified and preclinical or clinical trials are applied [71, 72].
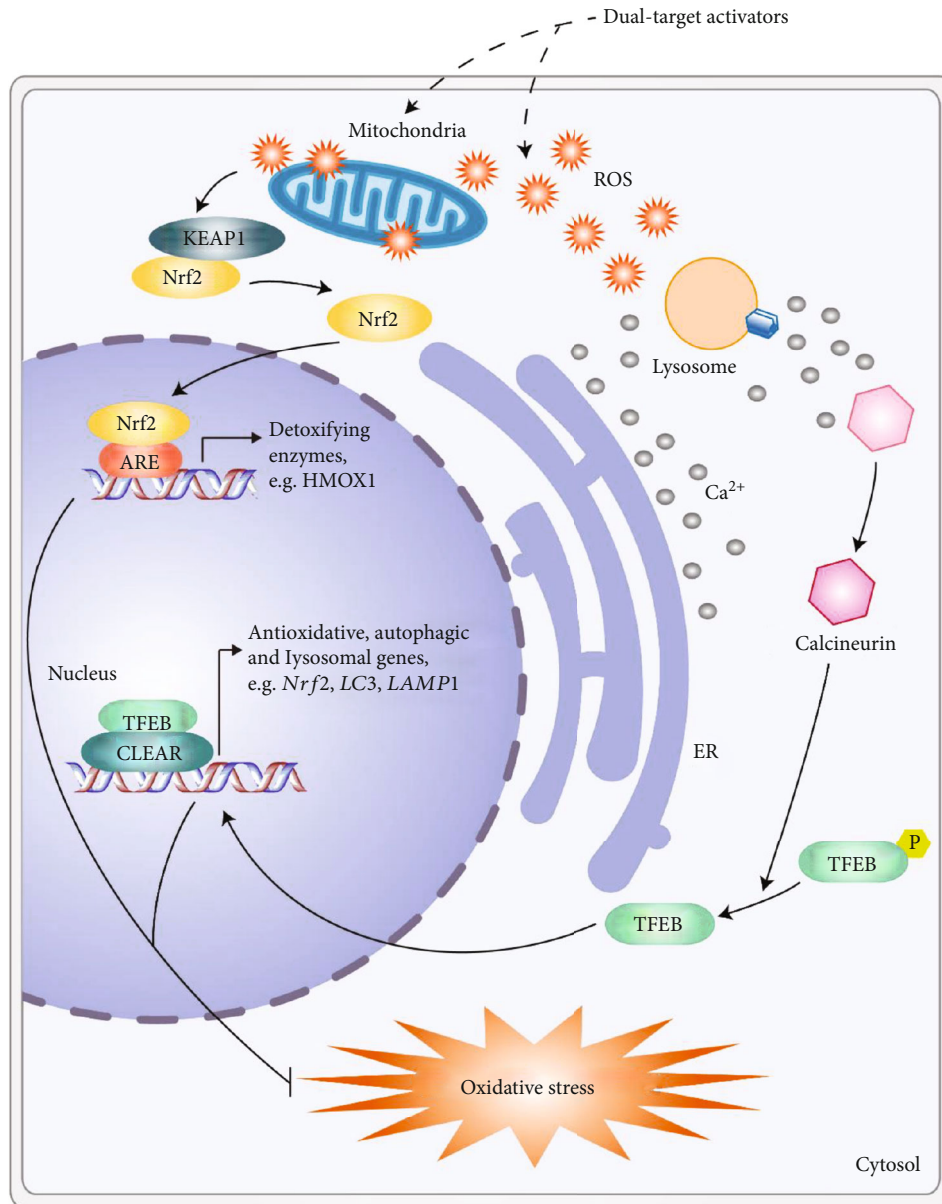
FIGURE 3: Dual-activating (antioxidant and autophagy) pathways. Dual-target activators such as sulforaphane induce a low level of ROS to activate the Nrf2-dependent antioxidant pathway and TFEB-dependent lysosomal biogenesis and autophagy, thereby helping to remove excess ROS [72]. A working model to illustrate the role of Nrf2/TFEB in sulforaphane-mediated enhancement of autophagic and lysosomal function. Sulforaphane (for example, through mitochondria and other sources) stimulates low level of ROS, which activates the Nrf2 pathway and the release of Ca^{2+}. Ca^{2+}-bound calcineurin dephosphorylates TFEB, causing TFEB nuclear translocation [129]. Nuclear Nrf2/TFEB then promotes the transcription of a unique set of genes related to detoxifying enzymes, autophagy induction, and autophagic and lysosomal biogenesis [130]. Subsequently, the cells are promoted to remove damaged mitochondria and excess ROS (the figure is adapted from Li et al. [72]).

4.2. The Effects of Autophagy Activators. Mammalian target of rapamycin (mTOR), a critical nutrient sensor, can regulate TFEB [73]. Under nutrient-rich conditions, mTOR phosphorylates TFEB on serine residues of S142 and S211 and phosphorylated TFEB is retained in the cytosol [74]. Upon starvation, mTOR is inhibited and TFEB is activated and translocated into the nucleus [75]. Torin1, 3,4-dimethoxychalcone, fisetin, and rapamycin are mTOR inhibitors [76–79].

Rapamycin has been shown to upregulate autophagy in cell models, fruit fly models, and mouse models of neurodegenerative diseases, respectively [80–83]. In the model of Huntington's disease (HD), rapamycin treatment can simultaneously reduce the soluble mutant huntingtin and the aggregation products of the protein, thereby protecting the cells from damage. A similar situation also appears in the PD model [83]. However, in early trials, high-dose treatment of rapamycin causes frequent side effects including slow

TABLE 1: Summary of phytochemicals related to ROS scavenging.

Phytochemicals	Sources	Main properties
Sulforaphane	Cruciferous plants such as broccoli [72]	Induce the expression of genes required for lysosomal biogenesis, promote autophagic flux, and induce TFEB nuclear translocation [72]
Flavonoids	Citrus [95], rutin, and so on	Antioxidant, suppression of carcinogenesis [94], and anti-inflammation [95]
Isoflavones	Legumes from the family *Fabaceae* [102], namely, soybean	Antioxidant, induction of autophagy, antitumor effect [103], and anti-inflammation [123]
Resveratrol	Red grape skins, peas, and so on	Antiaging [109], anticancer [106], anti-inflammation, and prevention of cardiovascular diseases
Curcumin	Rhizomes of some plants such as *Zingiberaceae*	Anticancer, anti-inflammatory, and antioxidant [118]

wound healing and hyperlipidemia [84]. In addition, high-dose or long-term use of rapamycin in patients causes severe infection, hemolytic uremic syndrome, cancer, leukopenia, bone atrophy, and even noninfectious interstitial pneumonia [85].

Lithium can negatively regulate the activity of GSK-3β, leading to the stimulation of mTOR kinase and the inhibition of autophagy. Recently, the combined use of lithium and rapamycin is found to be much more effective than rapamycin alone [86]. In addition, due to the limited absorption of rapamycin, its derivatives have been developed such as temsirolimus, everolimus, and lidformolimus [87, 88].

5. ROS as a Link to Connect Autophagy and Antioxidant Pathways

Many diseases such as NPC are associated with both oxidative stress and autophagy dysfunction. So far, none of single therapy against one target is shown to be effective. Thus, the dual-target therapeutic drugs will shed new light on the future directions. A number of natural compounds are identified to reduce oxidative stress and promote autophagy. Moreover, preclinical and clinical studies have shown that natural compounds, such as resveratrol, have therapeutic potential in several diseases including diabetes, aging, neuropathy, cardiovascular diseases, and cancer [89].

Sulforaphane, an Nrf2 activator enriched in cruciferous vegetables, has several biological activities such as reduction of oxidative stress and inflammation in several diseases including AD, sclerosis, and traumatic brain injury [90–93]. Recently, we found that sulforaphane is also a TFEB agonist [72]. Sulforaphane activates TFEB via stimulating low level of ROS, then inducing the expression of genes required for lysosomal biogenesis, autophagosome formation, and detoxification. A genetic interaction between Nrf2 and TFEB is also identified. Altogether, sulforaphane is a dual-target candidate for diseases with excessive ROS and autophagy dysfunction (Figure 3). Other phytochemicals with dual-target therapeutic effects are also summarized as follows (Table 1).

Flavonoids, a family of natural products enriched in fruits, have biological activities including anticancer, antiproliferation, antioxidant, and anti-inflammation via regulation of the cell cycle, induction of apoptosis, and inhibition of extracellular protein kinase phosphorylation [94]. Flavonoids have therapeutic effects on several diseases such as diabetes,

cancer, and cardiovascular diseases [95]. Kaempferol, a flavonoid, induces autophagic cell death in gastric cancer cells through epigenetic changes [96]. Quercetin provides neuroprotection by stimulating Nrf2-ARE antioxidant defenses and inducing autophagy induced via SIRT1 [97]. Modifications of flavonoids, such as hydroxylation, glycosylation, methylation, and acylation, have been shown to improve their biological activity [98–101].

Isoflavones are a variety of secondary metabolites mainly distributed in legumes [102]. They regulate the expression of antioxidant proteins and induce autophagy, thus eliminating the damaged or dysfunctional organellesand playing a cytoprotective role in maintaining cell homeostasis. Genistein, a soy-derived isoflavonoid with antitumor activity, involves the regulation of antioxidant enzymes and the expression of apoptotic signals, leading to the progression of cell apoptosis and autophagy [103].

Resveratrol, a ROS scavenger extracted from red grape skins and peas [104, 105], has many activities including antiaging and anticancer [106–110]. Studies have shown that resveratrol activates SIRT1, which may rely on the upstream of calmodulin kinase II to activate the AMPK-dependent increase in the ratio of NAD/NADH, thereby inducing SIRT1 activity. Resveratrol can promote p53 deacetylation and downregulate Akt phosphorylation, then increasing SIRT1 expression [111, 112]. Resveratrol inhibitscancer cell growth through autophagic initiation. Resveratrol also increases the chemotherapeutic efficiency of gemcitabine via Nrf2 signaling [113]. In addition, the anticancer activity of resveratrol is related to the activation of FoxOs. Resveratrol inhibits PI3K/Akt phosphorylation, resulting in a decrease in FoxO3 phosphorylation and an increase in FoxO3 nuclear transport, DNA binding affinity, and transcriptional activity [114]. In clinical trials, resveratrol can alleviate clinical parameters of cardiovascular diseases [115–117].

Curcumin, a major active component of turmeric (Curcuma longa, L.), has anticancer, anti-inflammatory, and antioxidant effects and has been applied to cancer, atherosclerosis, and neurodegenerative diseases [118–120]. Low dose of curcumin induces adaptive oxidative stress responses, while high dose of curcumin induces acute responses such as autophagy and mitochondrial destabilization [121]. This phenomenon is often referred to as hormesis. However, curcumin has poor bioavailability. Curcumin analogs, such as the neoketene curcumin, have stronger

clearance capabilities and become potential drugs under different pathological conditions [122].

6. Conclusions

Excessive ROS have been implicated in many diseases including cancer, neurodegenerative diseases and aging. Low/mild levels of ROS have been identified as important cellular signals, which can induce autophagy and antioxidant pathways under both physiological and pathological conditions. Increasing evidence suggests that there may be an important link ROS, antioxidant pathways, and autophagy. The detailed molecular mechanism underlying this linkage remains elusive. Antioxidants or autophagy activator alone is not ideal treatment for diseases characterized by both oxidative stress and autophagy dysfunction. Natural compounds with dual targeting of antioxidant and autophagy such as sulforaphane could be the potential therapeutic drug and direction for future research.

Abbreviations

AD: Alzheimer's disease
ARE: Antioxidant response element
C-I: Complex I
CLEAR: Coordinated lysosomal expression and regulation
CUL3:   Cullin 3
FoxO: Forkhead box, subgroup O
GSH: Glutathione
HD: Huntington's disease
IKK: IκB kinase
Keap1:   Kelch-like ECH-associated protein 1
mTOR: Mammalian target of rapamycin
NAC: N-Acetylcysteine
NPC: Niemann-Pick disease type C
Nrf2:   Nuclear factor E2-related factor 2
PD: Parkinson's disease
ROS: Reactive oxygen species
SIRT1:   Sirtuin 1
TFEB: Transcription factor EB.

Data Availability

Not applicable-no new data generated in this study.

Conflicts of Interest

The authors declare that they have no conflicts of interest.

Acknowledgments

References

[1] T. Fukai and M. Ushio-Fukai, "Cross-talk between NADPH oxidase and mitochondria: role in ROS signaling and angiogenesis," *Cell*, vol. 9, no. 8, 2020.

[2] A. V. Snezhkina, A. V. Kudryavtseva, O. L. Kardymon et al., "ROS generation and antioxidant defense systems in normal and malignant cells," *Oxidative Medicine and Cellular Longevity*, vol. 2019, Article ID 6175804, 17 pages, 2019.

[3] E. Dubois-Deruy, V. Peugnet, A. Turkieh, and F. Pinet, "Oxidative stress in cardiovascular diseases," *Antioxidants*, vol. 9, no. 9, p. 864, 2020.

[4] Y. R. Chen and J. L. Zweier, "Cardiac mitochondria and reactive oxygen species generation," *Circulation Research*, vol. 114, no. 3, pp. 524–537, 2014.

[5] J. M. Bravo-San Pedro, "Autophagy and mitophagy in cardiovascular disease," *Circulation Research*, vol. 120, no. 11, pp. 1812–1824, 2017.

[6] N. D. Georgakopoulos, G. Wells, and M. Campanella, "The pharmacological regulation of cellular mitophagy," *Nature Chemical Biology*, vol. 13, no. 2, pp. 136–146, 2017.

[7] A. Brunet, L. B. Sweeney, J. F. Sturgill et al., "Stress-dependent regulation of FOXO transcription factors by the SIRT1 deacetylase," *Science*, vol. 303, no. 5666, pp. 2011–2015, 2004.

[8] L. M. Williams and T. D. Gilmore, "Looking down on NF-κB," *Molecular and Cellular Biology*, vol. 40, no. 15, 2020.

[9] I. Bellezza, I. Giambanco, A. Minelli, and R. Donato, "Nrf2-Keap1 signaling in oxidative and reductive stress," *Biochimica et Biophysica Acta (BBA) - Molecular Cell Research*, vol. 1865, no. 5, pp. 721–733, 2018.

[10] G. Pizzino, N. Irrera, M. Cucinotta et al., "Oxidative stress: harms and benefits for human health," *Oxidative Medicine and Cellular Longevity*, vol. 2017, Article ID 8416763, 13 pages, 2017.

[11] L. Zhang, K. Wang, Y. Lei, Q. Li, E. C. Nice, and C. Huang, "Redox signaling: potential arbitrator of autophagy and apoptosis in therapeutic response," *Free Radical Biology & Medicine*, vol. 89, pp. 452–465, 2015.

[12] R. Scherz-Shouval, E. Shvets, E. Fass, H. Shorer, L. Gil, and Z. Elazar, "Reactive oxygen species are essential for autophagy and specifically regulate the activity of Atg4," *The EMBO Journal*, vol. 26, no. 7, pp. 1749–1760, 2007.

[13] R. Scherz-Shouval and Z. Elazar, "Regulation of autophagy by ROS: physiology and pathology," *Trends in Biochemical Sciences*, vol. 36, no. 1, pp. 30–38, 2011.

[14] J. Dan Dunn, L. A. J. Alvarez, X. Zhang, and T. Soldati, "Reactive oxygen species and mitochondria: a nexus of cellular homeostasis," *Redox Biology*, vol. 6, pp. 472–485, 2015.

[15] S. W. Zhang, F. E. Jiang-Nan, C. A. Yi, M. E. Li-Ping, and W. A. Shu-Lin, "Autophagy prevents autophagic cell death in Tetrahymena in response to oxidative stress," *Zoological Research*, vol. 36, no. 3, pp. 167–173, 2015.

[16] B. L. Baechler, D. Bloemberg, and J. Quadrilatero, "Mitophagy regulates mitochondrial network signaling, oxidative stress, and apoptosis during myoblast differentiation," *Autophagy*, vol. 15, no. 9, pp. 1606–1619, 2019.

[17] Q. F. Qin, X. J. Li, Y. S. Li et al., "AMPK-ERK/CARM1 signaling pathways affect autophagy of hepatic cells in samples of liver cancer patients," *Frontiers in Oncology*, vol. 9, p. 1247, 2019.

[18] C. Cabello-Verrugio, M. Ruiz-Ortega, M. Mosqueira, and F. Simon, "Oxidative stress in disease and aging: mechanisms and therapies 2016," *Oxidative Medicine and Cellular Longevity*, vol. 2017, Article ID 4310469, 2 pages, 2017.

[19] A. Bose and M. F. Beal, "Mitochondrial dysfunction and oxidative stress in induced pluripotent stem cell models of

Parkinson's disease," *European Journal of Neuroscience*, vol. 49, no. 4, pp. 525–532, 2019.

[20] B. D'Autréaux and M. B. Toledano, "ROS as signalling molecules: mechanisms that generate specificity in ROS homeostasis," *Nature Reviews. Molecular Cell Biology*, vol. 8, no. 10, pp. 813–824, 2007.

[21] A. Ahmad and H. Ahsan, "Biomarkers of inflammation and oxidative stress in ophthalmic disorders," *Journal of Immunoassay & Immunochemistry*, vol. 41, no. 3, pp. 257–271, 2020.

[22] G. S. Shadel and T. L. Horvath, "Mitochondrial ROS signaling in organismal homeostasis," *Cell*, vol. 163, no. 3, pp. 560–569, 2015.

[23] J. Wu, X. Luo, N. Thangthaeng et al., "Pancreatic mitochondrial complex I exhibits aberrant hyperactivity in diabetes," *Biochemistry and biophysics reports*, vol. 11, pp. 119–129, 2017.

[24] M. Rigoulet, E. D. Yoboue, and A. Devin, "Mitochondrial ROS generation and its regulation mechanisms involved in H2O2 signaling," *Antioxidants & redox signaling*, vol. 14, pp. 459–468, 2011.

[25] D. V. Pyatrikas, I. V. Fedoseeva, N. N. Varakina et al., "Relation between cell death progression, reactive oxygen species production and mitochondrial membrane potential in fermenting Saccharomyces cerevisiae cells under heat-shock conditions," *FEMS Microbiology Letters*, vol. 362, no. 12, 2015.

[26] I. V. Fedoseeva, D. V. Pyatrikas, A. V. Stepanov et al., "The role of flavin-containing enzymes in mitochondrial membrane hyperpolarization and ROS production in respiring *Saccharomyces cerevisiae* cells under heat-shock conditions," *Scientific Reports*, vol. 7, no. 1, p. 2586, 2017.

[27] V. I. Lushchak, "Free radicals, reactive oxygen species, oxidative stress and its classification," *Chemico-Biological Interactions*, vol. 224, pp. 164–175, 2014.

[28] I. Liguori, G. Russo, F. Curcio et al., "Oxidative stress, aging, and diseases," *Clinical Interventions in Aging*, vol. Volume 13, pp. 757–772, 2018.

[29] E. Fibach and M. Dana, "Oxidative stress in β-Thalassemia," *Molecular Diagnosis & Therapy*, vol. 23, no. 2, pp. 245–261, 2019.

[30] K. Jomova and M. Valko, "Advances in metal-induced oxidative stress and human disease," *Toxicology*, vol. 283, no. 2-3, pp. 65–87, 2011.

[31] F. Pohl and P. Kong Thoo Lin, "The potential use of plant natural products and plant extracts with antioxidant properties for the prevention/treatment of neurodegenerative diseases: in vitro, in vivo and clinical trials," *Molecules*, vol. 23, no. 12, 2018.

[32] C. Hwang, A. J. Sinskey, and H. F. Lodish, "Oxidized redox state of glutathione in the endoplasmic reticulum," *Science*, vol. 257, no. 5076, pp. 1496–1502, 1992.

[33] L. Cao, G. Wu, J. Zhu et al., "Genotoxic stress-triggered β-catenin/JDP2/PRMT5 complex facilitates reestablishing glutathione homeostasis," *Nature Communications*, vol. 10, no. 1, p. 3761, 2019.

[34] P. Diaz-Vivancos, A. de Simone, G. Kiddle, and C. H. Foyer, "Glutathione - linking cell proliferation to oxidative stress," *Free Radical Biology & Medicine*, vol. 89, pp. 1154–1164, 2015.

[35] S. Le Rossignol, N. Ketheesan, and N. Haleagrahara, "Redox-sensitive transcription factors play a significant role in the development of rheumatoid arthritis," *International Reviews of Immunology*, vol. 37, no. 3, pp. 129–143, 2018.

[36] Y. M. Lim, Y. Yagi, and L. Tsuda, "Cellular defense and sensory cell survival require distinct functions of ebi in Drosophila," *PLoS One*, vol. 10, no. 11, article e0141457, 2015.

[37] D. Pu, Y. Zhao, J. Chen et al., "Protective effects of sulforaphane on cognitive impairments and AD-like lesions in diabetic mice are associated with the upregulation of Nrf2 transcription activity," *Neuroscience*, vol. 381, pp. 35–45, 2018.

[38] T. Suzuki and M. Yamamoto, "Stress-sensing mechanisms and the physiological roles of the Keap1-Nrf2 system during cellular stress," *The Journal of Biological Chemistry*, vol. 292, no. 41, pp. 16817–16824, 2017.

[39] J. Zhang, X. Wang, V. Vikash et al., "ROS and ROS-mediated cellular signaling," *Oxidative Medicine and Cellular Longevity*, vol. 2016, Article ID 4350965, 18 pages, 2016.

[40] R. Santín-Márquez, A. Alarcón-Aguilar, N. E. López-Diazguerrero, N. Chondrogianni, and M. Königsberg, "Sulforaphane - role in aging and neurodegeneration," *Geroscience*, vol. 41, no. 5, pp. 655–670, 2019.

[41] T. I. Adelusi, L. du, M. Hao et al., "Keap1/Nrf2/ARE signaling unfolds therapeutic targets for redox imbalanced- mediated diseases and diabetic nephropathy," *Biomedicine & Pharmacotherapy*, vol. 123, p. 109732, 2020.

[42] P. Shaw and A. Chattopadhyay, "Nrf2–ARE signaling in cellular protection: mechanism of action and the regulatory mechanisms," *Journal of Cellular Physiology*, vol. 235, no. 4, pp. 3119–3130, 2020.

[43] J. Ma, S. Matkar, X. He, and X. Hua, "FOXO family in regulating cancer and metabolism," *Seminars in Cancer Biology*, vol. 50, pp. 32–41, 2018.

[44] C. Rohrl and H. Stangl, "Cholesterol metabolism-physiological regulation and pathophysiological deregulation by the endoplasmic reticulum," *Wiener Medizinische Wochenschrift (1946)*, vol. 168, no. 11-12, pp. 280–285, 2018.

[45] L. A. Donehower, M. Harvey, B. L. Slagle et al., "Mice deficient for p53 are developmentally normal but susceptible to spontaneous tumours," *Nature*, vol. 356, no. 6366, pp. 215–221, 1992.

[46] T. Jacks, L. Remington, B. O. Williams et al., "Tumor spectrum analysis in p53-mutant mice," *Current Biology*, vol. 4, no. 1, pp. 1–7, 1994.

[47] Z. Cheng, "The FoxO-autophagy axis in health and disease," *Trends in Endocrinology and Metabolism*, vol. 30, no. 9, pp. 658–671, 2019.

[48] A. K. Brown and A. E. Webb, "Regulation of FOXO factors in mammalian cells," *Current Topics in Developmental Biology*, vol. 127, pp. 165–192, 2018.

[49] G. Milan, V. Romanello, F. Pescatore et al., "Regulation of autophagy and the ubiquitin-proteasome system by the FoxO transcriptional network during muscle atrophy," *Nature Communications*, vol. 6, no. 1, p. 6670, 2015.

[50] G. Tardiolo, P. Bramanti, and E. Mazzon, "Overview on the effects of N-acetylcysteine in neurodegenerative diseases," *Molecules*, vol. 23, no. 12, 2018.

[51] Y. Pei, H. Liu, Y. Yang et al., "Biological activities and potential oral applications of N-acetylcysteine: progress and prospects," *Oxidative Medicine and Cellular Longevity*, vol. 2018, Article ID 2835787, 14 pages, 2018.

[52] G. F. Rushworth and I. L. Megson, "Existing and potential therapeutic uses for N-acetylcysteine: the need for conversion

to intracellular glutathione for antioxidant benefits," *Pharmacology & Therapeutics*, vol. 141, no. 2, pp. 150–159, 2014.

[53] G. Aldini, A. Altomare, G. Baron et al., "N-Acetylcysteine as an antioxidant and disulphide breaking agent: the reasons why," *Free Radical Research*, vol. 52, no. 7, pp. 751–762, 2018.

[54] F. Roubille and A. Lacampagne, "New drug avenues for cardioprotection in patients with acute myocardial infarction," *American Journal of Cardiovascular Drugs*, vol. 14, no. 1, pp. 73–77, 2014.

[55] S. Kostić, Ž. Mićovic, L. Andrejević et al., "The effects of L-cysteine and N-acetyl-L-cysteine on homocysteine metabolism and haemostatic markers, and on cardiac and aortic histology in subchronically methionine-treated Wistar male rats," *Molecular and Cellular Biochemistry*, vol. 451, no. 1-2, pp. 43–54, 2019.

[56] M. Marí, F. Caballero, A. Colell et al., "Mitochondrial free cholesterol loading sensitizes to TNF- and Fas-mediated steatohepatitis," *Cell Metabolism*, vol. 4, no. 3, pp. 185–198, 2006.

[57] S. Torres, N. Matías, A. Baulies et al., "Mitochondrial GSH replenishment as a potential therapeutic approach for Niemann Pick type C disease," *Redox Biology*, vol. 11, pp. 60–72, 2017.

[58] G. Filomeni, D. De Zio, and F. Cecconi, "Oxidative stress and autophagy: the clash between damage and metabolic needs," *Cell Death and Differentiation*, vol. 22, no. 3, pp. 377–388, 2015.

[59] G. P. Kaushal, K. Chandrashekar, and L. A. Juncos, "Molecular interactions between reactive oxygen species and autophagy in kidney disease," *International Journal of Molecular Sciences*, vol. 20, no. 15, p. 3791, 2019.

[60] X. Zhang, L. Yu, and H. Xu, "Lysosome calcium in ROS regulation of autophagy," *Autophagy*, vol. 12, no. 10, pp. 1954-1955, 2016.

[61] K. Pant, A. Saraya, and S. K. Venugopal, "Oxidative stress plays a key role in butyrate-mediated autophagy via Akt/mTOR pathway in hepatoma cells," *Chemico-Biological Interactions*, vol. 273, pp. 99–106, 2017.

[62] Y. Wang, Y. Nartiss, B. Steipe, G. A. McQuibban, and P. K. Kim, "ROS-induced mitochondrial depolarization initiates PARK2/PARKIN-dependent mitochondrial degradation by autophagy," *Autophagy*, vol. 8, no. 10, pp. 1462–1476, 2012.

[63] S. M. Yoo and Y. K. Jung, "A molecular approach to mitophagy and mitochondrial dynamics," *Molecules and Cells*, vol. 41, no. 1, pp. 18–26, 2018.

[64] P. H. Reddy, "Misfolded proteins, mitochondrial dysfunction, and neurodegenerative diseases," *Biochimica et Biophysica Acta*, vol. 1842, no. 8, p. 1167, 2014.

[65] C. Pitcairn, W. Y. Wani, and J. R. Mazzulli, "Dysregulation of the autophagic-lysosomal pathway in Gaucher and Parkinson's disease," *Neurobiology of Disease*, vol. 122, pp. 72–82, 2019.

[66] N. Raben and R. Puertollano, "TFEB and TFE3: linking lysosomes to cellular adaptation to stress," *Annual Review of Cell and Developmental Biology*, vol. 32, no. 1, pp. 255–278, 2016.

[67] J. A. Martina and R. Puertollano, "Protein phosphatase 2A stimulates activation of TFEB and TFE3 transcription factors in response to oxidative stress," *The Journal of Biological Chemistry*, vol. 293, no. 32, pp. 12525–12534, 2018.

[68] J. A. Martina, H. I. Diab, O. A. Brady, and R. Puertollano, "TFEB and TFE3 are novel components of the integrated stress response," *The EMBO Journal*, vol. 35, no. 5, pp. 479–495, 2016.

[69] X. Zhang, X. Cheng, L. Yu et al., "MCOLN1 is a ROS sensor in lysosomes that regulates autophagy," *Nature Communications*, vol. 7, no. 1, p. 12109, 2016.

[70] R. David, "TFEB perfects multitasking," *Nature Reviews. Molecular Cell Biology*, vol. 12, no. 7, p. 404, 2011.

[71] C. Wang, H. Niederstrasser, P. M. Douglas et al., "Small-molecule TFEB pathway agonists that ameliorate metabolic syndrome in mice and extend C. elegans lifespan," *Nature communications*, vol. 8, no. 1, article 2270, 2017.

[72] D. Li, R. Shao, N. Wang et al., "Sulforaphane activates a lysosome-dependent transcriptional program to mitigate oxidative stress," *Autophagy*, vol. 17, pp. 872–887, 2020.

[73] S. Peña-Llopis, S. Vega-Rubin-de-Celis, J. C. Schwartz et al., "Regulation of TFEB and V-ATPases by mTORC1," *The EMBO Journal*, vol. 30, no. 16, pp. 3242–3258, 2011.

[74] G. Napolitano, A. Esposito, H. Choi et al., "mTOR-dependent phosphorylation controls TFEB nuclear export," *Nature Communications*, vol. 9, no. 1, 2018.

[75] G. Napolitano and A. Ballabio, "TFEB at a glance," *Journal of Cell Science*, vol. 129, no. 13, pp. 2475–2481, 2016.

[76] G. Chen, W. Xie, J. Nah et al., "3,4-Dimethoxychalcone induces autophagy through activation of the transcription factors TFE3 and TFEB," *EMBO Molecular Medicine*, vol. 11, no. 11, article e10469, 2019.

[77] S. Kim, K. J. Choi, S. J. Cho et al., "Fisetin stimulates autophagic degradation of phosphorylated tau via the activation of TFEB and Nrf2 transcription factors," *Scientific Reports*, vol. 6, no. 1, p. 24933, 2016.

[78] K. Abe, T. Yano, M. Tanno et al., "mTORC1 inhibition attenuates necroptosis through RIP1 inhibition-mediated TFEB activation," *Biochimica et Biophysica Acta - Molecular Basis of Disease*, vol. 1865, no. 12, p. 165552, 2019.

[79] S. Avniel-Polak, G. Leibowitz, Y. Riahi, B. Glaser, D. J. Gross, and S. Grozinsky-Glasberg, "Abrogation of autophagy by chloroquine alone or in combination with mTOR inhibitors induces apoptosis in neuroendocrine tumor cells," *Neuroendocrinology*, vol. 103, no. 6, pp. 724–737, 2016.

[80] Z. G. Xie, Y. Xie, and Q. R. Dong, "Inhibition of the mammalian target of rapamycin leads to autophagy activation and cell death of MG63 osteosarcoma cells," *Oncology Letters*, vol. 6, no. 5, pp. 1465–1469, 2013.

[81] A. Sotthibundhu, K. McDonagh, A. von Kriegsheim et al., "Rapamycin regulates autophagy and cell adhesion in induced pluripotent stem cells," *Stem Cell Research & Therapy*, vol. 7, no. 1, pp. 1–6, 2016.

[82] W. Zhou and S. Ye, "Rapamycin improves insulin resistance and hepatic steatosis in type 2 diabetes rats through activation of autophagy," *Cell Biology International*, vol. 42, no. 10, pp. 1282–1291, 2018.

[83] B. Ravikumar, C. Vacher, Z. Berger et al., "Inhibition of mTOR induces autophagy and reduces toxicity of polyglutamine expansions in fly and mouse models of Huntington disease," *Nature Genetics*, vol. 36, no. 6, pp. 585–595, 2004.

[84] G. K. C. O'Farrelly, "Taking the rap multiple effects of blocking mammalian target of rapamycin," *Hepatology*, vol. 57, no. 1, pp. 1–3, 2013.

[85] K. Pierzynowska, L. Gaffke, Z. Cyske et al., "Autophagy stimulation as a promising approach in treatment of neurodegenerative diseases," *Metabolic Brain Disease*, vol. 33, no. 4, pp. 989–1008, 2018.

[86] Y. Watanabe, K. Taguchi, and M. Tanaka, "Ubiquitin, autophagy and neurodegenerative diseases," *Cell*, vol. 9, no. 9, 2020.

[87] H. Park, J.-H. Kang, and S. Lee, "Autophagy in neurodegenerative diseases: a hunter for aggregates," *International Journal of Molecular Sciences*, vol. 21, no. 9, p. 3369, 2020.

[88] F. Guo, X. Liu, H. Cai, and W. le, "Autophagy in neurodegenerative diseases: pathogenesis and therapy," *Brain Pathology*, vol. 28, no. 1, pp. 3–13, 2018.

[89] S.-F. Zhang, X. L. Wang, X. Q. Yang, and N. Chen, "Autophagy-associated targeting pathways of natural products during cancer treatment," *Asian Pacific Journal of Cancer Prevention*, vol. 15, no. 24, pp. 10557–10563, 2015.

[90] T. Ma, D. Zhu, D. Chen et al., "Sulforaphane, a natural isothiocyanate compound, improves cardiac function and remodeling by inhibiting oxidative stress and inflammation in a rabbit model of chronic heart failure," *Medical Science Monitor*, vol. 24, pp. 1473–1483, 2018.

[91] D. Michaličková, T. Hrnčíř, N. K. Canová, and O. Slanař, "Targeting Keap1/Nrf2/ARE signaling pathway in multiple sclerosis," *European Journal of Pharmacology*, vol. 873, p. 172973, 2020.

[92] M. S. Uddin, A. A. Mamun, M. Jakaria et al., "Emerging promise of sulforaphane-mediated Nrf2 signaling cascade against neurological disorders," *Science of the Total Environment*, vol. 707, p. 135624, 2020.

[93] A. Vanduchova, P. Anzenbacher, and E. Anzenbacherova, "Isothiocyanate from broccoli, sulforaphane, and its properties," *Journal of Medicinal Food*, vol. 22, no. 2, pp. 121–126, 2019.

[94] E. Meiyanto, A. Hermawan, and A. Anindyajati, "Natural products for cancer-targeted therapy: citrus flavonoids as potent chemopreventive agents," *Asian Pacific Journal of Cancer Prevention*, vol. 13, no. 2, pp. 427–436, 2012.

[95] N. Braidy, S. Behzad, S. Habtemariam et al., "Neuroprotective effects of citrus fruit-derived flavonoids, nobiletin and tangeretin in Alzheimer's and Parkinson's disease," *CNS & Neurological Disorders Drug Targets*, vol. 16, no. 4, pp. 387–397, 2017.

[96] T. W. Kim, S. Y. Lee, M. Kim, C. Cheon, and S. G. Ko, "Kaempferol induces autophagic cell death via IRE1-JNK-CHOP pathway and inhibition of G9a in gastric cancer cells," *Cell Death & Disease*, vol. 9, no. 9, p. 875, 2018.

[97] L. G. Costa, J. M. Garrick, P. J. Roquè, and C. Pellacani, "Mechanisms of neuroprotection by quercetin: counteracting oxidative stress and more," *Oxidative Medicine and Cellular Longevity*, vol. 2016, Article ID 2986796, 10 pages, 2016.

[98] A. N. Panche, A. D. Diwan, and S. R. Chandra, "Flavonoids: an overview," *Journal of nutritional science*, vol. 5, article e47, 2016.

[99] L. Chen, H. Teng, Z. Xie et al., "Modifications of dietary flavonoids towards improved bioactivity: an update on structure-activity relationship," *Critical Reviews in Food Science and Nutrition*, vol. 58, no. 4, pp. 513–527, 2018.

[100] H. Ishihara, T. Tohge, P. Viehöver, A. R. Fernie, B. Weisshaar, and R. Stracke, "Natural variation in flavonol accumulation in Arabidopsis is determined by the flavonol glucosyltransferase BGLU6," *Journal of Experimental Botany*, vol. 67, no. 5, pp. 1505–1517, 2016.

[101] S. Alseekh, L. Perez de Souza, M. Benina, and A. R. Fernie, "The style and substance of plant flavonoid decoration; towards defining both structure and function," *Phytochemistry*, vol. 174, p. 112347, 2020.

[102] D. C. Vitale, C. Piazza, B. Melilli, F. Drago, and S. Salomone, "Isoflavones: estrogenic activity, biological effect and bioavailability," *European Journal of Drug Metabolism and Pharmacokinetics*, vol. 38, no. 1, pp. 15–25, 2013.

[103] R. F. Prietsch, L. D. Monte, F. A. Da Silva et al., "Genistein induces apoptosis and autophagy in human breast MCF-7 cells by modulating the expression of proapoptotic factors and oxidative stress enzymes," *Molecular and Cellular Biochemistry*, vol. 390, no. 1-2, pp. 235–242, 2014.

[104] M. Hasan and H. Bae, "An overview of stress-induced resveratrol synthesis in grapes: perspectives for resveratrol-enriched grape products," *Molecules*, vol. 22, no. 2, 2017.

[105] J. Song, Y. Huang, W. Zheng et al., "Resveratrol reduces intracellular reactive oxygen species levels by inducing autophagy through the AMPK-mTOR pathway," *Frontiers in Medicine*, vol. 12, no. 6, pp. 697–706, 2018.

[106] L. G. Carter, J. A. D'Orazio, and K. J. Pearson, "Resveratrol and cancer: focus on in vivo evidence," *Endocrine-Related Cancer*, vol. 21, no. 3, pp. R209–R225, 2014.

[107] D. C. Ferraz da Costa, E. Fialho, and J. L. Silva, "Cancer chemoprevention by resveratrol the p53 tumor suppressor protein as a promising molecular target," *Molecules*, vol. 22, no. 6, p. 1014, 2017.

[108] Q. Xu, L. Zong, X. Chen et al., "Resveratrol in the treatment of pancreatic cancer," *Annals of the New York Academy of Sciences*, vol. 1348, no. 1, pp. 10–19, 2015.

[109] L. Huang, S. Zhang, J. Zhou, and X. Li, "Effect of resveratrol on drug resistance in colon cancer chemotherapy," *RSC Advances*, vol. 9, no. 5, pp. 2572–2580, 2019.

[110] Y. R. Li, S. Li, and C. C. Lin, "Effect of resveratrol and pterostilbene on aging and longevity," *BioFactors*, vol. 44, no. 1, pp. 69–82, 2018.

[111] J. H. Lee, J. S. Kim, S. Y. Park, and Y. J. Lee, "Resveratrol induces human keratinocyte damage via the activation of class III histone deacetylase, Sirt1," *Oncology Reports*, vol. 35, no. 1, pp. 524–529, 2016.

[112] S. J. Park, F. Ahmad, A. Philp et al., "Resveratrol ameliorates aging-related metabolic phenotypes by inhibiting cAMP phosphodiesterases," *Cell*, vol. 148, no. 3, pp. 421–433, 2012.

[113] L. Cheng, Z. Jin, R. Zhao, K. Ren, C. Deng, and S. Yu, "Resveratrol attenuates inflammation and oxidative stress induced by myocardial ischemia-reperfusion injury: role of Nrf2/ARE pathway," *International Journal of Clinical and Experimental Medicine*, vol. 8, no. 7, pp. 10420–10428, 2015.

[114] M. Sandri, C. Sandri, A. Gilbert et al., "Foxo transcription factors induce the atrophy-related ubiquitin ligase atrogin-1 and cause skeletal muscle atrophy," *Cell*, vol. 117, no. 3, pp. 399–412, 2004.

[115] F. Haghighatdoost and M. Hariri, "Effect of resveratrol on lipid profile: an updated systematic review and meta-analysis on randomized clinical trials," *Pharmacological Research*, vol. 129, pp. 141–150, 2018.

[116] F. Haghighatdoost and M. Hariri, "Can resveratrol supplement change inflammatory mediators? A systematic review and meta-analysis on randomized clinical trials," *European Journal of Clinical Nutrition*, vol. 73, no. 3, pp. 345–355, 2019.

[117] A. Rašković, V. Ćućuz, L. Torović et al., "Resveratrol supplementation improves metabolic control in rats with induced

hyperlipidemia and type 2 diabetes," *Saudi Pharmaceutical Journal*, vol. 27, no. 7, pp. 1036–1043, 2019.

[118] Y. J. Lee, N. Y. Kim, Y. A. Suh, and C. H. Lee, "Involvement of ROS in curcumin-induced autophagic cell death," *The Korean Journal of Physiology and Pharmacology*, vol. 15, no. 1, pp. 1–7, 2011.

[119] S. Deng, M. K. Shanmugam, A. P. Kumar, C. T. Yap, G. Sethi, and A. Bishayee, "Targeting autophagy using natural compounds for cancer prevention and therapy," *Cancer*, vol. 125, no. 8, pp. 1228–1246, 2019.

[120] A. A. Momtazi-Borojeni, E. Abdollahi, B. Nikfar, S. Chaichian, and M. Ekhlasi-Hundrieser, "Curcumin as a potential modulator of M1 and M2 macrophages: new insights in atherosclerosis therapy," *Heart Failure Reviews*, vol. 24, no. 3, pp. 399–409, 2019.

[121] N. E. Rainey, A. Moustapha, and P. X. Petit, "Curcumin, a multifaceted hormetic agent, mediates an intricate crosstalk between mitochondrial turnover, autophagy, and apoptosis," *Oxidative Medicine and Cellular Longevity*, vol. 2020, Article ID 3656419, 23 pages, 2020.

[122] L. Arshad, M. A. Haque, S. N. Abbas Bukhari, and I. Jantan, "An overview of structure–activity relationship studies of curcumin analogs as antioxidant and anti-inflammatory agents," *Future medicinal chemistry*, vol. 9, no. 6, pp. 605–626, 2017.

[123] B. Ahmad, S. Khan, Y. Liu et al., "Molecular mechanisms of anticancer activities of puerarin," *Cancer Management and Research*, vol. Volume 12, pp. 79–90, 2020.

[124] K. Maiese, "FoxO proteins in the nervous system," *Analytical Cellular Pathology (Amsterdam)*, vol. 2015, article 569392, pp. 1–15, 2015.

[125] C. H. Lin, C. C. Lin, W. J. Ting et al., "Resveratrol enhanced FOXO3 phosphorylation via synergetic activation of SIRT1 and PI3K/Akt signaling to improve the effects of exercise in elderly rat hearts," *Age (Dordrecht, Netherlands)*, vol. 36, no. 5, p. 9705, 2014.

[126] X. Ou, M. R. Lee, X. Huang, S. Messina-Graham, and H. E. Broxmeyer, "SIRT1 positively regulates autophagy and mitochondria function in embryonic stem cells under oxidative stress," *Stem Cells*, vol. 32, no. 5, pp. 1183–1194, 2014.

[127] S. Galati, C. Boni, M. C. Gerra, M. Lazzaretti, and A. Buschini, "Autophagy: a player in response to oxidative stress and DNA damage," *Oxidative Medicine and Cellular Longevity*, vol. 2019, Article ID 5692958, 12 pages, 2019.

[128] S. Ravi, K. A. Peña, C. T. Chu, and K. Kiselyov, "Biphasic regulation of lysosomal exocytosis by oxidative stress," *Cell Calcium*, vol. 60, no. 5, pp. 356–362, 2016.

[129] D. L. Medina, S. di Paola, I. Peluso et al., "Lysosomal calcium signalling regulates autophagy through calcineurin and TFEB," *Nature Cell Biology*, vol. 17, no. 3, pp. 288–299, 2015.

[130] I. C. Nnah, B. Wang, C. Saqcena et al., "TFEB-driven endocytosis coordinates MTORC1 signaling and autophagy," *Autophagy*, vol. 15, no. 1, pp. 151–164, 2019.

Research Article

α-Lipoic Acid Targeting PDK1/NRF2 Axis Contributes to the Apoptosis Effect of Lung Cancer Cells

Liduo Yue [ID],[1] **Yanbei Ren,**[1] **Qingxi Yue** [ID],[1,2] **Zhou Ding,**[1] **Kai Wang,**[1] **Tiansheng Zheng,**[1] **Guojie Chen,**[1] **Xiangyun Chen,**[1] **Ming Li** [ID],[1] **and Lihong Fan** [ID][1]

[1]*Department of Respiratory Medicine, Shanghai Tenth People's Hospital, Tongji University School of Medicine, 200072 Shanghai, China*
[2]*Department of Oncology, Shanghai 9th People's Hospital, Shanghai Jiao Tong University School of Medicine, 201999 Shanghai, China*

Correspondence should be addressed to Liduo Yue; 2216443774@qq.com, Ming Li; mlid163@163.com, and Lihong Fan; fanlih@aliyun.com

As an antioxidant, α-lipoic acid (LA) has attracted much attention to cancer research. However, the exact mechanism of LA in cancer progression control and prevention remains to be unclear. In this study, we demonstrated that α-lipoic acid has inhibitory effects on the proliferation, migration, and proapoptotic effects of non-small-cell lung cancer (NSCLC) cell lines A549 and PC9. LA-induced NSCLC cell apoptosis was mediated by elevated mitochondrial reactive oxygen species (ROS). Further study confirmed that it is by downregulating the expression of PDK1 (the PDH kinase), resulted in less phospho-PDH phenotype which could interact with Keap1, the negative controller of NRF2, directly leading to NRF2 decrease. Thus, by downregulating the NRF2 antioxidant system, LA plays a role in promoting apoptosis through the ROS signaling pathway. Moreover, LA could enhance other PDK inhibitors with the proapoptosis effect. In summary, our study shows that LA promotes apoptosis and exerts its antitumor activity against lung cancer by regulating mitochondrial energy metabolism enzyme-related antioxidative stress system. Administration of LA to the tumor-bearing animal model further supported the antitumor effect of LA. These findings provided new ideas for the clinical application of LA in the field of cancer therapy.

1. Introduction

Cancer cells exhibit increased ROS levels, partly due to onco-genic stimulation compared to normal cells, increasing their metabolic activity [1–3]. On the one hand, ROS could increase the membrane potential, leading to changes in the membrane permeability, release of cytochrome C, and inducing apoptosis [4]. On the other hand, the cancer cells could upregulate nuclear factor erythroid 2-related factor 2 (NRF2), the antioxidant system to inhibit the apoptotic pathway [5]. Under persistent oxidative stress, cancer cells become well adapted to such stress through a set of mechanisms that activate ROS-scavenging systems, including NRF2-Keap1-ARE system, and inhibit apoptosis [6].

Proteasomes rapidly degrade the nuclear factor erythroid 2-related factor 2 (NRF2) under a basal condition in a Keap1-dependent manner. ROS oxidatively modifies Keap1 to release NRF2 and allow its nuclear translocation [7]. It then binds to the antioxidant response element to regulate down-stream gene transcription. The NRF2 antioxidant system is the key to oxidative stress, maintaining redox homeostasis [8–10]. With increasing oxidative stress, the NRF2 is highly expressed, antioxidant proteins are upregulated, and then the cells escape from apoptosis. Meanwhile, higher NRF2 constantly interacts with the surrounding immune environment, resulting in the proliferation of cancer cells, immune escape, and malignant transformation [11, 12]. Several lines of evidence suggest that NRF2 is involved in cancer development and recurrence and resistance to anticancer drugs [9, 13, 14]. Therefore, understanding the mechanisms of ROS regulation is essential to kill cancer cells and overcome drug resistance efficiently.

α-Lipoic acid (LA) is a substance containing disulfide, known as 1,2,3-disulfide heterocyclic pentane pentanoic acid [15]. It is synthesized in the mitochondria. LA is a natural coenzyme in the mitochondrial pyruvate dehydrogenase (PDH) complex. PDH complex catalyzes the oxidative decarboxylation of α-keto acids, such as pyruvate and α-ketoglutarate [16]. It also regulates various metabolic enzymes in glucose catabolism [17]. LA forms a covalent bond with the side chain of a lysine residue within the E2 subunit of the PDH complex and promotes the enzyme activity of pyruvate dehydrogenase (PDH) [18]. PDH complex is the critical switch from glycolysis to oxidative phosphorylation (OXPHOS). Also, LA has been reported to promote apoptosis in several cancer subtypes [19–21]. It can induce ROS production and lead to cancer apoptosis [22, 23]. However, the molecular mechanism still remains to be unclear. Hence, in this study, the underlying relationship between the switching of glycolysis to OXPHOS and proapoptosis of LA was investigated.

Finally, based on the widely accepted theory of the Nobel Prize winner Warburg, "the tumor is a kind of metabolic disease," most lung cancer relies on glycolysis to generate energy, including the big lung cancer [24]. Because PDK1 suppresses the switch of glycolysis to OXPHOS by phosphorylation of Ser 293 of PDH [25], it has been regarded as an anticancer target [26, 27]. Nevertheless, the clinical effect and application still need to be evaluated. The NSCLC cell lines A549 and PC9 have been reported to prefer glycolysis for energy supply [28]. So, we test if LA could influence the metabolic feature and directly regulate the antioxidant system to promote apoptosis on these two cell lines.

2. Result

2.1. LA Inhibits Proliferation and Induces Apoptosis in A549 and PC9 Lung Cancer Cells.
To explore the antitumor effects of LA (Figure 1(a)) in lung cancer cells, A549 and PC9 lung cancer cell lines were treated with different concentrations of LA for 24 h or 48 h, respectively. Cell proliferation was evaluated by CCK8 assay (Figure 1(b)). The results showed that LA could inhibit the proliferation of lung cancer cells A549 and PC9 with IC50 at 3-6 mM. Under the bright-field view of the cells that are processed with different concentrations of LA, 1.5 mM LA showed noticeable apoptotic features (cell becomes longer) but not much cell death (Figure 1(c)). 1.5 mM LA could also effectively inhibit the shift of lung cancer cells (Figure 1(d)), coinciding with the antiproliferative effects. So, 1.5 mM LA was used for testing the mechanism of apoptosis in this work. A549 and PC9 cells were exposed to 1.5 mM LA for 24 h and 48 h. LA treatment increased the percentage of apoptotic cells (Figure 1(e)). Moreover, the longer the time of LA incubation, the more pronounced was the apoptosis.

2.2. LA Promotes Apoptosis of Lung Cancer Cells by Elevating ROS Signaling.
Using the MitoSOX red probe to label the mitochondrial ROS, we confirmed that the ROS of the two lung cancer cell were remarkably increased after exposed to LA. Moreover, the ROS was elevated in a time-dependent manner (Figure 2(a)). The apoptosis protein was examined by western blotting, either. The results show that the antiapoptotic protein Bcl-2 was significantly decreased, and apoptotic protein caspase-9 was increased accordingly in a time-dependent manner (Figure 2(b)). It indicates that the apoptosis of the lung cancer cell coincided with elevated ROS. It has been reported that ROS scavenger N-acetylcysteine (NAC) could quench ROS and the subsequent apoptosis [4]. In truth, NAC in this study could reverse this LA-induced ROS (Figure 2(c)) and the corresponding proapoptotic effect (Figure 2(d)), indicating that LA could induce apoptosis also through the induction of ROS-apoptosis signaling.

2.3. Increment of ROS by the Degradation of NRF2 Contributes to the Proapoptosis of LA.
Herein, the ROS leads to apoptosis upon LA exposure, so we hypothesized that LA induces apoptosis by downregulating the antioxidant system. Furthermore, as NRF2 has been broadly reported to keep redox homeostasis [25], it could control the antioxidant enzyme expression to battle the oxidative press. NRF2 protein levels of the two lung cancer cell lines were measured after LA exposure. As assumed, the protein levels of NRF2 were downregulated in a dose- and time-dependent manner (Figure 3(a)). To test if it is NRF2 downregulation that resulted in apoptosis, the NRF2 expression plasmid was transfected with cells after LA exposure. The results show that the downregulation of NRF2 protein could be elevated, and caspase-9 could be downregulated (Figure 3(b)). Also, the ROS and apoptosis induced by LA could be attenuated by NRF2 transfection (Figures 3(c) and 3(d)), indicating the apoptosis was negatively controlled by NRF2 expression. On the contrary, as LA could inhibit NRF2 leading to apoptosis, siRNA of NRF2 also results in elevated ROS and apoptosis (Figure 3(e)). All the data indicated that LA inhibits NRF2 to release ROS, initiating the apoptosis pathway.

2.4. LA Downregulates NRF2 by Suppressing PDK1 Expression.
As LA acts as a cofactor of PDH, the latter switches the glycolysis to OXPHOS. According to the Warburg effect, most cancer cells tend to undergo glycolysis, including A549 and PC9 lung cancer cell lines [28], so we assume that LA influences the antioxidant system by regulating the mitochondrial metabolic enzymes. As assumed, PDK1 (the PDH kinase, which could phosphorylate PDH and rendering its inactivity), when processed with LA, could be inhibited in both the cell lines in a dose-dependent manner (Figure 4(a)). However, LA does not affect the total PDH protein level, and as expected, the PDH enzyme activity was slightly elevated (Figure 4(b)), which might be due to PDK1 inhibition. Furthermore, we measured glycolytic activity in real time by monitoring the extracellular acidification rate (ECAR) using the XF96 Seahorse apparatus (Figure 4(c)). Accordingly, we observed that basal glycolytic activity (glycolysis rate and the ratio of ECAR/OCR) was significantly reduced in A549 and PC9 cells upon LA exposure, which further confirmed PDK1 inhibition after LA exposure. Thus, we are curious about if there is some relationship between PDK1 inhibition and NRF2 downregulation.

By the siRNA-PDK1 interference technique, PDK1 downregulation was confirmed to inhibit NRF2 expression (Figure 4(d)). Of the three designed siRNAs, the third siRNA works best to inhibit PDK1 expression and inhibit NRF2 more robustly. This data indicated that LA downregulates PDK1 protein expression to inhibit NRF2. It has been checked that LA has no direct inhibitory effect to the purified PDK1 enzyme (data not shown) but just to PDK1 enzyme protein.

Interestingly, LA could coordinate with the well-known PDK1 inhibitor, dichloroacetate (DCA), which was reported inducing ROS and promote apoptosis of several cancer cells [29, 30]. Although LA inhibits lung cancer at high concentration with an average IC50 of about 3-6 mM, it enhances other antitumor agents such as DCA in the two lung cancer cells, indicating the clinical application prospects of LA (Figure 4(e)). Also, we noticed that siRNA PDK1 could result in apoptosis robustly (Figure 4(e)), indicating that PDK1 inhibition could lead to apoptosis.

As that PDK1 inhibition could downregulate NRF2 to promote apoptosis, it is necessary to know the mechanism of PDK1 inhibition regulating NRF2 inhibition. So, the interaction between phosphor-PDH (p-PDH) and the Keap1 (the specific NRF2 negative regulator) was tested by the co-IP technique, and the results showed that p-PDH could interact with Keap1 protein directly (Figure 4(f)). The antibody of human p-PDH or Keap1 was bound to beads. The cell lysis was incubated with the beads. After incubation, the flow-throughs were collected, the beads were washed, and the flowthrough and the elution were tested by western blotting for Keap1 and p-PDH binding separately. It is concluded that p-PDH would decrease upon PDK1 inhibition; then, the released Keap1 will result in NRF2 inhibition.

2.5. LA Inhibits Lung Carcinoma via Reducing PDK1 and NRF2 Expression In Vivo. To further demonstrate the anticancer effects of LA *in vivo* and the inhibition of NRF2 and PDK1, a tumor-bearing mouse (C57BL/6, black) model was constructed. Compared to the control group, intraperitoneal administration of LA (91 mg/kg) could significantly decrease the size (Figures 5(a) and 5(b)) and weight (Figure 5(c)) of the tumors formed by LLC cells (mouse lung cancer cells). In addition, the mice were tolerant to LA at the concentration used (Figure 5(d)). This could be due to the inhibition of cell proliferation and increase in cell apoptosis, which was revealed by a decrease in Ki67 staining (an antigen marker of cell proliferation which has usually been checked to indicate the proliferating ability of cancer cells) (Figure 5(e)) and decrease in Bcl-2 expression and, on the contrary, an increase in caspase-9 expression (Figure 5(f)). Consistent with the effect of LA on PDK1 and NRF2 inhibition *in vitro*, LA treatment also reduced the expression of PDK1 and NRF2 *in vivo* (Figure 5(e)). These results further support that LA could suppress lung cancer cell growth and promote apoptosis *in vivo*.

3. Discussion

Lung cancer is the most common primary cancer. Despite an increase in the 5-year survival rate over the past 40 years, no

substantial improvement was seen since the 1980s [31, 32]. So, it is necessary to find novel therapeutic agents to combat this disease. In this study, we demonstrated that inducing degradation of NRF2 by inhibiting PDK1 is a promising strategy to combat lung cancer. LA (α-lipoic acid) is a novel PDK1 inhibitor for the treatment of lung cancer.

With the progression of cancer development, ROS rises with redox press. The strategy of cell adaptation to the redox press involves NRF2 to conquer the ROS press, and cell transformed for survival, striving for redox homeostasis. If ROS/apoptosis pathway should be activated, one should raise the ROS, but the NRF2 will combat the ROS. The metabolic will shift from oxidative phosphorylation to glycolysis leading to carcinogenesis [33]. An alternative strategy involves suppression of the antioxidant system, such as inhibition of NRF2 [34]. In this study, after LA exposure, the NRF2 was decreased, and ROS was increased.

In the past decades, LA has been reported the anticancer effects in broad aspects of cancer [16, 21]. Besides the anticancer, LA plays broad roles in physiological environment, including function in mitochondrial energy metabolism. LA is also known for its powerful antioxidative effects and has been used for the treatment of chronic diseases associated with high levels of oxidative stress, such as diabetic polyneuropathy and Alzheimer's disease. A growing number of studies have demonstrated that LA and its derivatives thereof are capable of suppressing the growth of various cancer cell lines, while nontransformed primary cells were hardly affected. The action mode of LA and its derivatives in cancer cells are described in detail, and promising results from recent preclinical studies are presented [35].

It seems a paradox that LA functions as both antioxidant and prooxidant. LA functions the prooxidant only in special cancer cells, such as A549 and PC9 cells which should show high-level NRF2 expression and high glycolytic level. In this study, through inhibiting PDK1 to further prohibit NRF2; LA functions as anticancer prooxidant. Moreover, LA exerted its antitumor effects at high concentration in this research work, which indicates potential antioxidant of LA at low dose and prooxidant of LA at high dose. The off-target effect of LA as anticancer prooxidant needs further study.

It could be noticed that the classic ROS generation pathway, such as PDH activity, showed slightly elevated (Figure 4(b)), indicating that a part of increased ROS, resulting from PDH activity improvement, but through the results of NRF2 overexpression, most of ROS generated by LA exposure could be ruined indicating that the induced ROS was due to NRF2 inhibition.

Many transactivation factors have been involved in the pathogenesis of cancer and were considered as drug targets. The agonist or antagonist is very difficult to develop as therapeutic targets [36]. Theoretically, the Keap1 binding to NRF2 will initiate the ubiquitin-proteasome degradation of NRF2. It was reported that the phosphorylation of Keap1 destroys the binding between NRF2 and Keap1 [7, 37]. It is very complicated to design small molecular inhibitors that target the phosphorylation process. A kind of ROS-inducing reagents that have proapoptotic effects assists in

(a)

(b)

(c)

(d)
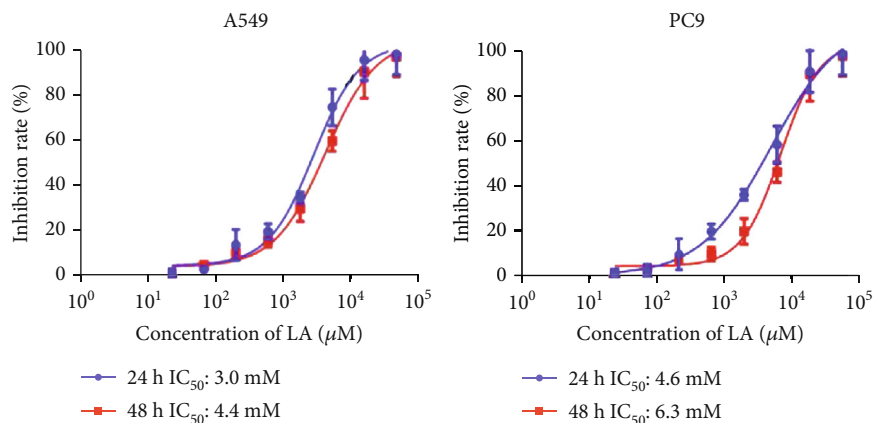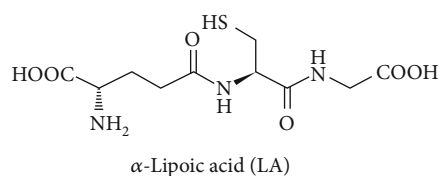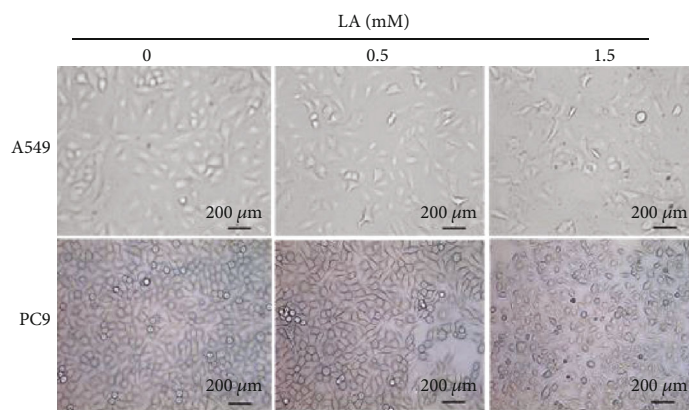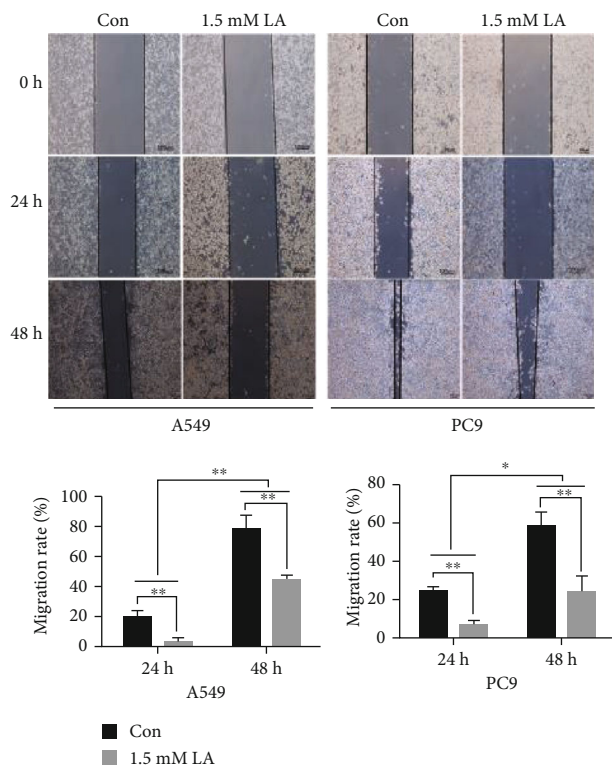
FIGURE 1: Continued.
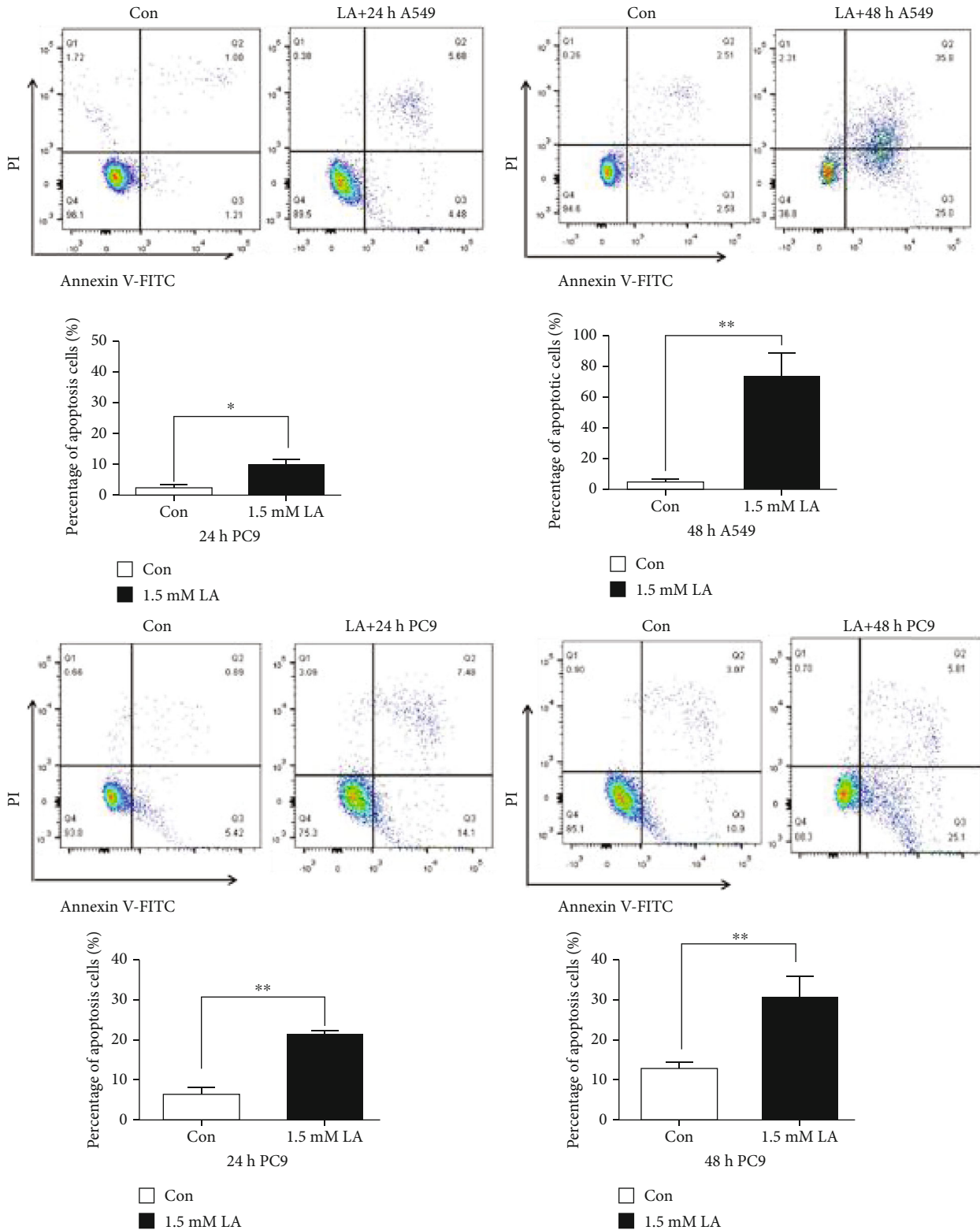
(e)

Figure 1: LA inhibits proliferation, induces apoptosis, and inhibits shift rate in lung cancer cells. (a) Chemical structure of LA. (b) Lung cancer cell lines were treated with different doses of LA for 24 h or 48 h. Cell proliferation was examined by CCK8 assay, and the IC50 values of LA were calculated by GraphPad (Prism) software. (c) Cell morphology were captured under the bright field of microscope exposed to different doses of LA. (d) LA inhibits the shift of A549and PC9 cells in a time-dependent manner. (e) The cells were exposed to 1.5 mM of LA for 24 h and 48 h, and then, Annexin/PI double staining was used to evaluate the apoptotic rates. Results were shown as the mean ± s.d. The symbol ∗ indicates $P < 0.05$; ∗∗ indicates $P < 0.01$.
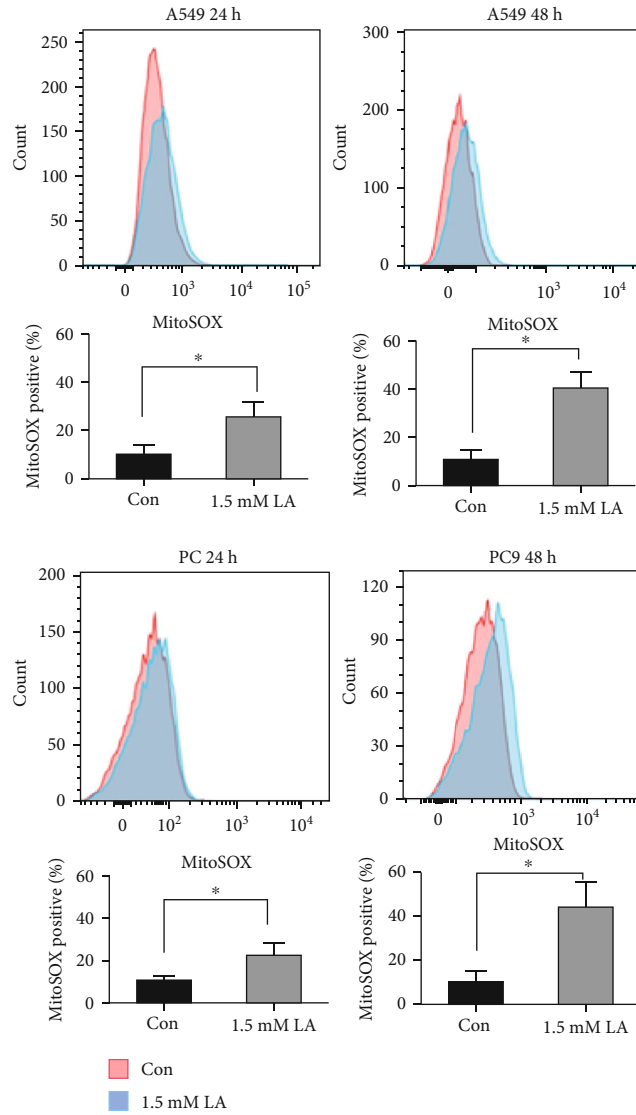
(a)
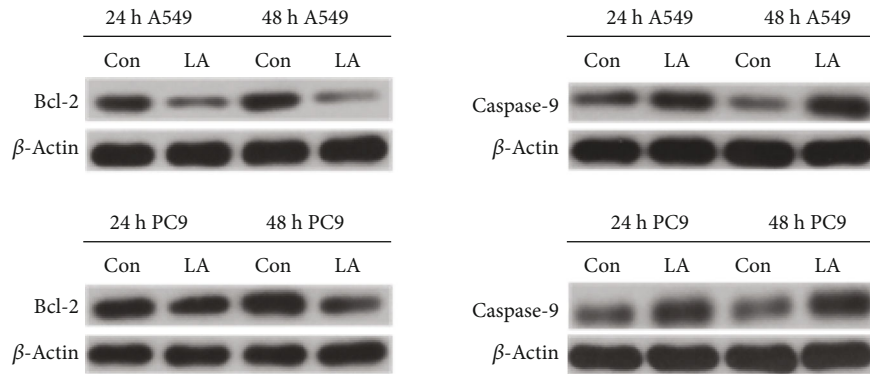
(b)

FIGURE 2: Continued.

(c)

(d)
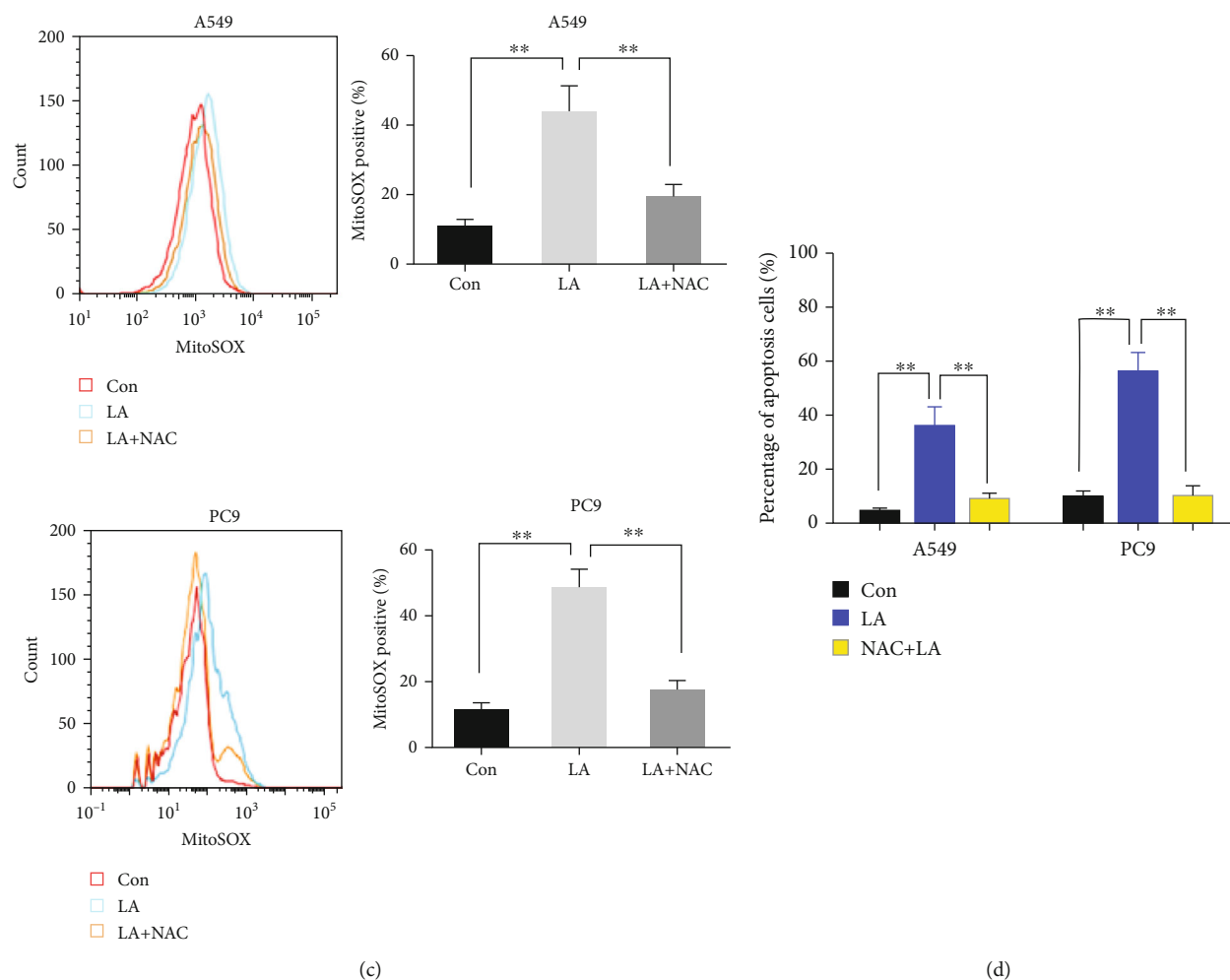
FIGURE 2: LA can induce mitochondrial ROS level of lung cancer cells. (a) The cells were incubated with 1.5 mM LA for 24 h and 48 h, and the mitochondria ROS was measured using MitoSOX red probe. (b) After incubation with 1.5 mM LA for 24 h and 48 h, the apoptotic proteins Bcl-2 and caspase-9 were examined by western blotting. (c) NAC quenched the ROS induced by LA. (d) NAC abbreviated the apoptotic effect induced by LA. Results are shown as the mean ± s.d. ∗ indicates $P < 0.05$; ∗∗ indicates $P < 0.01$.

conquering cancer [38]. LA and DCA have been reported as ROS inducers with proapoptosis effect [23]. In this study, as a cofactor of PDH in the mitochondria, LA was found to be the PDK1 inhibitor and can decrease the transactivation factor NRF2, leading to the activation of the ROS/apoptosis pathway.

It is well known now that phosphorylation and nonphosphorylation state could play different roles [39]. PDK1, as a gatekeeping gene that assists in regulating the PDH activity, is the regulator for the PDH activity [33]. The phosphorylation state of PDH (p-PDH) broadly exists in the cancer cells. We speculate that phosphorylation of PDH serves as the regulator of the metabolism of energy and the redox homeostasis. In the study, we found that p-PDH can directly bind to Keap1, which is the negative controller of NRF2. Once PDK1 was inhibited, p-PDH (the product of PDK1) would be decreased, releasing the binding Keap1. Then, Keap1 is more feasible to destroy NRF2, thus elaborately regulating the ROS/apoptosis pathway. The detailed regulation process was summarized in the below scheme (Figure 6).

From the co-IP result, we find that the phosphorylated PDH could bind to Keap1. As many reported PDK1 inhibitors need large doses to induce ROS, also the apoptosis of cells seems to be reversible to grow well. We guess that the binding of p-PDH with Keap1 is a reversible process. The detailed mechanism still requires investigation. Nevertheless, how to develop powerful agents based on this result is still hopeful and exciting. When small doses were administered, LA functions as a cofactor of PDH to participate in pyruvate metabolism during cancer development. If it exceeds the physiologic threshold, it could function as an anticancer agent or cooperate with other proapoptosis reagents to function best. So, high doses of LA act as PDK1 inhibitor. On the other hand, PDK1 usually is little expressed in normal cells. So, LA is associated with meager side effects on clinical application. Also, for cancers that do not rely on PDK1 to hold switching between glycolysis and OXPHOS, the antitumor effects of LA still need to be investigated.

In summary, as a natural molecule, LA has a wide range of therapeutic effects, and it promotes apoptosis, showing

(a)

(b)

(c)
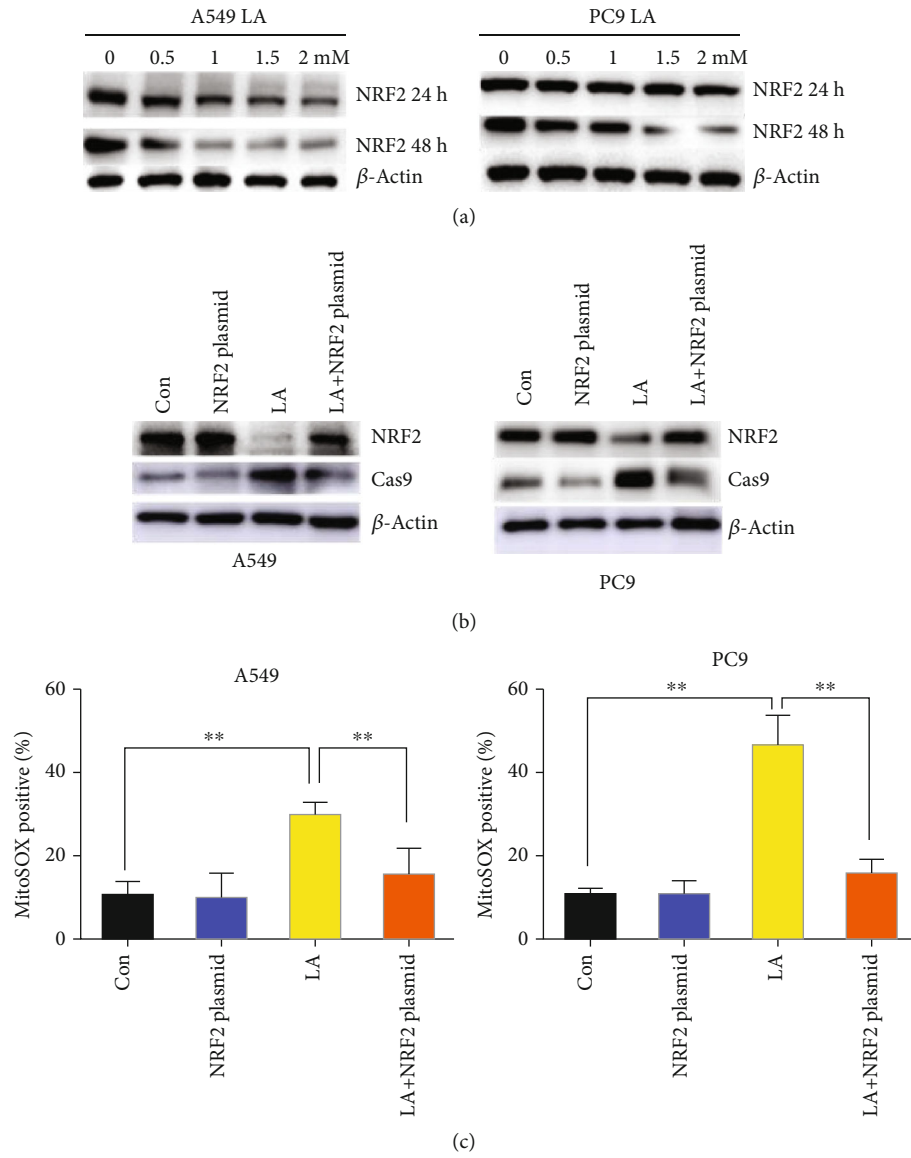
FIGURE 3: Continued.
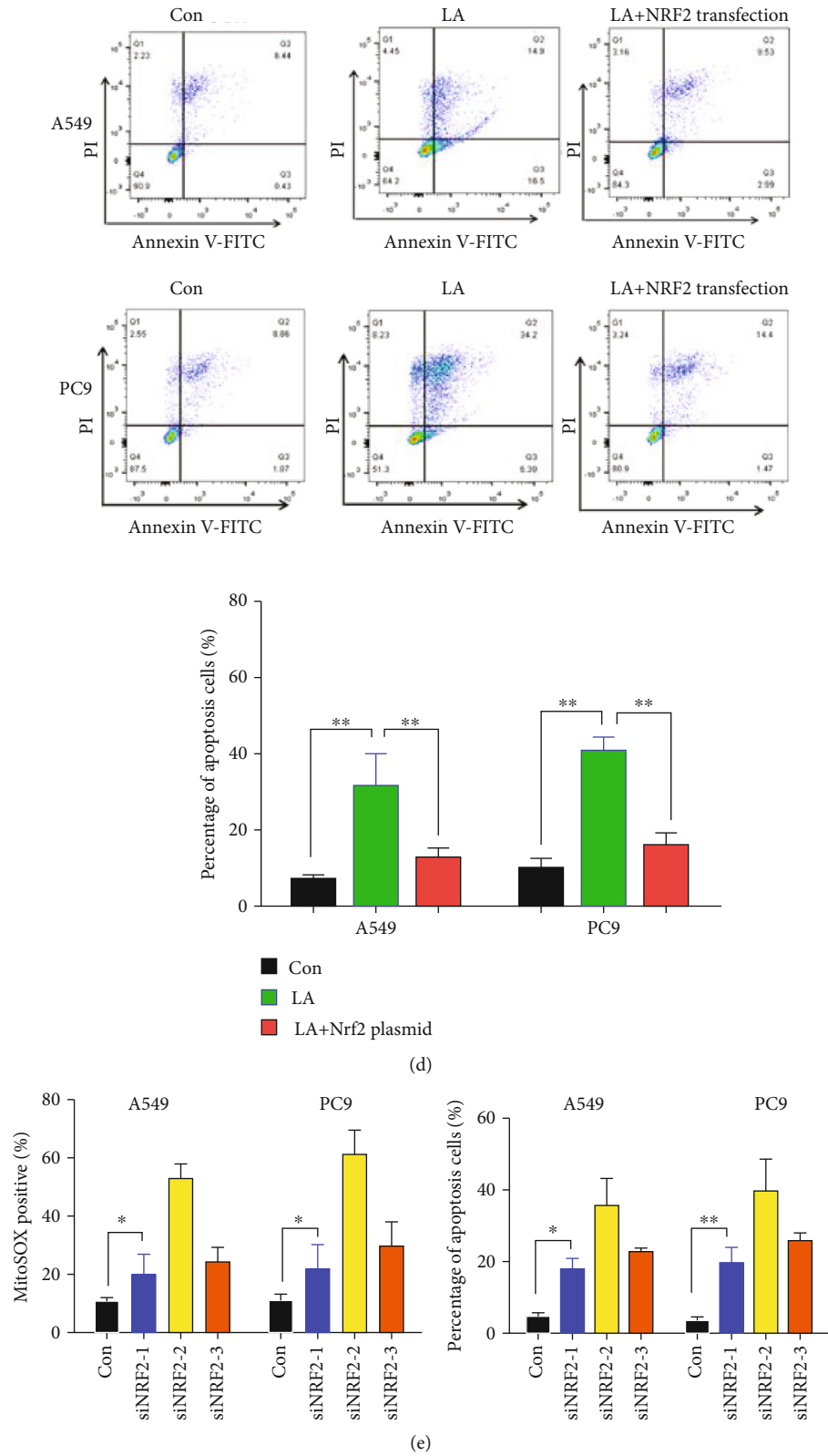
FIGURE 3: Downregulation of NRF2 by LA-induced apoptosis of A549 and PC9 cells. (a) NRF2 protein was downregulated in a dose- and time-dependent manner. (b) NRF2 and caspase-9 were examined in NRF2 expression plasmid transfected cells by western blotting. (c) Mitochondria ROS was measured by the MitoSOX red probe upon cells transfected with NRF2 expression plasmid after LA exposure. (d) NRF2 overexpression attenuated the LA-induced apoptosis in A549 and PC9 cells. (e) siRNA of NRF2-induced mitochondrial ROS and apoptosis. Results are shown as the mean $\pm$ s.d. $**$ indicates $P < 0.01$.

(a)

(b)

(c)

(d)

(e)

Figure 4: Continued.

(f)
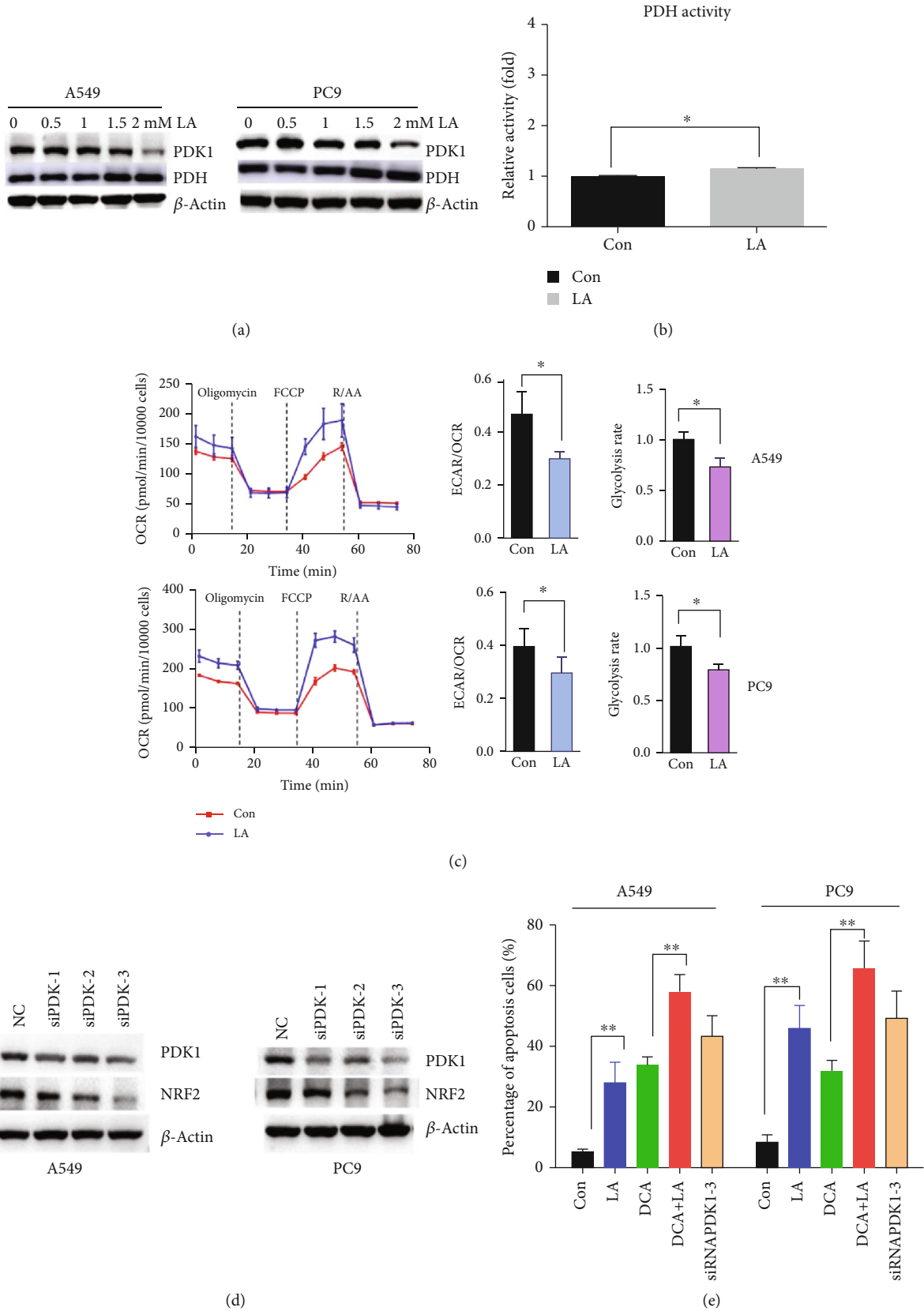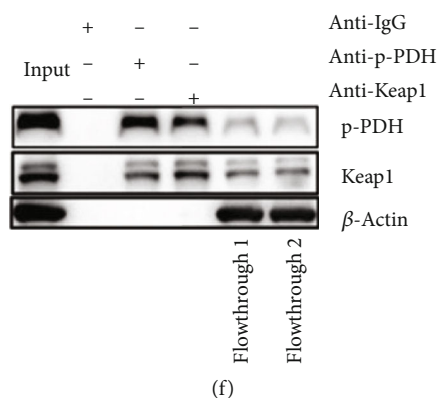
FIGURE 4: PDK1 inhibition by LA exerts proapoptotic effects through downregulating NRF2. (a) WB analysis of PDK1 and PDH expression in A549 and PC9 cells after LA exposure for 24 h. (b) LA (1.5 mM) slightly improves pyruvate dehydrogenase activity of A549 cells. (c) Glycolysis rate and oxygen consumption rate (OCR) were measured using glycolysis rate assay kit and Mito Stress Test kit. Calculated parameters of the assays are indicated in bar graphs. (d) Silencing of PDK1 by siRNA downregulates NRF2 expression. (e) PDK1 inhibition results in apoptosis and LA (1.5 mM) could enhance the proapoptosis effect of DCA (5 mM). Results are shown as the mean ± s .d.$^*P < 0.05$; $^{**}P < 0.01$. (f) Endogenous coimmunoprecipitation between phosphorylated PDH and Keap1 in human lung cancer cells. A549 cells were collected and lysed to undergo Co-IP assay according to the manufacturer's protocol. After incubating with anti-P-PDH and anti-Keap1 beads, the elutes and flowthroughs (flowthrough 1 from anti-p-PDH beads; flowthrough 2 from anti-Keap beads) were checked by western blotting assay.

fewer side effects. With a clearer molecular mechanism of LA proapoptosis, researchers can have a drug design scheme based on it to improve curative effect best.

4. Material and Methods

4.1. Reagents. LA and DCA were purchased from MedChem-Express⊠MCE, the USA⊠, and anti-human PDH, NRF2, Keap1, PDK1, and phosphor-PDH antibodies were purchased from the Cell Signaling Technology. Bcl-2, Caspase9 and β-actin antibodies were from Abcam. The LA and DCA were dissolved in dimethyl sulfoxide (DMSO). Dulbecco's modified Eagle's medium (DMEM) was obtained from Gibco. NAC (N-acetylcysteine) was purchased from SolarBio (Cat. No: IA0050).

4.2. Cell Culture. Human lung cancer cells A549 and PC9 (Shanghai Zhongqiao.com, Shanghai, China) were cultured in RPMI 1640 (Gibco) containing 10% FBS (Gibco) and 1% penicillin/streptomycin (Hyclone) in a 37°C, 5% CO$_2$ incubator. Mouse cell line LLC (Shanghai Zhongqiao.com) was cultured in DMEM (Gibco, high glucose) containing 10% FBS (Gibco) and 1% penicillin/streptomycin (Hyclone) in a 37°C, 5% CO$_2$ incubator.

4.3. Cell Viability Assay. Cell viability was detected using a CCK-8 kit (Cat. No. 40203ES60, Yeasen, Shanghai, China). Briefly, 5×10^3 cells/well were seeded into 96-well plates, treated with different concentrations of LA, followed by addition of CCK-8 to each well at 24 h and 48 h. The optical density (OD) was measured after 2 h incubation at 37°C in an incubator. The data were processed using GraphPad Prism software by nonlinear regression curve fitting "log{inhibitor vs. response-variable slope four parameter", and the formula was $Y = \text{Bottom} + (\text{Top} - \text{Bottom})/(1 + 10^{((\text{LogIC50}-X)*\text{HillSlope})})$.

4.4. Flow Cytometry Analysis for Apoptosis. For apoptosis analysis, A549 and PC9 cells were treated with different concentration of LA for 24 h and 48 h, washed with cold PBS, and then collected. A mixture of Annexin V-FITC/PI (Cat. No. 556547, BD, San Jose, CA) was added. The cells were then analyzed by flow cytometry (BD Biosciences, USA) immediately after incubation at room temperature for 20 min in the dark.

4.5. Flow Cytometry Analysis for Mitochondrial ROS. For MitoSOX staining, cells were incubated in phenol red-free medium containing 10% serum and 2.5 μM MitoSOX Red (Cat. No. M36008, Thermo Fisher Scientific) at 37°C for 10 min. Cells were then trypsinized, rinsed once with cold PBS, and resuspended in PBS supplemented with 0.1% serum. MitoSOX samples were immediately analyzed using a BD FACSCanto II flow cytometry system (BD Biosciences). For gating, cells were first gated by size using FSC and SSC and then by FSC height × FSC area to exclude doublets before measuring the fluorescence. Universally, the intensity threshold was set by which there are 10% positive cells of the control sample (without LA). The cell with signal beyond the threshold was regarded as the MitoSOX-positive cells, using the positive percentage to make the bar graphs. The MitoSOX quantification methods were done according to the reported methods [11].

4.6. siRNA Analysis. Human PDK1 siRNA and NRF2 siRNA (Hanheng Biotechnology, Shanghai, China) were used to investigate PDK1 and NRF2 expression profiles. The fragmented RNA was loaded onto the cells to operate according to the product protocol.

4.7. Cell Transfection. A549 or PC9 lung cancer cells were seeded in culture plates in serum-free DMEM. Three siRNAs (siRNA-1, siRNA-2, and siRNA-3) were designed and

(a)

(b)

(c)

(d)

(e)
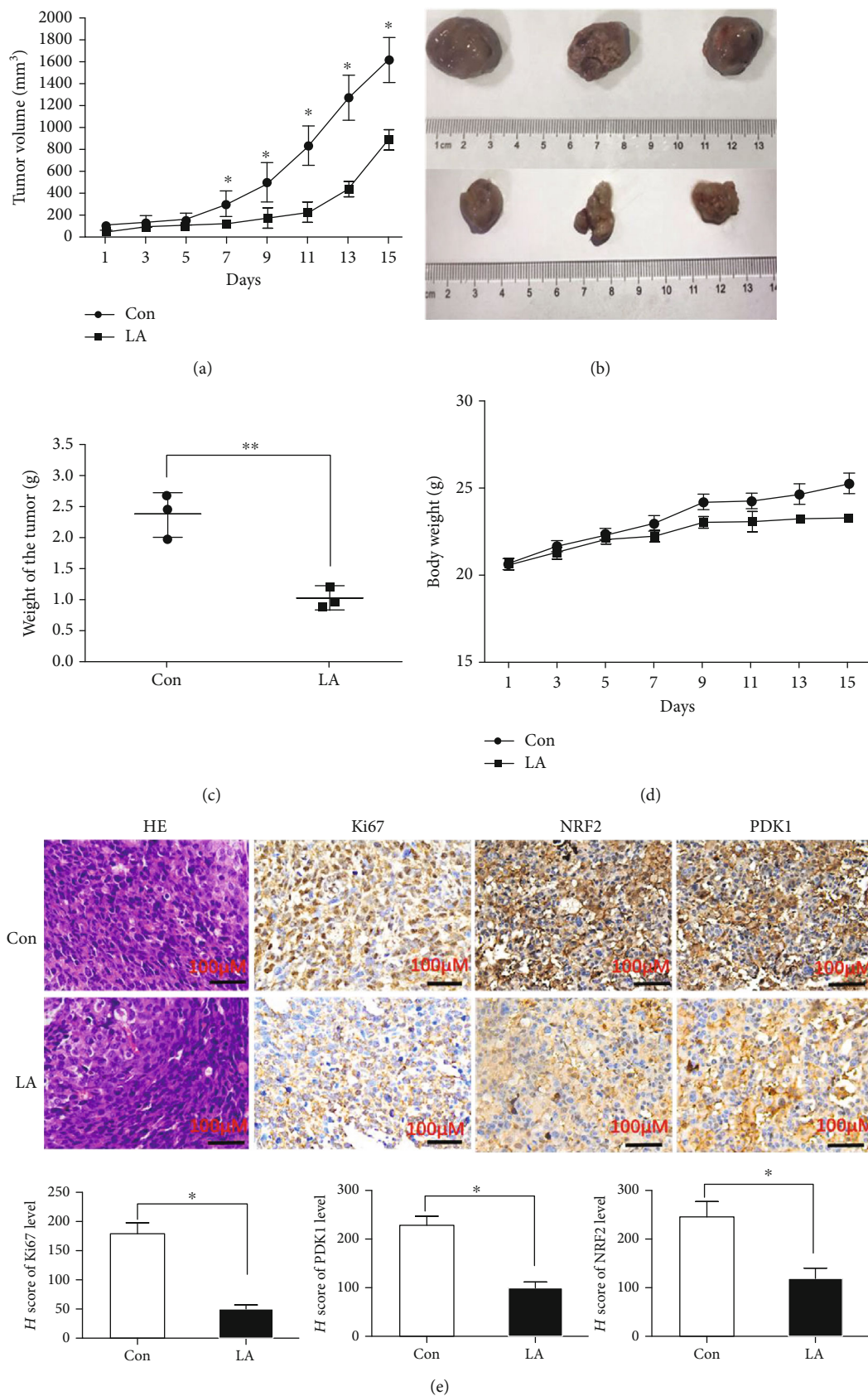
Figure 5: Continued.

(f)
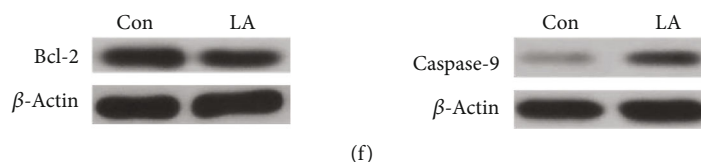
FIGURE 5: LA inhibits lung cancer growth and reduces NRF2 and PDK1 expression *in vivo*. (a) C57BL/6 mice bearing LLC tumor were treated with vehicle or LA (every other day by intraperitoneal injection) for 15 days, and then, tumor volume was recorded. It showed statistically significant differences in volume between the Con group and LA group ($P < 0.05$). (b) Image of tumors treated with LA or vehicle on day 16. (c) Comparison of tumor weight on day 16. (d) Effect of LA on mouse body weight. (e) The expression of patterns of Ki67, NRF2, and PDK1 was tested by immunohistochemical analysis in the tumors on day 16 in the control group and LA group. (f) Apoptotic protein Bcl-2 and caspase-9 expressions were analyzed in each tumor group. Results are shown as the mean ± s.d. ∗ indicates $P < 0.05$; ∗∗$P < 0.01$.
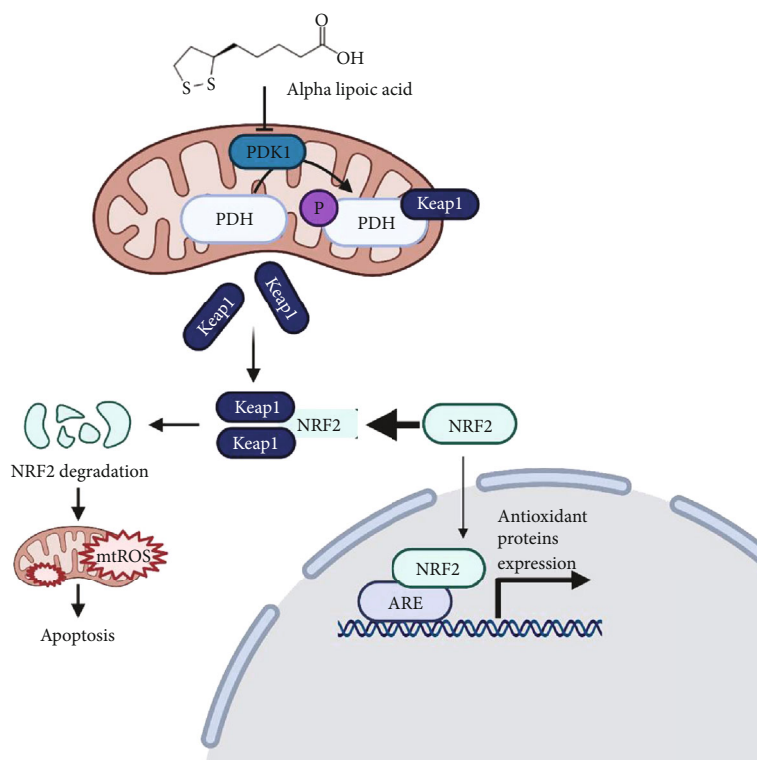
FIGURE 6: Schematic illustration of the apoptotic effect of LA in human lung cancer cells. LA inhibits PDK1, releasing Keap1 binded by p-PDH. NRF2 is then recaptured by Keap1 for degradation, initiating the ROS-induced apoptosis.

synthesized targeting PDK1, as well as a nonspecific siRNA (NC) and a GAPDH siRNA (siRNA-NC), and then were transfected into separate groups of A549 or PC9 lung cancer cells. siRNA-3 was evaluated as the most effective PDK1 siRNA. The sequences of the three PDK1 siRNAs were siRNA-1: 5′-GGAUCAGAAACCGACACAATT-3′; siRNA-2: 5′-GCCAAUACAAGUGGUUUAUTT-3′; and siRNA-3: 5′-GCUAGGCGUCUGUGUGAUUTT-3′; 6 h after transfection, fresh medium was added to the transfected cells and incubated for 24 h. Finally, verifying the gene silence is by determining the expression of proteins using western blot. The sequences of the three NRF2 siRNAs were siRNA-1: 5′-GGUUGAGACUACCAUGGUUTT-3′; siRNA-2: 5′-CCUGAAAGCACAGCAGAAUTT-3′; and siRNA-3: 5′-GCAGUUCAAUGAAGCUCAATT-3′.

4.8. NRF2 Overexpression. The plasmids of NRF2 were obtained from Hanheng Biotechnology. The cells with or without LA exposure were mixed with the transfection mixture (Lipofectamine 2000 with vehicle vector or NRF2 plasmid). After six hours of incubation, the cells were rinsed and incubated for another 24 h before the following analysis.

4.9. Western Blotting Analysis. The pretreated cells were washed with cold PBS. The concentration and purity of total cellular proteins were determined after being lysed on ice in RIPA buffer containing the protease inhibitor. An equal amount of protein was then loaded onto a 10% or 12.5% SDS-PAGE gel, transferred to nitrocellulose membranes, and incubated with primary antibodies overnight at 4°C after blocking for 1 h with 3% BSA, using anti-p-PDH, anti-PDH, anti-PDK1, anti-NRF2, anti-Keap1, anti-Bcl-2, anti-caspase-9,

and anti-β-actin (1:500). After three washes with PBST, membranes were incubated with the HRP-conjugated secondary antibodies, and then visualized by chemiluminescence.

4.10. PDH Activity Assay. After processing with or without LA for 24 h, the A549 and PC9 cells were processed according to the PDH activity assay kit for measuring the PDH activity. The kit was purchased from Sigma (Cat. No MAK183).

4.11. Extracellular Flux Analysis. A549 and PC9 cells were plated at 7500 cells/well in XF96 microplates (Seahorse Bioscience, Billerica, MA, USA) in RPMI medium with 10% according to the manufacturer's recommendations 48 h prior to the assay. Treatment with 1.5 mM LA was performed for 24 h.

For Mito Stress Test, the medium was exchanged to XF base medium (Seahorse Bioscience, Billerica, MA, USA) with 1 mM pyruvate, 2 mM glutamine, and 10 mM glucose and incubated at 37°C without CO_2 1 h prior to the assay. During the assay, OCR was measured using a Seahorse XFe 96 analyzer. Mito Stress Test kit containing 1 μM oligomycin, 1 μM carbonyl cyanide-4-(trifluoromethoxy)phenylhydrazone (FCCP), and 0.5 μM rotenone/0.5 μM antimycin A was performed according to the manufacturer's protocol.

For glycolytic rate assay, the medium was exchanged to XF base medium without phenol red (Seahorse Bioscience, Billerica, MA, USA) with 2 mM glutamine, 10 mM glucose, 1 mM pyruvate, and 5 mM HEPES and incubated at 37°C without CO_2 1 h prior to the assay. During the assay, ECAR was measured using a Seahorse XFe 96 analyzer. Glycolytic rate assay kit containing 0.5 μM rotenone, 0.5 μM antimycin A, and 50 mM 2-desoxyglucose was performed according to the manufacturer's protocol. ECAR and OCR were calculated by Wave 2.6 (Seahorse Bioscience, Billerica, MA, USA) software after the assay and normalized to cell numbers.

4.12. Coimmunoprecipitation (Co-IP) Assay. The A549 cells were lysed in an immunoprecipitation lysis buffer containing a protease inhibitor and phosphatase inhibitor. After centrifugation, the collected supernatant was incubated with beads by covalent binding antibody (the coimmunoprecipitation kit was purchased from Thermo Fisher, Cat. No. 26149) at 4°C overnight. The beads were then rinsed, and the bound proteins were eluted and then evaluated using western blotting analysis.

4.13. Tumor-Bearing Model Construction. Male C57BL/6 black mice aged six weeks (Shanghai Laboratory Animal Center, Shanghai, China) were fed with a standard diet and had free access to water in the standard animal laboratory. After subcutaneous injection of 100 μl LLC mouse lung cancer cells (3×10^6, serum-free culture medium) into the abdomen of mice, 6 animals were equally and randomly divided into two groups: a control group (ordinary diet) and an LA group (91 mg/kg LA, abdominal administration for three times a week) and sacrificed 15 days after administration. The tumors were removed, paraffin-embedded, fixed in 4% paraformaldehyde for 24 h, and then sliced into 5 μm thick sections for immunohistochemical analysis.

4.14. Histology and Immunohistochemistry. Tumors were cut into 2 μm sections from at least 3 different planes and stained with haematoxylin and eosin. For Ki67, NRF2, and PDK1 immunoperoxidase staining, paraffin-embedded sections were dehydrated and antigenic epitopes were exposed using a 10 mM citrate buffer and microwaving. Sections were incubated with rabbit polyclonal anti-Ki67, anti-NRF2, and anti-PDK1 antibodies. Primary Ab staining was detected by peroxidase-conjugated anti-rabbit IgG. The images were acquired under a Leica DM 4000B fluorescence microscope equipped with a digital camera. For the quantitative analysis, a histoscore (H score) was calculated based on the staining intensity and percentage of stained cells. The intensity score was defined as such: 0, no appreciable staining in cells; 1, weak staining in cells comparable with stromal cells; 2, intermediate staining; and 3, strong staining. The fraction of positive cells was scored as 0–100%. The H score was calculated by multiplying the intensity score and the fraction score, producing a total range of 0–300. A cutoff of 30 was used for LA positivity. Tissue sections were examined and scored separately by two independent investigators blinded to the clinicopathologic data.

4.15. Statistical Analysis. The GraphPad was used for statistical analysis, and all the data were obtained from at least three independent experiments. The results were calculated using Student's t-test and one-way ANOVA. $^*P < 0.05$ and $^{**}P < 0.01$, compared to the control group (0.5% DMSO).

Data Availability

The data used to support the findings of this study are available from the corresponding authors upon request.

Conflicts of Interest

The authors declare that they have no conflicts of interest.

Authors' Contributions

Liduo Yue, Yanbei Ren, and Qingxi Yue contributed equally to this work.

Acknowledgments

References

[1] S. Reuter, S. C. Gupta, M. M. Chaturvedi, and B. B. Aggarwal, "Oxidative stress, inflammation, and cancer: how are they

linked?," *Free Radical Biology & Medicine*, vol. 49, no. 11, pp. 1603–1616, 2010.

[2] R. Visconti and D. Grieco, "New insights on oxidative stress in cancer," *Current Opinion in Drug Discovery & Development*, vol. 12, no. 2, pp. 240–245, 2009.

[3] G. Waris and H. Ahsan, "Reactive oxygen species: role in the development of cancer and various chronic conditions," *Journal of Carcinogenesis*, vol. 5, no. 1, p. 14, 2006.

[4] J. Moungjaroen, U. Nimmannit, P. S. Callery et al., "Reactive oxygen species mediate caspase activation and apoptosis induced by lipoic acid in human lung epithelial cancer cells through Bcl-2 down-regulation," *The Journal of Pharmacology and Experimental Therapeutics*, vol. 319, no. 3, pp. 1062–1069, 2006.

[5] P. Huang, L. Feng, E. A. Oldham, M. J. Keating, and W. Plunkett, "Superoxide dismutase as a target for the selective killing of cancer cells," *Nature*, vol. 407, no. 6802, pp. 390–395, 2000.

[6] D. Trachootham, J. Alexandre, and P. Huang, "Targeting cancer cells by ROS-mediated mechanisms: a radical therapeutic approach?," *Nature Reviews. Drug Discovery*, vol. 8, no. 7, pp. 579–591, 2009.

[7] E. B. Krall, B. Wang, D. M. Munoz et al., "Correction:KEAP1 loss modulates sensitivity to kinase targeted therapy in lung cancer," *eLife*, vol. 6, article e33173, 2017.

[8] P. Liu, W. Tian, S. Tao et al., "Non-covalent NRF2 activation confers greater cellular protection than covalent activation," *Cell Chemical Biology*, vol. 26, no. 10, pp. 1427–1435.e5, 2019.

[9] S. M. Swamy, N. S. Rajasekaran, and V. J. Thannickal, "Nuclear factor-erythroid-2-related factor 2 in aging and lung fibrosis," *The American Journal of Pathology*, vol. 186, no. 7, pp. 1712–1723, 2016.

[10] J. R. V. Hlouschek, V. Ritter, F. Wirsdörfer, D. Klein, V. Jendrossek, and J. Matschke, "Targeting SLC25A10 alleviates improved antioxidant capacity and associated radioresistance of cancer cells induced by chronic-cycling hypoxia," *Cancer Letters*, vol. 439, pp. 24–38, 2018.

[11] D. B. Fox, N. M. G. Garcia, B. J. McKinney et al., "NRF2 activation promotes the recurrence of dormant tumour cells through regulation of redox and nucleotide metabolism," *Nature Metabolism*, vol. 2, no. 4, pp. 318–334, 2020.

[12] M. M. Kaneda, K. S. Messer, N. Ralainirina et al., "PI3Kγ is a molecular switch that controls immune suppression," *Nature*, vol. 539, no. 7629, pp. 437–442, 2016.

[13] S. Taniguchi, A. Elhance, A. van Duzer, S. Kumar, J. J. Leitenberger, and N. Oshimori, "Tumor-initiating cells establish an IL-33–TGF-β niche signaling loop to promote cancer progression," *Science*, vol. 369, no. 6501, pp. 269–283, 2020.

[14] H. Wang, Z. Gao, X. Liu et al., "Targeted production of reactive oxygen species in mitochondria to overcome cancer drug resistance," *Nature Communications*, vol. 9, no. 1, p. 562, 2018.

[15] X. Y. Gao Ting, Z. Xiaoying, C. Zhong, and Y. Jianping, "Mechanism of regulation of cell energy metabolism by mitochondrial lipoic acid synthesis," *Chinese Journal of Cell Biology*, vol. 40, no. 10, pp. 1767–1773, 2018.

[16] B. Dörsam and J. Fahrer, "The disulfide compound α-lipoic acid and its derivatives: a novel class of anticancer agents targeting mitochondria," *Cancer Letters*, vol. 371, no. 1, pp. 12–19, 2016.

[17] J. Liu, "The effects and mechanisms of mitochondrial nutrient α-lipoic acid on improving age-associated mitochondrial and cognitive dysfunction: an overview," *Neurochemical Research*, vol. 33, no. 1, pp. 194–203, 2008.

[18] Y. Guo, W. Qiu, T. E. Roche, and M. L. Hackert, "Crystal structure of the catalytic subunit of bovine pyruvate dehydrogenase phosphatase," *Acta Cryst*, vol. 76, no. 7, pp. 292–301, 2020.

[19] P. Phiboonchaiyanan and P. Chanvorachote, "Suppression of a cancer stem-like phenotype mediated by alpha-lipoic acid in human lung cancer cells through down-regulation of β-catenin and Oct-4," *Cellular Oncology*, vol. 40, no. 5, pp. 497–510, 2017.

[20] M. C. Cimolai, V. Vanasco, T. Marchini, N. D. Magnani, P. Evelson, and S. Alvarez, "α-Lipoic acid protects kidney from oxidative stress and mitochondrial dysfunction associated to inflammatory conditions," *Food &Function*, vol. 5, no. 12, pp. 3143–3150, 2014.

[21] S. Park, S. K. Choi, Y. Choi, and H. S. Moon, "AMPK/p53 axis is essential for α-lipoic acid–regulated metastasis in human and mouse colon cancer cells," *Journal of Investigative Medicine*, vol. 63, no. 7, pp. 882–885, 2015.

[22] S. J. Kim, H. S. Kim, and Y. R. Seo, "Understanding of ROS-inducing strategy in anticancer therapy," *Oxidative Medicine and Cellular Longevity*, vol. 2019, Article ID 5381692, 12 pages, 2019.

[23] X.-J. Yan, P. Xie, X.-F. Dai et al., "Dichloroacetate enhances the antitumor effect of pirarubicin via regulating the ROS-JNK signaling pathway in liver cancer cells," *Cancer Drug Resistance*, vol. 3, 2020.

[24] P. L. Pedersen, "Tumor mitochondria and the bioenergetics of cancer cells," *Progress in Experimental Tumor Research*, vol. 22, pp. 190–274, 1978.

[25] F. Seifert, E. Ciszak, L. Korotchkina et al., "Phosphorylation of serine 264 impedes active site accessibility in the E1 component of the human pyruvate dehydrogenase multienzyme complex," *Biochemistry*, vol. 46, no. 21, pp. 6277–6287, 2007.

[26] X. Deng, Q. Wang, M. Cheng et al., "Pyruvate dehydrogenase kinase 1 interferes with glucose metabolism reprogramming and mitochondrial quality control to aggravate stress damage in cancer," *Journal of Cancer*, vol. 11, no. 4, pp. 962–973, 2020.

[27] W. Sun, Z. Xie, Y. Liu et al., "JX06 selectively inhibits pyruvate dehydrogenase kinase PDK1 by a covalent cysteine modification," *Cancer Research*, vol. 75, no. 22, pp. 4923–4936, 2015.

[28] J. Bao, W. Yan, K. Xu et al., "Oleanolic acid decreases IL-1β-induced activation of fibroblast-like synoviocytes via the SIRT3-NF-κB axis in osteoarthritis," *Oxidative Medicine and Cellular Longevity*, vol. 2020, Article ID 7517219, 10 pages, 2020.

[29] B. Li, Y. Zhu, Q. Sun et al., "Reversal of the Warburg effect with DCA in PDGF-treated human PASMC is potentiated by pyruvate dehydrogenase kinase-1 inhibition mediated through blocking Akt/GSK-3β signalling," *International Journal of Molecular Medicine*, vol. 42, no. 3, pp. 1391–1400, 2018.

[30] F. Peng, J. H. Wang, W. J. Fan et al., "Glycolysis gatekeeper PDK1 reprograms breast cancer stem cells under hypoxia," *Oncogene*, vol. 37, no. 8, pp. 1062–1074, 2018.

[31] R. S. Heist and J. A. Engelman, "SnapShot: non-small cell lung cancer," *Cancer Cell*, vol. 21, no. 3, pp. 448–448.e2, 2012.

[32] A. Warth, "Diagnose, prognose und prädiktion nicht-kleinzelliger lungenkarzinome," *Der Pathologe*, vol. 36, Supplement 2, pp. 194–200, 2015.

[33] J. Kaplon, L. Zheng, K. Meissl et al., "A key role for mitochondrial gatekeeper pyruvate dehydrogenase in oncogene-induced senescence," *Nature*, vol. 498, no. 7452, pp. 109–112, 2013.

[34] M. Dodson, M. R. de la Vega, A. B. Cholanians, C. J. Schmidlin, E. Chapman, and D. D. Zhang, "Modulating NRF2 in disease: timing is everything," *Annual Review of Pharmacology and Toxicology*, vol. 59, no. 1, pp. 555–575, 2019.

[35] D. Tibullo, G. Li Volti, C. Giallongo et al., "Biochemical and clinical relevance of alpha lipoic acid: antioxidant and anti-inflammatory activity, molecular pathways and therapeutic potential," *Inflammation Research*, vol. 66, no. 11, pp. 947–959, 2017.

[36] B. Cosimelli, G. Greco, S. Laneri et al., "Identification of novel indole derivatives acting as inhibitors of the Keap1-Nrf2 interaction," *Journal of Enzyme Inhibition and Medicinal Chemistry*, vol. 34, no. 1, pp. 1152–1157, 2019.

[37] M. J. Bollong, G. Lee, J. S. Coukos et al., "A metabolite-derived protein modification integrates glycolysis with KEAP1-NRF2 signalling," *Nature*, vol. 562, no. 7728, pp. 600–604, 2018.

[38] D. Lastra, R. Fernandez-Gines, G. Manda, and A. Cuadrado, "Perspectives on the clinical development of NRF2-targeting drugs," *Handbook of Experimental Pharmacology*, vol. 264, pp. 93–141, 2021.

[39] W. Zhang, J. Su, H. Xu et al., "Dicumarol inhibits PDK1 and targets multiple malignant behaviors of ovarian cancer cells," *PLoS One*, vol. 12, no. 6, article e0179672, 2017.

Research Article

Molecular Basis for the Interactions of Human Thioredoxins with Their Respective Reductases

Md Faruq Hossain [iD],[1] **Yana Bodnar** [iD],[1] **Calvin Klein,**[1] **Clara Ortegón Salas,**[1] **Elias S. J. Arnér** [iD],[2,3] **Manuela Gellert** [iD],[1] **and Christopher Horst Lillig** [iD][1]

[1]*Institute for Medical Biochemistry and Molecular Biology, University Medicine Greifswald, Germany*
[2]*Department for Biochemistry, Karolinska Institutet, Stockholm, Sweden*
[3]*Department of Selenoprotein Research, National Institute of Oncology, Budapest, Hungary*

Correspondence should be addressed to Christopher Horst Lillig; horst@lillig.de

The mammalian cytosolic thioredoxin (Trx) system consists of Trx1 and its reductase, the NADPH-dependent seleno-enzyme TrxR1. These proteins function as electron donor for metabolic enzymes, for instance in DNA synthesis, and the redox regulation of numerous processes. In this work, we analysed the interactions between these two proteins. We proposed electrostatic complementarity as major force controlling the formation of encounter complexes between the proteins and thus the efficiency of the subsequent electron transfer reaction. If our hypothesis is valid, formation of the encounter complex should be independent of the redox reaction. In fact, we were able to confirm that also a redox inactive mutant of Trx1 lacking both active site cysteinyl residues (C32,35S) binds to TrxR1 in a similar manner and with similar kinetics as the wild-type protein. We have generated a number of mutants with alterations in electrostatic properties and characterised their interaction with TrxR1 in kinetic assays. For human Trx1 and TrxR1, complementary electrostatic surfaces within the area covered in the encounter complex appear to control the affinity of the reductase for its substrate Trx. Electrostatic compatibility was even observed in areas that do not form direct molecular interactions in the encounter complex, and our results suggest that the electrostatic complementarity in these areas influences the catalytic efficiency of the reduction. The human genome encodes ten cytosolic Trx-like or Trx domain-containing proteins. In agreement with our hypothesis, the proteins that have been characterised as TrxR1 substrates also show the highest similarity in their electrostatic properties.

1. Introduction

The thioredoxin (Trx) family of proteins comprises many key enzymes in redox signalling that catalyse specific reversible redox reactions, e.g., dithiol-disulphide exchange, (de-)glutathionylation, transnitrosylation, or peroxide reduction. The name giving protein, Trx, was first described in 1964 as electron donor for ribonucleotide reductase in *E. coli* [1, 2]; at least one functional thioredoxin system was proposed to have been encoded in the genome of LUCA, the last universal common ancestor of all live forms today [3]. Other family members include the glutaredoxins (Grx) and peroxiredoxins (Prx), often expressed in multiple isoforms in essentially all tissues, cells, and organelles [4–7]. The Trx family of pro-

teins is defined by a common structural motif that, in its most basic form, consists of a central four-stranded β-sheet surrounded by three alpha helices—the thioredoxin fold [8, 9]. Most Trxs are small proteins of approximately 12 kDa size, characterised by their highly conserved CGPC active site motif located on a loop connecting sheet 1 and helix 1 (in the most basic representation of the fold) [10, 11]. Trxs catalyse reversible thiol-disulphide exchange reactions. The reduction of protein disulphides, for instance, is initiated by a nucleophilic attack of the more N-terminal active site cysteinyl residue, characterised by a particularly low pK_a value, on a sulphur atom of the disulphide in the target protein. This results in an intermediate mixed disulphide that, in the second reaction step, is reduced by the C-terminal

cysteinyl residue, leading to the release of the reduced substrate and the formation of oxidized Trx, and for more details, see for instance [5, 12, 13]. Mammalian genomes encode approx. 20 Trxs or Trx domain-containing proteins [14]. From these, the cytosolic Trx1 (gene: TXN) is the one studied the most. Besides its two active site cysteinyl residues, cytosolic Trx1 possesses three additional structural cysteinyl residues that were implicated in regulatory function and Trx1-dimer formation [15, 16]. Trx1 does not contain a nuclear localization signal nor a signal peptide for secretion, but it was observed to translocate into the nucleus under certain conditions and also to be secreted in a nonclassic way, independent of its redox state [17–21].

Trx-oxidized active sites are reduced at the expense of NADPH by FAD-containing thioredoxin reductases (TrxR) [22]. Evolution has given rise to two classes of NADPH-dependent TrxRs: the low molecular weight (approx. 35 kDa) type and the high molecular weight (approx. 55 kDa) type [23, 24]. Both classes function as homodimers. The low molecular weight type is found in archaea, bacteria, and some eukaryota. The high molecular weight type is encoded in the genomes of higher eukaryotes including humans. Mammalian genomes encode three TrxRs: cytosolic TrxR1 (gene: TXNRD1), mitochondrial TrxR2 (gene: TXNRD2), and the thioredoxin-glutathione reductase TGR or TrxR3 (gene: TXNRD3) [25, 26]. Mammalian TrxRs are selenoproteins that form homodimers in a head-to-tail conformation. They belong to a family of pyridine-nucleotide-disulphide oxidoreductases that also includes, *e.g.*, glutathione reductase and trypanothione reductase [27]. They possess two active sites: one C-terminal GCUG motif and the N-terminal CVNVGC motif adjacent to the FAD domain. In contrast to their small molecular weight counterparts which have a high specificity for their endogenous substrate(s), these TrxRs accept a broad range of substrates [28], for human TrxR1 for instance Trx1, Grx2, and selenite; see overviews in [25, 29]. Electrons are transferred from NADPH to FAD and then to the N-terminal active site. Subsequently, the electrons are transferred to the selenocysteinyl residue containing C-terminal active site of the second protein in the dimeric TrxR and eventually to the target protein disulphides [30–32].

Numerous functions have been described for Trxs; see, *e.g.*, [33]. However, the proteins cannot randomly reduce all possible protein disulphides. Instead, they show a broad but distinct substrate/target specificity, which may also be the reason for the various isoforms and Trx domain-containing proteins encoded in the genomes of higher eukaryotes. Hypotheses for the different activities and substrate specificities of Trx family proteins included differences in redox potential [34, 35], the pK$_a$ values, *i.e.*, the nucleophilicity, of their more N-terminal active site cysteinyl residue [36], differences in overall dipole moments [37], and an increase in entropy as the major recognition force for Trx family protein target interactions [38].

Based on the analysis of *E. coli* phosphoadenylyl sulfate reductase, we have proposed that the specificity of protein-protein interactions is based mainly on two factors: first is geometric compatibility, and the second is electrostatic compatibility [39]. Based on electrostatic similarity, we have developed a mathematical approach to categorize Trx family proteins and to predict functions [14].

In this work, we propose that also the interaction of Trxs with their reductases is controlled by electrostatic compatibility. To address this hypothesis, we have analysed the interaction of the mammalian-type Trx1 with its reductase TrxR1. We have generated a number of mutants with alterations in electrostatic properties and characterised their interaction with TrxRs both *in silico* and *in vitro*; the formation and properties of the Trx1-TrxR1 enzyme-substrate complex were analysed with both wild-type proteins as well as mutants that exclude the thiol-disulphide/selenosulphide exchange reaction.

2. Material and Methods

2.1. Materials. Chemicals and enzymes were purchased at analytical grade or better from Sigma-Aldrich (St. Louis, MO, USA) unless otherwise stated.

2.2. Structural Analysis. Structures were acquired from the RSCB PDB Protein Data Bank (http://www.rcsb.org), and ligands and water molecules were removed using Pymol. The most representative structure of NMR ensembles was identified using UCSF Chimera [40]. The selected *in silico* mutations were inserted with the Dunbrack rotamer library [41] within the rotamer tool of Chimera; the rotamers with the highest probability were selected. The energy of the structure was minimized using Amberff14SB force field [42] after inserting a mutation in Chimera. The electrostatic calculations were performed as described before [14]. All the structures were preoriented in a way so that N-terminal active site cysteinyl residues face towards the camera perspective. These preoriented protein structures were then used to compute the electrostatic potential and the isosurfaces of the electrostatic potential. The addition of missing atoms and hydrogens, as well as the assignment of atomic charges and radii, was performed using pdb2pqr [43] applying the Amber force-field. VMD (visual molecular dynamics) [44] and APBS (Adaptive Poisson-Boltzmann Solver) [45] were used to compute the electrostatic potential in an aqueous solution containing 150 mM mobile ions, solvent dielectric constant: 78.54 at a temperature of 298.15 K. The electrostatic potential was mapped to the water accessible surface of the proteins from -4 to 4 $k_B \cdot T \cdot e^{-1}$ represented in red and blue colours, respectively. The isosurfaces of the electrostatic potential were computed from -1 to 1 $k_B \cdot T \cdot e^{-1}$ and also depicted in red and blue, respectively.

2.3. Cloning of Expression Constructs. Recombinant selenocysteine-containing rat TrxR1 (E. S. [46]) was used for all enzymatic assays, and the human TrxR U498C mutant [47] was used for all spectroscopic interaction studies, *i.e.*, CD and DSF. Human Trx1 was prepared as described in [48]. *E. coli* Trx1 and *E. coli* TrxR cDNAs were amplified by PCR from human cDNA and *E. coli* XL1 blue, respectively, using specific primers which were designed to insert

restriction sites for NdeI and BamHI (see supplementary table 1). The insert was ligated into the expression vector pET15b (Merck, Germany). All constructs and mutations were verified by sequencing (Microsynth Seqlab, Göttingen, Germany).

2.4. Mutagenesis. Three different groups of mutants were produced. Group I includes 10 mutants with changes in those particular residues that lead to perturbation at the immediate contact area of hTrx1 and hTrxR. Group II lists the mutants that change the electrostatic properties both in the immediate contact area and outside the contact area of hTrx1 and hTrxR. Group III includes the mutant which changes the electrostatic properties far away from the active site and immediate contact area. Mutations of the amino acid sequence and amplification of the plasmids were performed by rolling circle PCR. We generated the mutants using the indicated primers and the reversible complementary counterparts. Oligonucleotides are listed in supplementary table 1.

2.5. Recombinant Expression and Purification. Plasmids for recombinant expression of His-tagged Trx1 variants, *E. coli* TrxR, and human TrxR U498C were transformed into *E. coli* BL21 DE3 pRIL cells (Life Technologies, UK). Transformed cells were grown at 37°C in LB medium (Roth, Germany) with appropriate antibiotics to an optical density of 0.5 to 0.7 at 600 nm. Protein expression was induced by the addition of 0.5 mM isopropyl-1-thio-β-d-galactopyranoside (IPTG, Roth, Germany). The proteins were purified via immobilized metal affinity chromatography [49]. Size and purity of recombinantly expressed proteins were confirmed by SDS-PAGE using precasted TGX stain-free gels (4–20%, BioRad, Hercules, CA, USA). Pictures were taken following a five-minute UV-light activation.

2.6. Reduction of Proteins. The purified hTrx1 and mutant proteins were reduced with 10 mM TCEP (tris(2-carboxyethyl)phosphine) for 30 minutes and subsequently rebuffered in TE (50 mM Tris-HCl and 2 mM EDTA, pH 7.5) buffer using NAP-5 columns (GE Healthcare, UK). The rebuffered proteins were stored and kept reduced using immobilized TCEP disulphide reducing gel (Thermo Scientific, MA, USA) with a 2 : 1 ratio of sample volume to TCEP reducing gel volume. The protein and gel suspension was incubated at least 30 minutes rotating and centrifuged at $1000 \times g$ for 1 minute. Protein concentration in the supernatant was determined based on molar absorptivity at 280 nm ($\varepsilon_{hTrx1} = 6990 \, M^{-1} \cdot cm^{-1}$ and $\varepsilon_{hTrxR} = 64290 \, M^{-1} \cdot cm^{-1}$).

2.7. Kinetics of Insulin Reduction by Trx. The activity of hTrx1 and different mutants was determined by a plate-based NADPH depletion assay adapted from (E. S. J. [50]). The final reaction mixtures of 200 μl contained 50 mM Tris-EDTA buffer (pH 7.5), 150 μM NADPH, 160 μM insulin, 1.25 nM recombinant rat selenocysteine-containing TrxR and variable concentrations of Trx1, and mutant proteins (0-25 μM). NADPH consumption was measured at 340 nm for 80 minutes using the Clariostar plate reader (BMG Labtech, Offenburg, Germany). The linear range of the decrease in absorption was determined for each reaction individually.

Only reduced proteins were used in this assay. The specific activity of the recombinant selenocysteine-containing enzyme was approx. 100 min^{-1}. This was lower than reported before [30] and likely the result of a low degree of selenocysteine incorporation into the enzyme.

2.8. Differential Scanning Fluorimetry. Differential scanning fluorimetry (DSF) was performed in the CFX96 real-time PCR detection system from BioRad (Hercules, CA, USA) to obtain the dissociation constant and the thermal stability of the complex as described in [51]. All the proteins were desalted and rebuffered in Tris-EDTA buffer (50 mM Tris and 1 mM EDTA, pH 7.4) after purification using NAP-5 columns (GE Healthcare, UK) prior to this assay. The final reaction mixture of 50 μl contained 10 μM hTrxR protein, hTrx1 with variable concentrations (from 0 to 100 μM), Sypro Orange (1 : 500 diluted), and Tris-EDTA buffer. The reaction mixture was then heated with 0.3°C increments from 10.5 to 80°C. The increase in fluorescence due to binding of the dye to hydrophobic regions exposed during denaturation was recorded using the instrument's "FRET"-settings.

The melting temperatures of the thioredoxin reductase were obtained by fitting the first denaturation step (from 25.5°C to 42.6°C) with the Boltzmann fit (Eq. (1)), where FU is the measured fluorescence signal, T_m is the melting temperature, T is the temperature, and s is the slope.

$$FU = \frac{1}{1 + \exp \left(T_m - T/s \right)}. \tag{1}$$

The calculated melting temperatures were then plotted against the concentration of thioredoxin to obtain the EC$_{50}$ value, which in turn can be used to calculate the dissociation constant K_d as described in ref. [52]. For more details, see supplementary information.

2.9. CD Spectroscopy. CD spectra were recorded in 300 mM NaCl and 50 mM sodium phosphate, pH 8, with the proteins hTrxR and hTrx1 at 10 and 20 μM concentrations, respectively, using a Jasco J-810 spectropolarimeter from 190 nm to 240 nm at 25°C. Buffer-only spectra were subtracted. A standard sensitivity of 100 mdeg was used with a data pitch of 1 nm, 50 nm/min scanning speed, and 0.2 nm band width. In total, 10 spectra were accumulated for each sample. All the purified proteins were desalted and rebuffered in phosphate buffer (50 mM sodium phosphate and 300 mM NaCl, pH 8) using NAP-5 columns (GE Healthcare, UK) prior to CD spectroscopy.

2.10. Tryptophan Fluorescence. Fluorescence quenching assays were performed using a Perkin Elmer LS50B fluorimeter. The fluorescence signal was acquired at 25°C at the wavelength range from 310 to 498 nm with excitation at 296 nm. The slit width for excitation and emission was 6 and 4 nm, respectively. All purified proteins were desalted and rebuffered in Tris-EDTA buffer (50 mM Tris and 1 mM EDTA, pH 7.4) using NAP-5 columns (GE Healthcare, UK) prior to fluorescence quenching measurements.

2.11. All-Atom Molecular Dynamics Simulations. The crystal structures of TrxR and TrxR-Trx complex were obtained from the RCSB Protein Data Bank (PDB: 2ZZ0 and 3qfa, respectively) and then prepared for the simulations with the DockPrep tool of UCSF Chimera [40]. The MD simulations were performed in Gromacs 2016.3 [53], with AMBER-99ff-ILDN force field. The proteins and complexes were solvated with TIP3P water [54] in a cubic box under periodic boundary conditions and at least 1 nm away from the edge of the box. Na^+ and Cl^- ions were added to neutralize the charge of the system. An initial energy minimization was performed using the steepest descent algorithm until the system converged to $1000 \, kJ \cdot mol^{-1} \cdot nm^{-1}$. System equilibration was performed for 100 ps at a constant number of molecules, volume, and temperature 300 K (NVT) and for a duration of 100 ps with constant number of molecules, 1 bar pressure, and temperature 300 K (NPT). The duration of each production simulation was 50-250 ns (2 fs time steps). Simulations were repeated three times. The bonded interactions of hydrogens were constrained with LINCS algorithm [55]. The Parrinello-Rahman [56] method was used for pressure coupling and the modified Berendsen thermostat—velocity rescale [57] for the temperature coupling. The Particle Mesh Ewald [58] method was used for the calculation of the long-range electrostatic interactions; for the short-range interactions, Verlet cut-off scheme with 1.5 nm cut-off distance was applied, for both Coulomb- and van-der-Waals interactions. The parametrisation of FAD was done with Antechamber tool of AmberTools and ACPYPE [59] script with GAFF force field and Gasteiger charge methods. The RMSD and RMSF analyses of simulated data were performed with GROMACS-intern tools.

2.12. Statistical Analysis. All the numerical data are reported as mean ± SD unless otherwise stated. Statistical analyses were performed using one-way ANOVA followed by Tukey HSD test (Statistics Kingdom, Melbourne, Australia). A value of $p < 0.05$ was considered statistically significant.

2.13. Additional Software. All numerical calculations (spectra and kinetics) were performed and visualized using Grace (https://plasma-gate.weizmann.ac.il/Grace/). Structures were depicted using UCSF Chimera [40]. Picture panels and reaction schemes were generated using Inkscape (https://inkscape.org/).

3. Results

Based on previously published structures of the complexes between human Trx1 and TrxR1 [60], we have analysed the molecular interactions between the two proteins (Figure 1, supplementary Fig. 1). We have also included, for comparison, E. coli Trx1 and TrxR [61]. E. coli TrxR has a much narrower substrate specificity compared to the mammalian enzyme and cannot reduce human Trx1, while the mammalian-type TrxR1 can reduce both bacterial and mammalian Trxs (E. S. J. [50]). The first striking observation is the lower amount of molecular interactions (suppl. Fig. 1) and the smaller area of interaction, 448 versus 561 $Å^2$, in the

human complex (Figure 1(b)) compared to the bacterial (Figure 1(e)). We have computed the electrostatic properties of the proteins as outlined before [14] (Figures 1(c) and 1(f)). The isosurfaces of the electrostatic potentials at $\pm 1 \, k_B \cdot T \cdot e^{-1}$ (± 25.8 mV) of the interaction surfaces show an almost perfect complementarity in the immediate contact areas. Moreover, for the human complex, where only the left half of the Trx is in direct contact, as depicted in Figure 1(b), this is even true for the parts of the proteins that do not form direct molecular interactions (other than long-range electrostatic interactions), but only face each other (right side of the marked areas of the proteins in Figure 1(c)).

3.1. Trx and TrxR Interact Independently of the Redox Reaction and the Redox State of Trx. We proposed that electrostatic complementarity is the major distinguishing feature that controls the specific interactions of Trx family proteins with their target proteins. The electrostatic landscape of Trx family proteins shows only minor differences between their reduced and oxidized forms (Figures 2(a) and 2(b), respectively). Interactions of the proteins, i.e., the formation of an encounter complex preceding the thiol or thiol-selenol disulphide exchange reactions, should therefore be independent of the subsequent redox reaction. To test this hypothesis, we have generated an inactive mutant of Trx1, in which both active site cysteinyl residues were exchanged for seryl residues (C32,35S). Figures 2(a)–2(c) depict the electrostatic characteristics of the interaction interface of reduced, oxidized, and C32,35S human Trx1 calculated from experimentally determined structures demonstrating their similarity. We have confirmed a previous report that the redox-inactive C32,35S mutant is an inhibitor of the reduction of wild-type Trx1 by TrxR1 [62]. The mutant protein inhibits the reaction by competing with the oxidized wild-type protein for binding to the reduced reductase in the insulin reduction assay (Figure 2(d)). From a secondary Lineweaver-Burk plot (inset of Figure 2(d)), the K_i was determined as 5.3 $\mu mol \cdot l^{-1}$. Next, we analysed the complex formation by differential scanning fluorimetry (DSF, Figures 2(e)–2(h)). This method allows to determine dissociation constants by monitoring how a binding event influences the thermal stability of a protein. By fitting the data to the Boltzmann equation and plotting the log [Trx] against the T_m in Hill plots, we have obtained K_d values of 13.6 ± 1.6 and $9.8 \pm 0.3 \, \mu mol \cdot l^{-1}$ for the wild-type and mutant proteins, respectively Table 1. For further details of this approach, we refer to the supplementary material. All together, these similarities provide further evidence that both wild-type and C32,35S Trx1 interact with TrxR in the same way. Apparently, the interaction of the two proteins does not require Trx to be oxidized, nor the thiol-disulphide/selenosulphide exchange reaction to occur.

Fritz-Wolf et al. have presented a complex structure of the mixed-disulphide intermediate snapshot between the mutant proteins Trx1 C35S and TrxR1 U498C [60]. Since this complex was enforced by using mutated proteins, which was also possible for various other permutations of point mutants of Trx1 and TrxR1 [63], we have prepared complex structures of reduced wild-type and C32,35S Trx1 with TrxR1 U498C and analysed them as well as the two Trxs

(a)   (b)   (c)

(d)   (e)   (f)
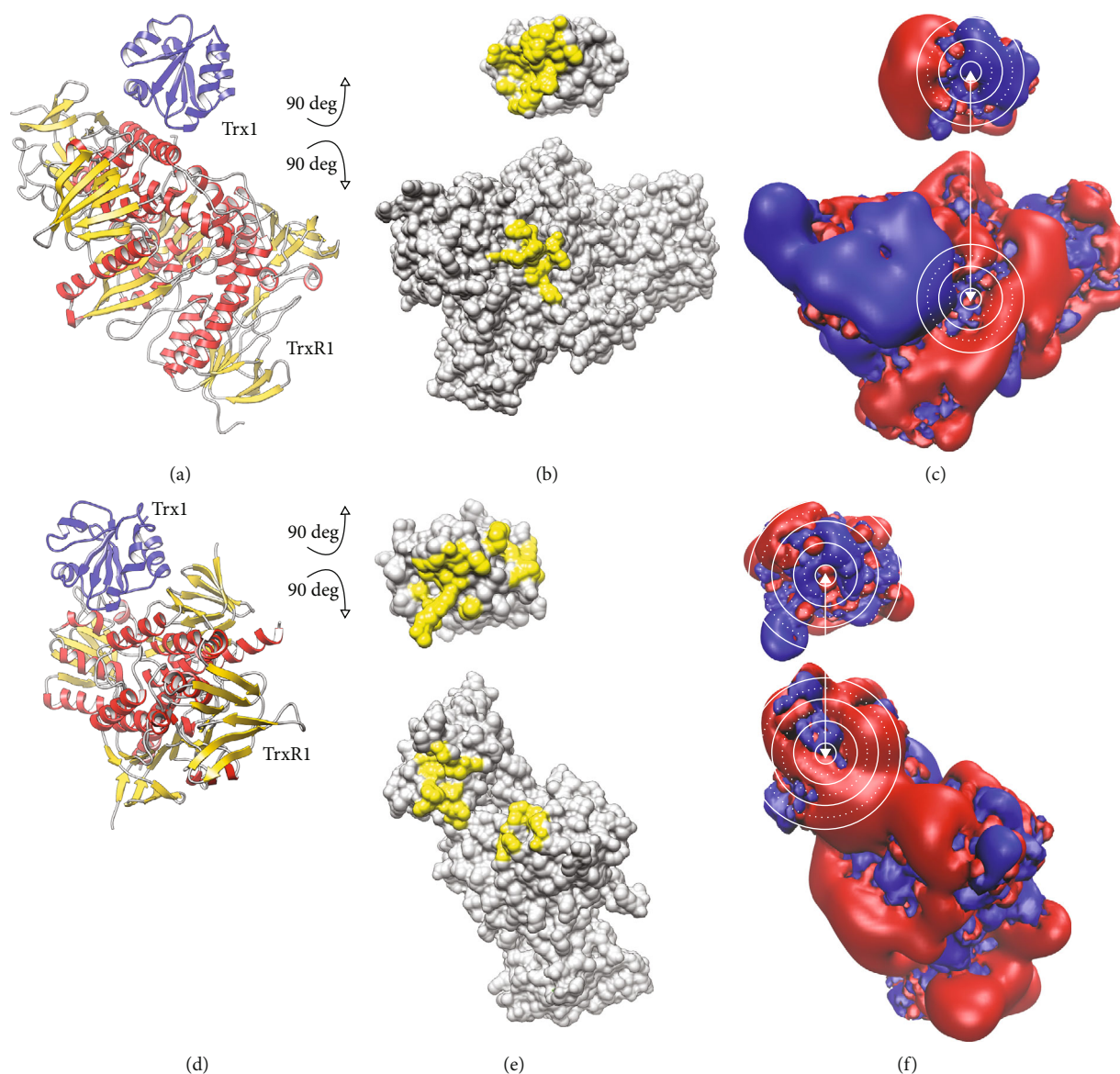
FIGURE 1: Molecular interaction surfaces of the human Trx1-TrxR1 and *E. coli* Trx1-TrxR complexes. Cartoon representation of the secondary structures of (a) human Trx1-TrxR1 complex PDB: 3qfa and (d) *E. coli* Trx1-TrxR complex PDB: 1f6m. The complex structure was opened by rotating both Trx and TrxR structures by 90° forward and backward, respectively. The contact patches with direct molecular contacts were highlighted in yellow using UCSF chimera (b, e). The isosurfaces of the electrostatic potential were depicted at ±1 $k_B \cdot T \cdot e^{-1}$ in blue (positive) and red (negative), respectively. The active site cysteinyl residues and interaction surfaces in the immediate contact area in both proteins were encircled in white lines (c, f).

alone by all-atom molecular dynamics simulations. Over the time course of 250 ns, both Trxs and both complexes behaved in a very similar way (Figures 3(a) and 3(b)). The average RMSD values of the Cα atoms during the last 150 ns of the simulations were 1.84 and 1.93 Å for the wild-type and C32,35S complexes, respectively. The RMSD between the two most representative complexes of wild-type and mutant was 2.42 Å (complexes are shown in Figure 3(d)). The fluctuation of the side chains was also very similar, both for the free redoxins as well as for the redoxins bound to TrxR1. In general, the fluctuations of the side chains within the contact area decreased in the complexes, especially in the area of the CxxC active site (Figure 3(c), RMSF).

Essentially all Trxs contain a tryptophanyl residue immediately before the N-terminal active site cysteinyl residue. TrxR1 residue W114 is located close to the active site selenocysteinyl (in our model system cysteinyl) residue. Binding of Trx1 to the reductase should thus decrease the solvent accessibility of these two indole ring systems. Compared to the simulation runs for the redoxins alone, the solvent accessible surface area of Trx1 W31 markedly decreased in the complexes from around 2 to 0.5 Å^2 (Figures 3(e) and 3(f)). Tryptophan indole ring systems exhibit solvatochromatic properties. In general, the fluorescence of tryptophanyl residues buried within a protein core or interaction surface is quenched due to aromatic-aromatic interactions or energy

(a)

(b)

(c)

(Trx1C32/35S)
- ● 0 μmol·l^{-1}
- ● 5 μmol·l^{-1}
- ● 10 μmol·l^{-1}

(d)

(e)

(f)

FIGURE 2: Continued.

(g)

(h)
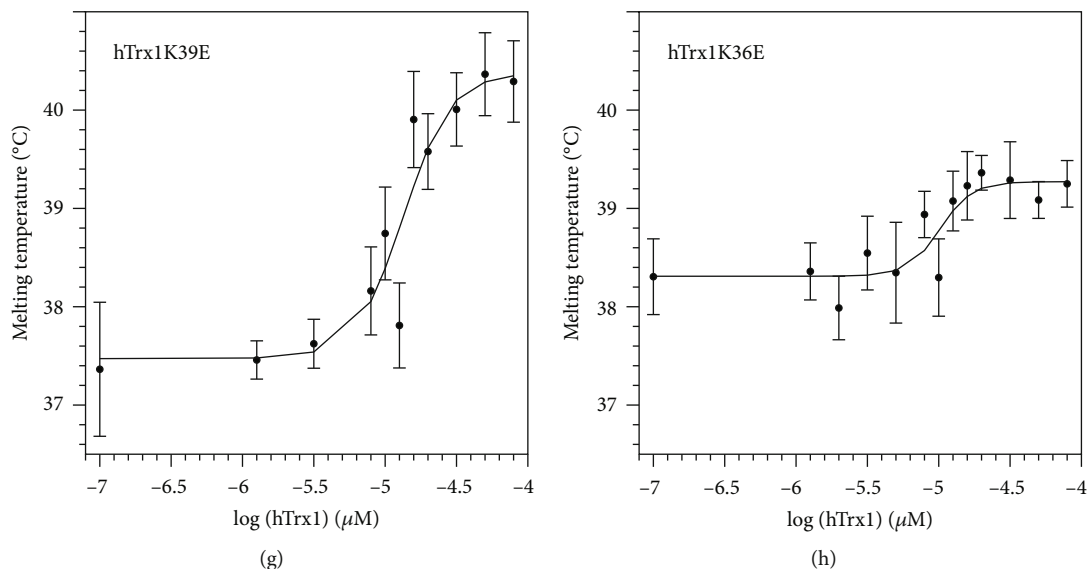
FIGURE 2: Comparison between the wild-type and double cysteinyl mutant of hTrx1 and its respective complex with hTrxR1. (a–c) Reduced and oxidized hTrx1WT compared to double cysteinyl mutant (a–c, respectively) in three different representations: (i) isosurfaces of the electrostatic potential at ± 1 $k_B \cdot T \cdot e^{-1}$ in blue (positive) and red (negative), (ii) electrostatic potential mapped on the solvent accessible surface at ± 4 $k_B \cdot T \cdot e^{-1}$, and (iii) secondary structure. (d) Lineweaver-Burk plot of inhibition kinetics measurements in the insulin reduction assay. The inset depicts the plot of the slope of the Lineweaver-Burk plots against the concentration of the redox-inactive mutant for the determination of the k_i. This assay was performed with the recombinant selenocysteine-containing TrxR. (e–h) Hill plots depicting the log [Trx] against the melting temperature (T_m) to determine the EC$_{50}$ and k_d values of the complexes. The T_m values were calculated form the original melting curves fitted to the Boltzmann equation; for further details, see supplementary material. These assays were performed using the U498C mutant of human TrxR1.

TABLE 1: Dissociation constants and binding energy determined for the interactions between Trx1 and TrxR1.

hTrx1 mutants	n	K_d μmol·l^{-1}	ΔG kJ·mol^{-1}	$\Delta\Delta G$ kJ·mol^{-1}
WT	12	13.60 ± 1.63	-27.79 ± 0.29	0
C32,35S	12	9.80 ± 0.31	-28.59 ± 0.2	-0.79
K36E	12	5.28 ± 0.08	-30.12 ± 0.03	-2.33
K39E	12	9.68 ± 1.25	-28.64 ± 0.31	-0.85

transfer to neighbouring charged groups; see for instance [64]. The decrease in solvent accessible area should thus quench the tryptophanyl fluorescence upon complex formation. We compared the changes of Trp fluorescence of both wild-type and C32,35S Trx1 upon complex formation with TrxR1 U498C. For both protein complexes, we recorded the expected fluorescence quenching (Figures 3(g) and 3(h)).

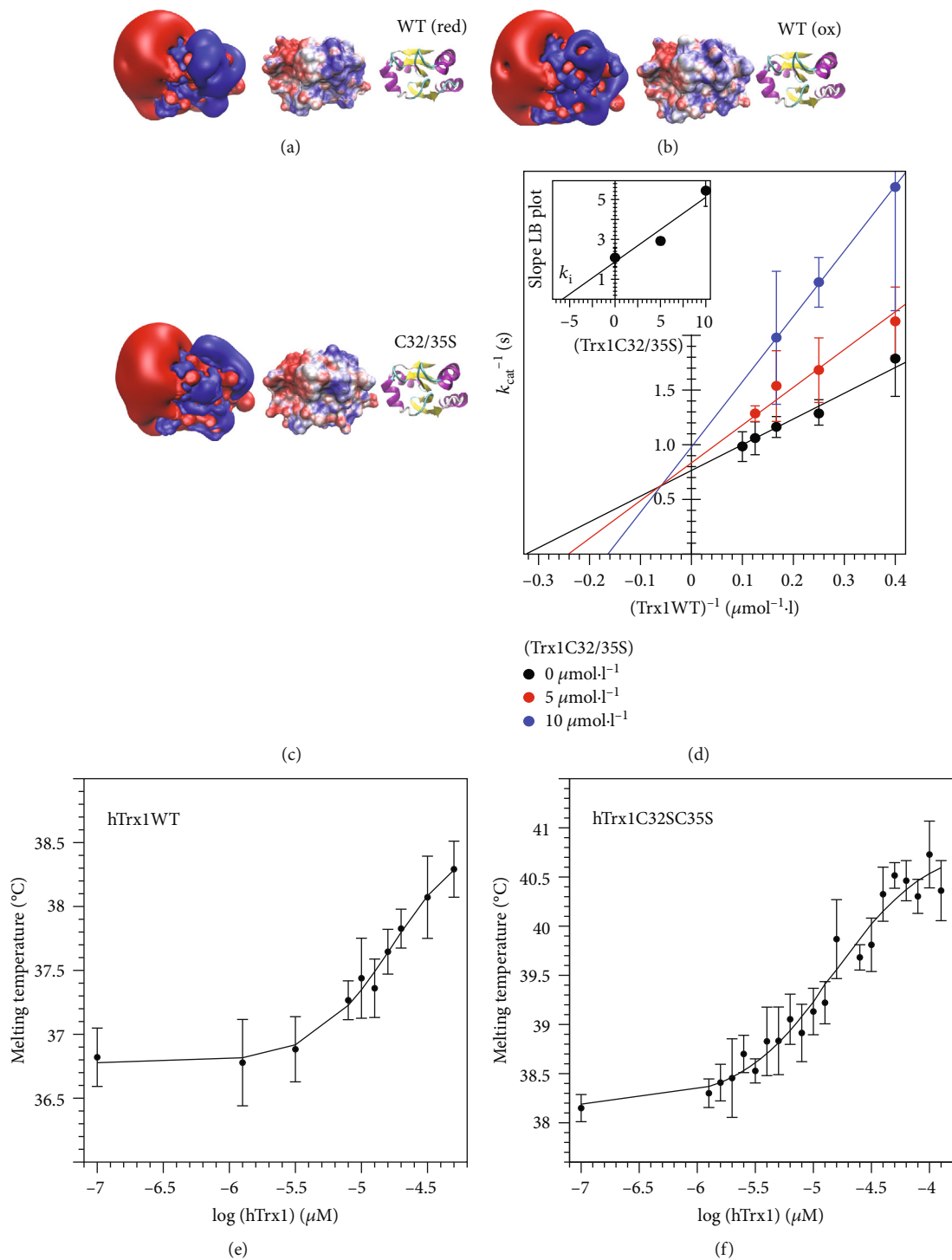Changes in the absorption properties of Trp residues may also induce changes in near and far UV circular dichroism (CD) spectra. We have thus analysed the binding of oxidized wild-type Trx1 and the active site cysteinyl double mutant to the selenocysteinyl to cysteinyl (U498C) mutant of TrxR by CD spectroscopy (supplementary Fig. 4). We have recorded the individual spectra of both proteins and compared the sum of both spectra to the ellipticity recorded for the proteins together, i.e., in an equilibrium reaction of the formation and dissociation of the enzyme-substrate complex. The insets of supplementary Fig. 4A and B depict the differences in ellipticity between the spectra of the complexes and the sum. Both

difference spectra do not display major differences; however, some smaller changes were found to be highly similar between the wild-type and C32,35S proteins when incubated with TrxR; these are slight increases in ellipticity at 205, 211, 217, and from 220 to 235 nm. While these changes do not prove complex formation per se, they provide further evidence that both the wild-type and mutant proteins interact with TrxR in a similar way.

3.2. Complementary Electrostatic Interaction Surfaces. To analyse the importance of complementary electrostatic interaction surfaces for the mammalian Trx1-TrxR redox couple, we have generated a number of Trx1 mutants that change the electrostatic potential (Figure 4): first, within the immediate contact area but, with one exception (K72), not involved in direct molecular interactions (for these, please see suppl. Fig. 2A-B); second, outside the immediate contact area but on the surface that faces the reductase; and third, one mutant with profound changes on the opposite side of the interaction surface (Figures 4(a) and 4(b)). Following recombinant expression in E. coli and purification applying immobilized metal affinity chromatography, we have confirmed the folding and stability of all mutants using differential scanning fluorimetry (suppl. Fig 3). Using a coupled assay with the reduction of insulin, to keep the Trx in the assay mix oxidized, we have analysed the reaction kinetics of recombinant selenocysteine-containing TrxR1 with these mutants as substrates, as summarized in Table 2 and Figure 5.

The mutations within or partly within the interaction surface (K36E; D60N; D58,60,61N; Q63R; and Q63R,K94E)

(a)

(b)

(c)

(d)

(e)

(f)

FIGURE 3: Continued.

(g)

(h)
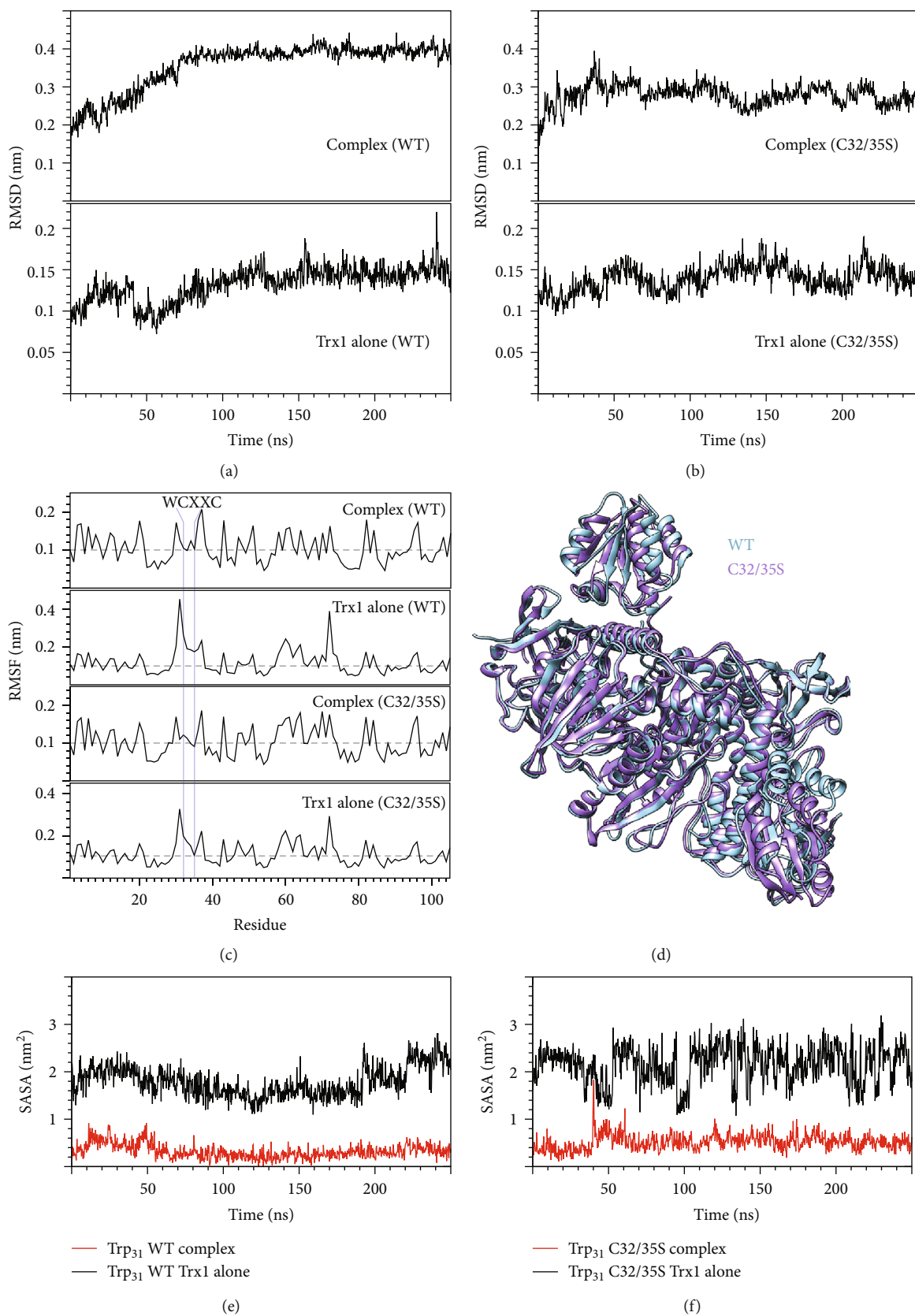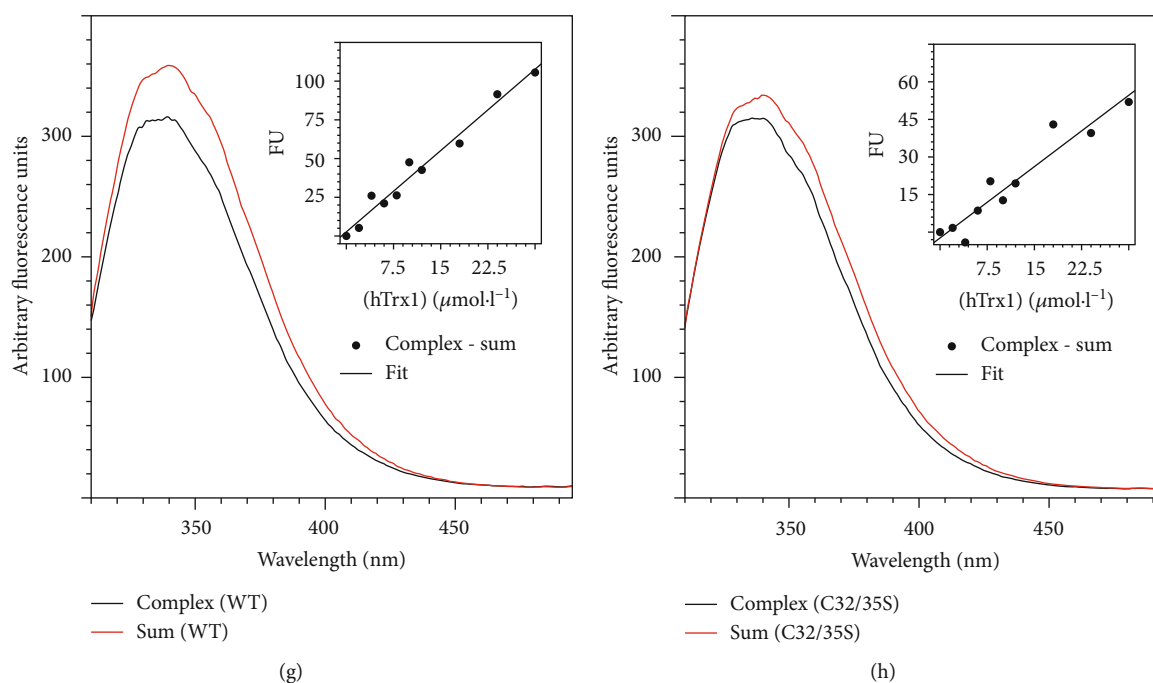
FIGURE 3: Molecular dynamics simulations of the TrxR-Trx complexes. (a, b) RMSD comparison of wild-type and C32,35S Trx alone (lower panels) and in complex with TrxR1 (top panels) over 250 ns. (c) Root-mean-square fluctuations of hTrx1 residues over 250 ns long MD simulation of wild-type and C32,35S Trx and the respective complexes with TrxR1. The active site cysteinyl residues are indicated (blue vertical lines). (d) Comparison of two representative structures from the 250 ns MD simulation of wild-type and cysteinyl double mutant complexes. The calculation of the representative structure was performed by Gromacs' clustering tool with RMSD cut-off of 0.2 nm. Superimpositioning was performed using UCSF Chimera's MatchMaker tool. (e, f) Solvent accessible surface area of W31 of hTrx1WT and hTrx1C32,35S in both complexes with hTrxR1 (red plot) and free (black plot) over 250 ns of MD simulation. (g, h) Fluorescence spectra of hTrx1-hTrxR1 U498C complexes (black) compared to the sum of the individually recorded spectra of hTrx1 and hTrxR1. The insets include the difference of the fluorescence signal between the complex- and sum spectra at 339.5 nm at different concentrations of thioredoxin.

mostly resulted in a significantly reduced catalytic efficiency of TrxR. This decreased efficiency was the result of an increase in K_M, i.e., a reduced affinity of TrxR for these proteins as substrates. The exception to this was the S67H mutation with only subtle changes to the electrostatic potential close to the N-terminal active site thiol (Figure 4). For this mutant, the catalytic efficiency did not change significantly. However, this was the result of both a significant decrease in K_M and k_{cat}. Two mutants with changes in their electrostatic characteristics outside the immediate contact surface but still facing TrxR (K39E and K94E) were analysed. For K39E, the catalytic efficiency did not change significantly. Again, this was the result of both a significant decrease in K_M and k_{cat}. The K94E mutant was the biggest surprise in our analysis. The changes (positive to negative) introduced here (see Figure 4) affected an area approx. 10 Å away from the active site thiol and the immediate contact area. Nevertheless, TrxR displayed the lowest catalytic efficiency with this mutant as a result of both an increase in K_M and a drop in k_{cat}. The double mutant Q63R,K94E that combines changes within and outside the area forming molecular interactions with TrxR (other than long-range electrostatic interactions) caused an increase in K_M and a decrease in k_{cat}, resulting in a catalytic efficiency comparable to those of the single mutants (Table 2). Changes in the electrostatic potential on the side opposite to the interaction surface of Trx1 (A17R,I53R) led to a small, but not significant, drop in k_{cat} and did not change the affinity of TrxR1 for this protein compared to the wild-type.

We have also tested some of our human Trx1 mutants, i.e., those that were more similar to E. coli Trx1 (Q63R,K94E; S67H; K72E; and K94E, see Figure 4 and suppl. Fig. 6) as substrate for the E. coli reductase. As the wild-type hTrx1, these failed to interact with the bacterial enzyme (suppl. Fig. 5).

3.3. Human Cytosolic Trxs and Trx Domains. The human genome encodes at least ten cytosolic Trxs or Trx domain-containing proteins, i.e., Trx1, Txndc2, 3, 6, 8, 9, and 17, Txnl1, and Nrx. To our knowledge, only Trx1, Txndc2, Txndc17 (also known as TRP14), and Txnl1 have been experimentally confirmed as substrates of TrxR1 [65–67]. Grx2, that is expressed in cytosolic and mitochondrial iso-forms [68], has also been characterised as substrate for TrxR1 [69]. Nrx (nucleoredoxin) has been suggested as TrxR1 inter-action partner [70]. Figure 6 summarizes the electrostatic similarity of these proteins. The highest similarity in the elec-trostatic properties was observed in the proteins that were
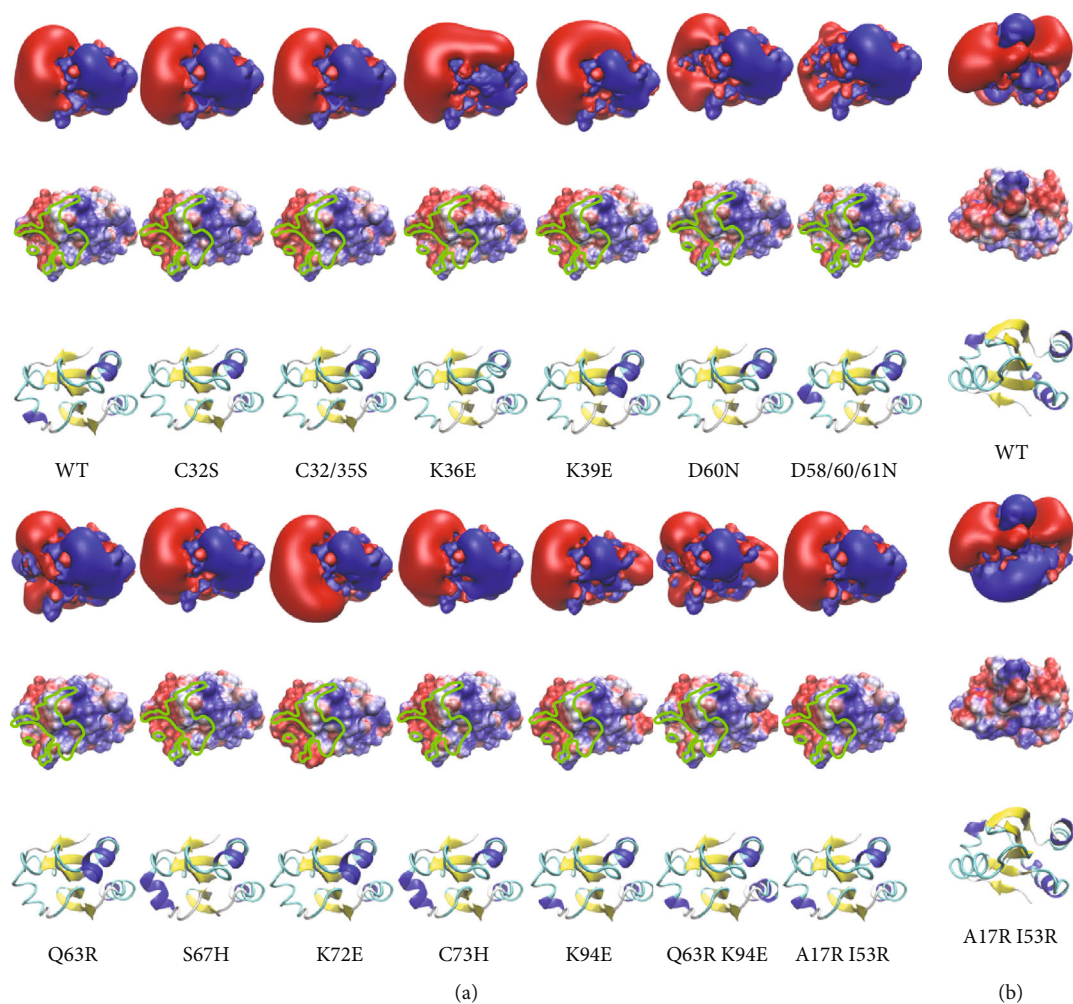
Figure 4: Overview of hTrx1 mutants in different representations. The first row shows the isosurfaces of the electrostatic potential at ±1 $k_B \cdot T \cdot e^{-1}$ in blue (positive) and red (negative), respectively. The second row shows the electrostatic potential mapped to the water accessible surface at ±4 $k_B \cdot T \cdot e^{-1}$. The third row displays the cartoon representation of the secondary structure of wild-type and mutant Trx1s (a, b). The immediate contact areas of interaction surfaces were circled in green in the second row of both panels (a). All the structures are oriented so that the N-terminal active site cysteinyl residues face towards the camera perspective (a) or rotated by 180° (b).

characterised as TrxR1 substrates before. Interestingly, Trxndc17 differs from the other redoxins significantly; however, it does show complementarity when rotated 180°, suggesting that this could reflect a unique mode of interaction with TrxR1 (suppl. Fig. 6).

4. Discussion

The results presented here confirm that the binding of Trx1 to TrxR1 is independent of a subsequent redox reaction between the proteins. Trx1 does not need to be in the oxidized disulphide form to bind to TrxR1. The redox-inactive Trx1 C32,35S, presumably always in a conformation that reflects reduced wild-type protein, binds to both reduced and oxidized TrxR1. The redox reaction-independent binding of Trx to its reductase has been reported before. In 1994, Oblong and coworkers first reported that human Trx1 C32,35S is a competitive inhibitor of the reduction of

wild-type Trx1 by TrxR with a K_i value of 6.7 μmol·l^{-1} [62], and the K_i of 5.3 μmol·l^{-1} estimated in this study is in good agreement with this. This value is close to the K_M of the enzyme for wild type Trx1 (2.4 μmol·l^{-1}), demonstrating that TrxR1 has similar affinities for both the wild-type and the redox-inactive mutant. Oblong and coworkers also reported detectable changes in CD spectra when wild-type and C32,C35S were bound to TrxR [62]. Subsequently, the C32,35S mutant has been characterised as a dominant negative mutant of the Trx system when overexpressed *in vivo*. For instance, in 1996, Gallegos et al. analysed the effect of Trx overexpression on the phenotype of breast cancer cells. They reported that wild-type Trx expression increased cell proliferation, but the expression of the C32,35S mutant inhibited cell growth and reversed the transformed phenotype of the cells. Xenografted into immunodeficient mice, wild-type Trx1 expression increased tumour formation, while expression of the redox-inactive mutant inhibited

TABLE 2: Kinetic analysis of the TrxR1 catalysed reduction of Trx1 variants in an insulin reduction-coupled assay.

Categories	hTrx1 mutants	n	K_M μmol·l^{-1}	k_{cat} s^{-1}	Catalytic efficiency %	mol·l^{-1}·s^{-1}
Wild-type	WT	43	2.43 ± 0.54	1.55 ± 0.42	100.00%	$6.38 \cdot 10^{-7}$
	K36E	13	$9.82 \pm 1.83^*$	1.33 ± 0.28	21.23%	$1.35 \cdot 10^{-7}$
	D60N	16	3.26 ± 1.76	1.19 ± 0.42	57.23%	$3.65 \cdot 10^{-7}$
	D58,60,61N	17	$5.83 \pm 2.05^*$	0.93 ± 0.16	25.01%	$1.6 \cdot 10^{-7}$
Inside or partly within the contact surface	Q63R	15	$6.37 \pm 1.57^*$	1.25 ± 0.57	30.76%	$1.96 \cdot 10^{-7}$
	S67H	18	$1.36 \pm 0.75^*$	$1.03 \pm 0.31^*$	118.73%	$7.57 \cdot 10^{-7}$
	K72E	18	2.22 ± 0.86	$1.99 \pm 0.39^*$	140.53%	$8.96 \cdot 10^{-7}$
	C73H	16	$1.24 \pm 0.36^*$	1.22 ± 0.17	154.25%	$9.84 \cdot 10^{-7}$
Mixed type	Q63R,K94E	15	$7.09 \pm 1.88^*$	$0.88 \pm 0.3^*$	19.46%	$1.24 \cdot 10^{-7}$
	K39E	18	$1.45 \pm 0.43^*$	$0.86 \pm 0.14^*$	92.98%	$5.93 \cdot 10^{-7}$
Outside the contact surface but facing TrxR	Q63R,K94E	15	$7.09 \pm 1.88^*$	$0.88 \pm 0.3^*$	19.46%	$1.24 \cdot 10^{-7}$
	K94E	6	$3.78 \pm 1.56^*$	$0.45 \pm 0.16^*$	18.66%	$1.19 \cdot 10^{-7}$
Opposite side	A17R,I53R	18	2.73 ± 0.49	1.24 ± 0.32	71.21%	$4.54 \cdot 10^{-7}$

tumour formation [71]. Yamamoto et al. reported in 2003 that transgenic cardiac-specific overexpression of the C32,35S mutant of Trx1 diminished the endogenous activity of Trx [72]. Oh et al. reported in 2004 the up- and downregulation of matrix metalloprotease 2 activities upon expression of wild-type and C32,35S Trx1, respectively, in human dermal fibroblasts [73]. More recently, Das reported on the effects of transgenic overexpression of both wild-type and C32,35S Trx1 in lung tissue. Wild-type Trx1 increased the resistance to hyperoxia-induced lung injury and increased the levels of reduced Trx in the lung. Overexpression of the redox-inactive mutant, however, decreased Trx activity and even increased the degree of oxidation of endogenous wild-type Trx in the tissue [74]. Taken together, these results demonstrate that the binding of Trx1 to TrxR is independent of the subsequent thiol-disulphide/selenosulphide exchange reaction and does not require Trx to be in the oxidized disulphide form.

Based on the analysis of the interaction of E. coli Trx and phosphoadenylyl sulfate (PAPS) reductase, Palde and Carroll suggested that Trxs recognize the oxidized form of its target proteins with higher selectivity compared to their reduced counterparts and that an increase in entropy may be a major recognition force for their interaction [38]. Based on this observation, the authors proposed a universal entropy-driven mechanism for thioredoxin-target recognition. It should, however, be mentioned that the Trx/PAPS redox couple may not be the most representative redox couple to study the importance of the individual redox states, because reduction and oxidation of PAPS reductase require extensive conformational changes of the protein [75–78]. For the Trx-TrxR redox couple discussed here, our results—as well as all the before mentioned evidence—imply that the redox state does not seem to have a major influence on the recognition and formation of a complex between the two proteins.

Peng et al. studied the reactivity of TrxA, TrxP, and TrxQ from Staphylococcus aureus with persulphidated pyruvate kinase as a model substrate. The three redoxins displayed small differences in substrate specificity that were also discussed to be the result of electrostatic differences in the area surrounding the N-terminal active site thiol [79]. We have previously proposed and provided evidence that the binding of Trx family proteins to their interaction partners and likely all protein-protein interactions in aqueous solution require geometrically compatible surfaces and, that given, are controlled by complementary electrostatic surfaces [14, 39, 80]. Here, we have engineered mutants of Trx1 with changes in their electrostatic potential landscape within and outside the contact patch with TrxR. In summary, the inversion of positive or negative potentials in areas that fell within the immediate contact area with TrxR1 decreased the affinity of the enzyme for its substrate without affecting k_{cat}. The subtle changes introduced with the S67H mutation close to the cysteinyl residue attacked by the selenol of TrxR in the reaction cycle decreased both K_M and k_{cat}. The effects of the reversals in the electrostatic potential outside the immediate contact surface but still facing TrxR depend on the positions. While the more negative potential "north" of the N-terminal active site cysteinyl residue (see Figures 1(c) and 2) did not change the catalytic efficiency of TrxR, and the positive to negative inversion 10 Å "east" of the active side (K94E) caused the largest decrease in catalytic efficiency. The positive potential of K94 faces complementary negative potentials on TrxR; however, the oxygen atoms of the hydroxyl and carboxy groups responsible for this negative potential are in 18-22 Å distance of the ε-amino group of K94. These distances exclude direct long-range electrostatic interactions as a potential explanation. Under the given conditions, these should only be significant until a distance of around 6 Å.
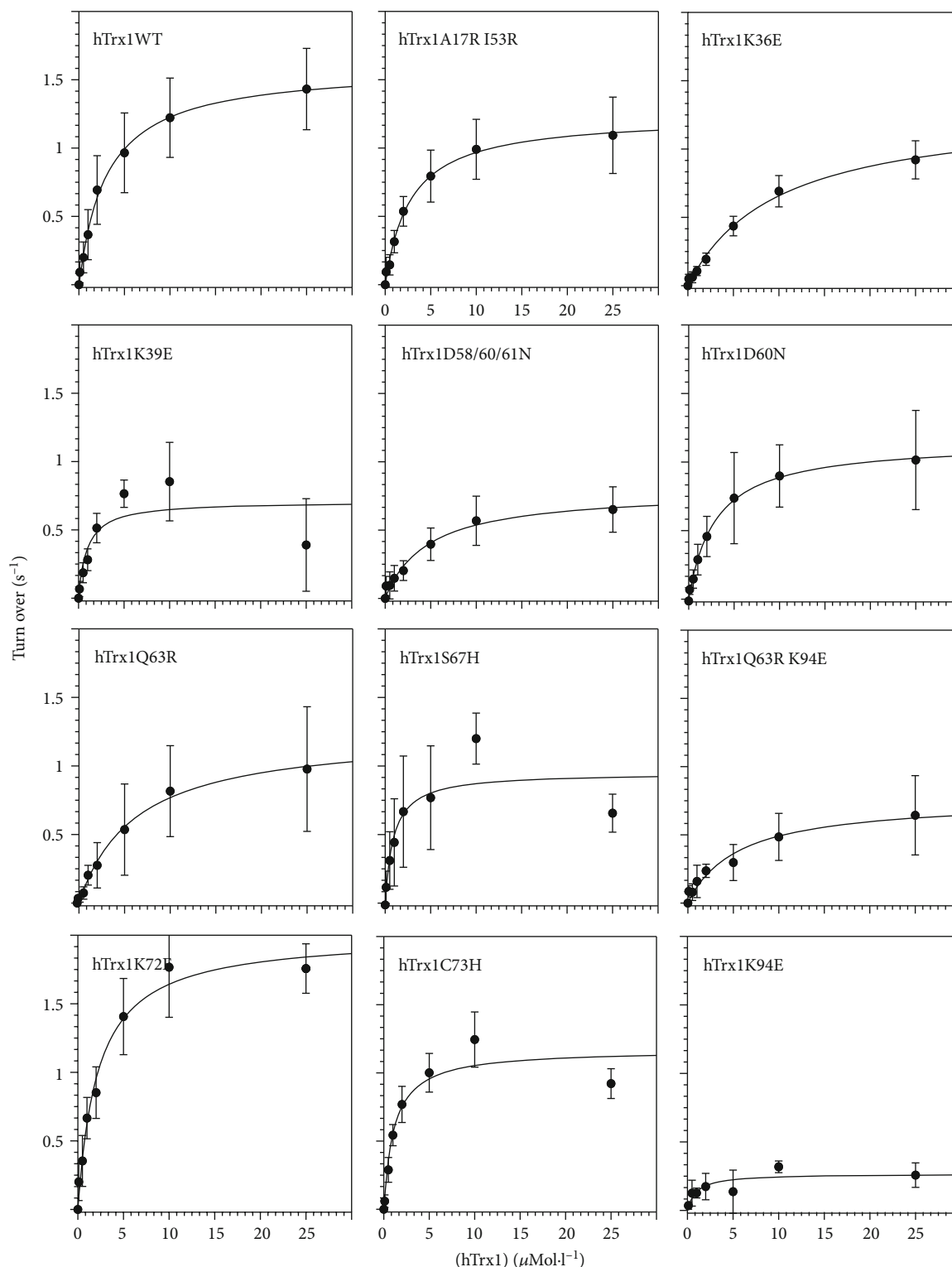
Figure 5: Kinetics of the reduction of the Trx1 mutants by TrxR. Michaelis-Menten plots for the proteins analysed. For details, *e.g.*, on statistics and number of independent experiments, see Table 1 of the main text. All data are shown as mean ± SD. The curves are the nonlinear curve fittings to the Michaelis-Menten equation from which the kinetic constants were obtained. These assays were performed with the recombinant selenocysteine-containing TrxR.

For our study, the tryptophanyl residues W31 and W114 of Trx1 and TrxR1, respectively, proved to be valuable for the analysis of the interaction between these two proteins. W114

of TrxR1 is an unusually reactive residue. If not part of the interaction surface with Trx, W114 is a solvent accessible residue susceptible to oxidation. It was suggested that this may
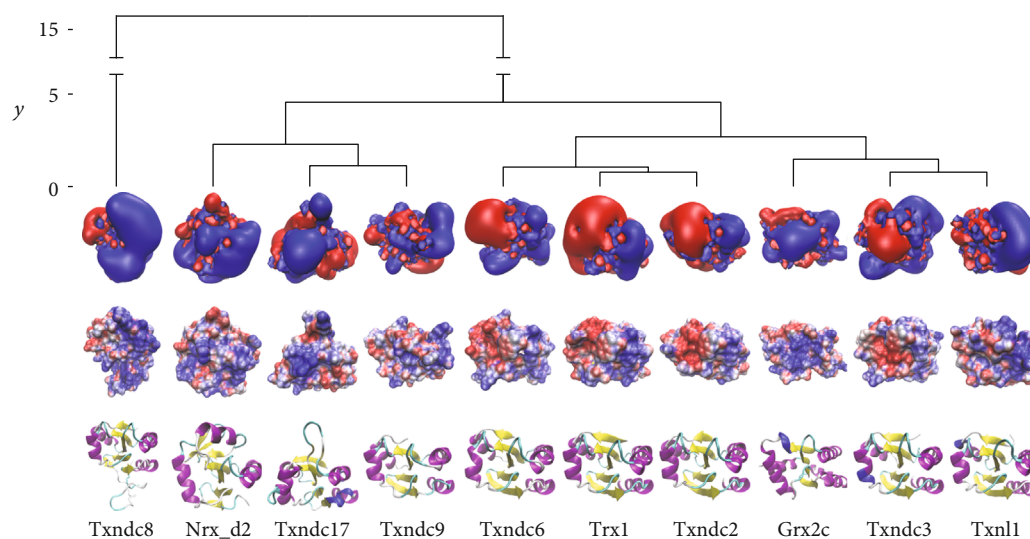
FIGURE 6: Electrostatic similarity of human cytosolic thioredoxins and thioredoxin domain-containing proteins. The tree of electrostatic similarity (on top) was prepared as described in [14]. The first row shows the isosurfaces of the electrostatic potential at $\pm 1\ k_B \cdot T \cdot e^{-1}$ in blue (positive) and red (negative), respectively. The second row shows the electrostatic potential mapped to the water accessible surface at $\pm 4\ k_B \cdot T \cdot e^{-1}$. The third row displays the cartoon representation of the secondary structure of wild-type and mutant Trxs. The orientation of the structures is the same as in Figures 1 and 4(a).

serve regulatory functions; it may also serve as an electron relay communicating with the FAD moiety. When oxidized, it facilitates oligomerisation of TrxR1 into tetramers that were also found in a crystal structure of TrxR1 [63]. Moreover, oxidatively modified W114 was suggested to contribute to covalently bonded, but not disulphide-linked, dimers between TRP14 and TrxR1 in cells [81].

Human and *E. coli* TrxR exhibit significant differences in their substrate specificities. While the human reductase accepts Trxs from different species and various low molecular weight compounds, *E. coli* TrxR is basically restricted to its endogenous Trx substrates, and for an overview, see (E. S. J. [50]). To some degree, especially for the reduction of low molecular weight compounds, this may be due to the higher reactivity of the selenolate active site in the human enzyme compared to the thiolate in its bacterial counterpart. Our study here provides a hypothesis for the distant specificities of the bacterial and mammalian reductases for Trxs. The *E. coli* enzyme requires significant more molecular interactions (see Figure 1 and suppl. Figs. 2C and D). The contact area is larger and concave. This requires a considerably higher degree of geometrical complementarity. Moreover, its electrostatic properties are more delicate and less binary compared to the human. The human genome encodes at least ten cytosolic Trxs or Trx domain-containing proteins, *i.e.*, Trx1, Txndc2, 3, 6, 8, 9, and 17, Txnl1, and Nrx. Trx1, Txndc2, and Txnl1 have been confirmed as substrates of TrxR1 [66, 67]. Txndc17 (also known as TRP14) was reported to be reduced efficiently by TrxR1 but not by TrxR2 ([65, 82], 14). This is in contrast to Trx1 that can be reduced by both reductases. Grx2, that is expressed in cytosolic and mitochondrial isoforms [68], has also been characterised as substrate for TrxR1 [69]. Nrx (nucleoredoxin) has been suggested as TrxR1 interaction partner [70]. Figure 6 summarizes the electrostatic similarity of these proteins. In

agreement with our hypothesis, the proteins that have been characterised as TrxR1 substrates also show the highest similarity in their electrostatic properties. The only exception to this is Txndc17 that is clearly more distant. In fact, the electrostatic properties of its interaction surface are basically the opposite to the other functional redoxins (see Figure 6 and suppl. Fig. 6). Since this ought to block any fruitful interaction with TrxRs, we propose that Txndc17 must interact in a different way with TrxR1 compared to the other proteins. If the orientation of the interaction surface of Txndc17 is rotated by 180°, a fruitful interaction may become possible (see suppl. Fig. 6). The lack of activity with TrxR2 may then be the result of geometric constrains that inhibit these alternative interactions, since the attack of the selenolate on the redoxin disulphide has to occur in an 180° angle in line with the disulphide. A high geometric and electrostatic complementarity is required for the binding of a Trx to *E. coli* TrxR. For the human TrxR1, the lower number of direct molecular interactions and its more protruding active site (see Figure 1(a)) may contribute to its ability to bind and reduce a greater variety of Trxs. With this decreased importance of geometric complementarity, the electrostatic compatibility may be the primary factor controlling the enzyme affinity for different redoxins as well as the efficiency of catalysis (see Figure 4 and Table 2). That is why the human enzyme also reduces *E. coli* Trx1 that only displays limited complementarity (see Figure 1 and suppl. Fig. 6), albeit with 14-fold lower affinity and 15.4-fold lower catalytic efficiency (E. S. J. [50]).

Conclusions

Our study provides new insights into the molecular interactions between human Trx1 and its reductase TrxR1. We confirmed that the transient protein-protein interactions, *i.e.*, the formation of an encounter complex between the proteins, are independent of the subsequent redox reaction. The

proteins must have an inherent affinity for each other in the area of the thiol-disulphide/selenosulphide exchange reaction controlling fruitful collisions in solution. The velocity of the reaction is too fast to be the result of random collisions between the proteins only. The only molecular forces that act in considerable distance in solution are electrostatic attraction and repulsion. For human Trx1 and TrxR1 electrostatic complementarity within the area covered in the encounter complex, it appears to control the affinity of the reductase for Trx, whereas electrostatic complementarity in areas outside this contact area can have a large influence on the catalytic efficiency.

Data Availability

All data not already contained with the manuscript will be made available by the corresponding author upon reasonable request.

Conflicts of Interest

The authors declare that they have no conflicts of interest.

Authors' Contributions

Md Faruq Hossain and Yana Bodnar contributed equally to this work.

Acknowledgments

Supplementary Materials

The following supplementary material is available separately: Supp. Table 1: oligonucleotides used in this study; further details on the K_d determination from the differential scanning fluorimetry data; Supp. Fig. 1: examples for the determination of T_m values; Supp. Fig. 2: molecular interactions between Trxs and their reductase; Supp. Fig. 3: thermal stability of the Trx mutants analysed in this study; Supp. Fig. 4: circular dichroism spectra of hTrx1-hTrxR1 complexes; Supp. Fig. 5: human Trx mutants as potential substrates of E. coli TrxR; Supp. Fig. 6: comparison of the electrostatic features of human TrxR1, TrxR2, E. coli TrxR, human Trx1, and Trp14, as well as E. coli Trx1; additional references. (Supplementary Materials)

References

[1] T. C. Laurent, E. C. Moore, and P. Reichard, "Enzymatic synthesis of deoxyribonucleotides. Iv. Isolation and characterization of thioredoxin, the hydrogen donor from *Escherichia coli* B," *The Journal of Biological Chemistry*, vol. 239, pp. 3436–3444, 1964.

[2] E. C. Moore, P. Reichard, and L. Thelander, "Enzymatic synthesis of deoxyribonucleotides.V. Purification and properties of thioredoxin reductase from *Escherichia coli* B," *The Journal of Biological Chemistry*, vol. 239, pp. 3445–3452, 1964.

[3] M. C. Weiss, F. L. Sousa, N. Mrnjavac et al., "The physiology and habitat of the last universal common ancestor," *Nature Microbiology*, vol. 1, no. 9, pp. 1–8, 2016.

[4] C. H. Lillig, C. Berndt, and A. Holmgren, "Glutaredoxin systems," *Biochimica et Biophysica Acta (BBA) - General Subjects*, vol. 1780, no. 11, pp. 1304–1317, 2008.

[5] C. H. Lillig and A. Holmgren, "Thioredoxin and related molecules from biology to health and disease," *Antioxidants & Redox Signaling*, vol. 9, no. 1, pp. 25–47, 2007.

[6] S. G. Rhee and H. A. Woo, "Multiple functions of peroxiredoxins: peroxidases, sensors and regulators of the intracellular messenger H_2O_2, and protein chaperones," *Antioxidants & Redox Signaling*, vol. 15, no. 3, pp. 781–794, 2011.

[7] M. D. Shelton, P. Boon Chock, and J. J. Mieyal, "Glutaredoxin: role in reversible protein S-glutathionylation and regulation of redox signal transduction and protein translocation," *Antioxidants & Redox Signaling*, vol. 7, no. 3–4, pp. 348–366, 2005.

[8] A. Holmgren, B. O. Söderberg, H. Eklund, and C. I. Brändén, "Three-dimensional structure of Escherichia coli thioredoxin-S2 to 2.8 A resolution," *Proceedings of the National Academy of Sciences of the United States of America*, vol. 72, no. 6, pp. 2305–2309, 1975.

[9] J. L. Martin, "Thioredoxin–a fold for all reasons," *Structure*, vol. 3, no. 3, pp. 245–250, 1995.

[10] A. Holmgren, "Thioredoxin. 6. The amino acid sequence of the protein from Escherichia coli B," *European Journal of Biochemistry/FEBS*, vol. 6, no. 4, pp. 475–484, 1968.

[11] A. Holmgren, "Thioredoxin," *Annual Review of Biochemistry*, vol. 54, no. 1, pp. 237–271, 1985.

[12] G. B. Kallis and A. Holmgren, "Differential reactivity of the functional sulfhydryl groups of cysteine-32 and cysteine-35 present in the reduced form of thioredoxin from *Escherichia coli*," *The Journal of Biological Chemistry*, vol. 255, no. 21, pp. 10261–10265, 1980.

[13] G. Roos, N. Foloppe, and J. Messens, "Understanding the pK(a) of redox cysteines: the key role of hydrogen bonding," *Antioxidants & Redox Signaling*, vol. 18, no. 1, pp. 94–127, 2013.

[14] M. Gellert, M. F. Hossain, F. J. F. Berens et al., "Substrate specificity of thioredoxins and glutaredoxins - towards a functional classification," *Heliyon*, vol. 5, no. 12, article e02943, 2019.

[15] S. I. Hashemy and A. Holmgren, "Regulation of the catalytic activity and structure of human thioredoxin 1 via oxidation and S-nitrosylation of cysteine residues," *The Journal of Biological Chemistry*, vol. 283, no. 32, pp. 21890–21898, 2008.

[16] A. Weichsel, J. R. Gasdaska, G. Powis, and W. R. Montfort, "Crystal structures of reduced, oxidized, and mutated human thioredoxins: evidence for a regulatory homodimer," *Structure*, vol. 4, no. 6, pp. 735–751, 1996.

[17] R. Bertini, O. M. Z. Howard, H.-F. Dong et al., "Thioredoxin, a redox enzyme released in infection and inflammation, is a unique chemoattractant for neutrophils, monocytes, and T cells," *The Journal of Experimental Medicine*, vol. 189, no. 11, pp. 1783–1789, 1999.

[18] K. Hirota, M. Murata, Y. Sachi et al., "Distinct roles of thioredoxin in the cytoplasm and in the nucleus. A two-step mechanism of redox regulation of transcription factor NF-KappaB," *The Journal of Biological Chemistry*, vol. 274, no. 39, pp. 27891–27897, 1999.

[19] A. Rubartelli, A. Bajetto, G. Allavena, E. Wollman, and R. Sitia, "Secretion of thioredoxin by normal and neoplastic cells through a leaderless secretory pathway," *The Journal of Biological Chemistry*, vol. 267, no. 34, pp. 24161–24164, 1992.

[20] M. Tanudji, S. Hevi, and S. L. Chuck, "The nonclassic secretion of thioredoxin is not sensitive to redox state," *American Journal of Physiology-Cell Physiology*, vol. 284, no. 5, pp. C1272–C1279, 2003.

[21] Y. Zhang, F. Chen, G. Tai et al., "TIGAR knockdown radiosensitizes TrxR1-overexpressing glioma in vitro and in vivo via inhibiting Trx1 nuclear transport," *Scientific Reports*, vol. 7, no. 1, article 42928, 2017.

[22] A. Holmgren and M. Björnstedt, "Thioredoxin and thioredoxin reductase," *Methods in Enzymology*, vol. 252, pp. 199–208, 1995.

[23] A. Holmgren, "Thioredoxin and glutaredoxin systems," *The Journal of Biological Chemistry*, vol. 264, no. 24, pp. 13963–13966, 1989.

[24] T. Sandalova, L. Zhong, Y. Lindqvist, A. Holmgren, and G. Schneider, "Three-dimensional structure of a mammalian thioredoxin reductase: implications for mechanism and evolution of a selenocysteine-dependent enzyme," *Proceedings of the National Academy of Sciences of the United States of America*, vol. 98, no. 17, pp. 9533–9538, 2001.

[25] E. S. J. Arnér, "Focus on mammalian thioredoxin reductases - important selenoproteins with versatile functions.," *Biochimica et Biophysica Acta*, vol. 1790, no. 6, pp. 495–526, 2009.

[26] J. Lu and A. Holmgren, "Selenoproteins," *Journal of Biological Chemistry*, vol. 284, no. 2, pp. 723–727, 2009.

[27] A. Argyrou and J. S. Blanchard, "Flavoprotein disulfide reductases: advances in chemistry and function," in *Progress in Nucleic Acid Research and Molecular Biology*, pp. 89–142, Academic Press, 2004.

[28] M. L. Tsang and J. A. Weatherbee, "Thioredoxin, glutaredoxin, and thioredoxin reductase from cultured HeLa cells," *Proceedings of the National Academy of Sciences of the United States of America*, vol. 78, no. 12, pp. 7478–7482, 1981.

[29] J. Lu, C. Berndt, and A. Holmgren, "Metabolism of selenium compounds catalyzed by the mammalian selenoprotein thioredoxin reductase," *Biochimica et Biophysica Acta (BBA) - General Subjects*, vol. 1790, no. 11, pp. 1513–1519, 2009.

[30] Q. Cheng, T. Sandalova, Y. Lindqvist, and E. S. J. Arnér, "Crystal structure and catalysis of the selenoprotein thioredoxin reductase 1," *Journal of Biological Chemistry*, vol. 284, no. 6, pp. 3998–4008, 2009.

[31] L. Zhong, E. S. J. Arnér, and A. Holmgren, "Structure and mechanism of mammalian thioredoxin reductase: the active site is a redox-active selenolthiol/selenenylsulfide formed from the conserved cysteine-selenocysteine sequence," *Proceedings of the National Academy of Sciences of the United States of America*, vol. 97, no. 11, pp. 5854–5859, 2000.

[32] L. Zhong and A. Holmgren, "Essential role of selenium in the catalytic activities of mammalian thioredoxin reductase revealed by characterization of recombinant enzymes with selenocysteine mutations," *Journal of Biological Chemistry*, vol. 275, no. 24, pp. 18121–18128, 2000.

[33] E.-M. Hanschmann, J. R. Godoy, C. Berndt, C. Hudemann, and C. H. Lillig, "Thioredoxins, glutaredoxins, and peroxiredoxins–molecular mechanisms and health significance: from cofactors to antioxidants to redox signaling," *Antioxidants & Redox Signaling*, vol. 19, no. 13, pp. 1539–1605, 2013.

[34] M. Hirasawa, P. Schürmann, J. P. Jacquot et al., "Oxidation-reduction properties of chloroplast thioredoxins, ferredoxin:thioredoxin reductase, and thioredoxin f-regulated enzymes," *Biochemistry*, vol. 38, no. 16, pp. 5200–5205, 1999.

[35] M. Huber-Wunderlich and R. Glockshuber, "A single dipeptide sequence modulates the redox properties of a whole enzyme family," *Folding & Design*, vol. 3, no. 3, pp. 161–171, 1998.

[36] K. S. Jensen, J. T. Pedersen, J. R. Winther, and K. Teilum, "The pKa value and accessibility of cysteine residues are key determinants for protein substrate discrimination by glutaredoxin," *Biochemistry*, vol. 53, no. 15, pp. 2533–2540, 2014.

[37] V. Bunik, G. Raddatz, S. Lemaire, Y. Meyer, J. P. Jacquot, and H. Bisswanger, "Interaction of thioredoxins with target proteins: role of particular structural elements and electrostatic properties of thioredoxins in their interplay with 2-oxoacid dehydrogenase complexes," *Protein Science: A Publication of the Protein Society*, vol. 8, no. 1, pp. 65–74, 1999.

[38] P. B. Palde and K. S. Carroll, "A universal entropy-driven mechanism for thioredoxin-target recognition," *Proceedings of the National Academy of Sciences of the United States of America*, vol. 112, no. 26, pp. 7960–7965, 2015.

[39] C. Berndt, J.-D. Schwenn, and C. H. Lillig, "The specificity of thioredoxins and glutaredoxins is determined by electrostatic and geometric complementarity," *Chemical Science*, vol. 6, no. 12, pp. 7049–7058, 2015.

[40] E. F. Pettersen, T. D. Goddard, C. C. Huang et al., "UCSF chimera–a visualization system for exploratory research and analysis," *Journal of Computational Chemistry*, vol. 25, no. 13, pp. 1605–1612, 2004.

[41] M. V. Shapovalov and R. L. Dunbrack Jr., "A smoothed backbone-dependent rotamer library for proteins derived from adaptive kernel density estimates and regressions," *Structure*, vol. 19, no. 6, pp. 844–858, 2011.

[42] J. A. Maier, C. Martinez, K. Kasavajhala, L. Wickstrom, K. E. Hauser, and C. Simmerling, "Ff14SB: improving the accuracy of protein side chain and backbone parameters from Ff99SB," *Journal of Chemical Theory and Computation*, vol. 11, no. 8, pp. 3696–3713, 2015.

[43] T. J. Dolinsky, P. Czodrowski, H. Li et al., "PDB2PQR: expanding and upgrading automated preparation of biomolecular structures for molecular simulations," *Nucleic Acids Research*, vol. 35, pp. W522–W525, 2007.

[44] W. Humphrey, A. Dalke, and K. Schulten, "VMD: visual molecular dynamics," *Journal of Molecular Graphics*, vol. 14, no. 1, pp. 33–38, 1996, 27–28.

[45] N. A. Baker, D. Sept, S. Joseph, M. J. Holst, and J. A. McCammon, "Electrostatics of nanosystems: application to microtubules and the ribosome," *Proceedings of the National Academy of Sciences of the United States of America*, vol. 98, no. 18, pp. 10037–10041, 2001.

[46] E. S. Arnér, H. Sarioglu, F. Lottspeich, A. Holmgren, and A. Böck, "High-level expression in Escherichia coli of selenocysteine-containing rat thioredoxin reductase utilizing gene fusions with engineered bacterial-type SECIS elements and co-expression with the selA, selB and selC genes," *Journal of Molecular Biology*, vol. 292, no. 5, pp. 1003–1016, 1999.

[47] S. Urig, J. Lieske, K. Fritz-Wolf, A. Irmler, and K. Becker, "Truncated mutants of human thioredoxin reductase 1 do not exhibit glutathione reductase activity," *FEBS Letters*, vol. 580, no. 15, pp. 3595–3600, 2006.

[48] D. Su, C. Berndt, D. E. Fomenko, A. Holmgren, and V. N. Gladyshev, "A conserved cis-proline precludes metal binding by the active site thiolates in members of the thioredoxin family of proteins," *Biochemistry*, vol. 46, no. 23, pp. 6903–6910, 2007.

[49] D. L. Wilkinson, N. T. Ma, C. Haught, and R. G. Harrison, "Purification by immobilized metal affinity chromatography of human atrial natriuretic peptide expressed in a novel thioredoxin fusion protein," *Biotechnology Progress*, vol. 11, no. 3, pp. 265–269, 1995.

[50] E. S. J. Arnér and A. Holmgren, "Measurement of thioredoxin and thioredoxin reductase," *Current Protocols in Toxicology*, vol. 24, no. 1, pp. 7.4.1–7.4.14, 2005.

[51] U. B. Ericsson, B. Martin Hallberg, G. T. Detitta, N. Dekker, and P. Nordlund, "Thermofluor-based high-throughput stability optimization of proteins for structural studies," *Analytical Biochemistry*, vol. 357, no. 2, pp. 289–298, 2006.

[52] N. Bai, H. Roder, A. Dickson, and J. Karanicolas, "Isothermal analysis of ThermoFluor data can readily provide quantitative binding affinities," *Scientific Reports*, vol. 9, no. 1, 2019.

[53] D. SpoelVan Der, E. Lindahl, B. Hess, G. Groenhof, A. E. Mark, and H. J. C. Berendsen, "GROMACS: fast, flexible, and free," *Journal of Computational Chemistry*, vol. 26, no. 16, pp. 1701–1718, 2005.

[54] K. Lindorff-Larsen, S. Piana, K. Palmo et al., "Improved side-chain torsion potentials for the Amber Ff99SB protein force field," *Proteins*, vol. 78, no. 8, pp. 1950–1958, 2010.

[55] B. Hess, H. Bekker, H. J. C. Berendsen, and J. G. E. M. Fraaije, "LINCS: a linear constraint solver for molecular simulations," *Journal of Computational Chemistry*, vol. 18, no. 12, pp. 1463–1472, 1997.

[56] M. Parrinello and A. Rahman, "Polymorphic transitions in single crystals: a new molecular dynamics method," *Journal of Applied Physics*, vol. 52, no. 12, pp. 7182–7190, 1981.

[57] G. Bussi, D. Donadio, and M. Parrinello, "Canonical sampling through velocity rescaling," *Journal of Chemical Physics*, vol. 126, no. 1, p. 014101, 2007.

[58] T. Darden, D. York, and P. Lee, "Particle mesh Ewald: an N·log (N) method for Ewald sums in large systems," *The Journal of Chemical Physics*, vol. 98, no. 12, pp. 10089–10092, 1993.

[59] S. da Silva, W. Alan, and W. F. Vranken, "ACPYPE - antechamber python parser interface," *BMC Research Notes*, vol. 5, no. 1, p. 367, 2012.

[60] K. Fritz-Wolf, S. Kehr, M. Stumpf, S. Rahlfs, and K. Becker, "Crystal structure of the human thioredoxin reductase-thioredoxin complex," *Nature Communications*, vol. 2, no. 1, p. 383, 2011.

[61] B. W. Lennon, C. H. Williams, and M. L. Ludwig, "Twists in catalysis: alternating conformations of Escherichia coli thioredoxin reductase," *Science*, vol. 289, no. 5482, pp. 1190–1194, 2000.

[62] J. E. Oblong, M. Berggren, P. Y. Gasdaska, and G. Powis, "Site-directed mutagenesis of active site cysteines in human thioredoxin produces competitive inhibitors of human thioredoxin reductase and elimination of mitogenic properties of thioredoxin," *The Journal of Biological Chemistry*, vol. 269, no. 16, pp. 11714–11720, 1994.

[63] J. Xu, S. E. Eriksson, M. Cebula et al., "The conserved Trp114 residue of thioredoxin reductase 1 has a redox sensor-like function triggering oligomerization and crosslinking upon oxidative stress related to cell death," *Cell Death & Disease*, vol. 6, no. 1, article e1616, 2015.

[64] G. Hernández-Alcántara, A. Rodríguez-Romero, H. Reyes-Vivas et al., "Unraveling the mechanisms of tryptophan fluorescence quenching in the triosephosphate isomerase from Giardia lamblia," *Biochimica et Biophysica Acta*, vol. 1784, no. 11, pp. 1493–1500, 2008.

[65] W. Jeong, H. W. Yoon, S.-R. Lee, and S. G. Rhee, "Identification and characterization of TRP14, a thioredoxin-related protein of 14 kDa. New insights into the specificity of thioredoxin function," *The Journal of Biological Chemistry*, vol. 279, no. 5, pp. 3142–3150, 2004.

[66] A. Miranda-Vizuete, J. A. Gustafsson, and G. Spyrou, "Molecular cloning and expression of a CDNA encoding a human thioredoxin-like protein," *Biochemical and Biophysical Research Communications*, vol. 243, no. 1, pp. 284–288, 1998.

[67] A. Miranda-Vizuete, J. Ljung, A. E. Damdimopoulos et al., "Characterization of Sptrx, a novel member of the thioredoxin family specifically expressed in human spermatozoa," *The Journal of Biological Chemistry*, vol. 276, no. 34, pp. 31567–31574, 2001.

[68] M. E. Lönn, C. Hudemann, C. Berndt et al., "Expression pattern of human glutaredoxin 2 isoforms: identification and characterization of two testis/cancer cell-specific isoforms," *Antioxidants & Redox Signaling*, vol. 10, no. 3, pp. 547–558, 2008.

[69] C. Johansson, C. H. Lillig, and A. Holmgren, "Human mitochondrial glutaredoxin reduces S-glutathionylated proteins with high affinity accepting electrons from either glutathione or thioredoxin reductase," *The Journal of Biological Chemistry*, vol. 279, no. 9, pp. 7537–7543, 2004.

[70] C. Urbainsky, R. Nölker, M. Imber et al., "Nucleoredoxin-dependent targets and processes in neuronal cells," *Oxidative Medicine and Cellular Longevity*, vol. 2018, Article ID 4829872, 11 pages, 2018.

[71] A. Gallegos, J. R. Gasdaska, C. W. Taylor et al., "Transfection with human thioredoxin increases cell proliferation and a dominant-negative mutant thioredoxin reverses the transformed phenotype of human breast cancer cells," *Cancer Research*, vol. 56, no. 24, pp. 5765–5770, 1996.

[72] M. Yamamoto, G. Yang, C. Hong et al., "Inhibition of endogenous thioredoxin in the heart increases oxidative stress and cardiac hypertrophy," *The Journal of Clinical Investigation*, vol. 112, no. 9, pp. 1395–1406, 2003.

[73] J.-H. Oh, A.-S. Chung, H. Steinbrenner, H. Sies, and P. Brenneisen, "Thioredoxin secreted upon ultraviolet A irradiation modulates activities of matrix metalloproteinase-2 and tissue inhibitor of metalloproteinase-2 in human dermal fibroblasts," *Archives of Biochemistry and Biophysics*, vol. 423, no. 1, pp. 218–226, 2004.

[74] K. C. Das, "Thioredoxin-deficient mice, a novel phenotype sensitive to ambient air and hypersensitive to hyperoxia-induced lung injury," *American Journal of Physiology-Lung Cellular and Molecular Physiology*, vol. 308, no. 5, pp. L429–L442, 2015.

[75] C. H. Lillig, A. Potamitou, J.-D. Schwenn, A. Vlamis-Gardikas, and A. Holmgren, "Redox regulation of 3'-phosphoadenylylsulfate reductase from Escherichia coli by

glutathione and glutaredoxins," *The Journal of Biological Chemistry*, vol. 278, no. 25, pp. 22325–22330, 2003.

[76] C. H. Lillig, A. Prior, J. D. Schwenn et al., "New thioredoxins and glutaredoxins as electron donors of 3'-phosphoadenylylsulfate reductase," *The Journal of Biological Chemistry*, vol. 274, no. 12, pp. 7695–7698, 1999.

[77] G. Montoya, C. Svensson, H. Savage, J. D. Schwenn, and I. Sinning, "Crystallization and preliminary X-ray diffraction studies of phospho-adenylylsulfate (PAPS) reductase from E. coli," *Acta Crystallographica Section D Biological Crystallography*, vol. 54, no. 2, pp. 281–283, 1998.

[78] J. D. Schwenn and U. Schriek, "PAPS-reductase from Escherichia coli: characterization of the enzyme as probe for thioredoxins," *Zeitschrift für Naturforschung C*, vol. 42, no. 1–2, pp. 93–102, 1987.

[79] H. Peng, Y. Zhang, J. C. Trinidad, and D. P. Giedroc, "Thioredoxin profiling of multiple thioredoxin-like proteins in Staphylococcus aureus," *Frontiers in Microbiology*, vol. 9, p. 2385, 2018.

[80] M. Deponte and C. H. Lillig, "Enzymatic control of cysteinyl thiol switches in proteins," *Biological Chemistry*, vol. 396, no. 5, pp. 401–413, 2015.

[81] S. Prast-Nielsen, M. Cebula, I. Pader, and E. S. J. Arnér, "Noble metal targeting of thioredoxin reductase–covalent complexes with thioredoxin and thioredoxin-related protein of 14 kDa triggered by cisplatin," *Free Radical Biology & Medicine*, vol. 49, no. 11, pp. 1765–1778, 2010.

[82] I. Pader, R. Sengupta, M. Cebula et al., "Thioredoxin-related protein of 14 kDa is an efficient L-cystine reductase and S-denitrosylase," *Proceedings of the National Academy of Sciences of the United States of America*, vol. 111, no. 19, pp. 6964–6969, 2014.

Review Article

HIF-1, the Warburg Effect, and Macrophage/Microglia Polarization Potential Role in COVID-19 Pathogenesis

Elisabetta Ferraro,[1] Maria Germanò,[2] Rocco Mollace,[3] Vincenzo Mollace,[3] and Natalia Malara [3]

[1]*Università di Pisa, Pisa, Italy*
[2]*Ospedale Sant'Anna, Como, Italy*
[3]*Università Magna Grecia, Catanzaro, Italy*

Correspondence should be addressed to Natalia Malara; nataliamalara@unicz.it

Despite the international scientific community's commitment to improve clinical knowledge about coronavirus disease 2019 (COVID-19), knowledge regarding molecular details remains limited. In this review, we discuss hypoxia's potential role in the pathogenesis of the maladaptive immune reaction against severe acute respiratory syndrome coronavirus-2 (SARS-CoV-2). The state of infection, with serious respiratory dysfunction, causes tissues to become hypoxic due to a discrepancy between cellular O_2 uptake and consumption similar to that seen within tumor tissue during the progression of numerous solid cancers. In this context, the heterogeneous clinical behavior and the multiorgan deterioration of COVID-19 are discussed as a function of the upregulated expression of the hypoxia-inducible factor-1 (HIF-1) and of the metabolic reprogramming associated with HIF-1 and with a proinflammatory innate immune response activation, independent of the increase in the viral load of SARS-CoV-2. Possible pharmacological strategies targeting O_2 aimed to improve prognosis are suggested.

1. Introduction

Coronavirus disease 2019 (COVID-19) has spread worldwide, causing overwhelming repercussions on daily and working life [1, 2]. The clinical severity of the severe acute respiratory syndrome coronavirus 2 (SARS-CoV-2) infection is determined by the multifaceted biological host response to the harmful virus that could be summarized as the succession of three prevalent pathogenic steps: (i) the direct damage of infected host cells, (ii) the early immune response characterized prevalently by cytokine release and complement activation, and (iii) the persistent inflammation in multiple tissue sites with progressive multiorgan deterioration [3–5]. An additional associated feature of COVID-19 is tissue hypoxia along with overexpression of the hypoxia-inducible factor-1 (HIF-1) along with their immunometabolic and immune-response consequences, which are the focus of this review.

2. HIF-1

HIFs are a family of highly conserved transcription factors activated by low O_2 partial pressure (pO_2). The HIF-1 complex is a heterodimer composed of two basic helix-loop-helix subunits: the HIF-1α and the HIF-1β subunits. HIF-1β is constitutively expressed whereas HIF-1α activity is posttranscriptionally regulated by O_2 sensors and O_2-dependent enzymes including prolyl hydroxylases (PHDs) [6, 7]. Under normoxia, when O_2 is available, O_2-dependent PHDs are active and lead to HIF-1α hydroxylation at conserved proline residues. This allows the recognition by the von Hippel-Lindau (pVHL) E3 ubiquitin ligase complex which causes HIF-1α's fast ubiquitination and its proteasomal degradation (Figure 1). Conversely, under hypoxia, PHDs are inhibited since PHDs need O_2 as a cosubstrate, and this reduces the PHD-dependent degradation of HIF-1α resulting
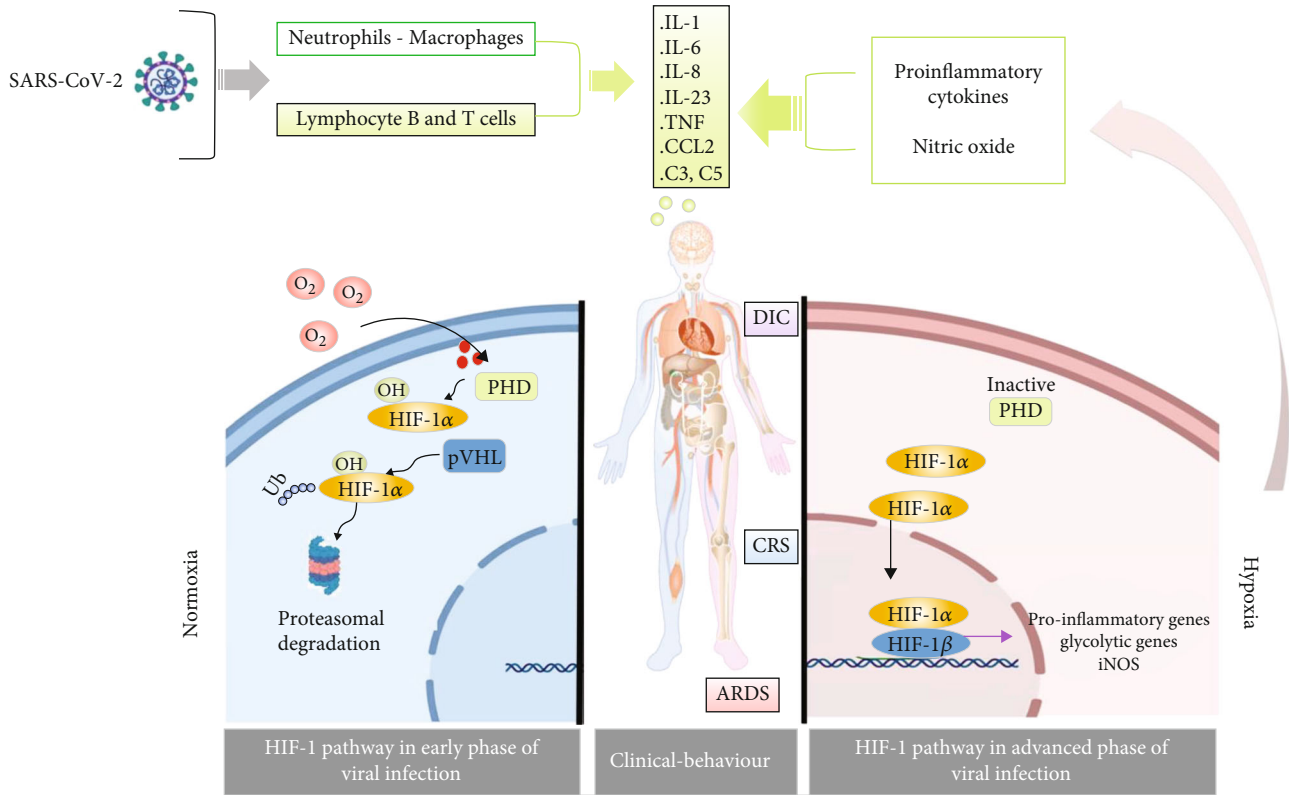
Figure 1: Severe SARS-CoV-2 syndrome as a result of hypoxia and HIF-1 signaling pathway activation. ARDS: acute respiratory distress syndrome; CCL: chemokine (C-C motif) ligand; CRS: cytokine release syndrome; DIC: disseminated intravascular coagulation; HIF-1: hypoxia-inducible factor; IL: interleukin; iNOS: inducible NO synthase; pVHL: von Hippel-Lindau tumor suppressor; SARS-CoV-2: severe acute respiratory syndrome coronavirus; TNF: tumor necrosis factor.

in its stabilization; once stabilized, HIF-1α dimerizes with HIF-1β and binds the promoters at hypoxia-responsive elements, thus inducing the expression of its target genes which are useful in hypoxia conditions. In fact, these target genes are involved not only in O_2-independent energy production (e.g., glycolytic genes) but also in angiogenesis (e.g., VEGF) and erythropoiesis, thereby increasing O_2 delivery to tissues [8, 9].

3. The Warburg Effect

All cells need a source of energy to maintain homeostasis. Glycolysis and mitochondrial respiration/oxidative phosphorylation (OxPhos) generate energy in the form of ATP. Under normoxic conditions, most cells use the pyruvate obtained by metabolizing glucose through cytosolic glycolysis to feed the Krebs cycle/tricarboxylic acid cycle (TCA). For this purpose, pyruvate enters the mitochondria where it is converted to acetyl coenzyme A (CoA) by the pyruvate dehydrogenase (PDH). Through the TCA cycle, acetyl CoA is oxidized to CO_2, and reducing equivalents (NADH and $FADH_2$) are produced. NADH and $FADH_2$ are then used and oxidized by the respiratory chain complexes and O_2 to generate the mitochondrial membrane proton gradient used by the ATPase to phosphorylate ADP to ATP. The OxPhos leads to the production of 36 molecules of ATP per molecule of glu-

cose. In conditions of O_2 deficiency (anaerobiosis), the activity of the mitochondrial OxPhos is reduced and the pyruvate deriving from glycolysis is directly converted in the cytosol into lactate; this glycolytic cycle is rapid and allows the formation of few ATP molecules per single molecule of glucose.

Some cells display an enhanced conversion of glucose to pyruvate, this then being metabolized to lactate even in the presence of abundant O_2; this aerobic glycolysis is called the Warburg effect [10]. In particular, this effect identifies the metabolic state of tumor cells and is highly important in antitumor treatments [11]. However, aerobic glycolysis is a metabolic condition also associated with pluripotency or observed in other cells; some of these belonging to the immune system [12, 13]. The Warburg effect reprogramming includes the overexpression of glucose transporters and glycolytic enzymes as well as the accumulation of glycolytic intermediates and lactate along with environmental acidification. This metabolic condition is characterized by a high-speed ATP production through the fast glycolytic flux and meets the energy demand of rapidly proliferating cells. In fact, the Warburg effect is a common feature of cells which exhibit a rapid proliferation rate and therefore switch to aerobic glycolysis to allow a rapid, often transitory, ATP production. *Vice versa*, the mitochondrial respiration prevalently supports stable and long-lasting processes, e.g., those related to cellular differentiation.

4. The Warburg Effect and HIF-1α in the Innate Immune Response

The innate immune response is characterized by macrophage (MΦ)/microglia cell (MG) activation toward a proinflammatory state which is often identified as M1-like activation. This first proinflammatory step is followed by a step involving anti-inflammatory and proregenerative MΦ/MG (M2-like polarized cells). One needs to take into account that this is an oversimplification; indeed, the proinflammatory M1 and the anti-inflammatory M2 MΦ/MG populations are the extremes of a wide range of intermediate activation states still not clearly defined.

M1 and M2 subsets express a different sensome and a different secretome; notably, different metabolic pathways are also enrolled by MΦ/MG in these two different activation states. In particular, the Warburg effect is typical of rapidly dividing proinflammatory M1 MΦ/MG [9]; ATP generation by enhanced aerobic glycolysis is associated with M1's rapid proliferation rate, with increased production of defense factors, with enhanced phagocytosis, and with the antigen-presenting function. Indeed, in these M1 proinflammatory cells as well as in cancer cells, the intracellular transport of glucose increases thanks to an increased expression of the glucose transporter GLUT1. In addition, the enzyme hexokinase, which catalyzes the first step of glycolysis and of the pentose phosphate pathway (PPP), is upregulated under this activation state. M1 subsets rearrange their metabolic flow and modify their intracellular production of ATP relying on glycolysis, necessary for their rapid activation, whereas the OxPhos decreases. The reduced activity of the respiratory chain allows the M1 subsets to employ the O_2 to produce reactive O_2 species (ROS) and nitric oxide (NO), whose generation also needs an upregulation of the PPP for the production of NADPH. NADPH is a substrate both for the NADPH oxidases (NOX), which produce ROS, and for inducible NO synthase (iNOS), which produces NO. In fact, another metabolic feature of M1 subsets is the enhanced PPP rate [14]. Moreover, some glycolytic enzymes such as 6-phospho-fructo-2-kinase/fructose-2,6-biphosphatase 3 (PFKFB3), pyruvate kinase M2 (PKM2), and α-enolase have been found to be crucial in supporting the proinflammatory function. Therefore, glycolysis is also necessary for M1 activation by providing signaling mediators which drive M1 polarization (reviewed by De Santa and collaborators [9]). In addition, although data are not clear and need further elucidation, M1 polarization also features flux discontinuities at several levels of the Krebs cycle, leading to the accumulation or reduction of some TCA intermediates which influence the inflammatory response. In particular, M1 subsets are characterized by an increase of proinflammatory succinate and citrate, immunoresponsive gene 1 (Irg1), isocitrate, and microbicidal itaconic acid and by the downregulation of isocitrate dehydrogenase 1 (Idh1) [9, 15]. Specifically, citrate, succinate, and itaconate are not only consequences but also a cause of M1 polarization.

Vice versa, rapid and acute activation is less important for the anti-inflammatory and regenerative M2 MΦ/MG whose role lasts longer to ensure proper tissue repair, producing ATP mainly by OxPhos. These observations led to the hypothesis that the OxPhos metabolic phenotype is more suitable for cells involved in long-term reparative roles (anti-inflammatory M2), while the aerobic glycolytic phenotype is necessary to produce rapid and transient responses (proinflammatory M1) [16, 17]. M2 are therefore characterized by a high and efficient OxPhos, which is required for M2 polarization, and also by an intact TCA cycle. The role of fatty acid β-oxidation in M2 activation is a matter of debate; in fact, it has been proposed that the overall oxidative metabolism, also fueled by glycolysis and not specifically by fatty acid β-oxidation, is crucial for M2 polarization (reviewed by De Santa and coworkers [9]). Finally, glutamine is also vital for M2 activation; the PPP rate decreases in M2 subsets whereas carbohydrate kinase-like (CARKL), a repressor of M1 activation, is upregulated.

During MΦ/MG activation, the metabolic adaptation is a key component required for polarization and not only its consequence [18]. It is now widely accepted that the metabolic phenotypic distinction between the M1 and M2 populations also drives the functional diversity of these two cellular effectors of the innate immunity. Paralleling the murine studies, the proinflammatory phenotype of human M1 MΦ, leading to an increased production of cytokines such as IL12p40, TNFα, or IL-6, is also characterized by an enhanced glycolytic energy pathway [16].

Notably, HIF-1α becomes activated during M1 polarization. This also occurs in an O_2-independent manner, in the presence of O_2 (normoxia). Indeed, PHD is downregulated in M1 by proinflammatory cytokines and by nuclear factor kB (NF-κB) binding to its promoter. In addition, succinate, which is highly expressed in M1 subsets, inhibits PHD activation, thus stabilizing HIF-1α in the presence of O_2 (the so-called pseudohypoxia). Finally, ROS and NO reduce PHD activity and also promote HIF-1α expression under normoxia [9].

HIF-1 plays a crucial role in orchestrating part of the M1 polarization, since it enhances the expression of the proinflammatory IL-1β and of other proinflammatory genes [9], downregulates the M2 marker CD206, and also induces iNOS expression. In addition, HIF-1 typically stimulates glucose uptake and the expression of key glycolytic enzymes as well as of pyruvate dehydrogenase kinase-1 (PDK1), thus promoting the metabolic reprogramming leading to M1 polarization [19–21]. In M1 subsets, besides being normoxic, the activation of HIF-1 transcription might also be typically hypoxic; in fact, M1 MΦ/MG are likely to be exposed to hypoxic environments during an infection. In addition, HIF-1 promotes stemness and stem cells reside within hypoxic regions. HIF-1 is involved in their homeostasis by decreasing their reliance on oxidative metabolism; it also maintains stemness in cancer stem cells.

5. HIF-1, the Warburg Effect, and the Innate Immune Response in COVID-19

During RNA virus lung infection such as coronavirus, viral RNAs are detected by sensors, thus inducing IFN-regulatory factor- (IRF-) 3, IRF-7, and NF-κB-mediated

expression of interferon- (IFN-) α and IFN-β as well as of other proinflammatory cytokines [22]. In SARS-CoV and MERS-CoV infections, the antiviral response is type-I IFN-mediated [23]. IFNs binding to their receptors lead to the phosphorylation of signal transducer and activator of transcription- (STAT-) 1 and STAT-2 transcription factors; this allows their migration to the nucleus where they bind to the promoter region of target genes, including iNOS and IL-12, associated with proinflammatory MΦ/MG activation [24]. In line with this, it has been demonstrated that STAT-1 is required for M1 polarization [25]. Interestingly, IFN-α/β signaling is essential for limiting virus dissemination throughout the central nervous system (CNS) thanks to the interaction between the IFN-α/β and the IFN-γ pathways, these being essential components of virus control in achieving optimal IFN-γ antiviral MΦ/MG responsiveness [26]. Notably, the clinical outcome of COVID-19 can be influenced by the time and the extent of the IFN response; in fact, mild and moderate SARS-CoV-2 infection has been associated with a stronger early type-I IFN response, compared to the lower IFN response observed in severe patients [27].

Type-I IFN-induced high expression of STAT-1 and STAT-2 leads to M1-like MΦ polarization. It has been proposed that the polarization of pulmonary MΦ towards the proinflammatory phenotype contributes to controlling viral replication. Indeed, in various viral respiratory diseases such as SARS and influenza, viral infection causes significant depletion of M1 MΦ through apoptosis and necrosis facilitating viral replication [28]. However, it is also known that, although M1 are important in fighting the virus, a balanced activation of the M2 MΦ subsets is essential for limiting immunopathological reactions. Liao et al. indicated that bronchoalveolar lavage fluid (BALF) from patients with severe COVID-19 infection had elevated M1 MΦ, while BALF from moderately infected patients and healthy controls contained a higher frequency of M2-like MΦ [29]. The initial impact of the viral infection and the response of the pulmonary parenchyma innate immunity is closely linked to the presence of M1 MΦ and also to the subsequent appearance of local M2 MΦ. In fact, the action of M1 subsets to counteract viral infection is necessary, even though their excessive and persistent presence can lead to severe forms of pneumonia by self-feeding the lung inflammation.

The SARS-CoV-2 virus affects the lungs and blood vessels and also the CNS where it mainly induces a chronic and pronounced inflammatory response and a cytokine storm that indirectly damages the CNS [30]. SARS-CoV-2 is neuroinvasive and may spread from the periphery to the brain, probably by the retrograde axonal transport through the vagus nerve and the olfactory nerve but also through the enteric nervous system and the hematogenous pathway. The angiotensin-converting enzyme-2 (ACE-2) receptor for SARS-CoV-2 is expressed in the capillary endothelium of the CNS; therefore, SARS-CoV-2 could bind and break the blood-brain barrier (BBB) to enter the CNS similarly to previous SARS coronaviruses. Moreover, it has been found that ACE-2 receptors are also expressed on various neuronal types, on astrocytes, and on microglia.

Although the pathological basis of the neurological damage in COVID-19 is still poorly understood, it seems that the neurological symptoms of COVID-19 infection are due to the massive systemic immune response and the subsequent proinflammatory cytokines and cytotoxic T lymphocyte infiltration into the CNS through the BBB, as well as to the strong activation of the resident immune cells, i.e., MG and astrocytes. In particular, it has been proposed that cytokines produced by MG contribute to disrupting the homeostasis of the CNS more than systemic inflammatory molecules do. Notably, if MG is in a "primed status," e.g., by conditions which contribute to systemic inflammation such as diabetes, ischemic conditions, and arthritis (all particularly frequent in the elderly), then a secondary stimulus such as a viral infection might further activate "primed" MG. This might explain why the elderly have a higher risk of experiencing neurological and cognitive disabilities in COVID-19 [31, 32]. As stated, the excessive proinflammatory MG activation seems to be the main cause of neuropathological damage in COVID-19 patients. Indeed, although SARS-CoV-2 could be detected in the brains of most examined patients where it might, in principle, have direct cytopathic effects disrupting the complex neural circuits, such effects are rare [33]. Moreover, the activation of the glycolytic pathway in chronic activated M1 MG might cause acidosis in the brain which can contribute to the neuropathological manifestations of COVID-19.

Neuropathological manifestations in COVID-19 are long-term secondary or bystander pathologies developing much later than the primary disease. They include anosmia, hypogeusia, headache, nausea and altered consciousness, seizures, stroke and acute cerebrovascular accidents, encephalitis and demyelinating disease, and, possibly, loss of control of respiration exacerbating hypoxemia. The lack of O_2 caused by damaged lung epithelial cells may cause—in critical COVID-19 patients—hypoxia disorders in the entire body including the CNS and subsequent cerebral damage.

As above stated, the M1 MΦ polarization is strictly dependent on the metabolic shift to glycolysis and to HIF-1α signaling. Therefore, although specific studies are necessary and the details of MΦ/MG polarization kinetics during the various stages of COVID-19 and its association with pathogenesis need to be unraveled, it is highly probable that MΦ/MG involved in the first phases of SARS-CoV-2 infection are M1-polarized and HIF-1α expressing and perform aerobic glycolysis. Notably, underlining the connection between viral infection, IFN production, STAT-1/2 activation, and M1 polarization, it has been found that sixteen enzymes involved in the glycolytic pathway are upregulated by STAT-1, which is typically induced by the virus [34]. Moreover, the increased glycolysis in a single COVID-19 patient has been explored by using 18F-fluorodeoxyglucose positron emission tomography (FDG PET) which identified FDG accumulation in the right paratracheal, right hilar lymph nodes, and bone marrow [35]. Ayres provides an interesting speculative dissertation on the relationship between metabolism and COVID-19 and on the potential relevance of glycolysis, using as his basis a parallelism between the pathophysiology of some metabolic abnormalities and the disease course of COVID-19 [36].

6. Hypoxia-Dependent Mechanisms in Cancer and Speculation on COVID-19 Pathogenesis

Besides the induction of the M1 proinflammatory response triggered by the virus through IFNs and STAT-1/2 and leading to normoxic HIF-1 activation and to aerobic glycolysis, COVID-19 infection also induces severe hypoxia conditions. Hypoxia, in turn, is the classical inducer of HIF-1 with subsequent inflammatory cytokine production and glycolysis enhancement. Therefore, the COVID-19 hypoxic conditions and the following HIF-1-dependent gene expression likely potentiate and exacerbate M1 polarization and the degree of inflammation of ACE-2-positive tissues [37], thus possibly reducing or delaying the shift to M2 MΦ subsets necessary for tissue repair. Hypoxia might therefore be considered pathogenic for COVID-19 and also for the complications in noble tissues sensitive to the degree of tissue oxygenation, such as in the brain, found in severe forms of COVID-19 [38].

In COVID-19, besides the alveolar damage, viral attack involves the endothelium and causes coagulation. Autopsy data have confirmed that the lung parenchyma injury is characterized by alveolar wall thickening, vascular hyperpermeability, and inflammatory cell infiltration [39]. Massive pulmonary embolism and deep thrombosis in the prostatic venous plexus have also been described due to fibrin thrombi associated with high levels of D-dimers in the blood configuring the disseminated intravascular coagulation (DIC) [39]. The microthrombi were prevalently identified in the areas of diffuse alveolar disruption and were associated with diffuse endothelial damage, thus helping to explain the severe hypoxemia characterizing the acute respiratory distress syndrome (ARDS) in COVID-19 patients [4, 19]. The hypoxemia favors tissue hypoxia at the sites of infection where the amount of O_2 available for each cell is reduced [37].

Although the transcriptionally regulated tissue adaptation to hypoxia in the pathophysiology of SARS-CoV-2 infection requires fuller investigation, our knowledge of the hypoxia-mediated immunoescape mechanisms occurring in tumor cells corroborates speculation concerning the potential role of hypoxia-mediated mechanisms in causing inadequate immune response against SARS-CoV-2 at the infection site. The hypoxic microenvironment is a pathophysiologic condition generated during SARS-CoV-2 infection which recalls that occurring in cancer disease. Hypoxia arises in cancer tissue through the uncontrolled and rapid proliferation of cancer cells; the parallel lack of sufficient vascularization leads cancer cells to rapidly consume O_2 and nutrients and to create a hypoxic microenvironment [40]. Similarly, hypoxia arises in tissues infected by SARS-CoV-2 through the diffusion of a rapid and uncontrolled inflammation and through a parallel lack of O_2 caused by the thrombotic event and by the alveolar damage, all inducing a hypoxic microenvironment. Interestingly, hypoxia stabilizes HIF-1α and promotes the glycolytic phenotype in cancer cells whereas, in the surrounding nontumor tissue, the prolonged lack of O_2 inhibits regular cell function [7]. Moreover, it has recently been found that hypoxia-induced HIF-1 enhances the overexpression of programmed death ligand-1 (PDL-1) on the tumor cell surface. PDL-1 binds to programmed cell death protein 1 (PD-1) which is expressed by T-cells, thus pre-

venting the cytotoxic activation of tumor-infiltrating T-cells and promoting tumor cell survival thanks to immune system surveillance escape [5, 41]. Recently, it has been suggested that similar mechanisms of hypoxia-dependent immune system escape based on the PD pathway might also occur in COVID-19 [42–44]. Further studies in this regard—e.g., aimed at evaluating PDL-1/PD-1 modulation in COVID-19 patients—might be desirable in order to clarify this important issue and to gain insight into why in COVID-19 patients with an altered immune response the occurrence of hypoxia and inflammation (also present in other diseases such as severe influenza) leads to an undesirable outcome.

In this context, it is interesting to note that some researchers have observed that cancer patients undergoing treatment with inhibitors of the PD pathway—immune checkpoint inhibitors (ICI) used to treat solid tumors such as melanoma, lung cancer, renal carcinoma, urothelial cancers, and head and neck carcinoma—could be more immunocompetent than cancer patients undergoing chemotherapy [41]. Notably, the evaluation of the potential therapeutic value of ICI recently tested for cancer treatment in restoring cellular immunocompetence in COVID-19 is attracting interest; indeed, a trial with the ICI anti-PD1 camrelizumab is ongoing in SARS-CoV-2-infected patients [45].

Here, we wish to emphasize these similarities with other known conditions of hypoxia since they might provide useful insight during the disease's late aggressive stages (characterized by high hypoxia and inflammation and by a high viral burden overcoming the patient immune response) and when alternative routes aimed at counteracting the pO_2 lowering are required.

Notably, comparative evaluation between COVID-19 and non-COVID-19 pneumonia patients suggested an impact of the SARS-CoV-2 infection on lymphocyte subset count which decreases in COVID-19. In particular, in SARS-CoV-2 patients, the B lymphocyte subset exhibits the most significant decrease compared to in non-SARS-CoV-2 pneumonia-infected patients and may fail to restrict the virus expansion [46]. The reduced levels of B lymphocytes in SARS-CoV-2 patients might be associated with HIF-1 activation [47]. In fact, hypoxia alters B cell physiology and function leading to reduced proliferation and increased B cell death. Moreover, hypoxia and the constitutive HIF-1 activation impair the generation of high-affinity IgG antibodies [48], and HIF-1α modulates recombinant Ig isotype variation in B cells, thus influencing memory recall. Therefore, the dysfunctional antibody production occurring in COVID-19 might possibly be related to B cell hypoxic damage [49]; a jammed antibody production by B cells caused by hypoxia and prolonged HIF-1 signaling activation could explain why some subjects, despite having contracted the virus, do not have a neutralization immunoconversion [50].

7. Potential Therapies for COVID-19 Targeting Hypoxia-Related Pathways

7.1. Targeting HIF-1 and/or Switching the Metabolism. Based on these premises, acting on aerobic glycolysis and/or on HIF-1 as possible therapeutic targets would have the effect of containing the presence and the activity of

proinflammatory M1, in the right context, while favoring M2 polarization, thus inducing the resolution of the inflammatory process and promoting tissue repair.

The concept of MΦ/MG reprogramming to promote anti-inflammatory/regenerative M2 polarization able to reduce inflammation might offer a new therapeutic approach to both promote tissue healing and reduce inflammation. Manipulating immune cell metabolism in order to regulate the immune cell development can enhance or temper the immune response and drive MΦ/MG polarization and function, which might be useful for the potential treatment of several diseases, including COVID-19 [16]. As reviewed by De Santa et al., calorie restriction stimulates adaptive metabolic changes with many positive effects such as lifespan extension and delayed age-associated disease onset. It has been found that calorie restriction in mice leads to M2 polarization. Moreover, nutrients impinging on metabolism such as resveratrol, vitamin D, pomegranate, and its polyphenols, grape seed-derived polyphenols (proanthocyanidolic oligomers), inhibit M1 activation and promote M2 activation. Also, some sirtuins seem to be able to modulate metabolism promoting an M1-to-M2 transition.

We also speculate that a possible pharmacological method for supporting the mitochondrial respiration could be the strong inhibition of the β-adrenergic receptors (β-ARs)/uncoupling protein 1 (UCP1) axis in the tissues where it is activated. β-ARs control thermogenesis by increasing the expression of UCP1 which is a member of the mitochondrial anion carrier family located on the internal mitochondrial membrane and predominantly expressed in brown adipocyte tissue [51]. β3-AR is the main trigger of UCP1 which uncouples the activity of the respiratory chain from the synthesis of ATP, thus releasing energy as heat for an adaptive thermogenesis [52]. The selective β3-AR antagonism, by using SR59230A, reduces heat production favoring the synthesis of ATP. Similar effects were observed with the use of genipin specifically inhibiting UCP2—ubiquitously expressed in tumor cells—which has been found to reduce the glycolytic pathway activation in cancer cells, shifting their metabolism toward the mitochondrial pathway [53].

7.2. Targeting Hypoxia.
The pathogenesis framework here described suggests that one of the pathophysiologic mechanisms in SARS-CoV-2 disease could be represented by the grade of hypoxia. The consolidation of a hypoxic microenvironment could be antagonized by opportune pharmacological actions aimed at improving O_2 supply (i) indirectly—by reducing the exuberance of the innate response and limiting the release of cytokines in the right time frame—and (ii) directly. Currently, no country has licensed any specific pharmaceutical treatments for COVID-19, in particular for the late aggressive stages of this disease characterized by high hypoxia and inflammation.

To limit hypoxia-inducible complications of SARS-CoV-2 pneumonia, the pO_2 in the plasma must increase [54]. To this end, O_2 supplementation via nasal cannulation/mechanical ventilation is performed. Although not used for pneumonia, an additional modality to increase the pO_2 in the plasma is the hyperbaric O_2 therapy (HBOT). By HBOT,

patients are treated with 100% O_2 at pressures greater than atmospheric pressure, this increasing the amount of O_2 dissolved in the plasma, thereby improving its delivery to stressed tissues reached by the blood flow [54]. Here, we discuss about another way to increase O_2 delivery to tissues which might be the administration of ozone (O_3) (*ozone therapy*) [55, 56]. O_3 has a short half-life and must be produced at the time of use by equipment which transforms medical O_2 into O_3. One of the most important routes of O_3 administration is direct intravenous by different delivery methods [55, 57, 58]. For example, a commonly accepted delivery method is the ozonated autohemotherapy by which a precisely controlled O_2/O_3 gaseous mixture is injected into the same volume of blood drawn from a patient and allowed to mix with it. The ozonized blood is then intravenously infused back into the same patient [59–61].

The main action of the *ozone therapy*—reported to be exceptionally safe—is the O_3 germicidal ability to reduce the infectivity of a wide range of pathogens including viruses, by lipid peroxidation, viral capsid damage, and inhibition of virus replication [57, 62]. Atoxic doses of O_3 have also been found to stimulate the innate immune system besides being a strong anti-inflammatory and antioxidant molecule counteracting the oxidative stress by upregulating the expression of antioxidant enzymes (glutathione peroxidase, catalase, and superoxide dismutase) [63–65]. Thus, many authors have recently proposed that the *ozone therapy* might be cytoprotective and improve clinical conditions caused by SARS-CoV-2 [60, 63, 66–68]. Moreover, besides these effects, various data describe the role of ozonated autohemotherapy in treating hypoxia by correcting the hypoxemia and improving O_2 delivery and tissue oxygenation [55, 58, 59, 68]. In fact, once in the blood, the O_3 reacts with organic compounds containing double bonds (i.e., polyunsaturated fatty acids) and generates messengers such as aldehydes derived from the unsaturated fatty acid peroxidation and hydrogen peroxide. The hydrogen peroxide increases the glycolysis rate into erythrocytes and enhances the production of 2,3 diphosphoglycerate deriving from 1,3-diphosphoglycerate obtained by glycolysis, thanks to the enzyme diphosphoglycerate mutase [68]. 2,3 di-phosphoglycerate, in turn, is able to reduce the affinity of the hemoglobin for the O_2, thus increasing the amount of O_2 released from hemoglobin to the tissues [65, 69, 70].

The reduction of the degree of hypoxemia is an important goal in the treatment of severe symptomatic SARS-CoV-2 patients; this review highlights the need to treat hypoxia. On the other hand, O_2 supply, if not properly calibrated, can determine side effects linked to an increased tissue oxidative damage by local release of ROS. Not only is the increment of ROS one of the immune system's strategies for fighting infections typically during the proinflammatory M1 phase but also it presents a serious risk of tissue damage, especially in noble parenchyma. In this context, it is necessary to concentrate on those patients whose oxidative system has previously collapsed through comorbidity or by aging. Accordingly, before O_2 supply, it would be useful to verify the health of the oxidative system in real time through a blood sample [71, 72]. For example, the accumulation of

methylglyoxal adducts indicates both a prevalent glycolytic metabolism and glutathione defensive system failure [72]. Through an oxidative screening of the blood, it would be possible to select the SARS-CoV-2 patients with a preserved antioxidant defense potentially benefitting from a therapy aimed at counteracting the oxidative mitochondrial phosphorylation shut down by hypoxia and inflammation. An oxidative screening on a blood sample will give information regarding all body tissues, whereas a specific analysis of the oxidative stress at each tissue level, although desirable, would require a tissue biopsy and would be invasive. In the future, the concomitant evaluation of tissue-specific markers in a blood sample might provide insights into a specific tissue. For example, the endothelial damage is typical of this disease; circulating endothelial cells (CEC) have been found in the blood of COVID-19 patients [73]. Therefore, the evaluation of the oxidative stress on CEC might be a way to evaluate the oxidative stress on specific cells by using a liquid biopsy. The analysis of specific exosomes, whose tissue origin could be identified by peculiar markers, would potentially shed light on that specific tissue's oxidative stress.

8. Concluding Remarks

Manifestations displayed by COVID-19 patients led us to consider the central role of HIF-1 and metabolic reprogramming in the inflammatory response typical of this disease, characterized by lung dysfunction. The side effects of the hypoxia/HIF-1 signaling triggered during the SARS-CoV-2 infection are a potentially important area of research for pharmacological applications. Hopefully, further studies will disclose MΦ/MG heterogeneity in COVID-19 and the metabolic pathways associated with MΦ/MG polarization, thus identifying novel immunometabolic molecular targets and contributing to therapeutic interventions. Cancer disease might provide insights into COVID-19 pathophysiology; however, defining the precise role of hypoxia in the development of the COVID-19 syndrome severity still requires further study. Nevertheless, we cannot avoid the conclusion that hypoxemia and hypoxia are sides of the same coin and that by trying to solve one, inevitably, we also affect the other.

Abbreviations

ACE-2: Angiotensin-converting enzyme 2
ARDS: Acute respiratory distress syndrome
BBB: Blood-brain barrier
β-ARs: β-Adrenergic receptors
CARKL: Carbohydrate kinase-like
CEC: Circulating endothelial cells
CNS: Central nervous system
COVID-19: Coronavirus disease 2019
DIC: Disseminated intravascular coagulation
FDG PET: 18F-fluorodeoxyglucose positron emission tomography
GLUT1: Glucose transporter type 1
HBOT: Hyperbaric O_2 therapy
HIF-1: Hypoxia-inducible factor-1
ICI: Immune checkpoint inhibitors
IRF: IFN-regulatory factor
Idh1: Isocitrate dehydrogenase 1
iNOS: Inducible NO synthase
IFN: Interferon
IL: Interleukin
Irg1: Immunoresponsive gene 1
MΦ: Macrophage
MG: Microglia
NF-κB: Nuclear factor kB
NO: Nitric oxide
NOX: NADPH oxidases
pO_2: Oxygen partial pressure
OxPhos: Oxidative phosphorylation
PDK1: Pyruvate dehydrogenase kinase-1
PFKFB3: Phosphofructo-2-kinase/fructose-2,6-biphosphatase 3
PHDs: Prolyl hydroxylases
PKM2: Pyruvate kinase M2
PPP: Pentose phosphate pathway
PD-1: Programmed cell death protein 1
PDL-1: Programmed death ligand-1
pVHL: von Hippel-Lindau tumor suppressor
ROS: Reactive O_2 species
SARS-CoV-2: Severe acute respiratory syndrome coronavirus
TNF: Tumor necrosis factor
STAT: Signal transducer and activator of transcription
TCA: Tricarboxylic acid cycle
UCP1: Uncoupling protein 1
VEGF: Vascular endothelial growth factor.

Conflicts of Interest

The authors declare that they have no conflicts of interest.

Authors' Contributions

The concept of this study was by NM; the draft was performed by EF, RM, GM, and NM; supervision was performed by EF, VM, and NM.

Acknowledgments

References

[1] X. Qian, R. Ren, Y. Wang et al., "Fighting against the common enemy of COVID-19: a practice of building a community with a shared future for mankind," *Infectious Diseases of Poverty*, vol. 9, no. 1, p. 34, 2020.

[2] I. Aquila, M. A. Sacco, L. Abenavoli et al., "SARS-CoV-2 pandemic: review of the literature and proposal for safe autopsy

practice," *Archives of Pathology & Laboratory Medicine*, vol. 144, no. 9, 2020.

[3] Y. Wan, J. Shang, R. Graham, R. S. Baric, and F. Li, "Receptor recognition by the novel coronavirus from Wuhan: an analysis based on decade-long structural studies of SARS coronavirus," *Journal of Virology*, vol. 94, no. 7, 2020.

[4] D. Giannis, I. A. Ziogas, and P. Gianni, "Coagulation disorders in coronavirus infected patients: COVID-19, SARS-CoV-1, MERS-CoV and lessons from the past," *Journal of Virology*, vol. 127, article 104362, 2020.

[5] A. Grifoni, D. Weiskopf, S. I. Ramirez et al., "Targets of T cell responses to SARS-CoV-2 coronavirus in humans with COVID-19 disease and unexposed individuals," *Cell*, vol. 181, no. 7, pp. 1489–1501.e15, 2020.

[6] G. Perozziello, R. La Rocca, G. Cojoc et al., "Microfluidic devices modulate tumor cell line susceptibility to NK cell recognition," *Small*, vol. 8, no. 18, pp. 2886–2894, 2012.

[7] S. E. Corcoran and L. A. O'Neill, "HIF1α and metabolic reprogramming in inflammation," *The Journal of Clinical Investigation*, vol. 126, no. 10, pp. 3699–3707, 2016.

[8] G. Donato, I. Presta, B. Arcidiacono et al., "Innate and adaptive immunity linked to recognition of antigens shared by neural crest-derived tumors," *Cancers (Basel)*, vol. 12, no. 4, p. 840, 2020.

[9] F. De Santa, L. Vitiello, A. Torcinaro, and E. Ferraro, "The role of metabolic remodeling in macrophage polarization and its effect on skeletal muscle regeneration," *Antioxidants & Redox Signaling*, vol. 30, pp. 1553–1598, 2019.

[10] S. Y. Lunt and M. G. Vander Heiden, "Aerobic glycolysis: meeting the metabolic requirements of cell proliferation," *Annual Review of Cell and Developmental Biology*, vol. 27, no. 1, pp. 441–464, 2011.

[11] P. Vaupel, H. Schmidberger, and A. Mayer, "The Warburg effect: essential part of metabolic reprogramming and central contributor to cancer progression," *International Journal of Radiation Biology*, vol. 95, no. 7, pp. 912–919, 2019.

[12] C. Patsch, L. Challet-Meylan, E. C. Thoma et al., "Generation of vascular endothelial and smooth muscle cells from human pluripotent stem cells," *Nature Cell Biology*, vol. 17, no. 8, pp. 994–1003, 2015.

[13] S. Varum, A. S. Rodrigues, M. B. Moura et al., "Energy metabolism in human pluripotent stem cells and their differentiated counterparts," *PLoS One*, vol. 6, no. 6, article e20914, 2011.

[14] C. Nagy and A. Haschemi, "Time and demand are two critical dimensions of immunometabolism: the process of macrophage activation and the pentose phosphate pathway," *Frontiers in Immunology*, vol. 6, p. 164, 2015.

[15] A. K. Jha, S. C. Huang, A. Sergushichev et al., "Network integration of parallel metabolic and transcriptional data reveals metabolic modules that regulate macrophage polarization," *Immunity*, vol. 42, no. 3, pp. 419–430, 2015.

[16] L. A. O'Neill and D. G. Hardie, "Metabolism of inflammation limited by AMPK and pseudo-starvation," *Nature*, vol. 493, no. 7432, pp. 346–355, 2013.

[17] P. Newsholme, R. Curi, S. Gordon, and E. A. Newsholme, "Metabolism of glucose, glutamine, long-chain fatty acids and ketone bodies by murine macrophages," *The Biochemical Journal*, vol. 239, no. 1, pp. 121–125, 1986.

[18] L. A. O'Neill and E. J. Pearce, "Immunometabolism governs dendritic cell and macrophage function," *The Journal of Experimental Medicine*, vol. 213, no. 1, pp. 15–23, 2016.

[19] E. Guadagno, I. Presta, D. Maisano et al., "Role of macrophages in brain tumor growth and progression," *International Journal of Molecular Sciences*, vol. 19, no. 4, p. 1005, 2018.

[20] L. Vitiello, E. Ferraro, S. De Simone et al., "CXCL12 prolongs naive CD4+ T lymphocytes survival via activation of PKA, CREB and Bcl2 and BclXl up-regulation," *International Journal of Cardiology*, vol. 224, pp. 206–212, 2016.

[21] G. Arango Duque and A. Descoteaux, "Macrophage cytokines: involvement in immunity and infectious diseases," *Frontiers in Immunology*, vol. 5, p. 491, 2014.

[22] B. X. Wang and E. N. Fish, "Global virus outbreaks: interferons as 1st responders," *Seminars in Immunology*, vol. 43, p. 101300, 2019.

[23] S. Shokri, S. Mahmoudvand, R. Taherkhani, and F. Farshadpour, "Modulation of the immune response by Middle East respiratory syndrome coronavirus," *Journal of Cellular Physiology*, vol. 234, no. 3, pp. 2143–2151, 2018.

[24] J. E. Darnell, I. M. Kerr, and G. R. Stark, "Jak-STAT pathways and transcriptional activation in response to IFNs and other extracellular signaling proteins," *Science*, vol. 264, no. 5164, pp. 1415–1421, 1994.

[25] C. M. Leopold Wager, C. R. Hole, K. L. Wozniak, M. A. Olszewski, and F. L. Wormley, "STAT1 signaling is essential for protection against Cryptococcus neoformans infection in mice," *Journal of Immunology*, vol. 193, no. 8, pp. 4060–4071, 2014.

[26] M. Hwang and C. C. Bergmann, "Neuronal ablation of alpha/beta interferon (IFN-α/β) signaling exacerbates central nervous system viral dissemination and impairs IFN-γ responsiveness in microglia/macrophages," *Journal of Virology*, vol. 94, no. 20, 2020.

[27] Y. Jamilloux, T. Henry, A. Belot et al., "Should we stimulate or suppress immune responses in COVID-19? Cytokine and anticytokine interventions," *Autoimmunity Reviews*, vol. 19, no. 7, p. 102567, 2020.

[28] Y. Sang, L. C. Miller, and F. Blecha, "Macrophage polarization in virus-host interactions," *Journal of Clinical and Cellular Immunology*, vol. 6, no. 2, 2015.

[29] M. Liao, Y. Liu, J. Yuan et al., "Single-cell landscape of bronchoalveolar immune cells in patients with COVID-19," *Nature Medicine*, vol. 26, no. 6, pp. 842–844, 2020.

[30] W. Y. Ong, M. L. Go, D. Y. Wang, I. K. Cheah, and B. Halliwell, "Effects of antimalarial drugs on neuroinflammation-potential use for treatment of COVID-19-related neurologic complications," *Molecular Neurobiology*, vol. 58, no. 1, pp. 106–117, 2021.

[31] R. Mishra and A. C. Banerjea, "Neurological damage by coronaviruses: a catastrophe in the queue!," *Frontiers in Immunology*, vol. 11, p. 565521, 2020.

[32] S. Al-Sarraj, C. Troakes, B. Hanley et al., "Invited review: the spectrum of neuropathology in COVID-19," *Neuropathology and Applied Neurobiology*, vol. 47, pp. 3–16, 2021.

[33] J. Matschke, M. Lütgehetmann, C. Hagel et al., "Neuropathology of patients with COVID-19 in Germany: a post-mortem case series," *Lancet Neurology*, vol. 19, no. 11, pp. 919–929, 2020.

[34] S. P. Pitroda, B. T. Wakim, R. F. Sood et al., "STAT1-dependent expression of energy metabolic pathways links tumour growth and radioresistance to the Warburg effect," *BMC Medicine*, vol. 7, no. 1, p. 68, 2009.

[35] S. Zou and X. Zhu, "FDG PET/CT of COVID-19," *Radiology*, vol. 296, no. 2, article E118, 2020.

[36] J. S. Ayres, "A metabolic handbook for the COVID-19 pandemic," *Nature Metabolism*, vol. 2, no. 7, pp. 572–585, 2020.

[37] M. Mahmudpour, J. Roozbeh, M. Keshavarz, S. Farrokhi, and I. Nabipour, "COVID-19 cytokine storm: the anger of inflammation," *Cytokine*, vol. 133, p. 155151, 2020.

[38] M. Lang, K. Buch, M. D. Li et al., "Leukoencephalopathy associated with severe COVID-19 infection: sequela of hypoxemia?," *AJNR. American Journal of Neuroradiology*, vol. 41, no. 9, pp. 1641–1645, 2020.

[39] R. M. Golonka, P. Saha, B. S. Yeoh et al., "Harnessing innate immunity to eliminate SARS-CoV-2 and ameliorate COVID-19 disease," *Physiological Genomics*, vol. 52, no. 5, pp. 217–221, 2020.

[40] R. Huber, B. Meier, A. Otsuka et al., "Tumour hypoxia promotes melanoma growth and metastasis via high mobility group box-1 and M2-like macrophages," *Scientific Reports*, vol. 6, no. 1, article 29914, 2016.

[41] M. Bersanelli, S. Scala, P. Affanni et al., "Immunological insights on influenza infection and vaccination during immune checkpoint blockade in cancer patients," *Immunotherapy*, vol. 12, no. 2, pp. 105–110, 2020.

[42] R. J. Sullivan, D. B. Johnson, B. I. Rini et al., "COVID-19 and immune checkpoint inhibitors: initial considerations," *Journal for ImmunoTherapy of Cancer*, vol. 8, no. 1, article e000933, 2019.

[43] M. Bersanelli, "COVID-19 and the newly rediscovered multidisciplinarity," *Immunotherapy*, vol. 12, no. 15, pp. 1101–1103, 2020.

[44] S. Di Cosimo, A. Malfettone, J. M. Pérez-García et al., "Immune checkpoint inhibitors: a physiology-driven approach to the treatment of coronavirus disease 2019," *European Journal of Cancer*, vol. 135, pp. 62–65, 2020.

[45] L. Gatto, E. Franceschi, V. D. Nunno, and A. A. Brandes, "Potential protective and therapeutic role of immune checkpoint inhibitors against viral infections and COVID-19," *Immunotherapy*, vol. 12, no. 15, pp. 1111–1114, 2020.

[46] Y. Zheng, Z. Hang, G. Yin et al., "Study of the lymphocyte change between COVID-19 and non-COVID-19 pneumonia cases suggesting other factors besides uncontrolled inflammation contributed to multi-organ injury," *med Rxiv*, vol. 1, pp. 1–7, 2020.

[47] K. Pieper, B. Grimbacher, and H. Eibel, "B-cell biology and development," *The Journal of Allergy and Clinical Immunology*, vol. 131, no. 4, pp. 959–971, 2013.

[48] S. H. Cho, A. L. Raybuck, K. Stengel et al., "Germinal centre hypoxia and regulation of antibody qualities by a hypoxia response system," *Nature*, vol. 537, no. 7619, pp. 234–238, 2016.

[49] R. K. Abbott, M. Thayer, J. Labuda et al., "Germinal center hypoxia potentiates immunoglobulin class switch recombination," *Journal of Immunology*, vol. 197, no. 10, pp. 4014–4020, 2016.

[50] M. Z. Tay, C. M. Poh, L. Rénia, P. A. MacAry, and L. F. P. Ng, "The trinity of COVID-19: immunity, inflammation and intervention," *Nature Reviews. Immunology*, vol. 20, no. 6, pp. 363–374, 2020.

[51] P. Puigserver, C. Picó, M. J. Stock, and A. Palou, "Effect of selective beta-adrenoceptor stimulation on UCP synthesis in primary cultures of brown adipocytes," *Molecular and Cellular Endocrinology*, vol. 117, no. 1, pp. 7–16, 1996.

[52] A. Fedorenko, P. V. Lishko, and Y. Kirichok, "Mechanism of fatty-acid-dependent UCP1 uncoupling in brown fat mitochondria," *Cell*, vol. 151, no. 2, pp. 400–413, 2012.

[53] G. Baffy, "Uncoupling protein-2 and cancer," *Mitochondrion*, vol. 10, no. 3, pp. 243–252, 2010.

[54] R. Choudhury, "Hypoxia and hyperbaric oxygen therapy: a review," *Int J Gen Med*, vol. Volume 11, pp. 431–442, 2018.

[55] R. J. Rowen, "Ozone and oxidation therapies as a solution to the emerging crisis in infectious disease management: a review of current knowledge and experience," *Medical Gas Research*, vol. 9, no. 4, pp. 232–237, 2019.

[56] I. Zanardi, E. Borrelli, G. Valacchi, V. Travagli, and V. Bocci, "Ozone: a multifaceted molecule with unexpected therapeutic activity," *Current Medicinal Chemistry*, vol. 23, no. 4, pp. 304–314, 2016.

[57] F. Cattel, S. Giordano, C. Bertiond et al., "Ozone therapy in COVID-19: a narrative review," *Virus Research*, vol. 291, p. 198207, 2021.

[58] R. J. Rowen and H. Robins, "Ozone therapy for complex regional pain syndrome: review and case report," *Current Pain and Headache Reports*, vol. 23, no. 6, p. 41, 2019.

[59] J. Wu, C. S. Tan, H. Yu et al., "Recovery of four COVID-19 patients via ozonated autohemotherapy," *Innovation (N Y)*, vol. 1, no. 3, article 100060, 2020.

[60] C. Tascini, G. Sermann, A. Pagotto et al., "Blood ozonization in patients with mild to moderate COVID-19 pneumonia: a single centre experience," *Internal and Emergency Medicine*, 2020.

[61] V. Bocci, I. Zanardia, G. Valacchi, E. Borrelli, and V. Travagli, "Validity of oxygen-ozone therapy as integrated medication form in chronic inflammatory diseases," *Cardiovascular & Hematological Disorders Drug Targets*, vol. 15, no. 2, pp. 127–138, 2015.

[62] B. K. Murray, S. Ohmine, D. P. Tomer et al., "Virion disruption by ozone-mediated reactive oxygen species," *Journal of Virological Methods*, vol. 153, no. 1, pp. 74–77, 2008.

[63] G. Martínez-Sánchez, A. Schwartz, and V. D. Donna, "Potential cytoprotective activity of ozone therapy in SARS-CoV-2/COVID-19," *Antioxidants (Basel)*, vol. 9, no. 5, p. 389, 2020.

[64] C. Scassellati, M. Ciani, A. C. Galoforo, R. Zanardini, C. Bonvicini, and C. Geroldi, "Molecular mechanisms in cognitive frailty: potential therapeutic targets for oxygen-ozone treatment," *Mechanisms of Ageing and Development*, vol. 186, p. 111210, 2020.

[65] R. di Mauro, G. Cantarella, R. Bernardini et al., "The biochemical and pharmacological properties of ozone: the smell of protection in acute and chronic diseases," *International Journal of Molecular Sciences*, vol. 20, no. 3, p. 634, 2019.

[66] A. Gavazza, A. Marchegiani, G. Rossi et al., "Ozone therapy as a possible option in COVID-19 management," *Frontiers in Public Health*, vol. 8, p. 417, 2020.

[67] Z. Zheng, M. Dong, and K. Hu, "A preliminary evaluation on the efficacy of ozone therapy in the treatment of COVID-19," *Journal of Medical Virology*, vol. 92, no. 11, pp. 2348–2350, 2020.

[68] A. M. Elvis and J. S. Ekta, "Ozone therapy: a clinical review," *J Nat Sci Biol Med*, vol. 2, no. 1, pp. 66–70, 2011.

[69] E. Borrelli and V. Bocci, "Visual improvement following ozonetherapy in dry age related macular degeneration; a review," *Med Hypothesis Discov Innov Ophthalmol*, vol. 2, no. 2, pp. 47–51, 2013.

[70] N. L. Smith, A. L. Wilson, J. Gandhi, S. Vatsia, and S. A. Khan, "Ozone therapy: an overview of pharmacodynamics, current research, and clinical utility," *Medical Gas Research*, vol. 7, no. 3, pp. 212–219, 2017.

[71] N. Malara, F. Gentile, N. Coppedè et al., "Superhydrophobic lab-on-chip measures secretome protonation state and provides a personalized risk assessment of sporadic tumour," *NPJ Precision Oncology*, vol. 2, no. 1, p. 26, 2018.

[72] M. L. Coluccio, I. Presta, M. Greco et al., "Microenvironment molecular profile combining glycation adducts and cytokines patterns on secretome of short-term blood-derived cultures during tumour progression," *International Journal of Molecular Sciences*, vol. 21, no. 13, p. 4711, 2020.

[73] C. Guervilly, S. Burtey, F. Sabatier et al., "Circulating endothelial cells as a marker of endothelial injury in severe COVID -19," *The Journal of Infectious Diseases*, vol. 222, no. 11, pp. 1789–1793, 2020.

Review Article

H₂O₂-Driven Anticancer Activity of Mn Porphyrins and the Underlying Molecular Pathways

Ines Batinic-Haberle [ID],[1] **Artak Tovmasyan** [ID],[1] **Zhiqing Huang** [ID],[2] **Weina Duan** [ID],[3]
Li Du [ID],[3] **Sharareh Siamakpour-Reihani** [ID],[4] **Zhipeng Cao** [ID],[3] **Huaxin Sheng** [ID],[3]
Ivan Spasojevic [ID],[4,5] **and Angeles Alvarez Secord** [ID][6]

[1]*Department of Radiation Oncology, Duke University School of Medicine, Durham, NC 27710, USA*
[2]*Department of Obstetrics and Gynecology, Division of Reproductive Sciences, Duke Cancer Institute, Duke University School of Medicine, Durham, NC 27710, USA*
[3]*Departments of Anesthesiology, Neurobiology, and Neurosurgery, Duke University School of Medicine, Durham, NC 27710, USA*
[4]*Department of Medicine, Duke University School of Medicine, Durham, NC 27710, USA*
[5]*Pharmacokinetics/Pharmacodynamics (PK/PD) Core Laboratory, Duke Cancer Institute, Duke University School of Medicine, Durham, NC 27710, USA*
[6]*Department of Obstetrics and Gynecology, Division of Gynecologic Oncology, Duke Cancer Institute, Duke University School of Medicine, Durham, NC 27710, USA*

Correspondence should be addressed to Ines Batinic-Haberle; ibatinic@duke.edu, Ivan Spasojevic; ivan.spasojevic@duke.edu, and Angeles Alvarez Secord; angeles.secord@duke.edu

Mn(III) *ortho-N*-alkyl- and *N*-alkoxyalkyl porphyrins (MnPs) were initially developed as superoxide dismutase (SOD) mimics. These compounds were later shown to react with numerous reactive species (such as ONOO⁻, H₂O₂, H₂S, CO₃•⁻, ascorbate, and GSH). Moreover, the ability of MnPs to oxidatively modify activities of numerous proteins has emerged as their major mechanism of action both in normal and in cancer cells. Among those proteins are transcription factors (NF-κB and Nrf2), mitogen-activated protein kinases, MAPKs, antiapoptotic bcl-2, and endogenous antioxidative defenses. The lead Mn porphyrins, namely, MnTE-2-PyP⁵⁺ (BMX-010, AEOL10113), MnTnBuOE-2-PyP⁵⁺ (BMX-001), and MnTnHex-2-PyP⁵⁺, were tested in numerous injuries of normal tissue and cellular and animal cancer models. The wealth of the data led to the progression of MnTnBuOE-2-PyP⁵⁺ into four Phase II clinical trials on glioma, head and neck cancer, anal cancer, and multiple brain metastases, while MnTE-2-PyP⁵⁺ is in Phase II clinical trial on atopic dermatitis and itch.

We have dedicated our review manuscript to a great colleague, dear friend, and exceptional scientist—Margaret Tome—who greatly influenced how we presently understand the in vivo mechanism of action of Mn porphyrin-based SOD mimics

1. Introduction

Besides summarizing the development and bioavailability of MnPs, we aimed herein to review the most recent knowledge on their impact on molecular pathways in normal and cancer cells in the presence of H₂O₂. Hydrogen peroxide plays a key role in cellular metabolism as well as in the actions of MnPs.

Anticancer effects of MnPs were explored with different sources of H₂O₂ in breast, ovarian, and head and neck cancers, glioma, melanoma, and hematological malignancies. Besides radiation and chemotherapy, an additional source of H₂O₂—exogenous ascorbate—was recently utilized in breast and ovarian cancers. In the case of ascorbate, MnP cycles with it catalytically, thus giving rise to large amounts

of H_2O_2. H_2O_2 subsequently couples with MnP and GSH to S-glutathionylate cysteines of numerous proteins, inactivating them and in turn inducing cancer cell death. The yield of the protein oxidation/S-glutathionylation, and therefore the therapeutic efficacy of MnPs, depends on the levels of reactants and their colocalization. MnPs prefer accumulation in cancer relative to normal cell/tissue. Further, cancer is under oxidative stress and has higher levels of H_2O_2 than normal cells; such scenario is in the origin of the differential effects of MnPs in inducing cancer cell death while suppressing damage from oxidative insult in a normal cell. We have summarized herein the strategies on the use of different sources of H_2O_2, including ascorbate, in breast and ovarian cancers. Ascorbate enhanced the tumor radiosensitizing ability of several cationic MnPs (including MnTnBuOE-2-PyP^{5+}) to suppress the viability of 4T1 breast cancer cells and 4T1 tumor growth, due primarily to the modified cellular redox status, massive protein oxidation, and preferred MnP accumulation in cancer cells/tissues. Recent studies on low-grade HOC7 and high-grade CAOV2 serous ovarian cancer cell lines recapitulated such ability of ascorbate to sensitize these cells to MnTnBuOE-2-PyP^{5+}. Mouse sc xenograft studies on the CAOV2 cancer cell line confirmed the therapeutic potential of MnTnBuOE-2-PyP^{5+}/ascorbate in ovarian cancer.

2. Design of Mn Porphyrins as SOD Mimics

Mn(III) substituted pyridylporphyrins (collectively abbreviated as MnPs) were initially developed as powerful mimics of the superoxide dismutase (SOD) family of enzymes [1–4]. The macrocyclic structure of the porphyrin ligand assures the integrity of the metal center where all reactions occurred—the very same reason nature has used the porphyrin ligand for numerous enzymes and proteins such as hemoglobin, myoglobin, cyt P450 family of enzymes, and nitric oxide synthases. The porphyrin ligand itself has redox chemistry outside the range that would have allowed its reactions with biomolecules; moreover, the porphyrin ligand is a powerful photosensitizer. Fe porphyrins were found inferior to Mn analogs for development as indicated at the end of this chapter. Substituted pyridylporphyrins were selected as ligands as they offer favorable thermodynamics and kinetics for the catalysis of $O_2^{\bullet-}$ dismutation. Structure-activity relationship (SAR) and the ability of MnPs to protect SOD-deficient *Escherichia coli* (*E. coli*) have guided us in their development. The *E. coli* assay has also been used as a major assessment of the toxicity of Mn porphyrins. SAR relates rate constants for the catalysis of superoxide, $O_2^{\bullet-}$ dismutation, $k_{cat}(O_2^{\bullet-})$ to the metal-centered reduction potentials, $E_{1/2}$ for the Mn^{III}/Mn^{II} redox couple. $E_{1/2}$ indicates whether the reaction can happen, while $k_{cat}(O_2^{\bullet-})$ indicates how fast the reaction happens. The first compounds that have extraordinarily high $k_{cat}(O_2^{\bullet-})$ of $\geq 7.1 \cdot 10^8$ M^{-1} s^{-1} (approaching that of SOD enzymes, $k_{cat}(O_2^{\bullet-}) \sim 10^9$ M^{-1} s^{-1}) were *meta* (3) and *para* (4) isomers of Mn(II) β-octabromo *meso*-tetrakis(*N*-methylpyridinium-3,4-yl)porphyrin, Mn^{II}Br$_8$TM(3 and 4)PyP^{4+}. Yet, both compounds have Mn in +2 oxidation states; thus, they are insufficiently stable and readily lose Mn at a biological pH of 7.4 [5]. However, these compounds provided the

proof of principle for establishing SAR and developing the powerful and stable porphyrin-based SOD mimics.

A very stable and potent SOD mimic, selected based on SAR, was Mn(III) *meso*-tetrakis(*N*-ethylpyridinium-2-yl)porphyrin, MnTE-2-PyP^{5+} (BMX-010, AEOL10113), with $E_{1/2}$ = +228 mV *vs.* NHE (normal hydrogen electrode) and log $k_{cat}(O_2^{\bullet-})$ = 7.76. This compound became our 1st lead drug from the *first generation of Mn(III) N-alkylpyridylporphyrins* [6] (Figure 1). Its hydrophilicity was thought to be a limiting factor for its distribution within cells and cellular organelles, most so within mitochondrion. A series of alkyl analogs with pyridyl substituents ranging from methyl to n-octyl were then synthesized to improve the lipophilicity and in turn biodistribution of MnPs [7]. Among those compounds, Mn(III) *meso*-tetrakis(*N*-n-hexylpyridinium-2yl)porphyrin MnTnHex-2-PyP^{5+} has balanced redox potency and bioavailability with minimal toxicity to normal cells/tissues [4, 8]; thus, it became our 2nd lead drug with $E_{1/2}$ = +314 mV *vs.* NHE and log $k_{cat}(O_2^{\bullet-})$ = 7.48 (Figure 1).

Further work was aimed at reducing toxicity to normal cells/tissues, while maintaining high lipophilicity and favorable redox properties. This was achieved by introducing oxygen atoms into *N*-alkylpyridyl chains and led to the creation of the *second generation of Mn(III) N-alkoxyalkylpyridylporphyrins* [9]. The 3rd lead drug emerged from that family of Mn porphyrins—Mn(III) *meso*-tetrakis(*N*-n-butoxyethylpyridinium-2yl)porphyrin MnTnBuOE-2-PyP^{5+} (BMX-001). It has an $E_{1/2}$ of +277 mV *vs.* NHE and a log $k_{cat}(O_2^{\bullet-})$ of 7.83 (Figure 1) [10]. The synthetic path leading to this compound was cumbersome; its mechanistic aspects were reported in [10, 11]. In addition, a hexoxy analog, Mn(III) *meso*-tetrakis(*N*-n-hexoxyethylpyridinium-2yl)porphyrin, MnTnHexOE-2-PyP^{5+}, was synthesized also [12]. For the large part of this review, we have focused on MnTnBuOE-2-PyP^{5+} due to its clinical relevance in cancer therapy. It was shown safe and well tolerated in Phase I clinical trial, where initial data suggest its efficacy [13–15]; it is now in several Phase II clinical trials.

A third generation of compounds has been recently developed where *N*-alkylpyridyl substituents were fluorinated (Figure 1). Fluorination of the drugs was known to result in more desirable pharmacokinetic and pharmacodynamic properties due to the increased polarity while at the same time increased lipophilicity and thus bioavailability [16–22]. Fluorine is the most electronegative element in the periodic system of elements. Such nature of fluorine limits our synthetic options when derivatizing porphyrins. Before embarking on the development of *N*-alkoxyalkylpyridylporphyrins, we attempted to replace 5 or 3 hydrogen atoms of MnTE-2-PyP^{5+}. Yet, we failed to synthesize a tri- or pentafluorinated ethyl analog, MnTE-2-PyP^{5+}. Due to the close proximity, the electronegative fluorines impose overwhelming electron-withdrawing effect on the pyridyl nitrogens. After completing characterization of oxygen-derivatized Mn(III) *N*-alkylpyridylporphyrins, we reassessed the fluorination of MnPs and succeeded in replacing only one hydrogen of MnTE-2-PyP^{5+} in Mn(III) *meso*-tetrakis(*N*-fluoroethylpyridinium-2yl)porphyrin, MnTFE-2-PyP^{5+} (BMX-002). We were
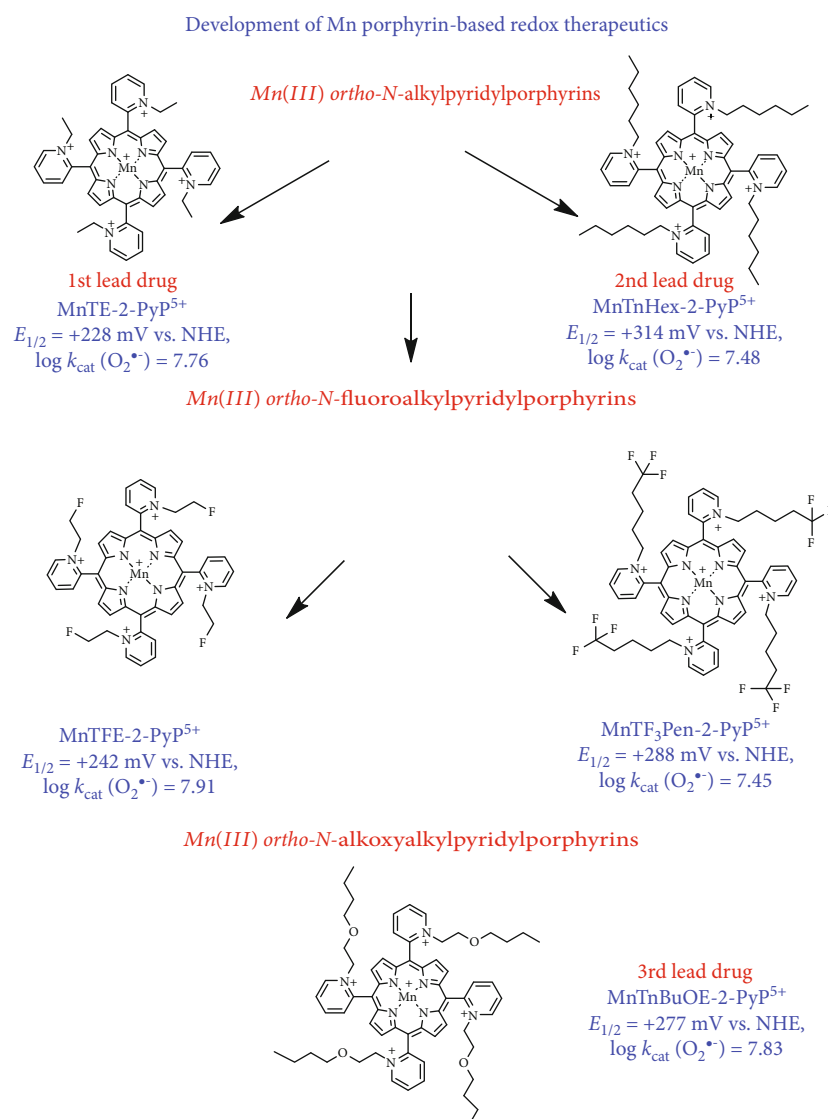
FIGURE 1: Development of Mn porphyrins towards analogs of optimized efficacy, bioavailability, and safety/toxicity [4, 25]. *Ortho* positions of *N*-pyridyl substituents, due to the vicinity to the Mn site and the cationic charge, afford the best thermodynamics and kinetics for the catalysis of $O_2^{\bullet-}$ dismutation in an SOD-like fashion; we named the key feature of such design the *ortho* effect. Based on the *ortho* effect, the first generation of powerful SOD mimics was synthesized [6, 26]. Among those, a hydrophilic, MnTE-2-PyP^{5+} (BMX-010), became our 1st lead drug. Its ethylpyridyl chains were subsequently lengthened from up to 8 carbon atoms in order to increase the lipophilicity of the molecule [7]. Among those compounds, MnTnHex-2-PyP^{5+} has the best balance between the lipophilicity (that would not damage cellular membranes at low clinically relevant concentrations) and its SOD-like potency and became our 2nd lead drug. To further diminish the toxicity of MnTnHex-2-PyP^{5+}, we introduced the oxygen atoms into hexyl chains deep into the porphyrin cavity. The butoxyethyl analog was created, MnTnBuOE-2-PyP^{5+} (BMX-001), and this became our 3rd lead drug. The approach was similar to the one where ether of sodium dodecyl sulfate (SDS) was synthesized to reduce the toxicity of SDS [10]. Based on the same principles of the *ortho* effect, the *N*-alkylpyridyl groups were fluorinated and two analogs were created: Mn(III) *meso*-tetrakis(*N*-fluoroethylpyridinium-2-yl)porphyrin, MnTFE-2-PyP^{5+} (BMX-002), and Mn(III) *meso*-tetrakis(*N*-trifluoropentylpyridinium-2-yl)porphyrin, MnTF$_3$Pen-2-PyP^{5+} (BMX-003). Aqueous chemistry data suggest improved safety/toxicity and efficacy profiles of fluorinated *vs.* nonfluorinated analogs. Initial studies confirmed their potency in radioprotecting normal tissue and radio- and chemosensitizing the 4T1 mouse breast cancer cell line in cellular and animal models [23, 24]. Below each of the structures, the metal-centered reduction potential for the Mn(III)/Mn(II) redox couple and log $k_{cat}(O_2^{\bullet-})$ for the catalysis of $O_2^{\bullet-}$ dismutation are listed.

then able to replace three hydrogens with fluorines in a pentyl analog as those fluorines were far away from the nitrogen atoms of the *meso* pyridyl rings. Such strategy gave rise to Mn(III) *meso*-tetrakis(*N*-trifluoropentylpyridinium-2yl)porphyrin MnTF$_3$Pen-2-PyP^{5+} (BMX-003). As anticipated, both

compounds have increased lipophilicity and reduced toxicity relative to nonfluorinated analogs as assessed in an *E. coli* assay [23, 24]. Another example of the reduced toxicity relates to the blood pressure drop, which imposes a limitation to the dosing of MnPs. Both MnTFE-2-PyP^{5+} and MnTF$_3$Pen-2-

PyP^{5+} exhibit a significantly lower blood pressure drop than $MnTnBuOE-2-PyP^{5+}$ [23].

In combination with ascorbate and radiation, two fluorinated porphyrins were already tested in the 4T1 breast cancer mouse subcutaneous flank model: $MnTFE-2-PyP^{5+}$ (BMX-002) and $MnTF_3Pen-2-PyP^{5+}$ (BMX-003). Data showed that ascorbate enhances the ability of those compounds to radiosensitize tumor. Also, $MnTF_3Pen-2-PyP^{5+}$/ascorbate proved efficacious in the radioprotection of prostate and erectile function. Their efficacy is comparable to the efficacy of earlier analogs, which warrants their progression to the clinic [23, 24].

There are a number of Mn complexes, other than *ortho-N*-alkyl- or alkoxyalkylpyridyl porphyrins, that have been also explored and discussed in a number of our reviews [2–4, 27, 28]. Among those, the most frequently studied have been Mn(III) corroles [29], Mn(III) salen (EUK) series of compounds [30], anionic Mn(III) porphyrin $MnTBAP^{3-}$ and cationic Mn(III) *meso*-tetrakis(*N,N* ′-dialkyl- and *N,N* ′-dimethoxyethyl imidazolium-2-yl)porphyrins, with $MnTDE-2-ImP^{5+}$ (AEOL10150) being the most frequently studied compound. $MnTDE-2-ImP^{5+}$ is also progressing towards the clinic for the radioprotection of normal tissue [9, 31–34]. Several members of the family of Mn cyclic polyamines [35] and Mn complexes whose structures have been inspired by the active site of SOD protein have been also explored [36]. Finally, the Gd and Lu complexes with extended porphyrins—texaphyrins—have been investigated [37]. The anionic Mn(III) *meso*-tetrakis(*p*-carboxylatophenyl)porphyrin, $MnTBAP^{3-}$, is not an SOD mimic. It has negligible catalase and GPx-like activities as well as the ability to oxidize ascorbate and ~300-fold lower ability to reduce peroxynitrite than $MnTnBuOE-2-PyP^{5+}$ and $MnTE-2-PyP^{5+}$ which all account for the therapeutic effects of cationic Mn porphyrins [4, 38]. Though the therapeutic effects of $MnTBAP^{3-}$ were reported by us and others, based on its aqueous chemistry, the origin of such effects cannot be fully understood and were discussed in several of our manuscripts [38–42]. Mn salen compounds have low SOD-like activity, and following activities are negligible: catalase-like activity, ability to oxidize ascorbate and GPx-like activity [43]. Yet in our own hands, in a study on *Cryptococcus neoformans* MnSOD-knockout, EUK-8 was the only compound protective against temperature-induced assault; no other cationic or anionic Mn porphyrin, Tempol, or $MnCl_2$ were efficacious [44]. Among the Mn salen EUK series, Mn EUK-134 is in use in humans—in Estee Lauder cosmetic products [30, 43]. The study on *Cryptococcus neoformans* is one of many that clearly indicates that so much is left to comprehend with regard to the interaction of redox-active compounds with components of the redox biology of a cell.

In addition to the Mn porphyrins, their Fe analogs have been extensively studied also [26, 45]. Analogous Fe porphyrins are as powerful SOD mimics as Mn analogs, yet more prone to oxidative degradation [45]. Moreover, they differ with regard to their coordination chemistry [26, 45]. Due to the propensity of the Fe center towards axial coordination, in an aqueous solution Fe porphyrin exists as a monohydroxo/monoaqua species, while Mn porphyrin exists as diaqua species (water molecules are usually not shown). Yet in a rich cellular milieu, Fe por-

phyrin would readily coordinate biomolecules. This would in turn prevent its Fe center to react with reactive species, precluding therapeutic effects of Fe porphyrins [26, 45]. We have tested $MnTnHex-2-PyP^{5+}$ ($\log k_{cat}(O_2^{\bullet-}) = 7.48$) and $(OH)FeTnHex-2-PyP^{4+}$ ($\log k_{cat}(O_2^{\bullet-}) = 7.53$) in a rodent stroke model [46]. Despite favorable plasma pharmacokinetics of the Fe analog and brain levels as high as those of the Mn analog, only Mn porphyrin was efficacious in a rodent stroke model [46]. In addition, the effects of Fe porphyrins were studied in a SOD-deficient *Escherichia coli* in comparison to Mn analogs [26, 45]. $(OH)FeTE-2-PyP^{4+}$ protects SOD-deficient *E. coli* in a concentration range of $0.01-1 \mu M$, but exhibits toxicity at concentrations higher than $1 \mu M$. Mn analog starts to become efficacious at concentrations higher than $5 \mu M$. Due to different growth patterns, further studies were conducted and it was demonstrated that Fe porphyrin works *via* delivering Fe to the cell [45]. Taken together, our data on Fe porphyrins indicate that more studies are needed before the progress of Fe porphyrins towards the clinic may be considered.

3. Bioavailability of Mn Porphyrins

Extensive studies on cationic Mn(III) porphyrins showed their high bioavailability in different cells, cellular organelles, and organs (reviewed in [4]). Their distribution is primarily governed by the positive charges which drive them towards anionic phosphate groups in plasma membrane, mitochondrial membranes, and the nucleus. Their bioavailability is further enhanced by their lipophilicity [4]. The tetracationic Zn analogs were also explored for their biodistribution and were additionally found in lysosomes, membranes, and endoplasmic reticulum [47] indicating that similar distribution may also be true for pentacationic MnPs. The studies on ZnPs demonstrated that the increase in the length of the alkyl chains, and their positions on pyridyl rings affecting the bulkiness/planarity of the molecule, directed the distribution of ZnPs from predominantly lysosomal (ZnTM-2-PyP^{4+}) to mitochondrial sites (ZnTnHex-2-PyP^{4+}).

$MnTE-2-PyP^{5+}$, $MnTnHex-2-PyP^{5+}$, and $MnTnBuOE-2-PyP^{5+}$ were most closely explored with regard to their bioavailability and pharmacokinetics (PK) (reviewed in [4]). The mitochondrial distribution of MnPs was also explored given the central role of the mitochondria in cellular metabolism under physiological and pathological conditions. $MnTE-2-PyP^{5+}$ was found to preferentially distribute in heart mitochondria relative to cytosol at a 1.6 : 1 ratio [48–51]. Yet, it was only found in brain cytosol, but not in brain mitochondria. The other two lipophilic MnPs prefer heart mitochondria to cytosol at a ratio of ~3 : 1. Moreover, they were found in brain mitochondria *vs.* cytosol at a similar ratio of ~2 : 1 [51, 52]. Such preferential mitochondrial distribution accounts for numerous therapeutic effects of MnPs, many of which are detailed in [27].

All three MnPs are available when given to the mouse subcutaneously (sc), intravenously (iv), intraperitoneally (ip), and topically [4, 28, 49, 53–57]. They have poor oral availability: 0.6, 2.9, and 3.9% for $MnTE-2-PyP^{5+}$,

MnTnHex-2-PyP^{5+}, and MnTnBuOE-2-PyP^{5+}, respectively [4]. Data obtained on MnTnHex-2-PyP^{5+} suggest excellent availability of MnPs if given *via* inhalation [4]. These three MnPs are distributed in all organs, brain included, and to the highest level in the liver and kidney, which serve as depot organs for redistribution in other tissues. The best tissue penetration and retention distribution were found for the most lipophilic MnTnHex-2-PyP^{5+}. The initial PK profiles of MnPs were obtained *via* ip and iv routes, at 2 mg/kg for the lipophilic analog MnTnHex-2-PyP^{5+} and at a 5-fold higher dose of 10 mg/kg for the hydrophilic MnTE-2-PyP^{5+}. The PK of MnTnHex-2-PyP^{5+} was characterized by higher plasma t_{max} (1 h), similar plasma C_{max} (1.52 μM), higher plasma C_{24} (0.01 μM), slower plasma $t_{1/2}$ of elimination (3.8 h), and higher body exposure in many organs, described by the area under the curve (AUC) than MnTE-2-PyP^{5+} (t_{max} (0.17 h), C_{max} (11.57 μM), C_{24} (0.005 μM) and $t_{1/2}$ of elimination (6.4 h)) [49, 53, 55]. The plasma AUC_{ip} was 83% of AUC_{iv} for MnTE-2-PyP^{5+} and 84% for MnTnHex-2-PyP^{5+}.

The mouse PK of MnTnBuOE-2-PyP^{5+} was done *via* the sc route at 10 mg/kg in comparison with the iv route at 2 mg/kg [28, 54, 56, 57]. The following PK parameters for sc PK were calculated: plasma t_{max} (1.3 h), plasma C_{max} (6.2 μM), and plasma AUC (23.58 μM·h). The high body exposure was achieved *via* the sc route of administration, which also affords the safest delivery of MnP compared to the iv route with a lesser dose-limiting side effect—blood pressure drop. Again, the highest levels of the drug were found in the liver and kidney. Comprehensive mouse brain PK of MnTnBuOE-2-PyP^{5+} was also performed *via* the sc route in the olfactory bulb, brainstem, cerebellum, thalamus, hippocampus, and cortex [58]. After 10 days of sc administration of 1.5 mg/kg twice daily, the brain levels of lipophilic MnTnBuOE-2-PyP^{5+} and MnTnHex-2-PyP^{5+} were between 15 and 160 nM. Much lower levels in brain parts were found for MnTE-2-PyP^{5+} (ranging from 0.8 to 36 nM) [58]. In a dog PK study, MnTnBuOE-2-PyP^{5+} was injected sc for 3 weeks at 0.25 mg/kg three times per week [4, 59]. The highest levels were found in peripheral lymph nodes (ranging from 4 to 6 μM), followed by the levels in the liver (2.5 μM) and kidney (2.0 μM) [4]. Such bioavailability suggests the therapeutic potential of MnTE-2-PyP^{5+} in the treatment of lymphoma [60, 61].

Out of the 3 MnPs, MnTE-2-PyP^{5+} has the safest toxicity profile, but the data demonstrate that MnTnBuOE-2-PyP^{5+} poses no genotoxic risk to humans [55, 56]. Both compounds proved to be safe and well tolerated in Phase I, and both progressed to the Phase II clinical trials [13–15].

4. Mn Porphyrins as Redox-Active Compounds

4.1. Reactivity of Mn Porphyrins with Low-Molecular-Weight Reactive Species.
While initially developed as SOD mimics, MnPs do not possess the quaternary structure of an enzyme to be specific for the reaction with superoxide ($O_2^{\bullet-}$). MnPs are small molecules with no steric hindrance towards incoming reactive species. Indeed, they are almost as reactive with peroxynitrite (ONOO$^-$), as with $O_2^{\bullet-}$ [62]. Our insight into their reactivities matured along with mounting knowledge on the redox biology. The very first insight into MnPs' reactivity, other than towards $O_2^{\bullet-}$, was provided in collaboration with Radi et al.; the reactions towards peroxynitrite (ONOO$^-$) and carbonate radical ($CO_3^{\bullet-}$) were explored [63, 64]. A decade later, the same collaboration showed a high activity of MnPs towards hypochlorite, (ClO$^-$) [65]. In essence, MnPs are reactive with any reactive species we have thus far explored which in addition to ONOO$^-$ and $O_2^{\bullet-}$ include hydrogen peroxide (H_2O_2), ClO$^-$, nitric oxide ($^{\bullet}$NO), glutathione (GSH), ascorbate, hydrogen sulfide (H_2S) [66, 67], oxygen (O_2), sulfite (SO_3^{2-}), tetrahydrobiopterin (BH_4), and protein (cysteine) thiols (R-SH) [4, 62]. Due to the complex chemistry of MnPs with 4 oxidation states available for *in vivo* reactions, and complex biological milieu, many more reactions are to be uncovered. The important message from studies in aqueous milieu is that the more potent the SOD mimic Mn porphyrin is, the more potent it is also in undergoing redox reactions with reactive species thus far explored other than $O_2^{\bullet-}$, namely, ONOO$^-$, ClO$^-$, H_2S, ascorbate, H_2O_2, and thiols via the GPx-like reactivity [4, 48, 49, 65–67]. Numerous efficacy studies further demonstrated that the more potent the SOD mimic Mn porphyrin is, the more efficacious therapeutic it tends to be [2–4, 62, 68, 69].

The critical role of the SOD enzyme in tumorigenesis staged grounds for the exploration of SOD mimics in cancer [27, 70, 71]. We have early on demonstrated that MnPs inhibit transcription factors, such as hypoxia-inducible factor (HIF-1α), activator protein (AP-1), and specificity protein (SP-1) [3, 4, 62]. We had no clue, until more than 10 years later, what was really happening, *i.e.*, how a small molecule such as MnP interacts with a huge protein structure and in the process inhibits its activity. The first explanation was that MnP removes reactive species, such as $O_2^{\bullet-}$ and ONOO$^-$ (in antioxidative fashion), which would have otherwise served as a signal for the activation of proteins involved in apoptotic/proliferative pathways. We knew early on that MnP reacts with endogenous small-molecular-weight antioxidants, oxidizing ascorbate one-electronically into ascorbyl radical [26] and glutathione into glutathione radical [48]. We have overlooked the seemingly obvious fact that during the dismutation process, MnP does act as a prooxidant in the 1st step of the process, oxidizing $O_2^{\bullet-}$ into oxygen. Despite such evidence, we have not for a long while considered that the prooxidative action of MnP happens *in vivo* and may play a major role in the overall mechanism of action of MnPs. The very first suggestion of a prooxidative action of MnP from *in vivo* studies came from our colleague Jon Piganelli; he suggested that MnTE-2-PyP^{5+} oxidizes the p50 subunit of nuclear factor-κB (NF-κB) in the nucleus, preventing its transcription [72]. The subsequent collaborative study demonstrated the feasibility of such notion due to ~3-fold higher accumulation of MnTE-2-PyP^{5+} in the nucleus than in cytosol [48]. Still, at that point in time, we did not understand the type of reaction/s behind such event.
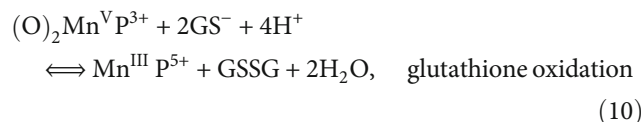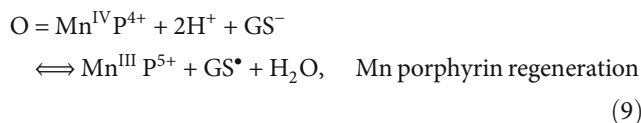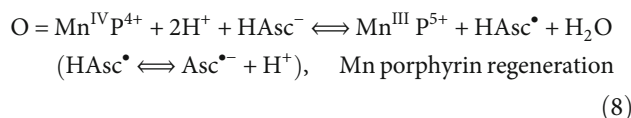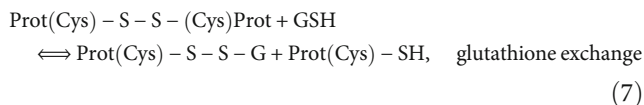
4.2. Reactivity of Mn Porphyrins towards Protein Cysteines -Thiol Signaling.
Independent studies by Tome's lab were crucial to understand the nature of the major action/s of MnPs *in vivo*, and in particular in *cancer cells* [60, 61, 73].

Her studies on the lymphoma cellular model showed that MnTE-2-PyP^{5+} alone (cycling with cellular reductants such as ascorbate as described in equations (1)–(3)), and more so in the presence of dexamethasone, increases the levels of H$_2$O$_2$ [74]. In the next step, MnP employs H$_2$O$_2$ to undergo oxidation into high-valent and highly oxidizing Mn(IV) [starting from reduced Mn(II)P, not shown] and Mn(V) oxo species [starting from Mn(III)P, equation (4)]. These species [shown for Mn(III)P] can subsequently oxidize the protein cysteine residue, Prot-Cys-S$^-$, into the Prot-Cys-S$^•$ radical (equation (5)). The Prot-Cys-S$^•$ radical then couples with another radical to make disulfide. Disulfide exchanges glutathione in the presence of GSH (equation (6)) and gets S-glutathionylated (equation (7)) [60, 61]. The high-oxo MnP gets recycled back into its resting state, Mn^{III}P^{5+}, with a cellular reductant such as ascorbate and glutathione (equations (8) and (9)). The kinetics of the reaction of O = Mn^{IV}TM − (2, 3 and 4)PyP^{4+} with tyrosine, glutathione, and ascorbate was reported by Radi's team [63]. High-valent MnPs can also oxidize GSH giving rise to GSSG (equation (10)). Several reactions, in addition to those shown below, can also account for the protein S-glutathionylation (see other possibilities in [4, 43, 74]). In one of those scenarios, instead of reacting with another Pr(Cys)-S$^•$ radical to form disulfide (equation (6)), Pr(Cys)-S$^•$ reacts with GSH. Such reaction results in the formation of a Prot(Cys)-S-S-G$^{•-}$ anion radical, which then reacts with oxygen giving rise to glutathionylated protein, Prot(Cys)-S-S-G [43]. The high-valent Mn(V) dioxo species can also oxidize its own porphyrin ligand giving rise to the Mn(IV) porphyrin π-cation radical, O = Mn(IV)P$^{•+}$, which would result in the degradation of the Mn complex [75]. The involvement of H$_2$S/MnP in the S-glutathionylation of proteins was also implicated [66, 67]. In the study of Tome's lab, MnP oxidizes primarily cys38 of the p65 subunit of NF-κB and to a lesser degree cys62 of the p50 subunit. Her team provided unambiguous evidence that H$_2$O$_2$ and GSH are necessary for such protein oxidative modification to occur. The team showed that no S-glutathionylation happened when catalase was overexpressed or GHS synthesis inhibited [74]. Finally, Tome's team provided direct evidence that S-glutathionylation was the type of oxidative damage to NF-κB inflicted by MnP [61]. Such work helped us understand how the small Mn porphyrin molecule reacts with cysteines exposed at the surface of proteins, and in turn affects the cellular signaling pathways.

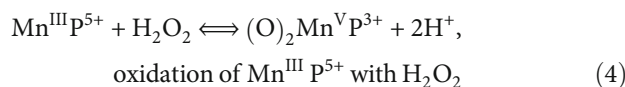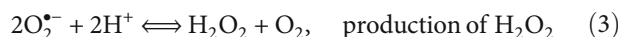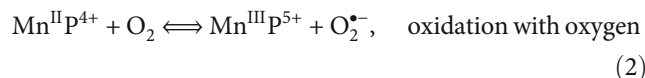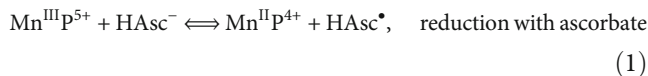In addition to NF-κB, Tome's lab showed that complexes I, III, and IV of the mitochondrial respiration were also oxidized by MnP/H$_2$O$_2$/GSH. Complexes I and III, but not complex IV, were inactivated by such oxidative modification. Data suggest that some proteins involved in glycolysis may also be oxidized by the action of MnP/H$_2$O$_2$/GSH [60]. Importantly, MnP did not oxidize proteins in normal lymphocytes [60].

In addition to the glucocorticoid, dexamethasone, Tome's team also demonstrated that MnPs have potential for use in hematologic malignancies that are treated with cyclophosphamide and doxorubicin [73]. While MnTE-2-PyP^{5+} sensitized murine thymic lymphoma cells to cyclophosphamide, it protected H9c2 cardiomyocytes from doxorubicin toxicity [73].

Jones referred to S-glutathionylation as a major *in vivo* thiol oxidative modification [76, 77]. MnP gets involved in thiol signaling, *via* reversible S-glutathionylation, providing an on/off switch for an individual protein. More details on the proteins, which activities are thus far found modified by MnPs, are listed below under "Molecular Pathways Affected by Mn Porphyrins in Cancer and Normal Cell" :

$$Mn^{III}P^{5+} + HAsc^- \Longleftrightarrow Mn^{II}P^{4+} + HAsc^•, \quad \text{reduction with ascorbate} \tag{1}$$

$$Mn^{II}P^{4+} + O_2 \Longleftrightarrow Mn^{III}P^{5+} + O_2^{•-}, \quad \text{oxidation with oxygen} \tag{2}$$

$$2O_2^{•-} + 2H^+ \Longleftrightarrow H_2O_2 + O_2, \quad \text{production of } H_2O_2 \tag{3}$$

$$Mn^{III}P^{5+} + H_2O_2 \Longleftrightarrow (O)_2Mn^VP^{3+} + 2H^+,$$
$$\text{oxidation of } Mn^{III}P^{5+} \text{ with } H_2O_2 \tag{4}$$

$$(O)_2Mn^VP^{3+} + 2H^+ + Prot(Cys) - S^-$$
$$\Longleftrightarrow O = Mn^{IV}P^{4+} + Prot(Cys) - S^• + H_2O, \tag{5}$$
$$\text{oxidation of protein cysteine}$$

$$Prot(Cys) - S^• + Prot(Cys) - S^•$$
$$\Longleftrightarrow Prot(Cys) - S - S - (Cys)Prot, \quad \text{disulfide formation} \tag{6}$$

$$Prot(Cys) - S - S - (Cys)Prot + GSH$$
$$\Longleftrightarrow Prot(Cys) - S - S - G + Prot(Cys) - SH, \quad \text{glutathione exchange} \tag{7}$$

$$O = Mn^{IV}P^{4+} + 2H^+ + HAsc^- \Longleftrightarrow Mn^{III}P^{5+} + HAsc^• + H_2O$$
$$(HAsc^• \Longleftrightarrow Asc^{•-} + H^+), \quad \text{Mn porphyrin regeneration} \tag{8}$$

$$O = Mn^{IV}P^{4+} + 2H^+ + GS^-$$
$$\Longleftrightarrow Mn^{III}P^{5+} + GS^• + H_2O, \quad \text{Mn porphyrin regeneration} \tag{9}$$

$$(O)_2Mn^VP^{3+} + 2GS^- + 4H^+$$
$$\Longleftrightarrow Mn^{III}P^{5+} + GSSG + 2H_2O, \quad \text{glutathione oxidation} \tag{10}$$

MnP does not discriminate cancer cells from normal cells. Thus, the same type of reactions would occur in both normal and cancer cells, but at different yields controlled by much higher levels of H$_2$O$_2$ and MnP in cancer cells than in normal cells [43]. High yields of oxidation of proteins in cancer, such as NF-κB and mitogen-activated protein kinases (MAPKs) would subsequently result in massive apoptosis of cancer cells (see below under "Molecular Pathways Affected by Mn Porphyrins in Cancer and Normal Cell").

In a *normal cell*, H$_2$O$_2$ (endogenously formed in many processes) is, however, kept at nM level with abundant enzymes, such as catalase, glutathione peroxidase, and

peroxiredoxins and their partner proteins, thioredoxins. Under an oxidative insult, MnP^{5+} would cycle in the cell with cellular reductants such as ascorbate (equations (1)–(3)) and glutathione or protein cysteines and would be reduced to $Mn^{II}P^{4+}$, which would then be reoxidized to $Mn^{III}P^{5+}$, thereby reducing oxygen to $O_2^{\bullet-}$. $O_2^{\bullet-}$ would in turn enzymatically or spontaneously dismute to H_2O_2 and O_2 (equation (3)). The production of H_2O_2, while not excessive in a normal cell, would just be sufficient to be employed by MnP for the catalysis of oxidation and inhibition of NF-κB, oxidation of Kelch-like ECH-associated protein 1 (Keap1), and activation of nuclear factor E2-related factor 2 (Nrf2) [4]. Moderate inhibition of NF-κB would in turn suppress exccessive inflammatory responses. The activation of Nrf2 would result in the upregulation of cellular endogenous antioxidant defenses including MnSOD, catalase, and glutathione-S-transferase that would remove $O_2^{\bullet-}$ and H_2O_2. Thus, in a normal but diseased tissue/cell, modest inhibition of NF-κB and activation of Nrf2 would jointly restore the cellular physiological redox environment.

5. Molecular Pathways Affected by Mn Porphyrins in Cancer and Normal Cell

The MnP-driven oxidation of NF-κB was explored in both normal cell/tissue [72, 78, 79] and cancer and seems to be at least one of the major pathways contributing to the therapeutic effects of MnPs [4, 60, 61, 80, 81]. Yet, the impact on Nrf2 was thus far only explored in normal tissue [82]. Several other pathways affected by MnPs were also explored in cancer but not in normal cells, and were detailed below and listed in Figure 2. Abbreviations of signaling proteins affected by MnPs are described in the legend of Figure 2.

5.1. Cancer Cell. The redox proteomics of the *mouse breast 4T1 cancer cell line*, exposed to excessive levels of H_2O_2 produced *via* cycling of MnTE-2-PyP^{5+} with ascorbate (equations (1)–(3)), demonstrated that 3605 peptidyl cysteines (Cys) were affected in total, out of which 1577 were oxidized 1.3-fold or higher compared with control, untreated 4T1 breast cancer cells [80]. While cancer cells may be under oxidative stress and have Nrf2 already activated, our data provide clear evidence that the MnP/Asc system oxidized Keap1 which may lead us to assume that this would activate the Nrf2 pathway. The MnP/Asc system affected 1762 proteins in total, among which 942 proteins were associated with >1.3-fold oxidized peptidyl Cys. Such massive oxidative modification of proteins, driven by MnP/ascorbate, promoted apoptotic pathways in tumor cells. The pathways affected were those associated with the regulation of cytoskeleton rearrangement, transcription-mRNA processing, translation, protein folding, cell cycle, and adhesion. Most affected was the toll-like receptor signaling (TLR) with the largest number of pathways involved, the components of which are listed below. The fold oxidation, imposed by MnP/ascorbate relative to nontreated 4T1 cells, is given in parenthesis: NF-κB (1.39-fold), Keap1 (3.73-fold), p38 MAPK (1.36-fold), p38a (MAPK14) (6.84-fold), and heat shock protein HSP60 (4.26-fold). The protein kinase

PKCσ (1.39-fold) and PKCι (2.74-fold) as well as serine/-threonine protein phosphatase 2A subunit A (1.51-fold) have a critical impact on the TLR pathway [80, 83–85]. In addition to HSP60, several other HSPs were found oxidized also. Of our immediate interest, redox proteomics indicated that cysteines of numerous endogenous antioxidative defenses were oxidized, such as glutaredoxin 3 (1.85-fold) and glutaredoxin 5 (2.62-fold); glutathione-S-transferase o1 (1.64-fold); isocitrate dehydrogenases 1 (1.87-fold), 2 (1.68), and 3 (2.46-fold); peroxiredoxins 4 (2.26-fold), 5 (1.99-fold), and 6 (1.47-fold); thioredoxin 1 (1.72-fold), and thioredoxin domain containing proteins 5 (1.36-fold) and 6 (2.46-fold). Based on the results from Tome's lab (see under "Reactivity of Mn Porphyrins towards Protein Cysteine-Thiol Signaling") and our data from the mouse breast cancer study (see under "Breast Cancer"), we may safely assume that S-glutathionylation is the type of oxidative modification. Reportedly, such oxidative modification results in protein inactivation [61, 74, 86–90]. In addition, Cu,ZnSOD and catalase were oxidized also.

In a collaborative mouse study with Park's team's a lipophilic analog with similar redox properties , MnTnHex-2-PyP^{5+}, radiosensitized 4T1 breast cancer cell line resulting in a large suppression of tumor growth. In accompaning cellular study, MnTnHex-2-PyP^{5+} suppressed the antiapoptotic pathways NF-κB, bcl-2, and mcl-1, while promoting the proapoptotic pathways bim, bak, cleaved PARP, and cleaved caspase 3 (Figure 2) [91]. The authors also found that the radiation-induced activation of several MAPKs (ERK, JNK, AKT and p38 MAPK), was greatly suppresed by MnP; such data are in agreement with the study on redox proteomics of a 4T1 breast cancer cell line exposed to MnP/ascorbate. Finally, the authors reported also the radiosensitization of the B16 melanoma cell line by MnTnHex-2-PyP^{5+} in a mouse model [91].

The effect of MnTE-2-PyP^{5+}/ascorbate upon NF-κB, ERK1/2, and p38 MAPK was also seen in a study of the rare and highly aggressive inflammatory breast cancer (IBC) cell line SUM149 (basal type) [92]. MnTE-2-PyP^{5+} significantly depleted glutathione levels and reduced phosphorylated NF-κB, ERK1/2, and p38 MAPK. MnTE-2-PyP^{5+}/ascorbate induced the release of the apoptosis inducible factor, AIF, from mitochondria which was followed by its translocation into the nucleus. This event is known to induce caspase-independent cell death. The decreased X-linked inhibitor of apoptosis protein, XIAP, and the increase in cleaved PARP by MnTE-2-PyP^{5+}/ascorbate was also demonstrated, revealing apoptosis-mediated cytotoxicity in cells [69]. Both MnTE-2-PyP^{5+} and MnTnBuOE-2-PyP^{5+} combined with ascorbate suppressed the viability of the SUM190 (erb-b2, receptor tyrosine kinase 2, overexpressor cell line), SUM149, and even rSUM149 cell lines. The rSUM149 cell line is an isogenic derivative of SUM149 that shows significant resistance to reactive species-mediated apoptosis due to high levels of GSH, Cu,ZnSOD, and MnSOD.

The effect of MnTnBuOE-2-PyP^{5+}, MnTE-2-PyP^{5+}, and MnTnHex-2-PyP^{5+} was also explored in studies on *hematologic malignancies* (lymphoma, multiple myeloma, and the activated B cell subtype of diffuse large B cell lymphoma)
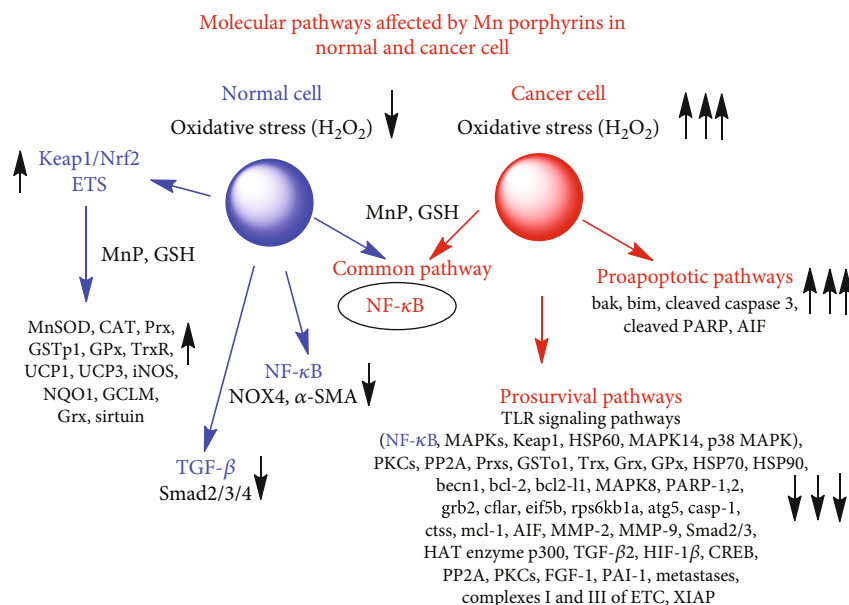
FIGURE 2: Molecular pathways affected by Mn porphyrins in normal and cancer cell. Most of the data were derived from breast cancer and glioma studies. Two major pathways, affected by Mn porphyrins, have been explored: nuclear factor-κB (NF-κB) and Keap1/nuclear factor E2-related factor 2 (Nrf2). In both tumor and normal tissue injury, NF-κB was inactivated by the MnP-driven catalysis of p50 and p65 cysteine oxidation in the presence of H_2O_2 and GSH. The yield of inactivation depends upon MnP and H_2O_2 levels, both of which are higher in tumor than in normal cell *Normal cell. Hematopoietic stem/progenitor cells.* The nuclear factor E2-related factor 2 (Nrf2) pathway was activated, and it upregulated endogenous antioxidative defenses such as MnSOD, catalase (CAT), glutathione peroxidase (GPx), peroxiredoxin (Prx), glutaredoxin (Grx), glutathione-*S*-transferase (GSTp1), NAD(P)H quinone dehydrogenase (NQO1), uncoupling proteins 1 and 3 (UCP1 and UCP3), and glutamate cysteine ligase regulatory subunit (GCLM). In the study, the ETS transcription activity, which plays role in hematopoiesis, was also increased. The ETS family of transcription factors is among the end effector molecules of the signal transduction pathway. Phosphorylation of ETS modulates DNA binding, protein-protein interaction, transcriptional activation, and subcellular localization. ETS stands for E26 transformation specific or E26, as the ETS sequence (v-ets) was first identified in the genome of the avian retrovirus E26. *Normal colorectal and prostate fibroblasts.* The effect of MnP on NADPH oxidase 4 (NOX4) and α-smooth muscle actin (α-SMA), Nrf2, NF-κB, and TGF-β molecular with a subsequent effect on Smad 2/3 was reported. Smad 2/3 is the main signal transducer for receptors of the transforming growth factor beta (TGF-β) superfamily. The abbreviation stands for an acronym from the fusion of *Caenorhabditis elegans* Sma and the *Drosophila* Mad (Mothers against decapentaplegic) genes. *Cancer. 4T1 breast cancer.* NF-κB, a part of the TLR molecular pathway, is the major pathway affected by MnP/ascorbate in 4T1 cells as found by redox proteomics. In addition, and as a part of the TLR pathway, MnP/ascorbate oxidized cysteines of different mitogen-activated protein kinases (MAPKs) (p38 mitogen-activated protein kinase (p38 MAPK) and MAPK14) and protein kinase C (PKC ι and δ). We have also seen the oxidation of Kelch-like ECH-associated protein 1 (Keap1) as part of the TLR pathway. In addition, endogenous antioxidative defenses were oxidized, such as Cu,ZnSOD, glutathione-*S*-transferase (GSTo1), peroxiredoxins (Prxs), thioredoxin, thioredoxin 1 (Trx1), and heat shock proteins (HSPs). In another 4T1 breast cancer study, the inactivation of c-Jun N-terminal kinase (JNK), extracellular signal-regulated kinase (ERK), and protein kinase B (AKT) by MnP/RT was seen. Also, the suppression of antiapoptotic NF-κB, bcl-2, and mcl-1; the promotion of proapoptotic pathways, bak and bim; and the increase of cleaved PARP and cleaved caspase 3 were demonstrated. *Inflammatory breast cancer.* In SUM149 cells, the inhibitory effect of MnTE-2-PyP^{5+} on NF-κB, p38 MAPK, ERK1/2, XIAP (X-linked inhibitor of apoptosis protein); the activation of apoptosis-inducing factor (AIF); and the increase in PARP cleavage were seen. *Glioblastoma multiforme/glioma.* In glioma tissue from a subcutaneous xenograft mouse study, the cell death array showed a number of genes downregulated by MnP/RT (fold difference *vs.* RT alone listed in parenthesis). Among the most affected genes are those that regulate the following proteins (listed from most affected to less affected): eif5b, eukaryotic translation initiation factor 5B (-408.8-fold); rps6kb1a, serine/threonine kinase that acts downstream of PIP3 (phosphatidylinositol (3,4,5)-trisphosphate) and phosphoinositide-dependent kinase-1 in the PI3 kinase pathway (-176.6-fold); bcl2-l1, a potent inhibitor of apoptosis (-59-fold); ctss, cathepsin S (-59-fold); grb2, growth receptor bound protein-2, an adaptor protein involved in signal transduction/cell communication (-45.5-fold); atg5, autophagy-related protein (-43-fold); cflar, CFLAR, CASP8, and FADD-like apoptosis regulator (-38.7-fold); casp1, inflammasome mediates activation of caspase-1 which promotes the secretion of the proinflammatory cytokines IL-1β, IL-18, and pyroptosis (-37-fold); CD40, cluster of differentiation 40, member of the TNF superfamily essential to a broad array of immune and inflammatory responses (-21-fold); becn1, plays critical role in autophagy and cell death (-16-fold); NF-κB p105 subunit (-13.6-fold); MAPK8 (also known as JNK1), mitogen-activated kinase which plays a key role in T cell proliferation, apoptosis, and differentiation (-7.8-fold); PARP-1 and PARP-2, poly(ADP-ribose) polymerase-1 and 2 (-5.4-fold and -3.3-fold, respectively). *Prostate cancer.* The effect of MnP was seen on histone acetyltransferase p300 (HAT p300), cAMP response element-binding protein (CREB), fibroblast growth factor (FGF), hypoxia-inducible factor 1β(HIF-1β), and plasminogen activator inhibitor-1 (PAI-1). *Colorectal cancer.* MnP-driven suppression of transforming growth factor (TGF-β) and in turn matrix-metalloproteinases 2 and 9 (MMP-2 and MMP-9) and Smad 2/3 was reported. *Hematologic malignancies.* NF-κB and complexes I, III, and IV of the mitochondrial electron-transport chain (ETC) were oxidized by MnP.

(see under "Reactivity of Mn Porphyrins towards Protein Cysteine-Thiol Signaling" and Figure 2) [4, 60, 61, 91].

The tumor radio- and chemosensitization was demonstrated in a mouse subcutaneous 245-MG *glioblastoma multiforme* xenograft model when mice were treated with radiation, temozolomide, and either MnTnBuOE-2-PyP^{5+} or MnTnHex-2-PyP^{5+} [3, 93]. A cell death gene array demonstrated a significant decrease in gene expression in tumors of mice treated with MnTnBuOE-2-PyP^{5+}/radiation in comparison to radiation only [3, 94]. The metastatic pathways (*ctss* (-58-fold *beclin1*)) were largely downregulated, as were the antiapoptotic and NF-κB pathways (*Bcl2-l1* (-59-fold), *mcl-1* (-8.7-fold), *Nfkb1* (-13.6-fold), and PI3kinase and mTOR (*Rsp6kb1* (-177-fold)); fold decrease is listed in parentheses next to the name of the gene. The protein translation changes were also implicated as *Eif5b* was downregulated by -408.8-fold (Figure 2).

The impact of MnTnBuOE-2-PyP^{5+} combined with radiation was demonstrated in the suppression of the *FaDu human epithelial cell line from squamous cell carcinoma* of the hypopharynx in a mouse sc flank xenograft model. The tumor radiosensitizing effect of MnP was discussed with regard to the significant influx of tumoricidal M1 tumor-associated macrophages [54, 95]. Further, MnTnBuOE-2-PyP^{5+} reduced radiation-mediated mucositis, xerostomia, and fibrosis of salivary glands.

In prostate cancer studies, post radiation, MnTE-2-PyP^{5+} significantly reduced the overall HAT activity altering the p300 DNA binding, which resulted in the inhibition of HIF-1β and CREB signaling pathways as the expression of 3 of their genes, namely, TGF-β, FGF-1, and PAI-1, was reduced [96]. The HAT enzyme, p300, acetylates histones and increases overall transcription. The authors speculate that Mn porphyrin may not only be altering activity of transcription factors directly but may also be affecting transcription globally. Such effect may occur *via* modification of the redox transcription factor enhancer, p300 [96]. In another prostate cancer study, authors speculate that the anticancer effect of MnTE-2-PyP^{5+} on growth inhibition may occur through protein oxidative modifications and mitotic catastrophes in the PC3 prostate cancer cell line, while it may occur through tumor cell quiescence or cell death in the LNCaP prostate cancer cell line [97].

The impact of MnPs on metastases was reported by Oberley-Deegan et al. on colorectal cancer and Fernandes et al. on breast cancer (see below) [98]. *In colorectal cancer*, MnTE-2-PyP^{5+} significantly reduced the expression of mesenchymal markers, suppressing the phosphorylated Smad2/3 protein levels induced by TGF-β in SW480 cells. It also suppressed the TGF-β-mediated cell migration and invasion and the expression of matrix metalloproteinase 2 (MMP-2) and MMP-9 in colorectal cells [99, 100].

The human breast cancer cell lines, MCF-7 and MDA-MB-231, were studied by Flórido et al. [98]. Both cells are invasive ductal/breast carcinomas. While MDA-MB-231 is triple negative to estrogen and progesterone receptor and does not have HER2 amplification (human epidermal growth factor receptor 2), it is multidrug resistant and present in about 15% to 20% of all breast cancer cases. MCF-7 is an estrogen and progesterone receptor-positive cell line. MnTnHex-2-PyP^{5+} enhanced the cytotoxicity of doxorubicin to those breast cancer cells, *via* increasing H$_2$O$_2$ levels and reducing collective cell migration and chemotaxis thereby affecting their metastatic potential [98]. The reduction in a doxorubicin-induced increase in random migration and proteolytic invasion of MDA-MB-231 cells by MnP was also seen [98]. Breast cancer patients treated with doxorubicin, cyclophosphamide, and paclitaxel frequently exhibit brain toxicity, often described by cancer survivors as chemo brain. In a mouse study, McElroy et al. showed that MnTnBuOE-2-PyP^{5+} ameliorates effects on mature dendrite morphology and neurocognition [101]. The proteomic analysis suggested mitochondrial dysfunction, oxidative stress, and energy metabolism as possible mechanisms behind chemo brain. The most affected pathways by MnP/chemotherapy *vs.* chemotherapy include 3-phosphoinositide degradation, the super pathway of inositol phosphate compounds, the mitochondrial L-carnitine shuttle pathway, polyamine regulation, and Sirtuin signaling. The top network has functions associated with the cardiovascular system and cell morphology.

Driven by H$_2$O$_2$, MnP also has a beneficial impact on reducing cell viability and chemotactic migration of *human clear renal cancer cells* [102].

5.2. Normal Cell.

The very first evidence of the possible involvement of the Nrf2 pathway in the therapeutic effects of metalloporphyrins was reported by Konorev et al. [103] in a study on doxorubicin-induced toxicity to cardiomyocytes. One of the genes controlled by Nrf2 is heme oxygenase-1. Konorev et al. demonstrated that anionic metalloporphyrins, (OH)FeTBAP^{4-} and CoTBAP^{3-}, induced heme oxygenase-1 and protected cardiomyocytes from DOX-induced apoptosis [103]. MnTBAP^{3-} and ZnTBAP^{4-} were less efficacious. The reasoning behind the SOD-independent (but H$_2$O$_2$-dependent) suppression of DOX-induced toxicity to cardiomyocytes by Fe and Co porphyrins is as follows. (OH)FeTE-2-PyP^{4+} is ~13-fold better catalase mimic than its Mn analog, MnTE-2-PyP^{5+} [104]. Based on such analogy, and with MnTBAP^{3-} having $k_{cat}(H_2O_2) = 5.84$, the (OH)FeTBAP^{4-} would have $k_{cat}(H_2O_2)$ of ~76, slightly higher than the $k_{cat}(H_2O_2)$ of MnTE-2-PyP^{5+}, which is 63.32; our data show that the latter value allows for the efficient cycling of MnP with H2O2. This in turn implies that (OH)FeTBAP^{4-} could have been oxidized with H$_2$O$_2$ to the (O$_2$)Fe(V) species in the 1st step of the H$_2$O$_2$ dismutation process. This species of high oxidizing power could have in turn oxidized Keap1 and activated Nrf2.

In a *kidney ischemia/reperfusion model*, rats were treated with the cocktail containing MnTnHex-2-PyP^{5+}. 100 μg/kg/day of Mn porphyrin was given at -24, 0, and +24 h after clamping the left renal artery. Ischemia lasted 40 min, followed by 48 h of reperfusion. In comparison to nontreated rats, the real-time quantitative polymerase chain reaction for oxidative stress-related genes showed that numerous antioxidative enzymes were upregulated, such as MnSOD (10.2-fold); extracellular SOD (ECSOD) (12.3-fold); peroxiredoxins 2 (9.6-fold), 3 (9.8-fold), and 5 (6.6-fold);

GPx 1 (9.8-fold) and 3 (23.9-fold); and thioredoxin reductase 1 (6.9-fold) [105]. Such data suggested the role of Nrf2 in the protective mechanism of action of Mn porphyrin. This was the first study to suggest that MnP does not act as a SOD mimic in vivo, but rather upregulates the SOD enzyme.

Subsequently, St. Clair et al. provided the first direct evidence on the MnP-driven activation of the Nrf2 pathway. In a study on *hematopoietic stem/progenitor cells (HSPC)*, MnTnBuOE-2-PyP^{5+} enhanced the number and function of those cells under physiological conditions and improved the function of long-term engraftment and multilineage differentiation of HSC. *Via* activation of Nrf2/ARE (antioxidant response element) and ETS transcription activities, MnTnBuOE-2-PyP^{5+} regulated intracellular redox homeostasis, supporting quiescence and possibly affecting bone marrow HSPC regulation. The ETS family of transcription factors, comprising more than 26 genes in vertebrates, have been implicated in the regulation of hematopoiesis. Reduction in Nrf2 activity, however, was shown to enhance the differentiation of hematopoietic stem cells, while the reversal of Nrf2 knockdown increases pluripotency [106]. The upregulation of the following Nrf2-controlled genes was demonstrated by the action of MnP: MnSOD, catalase, glutathione-S-transferase p1 (GSTp1), NAD(P)H quinone dehydrogenase (NQO1), uncoupling proteins 1 and 3, and glutamate cysteine ligase regulatory subunit. Finally, the increased expression of MnSOD, catalase, GSTp1, and UCP3 proteins was demonstrated [82]. The data clearly demonstrate that MnP does not act as an SOD mimic but upregulates the SOD enzyme.

The MnP-driven activation of Nrf2 (with upregulation of MnSOD, NQO1, and sirtuin) and the inhibition of NF-κB (accompanied by suppression of NOX4 and α-SMA) was subsequently reported by Oberley-Deegan et al. to play a critical role in the radioprotection of *prostate* [107–109]. Further, her team demonstrated that the TGF-β pathway also plays a role in MnP-mediated protection of prostate fibroblasts from radiation-induced damage. Thus, MnTE-2-PyP^{5+} downregulates the expression of TGF-β receptor 2, with subsequent reduction in activation and/or expression of Smad2, Smad3, and Smad4. Consequently, Smad2/3-mediated transcription of profibrotic markers was reduced [108].

The impact of MnPs on the Keap1/Nrf2 pathway in cancer has not yet been studied. However, in the redox proteomics study of the 4T1 breast cancer cell line, where cells were treated with MnP/ascorbate, Keap1 was 3.73-fold oxidized relative to nontreated cells [4, 80]. Three scenarios may possibly account for such data: (i) Nrf2 might have been regulated by a different mechanism other than by MnP-driven oxidation of Keap1 (summarized in reference [4]), or (ii) activation of this pathway by MnP could have lessened the anticancer effect of MnP; or, most likely, (iii) Nrf2 might have been activated, and endogenous antioxidative defenses subsequently upregulated, but oxidized by the action of MnP/H_2O_2 (as found by redox proteomics and detailed above). In turn, those antioxidants would be inactive and could not protect tumor from excessive oxidative stress and therefore cannot allow for its proliferation.

Finally, it may be obvious, but still important to note, that if the normal cell is under immense oxidative stress approaching the state of inflammation similar to that of a cancer, Mn porphyrins would have plenty of H_2O_2 to catalyze the oxidation of protein thiols, inactivate numerous proteins, and in turn aggravate the existing condition, rather than heal the diseased cell. We have reported such cases in a study on advanced diabetes and excessive radiation-induced rectum injury of a rat [110, 111]. In the former case, in a streptozotocin mouse model of diabetes, the methyl analog, MnTM-2-PyP^{5+} protected kidneys when the treatment started at the onset of diabetes, but induced kidney damage when the treatment started once diabetes already progressed [111]. In the latter case, when the rectum of rats was exposed to 20-30 Gy of radiation, MnTE-2-PyP^{5+} was protective and reduced the fraction of rats with proctitis. However, at doses higher than 30 Gy, Mn porphyrin amplified the cytotoxic effect of radiation [110].

6. MnTnBu-2-PyP^{5+}, a Clinical Candidate, as a Cancer Radio- and Chemosensitizer while a Protector of Normal Tissue

Due to its progression into clinical trials, we have herein summarized primarily the therapeutic effects of MnTnBuOE-2-PyP^{5+} (Figure 3). Therapeutic effects of other MnPs were reviewed elsewhere [3, 25, 28, 68, 69, 74]. In cancer cells relative to normal cells, H_2O_2 metabolism is perturbed, resulting in elevated levels of H_2O_2. Either the production of H_2O_2 is increased or the enzymatic systems that should have maintained the physiological levels of H_2O_2 are downregulated or excessively oxidized/S-glutathionylated and thus are no longer active [3, 4, 74]. In turn, cancer is under oxidative stress and vulnerable to any further increase in it. It is thus no wonder that tumors were treated with therapies (such as radiation, chemotherapy, or ascorbate) that increase their oxidative stress and plunge them into apoptosis [27]. We and others have applied such therapies where different MnPs were combined with one or all of those treatments in cellular and animal models of breast and ovarian cancer, glioblastoma multiforme, head and neck cancer, hematologic malignancies, prostate cancer, and colorectal cancer. Anticancer effects were demonstrated, while normal tissue was protected by MnPs, see also under "Molecular Pathways Affected by Mn Porphyrins in Cancer and Normal Cell" [3, 68, 112, 113].

MnTnBuOE-2-PyP^{5+}was found safe and well-tolerated in Phase I clinical trial on glioma [13] and is now in four Phase II clinical trials with the primary goal of demonstrating the radioprotection of normal tissues with cancer patients (Figure 4). Its efficacy is being tested in Phase II trials on the radioprotection of normal tissue with glioma patients (in combination with radiation and temozolomide, NCT02655601), head and neck cancer patients (in combination with radiation and cisplatin, NCT02990468), and anal squamous cell carcinoma patients (in combination with 5-fluorouracil/mitomycin, NCT03386500), as well as on the radioprotection of normal brain in cancer patients who suffer
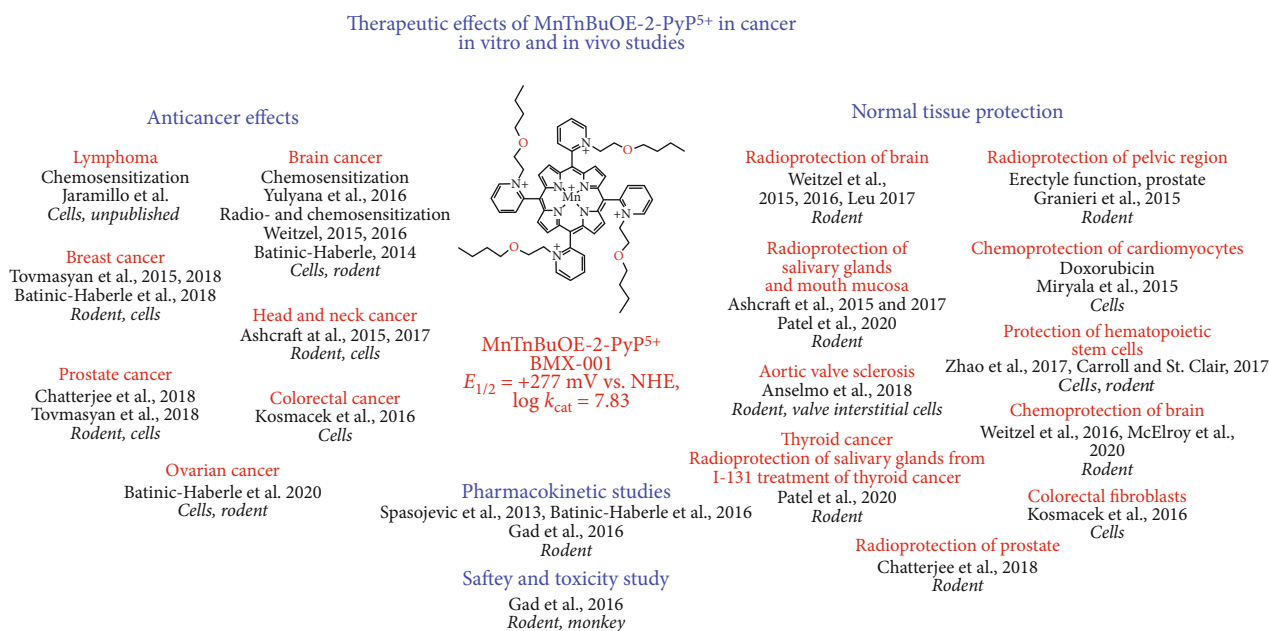
Figure 3: Therapeutic effects of MnTnBuOE-2-PyP^{5+} in suppressing cancer and protecting normal tissue [3, 4, 12, 24, 43, 54, 56, 58, 60, 82, 93, 100, 101, 114–122]. Such effects are driving progress of MnTnBuOE-2-PyP^{5+} into clinical trials. We have also listed here those beneficial effects upon normal tissue that are of relevance to cancer therapy. Such is the effect of MnTnBuOE-2-PyP^{5+} on suppression of aortic sclerosis/stenosis in cellular and mouse models, *via* reducing oxidative stress [123]. The effect is relevant to cancer patients subjected to chemotherapy as it increases the likelihood of plagues in their vasculature. Radiation of cancer patients often damages bone marrow, a source of hematopoietic stem/progenitor cells; the ability of MnTnBuOE-2-PyP^{5+} to enhance the number and function of those cells was reported [82]. Indeed, related to the ability of MnP to protect bone marrow, it was observed that none of the nine patients receiving MnTnBuOE-2-PyP^{5+}/temozolomide in a Phase I glioma clinical trial developed dose-limiting thrombocytopenia [14].
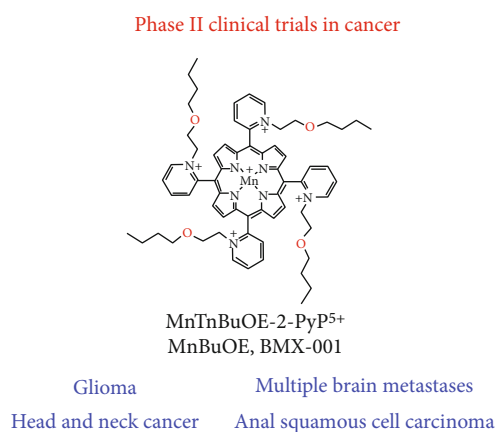

Figure 4: MnTnBuOE-2-PyP^{5+} (BMX-001) in four Phase II clinical trials. MnTnBuOE-2-PyP^{5+} was shown safe and well tolerated in a Phase I trial on glioma patients [13] and was then forwarded into Phase II trials. Initial data from the Phase I trial suggest the therapeutic potential of MnTnBuOE-2-PyP^{5+} with glioma patients [14, 15]. None of the nine patients receiving MnTnBuOE-2-PyP^{5+}/temozolomide developed dose-limiting thrombocytopenia in the Phase I clinical trial [14]. Three other trials are ongoing on the radioprotection of normal tissue with head and neck cancer patients, anal squamous cell carcinoma patients, and patients with multiple brain metastases.

from brain metastases (in combination with radiation, NCT03608020). It is important to note that BMX-001 does not protect cancer cells or cancerous tissues but acts as a tumor radio- and chemosensitizer [3, 4]. A second porphyrin analog, MnTE-2-PyP^{5+} (AEOL10113, BMX-010), is being tested in a Phase II trial for a noncancer application—atopic dermatitis and itch (NCT03381625).

7. Ascorbate Enhances the Anticancer Radio- and Chemosensitizing Effects of MnTnBuOE-2-PyP^{5+}

The treatment with MnP/ascorbate was thus far only investigated in cellular and mouse models of breast and ovarian cancers in combination with chemo- and radiotherapy. Herein, we are providing the overview of the reported data on MTE-2-PyP^{5+} and MnTnBuOE-2-PyP^{5+} in the 4T1 breast cancer cell line and MnTnBuOE-2-PyP^{5+} in CAOV2 and HOC7 ovarian cancer cell lines. It is noteworthy that MnP/ascorbate is not toxic to normal cells such as the human epithelial breast cell line, HBL-100 [12]; normal human astrocytes, iNHA; primary normal human dermal fibroblasts, NHDF; and the nontumorigenic epithelial breast cell line, MCF-10A [3, 28].

7.1. Breast Cancer. The impact of MnPs (combined with different sources of H_2O_2) on signaling pathways involved in the 4T1 mouse breast cancer cell line [4, 12, 43, 91],

inflammatory aggressive breast cancer SUM149 and SUM190 cell lines [92], and MCF-7 and MDA-MB-231 met-astatic breast cancer cell lines [98] were extensively studied. Data are summarized under "Molecular Pathways Affected by Mn Porphyrins in Normal and Cancer Cell" and Figure 2. In 4T1 mouse breast cancer cells and inflammatory breast cancer cells, NF-κB and MAPK signaling pathways were the major ones affected by MnP when combined with radiation- and ascorbate-derived sources of H_2O_2 [4, 80]. The impact of MnPs on the Nrf2 pathway in cancer cells has not yet been reported.

We have most frequently utilized a 4T1, triple negative, metastatic mouse breast cancer cell line for therapeutic and mechanistic purposes in cellular studies and in the immuno-competent balb/c mouse. We have tested a variety of Mn por-phyrins (MnTE-2-PyP^{5+}, MnTnHex-2-PyP^{5+}, MnTnBuOE-2-PyP^{5+}, MnTFE-2-PyP^{5+}, and MnTF$_3$Pen-2-PyP^{5+}), in combination with ascorbate and radiation (RT), on the impact of their different redox and bioavailability properties on anticancer efficacies [4, 12, 23, 43]. The chemistry behind such efficacies is elaborated under "Reactivity of Mn Porphy-rins towards Protein Cysteines -Thiol Signaling," and briefly summarized below.
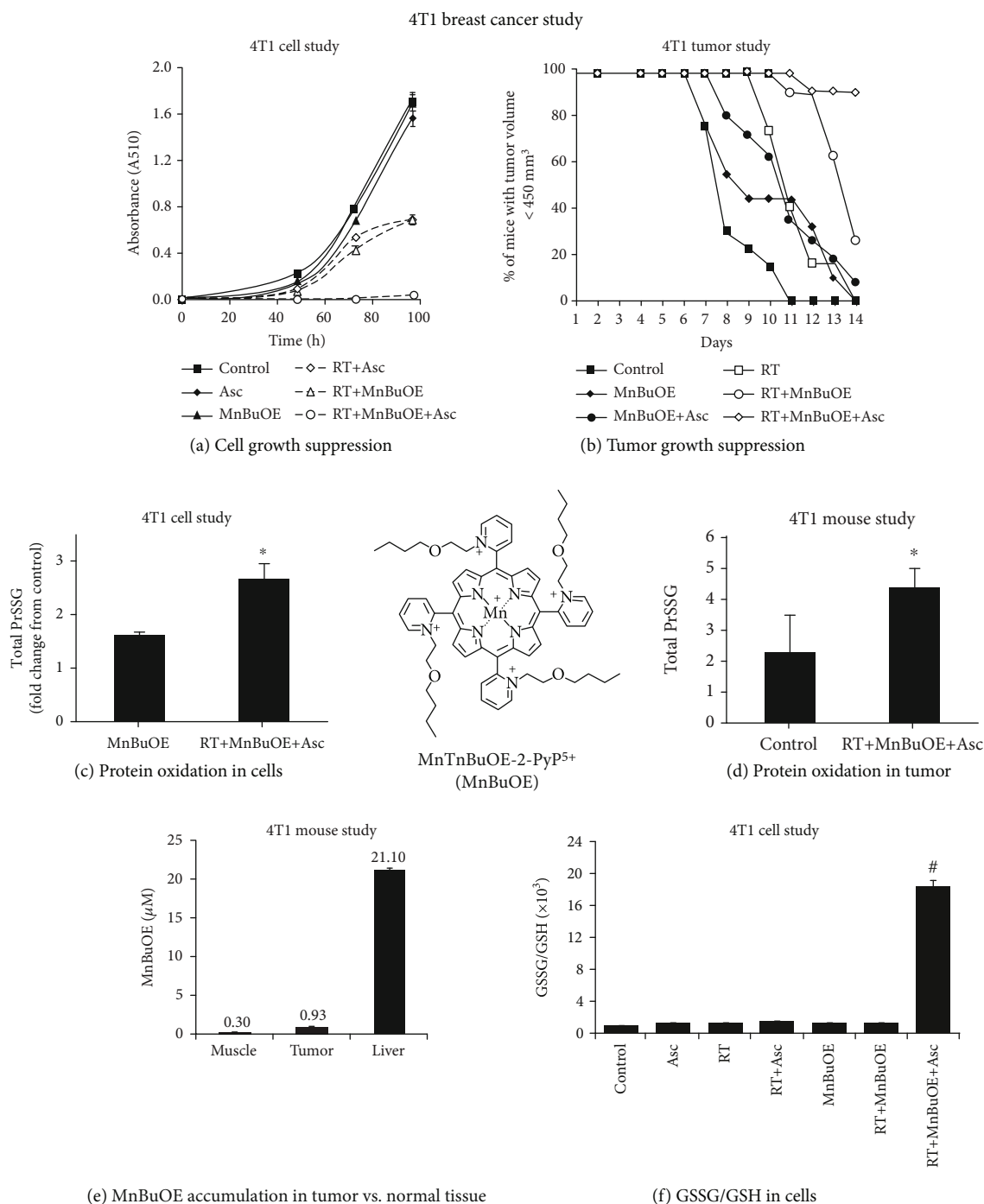
MnTnBuOE-2-PyP^{5+} was reduced with ascorbate and reoxidized with oxygen in a catalytic cycle, thereby producing excessive levels of superoxide/H_2O_2. H_2O_2 levels were further increased by the addition of radiation (RT) (equations (1)–(3)). Subsequently, MnTnBuOE-2-PyP^{5+} reacts with H_2O_2 and is oxidized to highly oxidizing Mn(V) dioxo spe-cies (equation (4)). This species in turn oxidizes/S-glutathio-nylates cysteines of signaling proteins (equations (5)–(7)). The yield of oxidized/S-glutathionylated proteins is high (Figures 5(c) and 5(d)) when the levels of colocalized reac-tants, MnTnBuOE-2-PyP^{5+} (Figure 5(e)) and H_2O_2, are high, giving rise also to high levels of oxidized glutathione, GSSG (Figure 5(f)). The high level of protein oxidation results in the promotion of apoptotic processes [4, 12, 43]. Due to the role of Mn porphyrin as a catalyst, in 4T1 mouse breast can-cer studies we were able to obtain the therapeutic effects of the same magnitude with 2 mg/kg/day and 0.2 mg/kg/day [4, 12]. Such findings are clinically relevant as the lower dose is similar to the dose used in clinical trials.

In initial 4T1 mouse breast cancer studies, we only looked at the anticancer effect of MnTE-2-PyP^{5+} in its own right. The significant suppression of tumor growth was only achieved when it was given subcutaneously at 15 mg/kg/day throughout the study, but not at 2 mg/kg/day. At that point in time, we did not fully comprehend the mechanism of the anticancer action of MnPs [124]. We now know that MnP couples with endogenous sources of H_2O_2, including the H_2O_2 produced by its cycling with endogenous ascorbate. Even with levels of MnP as high as 15 mg/kg/day, the endog-enous H_2O_2 levels sufficed only for the modest anticancer effect of MnP [124]. We needed much higher levels of MnP as a single agent, to suppress tumor growth, than when it is combined with exogenous sources of H_2O_2. In a subsequent study, a larger anticancer effect was seen when MnP was administered at 0.2 or 2 mg/kg/day concurrent with intraper-itoneal ascorbate at 4 g/kg/day [12]. The largest anticancer

effect on cellular viability and tumor growth was seen when Mn porphyrin was combined with two sources of H_2O_2—as-corbate and radiation (Figures 5(a) and 5(b)) [43]. When combined with ascorbate, MnTnBuOE-2-PyP^{5+} reduced cel-lular viability dose-dependently by up to 98%, and tumor growth by 36% vs. control. Further, ascorbate enhanced the radiosensitizing ability of MnTnBuOE-2-PyP^{5+} to suppress the cell viability dose-dependently by up to 98%, and tumor growth by 100% vs. control [4, 12, 43]. MnTnBuOE-2-PyP^{5+} and ascorbate, at doses used in cytotoxicity experi-ments (Figure 5(a)), have shown no toxicity when applied alone, whereas their combination have shown statistically significant anticancer effects compared to their respective single treatment cohorts. Moreover, both MnTnBuOE-2-PyP^{5+} and ascorbate sensitize cancer cells towards RT. The results indicate possible synergism between the treatment components.

In cellular and mouse 4T1 breast cancer studies, we have also compared the effects of MnTE-2-PyP^{5+} and MnTnBuOE-2-PyP^{5+} to EUK-8, MnTBAP^{3-}, and M40403. M40403 is the Mn(II) cyclic polyamine whose enantiomer, GC4419, is in a clinical trial for an identical application as MnTnBuOE-2-PyP^{5+} [4, 43]. Only MnTE-2-PyP^{5+} and MnTnBuOE-2-PyP^{5+} exhibited anticancer effects in cellular and mouse models (Figure 5) and restored the cellular physi-ological environment as measured via GSSG/GSH redox cou-ple and levels of S-glutathionylated proteins (Figures 5(c), 5(d), and 5(f)) [43]. The origin of the effects with cationic Mn porphyrins and the lack of those with other compounds were discussed in detail elsewhere [4, 43]. Briefly, based on low catalase-like activities, EUK-8, MnTBAP^{3-}, and M40403 have no ability to cycle with H_2O_2. Further, they have a low ability to oxidize ascorbate. Finally, all 3 compounds have low (MnTBAP^{3-}, EUK-8) or no GPx-like activity (M40403). Those properties are essential when coupling with ascorbate and subsequently with H_2O_2 in order to give rise to high-valent Mn compounds that would in turn oxidize protein thiols.

7.2. Ovarian Cancer. Epithelial cancers of the ovary, fallopian tube, and peritoneum (collectively known as epithelial ovar-ian cancer cells (EOCs)) represent 85% to 90% of all ovarian cancers and are treated in a similar manner. The majority of EOCs are aggressive *high-grade serous cancers (HGSCs)* and are associated with a worse clinical outcome [125, 126]. Fur-ther, HGSCs are especially challenging due to their primary and secondary chemoresistance. HGSCs almost always har-bor tumor protein TP53 mutation and lack obvious benign and/or borderline tumors, except in rare cases [127]. Recent data suggest that TP53 dysfunction in the fallopian tubal cells triggers high-grade serous carcinogenesis [128]. Also, *bcl-2* (a major regulator of apoptosis and tumor pathogenesis, pro-gression, and resistance to treatment) was overexpressed in HGSC specimen from women with shorter overall survival of >3 years ($p = 0.007$) in comparison with women with a longer overall survival of >7 years [129]. Findings were confirmed using an external HGSC database, GSE26712 (Siamakpour-Reihani), showing that women with high *bcl-2* tumor expression had significantly worse survival

(a) Cell growth suppression

(b) Tumor growth suppression

(c) Protein oxidation in cells

MnTnBuOE-2-PyP^{5+}
(MnBuOE)

(d) Protein oxidation in tumor

(e) MnBuOE accumulation in tumor vs. normal tissue

(f) GSSG/GSH in cells

FIGURE 5: Ascorbate enhances the radiosensitizing ability of MnTnBuOE-2-PyP^{5+} to suppress cancer growth. *In a cellular study* (a), 4T1 cells were treated with 1 mM ascorbate (Asc) and 2.5 μM MnTnBuOE-2-PyP^{5+} (MnBuOE). The 5 Gy radiation (RT) was delivered to cells at 1.81 Gy/min, and cell growth was followed during 96 h. Cell proliferation was assessed by sulforhodamine B assay, and measured as absorbance at 510 nm. Experiments were done in triplicate. Values are mean ± SEM. *In a mouse study*, 10^6 tumor cells in 100 μL were subcutaneously (sc) injected into a mouse flank. MnP was given sc at 2 mg/kg/day to balb/c mice for the duration of the study. Ascorbate was injected intraperitoneally for 5 days at 4 mg/kg/day, followed by 1 g/kg/day for the rest of the study. Treatment with MnP and ascorbate started one day before RT. Radiation started once the mice reached a tumor volume of ~80 mm^3. RT was given at 2.5 Gy/day for 3 days. The number of mice per group was 12 [43]. On day 11 (b), >90% of mice treated with MnBuOE/Asc/RT had tumors less than 450 mm^3 in size. The impact of MnP on the cellular (c) and tumor (d) redox status was demonstrated with the highest levels of total oxidized/*S*-glutathionylated proteins (PrSSG) when it was combined with both radiation and ascorbate—the system that induces the highest production of H$_2$O$_2$. The accumulation of MnP in the tumor, relative to the muscle from the leg opposite to tumor-bearing leg and liver (which were both not exposed to radiation), was measured by LC-MS/MS (e). An increase in the oxidative cellular redox environment by the action of MnP/ascorbate/radiation was demonstrated by the increase in the ratio of (GSSG)/(GSH) in 4T1 cells (f).
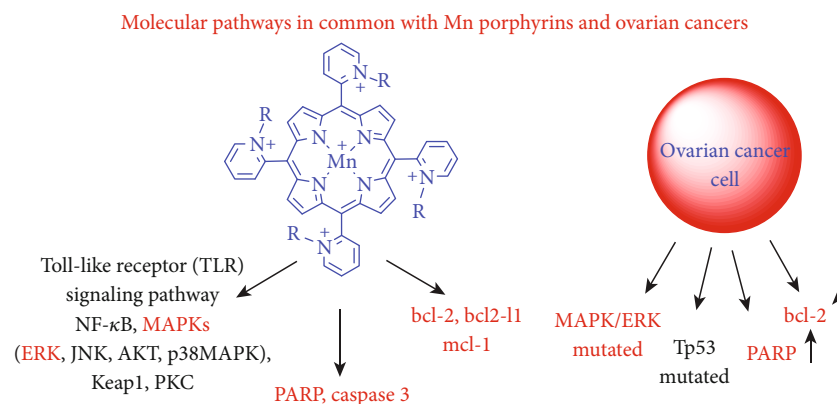
FIGURE 6: Molecular pathways upregulated in ovarian cancer cells that coincide with those which are affected by Mn(III) N-substituted pyridylporphyrins. Common pathways are indicated in red. In breast cancer studies, MnPs were found to operate predominantly *via* the TLR pathway with NF-κB, p38 MAPK, MAPK14, and HSP60 being components of it. It was also found that MnP inhibits the antiapoptotic proteins, bcl-2 and mcl-1, which are overexpressed in high-grade serous cancer cells [129], thus promoting apoptotic pathways (see Figure 2). PARP is also overexpressed in several types of ovarian cancer cells, and MnP was found to suppress its activity *via* increasing levels of inactive cleaved PARP (Figure 2) [137]. MnP was also found to increase the levels of activated, cleaved caspase 3 [137]. TP53 and MAPK/ERK are mutated in low-grade serous cancer [127] allowing for the therapeutic interventions with their inhibitors, MnPs prospectively being one of those. R in the structure of MnPs indicates *ortho-N*-alkyl- or *N*-alkoxyalkylpyridyl substituents.

($p = 0.002$) and approximately 2-fold higher risk of death. The *bcl-2* gene was transcriptionally regulated by NF-κB and directly links the tumor necrosis factor α, TNF-α/NF-κB signaling pathway with bcl-2 expression and its prosurvival response in human prostate carcinoma cells [130]. DNase I footprinting, gel retardation, and supershift analysis identified an NF-κB site in the bcl-2 p2 promoter [130]. Several studies in different cell types have shown that treatment with known activators of NF-κB often results in an increase in prosurvival factors such as bcl-2, bcl-xL, and bfl-1/A1 [131–134]. Conversely, *low-grade serous cancers* (*LGSCs*) often intermingle with the benign and borderline serous tumor component and exhibit low cellular proliferation. LGSC and serous borderline tumors have relatively frequent point mutations in the *KRAS* and *BRAF* genes [135, 136] which participate in RAS-RAF-MEK-ERK signaling (also known as MAPK/ERK). Thus, the occurrence of these 2 mutational events in low-grade serous carcinogenesis is mutually exclusive [127]. Reportedly, mutations occur at codon 599 of *BRAF* and codons 12 and 13 of *KRAS* [136]. Either of those, but not both, are present in 15 out of 22 (68%) invasive low-grade micropapillary serous carcinomas (MPSC), and in 31 out of 51 (61%) serous borderline tumors, precursors to MPSC. Mutations are specific for LGSC and none were found in 72 conventional HGSCs [136].

We have demonstrated that Mn(III) N-substituted pyridylporphyrins favorably affect pathways that are involved in LGSC or HGSC such as bcl-2/NF-κB, and MAPK/ERK (see more under "Molecular Pathways Affected by Mn Porphyrins in Cancer and Normal Cells" and Figures 2 and 6) [3, 4, 74, 80, 91, 92, 94]. Such data have provided strong basis for exploring the therapeutic potential of MnPs in ovarian cancer.

The impact of MnTnBuOE-2-PyP^{5+}, combined with ascorbate and chemotherapy, was explored in two ovarian cancer cell lines, each representative of low- (HOC7) and high-grade (CAOV2) carcinomas [138, 139]. Data show the impressive ability of MnTnBuOE-2-PyP^{5+} (MnBuOE)/ascorbate (Asc) to suppress the growth of both ovarian cancer cells (Figure 7) [138, 139]. Ascorbate sensitized CAOV2 and HOC7 ovarian cancer cells to MnTnBuOE-2-PyP^{5+}, reducing cellular viability by 75% and 42%, respectively (Figure 7)[139]. The data pointed to the critical role that catalytic redox cycling of Mn porphyrin with ascorbate plays in MnP-driven tumor suppression giving rise to excess peroxide. The mouse tumor growth studies on CAOV2 cell line demonstrated the strong anticancer potential of MnTnBuOE-2-PyP^{5+}/ascorbate [138]. Such results agree well with effects seen in 4T1 breast cancer cellular and mouse studies ([12, 43]. At least in part, such effects are orchestrated through common signaling pathways comprised of NF-κB, bcl-2, MAPK/ERK, PARP, and caspase 3; see also under "Molecular Pathways Affected by Mn Porphyrins in Normal and Cancer Cell" (Figures 2 and 6) [3, 91, 92].

Paclitaxel and carboplatin are standard-of-care therapy for ovarian cancer [140]. However, paclitaxel and carboplatin are associated with significant toxicities that include grade 3-4 thrombocytopenia, grade 3-4 neutropenia, grade 2-4 neurotoxicity [140–142], and a decline in cognitive functions [143]. In a Phase I glioma clinical trial on the radioprotection of normal tissue with glioma patients (Figure 4), [13] none of the nine patients receiving MnTnBuOE-2-PyP^{5+}/temozolomide developed dose-limiting thrombocytopenia [14], which is associated with chemotherapy in up to 39% of patients [140]. This effect of MnTnBuOE-2-PyP^{5+} is related to its ability to protect the bone marrow from radiation, and seems to be at least in part related to the MnP-driven inhibition of NF-κB and activation of Nrf2 [82, 144, 145]. MnTnBuOE-2-PyP^{5+} was found to enhance the number and function of hematopoietic stem/progenitor cells isolated from the bone marrow *via* activation of the Nrf2 transcription factor and upregulation of its
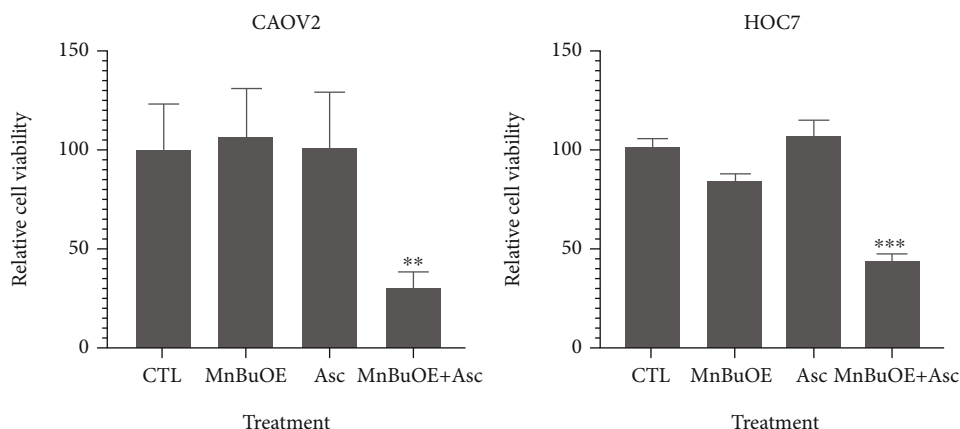
Figure 7: Ascorbate sensitizes high- (CAOV2) and low-grade (HOC7) ovarian cancer cells to MnTnBuOE-2-PyP^{5+}. Cancer cells were seeded onto a 96-well plate with RPMI 1640 medium plus 10% fetal bovine serum and 1% penicillin and streptomycin. The drugs were added onto cells after 24 hours of plating; treatment was applied for 72 hours. The cell viability was assessed using CellTiter-Glo® Luminescent Cell Viability Assay (Promega) according to the manufacturer's protocol. Relative cell viability was calculated against mock treatment (CTL). The average values at each dose were calculated from 4 replicates and normalized against control values (CTL). *Statistics*: the paired Student t-test was performed. The p values are shown here as $^{**}p < 0.01$, and $^{***}p < 0.001$ relative to control. *Abbreviations*: MnBuOE: MnTnBuOE-2-PyP^{5+}; Asc: ascorbate; CTL: control. *Concentrations of drugs for COAV2 cells*: MnBuOE = 2.5 μM, Asc = 0.25 mM. *Concentrations of drugs for HOC7 cells*: MnBuOE = 5 μM, Asc = 0.25 mM [138, 139].

endogenous antioxidative genes (see also "Molecular Pathways Affected by Mn Porphyrins in Normal and Cancer Cell" and Figure 2) [82].

8. Future Perspectives

Mn porphyrins are now in clinical trials on several types of cancer: glioma, head and neck cancer, anal squamous cell carcinoma, and multiple brain metastases emerging from different primary cancers. We have summarized here the therapeutic effects of MnPs, and in particular, the anticancer efficacy of the MnP/ascorbate system. Thus far, we explored such system in the treatment of breast and ovarian cancer in preclinical models. In a breast cancer study, ascorbate further amplified the anticancer effect of MnP/radiation. In the treatment of ovarian cancer, data suggest that the MnP/ascorbate system may be an anticancer agent as powerful as paclitaxel—a standard-of-care therapy.

Ascorbate was used in preclinical models in combination with chemo- and radiotherapy for several different cancers [113, 146–148]. Ascorbate has reached clinical trials as an adjuvant to standard-of-care therapy in a number of cancers such as glioma, pancreatic cancer, prostate cancer, kidney cancer, hematologic malignancies, bone sarcomas, and non-small-cell lung cancer [113, 149]. It was combined with temozolomide and radiotherapy in a Phase I clinical trial of newly diagnosed glioblastoma; the system was found safe and with promising clinical outcome and warranted further investigation in an ongoing Phase II trial (NCT02344355) [150]. Ascorbate is in progress in a Phase II trial (NCT02905578) for the treatment of pancreatic cancer in combination with nab-paclitaxel and gemcitabine standard-of-care therapy [151, 152]. Thus far, only one pilot Phase I/IIa trial on ascorbate in ovarian cancer was conducted on patients diagnosed with stage III or

IV ovarian cancer. 27 patients were randomized into either a paclitaxel/carboplatin group or a paclitaxel/carboplatin/ascorbate group [153]. Treatment with ascorbate reduced chemotherapy-related toxicity. There was an 8.75-month increase in progression-free survival and an improved trend in overall survival in the ascorbate-treated arm. Ascorbate is now in a Phase I clinical trial for the treatment of pneumonia with COVID-19 patients (NCT04264533).

The mechanism of action of ascorbate (in the absence of MnPs) is reportedly based on its coupling with metal centers of endogenous proteins/enzymes, giving rise to H_2O_2 [146, 147, 154]. Yet, those metalloproteins are optimized neither on kinetic nor thermodynamic grounds for reaction with ascorbate. The MnPs are, however, optimized to couple with ascorbate. In a catalytic fashion, MnPs produce large amounts of H_2O_2 which can then be employed (again in a catalytic fashion) to oxidize and inactivate cellular proteins. We thus hope that the MnP/ascorbate system will eventually progress into clinical trials.

For the first time in drug development, redox-active metal complexes that affect cellular redox environment, but do not act on a particular biomolecule, are in clinical trials: two Mn porphyrins (MnTnBuOE-2-PyP^{5+}, BMX-001 and MnTE-2-PyP^{5+}, BMX-010) and Mn cyclic polyamine (GC4419). Moreover, BMX-001 and GC4419 are presently tested for the same clinical application: radioprotection of the normal tissue with head and neck cancer patients. (NCT03689712). The results from the Phase II trial on GC4419 were reported [155], indicating significant, clinically meaningful reduction in severe oral mucositis duration, incidence and severity with acceptable safety at dose of 90 mg [155]. The Phase III trial on GC4419 has begun (NCT03689712). The outcome of the trial could advance our understanding of the role redox chemistry has in cellular biology under pathological and physiological conditions and

further clinical development of the new class of therapeutics. While BMX-001 and GC4419 are similarly potent SOD mimics, these compounds have a different chemistry and therefore may undergo different reactions in the cellular environment. With their Mn center in +2 oxidation state, Mn(II) cyclic polyamines are not very stable complexes and are prone to demetallation, whereas Mn(III) porphyrins with their Mn in +3 oxidation state are stable compounds. Indeed, Weekley et al. demonstrated that the enantiomer of GC4419, M40403, undergoes demetallation *in vivo* [35]. Such difference in the oxidation state of the Mn center also controls their reactivities. Data show that rather than acting as SOD mimics in both normal ant tumor cell/tissue, Mn porphyrins cycle with ascorbate, and at the expense of oxygen, give rise to H_2O_2. In a subsequent step, H_2O_2 is employed by Mn porphyrin in a catalysis of oxidation of protein cysteines. Such oxidative modification of proteins modifies their activities and affect cellular metabolism. The reactivity of GC4419 towards ascorbate was reported, but its mechanism was not readily understood [156]. The Mn +2 state of GC4419 reacts with $O_2^{\bullet-}$ in a 1st step to give rise to the Mn +3 state (and H_2O_2) and cycles back to Mn +2 either with $O_2^{\bullet-}$ or with ascorbate, whereby either oxygen or ascorbyl radical, respectively, are formed. The Mn +2 state is a resting state of GC4419 and is not expected to react with oxygen in a reaction which would give rise to $O_2^{\bullet-}$ and subsequently H_2O_2, and thus enable the anticancer action of GC4419 *via* its high-valent oxidation state capable of oxidizing protein thiols. The reaction of the Mn +3 state of GC4419 with ascorbate instead of with $O_2^{\bullet-}$, to close the catalytic cycle, may enhance the reactivity of GC4419 as an SOD mimic. Yet, the yield of H_2O_2 (and the Mn +3 state) in the 1st step, to allow for the 2nd step reaction of Mn +3 with ascorbate, is limited by the levels of superoxide. For the same reason, the oxidation of GC4419 with H_2O_2 to a high-valent Mn +4 oxidation state would also occur with a low yield; moreover, such reaction would likely give rise to the degradation of the complex [35]. The yield of H_2O_2 in the case of MnPs, however, is controlled by the amount of oxygen and ascorbate, both of which are abundant.

Our studies have demonstrated that M40403, an enantiomer of GC4419, has no GPx-like activity [4, 157], low activity towards ascorbate [43] and H_2O_2 [104], and has no anticancer efficacy in the presence of ascorbate in suppressing tumor growth in 4T1 mouse breast cancer model [4, 43]. Based on our present knowledge, the ability of MnPs to protect normal tissue relates to their ability to catalyze the oxidative modifications of signaling proteins such as NF-κB and Keap1 of Nrf2. Yet, the mechanism behind the protective actions of GC4419 is not fully understood. Therefore, more studies are needed to clarify the mechanism of anticancer actions of Mn(II) cyclic polyamines in the presence and absence of ascorbate.

With regard to the use of Mn porphyrin/ascorbate treatment for the protection of the normal tissue, the concern may be whether the H_2O_2 originating from MnP/ascorbate cycling will induce cytotoxicity. We have performed a study with $MnTF_3Pen-2-PyP^{5+}$ on the radioprotection of the prostate and erectile function in the presence of ascorbate. No

toxicity to normal tissue was seen [24]. Lack of the toxicity arises from the ability of normal tissue to maintain H_2O_2 at the physiological levels due to the abundant and functional endogenous enzymes and small-molecular-weight antioxidants (see "Molecular Pathways Affected by Mn Porphyrins in Cancer and Normal Cell"). Yet, more studies on different animal models are needed for further evaluation of such system in the radioprotection of normal tissue.

While we have fully characterized the aqueous chemistry of two members of the newest class of Mn(III) fluorinated *N*-alkylpyridylporphyrins, a lot is left to be done on their *in vitro* and *in vivo* therapeutic effects. Thus far, we demonstrated that they are anticancer drugs at least as good as $MnTE-2-PyP^{5+}$ and $MnTnBuOE-2-PyP^{5+}$in a 4T1 mouse breast cancer model in the presence of radiation and ascorbate [23]. Data also show that, in the presence of ascorbate, they possess the ability to radioprotect normal tissue [24]. The efficacy in other cancer cell lines and other inflammatory diseases are yet to be performed.

Given the rich redox chemistry of MnPs and the redox biology of a cell, much is left to be explored. On the level of a mechanism of action, the question that is still left unanswered is how MnPs affect Nrf2 regulation in a tumor. Nrf2 was activated by MnP in hematopoietic stem/progenitor cells [82]. Activation of Nrf2 was followed by the upregulation of MnSOD, catalase, glutathione-*S*-transferase p1, NAD(P)H quinone dehydrogenase 1, and uncoupling proteins. Redox proteomics of 4T1 breast cancer cells treated with MnP and ascorbate (as exogenous source of H_2O_2) showed that Keap1 is oxidized, thus Nrf2 is likely activated. The subsequent upregulation of antioxidants should have promoted tumor growth, but such impact on tumor growth by MnPs has not been reported [3, 4]. A possible explanation lies in the fact that MnP, combined with sources of H_2O_2, oxidizes antioxidant enzymes. Thus, despite their upregulation by the activated Nrf2, such antioxidants would likely be inactivated and thus would not diminish the anticancer potential of MnP.

9. Conclusions

Stable and redox-active Mn porphyrins were thus far developed, all of which carry positive charges on each of four *ortho* pyridyl nitrogens. Those charges provide thermodynamic and kinetic facilitation for the reactions of MnPs with biomolecules. MnPs were initially developed as powerful SOD mimics with the k_{cat} for the catalysis of $O_2^{\bullet-}$ dismutation as high as $7 \times 10^8\ M^{-1}\ s^{-1}$. Yet, their rich redox chemistry, originating from 4 biologically assessable oxidation states, +2, +3, +4, and +5, enables MnPs to couple with numerous components of the rich redox biology of the cell. Many more reactions of MnPs might be envisioned to emerge in the future.

Driven by the pentacationic charge, lipophilic *N*-alkylpyridyl substituents, and abundant anionic phosphates of the cell, MnPs distribute in various cellular organelles, mitochondria and nucleus included. MnPs distribute in all organs, including the brain and brain compartments. Finally, MnPs prefer tumor to normal cell/tissue accumulation.

On a therapeutic level, MnPs were found to act as anti-inflammatory drugs. Recently, most of the studies were concentrated on their efficacy as anticancer drugs, in combination with chemo- and radiation therapy, and as radioprotectors of normal tissue with cancer patients. The wealth of effects *in vitro* and *in vivo* has driven the progress of MnPs into clinical trials.

While direct reactivity with $O_2^{\bullet-}$ cannot be fully excluded as their mechanism of action, numerous *in vitro* and *in vivo* studies suggest that therapeutic effects in both normal and tumor cells/tissues arise from the ability of MnPs to modify activities of cellular signaling proteins and thus affect proliferative and apoptotic pathways. Such studies, along with redox proteomics, helped us understand the mechanism below the ability of MnPs to affect signaling proteins. In the presence of H_2O_2 and glutathione, MnPs catalytically *S*-glutathionylate cysteines of numerous endogenous proteins, such as NF-κB, Keap1, and MAPKs, and endogenous antioxidative defenses such as peroxiredoxins, glutathione-*S*-transferase, and isocitrate dehydrogenase. Such oxidative modifications result in the modification of the activities of proteins. The yield of oxidative modifications of proteins would depend upon the levels of MnPs and H_2O_2, both of which are at much higher levels in tumors than in normal tissues. Consequently, massive oxidation of tumor biomolecules would promote apoptotic processes. Conversely, lesser inhibition of NF-κB and activation of Nrf2 (upon oxidation of Keap1) would restore the physiological environment of diseased but normal cell. The impact of MnPs on both NF-κB and Nrf2 was investigated in normal cells/tissues, but only the effect on NF-κB was thus far reported in tumors.

In summary, the ability of MnPs to modulate activities of major signaling proteins, along with high cellular, mitochondrial, and tissue bioavailability and stability, resulted in favorable therapeutic effects, which enabled their progress into several Phase II clinical trials.

Data Availability

This is a review manuscript and all the data that are described here are from published material and can be found under the list of references.

Conflicts of Interest

IBH, IS, AT, and Duke University have patent rights and have licensed technologies to BioMimetix JV, LLC. IBH and IS are consultants with BioMimetix JV, LLC. Duke University and IBH and IS hold equities in BioMimetix JV, LLC.

Acknowledgments

References

[1] G. DeFreitas-Silva, J. S. Rebouças, I. Spasojević, L. Benov, Y. M. Idemori, and I. Batinić-Haberle, "SOD-like activity of Mn(II) β-octabromo-meso-tetrakis(N-methylpyridinium-3-yl)porphyrin equals that of the enzyme itself," *Archives of Biochemistry and Biophysics*, vol. 477, no. 1, pp. 105–112, 2008.

[2] I. Batinic-Haberle, J. S. Rebouças, and I. Spasojevic, "Superoxide dismutase mimics: chemistry, pharmacology, and therapeutic potential," *Antioxidants & Redox Signaling*, vol. 13, no. 6, pp. 877–918, 2010.

[3] I. Batinic-Haberle, A. Tovmasyan, E. R. H. Roberts, Z. Vujaskovic, K. W. Leong, and I. Spasojevic, "SOD therapeutics: latest insights into their structure-activity relationships and impact on the cellular redox-based signaling pathways," *Antioxidants & Redox Signaling*, vol. 20, no. 15, pp. 2372–2415, 2014.

[4] I. Batinic-Haberle, A. Tovmasyan, and I. Spasojevic, "Mn porphyrin-based redox-active drugs: differential effects as cancer therapeutics and protectors of normal tissue against oxidative injury," *Antioxidants & Redox Signaling*, vol. 29, no. 16, pp. 1691–1724, 2018.

[5] I. Batinić-Haberle, S. I. Liochev, I. Spasojević, and I. Fridovich, "A potent superoxide dismutase mimic: manganese β-octabromo-meso-tetrakis-(N-methylpyridinium-4-yl) porphyrin," *Archives of Biochemistry and Biophysics*, vol. 343, no. 2, pp. 225–233, 1997.

[6] I. Batinic-Haberle, L. Benov, I. Spasojevic, and I. Fridovich, "The ortho effect makes manganese(III) meso-tetrakis(N-methylpyridinium-2-yl)porphyrin a powerful and potentially useful superoxide dismutase mimic," *The Journal of Biological Chemistry*, vol. 273, no. 38, pp. 24521–24528, 1998.

[7] I. Batinić-Haberle, I. Spasojević, R. D. Stevens, P. Hambright, and I. Fridovich, "Manganese(III) meso-tetrakis(ortho-N-alkylpyridyl)porphyrins. Synthesis, characterization, and catalysis of $O_2^{\bullet-}$ dismutation," *Dalton Transactions*, vol. 13, pp. 2689–2696, 2002.

[8] J. M. Pollard, J. S. Rebouças, A. Durazo et al., "Radioprotective effects of manganese-containing superoxide dismutase mimics on ataxia-telangiectasia cells," *Free Radical Biology & Medicine*, vol. 47, no. 3, pp. 250–260, 2009.

[9] I. Batinić-Haberle, I. Spasojević, R. D. Stevens et al., "New class of potent catalysts of $O_2^{\bullet-}$ dismutation. Mn(III) ortho-methoxyethylpyridyl- and di-ortho-methoxyethylimidazolyl-porphyrins," *Dalton Transactions*, vol. 11, pp. 1696–1702, 2004.

[10] Z. Rajic, A. Tovmasyan, I. Spasojevic et al., "A new SOD mimic, Mn(III) *ortho* N -butoxyethylpyridylporphyrin, combines superb potency and lipophilicity with low toxicity," *Free Radical Biology & Medicine*, vol. 52, no. 9, pp. 1828–1834, 2012.

[11] Z. Rajic, A. Tovmasyan, O. L. de Santana et al., "Challenges encountered during development of Mn porphyrin-based, potent redox-active drug and superoxide dismutase mimic, MnTnBuOE-2-PyP^{5+}, and its alkoxyalkyl analogues," *Journal of Inorganic Biochemistry*, vol. 169, pp. 50–60, 2017.

[12] A. Tovmasyan, R. S. Sampaio, M.-K. Boss et al., "Anticancer therapeutic potential of Mn porphyrin/ascorbate system,"

Free Radical Biology & Medicine, vol. 89, pp. 1231–1247, 2015.

[13] K. Peters, J. Kirkpatrick, I. Batinic-Haberle et al., "ACTR-28. Phase 1 dose escalation trial of the safety of BMX-001 concurrent with radiation therapy and temozolomide in newly diagnosed patients with high-grade gliomas," *Neuro-Oncology*, vol. 20, article vi17, Supplement 6, 2018.

[14] K. B. Peters, J. P. Kirkpatrick, I. Batinic-Haberle et al., "First in human clinical trial of a metalloporphyrin dual radioprotectant and radiosensitizer, BMX-001, in newly diagnosed high-grade glioma undergoing concurrent chemoradiation," *International Journal of Radiation Oncology • Biology • Physics*, vol. 105, no. 1, article E106, 2019.

[15] K. Peters, J. Kirkpatrick, I. Batinic-Haberle et al., "MASCC20-ABS-1534. Cognitive outcomes of Phase 1 trial of novel metalloporphyrin radioprotectant and radiosensitizer in newly diagnosed high grade glioma patients," in *Annual Meeting on Supportive Care in Cancer*, Seville, Spain, 2021.

[16] B. Gaye and A. Adejare, "Fluorinated molecules in the diagnosis and treatment of neurodegenerative diseases," *Future Medicinal Chemistry*, vol. 1, no. 5, pp. 821–833, 2009.

[17] J. S. Driscoll, V. E. Marquez, J. Plowman, P. S. Liu, J. A. Kelley, and J. J. Barchi, "Antitumor properties of 2(1H)-pyrimidinone riboside (zebularine) and its fluorinated analogues," *Journal of Medicinal Chemistry*, vol. 34, no. 11, pp. 3280–3284, 1991.

[18] R. Filler and R. Saha, "Fluorine in medicinal chemistry: a century of progress and a 60-year retrospective of selected highlights," *Future Medicinal Chemistry*, vol. 1, no. 5, pp. 777–791, 2009.

[19] U. Gravemann, J. Volland, and H. Nau, "Hydroxamic acid and fluorinated derivatives of valproic acid: anticonvulsant activity, neurotoxicity and teratogenicity," *Neurotoxicology and Teratology*, vol. 30, no. 5, pp. 390–394, 2008.

[20] A. S. Kiselyov, "Chemistry of N-fluoropyridinium salts," *Chemical Society Reviews*, vol. 34, no. 12, pp. 1031–1037, 2005.

[21] P. V. Ramachandran, "Welcome to "fluorine in medicinal chemistry"," *Future Medicinal Chemistry*, vol. 1, no. 5, pp. 771–772, 2009.

[22] P. Shah and A. D. Westwell, "The role of fluorine in medicinal chemistry," *Journal of Enzyme Inhibition and Medicinal Chemistry*, vol. 22, no. 5, pp. 527–540, 2007.

[23] A. Tovmasyan, J. C. Bueno-Janice, I. Spasojevic, and I. Batinic-Haberle, "Novel fluorinated Mn porphyrin as a powerful SOD mimic and catalyst for ascorbate-coupled anticancer therapy," *Free Radical Biology and Medicine*, vol. 112, Supplement 1, pp. 36-37, 2017.

[24] A. Tovmasyan, I. Spasojevic, H. Sheng et al., "Protection of rat prostate and erectile function from radiation-induced damage by novel Mn(III) N-substituted pyridylporphyrin and ascorbate," *Free Radical Biology and Medicine*, vol. 112, Supplement 1, pp. 35-36, 2017.

[25] I. Batinic-Haberle and I. Spasojevic, "25 years of development of Mn porphyrins—from mimics of superoxide dismutase enzymes to thiol signaling to clinical trials: the story of our life in the USA," *Journal of Porphyrins and Phthalocyanines*, vol. 23, no. 11n12, pp. 1326–1335, 2019.

[26] I. Batinić-Haberle, I. Spasojević, P. Hambright, L. Benov, A. L. Crumbliss, and I. Fridovich, "Relationship among redox potentials, proton dissociation constants of pyrrolic nitro-

[27] S. Miriyala, I. Spasojevic, A. Tovmasyan et al., "Manganese superoxide dismutase, MnSOD and its mimics," *Biochimica et Biophysica Acta*, vol. 1822, no. 5, pp. 794–814, 2012.

[28] I. Batinić-Haberle, A. Tovmasyan, and I. Spasojević, "Mn porphyrin-based redox-active therapeutics," in *Redox-Active Therapeutics*, I. Batinić-Haberle, J. S. Rebouças, and I. Spasojević, Eds., pp. 165–212, Springer International Publishing, Cham, 2016.

[29] R. D. Teo, S. S. Dong, Z. Gross, H. B. Gray, and W. A. Goddard, "Computational predictions of corroles as a class of Hsp90 inhibitors," *Molecular BioSystems*, vol. 11, no. 11, pp. 2907–2914, 2015.

[30] S. R. Doctrow et al., "Salen manganese complexes mitigate radiation injury in normal tissues through modulation of tissue environment, including through redox mechanisms," in *Redox-Active Therapeutics*, I. Batinić-Haberle, J. S. Rebouças, and I. Spasojević, Eds., pp. 265–285, Springer International Publishing, Cham, 2016.

[31] X. R. Zhang, W. X. Zhou, and Y. X. Zhang, "Improvements in SOD mimic AEOL-10150, a potent broad-spectrum antioxidant," *Military Medical Research*, vol. 5, no. 1, p. 30, 2018.

[32] N. Tewari-Singh, S. Inturi, A. K. Jain et al., "Catalytic antioxidant AEOL 10150 treatment ameliorates sulfur mustard analog 2-chloroethyl ethyl sulfide-associated cutaneous toxic effects," *Free Radical Biology & Medicine*, vol. 72, pp. 285–295, 2014.

[33] H. Sheng, W. Yang, S. Fukuda et al., "Long-term neuroprotection from a potent redox-modulating metalloporphyrin in the rat," *Free Radical Biology & Medicine*, vol. 47, no. 7, pp. 917–923, 2009.

[34] J. N. Pearson-Smith, L.-P. Liang, S. D. Rowley, B. J. Day, and M. Patel, "Oxidative stress contributes to status epilepticus associated mortality," *Neurochemical Research*, vol. 42, no. 7, pp. 2024–2032, 2017.

[35] C. M. Weekley, I. Kenkel, R. Lippert et al., "Cellular fates of manganese(II) pentaazamacrocyclic superoxide dismutase (SOD) mimetics: fluorescently labeled MnSOD mimetics, X-ray absorption spectroscopy, and X-ray fluorescence microscopy studies," *Inorganic Chemistry*, vol. 56, no. 11, pp. 6076–6093, 2017.

[36] C. Policar and S. O. D. Mimicking, "Why and how: bioinspired manganese complexes as SOD mimic," in *Redox-Active Therapeutics*, I. Batinić-Haberle, J. S. Rebouças, and I. Spasojević, Eds., pp. 125–164, Springer International Publishing, Cham, 2016.

[37] C. Preihs, J. F. Arambula, D. Magda et al., "Recent developments in texaphyrin chemistry and drug discovery," *Inorganic Chemistry*, vol. 52, no. 21, pp. 12184–12192, 2013.

[38] J. S. Reboucas, I. Spasojevic, and I. Batinic-Haberle, "Pure manganese(III) 5,10,15,20-tetrakis(4-benzoic acid)porphyrin (MnTBAP) is not a superoxide dismutase mimic in aqueous systems: a case of structure-activity relationship as a watchdog mechanism in experimental therapeutics and biology," *Journal of Biological Inorganic Chemistry*, vol. 13, no. 2, pp. 289–302, 2008.

[39] I. Batinić-Haberle, S. Cuzzocrea, J. S. Rebouças et al., "Pure MnTBAP selectively scavenges peroxynitrite over superoxide: comparison of pure and commercial MnTBAP samples

gens, and in vivo and in vitro superoxide dismutating activities of manganese(III) and iron(III) water-soluble porphyrins," *Inorganic Chemistry*, vol. 38, no. 18, pp. 4011–4022, 1999.

to MnTE-2-PyP in two models of oxidative stress injury, an SOD-specific Escherichia coli model and carrageenan-induced pleurisy," *Free Radical Biology & Medicine*, vol. 46, no. 2, pp. 192–201, 2009.

[40] X. Zhou, M. Li, M. Xiao et al., "ERbeta accelerates diabetic wound healing by ameliorating hyperglycemia-induced persistent oxidative stress," *Frontiers in Endocrinology*, vol. 10, p. 499, 2019.

[41] J. Brestoff and T. H. Reynolds, "The antioxidant MnTBAP induces weight loss and enhances insulin sensitivity in mice fed a normal chow diet or a high fat diet," *The FASEB Journal*, vol. 22, no. S2, pp. 110–110, 2008.

[42] K. M. Pires, O. Ilkun, M. Valente, and S. Boudina, "Treatment with a SOD mimetic reduces visceral adiposity, adipocyte death, and adipose tissue inflammation in high fat-fed mice," *Obesity (Silver Spring)*, vol. 22, no. 1, pp. 178–187, 2014.

[43] A. Tovmasyan, J. C. Bueno-Janice, M. C. Jaramillo et al., "Radiation-mediated tumor growth inhibition is significantly enhanced with redox-active compounds that cycle with ascorbate," *Antioxidants & Redox Signaling*, vol. 29, no. 13, pp. 1196–1214, 2018.

[44] S. S. Giles, I. Batinić-Haberle, J. R. Perfect, and G. M. Cox, "Cryptococcus neoformans mitochondrial superoxide dismutase: an essential link between antioxidant function and high-temperature growth," *Eukaryotic Cell*, vol. 4, no. 1, pp. 46–54, 2005.

[45] A. Tovmasyan, T. Weitner, H. Sheng et al., "Differential coordination demands in Fe versus Mn water-soluble cationic metalloporphyrins translate into remarkably different aqueous redox chemistry and biology," *Inorganic Chemistry*, vol. 52, no. 10, pp. 5677–5691, 2013.

[46] L. Li, A. Tovmasyan, H. Sheng et al., "Fe porphyrin-based SOD mimic and redox-active compound, $(OH)FeTnHex-2-PyP^{4+}$, in a rodent ischemic stroke (MCAO) model: efficacy and pharmacokinetics as compared to its Mn analogue, $(H_2O)MnTnHex-2-PyP^{5+}$," *Antioxidants (Basel)*, vol. 9, no. 6, 2020.

[47] R. Ezzeddine, A. Al-Banaw, A. Tovmasyan, J. D. Craik, I. Batinic-Haberle, and L. T. Benov, "Effect of molecular characteristics on cellular uptake, subcellular localization, and phototoxicity of Zn(II) N-alkylpyridylporphyrins," *The Journal of Biological Chemistry*, vol. 288, no. 51, pp. 36579–36588, 2013.

[48] I. Batinic-Haberle, I. Spasojevic, H. M. Tse et al., "Design of Mn porphyrins for treating oxidative stress injuries and their redox-based regulation of cellular transcriptional activities," *Amino Acids*, vol. 42, no. 1, pp. 95–113, 2012.

[49] T. Weitner, I. Kos, H. Sheng et al., "Comprehensive pharmacokinetic studies and oral bioavailability of two Mn porphyrin-based SOD mimics, $MnTE-2-PyP^{5+}$ and $MnTnHex-2-PyP^{5+}$," *Free Radical Biology & Medicine*, vol. 58, pp. 73–80, 2013.

[50] I. Spasojević, Y. Chen, T. J. Noel et al., "Mn porphyrin-based superoxide dismutase (SOD) mimic, $Mn^{III}TE-2-PyP^{5+}$, targets mouse heart mitochondria," *Free Radical Biology & Medicine*, vol. 42, no. 8, pp. 1193–1200, 2007.

[51] T. Weitner, H. Sheng, S. Miriyala et al., "Comprehensive pharmacokinetic studies and biodistribution of two cationic Mn porphyrin-based catalysts, $MnTE-2-PyP^{5+}$ and $MnTnHex-2-PyP^{5+}$: plasma and organ oral availability, mitochondrial, cytosolic, whole brain, Hippocampus and Cortex

Distribution," *Free Radical Biology and Medicine*, vol. 53, p. S118, 2012.

[52] I. Spasojevic, S. Miriyala, A. Tovmasyan et al., "Lipophilicity of Mn(III) N-alkylpyridylporphyrins dominates their accumulation within mitochondria and therefore in vivo efficacy: a Mouse Study," *Free Radical Biology and Medicine*, vol. 51, p. S98, 2011.

[53] I. Spasojević, Y. Chen, T. J. Noel et al., "Pharmacokinetics of the potent redox-modulating manganese porphyrin, $MnTE-2-PyP^{5+}$, in plasma and major organs of B6C3F1 mice," *Free Radical Biology & Medicine*, vol. 45, no. 7, pp. 943–949, 2008.

[54] K. A. Ashcraft, M.-K. Boss, A. Tovmasyan et al., "Novel manganese-porphyrin superoxide dismutase-mimetic widens the therapeutic margin in a preclinical head and neck cancer model," *International Journal of Radiation Oncology • Biology • Physics*, vol. 93, no. 4, pp. 892–900, 2015.

[55] S. C. Gad, D. W. Sullivan, J. D. Crapo, and C. B. Spainhour, "A nonclinical safety assessment of MnTE-2-PyP, a manganese porphyrin," *International Journal of Toxicology*, vol. 32, no. 4, pp. 274–287, 2013.

[56] S. C. Gad, D. W. Sullivan Jr., I. Spasojevic, C. V. Mujer, C. B. Spainhour, and J. D. Crapo, "Nonclinical safety and toxicokinetics of MnTnBuOE-2-PyP5+ (BMX-001)," *International Journal of Toxicology*, vol. 35, no. 4, pp. 438–453, 2016.

[57] I. Spasojevic, T. Weitner, A. Tovmasyan et al., "Pharmacokinetics, brain hippocampus and cortex, and mitochondrial accumulation of a new generation of lipophilic redox-active therapeutic, Mn(III) meso tetrakis(N-n-butoxyethylpyridinium-2-yl)porphyrin, MnTnBuOE-2-PyP5+, in comparison with its ethyl and N-hexyl analogs, MnTE-2-PyP5+ and MnTnHex-2-PyP5+," *Free Radical Biology and Medicine*, vol. 65, p. S132, 2013.

[58] D. Leu, I. Spasojevic, H. Nguyen et al., "CNS bioavailability and radiation protection of normal hippocampal neurogenesis by a lipophilic Mn porphyrin-based superoxide dismutase mimic, $MnTnBuOE-2-PyP^{5+}$," *Redox Biology*, vol. 12, pp. 864–871, 2017.

[59] M. K. Boss, M. W. Dewhirst, R. S. Sampaio et al., "Potential for a novel manganese porphyrin compound as adjuvant canine lymphoma therapy," *Cancer Chemotherapy and Pharmacology*, vol. 80, no. 2, pp. 421–431, 2017.

[60] M. C. Jaramillo, M. M. Briehl, I. Batinic-Haberle, and M. E. Tome, "Manganese (III) meso-tetrakis N-ethylpyridinium-2-yl porphyrin acts as a pro-oxidant to inhibit electron transport chain proteins, modulate bioenergetics, and enhance the response to chemotherapy in lymphoma cells," *Free Radical Biology & Medicine*, vol. 83, pp. 89–100, 2015.

[61] M. C. Jaramillo, M. M. Briehl, J. D. Crapo, I. Batinic-Haberle, and M. E. Tome, "Manganese porphyrin, $MnTE-2-PyP^{5+}$, acts as a pro-oxidant to potentiate glucocorticoid-induced apoptosis in lymphoma cells," *Free Radical Biology & Medicine*, vol. 52, no. 8, pp. 1272–1284, 2012.

[62] I. Batinic-Haberle, A. Tovmasyan, and I. Spasojevic, "An educational overview of the chemistry, biochemistry and therapeutic aspects of Mn porphyrins–from superoxide dismutation to H_2O_2-driven pathways," *Redox Biology*, vol. 5, pp. 43–65, 2015.

[63] G. Ferrer-Sueta, I. Batinić-Haberle, I. Spasojević, I. Fridovich, and R. Radi, "Catalytic scavenging of peroxynitrite by isomeric Mn(III) N-methylpyridylporphyrins in the presence of reductants," *Chemical Research in Toxicology*, vol. 12, no. 5, pp. 442–449, 1999.

[64] G. Ferrer-Sueta, D. Vitturi, I. Batinić-Haberle et al., "Reactions of manganese porphyrins with peroxynitrite and carbonate radical anion," *The Journal of Biological Chemistry*, vol. 278, no. 30, pp. 27432–27438, 2003.

[65] S. Carballal, V. Valez, I. Batinic-Haberle, G. Ferrer-Sueta, and R. Radi, "Reactivity and cytoprotective capacity of the synthetic catalytic antioxidants Mn porphyrins towards peroxynitrite and hypochlorite," *Free Radical Biology & Medicine*, vol. 65, pp. S121–S122, 2013.

[66] K. R. Olson, Y. Gao, F. Arif et al., "Manganese porphyrin-based SOD mimetics produce polysulfides from hydrogen sulfide," *Antioxidants (Basel)*, vol. 8, no. 12, 2019.

[67] K. R. Olson, Y. Gao, A. K. Steiger et al., "Effects of manganese porphyrins on cellular sulfur metabolism," *Molecules*, vol. 25, no. 4, 2020.

[68] I. Batinic-Haberle, Z. Rajic, A. Tovmasyan et al., "Diverse functions of cationic Mn(III) N-substituted pyridylporphyrins, recognized as SOD mimics," *Free Radical Biology & Medicine*, vol. 51, no. 5, pp. 1035–1053, 2011.

[69] I. Batinic-Haberle and A. Tovmasyan, "Superoxide dismutase mimics and other redox-active therapeutics," in *Oxidative Stress and Antioxidant Protection: The Science of Free Radical Biology and Disease*, D. Armstrong and R. D. Stratton, Eds., pp. 415–470, John Wiley & Sons, Inc., Hoboken, New Jersey, 2016.

[70] S. Kaewpila, S. Venkataraman, G. R. Buettner, and L. W. Oberley, "Manganese superoxide dismutase modulates hypoxia-inducible factor-1 alpha induction via superoxide," *Cancer Research*, vol. 68, no. 8, pp. 2781–2788, 2008.

[71] C. J. Weydert, T. A. Waugh, J. M. Ritchie et al., "Overexpression of manganese or copper-zinc superoxide dismutase inhibits breast cancer growth," *Free Radical Biology & Medicine*, vol. 41, no. 2, pp. 226–237, 2006.

[72] J. D. Piganelli, S. C. Flores, C. Cruz et al., "A metalloporphyrin-based superoxide dismutase mimic inhibits adoptive transfer of autoimmune diabetes by a diabetogenic T-cell clone," *Diabetes*, vol. 51, no. 2, pp. 347–355, 2002.

[73] M. C. Jaramillo, J. B. Frye, J. D. Crapo, M. M. Briehl, and M. E. Tome, "Increased manganese superoxide dismutase expression or treatment with manganese porphyrin potentiates dexamethasone-induced apoptosis in lymphoma cells," *Cancer Research*, vol. 69, no. 13, pp. 5450–5457, 2009.

[74] I. Batinic-Haberle and M. E. Tome, "Thiol regulation by Mn porphyrins, commonly known as SOD mimics," *Redox Biology*, vol. 25, article 101139, 2019.

[75] I. Spasojević, O. M. Colvin, K. R. Warshany, and I. Batinić-Haberle, "New approach to the activation of anti-cancer pro-drugs by metalloporphyrin-based cytochrome P450 mimics in all-aqueous biologically relevant system," *Journal of Inorganic Biochemistry*, vol. 100, no. 11, pp. 1897–1902, 2006.

[76] D. P. Jones, "Radical-free biology of oxidative stress," *American Journal of Physiology. Cell Physiology*, vol. 295, no. 4, pp. C849–C868, 2008.

[77] D. P. Jones, "Redox sensing: orthogonal control in cell cycle and apoptosis signalling," *Journal of Internal Medicine*, vol. 268, no. 5, pp. 432–448, 2010.

[78] H. Sheng, R. E. Chaparro, T. Sasaki et al., "Metalloporphyrins as therapeutic catalytic oxidoreductants in central nervous system disorders," *Antioxidants & Redox Signaling*, vol. 20, no. 15, pp. 2437–2464, 2014.

[79] H. Sheng, I. Spasojevic, H. M. Tse et al., "Neuroprotective efficacy from a lipophilic redox-modulating Mn(III) N-Hexylpyridylporphyrin, MnTnHex-2-PyP: rodent models of ischemic stroke and subarachnoid hemorrhage," *The Journal of Pharmacology and Experimental Therapeutics*, vol. 338, no. 3, pp. 906–916, 2011.

[80] A. Tovmasyan, Y.-M. Go, D. Jones, I. Spasojevic, and I. Batinic-Haberle, "Redox proteomics of 4T1 breast cancer cell after treatment with MnTE-2-PyP5+/ascorbate system," *Free Radical Biology and Medicine*, vol. 100, pp. S112–S113, 2016.

[81] A. Flórido, N. Saraiva, S. Cerqueira et al., "Impact of the SOD mimic MnTnHex-2-PyP on the adhesion and migration of doxorubicin-treated MDA-MB-231 cells," *Toxicology Letters*, vol. 238S, p. S241, 2015.

[82] Y. Zhao, D. W. Carroll, Y. You et al., "A novel redox regulator, MnTnBuOE-2-PyP^{5+}, enhances normal hematopoietic stem/progenitor cell function," *Redox Biology*, vol. 12, pp. 129–138, 2017.

[83] A. R. Clark and M. Ohlmeyer, "Protein phosphatase 2A as a therapeutic target in inflammation and neurodegeneration," *Pharmacology & Therapeutics*, vol. 201, pp. 181–201, 2019.

[84] M. Serrero, R. Planes, and E. Bahraoui, "PKC-δ isoform plays a crucial role in Tat-TLR4 signalling pathway to activate NF-κB and CXCL8 production," *Scientific Reports*, vol. 7, no. 1, p. 2384, 2017.

[85] L. Xie, C. Liu, L. Wang et al., "Protein phosphatase 2A catalytic subunit alpha plays a MyD88-dependent, central role in the gene-specific regulation of endotoxin tolerance," *Cell Reports*, vol. 3, no. 3, pp. 678–688, 2013.

[86] J. V. Cross and D. J. Templeton, "Oxidative stress inhibits MEKK1 by site-specific glutathionylation in the ATP-binding domain," *The Biochemical Journal*, vol. 381, no. 3, pp. 675–683, 2004.

[87] C. A. Bonham and P. O. Vacratsis, "Redox regulation of the human dual specificity phosphatase YVH1 through disulfide bond formation," *The Journal of Biological Chemistry*, vol. 284, no. 34, pp. 22853–22864, 2009.

[88] H. M. Tse, M. J. Milton, and J. D. Piganelli, "Mechanistic analysis of the immunomodulatory effects of a catalytic antioxidant on antigen-presenting cells: implication for their use in targeting oxidation-reduction reactions in innate immunity," *Free Radical Biology & Medicine*, vol. 36, no. 2, pp. 233–247, 2004.

[89] D. Raman and S. Pervaiz, "Redox inhibition of protein phosphatase PP2A: potential implications in oncogenesis and its progression," *Redox Biology*, vol. 27, article 101105, 2019.

[90] Y. Xiong, J. D. Uys, K. D. Tew, and D. M. Townsend, "S-glutathionylation: from molecular mechanisms to health outcomes," *Antioxidants & Redox Signaling*, vol. 15, no. 1, pp. 233–270, 2011.

[91] S.-W. Shin, C. Choi, G.-H. Lee et al., "Mechanism of the antitumor and radiosensitizing effects of a manganese porphyrin, MnHex-2-PyP," *Antioxidants & Redox Signaling*, vol. 27, no. 14, pp. 1067–1082, 2017.

[92] M. K. Evans, A. Tovmasyan, I. Batinic-Haberle, and G. R. Devi, "Mn porphyrin in combination with ascorbate acts as a pro-oxidant and mediates caspase-independent cancer cell death," *Free Radical Biology & Medicine*, vol. 68, pp. 302–314, 2014.

[93] D. H. Weitzel, A. Tovmasyan, K. A. Ashcraft et al., "Neurobehavioral radiation mitigation to standard brain cancer therapy regimens by Mn(III) n-butoxyethylpyridylporphyrin-based redox modifier," *Environmental and Molecular Mutagenesis*, vol. 57, no. 5, pp. 372–381, 2016.

[94] R. E. Oberley-Deegan and J. D. Crapo, "Mechanisms by which manganese porphyrins affect signaling in cancer cells," in *Redox-Active Therapeutics*, I. Batinić-Haberle, J. S. Rebouças, and I. Spasojević, Eds., pp. 405–431, Springer International Publishing, Cham, 2016.

[95] S. R. Birer, C.-T. Lee, K. R. Choudhury et al., "Inhibition of the continuum of radiation-induced normal tissue injury by a redox-active Mn porphyrin," *Radiation Research*, vol. 188, no. 1, pp. 94–104, 2017.

[96] Q. Tong, M. R. Weaver, E. A. Kosmacek et al., "MnTE-2-PyP reduces prostate cancer growth and metastasis by suppressing p300 activity and p300/HIF-1/CREB binding to the promoter region of the PAI-1 gene," *Free Radical Biology & Medicine*, vol. 94, pp. 185–194, 2016.

[97] Y. Zhu, E. A. Kosmacek, A. Chatterjee, and R. E. Oberley-Deegan, "MnTE-2-PyP suppresses prostate cancer cell growth via H_2O_2 production," *Antioxidants (Basel)*, vol. 9, no. 6, p. 490, 2020.

[98] A. Flórido, N. Saraiva, S. Cerqueira et al., "The manganese(III) porphyrin MnTnHex-2-PyP^{5+} modulates intracellular ROS and breast cancer cell migration: impact on doxorubicin-treated cells," *Redox Biology*, vol. 20, pp. 367–378, 2019.

[99] Y. Yang, P. Zhang, R. Yan et al., "MnTE-2-PyP attenuates TGF-β-induced epithelial-mesenchymal transition of colorectal cancer cells by inhibiting the Smad2/3 signaling pathway," *Oxidative Medicine and Cellular Longevity*, vol. 2019, Article ID 8639791, 11 pages, 2019.

[100] E. A. Kosmacek, A. Chatterjee, Q. Tong, C. Lin, and R. E. Oberley-Deegan, "MnTnBuOE-2-PyP protects normal colorectal fibroblasts from radiation damage and simultaneously enhances radio/chemotherapeutic killing of colorectal cancer cells," *Oncotarget*, vol. 7, no. 23, pp. 34532–34545, 2016.

[101] T. McElroy, T. Brown, F. Kiffer et al., "Assessing the effects of redox modifier MnTnBuOE-2-PyP 5+ on cognition and hippocampal physiology following doxorubicin, cyclophosphamide, and paclitaxel treatment," *International Journal of Molecular Sciences*, vol. 21, no. 5, 2020.

[102] J. G. Costa, N. Saraiva, I. Batinic-Haberle, M. Castro, N. G. Oliveira, and A. S. Fernandes, "The SOD mimic MnTnHex-2-PyP^{5+} reduces the viability and migration of 786-O human renal cancer cells," *Antioxidants (Basel)*, vol. 8, no. 10, 2019.

[103] E. A. Konorev, S. Kotamraju, H. Zhao, S. Kalivendi, J. Joseph, and B. Kalyanaraman, "Paradoxical effects of metalloporphyrins on doxorubicin-induced apoptosis: scavenging of reactive oxygen species versus induction of heme oxygenase-1," *Free Radical Biology & Medicine*, vol. 33, no. 7, p. 988, 2002.

[104] A. Tovmasyan, C. G. C. Maia, T. Weitner et al., "A comprehensive evaluation of catalase-like activity of different classes of redox-active therapeutics," *Free Radical Biology & Medicine*, vol. 86, pp. 308–321, 2015.

[105] T. Dorai, A. I. Fishman, C. Ding, I. Batinic-Haberle, D. S. Goldfarb, and M. Grasso, "Amelioration of renal ischemia-reperfusion injury with a novel protective cocktail," *The Journal of Urology*, vol. 186, no. 6, pp. 2448–2454, 2011.

[106] J. Jang, Y. Wang, H.-S. Kim, M. A. Lalli, and K. S. Kosik, "Nrf2, a regulator of the proteasome, controls self-renewal and pluripotency in human embryonic stem cells," *Stem Cells*, vol. 32, no. 10, pp. 2616–2625, 2014.

[107] S. Shrishrimal, A. Chatterjee, E. A. Kosmacek, P. J. Davis, J. T. McDonald, and R. E. Oberley-Deegan, "Manganese porphyrin, MnTE-2-PyP, treatment protects the prostate from radiation-induced fibrosis (RIF) by activating the NRF2 signaling pathway and enhancing SOD2 and sirtuin activity," *Free Radical Biology & Medicine*, vol. 152, pp. 255–270, 2020.

[108] A. Chatterjee, E. A. Kosmacek, and R. E. Oberley-Deegan, "MnTE-2-PyP treatment, or NOX4 inhibition, protects against radiation-induced damage in mouse primary prostate fibroblasts by inhibiting the TGF-beta 1 signaling pathway," *Radiation Research*, vol. 187, no. 3, pp. 367–381, 2017.

[109] A. Chatterjee, E. A. Kosmacek, S. Shrishrimal, J. T. McDonald, and R. E. Oberley-Deegan, "MnTE-2-PyP, a manganese porphyrin, reduces cytotoxicity caused by irradiation in a diabetic environment through the induction of endogenous antioxidant defenses," *Redox Biology*, vol. 34, article 101542, 2020.

[110] J. O. Archambeau, A. Tovmasyan, R. D. Pearlstein, J. D. Crapo, and I. Batinic-Haberle, "Superoxide dismutase mimic, MnTE-2-PyP^{5+} ameliorates acute and chronic proctitis following focal proton irradiation of the rat rectum," *Redox Biology*, vol. 1, no. 1, pp. 599–607, 2013.

[111] D. K. Ali, M. Oriowo, A. Tovmasyan, I. Batinic-Haberle, and L. Benov, "Late administration of Mn porphyrin-based SOD mimic enhances diabetic complications," *Redox Biology*, vol. 1, no. 1, pp. 457–466, 2013.

[112] K. A. Mapuskar, C. M. Anderson, D. R. Spitz, I. Batinic-Haberle, B. G. Allen, and R. E. Oberley-Deegan, "Utilizing superoxide dismutase mimetics to enhance radiation therapy response while protecting normal tissues," *Seminars in Radiation Oncology*, vol. 29, no. 1, pp. 72–80, 2019.

[113] J. D. Schoenfeld, M. S. Alexander, T. J. Waldron et al., "Pharmacological ascorbate as a means of sensitizing cancer cells to radio-chemotherapy while protecting normal tissue," *Seminars in Radiation Oncology*, vol. 29, no. 1, pp. 25–32, 2019.

[114] Y. Yulyana, A. Tovmasyan, I. A. W. Ho et al., "Redox-active Mn porphyrin-based potent SOD mimic, MnTnBuOE-2-PyP^{5+}, enhances carbenoxolone-mediated TRAIL-induced apoptosis in glioblastoma multiforme," *Stem Cell Reviews*, vol. 12, no. 1, pp. 140–155, 2016.

[115] D. H. Weitzel, A. Tovmasyan, K. A. Ashcraft et al., "Radioprotection of the brain white matter by Mn(III) n-butoxyethylpyridylporphyrin-based superoxide dismutase mimic MnTnBuOE-2-PyP5+," *Molecular Cancer Therapeutics*, vol. 14, no. 1, pp. 70–79, 2015.

[116] A. Tovmasyan, H. Sheng, T. Weitner et al., "Design, mechanism of action, bioavailability and therapeutic effects of Mn porphyrin-based redox modulators," *Medical Principles and Practice*, vol. 22, no. 2, pp. 103–130, 2013.

[117] K. A. Ashcraft and M. W. Dewhirst, "Anticancer action of Mn porphyrins in head and neck cancer," in *Redox-Active Therapeutics*, I. Batinić-Haberle, J. S. Rebouças, and I. Spasojević, Eds., pp. 469–484, Springer International Publishing, Cham, 2016.

[118] M. Granieri, A. Tovmasyan, H. Yan et al., "Radioprotection of erectile function using novel anti-oxidant in the rat," *The Journal of Sexual Medicine*, vol. 12, Supplement 2, pp. 178-179, 2015.

[119] A. Patel, E. A. Kosmacek, K. W. Fisher, W. Goldner, and R. E. Oberley-Deegan, "MnTnBuOE-2-PyP treatment protects from radioactive iodine (I-131) treatment-related side effects in thyroid cancer," *Radiation and Environmental Biophysics*, vol. 59, no. 1, pp. 99–109, 2020.

[120] S. Miriyala, C. Thippakorn, L. Chaiswing et al., "Novel role of 4-hydroxy-2-nonenal in AIFm2-mediated mitochondrial stress signaling," *Free Radical Biology & Medicine*, vol. 91, pp. 68–80, 2016.

[121] D. Carroll and D. K. S. Clair, "Hematopoietic stem cells: normal versus malignant," *Antioxidants & Redox Signaling*, vol. 29, 2017.

[122] A. Chatterjee, Y. Zhu, Q. Tong, E. Kosmacek, E. Lichter, and R. Oberley-Deegan, "The addition of manganese porphyrins during radiation inhibits prostate cancer growth and simultaneously protects normal prostate tissue from radiation damage," *Antioxidants (Basel)*, vol. 7, no. 1, 2018.

[123] W. Anselmo, E. Branchetti, J. B. Grau et al., "Porphyrin-based SOD mimic MnTnBu OE-2-PyP^{5+} inhibits mechanisms of aortic valve remodeling in human and murine models of aortic valve sclerosis," *Journal of the American Heart Association*, vol. 7, no. 20, article e007861, 2018.

[124] Z. N. Rabbani, I. Spasojevic, X. Zhang et al., "Antiangiogenic action of redox-modulating Mn(III) meso-tetrakis(N-ethyl-pyridinium-2-yl)porphyrin, MnTE-2-PyP^{5+}, via suppression of oxidative stress in a mouse model of breast tumor," *Free Radical Biology & Medicine*, vol. 47, no. 7, pp. 992–1004, 2009.

[125] A. Berchuck, E. S. Iversen, J. Luo et al., "Microarray analysis of early stage serous ovarian cancers shows profiles predictive of favorable outcome," *Clinical Cancer Research*, vol. 15, no. 7, pp. 2448–2455, 2009.

[126] B. J. Monk, M. F. Brady, C. Aghajanian et al., "A phase 2, randomized, double-blind, placebo- controlled study of chemo-immunotherapy combination using motolimod with pegylated liposomal doxorubicin in recurrent or persistent ovarian cancer: a Gynecologic Oncology Group partners study," *Annals of Oncology*, vol. 28, no. 5, pp. 996–1004, 2017.

[127] Y. Hatano, K. Hatano, M. Tamada et al., "A comprehensive review of ovarian serous carcinoma," *Advances in Anatomic Pathology*, vol. 26, no. 5, pp. 329–339, 2019.

[128] F. Medeiros, M. G. Muto, Y. Lee et al., "The tubal fimbria is a preferred site for early adenocarcinoma in women with familial ovarian cancer syndrome," *The American Journal of Surgical Pathology*, vol. 30, no. 2, pp. 230–236, 2006.

[129] S. Siamkpour-Reihani, K. Owzar, C. Jiang et al., "Prognostic significance of differential expression of angiogenic genes in women with high-grade serous ovarian carcinoma," *Gynecologic Oncology*, vol. 139, no. 1, pp. 23–29, 2015.

[130] S. D. Catz and J. L. Johnson, "Transcriptional regulation of bcl-2 by nuclear factor κB and its significance in prostate cancer," *Oncogene*, vol. 20, no. 50, pp. 7342–7351, 2001.

[131] C. A. Heckman, J. W. Mehew, and L. M. Boxer, "NF-κB activates Bcl-2 expression in t(14;18) lymphoma cells," *Oncogene*, vol. 21, no. 24, pp. 3898–3908, 2002.

[132] Z. Feng and A. G. Porter, "NF-κB/Rel proteins are required for neuronal differentiation of SH-SY5Y neuroblastoma cells," *The Journal of Biological Chemistry*, vol. 274, no. 43, pp. 30341–30344, 1999.

[133] J. Lee, C. Godon, G. Lagniel et al., "Yap1 and Skn7 control two specialized oxidative stress response regulons in yeast," *The Journal of Biological Chemistry*, vol. 274, no. 23, pp. 16040–16046, 1999.

[134] M. Tamatani, Y. H. Che, H. Matsuzaki et al., "Tumor necrosis factor induces Bcl-2 and Bcl-x expression through NFκB activation in primary hippocampal neurons," *The Journal of Biological Chemistry*, vol. 274, no. 13, pp. 8531–8538, 1999.

[135] S. Jones, T. L. Wang, R. J. Kurman et al., "Low-grade serous carcinomas of the ovary contain very few point mutations," *The Journal of Pathology*, vol. 226, no. 3, pp. 413–420, 2012.

[136] G. Singer, R. Oldt, Y. Cohen et al., "Mutations in BRAF and KRAS characterize the development of low-grade ovarian serous carcinoma," *Journal of the National Cancer Institute*, vol. 95, no. 6, pp. 484–486, 2003.

[137] R. Ambur Sankaranarayanan, S. Kossatz, W. Weber, M. Beheshti, A. Morgenroth, and F. M. Mottaghy, "Advancements in PARP1 targeted nuclear imaging and theranostic probes," *Journal of Clinical Medicine*, vol. 9, no. 7, 2020.

[138] I. Batinic-Haberle, W. Duan, L. Du et al., "MnTnBuOE-2-PyP^{5+}/ascorbate in treatment of ovarian cancer," *Free Radical Biology and Medicine*, vol. 159, p. S51, 2020.

[139] I. Batinic-Haberle, A. Tovmasyan, A. Veade, I. Spasojevic, S. Reihani, and A. Secord, "Mn porphyrin/ascorbate sensitizes serous epithelial ovarian cancer to chemotherapy," *Free Radical Biology and Medicine*, vol. 128, pp. S74–S75, 2018.

[140] R. F. Ozols, B. N. Bundy, B. E. Greer et al., "Phase III trial of carboplatin and paclitaxel compared with cisplatin and paclitaxel in patients with optimally resected stage III ovarian cancer: a Gynecologic Oncology Group study," *Journal of Clinical Oncology*, vol. 21, no. 17, pp. 3194–3200, 2003.

[141] R. A. Burger, M. F. Brady, M. A. Bookman et al., "Incorporation of bevacizumab in the primary treatment of ovarian cancer," *The New England Journal of Medicine*, vol. 365, no. 26, pp. 2473–2483, 2011.

[142] Group, GO, "Statistical report GOG-0218," 2009, 2017, https://gogmember.gog.org/GOG/StatReports/Reports/January_2009/Ovary/0218.PDF.

[143] L. M. Hess, H. Q. Huang, A. L. Hanlon et al., "Cognitive function during and six months following chemotherapy for front-line treatment of ovarian, primary peritoneal or fallopian tube cancer: an NRG oncology/gynecologic oncology group study," *Gynecologic Oncology*, vol. 139, no. 3, pp. 541–545, 2015.

[144] H. Li, Y. Wang, S. K. Pazhanisamy et al., "Mn(III) meso-tetrakis-(N-ethylpyridinium-2-yl) porphyrin mitigates total body irradiation-induced long-term bone marrow suppression," *Free Radical Biology & Medicine*, vol. 51, no. 1, pp. 30–37, 2011.

[145] S. K. Pazhanisamy, H. Li, Y. Wang, I. Batinic-Haberle, and D. Zhou, "NADPH oxidase inhibition attenuates total body irradiation-induced haematopoietic genomic instability," *Mutagenesis*, vol. 26, no. 3, pp. 431–435, 2011.

[146] Q. Chen, M. G. Espey, M. C. Krishna et al., "Pharmacologic ascorbic acid concentrations selectively kill cancer cells: action as a pro-drug to deliver hydrogen peroxide to tissues," *Proceedings of the National Academy of Sciences of the United States of America*, vol. 102, no. 38, pp. 13604–13609, 2005.

[147] Q. Chen, M. G. Espey, A. Y. Sun et al., "Ascorbate in pharmacologic concentrations selectively generates ascorbate radical and hydrogen peroxide in extracellular fluid in vivo," *Proceedings of the National Academy of Sciences of the United States of America*, vol. 104, no. 21, pp. 8749–8754, 2007.

[148] Q. Chen, M. G. Espey, A. Y. Sun et al., "Pharmacologic doses of ascorbate act as a prooxidant and decrease growth of aggressive tumor xenografts in mice," *Proceedings of the National Academy of Sciences of the United States of America*, vol. 105, no. 32, pp. 11105–11109, 2008.

[149] "Clinical Trials Using Ascorbic Acid, National Cancer Institute," https://www.cancer.gov/about-cancer/treatment/clinical-trials/intervention/ascorbic-acid.

[150] B. G. Allen, K. L. Bodeker, M. C. Smith et al., "First-in-human phase I clinical trial of pharmacologic ascorbate combined with radiation and temozolomide for newly diagnosed glioblastoma," *Clinical Cancer Research*, vol. 25, no. 22, pp. 6590–6597, 2019.

[151] D. A. Monti, E. Mitchell, A. J. Bazzan et al., "Phase I evaluation of intravenous ascorbic acid in combination with gemcitabine and erlotinib in patients with metastatic pancreatic cancer," *PLoS One*, vol. 7, no. 1, article e29794, 2012.

[152] J. L. Welsh, B. A. Wagner, T. J. Van't Erve et al., "Pharmacological ascorbate with gemcitabine for the control of metastatic and node-positive pancreatic cancer (PACMAN): results from a phase I clinical trial," *Cancer Chemotherapy and Pharmacology*, vol. 71, no. 3, pp. 765–775, 2013.

[153] G. Nauman, J. C. Gray, R. Parkinson, M. Levine, and C. J. Paller, "Systematic review of intravenous ascorbate in cancer clinical trials," *Antioxidants (Basel)*, vol. 7, no. 7, 2018.

[154] N. Shenoy, E. Creagan, T. Witzig, and M. Levine, "Ascorbic acid in cancer treatment: let the phoenix fly," *Cancer Cell*, vol. 34, no. 5, pp. 700–706, 2018.

[155] C. M. Anderson, C. M. Lee, D. P. Saunders et al., "Phase IIb, randomized, double-blind trial of GC4419 versus placebo to reduce severe oral mucositis due to concurrent radiotherapy and cisplatin for head and neck cancer," *Journal of Clinical Oncology*, vol. 37, no. 34, pp. 3256–3265, 2019.

[156] G. Nauman, J. C. Gray, R. Parkinson, M. Levine, and C. J. Paller, "Superoxide dismutase mimetic GC4419 enhances the oxidation of pharmacological ascorbate and its anticancer effects in an H_2O_2-dependent manner," *Antioxidants (Basel)*, vol. 7, no. 1, 2018.

[157] J. C. Bueno-Janice, A. Tovmasyan, and I. Batinic-Haberle, "Comprehensive study of GPx activity of different classes of redox-active therapeutics—implications for their therapeutic actions," *Free Radical Biology and Medicine*, vol. 87, pp. S86–S87, 2015.

Research Article

Manoalide Shows Mutual Interaction between Cellular and Mitochondrial Reactive Species with Apoptosis in Oral Cancer Cells

Hui-Ru Wang,[1] **Ping-Ho Chen** ⬭,[2,3] **Jen-Yang Tang** ⬭,[4,5] **Ching-Yu Yen** ⬭,[6,7]
Yong-Chao Su ⬭,[1] **Ming-Yii Huang** ⬭,[4,5] **and Hsueh-Wei Chang** ⬭[1,3,8]

[1]*Department of Biomedical Science and Environmental Biology, PhD Program of Life Science, College of Life Science, Kaohsiung Medical University, Kaohsiung, Taiwan*
[2]*School of Dentistry, College of Dental Medicine, Kaohsiung Medical University, Kaohsiung, Taiwan*
[3]*Cancer Center, Kaohsiung Medical University Hospital, Kaohsiung, Taiwan*
[4]*Department of Radiation Oncology, Kaohsiung Medical University Hospital, Kaohsiung, Taiwan*
[5]*Department of Radiation Oncology, Faculty of Medicine, College of Medicine, Kaohsiung Medical University, Kaohsiung, Taiwan*
[6]*Department of Oral and Maxillofacial Surgery, Chi-Mei Foundation Medical Center, Tainan, Taiwan*
[7]*School of Dentistry, Taipei Medical University, Taipei, Taiwan*
[8]*Center for Cancer Research, Kaohsiung Medical University, Kaohsiung, Taiwan*

Correspondence should be addressed to Ming-Yii Huang; miyihu@kmu.edu.tw and Hsueh-Wei Chang; changhw@kmu.edu.tw

We previously found that marine sponge-derived manoalide induced antiproliferation and apoptosis of oral cancer cells as well as reactive species generations probed by dichloro-dihydrofluorescein diacetate (DCFH-DA) and MitoSOX Red. However, the sources of cellular and mitochondrial redox stresses and the mutual interacting effects between these redox stresses and apoptosis remain unclear. To address this issue, we examined a panel of reactive species and used the inhibitors of cellular reactive species (N-acetylcysteine (NAC)), mitochondrial reactive species (MitoTEMPO), and apoptosis (Z-VAD-FMK; ZVAD) to explore their interactions in manoalide-treated oral cancer Ca9-22 and CAL 27 cells. Hydroxyl ($^\cdot OH$), nitrogen dioxide ($NO_2{}^\cdot$), nitric oxide ($^\cdot NO$), carbonate radical-anion ($CO_3{}^{\cdot-}$), peroxynitrite ($ONOO^-$), and superoxide ($O_2{}^{\cdot-}$) were increased in oral cancer cells following manoalide treatments in terms of fluorescence staining and flow cytometry. Cellular reactive species ($^\cdot OH$, $NO_2{}^\cdot$, $^\cdot NO$, $CO_3{}^{\cdot-}$, and $ONOO^-$) as well as cellular and mitochondrial reactive species ($O_2{}^{\cdot-}$) were induced in oral cancer cells following manoalide treatment for 6 h. NAC, MitoTEMPO, and ZVAD inhibit manoalide-induced apoptosis in terms of annexin V and pancaspase activity assays. Moreover, NAC inhibits mitochondrial reactive species and MitoTEMPO inhibits cellular reactive species, suggesting that cellular and mitochondrial reactive species can crosstalk to regulate each other. ZVAD shows suppressing effects on the generation of both cellular and mitochondrial reactive species. In conclusion, manoalide induces reciprocally activation between cellular and mitochondrial reactive species and apoptosis in oral cancer cells.

1. Introduction

Oral cancer is a global disease with approximately 710,000 new cases of cancers of the oral cavity and pharynx per year and over 359,000 deaths worldwide [1]. In the world, cancers of the oral cavity and pharynx rank as the 7th

more prevalent cancer and rank as the 9th cause of cancer death. To date, the incidence rate of oral and pharynx cancers among Taiwanese men ranks the highest worldwide [1, 2]. In Taiwan, cancers of the oral cavity and pharynx were the fourth most prevalent cancer among males [3]. At present, oral cancer is primarily treated by

surgical resection, radiation therapy, chemotherapy, or a combination of the above therapies [4]. The anticancer drug development for oral cancer cells is still imperative.

Marine natural products are abundant resources for identifying anticancer drugs [5–8]. Manoalide, a marine sponge-derived sesterterpenoid [9], has antibiotic, analgesic, anti-inflammatory [10], and anticancer effects [11, 12]. In 1993, the first anticancer effect for antiproliferation by manoalide had been reported in human epidermoid carcinoma KB cells [13] but only the IC_{50} value was provided without investigating detailed mechanisms [11]. Manoalide has been used for Phase II (antipsoriatic) clinical trial but ceased by formulation problems [14].

Recently, we reported that manoalide exhibited antiproliferation, apoptosis, and DNA damage effects against oral cancer cells by inducing the cellular reactive species as probed by dichloro-dihydrofluorescein diacetate (DCFH-DA) [12]. However, the DCFH-DA was reported to be unreliable probe to detect H_2O_2 and other kind of ROS [15, 16]. Moreover, superoxide anion was reported to be incapable of crossing the mitochondrial membrane [17]. However, our previous study showed that MitoTEMPO (MT) [18], an mitochondrial superoxide (MitoSOX) inhibitor, suppressed manoalide-induced DNA damages (γH2AX and 8-oxodG) [12], suggesting that MitoSOX may cross the mitochondrial membrane to induce DNA damage in oral cancer cells. Accordingly, the MitoSOX traffic to exit mitochondria is controversial. Therefore, the traffic between manoalide-induced cellular and mitochondrial reactive species remains unclear. It warrants for detailed investigation for the involvement of more different cellular and mitochondrial reactive species after manoalide treatment.

In the present study, we aimed to determine the changes of several types of reactive species using several available probes [19] in oral cancer Ca9-22 and CAL 27 cells following manoalide treatment. Levels of the cellular reactive species such as nitrogen dioxide ($NO_2^{\cdot}$), carbonate radical-anion ($CO_3^{\cdot-}$), hydroxyl ($^{\cdot}OH$), peroxynitrite ($ONOO^-$), and nitric oxide ($^{\cdot}NO$) as well as the cellular and mitochondrial superoxide ($O_2^{\cdot-}$) were estimated.

Using the inhibitors for cellular and mitochondrial oxidative stresses (N-acetylcysteine (NAC) and MitoTEMPO (MT)), the sources of cellular and mitochondrial reactive species and its apoptosis-modulating effect in oral cancer cells after manoalide treatment were analyzed. Using the inhibitors for apoptosis (Z-VAD-FMK; ZVAD), the cellular and mitochondrial reactive species-modulating effect of apoptosis in oral cancer cells after manoalide treatment was explored. Therefore, the possibility that manoalide induced the mutual interaction between cellular and mitochondrial reactive species and apoptosis in oral cancer cells were examined in the current study.

2. Materials and Methods

2.1. Cell Culture, Cell Viability, Apoptosis, Manoalide, and Inhibitors. The human oral cancer cell lines (Ca9-22 and CAL 27), collected from Health Science Research Resources Bank (HSRRB; Osaka, Japan) and American Type Culture

Collection (ATCC; Manassas, VA, USA), were maintained in DMEM formula (Gibco, Grand Island, NY, USA) with 10% fetal bovine serum as previously described [20]. Cell viability for 6 h manoalide treatment ($10\,\mu M$) was determined by MTS assay [12]. Apoptosis was determined by both annexin V/7-aminoactinmycin D (7AAD) (Strong Biotech Corporation, Taipei, Taiwan) and pancaspase activity (Abcam, Cambridge, UK) [21] assays as previously described.

Manoalide, mitochondrial superoxide inhibitor MT [18] (Cayman Chemical, Ann Arbor, MI, USA), and panapoptosis inhibitor ZVAD [22] (http://Selleckchem.com/; Houston, TX, USA) were dissolved in DMSO. A cellular reactive species inhibitor NAC [23, 24] (Sigma-Aldrich; St Louis, MO, USA) was dissolved in double distilled water.

2.2. Probes for Several Reactive Species. Measurements for several reactive species could be detected using several probes (Sigma, St Louis, MO, USA) as follows [19]. DCFH-DA is a probe for $NO_2^{\cdot}$, $CO_3^{\cdot-}$, and $^{\cdot}OH$. Hydroxyphenyl fluorescein (HPF) is a probe for $^{\cdot}OH$ and ONOO-. 4-amino-5-methylamino-2$'$,7$'$-difluorofluorescein (DAF-FM) is a probe for $^{\cdot}NO$. Dihydroethidium (DHE) and MitoSOX Red are probes for cellular and mitochondria $O_2^{\cdot-}$, respectively [16]. These probes were dissolved in DMSO and all experiments with or without probes had the same concentration of 0.1% DMSO.

2.3. Fluorescence Staining for Several Reactive Species. After manoalide treatment for 6 h, cells were stained with DCFH-DA (10 mM, 30 min), DHE ($50\,\mu M$, 30 min), MitoSOX Red (2.5 mM, 10 min), DAF-FM ($100\,\mu M$, 30 min), or HPF ($100\,\mu M$, 30 min) [19] and washed with 1x PBS before microscopy. DCFH-DA, DAF-FM, and HPF were observed by Leica DMi8 fluorescence microscope at excitation (ex)/emission (em) 488/525 nm while DHE and MitoSOX Red were observed by Olympus FV1000 confocal microscope at ex/em for 405/605 nm [25].

2.4. Flow Cytometry for Several Reactive Species. After manoalide treatment for 6 h, cells were stained with DCFH-DA [26] (1 mM, 30 min), DHE [27] ($5\,\mu M$, 30 min), MitoSOX Red [28] (0.25 mM, 10 min), DAF-FM [29] ($10\,\mu M$, 30 min), or HPF [30] ($10\,\mu M$, 30 min), and washed with 1x PBS. Subsequently, DCFH-DA, DAF-FM, and HPF were observed by Guava® easyCyte flow cytometer (Merck KGaA; Darmstadt, Germany) at ex/em for 488/525 nm. DHE and MitoSOX Red were observed by LSR II flow cytometer (Becton-Dickinson, Mansfield, MA, USA) at ex/em for 405/585 nm to avoid the nonspecific superoxide detection under 488 nm excitation [25]. Data were analyzed by Flow Jo (FlowJo LLC, Ashland, OR, USA).

To evaluate the suppression powder of inhibitors on manoalide-induced reactive species, we use the formula of suppression (fold) to calculate as follows: Suppression fold of reactive species inhibitors = (mean intensity of manoalide / mean intensity of control) / (mean intensity of inhibitors and manoalide / mean intensity of inhibitors), where

inhibitors can be NAC, MT, and ZVAD. When manoalide concentration is zero, the suppression (fold) of inhibitor is 1.

2.5. *Statistics.* The significance of the difference in multiple comparisons were analyzed by one-way ANOVA with Tukey HSD post hoc test (JMP® 12 software). Results from different treatments are considered significantly different for multiple comparison (indicated via different letters without overlapping) if $p < 0.05$.

3. Results

3.1. *Several Reactive Species Were Detectable in Oral Cancer Cells after Manoalide Treatment.* As shown in Figure 1(a), cellular reactive species ($NO_2^{\cdot}$, $CO_3^{\cdot-}$, $^{\cdot}OH$, $ONOO^-$, $^{\cdot}NO$, and $O_2^{\cdot-}$) in manoalide-treated oral cancer cells were detected by using available probes such as DCFH-DA, HPF, DAF-FM, and DHE). Mitochondrial $O_2^{\cdot-}$ reactive species was probed by MitoSOX Red. Both cellular and mitochondrial reactive species showed positive fluorescent staining in oral cancer Ca9-22 and CAL 27 cells after manoalide treatment ($10\,\mu M$, 6 h), demonstrating that the radical probes DCFH-DA, HPF, DAF-FM, DHE, and MitoSOX Red were able to qualitatively detect their reactive species. The relative quantitative analyses were analyzed by flow cytometer as shown in the following experiments. Under manoalide treatment ($10\,\mu M$, 6 h), oral cancer Ca9-22 and CAL 27 cells showed about 76% cell viability (Figure 1(b)), suggesting short-term exposure of manoalide exhibited a detectable cell killing effect to oral cancer cells.

3.2. *Several Reactive Species Were Differentially Generated in Oral Cancer Cells after Manoalide Treatment.* Using flow cytometry, the levels of several reactive species were measured in manoalide-treated oral cancer cells by using available probes (Figure 2(a)). Since free radicals were short-lived intermediates [16, 31], all test probes (DCFH-DA, HPF, DAF-FM, DHE, and MitoSOX Red) were detected in short time (0, 10 min, 1 h, and 6 h). These test probes showed differential increase for their corresponding reactive radicals in a time-dependent manner to oral cancer Ca9-22 and CAL 27 cells after manoalide treatment ($10\,\mu M$) (Figure 2(b)). Moreover, cellular reactive species (probed by DCFH-DA, HPF, DAF-FM, and DHE) and mitochondrial reactive species (probed by MitoSOX Red) were differentially induced in manoalide-treated oral cancer cells. Since 6 h manoalide treatment ($10\,\mu M$) showed the highest intensity for all reactive species ranging from 0 to 6 h, the following experiments were performed according to this condition.

3.3. *Manoalide-Induced Apoptosis Was Differentially Suppressed by NAC, MT, and ZVAD in Oral Cancer Cells.* Following pretreatments of inhibitors for cellular reactive species, mitochondrial reactive species, and apoptosis, i.e., *N*-acetylcysteine (NAC), MitoTEMPO (MT), and apoptosis (ZVAD), the flow cytometry patterns of annexin V/7AAD and pancaspase activity-detected apoptosis in manoalide ($10\,\mu M$, 6 h) posttreated oral cancer Ca9-22 and CAL 27 cells were provided (Figures 3(a) and 3(c)). As shown in Figures 3(b) and 3(d), annexin V- and pancaspase activity-

detected apoptosis was highly induced by manoalide in oral cancer cells, which was suppressed by pretreatments of NAC, MT, and ZVAD.

3.4. *DCFH-DA-Detected Cellular Reactive Species Were Differentially Suppressed by NAC, MT, and ZVAD in Manoalide-Treated Oral Cancer Cells.* Following pretreatments of inhibitors for cellular reactive species, mitochondrial reactive species, and apoptosis, i.e., NAC, MT, and ZVAD, the flow cytometry patterns of DCFH-DA-detected reactive species in manoalide posttreated oral cancer Ca9-22 and CAL 27 cells were provided (Figure 4(a)). As shown in Figure 4(b), DCFH-DA-detected cellular reactive species were highly induced by manoalide in oral cancer cells, which were suppressed by pretreatments of NAC, MT, and ZVAD.

3.5. *HPF-Detected Cellular Reactive Species Were Differentially Suppressed by NAC, MT, and ZVAD in Manoalide-Treated Oral Cancer Cells.* Following pretreatments of NAC, MT, and ZVAD, the flow cytometry patterns of HPF-detected reactive species in manoalide posttreated oral cancer Ca9-22 and CAL 27 cells were provided (Figure 5(a)). As shown in Figure 5(b), HPF-detected cellular reactive species were highly induced by manoalide in oral cancer cells, which were suppressed by pretreatments of NAC, MT, and ZVAD.

3.6. *DAF-FM-Detected Cellular Reactive Species Were Differentially Suppressed by NAC, MT, and ZVAD in Manoalide-Treated Oral Cancer Cells.* Following pretreatments of NAC, MT, and ZVAD, the flow cytometry patterns of DAF-FM-detected reactive species in manoalide posttreated oral cancer Ca9-22 and CAL 27 cells were provided (Figure 6(a)). As shown in Figure 6(b), DAF-FM-detected cellular reactive species were highly induced by manoalide in oral cancer cells, which were suppressed by pretreatments of NAC, MT, and ZVAD.

3.7. *DHE-Detected Cellular Reactive Species Were Differentially Suppressed by NAC, MT, and ZVAD in Manoalide-Treated Oral Cancer Cells.* Following pretreatments of NAC, MT, and ZVAD, the flow cytometry patterns of DHE-detected reactive species in manoalide posttreated oral cancer Ca9-22 and CAL 27 cells were provided (Figure 7(a)). As shown in Figure 7(b), DHE-detected cellular $O_2^{\cdot-}$ reactive species were highly induced by manoalide in oral cancer cells, which were suppressed by pretreatments of NAC, MT, and ZVAD.

3.8. *MitoSOX Red-Detected Mitochondrial Reactive Species Were Differentially Suppressed by NAC, MT, and ZVAD in Manoalide-Treated Oral Cancer Cells.* Following pretreatments of NAC, MT, and ZVAD, the flow cytometry patterns of MitoSOX Red-detected reactive species in manoalide posttreated oral cancer Ca9-22 and CAL 27 cells were provided (Figure 8(a)). As shown in Figure 8(b), MitoSOX Red-detected mitochondrial $O_2^{\cdot-}$ reactive species were highly induced by manoalide in oral cancer cells, which were suppressed by pretreatments of NAC, MT, and ZVAD.
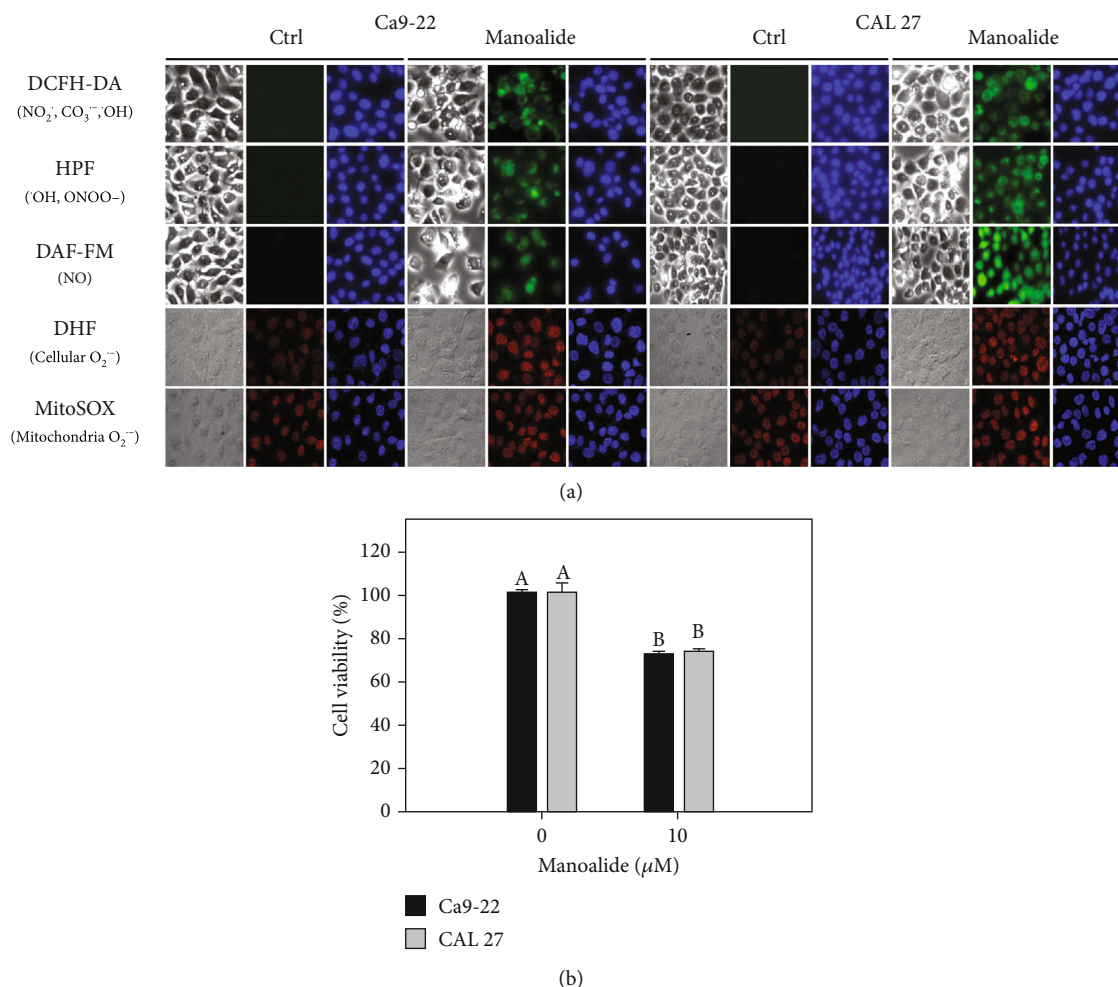
(a)

(b)

FIGURE 1: Detection of several kinds of reactive species and cell viability in oral cancer cells after 6 h manoalide treatment. Cells were treated under control (0.1% DMSO only) and manoalide (10 μM) treatments for 6 h. All experiments had the same concentration of DMSO. (a) Fluorescence staining images of cellular and mitochondrial radical probes with DCFH-DA, HPF, DAF-FM, DHE, and MitoSOX Red in manoalide-treated oral cancer (Ca9-22 and CAL 27) cells. For each treatment, the light microscope, radical probe, and Hoechst 33342 (2'-[4-ethoxyphenyl]-5-[4-methyl-1-piperazinyl]-2,5'-bi-1H-benzimidazole trihydrochloride trihydrate) counterstaining images were provided. DCFH-DA-, HPF-, and DAF-FM-probed images were captured by Leica DMi8 fluorescence microscope. DHE- and MitoSOX-probed images were captured by Olympus FV1000 confocal microscope. (b) MTS assay for cell viability determination. Results between control and manoalide treatment of the same cells are considered significantly different (indicated via different letters without overlapping) ($p < 0.0001$). Data, means $\pm$ SDs ($n = 3$ independent experiments, each experiment was performed with three replications).

4. Discussion

Drugs with redox-modulating ability have the potential for selective killing on cancer cells [32–34]. Manoalide was validated to have this redox-modulating ability for selective killing on oral cancer cells [12]; however, its redox evidence of manoalide relies on DCFH-DA and MitoSOX Red-detected reactive species. Moreover, the DCFH-DA was reported to be unreliable probe to detect H_2O_2 ($\cdot$OH) [15, 16]. DCFH-DA also crossdetected $NO_2^{\cdot}$ and $CO_3^{\cdot-}$. Accordingly, more probes detecting other reactive species as indicated in Figure 1 are necessary to clarify the redox-modulating ability of manoalide.

In the present study, we investigated the sources of cellular and mitochondrial oxidative stresses in oral cancer cells

after manoalide treatment. Moreover, the interaction among these manoalide-induced reactive species and apoptosis in oral cancer cells were explored.

4.1. Cellular Reactive Species May Regulate Mitochondrial Reactive Species. Based on the finding using the inhibitor pretreatment (NAC) of cellular reactive species, the manoalide-induced cellular reactive species as probed by DCFH-DA, HPF, DAF-FM, and DHE were suppressed (Figures 4–7). Similarly, FasL-stimulated cellular reactive species as probed by dihydrorhodamine (DHR for H_2O_2 detection), HPF, and DHE were suppressed by NAC in Jurkat cells [35]. Thrombin-induced cellular reactive species as probed by DHE was suppressed by NAC in platelets *in vitro* [27]. Moreover, NAC pretreatment also suppressed the mitochondrial
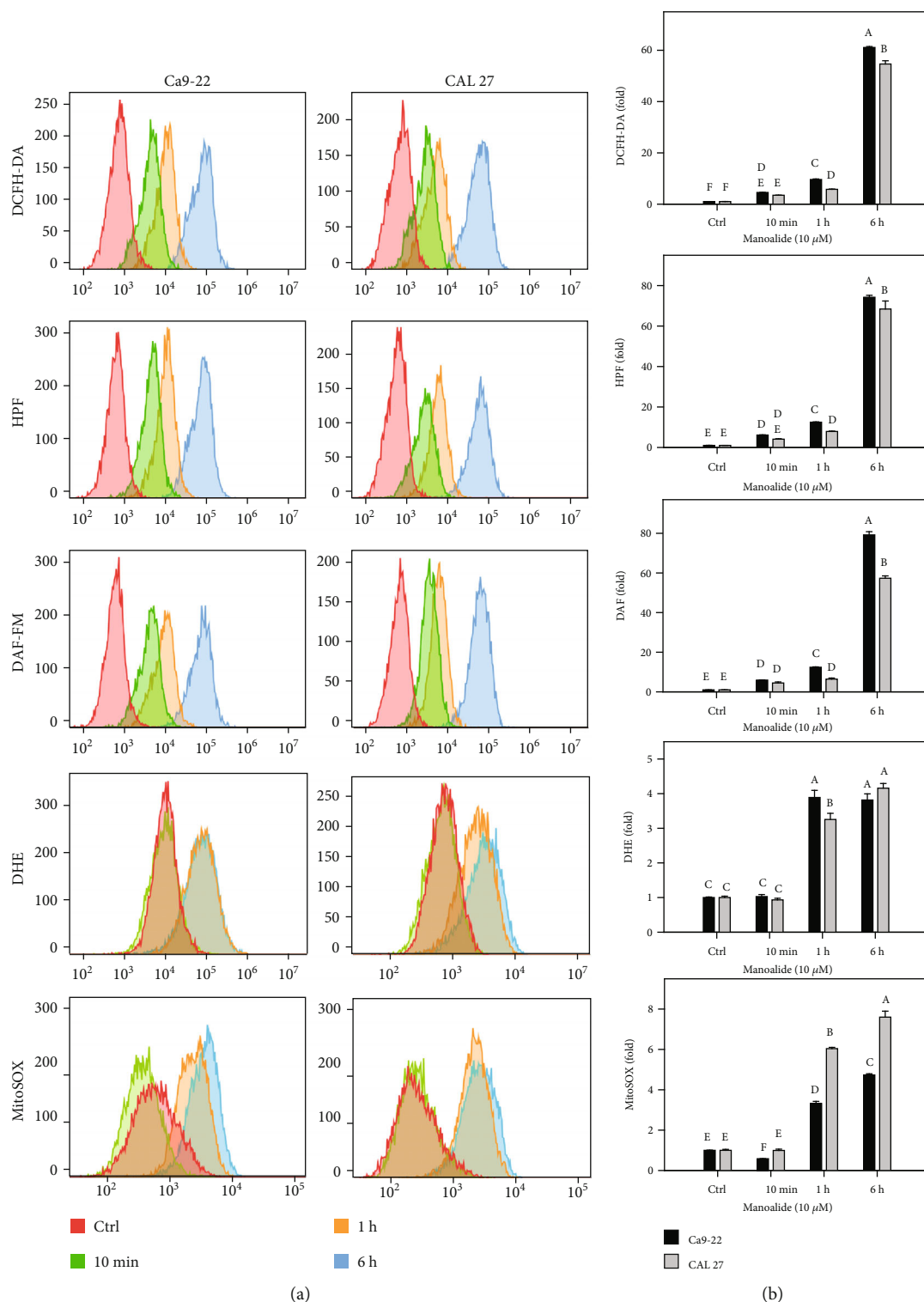
FIGURE 2: Flow cytometry of radical probes with DCFH-DA, HPF, DAF-FM, DHE, and MitoSOX Red in manoalide-treated oral cancer cells. Cells were treated with control (0.1% DMSO only) and manoalide (10 μM) for 0, 10 min, 1 h, and 6 h. All experiments had the same concentration of DMSO. (a) Flow cytometry patterns for manoalide-treated oral cancer cells (Ca9-22 and CAL 27). (b) Statistics. The reactive mean intensity for the control is set to 1. Results from different treatments are considered significantly different for multiple comparison (indicated via different letters without overlapping) ($p < 0.05$ to 0.0001). In the example of (b), the DCFH-DA fold for control, 10 min, 1 h, and 6 h show letters at top for "f," "de," "c," and "a" for Ca9-22 cells. Since they were marked with different letters without overlapping, all the treatments between each other for control, 10 min, 1 h, and 6 h differ significantly. Moreover, the DCFH-DA fold at 6 h for Ca9-22 and CAL 27 cells show letters at top for "a" and "b," indicating that they are significantly different. Data, means ± SDs ($n = 3$ independent experiments, each experiment collected with 10000 gated cell counts).
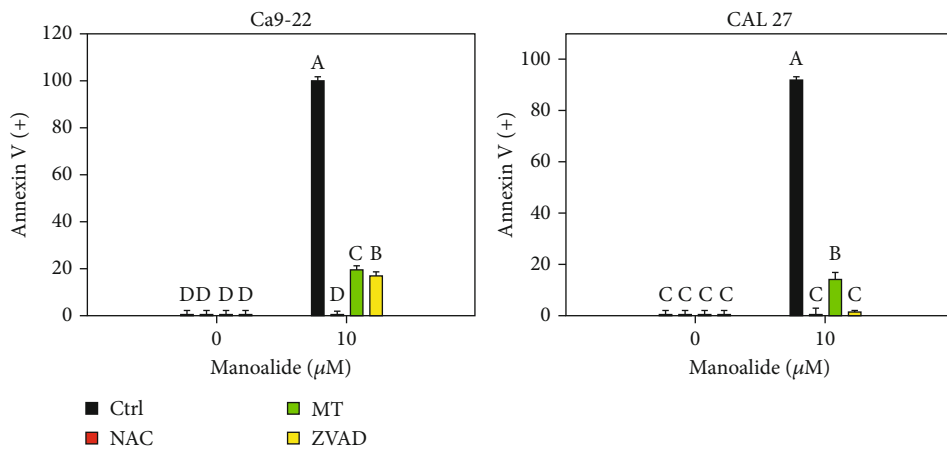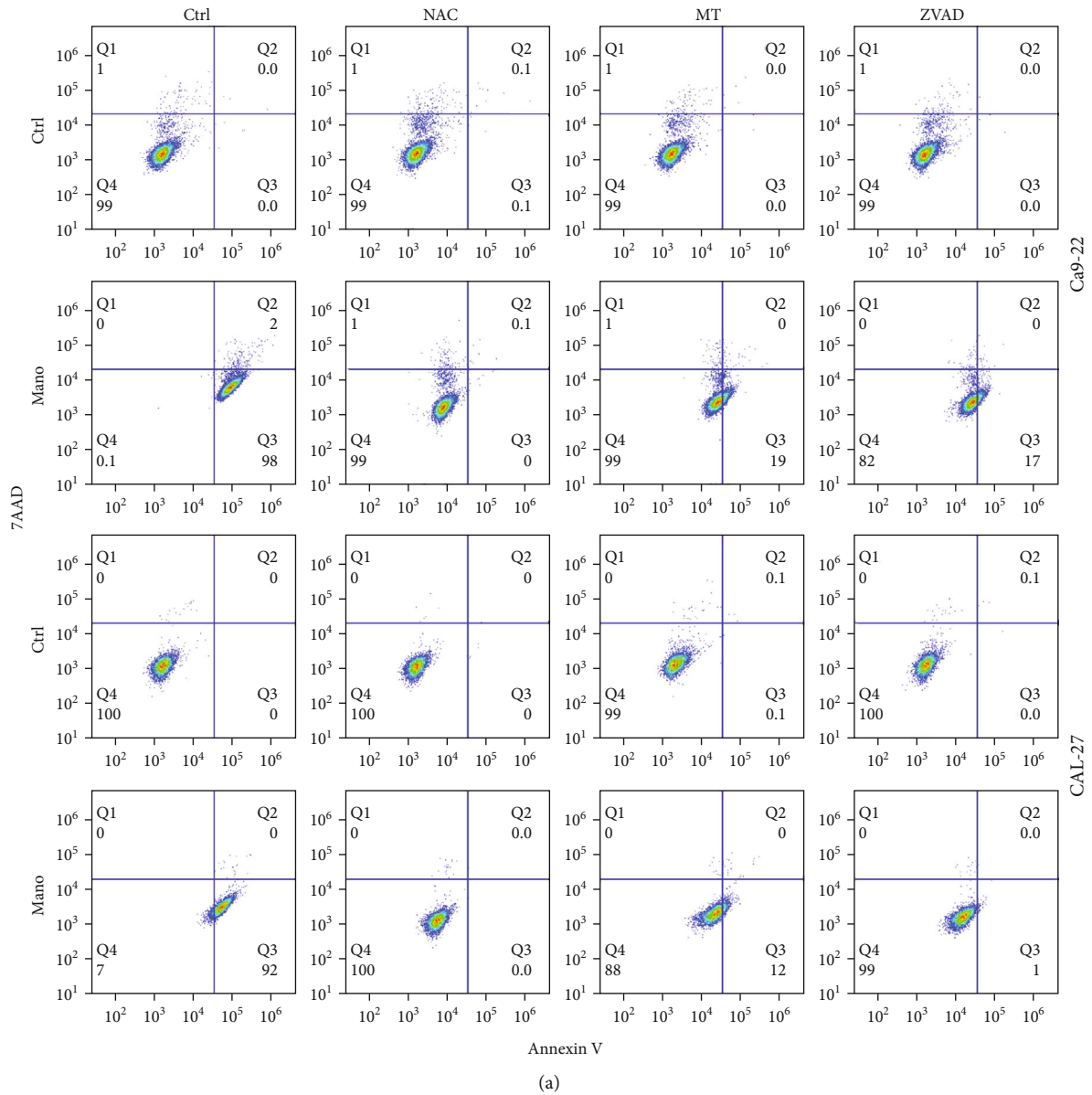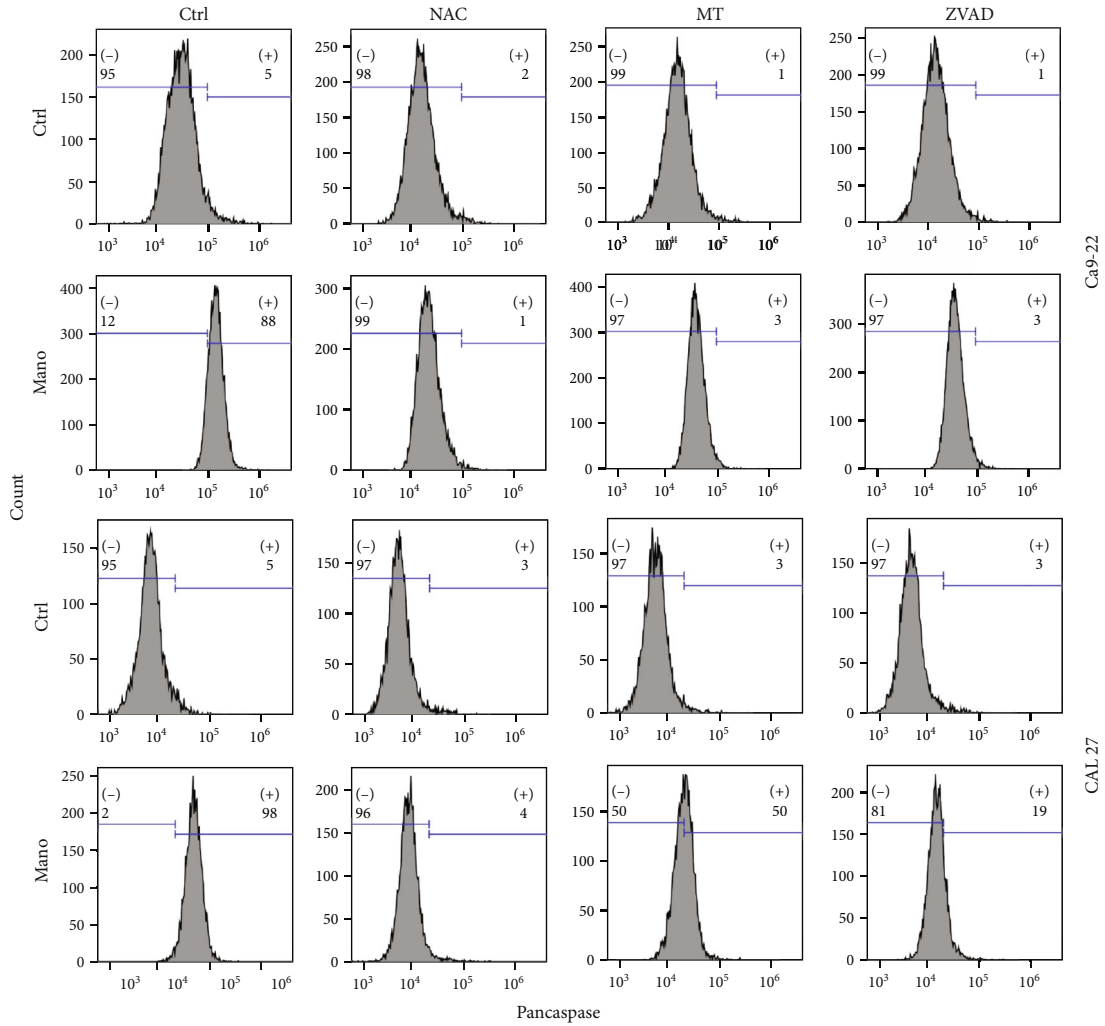
(a)

(b)

Figure 3: Continued.

(c)

(d)

FIGURE 3: Apoptosis effects of inhibitors for cellular reactive species, mitochondrial reactive species, and apoptosis (NAC, MT, and ZVAD) in manoalide-treated oral cancer cells. Cells (Ca9-22 and CAL 27) were pretreated with control (0.1% DMSO only), NAC (8 mM), MT (20 μM), and ZVAD (100 μM) for 2 h and posttreated with control and manoalide (10 μM) for 0 and 6 h. All experiments had the same concentration of DMSO. (a) Flow cytometry patterns of annexin V/7AAD staining for manoalide-treated oral cancer cells. (b) Statistics of (a). (c) Flow cytometry patterns of pancaspase activity for manoalide-treated oral cancer cells. (d) Statistics of (c). Results from different inhibitor treatments are considered significantly different compared to control (indicated via different letters without overlapping) ($p < 0.05$ to 0.0001). Data, means ± SDs ($n = 3$ independent experiments, each experiment collected with 10000 gated cell counts).
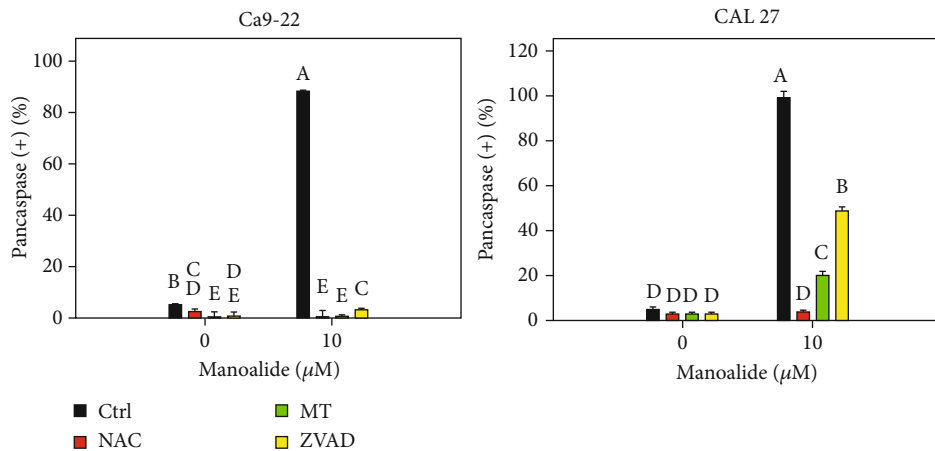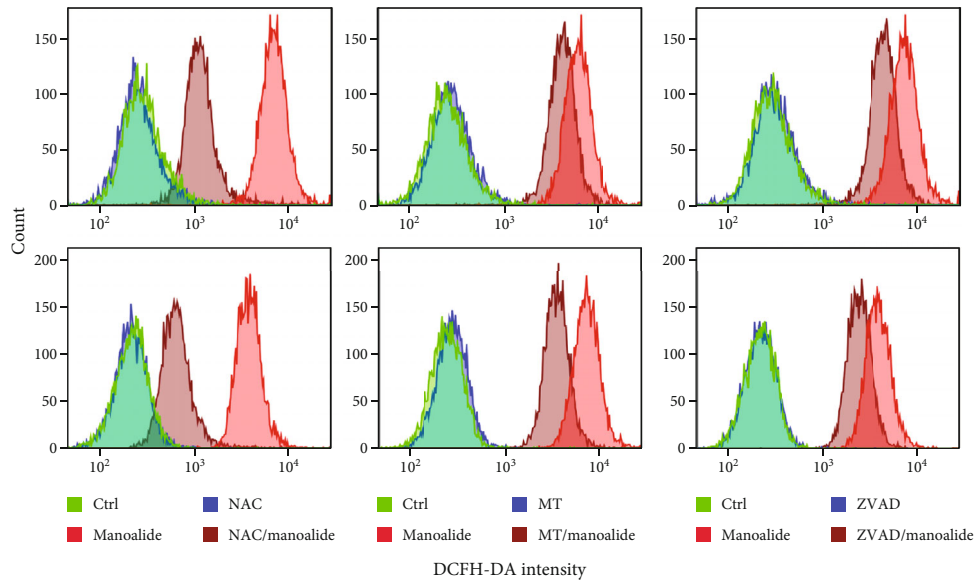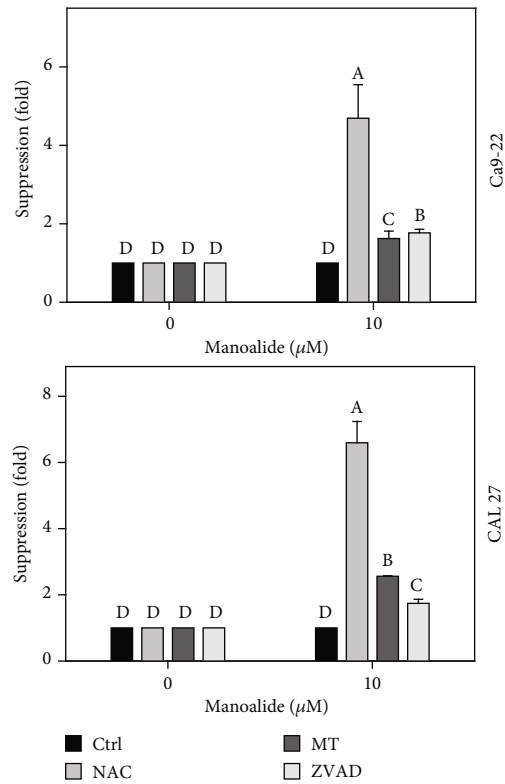
(a)

(b)

FIGURE 4: Effects of inhibitors for cellular reactive species, mitochondrial reactive species, and apoptosis (NAC, MT, and ZVAD) on flow cytometry of DCFH-DA ($NO_2^{\cdot}$, $CO_3^{\cdot-}$, and $\cdot OH$) in manoalide-treated oral cancer cells. Cells were pretreated with control (0.1% DMSO only), NAC (8 mM), MT (20 μM), and ZVAD (100 μM) for 2 h and posttreated with control and manoalide (10 μM) for 0 and 6 h. All experiments had the same concentration of DMSO. (a) Flow cytometry patterns for manoalide-treated oral cancer cells (Ca9-22 and CAL 27). (b) Statistics of suppression (fold). The suppression fold is defined in detail at Section 2.4. No suppression is defined at 1 (untreated control; 0.1% DMSO only). If the reactive species intensity determined by flow cytometry is decreased after inhibitor treatment, the suppression fold of inhibitors (NAC, MT, and ZVAD) is larger than 1. Results from different treatments are considered significantly different for multiple comparisons (indicated via different letters without overlapping) ($p < 0.0001$). In the example of Ca9-22 cells, the suppression fold for control, NAC, MT, and ZVAD show letters at top for "D," "A," "C," and "B" for Ca9-22 cells. Since they were marked with different letters without overlapping, all the treatments between each other (control, NAC, MT, or ZVAD) differ significantly. Data, means ± SDs ($n = 3$ independent experiments, each experiment collected with 10000 gated cell counts).
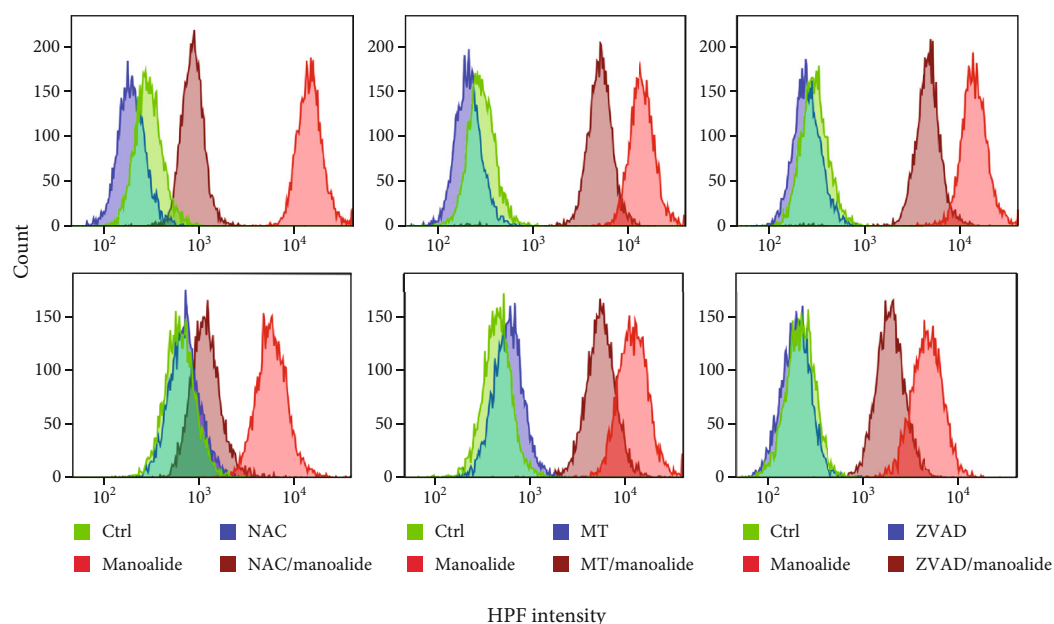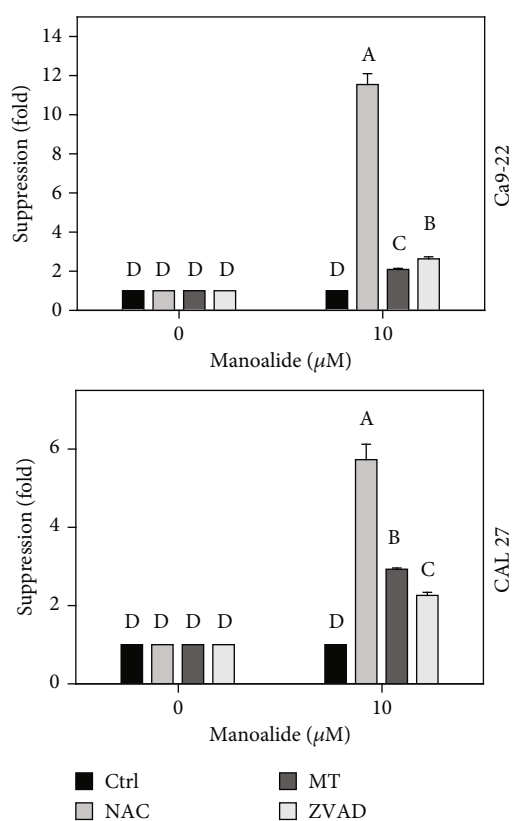
(a)

(b)

FIGURE 5: Effects of inhibitors for cellular reactive species, mitochondrial reactive species, and apoptosis (NAC, MT, and ZVAD) on flow cytometry of HPF ($\cdot$OH and ONOO-) in manoalide-treated oral cancer cells. Cells were pretreated with control (0.1% DMSO only), NAC (8 mM), MT (20 μM), and ZVAD (100 μM) for 2 h and posttreated with control and manoalide (10 μM) for 0 and 6 h. All experiments had the same concentration of DMSO. (a) Flow cytometry patterns for manoalide-treated oral cancer cells (Ca9-22 and CAL 27). (b) Statistics of suppression (fold). The suppression fold is defined in detail at Section 2.4. No suppression is defined at 1 (untreated control; 0.1% DMSO only). If the reactive species intensity determined by flow cytometry is decreased after inhibitor treatment, the suppression fold of inhibitors (NAC, MT, and ZVAD) is larger than 1. Results from different treatments are considered significantly different for multiple comparison (indicated via different letters without overlapping) ($p < 0.0001$). Data, means ± SDs ($n = 3$ independent experiments, each experiment collected with 10000 gated cell counts).

(a)

(b)

FIGURE 6: Effects of inhibitors for cellular reactive species, mitochondrial reactive species, and apoptosis (NAC, MT, and ZVAD) on flow cytometry of DAF-FM (˙NO) in manoalide-treated oral cancer cells. Cells were pretreated with control (0.1% DMSO only), NAC (8 mM), MT (20 μM), and ZVAD (100 μM) for 2 h and posttreated with control and manoalide (10 μM) for 0 and 6 h. All experiments had the same concentration of DMSO. (a) Flow cytometry patterns for manoalide-treated oral cancer cells (Ca9-22 and CAL 27). (b) Statistics of suppression (fold). The suppression fold is defined in detail at Section 2.4. No suppression is defined at 1 (untreated control; 0.1% DMSO only). If the reactive species intensity determined by flow cytometry is decreased after inhibitor treatment, the suppression fold of inhibitors (NAC, MT, and ZVAD) is larger than 1. Results from different treatments are considered significantly different for multiple comparison (indicated via different letters without overlapping) ($p < 0.01$ to 0.0001). Data, means ± SDs ($n = 3$ independent experiments, each experiment collected with 10000 gated cell counts).
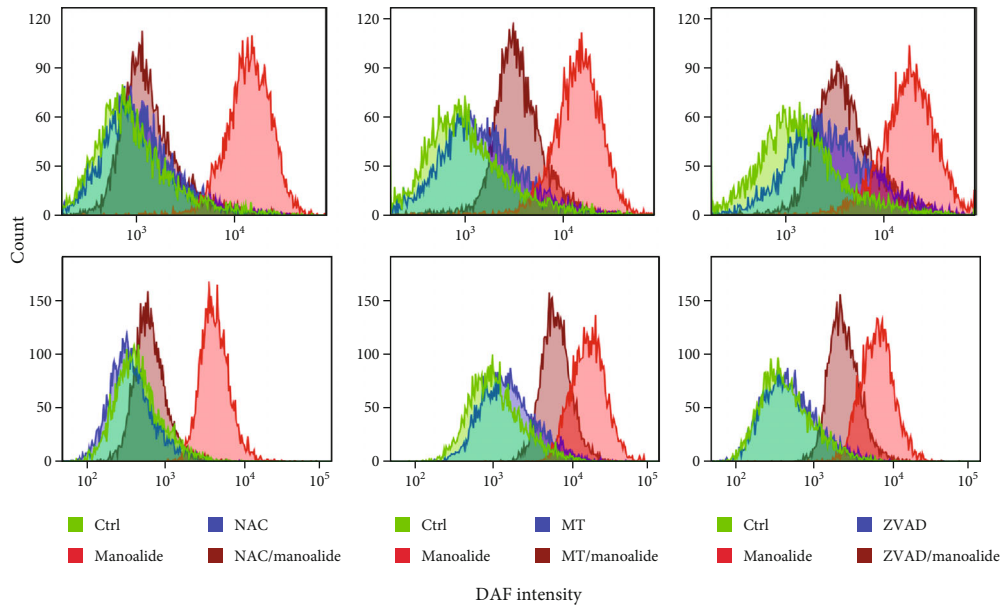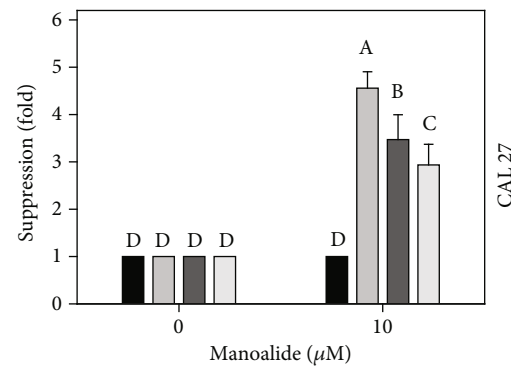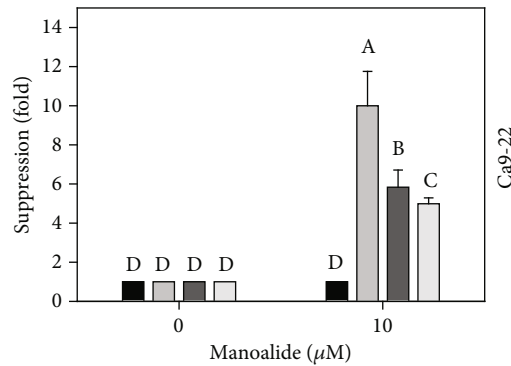
FIGURE 7: Effects of inhibitors for cellular reactive species, mitochondrial reactive species, and apoptosis (NAC, MT, and ZVAD) on flow cytometry of DHE (cellular $O_2^{\cdot-}$) in manoalide-treated oral cancer cells. Cells were pretreated with control (0.1% DMSO only), NAC (8 mM), MT (20 μM), and ZVAD (100 μM) for 2 h and posttreated with control and manoalide (10 μM) for 0 and 6 h. All experiments had the same concentration of DMSO. (a) Flow cytometry patterns for manoalide-treated oral cancer cells (Ca9-22 and CAL 27). (b) Statistics of suppression (fold). The suppression fold is defined in detail at Section 2.4. No suppression is defined at 1 (untreated control; 0.1% DMSO only). If the reactive species intensity determined by flow cytometry is decreased after inhibitor treatment, the suppression fold of inhibitors (NAC, MT, and ZVAD) is larger than 1. Results from different treatments are considered significantly different for multiple comparison (indicated via different letters without overlapping) ($p < 0.05$ to 0.0001). Data, means ± SDs ($n = 3$ independent experiments, each experiment collected with 10000 gated cell counts).
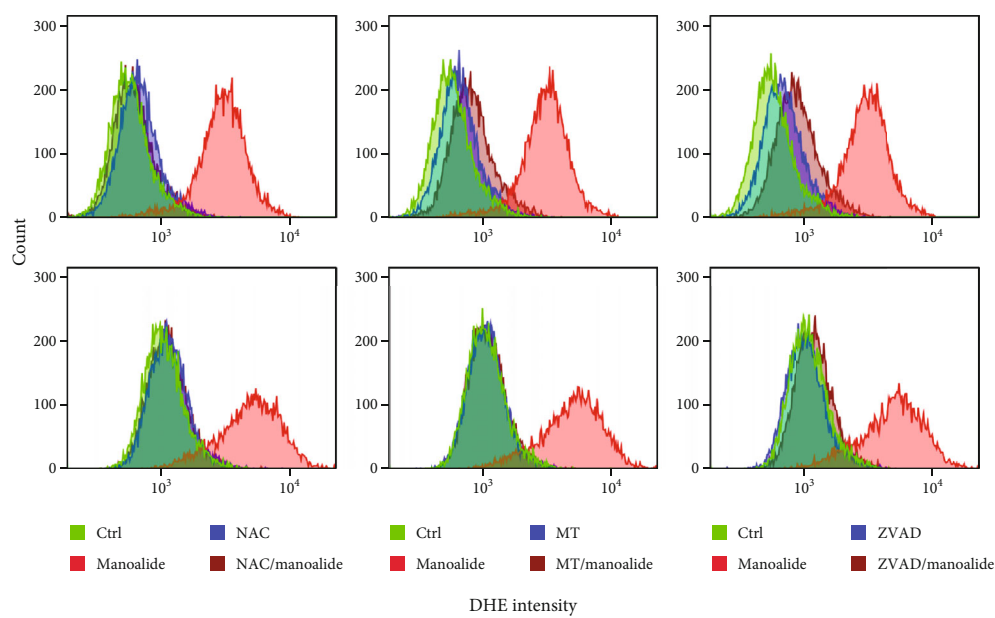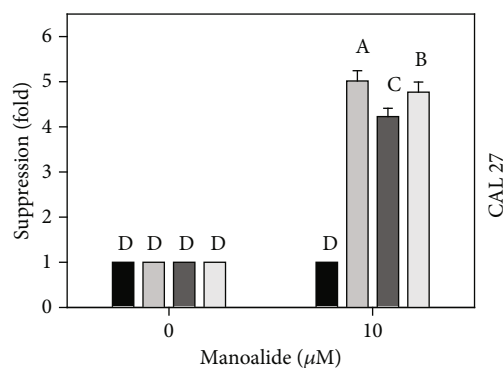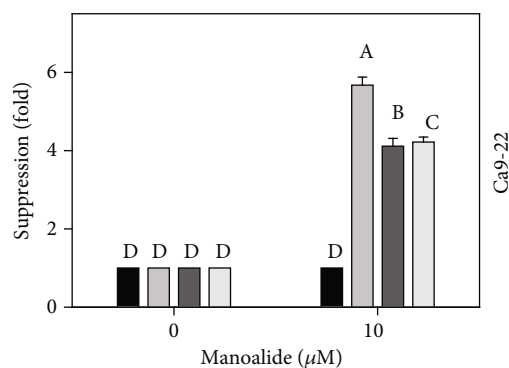
(a)

(b)

FIGURE 8: Effects of inhibitors for cellular reactive species, mitochondrial reactive species, and apoptosis (NAC, MT, and ZVAD) on flow cytometry of MitoSOX Red (mitochondrial $O_2^{\cdot-}$) in manoalide-treated oral cancer cells. Cells were pretreated with control (0.1% DMSO only), NAC (8 mM), MT (20 μM), and ZVAD (100 μM) for 2 h and posttreated with control and manoalide (10 μM) for 0 and 6 h. All experiments had the same concentration of DMSO. (a) Flow cytometry patterns for manoalide-treated oral cancer cells (Ca9-22 and CAL 27). (b) Statistics of suppression (fold). The suppression fold is defined in detail at Section 2.4. No suppression is defined at 1 (untreated control; 0.1% DMSO only). If the reactive species intensity determined by flow cytometry is decreased after inhibitor treatment, the suppression fold of inhibitors (NAC, MT, and ZVAD) is larger than 1. Results from different treatments are considered significantly different for multiple comparison (indicated via different letters without overlapping) ($p < 0.0001$). Data, means ± SDs ($n = 3$ independent experiments, each experiment collected with 10000 gated cell counts).

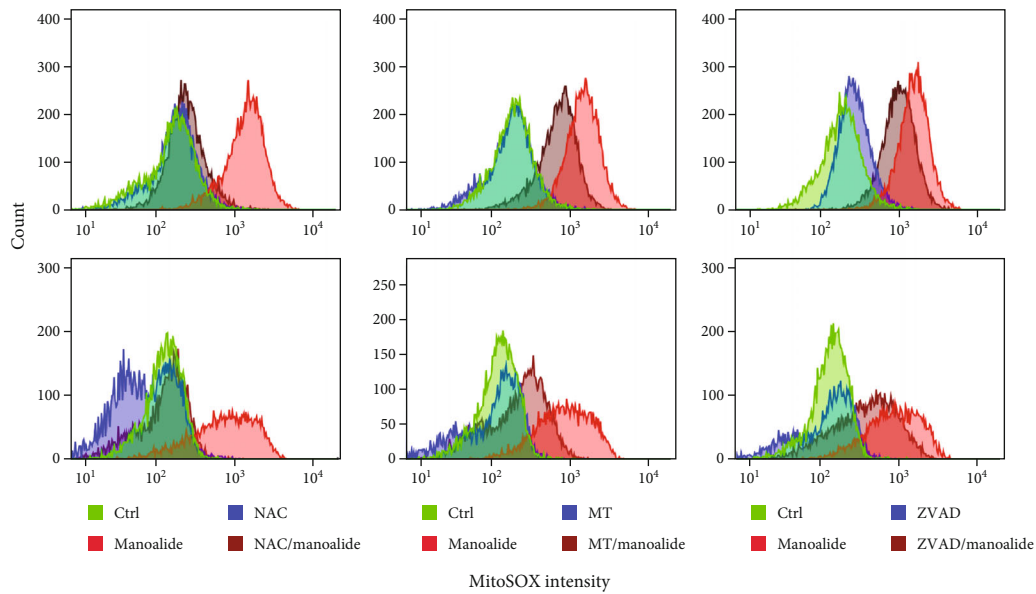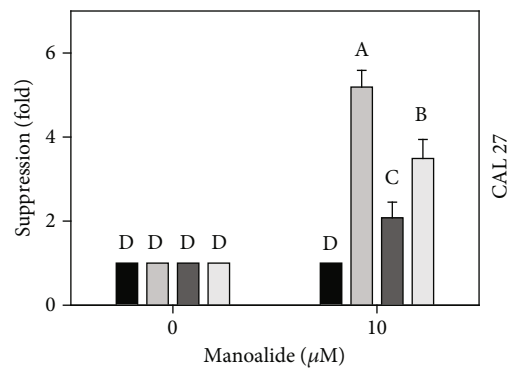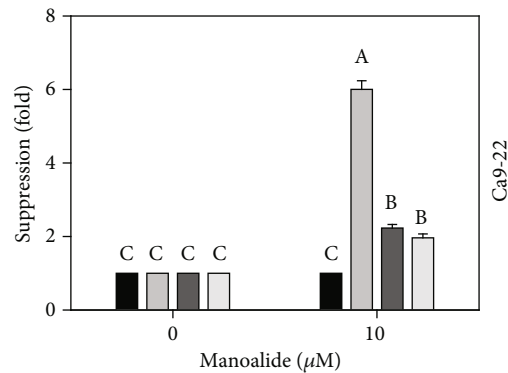reactive species (MitoSOX) (Figure 8). Similarly, antimycin A [36] and withanolide C [37] -induced MitoSOX generations were suppressed by NAC in oral and breast cancer cells, respectively. Therefore, cellular reactive species may induce mitochondrial reactive species generations in oral cancer cells.

4.2. Mitochondrial Reactive Species May Regulate Cellular Reactive Species.

Superoxide may be derived from the sources of NAPDH oxidase (NOX) [38] and mitochondria [39]. For mitochondria, complexes I and III are responsible for continuously producing reactive species during electron transfer [40]. Mitochondrial superoxide was reported to be highly membrane impermeable [41], which was supported by the finding that complex I-dependent superoxide is exclusively fluxed to matrix without escaping from mitochondria to cytoplasm [42]. However, this team also reported that that complex III can release superoxide to both the matrix and outer mitochondrial membrane [42], which may partly release to cytoplasm. Therefore, the traffic of mitochondrial reactive species to exit mitochondria is controversial.

Based on our findings using the inhibitor pretreatment (MT) of mitochondrial reactive species, the manoalide-induced mitochondrial reactive species as probed by Mito-SOX Red were suppressed (Figure 8). Moreover, MT pretreatment also suppressed cellular reactive species as probed by DCFH-DA, HPF, DAF-FM, and DHE (Figures 4–7). Therefore, manoalide-induced mitochondrial reactive species may induce cellular reactive species generations in oral cancer cells, suggesting that mitochondrial reactive species may exit from mitochondria to cytoplasm to regulate the cellular reactive species.

4.3. Both Cellular and Mitochondrial Reactive Species May Regulate Apoptosis.

At 6 h manoalide treatment, apoptosis is triggered in oral cancer Ca9-22 and CAL 27 cells. This manoalide-induced apoptosis was differentially suppressed by NAC, MT, and ZVAD in oral cancer cells (Figure 3). In addition to radical species scavenging (Figures 4–8), both NAC and MT can inhibit apoptosis after manoalide treatment in oral cancer cells. Therefore, cellular and mitochondrial reactive species can induce manoalide-induced apoptosis.

4.4. Apoptosis May Regulate Both Cellular and Mitochondrial Reactive Species.

It is well known that reactive species can induce apoptosis. However, the role of apoptosis in the induction of reactive species is rarely investigated. ZVAD, a common pancaspase inhibitor to suppress apoptosis, was used to investigate the modulating effect of apoptosis to reactive species response. For example, ZVAD inhibits etoposide-induced caspase activation and DCFH-DA-detected reactive species generation in cervical cancer HeLa cells [43]. ZVAD inhibits cytosine analogue ferropoptoside N69-induced DCFH-DA-detected reactive species generation in melanoma cells [44]. ZVAD also suppresses oxidized black carbon-induced DCFH-DA detected reactive species generation in lung cancer cells [45]. These studies suggest that sev-

Figure 9: Expected mechanism of multifaceted inductions for cellular and mitochondrial reactive species to apoptosis on manoalide-treated oral cancer cells. NAC is an inhibitor for cellular reactive species (as probed by DCFH-DA, HPF, DAF-FM, and DHE), MT is an inhibitor for mitochondrial reactive species (as probed by MitoSOX Red), and ZVAD is an inhibitor for apoptosis. We proposed a possible mechanism that manoalide ($10 \mu M$, 6 h) can induce (1) cellular and (2) mitochondrial reactive species. Moreover, (3) NAC inhibits manoalide-induced mitochondrial reactive species and (4) MT inhibits manoalide-induced cellular reactive species, suggesting that cellular and mitochondrial reactive species can reciprocally induce each other in manoalide-treated oral cancer cells. (5) Manoalide induces apoptosis, which are suppressed by (3) NAC, (4) MT, and (6) ZVAD, suggesting that (7) cellular and (8) mitochondrial radical species can trigger apoptosis. Interestingly, (6) ZVAD also inhibits both (7) cellular and (8) mitochondrial reactive species, suggesting that apoptosis may induce manoalide-induced cellular and mitochondrial reactive species in oral cancer cells. Therefore, manoalide exhibits reciprocally activation between cellular reactive species, mitochondrial reactive species, and apoptosis in oral cancer cells. Note: arrow and T symbol indicate the activating and inhibiting effects. DCFH-DA is the probe for $NO_2\cdot$, $CO_3\cdot^-$, and $\cdot OH$. HPF is the probe for $\cdot OH$ and ONOO-. DAF-FM is the probe for $\cdot NO$. DHE and MitoSOX Red are the probes for cellular and mitochondrial $O_2\cdot^-$.

eral drug-induced apoptosis can induce DCFH-DA-detected reactive species.

Similarly, we found that manoalide induced a number of cellular (Figures 4–7) and mitochondrial (Figure 8) reactive species generations, which were suppressed by ZVAD pretreatment in oral cancer cells. It shows that manoalide induces a caspase-dependent reactive species generation in oral cancer cells. These results suggest that apoptosis may trigger both manoalide-induced cellular and mitochondrial reactive species generations. Therefore, manoalide can induce apoptosis as well as cellular and mitochondrial reactive species in oral cancer cells, and they have the reciprocal activation between each other.

Moreover, many drug-induced apoptosis in cancer cell studies [46–49] also triggered oxidative stress but these studies only relied on the cellular reactive species detection by DCFH-DA. Our finding demonstrates that more cellular and mitochondrial reactive species as probed by DCFH-DA HPF, DAF-FM, DHE, and MitoSOX red also contribute to manoalide-induced redox changes to induce apoptosis. Therefore, multiple kinds of cellular and mitochondrial reactive species are suggested to be considered in drug-induced apoptosis studies.

5. Conclusions

In the present study, manoalide (10 μM, 6 h) induces DCFH-DA, HPF, DAF-FM, and DHE detected cellular reactive species and induces MitoSOX Red-detected mitochondrial reactive species, which are respectively inhibited by NAC and MT pretreatment. These cellular reactive species induce MitoSOX Red-detected mitochondrial reactive species, which are validated by the presence of NAC. These mitochondrial reactive species may induce cellular reactive species, which is validated by the presence of MT. It shows the reciprocally activation between cellular and mitochondrial reactive species after manoalide treatment in oral cancer cells. Moreover, manoalide induces apoptosis, which are suppressed by NAC, MT, and ZVAD, suggesting that cellular and mitochondrial radical species can trigger apoptosis. Apoptosis induces cellular and mitochondrial reactive species, which are validated by the presence of ZVAD. It shows the reciprocally activation between reactive species (cell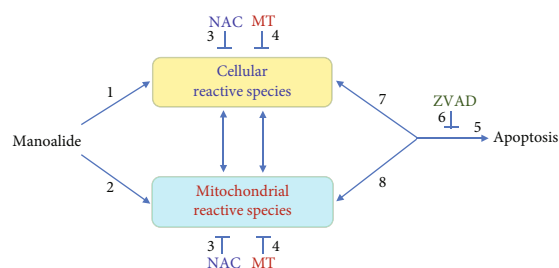ular and mitochondrial) and apoptosis. Therefore, we propose a mechanism of multifaceted inductions and interactions for cellular and mitochondrial reactive species to apoptosis on manoalide-treated oral cancer cells (Figure 9).

Data Availability

No data were used to support this study.

Conflicts of Interest

The authors declare no conflict of interest.

Authors' Contributions

Hui-Ru Wang and Ping-Ho Chen contributed equally to this work.

Acknowledgments

References

[1] K. M. Chan, N. F. Rajab, D. Siegel, L. B. Din, D. Ross, and S. H. Inayat-Hussain, "Goniothalamin induces coronary artery smooth muscle cells apoptosis: the p53-dependent caspase-2 activation pathway," *Toxicological Sciences*, vol. 116, no. 2, pp. 533–548, 2010.

[2] P. H. Chen, Q. Mahmood, G. L. Mariottini, T. A. Chiang, and K. W. Lee, "Adverse health effects of betel quid and the risk of oral and pharyngeal cancers," *BioMed Research International*, vol. 2017, Article ID 3904098, 2017.

[3] L. Dumitrescu, D. T. Mai Huong, N. Van Hung, B. Crousse, and D. Bonnet-Delpon, "Synthesis and cytotoxic activity of fluorinated analogues of Goniothalamus lactones. Impact of fluorine on oxidative processes," *European Journal of Medicinal Chemistry*, vol. 45, no. 7, pp. 3213–3218, 2010.

[4] A. K. D'Cruz, R. Vaish, and H. Dhar, "Oral cancers: current status," *Oral Oncology*, vol. 87, pp. 64–69, 2018.

[5] J. C. Lee, M. F. Hou, H. W. Huang et al., "Marine algal natural products with anti-oxidative, anti-inflammatory, and anti-cancer properties," *Cancer Cell International*, vol. 13, no. 1, p. 55, 2013.

[6] A. A. Farooqi, S. Fayyaz, M. F. Hou, K. T. Li, J. Y. Tang, and H. W. Chang, "Reactive oxygen species and autophagy modulation in non-marine drugs and marine drugs," *Marine Drugs*, vol. 12, no. 11, pp. 5408–5424, 2014.

[7] D. Matulja, K. Wittine, N. Malatesti et al., "Marine natural products with high anticancer activities," *Current Medicinal Chemistry*, vol. 27, no. 8, pp. 1243–1307, 2020.

[8] S. A. M. Khalifa, N. Elias, M. A. Farag et al., "Marine natural products: a source of novel anticancer drugs," *Marine Drugs*, vol. 17, no. 9, p. 491, 2019.

[9] E. D. de Silva and P. J. Scheuer, "Manoalide, an antibiotic sesterterpenoid from the marine sponge (polejaeff)," *Tetrahedron Letters*, vol. 21, no. 17, pp. 1611–1614, 1980.

[10] A. Soriente, M. M. De Rosa, A. Scettri et al., "Manoalide," *Current Medicinal Chemistry*, vol. 6, no. 5, pp. 415–431, 1999.

[11] J. Kobayashi, C. M. Zeng, M. Ishibashi, and T. Sasaki, "Luffariolides F and G, new manoalide derivatives from the Okinawan marine sponge Luffariella sp," *Journal of Natural Products*, vol. 56, no. 3, pp. 436–439, 1993.

[12] H. R. Wang, J. Y. Tang, Y. Y. Wang et al., "Manoalide preferentially provides antiproliferation of oral cancer cells by oxidative stress-mediated apoptosis and DNA damage," *Cancers*, vol. 11, no. 9, p. 1303, 2019.

[13] L. Vaughan, W. Glanzel, C. Korch, and A. Capes-Davis, "Widespread use of misidentified cell line KB (HeLa): incorrect attribution and its impact revealed through mining the scientific literature," *Cancer Research*, vol. 77, no. 11, pp. 2784–2788, 2017.

[14] A. Kijjoa and P. Sawangwong, "Drugs and cosmetics from the sea," *Marine Drugs*, vol. 2, no. 2, pp. 73–82, 2004.

[15] B. Kalyanaraman, V. Darley-Usmar, K. J. A. Davies et al., "Measuring reactive oxygen and nitrogen species with fluorescent probes: challenges and limitations," *Free Radical Biology and Medicine*, vol. 52, no. 1, pp. 1–6, 2012.

[16] S. I. Dikalov and D. G. Harrison, "Methods for detection of mitochondrial and cellular reactive oxygen species," *Antioxidants & Redox Signaling*, vol. 20, no. 2, pp. 372–382, 2014.

[17] M. Inoue, E. F. Sato, M. Nishikawa et al., "Mitochondrial generation of reactive oxygen species and its role in aerobic life," *Current Medicinal Chemistry*, vol. 10, no. 23, pp. 2495–2505, 2003.

[18] T. S. Wang, C. P. Lin, Y. P. Chen, M. R. Chao, C. C. Li, and K. L. Liu, "CYP450-mediated mitochondrial ROS production involved in arecoline N-oxide-induced oxidative damage in

liver cell lines," *Environmental Toxicology*, vol. 33, no. 10, pp. 1029–1038, 2018.

[19] C. Zhu, W. Hu, H. Wu, and X. Hu, "No evident dose-response relationship between cellular ROS level and its cytotoxicity – a paradoxical issue in ROS-based cancer therapy," *Scientific Reports*, vol. 4, 2015.

[20] Y. T. Chang, C. Y. Huang, K. T. Li et al., "Sinuleptolide inhibits proliferation of oral cancer Ca9-22 cells involving apoptosis, oxidative stress, and DNA damage," *Archives of Oral Biology*, vol. 66, pp. 147–154, 2016.

[21] S.-Y. Peng, Y.-Y. Wang, T.-H. Lan et al., "Low Dose Combined Treatment with Ultraviolet-C and Withaferin a Enhances Selective Killing of Oral Cancer Cells," *Antioxidants*, vol. 9, no. 11, p. 1120, 2020.

[22] C. Y. Chen, C. Y. Yen, H. R. Wang et al., "Tenuifolide B from Cinnamomum tenuifolium stem selectively inhibits proliferation of oral cancer cells via apoptosis, ROS generation, mitochondrial depolarization, and DNA damage," *Toxins*, vol. 8, no. 11, p. 319, 2016.

[23] C. H. Huang, J. M. Yeh, and W. H. Chan, "Hazardous impacts of silver nanoparticles on mouse oocyte maturation and fertilization and fetal development through induction of apoptotic processes," *Environmental Toxicology*, vol. 33, no. 10, pp. 1039–1049, 2018.

[24] C. F. Wu, M. G. Lee, M. El-Shazly et al., "Isoaaptamine induces T-47D cells apoptosis and autophagy via oxidative stress," *Marine Drugs*, vol. 16, no. 1, p. 18, 2018.

[25] T. Pearson, T. Kabayo, R. Ng, J. Chamberlain, A. McArdle, and M. J. Jackson, "Skeletal muscle contractions induce acute changes in cytosolic superoxide, but slower responses in mitochondrial superoxide and cellular hydrogen peroxide," *PLoS One*, vol. 9, no. 5, 2014.

[26] C. Y. Yen, C. C. Chiu, R. W. Haung et al., "Antiproliferative effects of goniothalamin on Ca9-22 oral cancer cells through apoptosis, DNA damage and ROS induction," *Mutation Research*, vol. 747, no. 2, pp. 253–258, 2012.

[27] A. A. Abubaker, D. Vara, I. Eggleston, I. Canobbio, and G. Pula, "A novel flow cytometry assay using dihydroethidium as redox-sensitive probe reveals NADPH oxidase-dependent generation of superoxide anion in human platelets exposed to amyloid peptide β," *Platelets*, vol. 30, no. 2, pp. 181–189, 2019.

[28] H. W. Huang, J. Y. Tang, F. Ou-Yang et al., "Sinularin selectively kills breast cancer cells showing G2/M arrest, apoptosis, and oxidative DNA damage," *Molecules*, vol. 23, no. 4, p. 849, 2018.

[29] J. Kepczynski and D. Cembrowska-Lech, "Application of flow cytometry with a fluorescent dye to measurement of intracellular nitric oxide in plant cells," *Planta*, vol. 248, no. 2, pp. 279–291, 2018.

[30] W. Paulander, Y. Wang, A. Folkesson, G. Charbon, A. Lobner-Olesen, and H. Ingmer, "Bactericidal antibiotics increase hydroxyphenyl fluorescein signal by altering cell morphology," *PLoS One*, vol. 9, no. 3, 2014.

[31] R. Radi, "Oxygen radicals, nitric oxide, and peroxynitrite: redox pathways in molecular medicine," *Proceedings of the National Academy of Sciences of the United States of America*, vol. 115, no. 23, pp. 5839–5848, 2018.

[32] J. Y. Tang, F. Ou-Yang, M. F. Hou et al., "Oxidative stress-modulating drugs have preferential anticancer effects - involving the regulation of apoptosis, DNA damage, endoplasmic reticulum stress, autophagy, metabolism, and migration," *Seminars in Cancer Biology*, vol. 58, pp. 109–117, 2019.

[33] X.-j. Wu and X. Hua, "Targeting ROS: Selective killing of cancer cells by a cruciferous vegetable derived pro-oxidant compound," *Cancer Biology & Therapy*, vol. 6, no. 5, pp. 646-647, 2014.

[34] S. J. Kim, H. S. Kim, and Y. R. Seo, "Understanding of ROS-Inducing Strategy in Anticancer Therapy," *Oxidative Medicine and Cellular Longevity*, vol. 2019, Article ID 5381692, 12 pages, 2019.

[35] R. Franco, M. I. Panayiotidis, and J. A. Cidlowski, "Glutathione depletion is necessary for apoptosis in lymphoid cells independent of reactive oxygen species formation," *The Journal of Biological Chemistry*, vol. 282, no. 42, pp. 30452–30465, 2007.

[36] T. J. Yu, C. Y. Hsieh, J. Y. Tang et al., "Antimycin a shows selective antiproliferation to oral cancer cells by oxidative stress-mediated apoptosis and DNA damage," *Environmental Toxicology*, vol. 35, no. 11, pp. 1212–1224, 2020.

[37] T.-J. Yu, J.-Y. Tang, L.-C. Lin et al., "Withanolide C Inhibits Proliferation of Breast Cancer Cells via Oxidative Stress-Mediated Apoptosis and DNA Damage," *Antioxidants*, vol. 9, no. 9, p. 873, 2020.

[38] M. E. Armitage, K. Wingler, H. H. H. W. Schmidt, and M. La, "Translating the oxidative stress hypothesis into the clinic: NOX versus NOS," *Journal of Molecular Medicine*, vol. 87, no. 11, pp. 1071–1076, 2009.

[39] A. V. Snezhkina, A. V. Kudryavtseva, O. L. Kardymon et al., "ROS Generation and Antioxidant Defense Systems in Normal and Malignant Cells," *Oxidative Medicine and Cellular Longevity*, vol. 2019, Article ID 6175804, 17 pages, 2019.

[40] R. Z. Zhao, S. Jiang, L. Zhang, and Z. B. Yu, "Mitochondrial electron transport chain, ROS generation and uncoupling (review)," *International Journal of Molecular Medicine*, vol. 44, no. 1, pp. 3–15, 2019.

[41] R. A. Gus'kova, I. I. Ivanov, V. K. Kol'tover, V. V. Akhobadze, and A. B. Rubin, "Permeability of bilayer lipid membranes for superoxide (O_2^-) radicals," *Biochimica et Biophysica Acta (BBA)-Biomembranes*, vol. 778, no. 3, pp. 579–585, 1984.

[42] F. L. Muller, Y. Liu, and H. Van Remmen, "Complex III releases superoxide to both sides of the inner mitochondrial membrane," *The Journal of Biological Chemistry*, vol. 279, no. 47, pp. 49064–49073, 2004.

[43] A. Dumay, V. Rincheval, P. Trotot, B. Mignotte, and J. L. Vayssiere, "The superoxide dismutase inhibitor diethyldithiocarbamate has antagonistic effects on apoptosis by triggering both cytochrome c release and caspase inhibition," *Free Radical Biology & Medicine*, vol. 40, no. 8, pp. 1377–1390, 2006.

[44] J. C. Franke, M. Plotz, A. Prokop, C. C. Geilen, H. G. Schmalz, and J. Eberle, "New caspase-independent but ROS-dependent apoptosis pathways are targeted in melanoma cells by an iron-containing cytosine analogue," *Biochemical Pharmacology*, vol. 79, no. 4, pp. 575–586, 2010.

[45] J. An, Q. Zhou, M. Wu et al., "Interactions between oxidative stress, autophagy and apoptosis in A549 cells treated with aged black carbon," *Toxicology In Vitro*, vol. 54, pp. 67–74, 2019.

[46] S. Jiménez, S. Gascón, A. Luquin, M. Laguna, C. Ancin-Azpilicueta, and M. J. Rodríguez-Yoldi, "Rosa canina extracts have antiproliferative and antioxidant effects on Caco-2 human colon cancer," *PLoS One*, vol. 11, no. 7, 2016.

[47] V. Ruiz-Torres, C. Rodriguez-Perez, M. Herranz-Lopez et al., "Marine invertebrate extracts induce colon cancer cell death

via ROS-mediated DNA oxidative damage and mitochondrial impairment," *Biomolecules*, vol. 9, no. 12, p. 771, 2019.

[48] V. Nanni, L. Canuti, A. Gismondi, and A. Canini, "Hydroalcoholic extract of Spartium junceum L. flowers inhibits growth and melanogenesis in B16-F10 cells by inducing senescence," *Phytomedicine*, vol. 46, pp. 1–10, 2018.

[49] R. Vaikundamoorthy, R. Sundaramoorthy, V. Krishnamoorthy, R. Vilwanathan, and R. Rajendran, "Marine steroid derived from Acropora formosa enhances mitochondrial-mediated apoptosis in non-small cell lung cancer cells," *Tumour Biology*, vol. 37, no. 8, pp. 10517–10531, 2016.

Review Article

Superoxide Dismutase 2 (SOD2) in Vascular Calcification: A Focus on Vascular Smooth Muscle Cells, Calcification Pathogenesis, and Therapeutic Strategies

You-Tien Tsai,[1] Hsiang-Yuan Yeh [ID],[2] Chia-Ter Chao [ID],[1,3,4] and Chih-Kang Chiang[4]

[1]*Nephrology Division, Department of Internal Medicine, National Taiwan University Hospital BeiHu Branch, Taipei, Taiwan*
[2]*School of Big Data Management, Soochow University, Taipei, Taiwan*
[3]*Nephrology Division, Department of Internal Medicine, National Taiwan University School of Medicine, Taipei, Taiwan*
[4]*Graduate Institute of Toxicology, National Taiwan University School of Medicine, Taipei, Taiwan*

Correspondence should be addressed to Chia-Ter Chao; b88401084@gmail.com

Vascular calcification (VC) describes the pathophysiological phenotype of calcium apatite deposition within the vascular wall, leading to vascular stiffening and the loss of compliance. VC is never benign; the presence and severity of VC correlate closely with the risk of myocardial events and cardiovascular mortality in multiple at-risk populations such as patients with diabetes and chronic kidney disease. Mitochondrial dysfunction involving each of vascular wall constituents (endothelia and vascular smooth muscle cells (VSMCs)) aggravates various vascular pathologies, including atherosclerosis and VC. However, few studies address the pathogenic role of mitochondrial dysfunction during the course of VC, and mitochondrial reactive oxygen species (ROS) seem to lie in the pathophysiologic epicenter. Superoxide dismutase 2 (SOD2), through its preferential localization to the mitochondria, stands at the forefront against mitochondrial ROS in VSMCs and thus potentially modifies the probability of VC initiation or progression. In this review, we will provide a literature-based summary regarding the relationship between SOD2 and VC in the context of VSMCs. Apart from the conventional wisdom of attenuating mitochondrial ROS, SOD2 has been found to affect mitophagy and the formation of the autophagosome, suppress JAK/STAT as well as PI_3K/Akt signaling, and retard vascular senescence, all of which underlie the beneficial influences on VC exerted by SOD2. More importantly, we outline the therapeutic potential of a novel SOD2-targeted strategy for the treatment of VC, including an ever-expanding list of pharmaceuticals and natural compounds. It is expected that VSMC SOD2 will become an important druggable target for treating VC in the future.

1. Introduction

Vascular calcification, the ectopic deposition of calcium apatite within the vascular wall, was previously thought to be a degenerative process predominantly involving individuals of advanced age. It is now well established that vascular calcification also affects those with diabetes mellitus (DM) and chronic kidney disease (CKD)/end-stage renal disease (ESRD) at an accelerated speed. The presence of vascular calcification confers detrimental cardiovascular influences through impairing vascular compliance and increasing stiffness, elevating systemic resistance and afterload, leading to

cardiac hypertrophy, myocardial remodeling, and a greater risk of heart failure-related hospitalization [1]. Mechanically, the stiffened vessels beget a greater cardiac pulsatile force and rising luminal shear stress, which correlates with endothelial dysfunction and atherogenesis involving coronary and peripheral arteries [2]. In addition, the transmission of the exaggerated pulsatile energy to susceptible end organs potentially contributes to dysregulated perfusion and functional disturbances [3]. Several meta-analyses have shown that aortic and coronary artery calcification is predictive of 2- to 3-fold increase in overall and cardiovascular mortality among at-risk populations [4, 5]. Moreover, patients having

vascular calcification are revealed to exhibit a significantly higher risk of developing frailty [6], osteoporosis with fragility fractures [7], and sarcopenia [8] compared to those without. Vascular calcification involving lower limbs is also conducive to peripheral artery occlusion, causing intermittent claudication and compromised wound healing [1]. These findings lend support to the notion that vascular calcification is pathologically important and warrants a greater understanding of its pathophysiology.

2. Vital Pathophysiological Pieces of Vascular Calcification: Mitochondrial Dysfunction

The recognition of vascular calcification pathogenesis has evolved rapidly over the past decades, expanding from the passive phenomenon of divalent ion imbalances with medial calcium deposition to the active process of well-orchestrated osteoid-like substance secretion by transdifferentiated vascular medial cells, especially vascular smooth muscle cells (VSMCs) [9]. Drivers of this VSMC phenotypic changes are complex; apart from precipitating factors such as advanced glycation end products (AGEs), protein-bound uremic toxins (indoxyl sulfate and p-cresyl sulfate), epigenetic effectors (e.g., microRNAs) [10, 11], and a high-phosphate environment, dysfunctional cellular organelles are also pinpointed as a critical contributor [12]. Lysosomal degradation abnormality can be accompanied by the accumulation of β-galactosidase and cellular senescence, while dysregulated endoplasmic reticulum (ER) function and nuclear processing will lead to unfolded protein response and DNA damages, respectively [13]. Most importantly, the perturbation of mitochondrial functioning frequently occurs during the course of vascular diseases including atherosclerosis and vascular calcification and is recognized as a cardinal feature in these disorders.

2.1. Mitochondrial Dysfunction: An Overview regarding Vascular Diseases. Mitochondria are widely known as the energy factory of a given cell based on its oxidative phosphorylation capacity. Mitochondrial dysfunction leads to the failure of this organelle to generate adequate ATP to meet cellular demand, culminating in energy failure, compromised cellular viability, and tissue remodeling. The spectrum of mitochondrial dysfunction includes but is not limited to mitochondrial dynamic perturbation, mitochondrial protein synthesis impairment, reduced mitophagy, uprising mitochondrial reactive oxygen species (mtROS), and mitochondrial DNA damages [14]. This phenomenon has been described in multiple degenerative disorders, ranging from malignancy, neurodegenerative disorders, DM, and cardiovascular diseases. Among vascular pathologies, prior studies mostly addressed the role of mitochondrial dysfunction in atherogenesis [15]. Mitochondrial dysfunction in endothelial cells (ECs) and VSMCs aggravates atherosclerosis in multiple ways. Anatomically, ECs in atherosclerotic plaques are shown to contain swollen mitochondria with a circular shape and architectural remodeling with loss of the internal structures [16]. Specifically, there is an ultrastructural reduction of cristae number and a detachment of cristae from the inner membrane, accompanied by membrane breakdown at the

cellular periphery [16]. In VSMCs residing in atherosclerotic plaques, their mitochondria are similarly enlarged and vacuolated, exhibiting a degenerative tendency [17].

Mitochondrial dysfunction lies at the core of vascular diseases, especially atherosclerosis. Disrupted mitochondria predispose affected ECs and VSMCs to developing oxidative damages following impaired defensive mechanisms (e.g., turnover through mitophagy), enhancing vascular inflammation and senescence [18]. For example, oxidized low-density lipoprotein (ox-LDL) is found to upregulate caspase-3/9 and trigger EC apoptosis through decreasing mitochondrial membrane potential and enhancing mitochondrial permeability [19]. Mitochondrial fusion and mitophagy are also impaired by ox-LDL by means of Opa-1 downregulation [19]. Plaque stabilization is also adversely influenced by the presence of an impaired autophagy efficiency involving culprit cells [20]. In light of these findings, defective mitochondria should be deemed an integral pathologic player in atherosclerosis.

2.2. Mitochondrial Dysfunction in Vascular Calcification: A Less Charted Field. Relatively few studies address the association between mitochondrial dysfunction and vascular calcification. Kim et al. first showed that a natural antioxidant termed α-lipoic acid capable of restoring mitochondrial health could effectively ameliorate phosphate-induced VSMC apoptosis through regulating the Gas6-Axl-Akt pathway [21]. Mitochondrial dynamics are also impaired during calcification progression; specimens from calcified human arteries showed an increased expression of dynamin-related protein 1 (Drp1), an integral mediator of mitochondrial fission, while Drp1 downregulation in valvular cells could attenuate their tendency of calcification [22]. Polyphenols such as quercetin are also effective against vascular calcification, potentially through inhibiting Drp1 and subsequent mitochondrial fission [23]. Metformin, a biguanide-type antidiabetic agent, is also shown to retard VSMC calcification through improving mitochondrial DNA damages, restoring mitochondrial membrane potential and energy production, presumably by upregulating AMPK signaling pathways [24]. Mitochondrial biogenesis-related proteins, such as nuclear factor erythroid 2-related factor-1 (Nrf-1) and peroxisome proliferator-activated receptor-γ coactivator-1α (PGC-1α), can also be upregulated by metformin treatment [24]. Although it is still inconclusive whether mitochondrial dysfunction directly participates in the pathogenesis of vascular calcification, the above results indirectly support that mitochondrial dysfunction is closely associated with the process of vascular calcification. Presumably targeting mitochondrial dysfunction may aid in the management of vascular calcification.

2.3. Superoxide Dismutase 2 (SOD2) and Mitochondrial ROS. mtROS is an important yet underrecognized pathogenic factor in vascular calcification pathogenesis, and not until a decade ago, mtROS was identified as a vital contributor to uremic vascular calcification [25]. High phosphate-induced VSMC calcification was shown to be accompanied by an increased production of mtROS following mitochondrial membrane potential elevation [25]. The rising mtROS is

related to the upregulation of Ca^{2+}-sensitive intracellular cysteine protease calpain-1, which leads to higher expressions of alkaline phosphatase and attenuates the expressions of ATP synthases and calcification inhibitors [26]. Higher levels of mtROS frequently ensue mitochondrial dysfunction, lower mitochondrial ATP generation, and aggravate the tendency of VSMC apoptosis as well as calcification in aging mice [27].

SOD2, or manganese SOD, is an important defensive mechanism wielded by cells to eliminate free radicals, especially superoxide [28]. Transcribed from *sod2* and synthesized in cytoplasm, SOD2 is subsequently relocated to the mitochondrial matrix, endowed with the responsibility to scavenge superoxide produced by respiratory chain enzymes and to contain mtROS [29]. This subcellular distribution of antioxidative enzymes is important particularly in vascular cells, since molecules activating ROS-defensive machineries may have differential influences on SOD subtypes. A prior study revealed that curcumin, a strong antioxidant, significantly reduced intracellular ROS levels but did not alter the expressions of SOD2 in VSMCs [30]. Judging from the pathologic importance of mtROS during the course of vascular calcification and the primary action of SOD2 in quenching mtROS, we surmise that SOD2 may potentially play a role in the pathophysiology of vascular calcification of different origins, besides that of SOD1.

In the following sections, we will provide a literature-based summary of the relationship between SOD2 and vascular calcification and the potential implications of a SOD2-targeted strategy for treating vascular calcification. We will put emphasis specifically on VSMCs, a *de facto* cellular component which is heavily involved in medial calcification but garners less research attention.

3. SOD2 and Vascular Calcification Involving VSMCs: Old Players with New Actions

3.1. Sod2-Knockout (KO) Mice and Vascular Diseases. Much insight has been gleaned from the vascular manifestations in Sod2-KO mice. Homozygous deletion of Sod2 leads to early lethality in rodents [31], and only mice with heterozygous Sod2 deletion can be harnessed for vascular phenotype observation. Heterozygous Sod2 deletion mice exhibited an exquisite susceptibility to oxidative stress and tended to have accelerated atherosclerosis due to prominent endothelial dysfunction [32, 33]. However, the influence of Sod2 deletion on the VSMC phenotype was previously unclear. Zhou et al. found that heterozygous Sod2 deletion mice had VSMCs with increased expressions of collagen and matrix metalloproteinase-2 (MMP-2) and decreased elastin levels, followed pathologically by increasing aortic oxidative stress, vascular remodeling, and rising aortic stiffness [34]. Importantly, deficient SOD2 levels in VSMCs contributed to lower expressions of cell survival-responsive genes including Akt and forkhead box O3a (FoxO3a), especially during chronological aging. These mice were inclined to developing extensive atherosclerosis when exposed to hyperlipidemic stimuli, with prominent plaque instability, necrosis, and hemorrhage [35]. Such phenotype was largely attributable to VSMC apoptosis and the upregulation of calpain and matrix degrada-

tion related to higher mtROS levels as compared to their wild-type littermates. Several of these upregulated molecules are also involved in the acceleration of vascular calcification, but none of the above knockout mouse studies addressed the extent of aortic calcification in these animals. It would be tempting to speculate whether germline Sod2 deletion predisposes animals to developing vascular calcification in addition to atherosclerosis, especially when they reach an advanced age.

3.2. SOD2 in Vascular Calcification: Effect Duality. The potential role of SOD2 in the pathogenesis of vascular calcification is not recognized until roughly a decade ago. Zhao et al. revealed that mtROS served as a trigger for phosphate-induced VSMC calcification and could be effectively counteracted by SOD mimics or SOD2 upregulation [25]. Although Sod2 expressions were not measured in their experiments, indirect evidence suggested that the substantial mtROS elevation at baseline could result from Sod2 downregulation. The suppression of SOD2 in valvular cells and possibly VSMCs nullifies cellular protection against mtROS-induced DNA damage, leading to significantly higher calcification severities [36]. Apart from this action, SOD2 seems to exhibit other influences on VSMC calcification propensity. Dai and colleagues showed that in cultured VSMCs, the activation of high phosphate-induced autophagy in the forms of autophagosome formation and LC3II upregulation was significantly attenuated by the overexpression of Sod2; the retardation of autophagy in VSMCs paradoxically predisposed these cells to developing calcification [37]. Similar findings were affirmed in CKD mice with aortic calcifications. The observed effect on calcification severity might be modified by the intensity of phosphate-induced apoptosis and the degree to which other autophagy-related genes (e.g., autophagy-related 5 (Atg5)) were altered within the affected VSMCs. Results from the above experiments thus support the duality of influences posed by SOD2 during the process of vascular calcification and the presence of a ROS-independent influence exerted by SOD2 in VSMCs.

Given the perceived importance of SOD2 in vascular calcification and its potential Janus-faced effect on calcification tendency, it would be interesting to examine the expressions of Sod2 in calcified vascular tissues *in vivo*. A prior study disclosed that in a CKD rat model with calcium/phosphate/-vitamin D-supplemented diet, calcified aortas harbored increased expressions of inflammatory cytokines (interleukins/tumor necrosis factor (TNF)) and NADPH oxidase and ROS levels but halved expressions of antioxidant enzymes including SOD2 [38]. SOD2 thus more likely assumes an anticalcific role in the vascular calcification pathogenesis. Apart from exerting a host effect, SOD2 also acts against a paracrine-related calcification effect from matrix vesicle (MV) release. Chen et al. in *in vitro* experiments showed that calcified primary VSMCs were able to release MVs capable of influencing their noncalcified neighbors, and recipient cells could respond to this tide of spreading calcification through upregulating Sod2 [39]. In their study, mitochondrial dysfunction or ROS levels were similarly unaltered in recipient cells despite an increase in

calcium deposition, echoing the potential existence of a ROS-unrelated influence introduced by SOD2.

During the quenching of mtROS, SOD2 activities generate the byproduct, hydroperoxide (H_2O_2), which diffuses out of mitochondria and potentially affects a diverse range of physiological and pathological processes [40]. Cytosolic hydrogen peroxide has been shown to modulate protein thiol, alter their activities, and thereby activate multiple signaling pathways including mitogen-activated protein (MAP) kinases, hypoxia-inducible factor (HIF)-1, and its downstream effectors, p53, Nrf2, nuclear factor-κB (NF-κB), etc. [41], all of which have been implicated in the initiation and progression of vascular calcification.

3.3. Effects of SOD2 Other Than ROS in Vascular Calcification: Plausible Candidates. Apart from the traditional belief that SOD2 is mainly responsible for lowering mtROS, SOD2 may have plausible influences on other signaling pathways irrespective of the extent of ROS elevation. VSMCs with Sod2 heterozygous deletion exhibit a constitutive activation of Janus kinase 2 (JAK2)/signal transducer and activator of transcription 3 (STAT3), leading to a greater propensity for continuous proliferation [42]. Sod2 overexpression in a carotid artery balloon injury model attenuated the phenomenon of neointima formation and reduced VSMC migration as well as proliferation through suppressing Akt phosphorylation [43]. SOD2 may also counteract VSMC senescence through its action against ROS and subsequent senescence-associated secretory phenotype emergence [44].

SOD2 may also be a surrogate of ambient oxygen concentration within tissues, and oxygen levels are potential modulators of mineralization tendency [45]. Prior studies suggested that the severity of body-wide hypoxia, in the form of serum HIF-1 levels, was independently associated with the presence and the degree of vascular calcification in diabetic patients [46]. It is proposed that a low oxygen level contributes directly to osteogenic differentiation of osteoblasts and VSMCs, presumably though the induction and perpetuation of proinflammatory stimuli and indirectly through its association with other comorbidities that set the groundwork of vascular calcification [47]. Along the same line, Sod2 expressions may additionally be reflective of the activation of several inflammation-related genes, including nicotinamide phosphoribosyltransferase (NAMPT) and cytokines such as interleukins and TNF-α [48], while vascular inflammation serves as a predecessor of subsequent vascular calcification. Downregulation of Sod2 can also be an indicator of the defective mitochondrial respiratory chain complex, indirectly contributing to mitochondrial dysfunction and impaired cell viability [49].

A brief summary of the above findings regarding the role of VSMC SOD2 in vascular calcification pathogenesis is provided in Figure 1.

4. Regulatory Mechanisms for SOD2 Expressions in VSMCs

SOD2 can be transcriptionally regulated in multiple ways. There are several transcriptional activator binding sites located upstream of the promoter of *sod2*, including those of FoxO3a, NF-κB, specific protein 1 (SP1), and activator protein 2 (AP2) [50]. Among these SOD2-regulating molecules, proinflammatory cytokines are the most renowned ones, including interleukin-1, interleukin-6, TNF-α, and interferon-γ [51]; the activation of SOD2 by cytokines serves as a reflex defensive mechanism during inflammation, ameliorating the damages introduced. ROS is another default modifier of Sod2 expressions. Superoxide radicals have been found to upregulate NF-κB and also Nrf2 levels, thereby inducing Sod2 expressions and enzymatic activities [52]. SIRT3, on the other hand, exerts posttranslational influences on SOD2 enzyme activity and attenuates mtROS [53]. Finally, Sod2 can be epigenetically targeted through CpG island hypermethylation conferred by DNA methyltransferase (DNMT); this methylation-related downregulation of Sod2 also promotes VSMC proliferation involving pulmonary circulation [54].

However, not all regulators of SOD2 found in other cell types have been demonstrated to be in action within VSMCs, and very few studies affirm the relevance of such event to the pathogenesis of vascular calcification. This represents an important research gap waiting to be filled. Contrary to our belief, high glucose exposure is found by some to have minimal influences on Sod2 expressions in VSMCs [55]. We summarized available reports focusing on the upstream regulatory molecules of SOD2 in VSMCs in (Figure 1). Using cultured VSMCs and calcified aortas from CKD rats, Feng et al. disclosed that SIRT3 upregulated Sod2 expressions, attenuated mtROS, and retarded VSMC calcification, while SIRT3 inhibition exhibited the reverse phenotypes [56]. They further discovered that PGC-1α was an important endogenous activator of SIRT3 and could effectively defend against vascular calcification through increasing SOD2 levels [56]. Similarly, PGC-1α overexpression has been shown to upregulate Sod2 and reduce mtROS production, suppressing VSMC migratory ability both *in vitro* and neointima development *in vivo* [57]. Another smooth muscle cell-specific molecule, SM22, whose function is to bind to actin and anchor the cytoskeleton, also modulates Sod2 expression through deactivating NF-κB. Shen and colleagues identified that primary VSMCs from SM22-KO mice exhibited prominent NADPH oxidase upregulation and NF-κB activation, followed by an increased expression of proinflammatory genes, ROS production, and the feedback upregulation of Sod2 [58]. An adipokine C1q and TNF-related protein 1 (C1QTNF1) is also found to regulate Sod2 expressions in VSMCs; through bioinformatic analyses, Kim et al. showed that VSMCs treated with C1QTNF1 had significant Sod2 upregulation accompanied by activations of interleukin-6 and adhesion molecules [59]. On the other hand, neuron-derived orphan receptor-1 (NOR-1), a ligand-independent transcription factor involved in various growth and inflammatory responses, also plays a role in regulating SOD2 levels. Alonso et al. revealed in VSMCs that NOR-1 induced an upregulation of NADPH oxidase 1 (Nox1) and suppressed Sod2 expressions through lowering p65 nuclear translocation, thereby increasing intracellular ROS levels [60]. Despite the above promising findings, more
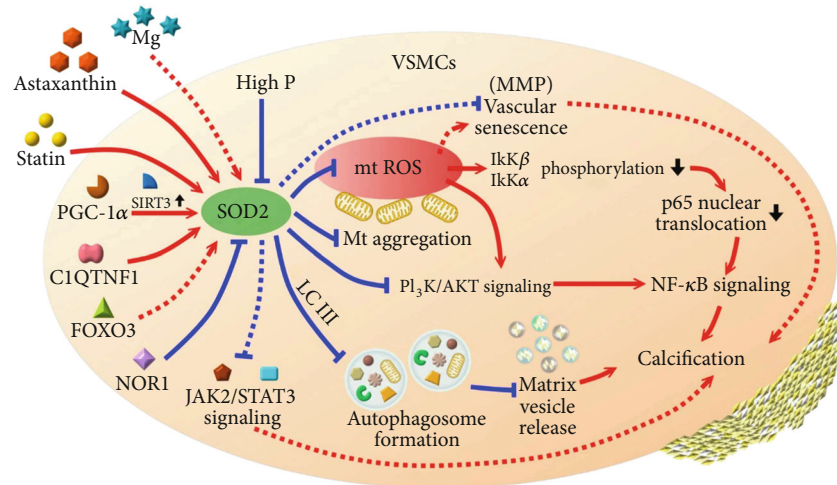
FIGURE 1: A summary diagram illustrating the regulatory molecules and the effectors of SOD2 in vascular smooth muscle cells demonstrated in the literature. Red arrows indicate activating stimuli, while blue lines indicate inhibitory or antagonistic effects. MMP: matrix metalloproteinase; mt: mitochondria; P: phosphate; ROS: reactive oxygen species; SOD2: superoxide dismutase 2; VSMC: vascular smooth muscle cells.

are needed to facilitate a better understanding of VSMC-specific SOD2 regulatory mechanisms.1

5. SOD2-Targeted Strategies in Vascular Calcification Management

5.1. Clinical Evidence of SOD2 Relevance in Vascular Calcification. Judging from the importance of VSMC SOD2 in vascular calcification, it is expected that SOD2 levels differ significantly between clinical specimens from patients with and without vascular calcification. Few studies report on this issue. A group from Italy showed that Sod2 expression levels in the peripheral blood mononuclear cells were significantly higher among patients with coronary artery calcification compared to those without, and this relationship persisted regardless of the patients' DM status [61]. Their findings agree with the experimental results that high glucose levels minimally affect SOD2 levels in VSMCs [55]. Another study reported that plasma obtained from the coronary arteries exhibited significantly greater SOD2 enzymatic activities than those from peripheral blood in patients with coronary atherosclerosis [62]; this suggests that there may be site-specific issues with regard to SOD2 level detection or enzyme activity determination. Andujar-Vera and colleagues examined the proteomic profiles of calcified and noncalcified femoral artery samples from patients with DM and found that Sod2 was an important hub gene that exhibited differential expressions in calcified arterial walls [63]. Based on the above clinical findings, it would be prudent to state that tissue SOD2 levels and circulatory SOD2 activities alter depending on vascular calcification status and severities, and SOD2 likely participates in the pathogenesis of vascular calcification.

5.2. Potential Vascular Calcification Treatment Strategies Targeting SOD2. Since SOD2 can be regulated by multiple endogenous molecules and potentially upregulated by exoge-

nous treatments (Figure 1), it would be tempting to repurpose a SOD2-targeted approach for managing vascular calcification. Several reports support the feasibility and potential usefulness of this idea. For instance, statin can be a plausible candidate. Crespo and colleagues demonstrated that VSMCs treated with simvastatin have a downregulation of NOR-1, a negative regulatory molecule of Sod2 [64], and others have indicated that statin can inhibit inflammation-induced vascular calcification *in vitro* [65]. Feresin et al. previously found that polyphenols from berry extracts could trickle up the expressions of Sod2 in treated VSMCs, decrease ROS severity, and ameliorate VSMC senescence, accompanied by the inhibition of Akt, MAPK, and extracellular-regulated protein kinase (ERK) signaling [66]. These effects are expected to improve vascular calcification through the intertwined connections between these pathways and calcification pathogenesis [44, 67]. Magnesium has also been shown to ameliorate oxidative stress and decrease vascular calcification severity through its effect on multiple pathways, including SM22 regulation [68]. Finally, using an *in vitro* model of VSMC calcification in combination with transcriptomic profiling, our research group recently discovered that astaxanthin, a carotenoid derivative with strong antioxidative property, exhibited a prominent anticalcific effect through specifically targeting SOD2 during treatment of calcified VSMCs [69]. Indeed, there are a handful of natural products or extracts exhibiting *in vitro* or *in vivo* effects of augmenting Sod2 expression and activities [70, 71], and testing these SOD2-targeted candidates in VSMCs regarding their anticalcific potential may be a fruitful approach for identifying new pharmaceuticals for treating vascular calcification.

6. Conclusion and Future Perspectives

Vascular calcification, although traditionally deemed as an innocent process of vascular aging, has gained tremendous

research and clinical attention due to its strong associations with adverse outcomes independent of other confounders. Mitochondrial dysfunction is an emerging pathogenic factor identified during the course of vascular calcification, and mitochondrial ROS lies at the epicenter of this detrimental phenotype. Through counteracting mitochondrial ROS and potentially modulating other signaling pathways, SOD2 acts as a critical gateway within VSMCs blocking the progression of subsequent calcification. Several available pharmaceuticals and natural compounds have been found to upregulate SOD2 specifically in VSMCs, a pivotal pathophysiologic player in vascular calcification, but studies addressing the potential utility of these candidates are scant. More data are needed for uncovering the potential of novel SOD2-targeted strategies for the treatment of vascular calcification.

Abbreviations

AGE: Advanced glycation end product
AP2: Activator protein 2
Atg5: Autophagy-related 5
C1QTNF1: C1q and TNF-related protein 1
CKD: Chronic kidney disease
DM: Diabetes mellitus
DNMT: DNA methyltransferase
Drp1: Dynamin-related protein 1
EC: Endothelial cell
ER: Endoplasmic reticulum
ERK: Extracellular-regulated protein kinase
ESRD: End-stage renal disease
FOXO3a: Forkhead box O3a
HIF: Hypoxia-inducible factor
JAK2: Janus kinase 2
KO: Knockout
MAP: Mitogen-activated protein
MMP: Matrix metalloproteinase
mtROS: Mitochondrial reactive oxygen species
MV: Matrix vesicle
NAMPT: Nicotinamide phosphoribosyltransferase
NF-κB: Nuclear factor-κB
NOR-1: Neuron-derived orphan receptor-1
Nox: NADPH oxidase
Nrf: Nuclear factor erythroid 2-related factor
ox-LDL: Oxidized low-density lipoprotein
PGC-1α: Peroxisome proliferator-activated receptor-γ coactivator-1α
ROS: Reactive oxygen species
SOD2: Superoxide dismutase 2
SP1: Specific protein 1
STAT3: Signal transducer and activator of transcription 3
TNF: Tumor necrosis factor
VSMC: Vascular smooth muscle cell.

Data Availability

No new data are generated from this review.

Disclosure

The sponsors have no role in the study design, data collection, analysis, and result interpretation of this study.

Conflicts of Interest

The authors have no relevant financial or nonfinancial conflicts of interests to declare in relation to this manuscript.

Authors' Contributions

HYY and CTC contributed to the study design. YTT, HYY, and CTC contributed to the data analysis. YTT, HYY, CTC, and CKC drafted the article. All authors approved the final version of the manuscript.

Acknowledgments

References

[1] R. R. Townsend, "Arterial stiffness and chronic kidney disease: lessons from the chronic renal insufficiency cohort study," *Current Opinion in Nephrology and Hypertension*, vol. 24, no. 1, pp. 47–53, 2015.

[2] C. Souilhol, J. Serbanovic-Canic, M. Fragiadaki et al., "Endothelial responses to shear stress in atherosclerosis: a novel role for developmental genes," *Nature Reviews Cardiology.*, vol. 17, no. 1, pp. 52–63, 2020.

[3] J. A. Chirinos, P. Segers, T. Hughes, and R. Townsend, "Large-artery stiffness in health and disease;," *Journal of the American College of Cardiology*, vol. 74, no. 9, pp. 1237–1263, 2019.

[4] Q. Niu, Y. Hong, C.-H. Lee, C. Men, H. Zhao, and L. Zuo, "Abdominal aortic calcification can predict all-cause mortality and CV events in dialysis patients: a systematic review and meta-analysis," *PLoS One*, vol. 13, no. 9, p. e0204526, 2018.

[5] X.-R. Wang, J.-J. Zhang, X.-X. Xu, and Y.-G. Wu, "Prevalence of coronary artery calcification and its association with mortality, cardiovascular events in patients with chronic kidney disease: a systematic review and meta-analysis," *Renal Failure*, vol. 41, no. 1, pp. 244–256, 2019.

[6] S.-Y. Lee, C.-T. Chao, J.-W. Huang, and K.-C. Huang, "Vascular calcification as an underrecognized risk factor for frailty in 1783 community-dwelling elderly individuals," *Journal of the American Heart Association*, vol. 9, no. 18, p. e017308, 2020.

[7] J. R. Lewis, C. J. Eggermont, J. T. Schousboe et al., "Association between abdominal aortic calcification, bone mineral density, and fracture in older women," *Journal of Bone and Mineral Research.*, vol. 34, no. 11, pp. 2052–2060, 2019.

[8] B.-J. Ko, Y. Chang, H.-S. Jung et al., "Relationship between low relative muscle mass and coronary artery calcification in healthy adults," *Arteriosclerosis, Thrombosis, and Vascular Biology.*, vol. 36, no. 5, pp. 1016–1021, 2016.

[9] S. Zununi Vahed, S. Mostafavi, S. M. Hosseiniyan Khatibi, M. M. Shoja, and M. Ardalan, "Vascular calcification: an important understanding in nephrology," *Vascular Health and Risk Management*, vol. 16, pp. 167–180, 2020.

[10] C.-T. Chao, Y.-P. Liu, S.-F. Su et al., "Circulating microRNA-125b predicts the presence and progression of uremic vascular calcification," *Arteriosclerosis, Thrombosis, and Vascular Biology.*, vol. 37, no. 7, pp. 1402–1414, 2017.

[11] Y.-C. Hou, C.-L. Lu, T.-H. Yuan, M.-T. Liao, C.-T. Chao, and K.-C. Lu, "The epigenetic landscape of vascular calcification: an integrative perspective," *International Journal of Molecular Sciences*, vol. 21, no. 3, p. 980, 2020.

[12] S. J. Lee, I.-K. Lee, and J.-H. Jeon, "Vascular calcification-new insights into its mechanism," *International Journal of Molecular Sciences*, vol. 21, no. 8, p. 2685, 2020.

[13] G. Machado-Oliveira, C. Ramos, A. R. A. Marques, and O. V. Vieira, "Cell senescence, *multiple organelle dysfunction and atherosclerosis*," *Cells*, vol. 9, no. 10, p. 2146, 2020.

[14] S. van der Rijt, M. Molenaars, R. L. McIntyre, G. E. Janssens, and R. H. Houtkooper, "Integrating the hallmarks of aging throughout the tree of life: a focus on mitochondrial dysfunction," *Frontiers in Cell and Developmental Biology*, vol. 8, p. 594416, 2020.

[15] E. Yu, J. Mercer, and M. Bennett, "Mitochondria in vascular disease," *Cardiovascular Research*, vol. 95, no. 2, pp. 173–182, 2012.

[16] I. Perrotta, "The microscopic anatomy of endothelial cells in human atherosclerosis: focus on ER and mitochondria," *Journal of Anatomy*, vol. 237, no. 6, pp. 1015–1025, 2020.

[17] Y.-X. Ru, H.-C. Shang, S.-X. Dong, S.-X. Zhao, H.-Y. Liang, and C.-J. Zhu, "Foam cell origination from degenerated vascular smooth muscle cells in atherosclerosis: an ultrastructural study on hyperlipidemic rabbits," *Ultrastructural Pathology.*, vol. 44, no. 1, pp. 103–115, 2020.

[18] T. Shemiakova, E. Ivanova, A. V. Grechko, E. V. Gerasimova, I. A. Sobenin, and A. N. Orekhov, "Mitochondrial dysfunction and DNA damage in the context of pathogenesis of atherosclerosis," *Biomedicine*, vol. 8, no. 6, p. 166, 2020.

[19] J. Zheng and C. Lu, "Oxidized LDL causes endothelial apoptosis by inhibiting mitochondrial fusion and mitochondria autophagy," *Frontiers in Cell and Development Biology*, vol. 8, p. 600950, 2020.

[20] B. Swaminathan, H. Goikuria, R. Vega, A. Rodríguez-Antigüedad, and A. López Medina, "Autophagic marker MAP1LC3B expression levels are associated with carotid atherosclerosis symptomatology," *PLoS One*, vol. 9, no. 12, p. e115176, 2014.

[21] H. Kim, H.-J. Kim, K. Lee et al., "α-Lipoic acid attenuates vascular calcification via reversal of mitochondrial function and restoration of Gas6/Axl/Akt survival pathway," *Journal of Cellular and Molecular Medicine*, vol. 16, no. 2, pp. 273–286, 2012.

[22] M. A. Rogers, N. Maldonado, J. D. Hutcheson et al., "Dynamin-related protein 1 inhibition attenuates cardiovascular calcification in the presence of oxidative stress," *Circulation Research*, vol. 121, no. 3, pp. 220–233, 2017.

[23] L. Cui, Z. Li, X. Chang, G. Cong, and L. Hao, "Quercetin attenuates vascular calcification by inhibiting oxidative stress and mitochondrial fission," *Vascular Pharmacology.*, vol. 88, pp. 21–29, 2017.

[24] W.-Q. Ma, X.-J. Sun, Y. Wang, Y. Zhu, X.-Q. Han, and N.-F. Liu, "Restoring mitochondrial biogenesis with metformin attenuates β-GP-induced phenotypic transformation of VSMCs into an osteogenic phenotype via inhibition of PDK4/oxidative stress-mediated apoptosis," *Molecular and Cellular Endocrinology.*, vol. 479, pp. 39–53, 2019.

[25] M.-M. Zhao, M.-J. Xu, Y. Cai et al., "Mitochondrial reactive oxygen species promote p65 nuclear translocation mediating high-phosphate-induced vascular calcification in vitro and in vivo," *Kidney International.*, vol. 79, no. 10, pp. 1071–1079, 2011.

[26] F. Tang, E. Chan, M. Lu et al., "Calpain-1 mediated disorder of pyrophosphate metabolism contributes to vascular calcification induced by oxLDL," *PLoS One*, vol. 10, no. 6, p. e0129128, 2015.

[27] R. Villa-Bellosta, "Dietary magnesium supplementation improves lifespan in a mouse model of progeria," *EMBO Molecular Medicine*, vol. 12, no. 10, p. e12423, 2020.

[28] J. M. McCord and I. Fridovich, "Superoxide dismutase: an enzymic function for erythrocuprein (hemocuprein)," *Journal of Biological Chemistry.*, vol. 244, no. 22, pp. 6049–6055, 1969.

[29] T. Fukai and M. Ushio-Fukai, "Superoxide dismutases: role in redox signaling, vascular function, and diseases," *Antioxidants & Redox Signaling*, vol. 15, no. 6, pp. 1583–1606, 2011.

[30] P. Roman-Garcia, S. Barrio-Vazquez, J. L. Fernandez-Martin, M. P. Ruiz-Torres, and J. B. Cannata-Andia, "Natural antioxidants and vascular calcification: a possible benefit," *Journal of Nephrology*, vol. 24, no. 6, pp. 669–672, 2011.

[31] Y. Li, T.-T. Huang, E. J. Carlson et al., "Dilated cardiomyopathy and neonatal lethality in mutant mice lacking manganese superoxide dismutase," *Nature Genetics*, vol. 11, no. 4, pp. 376–381, 1995.

[32] S. W. Ballinger, C. Patterson, C. A. Knight-Lozano et al., "Mitochondrial integrity and function in atherogenesis," *Circulation*, vol. 106, no. 5, pp. 544–549, 2002.

[33] M. Ohashi, S. Runge Marschall, M. Faraci Frank, and D. D. Heistad, "MnSOD deficiency increases endothelial dysfunction in ApoE-deficient mice," *Arteriosclerosis, Thrombosis, and Vascular Biology*, vol. 26, no. 10, pp. 2331–2336, 2006.

[34] R.-H. Zhou, A. E. Vendrov, I. Tchivilev et al., "Mitochondrial oxidative stress in aortic stiffening with age: the role of smooth muscle cell function," *Arteriosclerosis, thrombosis, and vascular biology.*, vol. 32, no. 3, pp. 745–755, 2012.

[35] A. E. Vendrov, M. D. Stevenson, S. Alahari et al., "Attenuated superoxide dismutase 2 activity induces atherosclerotic plaque instability during aging in hyperlipidemic mice," *Journal of the American Heart Association*, vol. 6, no. 11, p. e006775, 2017.

[36] E. Branchetti, R. Sainger, P. Poggio et al., "Antioxidant enzymes reduce DNA damage and early activation of valvular interstitial cells in aortic valve sclerosis," *Arteriosclerosis, thrombosis, and vascular biology.*, vol. 33, no. 2, pp. e66–e74, 2013.

[37] X.-Y. Dai, M.-M. Zhao, Y. Cai et al., "Phosphate-induced autophagy counteracts vascular calcification by reducing matrix vesicle release," *Kidney International.*, vol. 83, no. 6, pp. 1042–1051, 2013.

[38] M. Agharazii, R. St-Louis, A. Gautier-Bastien et al., "Inflammatory cytokines and reactive oxygen species as mediators of chronic kidney disease-related vascular calcification," *American Journal of Hypertension.*, vol. 28, no. 6, pp. 746–755, 2015.

[39] N. X. Chen, K. D. O'Neill, and S. M. Moe, "Matrix vesicles induce calcification of recipient vascular smooth muscle cells through multiple signaling pathways," *Kidney International.*, vol. 93, no. 2, pp. 343–354, 2018.

[40] M. D. Brand, "Riding the tiger –physiological and pathological effects of superoxide and hydrogen peroxide generated in the mitochondrial matrix," *Critical Reviews in Biochemistry and Molecular Biology.*, vol. 55, no. 6, pp. 592–661, 2020.

[41] R. Siauciunaite, N. S. Foulkes, V. Calabro, and D. Vallone, "Evolution shapes the gene expression response to oxidative stress," *International Journal of Molecular Sciences.*, vol. 20, no. 12, p. 3040, 2019.

[42] N. R. Madamanchi, S.-K. Moon, Z. S. Hakim et al., "Differential activation of mitogenic signaling pathways in aortic smooth muscle cells deficient in superoxide dismutase isoforms," *Arteriosclerosis, Thrombosis, and Vascular Biology.*, vol. 25, no. 5, pp. 950–956, 2005.

[43] J.-N. Wang, N. Shi, and S.-Y. Chen, "Manganese superoxide dismutase inhibits neointima formation through attenuation of migration and proliferation of vascular smooth muscle cells," *Free Radical Biology & Medicine*, vol. 52, no. 1, pp. 173–181, 2012.

[44] C.-T. Chao, H.-Y. Yeh, Y.-T. Tsai et al., "Natural and non-natural antioxidative compounds: potential candidates for treatment of vascular calcification," *Cell Death Discov.*, vol. 5, no. 1, p. 145, 2019.

[45] C. Nicolaije, M. Koedam, and J. P. T. M. van Leeuwen, "Decreased oxygen tension lowers reactive oxygen species and apoptosis and inhibits osteoblast matrix mineralization through changes in early osteoblast differentiation," *Journal of Cellular Physiology.*, vol. 227, no. 4, pp. 1309–1318, 2012.

[46] G. Li, W. H. Lu, R. Ai, J. H. Yang, F. Chen, and Z. Z. Tang, "The relationship between serum hypoxia-inducible factor 1α and coronary artery calcification in asymptomatic type 2 diabetic patients," *Cardiovascular Diabetology*, vol. 13, no. 1, p. 52, 2014.

[47] H. K. Eltzschig and P. Carmeliet, "Hypoxia and inflammation," *The New England Journal of Medicine*, vol. 364, no. 7, pp. 656–665, 2011.

[48] B. Halvorsen, M. Z. Espeland, G. Ø. Andersen et al., "Increased expression of NAMPT in PBMC from patients with acute coronary syndrome and in inflammatory M1 macrophages," *Atherosclerosis*, vol. 243, no. 1, pp. 204–210, 2015.

[49] S. Raffa, X. L. D. Chin, R. Stanzione et al., "The reduction of NDUFC2 expression is associated with mitochondrial impairment in circulating mononuclear cells of patients with acute coronary syndrome," *International Journal of Cardiology.*, vol. 286, pp. 127–133, 2019.

[50] L. Miao and D. K. St Clair, "Regulation of superoxide dismutase genes: implications in disease," *Free Radical Biology & Medicine*, vol. 47, no. 4, pp. 344–356, 2009.

[51] I. N. Zelko, T. J. Mariani, and R. J. Folz, "Superoxide dismutase multigene family: a comparison of the CuZn-SOD (SOD1), Mn-SOD (SOD2), and EC-SOD (SOD3) gene structures, evolution, and expression," *Free Radical Biology and Medicine.*, vol. 33, no. 3, pp. 337–349, 2002.

[52] M. Akashi, M. Hachiya, R. L. Paquette, Y. Osawa, S. Shimizu, and G. Suzuki, "Irradiation increases manganese superoxide dismutase mRNA levels in human fibroblasts," *Journal of Biological Chemistry.*, vol. 270, no. 26, pp. 15864–15869, 1995.

[53] Y. Chen, J. Zhang, Y. Lin et al., "Tumour suppressor SIRT3 deacetylates and activates manganese superoxide dismutase to scavenge ROS," *EMBO Reports*, vol. 12, no. 6, pp. 534–541, 2011.

[54] S. L. Archer, G. Marsboom, G. H. Kim et al., "Epigenetic attenuation of mitochondrial superoxide dismutase 2 in pulmonary arterial hypertension," *Circulation*, vol. 121, no. 24, pp. 2661–2671, 2010.

[55] M. Descorbeth and M. B. Anand-Srivastava, "Role of oxidative stress in high-glucose- and diabetes-induced increased expression of Gq/11α proteins and associated signaling in vascular smooth muscle cells," *Free Radical Biology and Medicine.*, vol. 49, no. 9, pp. 1395–1405, 2010.

[56] H. Feng, J.-Y. Wang, B. Yu et al., "Peroxisome proliferator-activated receptor-γ coactivator-1α inhibits vascular calcification through sirtuin 3-mediated reduction of mitochondrial oxidative stress," *Antioxidants & Redox Signaling*, vol. 31, no. 1, pp. 75–91, 2019.

[57] A. Qu, C. Jiang, M. Xu et al., "PGC-1α attenuates neointimal formation via inhibition of vascular smooth muscle cell migration in the injured rat carotid artery," *American Journal of Physiology-Cell Physiology.*, vol. 297, no. 3, pp. C645–C653, 2009.

[58] J. Shen, M. Yang, D. Ju et al., "Disruption of SM22 promotes inflammation after artery injury via nuclear factor κB activation," *Circulation Research*, vol. 106, no. 8, pp. 1351–1362, 2010.

[59] D. Kim and S.-Y. Park, "C1q and TNF related protein 1 regulates expression of inflammatory genes in vascular smooth muscle cells," *Genes & Genomics.*, vol. 41, no. 4, pp. 397–406, 2019.

[60] J. Alonso, L. Cañes, A. B. García-Redondo, P. G. de Frutos, C. Rodríguez, and J. Martínez-González, "The nuclear receptor NOR-1 modulates redox homeostasis in human vascular smooth muscle cells," *Journal of Molecular and Cellular Cardiology.*, vol. 122, pp. 23–33, 2018.

[61] T. Infante, E. Forte, M. Aiello, M. Salvatore, and C. Cavaliere, "In vivo and in vitro analysis in coronary artery disease related to type 2 diabetes," *Frontiers in Endocrinology*, vol. 8, p. 209, 2017.

[62] H. Gutiérrez-Leonard, E. Martínez-Lara, A. E. Fierro-Macías et al., "Pregnancy-associated plasma protein-A (PAPP-A) as a possible biomarker in patients with coronary artery disease," *Irish Journal of Medical Science*, vol. 186, no. 3, pp. 597–605, 2017.

[63] F. Andújar-Vera, C. García-Fontana, S. Lozano-Alonso et al., "Association between oxidative-stress-related markers and calcified femoral artery in type 2 diabetes patients," *Journal of Pharmaceutical and Biomedical Analysis.*, vol. 190, p. 113535, 2020.

[64] J. Crespo, J. Martínez-González, J. Rius, and L. Badimon, "Simvastatin inhibits NOR-1 expression induced by hyperlipemia by interfering with CREB activation," *Cardiovascular Research*, vol. 67, no. 2, pp. 333–341, 2005.

[65] A. Kizu, A. Shioi, S. Jono, H. Koyama, Y. Okuno, and Y. Nishizawa, "Statins inhibit in vitro calcification of human vascular smooth muscle cells induced by inflammatory mediators," *Journal of Cellular Biochemistry*, vol. 93, no. 5, pp. 1011–1019, 2004.

[66] R. G. Feresin, J. Huang, D. S. Klarich et al., "Blackberry, raspberry and black raspberry polyphenol extracts attenuate angiotensin II-induced senescence in vascular smooth muscle cells," *Food & Function.*, vol. 7, no. 10, pp. 4175–4187, 2016.

[67] C.-L. Lu, M.-T. Liao, Y.-C. Hou et al., "Sirtuin-1 and its relevance in vascular calcification," *International Journal of Molecular Sciences*, vol. 21, no. 5, p. 1593, 2020.

[68] A. D. ter Braake, M. Shanahan Catherine, and H. F. de Baaij Jeroen, "Magnesium counteracts vascular calcification," *Arteriosclerosis, Thrombosis, and Vascular Biology.*, vol. 37, no. 8, pp. 1431–1445, 2017.

[69] C.-T. Chao, H.-Y. Yeh, Y.-T. Tsai et al., "Astaxanthin counteracts vascular calcification in vitro through an early up-regulation of SOD2 based on a transcriptomic approach," *International Journal of Molecular Sciences*, vol. 21, no. 22, p. 8530, 2020.

[70] D. Disasa, L. Cheng, M. Manzoor et al., "Amarogentin from Gentiana rigescens Franch exhibits antiaging and neuroprotective effects through antioxidative stress," *Oxidative Medicine and Cellular Longevity*, vol. 2020, Article ID 3184019, 15 pages, 2020.

[71] Y. Lin, Y. Kotakeyama, J. Li et al., "Cucurbitacin B exerts anti-aging effects in yeast by regulating autophagy and oxidative stress," *Oxidative Medicine and Cellular Longevity*, vol. 2019, Article ID 4517091, 15 pages, 2019.

Research Article

W196 and the β-Hairpin Motif Modulate the Redox Switch of Conformation and the Biomolecular Interaction Network of the Apoptosis-Inducing Factor

Silvia Romero-Tamayo,[1,2] **Ruben Laplaza,**[3,4] **Adrian Velazquez-Campoy** ![ORCID],[1,2,5,6,7]
Raquel Villanueva ![ORCID],[1,2] **Milagros Medina** ![ORCID],[1,2] **and Patricia Ferreira** ![ORCID][1,2]

[1]*Departamento de Bioquímica y Biología Molecular y Celular, Facultad de Ciencias, Universidad de Zaragoza, Spain*
[2]*Instituto de Biocomputación y Física de Sistemas Complejos, BIFI (GBsC-CSIC and BIFI-IQFR Joint Units),*
 Universidad de Zaragoza, Spain
[3]*Sorbonne Université, CNRS, Laboratoire de Chimie Théorique, LCT, 75005 Paris, France*
[4]*Departamento de Química Física, Universidad de Zaragoza, 50009 Zaragoza, Spain*
[5]*Fundación ARAID, Diputación General de Aragón, Spain*
[6]*Aragon Institute for Health Research (IIS Aragon), Zaragoza, Spain*
[7]*Biomedical Research Networking Centre for Liver and Digestive Diseases (CIBERehd), Madrid, Spain*

Correspondence should be addressed to Milagros Medina; mmedina@unizar.es and Patricia Ferreira; ferreira@unizar.es

Academic Editor: Luciana Hannibal

The human apoptosis-inducing factor (hAIF) is a moonlight flavoprotein involved in mitochondrial respiratory complex assembly and caspase-independent programmed cell death. These functions might be modulated by its redox-linked structural transition that enables hAIF to act as a NAD(H/$^+$) redox sensor. Upon reduction with NADH, hAIF undergoes a conformational reorganization in two specific insertions—the flexible regulatory C-loop and the 190-202 β-harpin—promoting protein dimerization and the stabilization of a long-life charge transfer complex (CTC) that modulates its monomer-dimer equilibrium and its protein interaction network in healthy mitochondria. In this regard, here, we investigated the precise function of the β-hairpin in the AIF conformation landscape related to its redox mechanism, by analyzing the role played by W196, a key residue in the interaction of this motif with the regulatory C-loop. Mutations at W196 decrease the compactness and stability of the oxidized hAIF, indicating that the β-hairpin and C-loop coupling contribute to protein stability. Kinetic studies complemented with computational simulations reveal that W196 and the β-hairpin conformation modulate the low efficiency of hAIF as NADH oxidoreductase, contributing to configure its active site in a noncompetent geometry for hydride transfer and to stabilize the CTC state by enhancing the affinity for NAD$^+$. Finally, the β-hairpin motif contributes to define the conformation of AIF's interaction surfaces with its physiological partners. These findings improve our understanding on the molecular basis of hAIF's cellular activities, a crucial aspect for clarifying its associated pathological mechanisms and developing new molecular therapies.

1. Introduction

The human apoptosis-inducing factor (hAIF) was first described as a mitochondrial-released flavoprotein mediating caspase-independent programmed cell death [1]. Moreover, this ubiquitously expressed protein across eukaryotes also plays a vital role in cell development and survival [2]. These

survival functions rely on its FAD-dependent activities, which contribute to maintain the stability of the mitochondrial electron transfer chain, supercomplex organization, and transmembrane potential, as well as to control mitochondrial reactive oxygen species (ROS) [3]. In healthy mitochondria, the hAIF is processed and the hAIF$_{\Delta 1-53}$ mature protein anchors in the inner membrane (IM)—*via* its N-

terminal segment, facing the intermembrane space (IMS)—and folds in three domains (Figure 1(a)) [4–6]. Mammalian AIFs have two specific insertions, a regulatory C-terminal loop (aa 510-560 in hAIF) and a β-hairpin (aa 190-202 in hAIF), which connect the NADH and FAD domains to the C-terminal proapoptotic domain (Figure 1(a)).

hAIF conformation is dynamically influenced by coenzyme substrate binding and by the redox switch of its flavin cofactor, facts believed to modulate its biomolecular interaction network [7, 8]. In oxidized hAIF (hAIF$_{ox}$), the regulatory C-loop is stabilized in the protein core by direct interaction with the β-hairpin, particularly through stacking and H-bonding interactions of W196 and R201 residues with its 517-524 and 529-533 short helixes. Binding of one NADH molecule to AIF's active site (NADH$_A$) promotes FAD reduction, as well as the stabilization of a long-lived FADH$^-$/NAD$^+$ charge transfer complex (CTC). This CTC is inefficient in electron transfer, but capable of inducing a redox-linked protein conformational reorganization and its subsequent dimerization. CTC formation displaces the β-hairpin that triggers C-loop remodeling and its release to the solvent. These conformational changes induce (i) the allosteric formation of the second noncatalytic NADH binding site (NADH$_B$), where stacking interactions with reoriented W196 and F582 side chains facilitate NADH$_B$ accommodation and (ii) the dimerization of the protein (Figures 1(c) and 1(e)). These facts led to postulate AIF as a redox sensor of NAD(H/$^+$) cellular levels [9–11]. W196 substitution by alanine disrupts the interaction between the β-hairpin and the C-loop that unwinds the above mentioned 529-533 helix and releases the two specific AIF insertions to the solvent, promoting a permissive mutant dimerization in its oxidized state (W196A hAIF$_{\Delta 1\text{-}101ox}$, herein W196A$_{ox}$) (Figures 1(a) and 1(d)) [11]. However, W196A$_{ox}$ maintains an active-site architecture similar to that of WT hAIF$_{ox}$ for residues involved in NADH$_A$ binding with the only exceptions of E453 and H454 (Figure 1(b)). The β-hairpin release in W196A$_{ox}$ also induces the displacement of the central β-strand and the reorientation of E453 and H454 side chains (Figure S1D-E). Thus, H454 disrupts its interaction with S480, producing as a consequence the displacement of the H478 side chain—sited in the loop connecting the central β-strand and the His-rich helix—towards the C-loop, contributing to its release, and the exposition of the hydrophobic border at the dimerization interfaces in the W196A$_{ox}$ structure. Such last conformational changes are similar to those reported for the WT CTC structure (Figure S1E-F).

In healthy cells, hAIF is essential for mitochondrial bioenergetics, being its physical and functional interaction with human CHCHD4 (coiled-coil-helix-coiled-coil-helix domain containing 4) key in the assembly and/or stabilization of multisubunit respiratory transport chain complexes and supercomplexes [12–15]. In IMS, CHCHD4 controls the import and oxidative folding of a set of assembly factors and protein subunits of respiratory complexes, while hAIF would regulate CHCHD4 expression as well as its import and proper IMS localization. Consequently, downregulation or depletion of hAIF gives rise to major dysfunctions in oxi-

dative phosphorylation (OXPHOS), secondary to the deficiency of CHCHD4, causing severe neurodegenerative illnesses [12, 14, 16, 17]. The hAIF conformation—modulated by its redox NADH-dependent monomer-dimer equilibrium—is suggested to be critical for this interaction [7, 13, 18].

Upon lethal cellular stress, hAIF acts as a mediator of necrotic poly(ADP-ribose) polymerase- (PARP-) 1-dependent cell death (parthanatos) by its further processing into the soluble proapoptotic form (hAIF$_{\Delta 1\text{-}101}$) and its release into the cytosol. The regulatory mechanism by which AIF is released is unknown, but could be somehow modulated by its structural reorganization due to depletion of coenzyme levels during PARP-1 hyperactivation [19]. Once in the cytosol, its interaction with some endonucleases, as cyclophilin A (CypA), favors nuclear cotranslocation of the AIF:CypA complex [20, 21]. In this subcellular compartment, the association of this binary complex to the histone H2AX leads to the assembly of the AIF-mediated DNA degradation complex ("degradosome," AIF:CypA:H2AX:DNA), which provokes chromatin condensation and DNA fragmentation [21, 22].

Despite the emerging picture of the physiological functions of AIF being modulated by its conformational and redox states, we are only starting to depict the implications of the molecular mechanism regulating its activities. Thus, the molecular basis for the mechanism by which AIF regulates and pivots the redox-dependent interaction with CHCHD4, as well as those for the action of the degradosome complex as a death effector remain unknown. Nonetheless, we can envisage that AIF ability to stabilize both stable CTC and dimers—upon interaction with the coenzyme followed by FAD reduction—is surely a key feature to switch among its *in vivo* roles. In this context, the structural changes induced by CTC formation in native protein, but also shared by W196A$_{ox}$, suggest that W196 and/or the β-hairpin might be relevant for AIF cellular activities. Such hypothesis is further supported by the β-hairpin contributing to binding of the allosteric NADH$_B$, as well as by the fact that pathogenic mutations coursing with severe processes of neurodegeneration and early death have been reported at both the NADH$_B$ binding site and the β-hairpin itself.

In the present study, we particularly investigate the contribution of the β-hairpin to the regulation of hAIF structural stability, coenzyme binding, reductase activity, CTC stability, and interaction with its physiological partners, by generating W196A, W196L, and W196Y site-directed mutants (which progressively reduce aromatic and stacking interactions). Our results indicate that the W196 side chain is not only key to establish the β-hairpin and C-loop organization in the oxidized state, but also to regulate the stability and conformational landscape of the protein. Both facts seem to be relevant to determine AIF efficiency as a cellular redox sensor, as well as to the establishment of specific binary interactions with different partners.

2. Materials and Methods

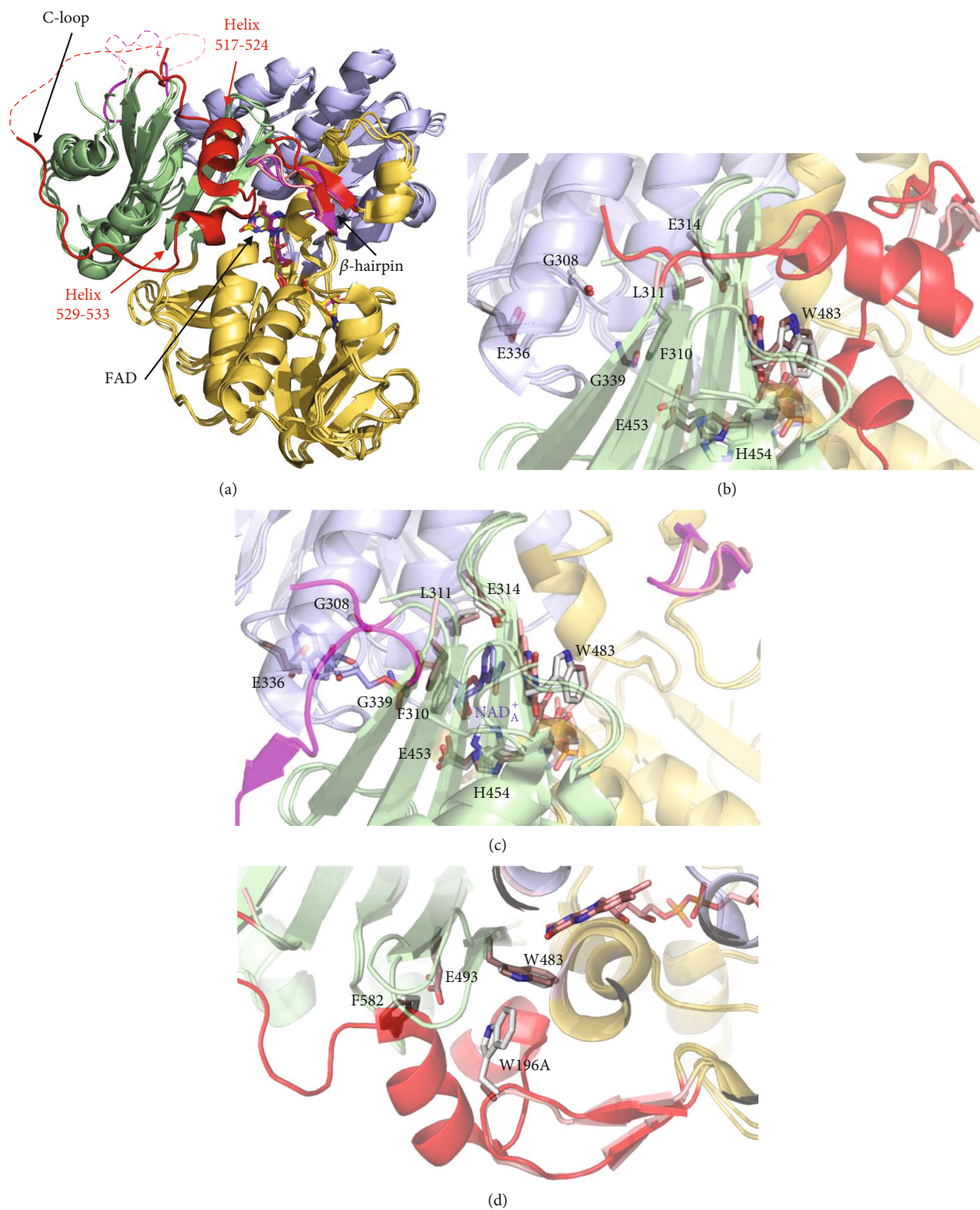*2.1. Expression and Production of Proteins.* The cDNA sequences encoding for W196Y, W196L, and W196A

(a)
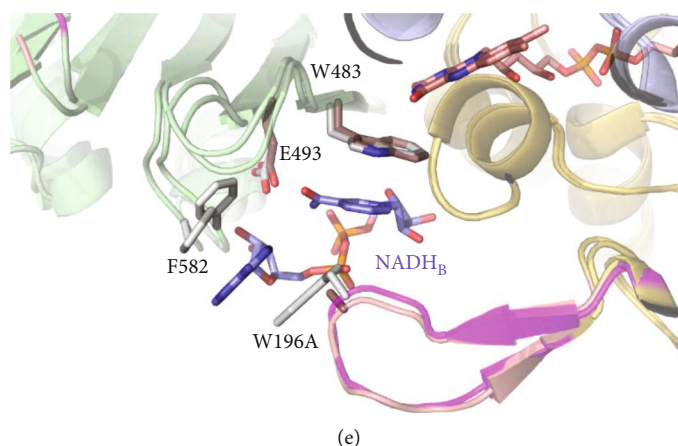
(b)

(c)

(d)

FIGURE 1: Continued.

(e)

Figure 1: Comparative overview of the crystallographic structures of WT hAIF$_{\Delta 1-101ox}$ (PDB 4BV6), WT CTC hAIF$_{\Delta 1-101rd}$:2NAD($^+$/H) (PDB 4BUR), and W196A$_{ox}$ variant (PDB 5KVH). (a) Cartoon superposition. FAD-, NADH-, and C-terminal domains colored in gold, light blue, and pale green, respectively. FAD drawn as sticks with C atoms in yellow, salmon, and magenta, respectively, for WT$_{ox}$, WT CTC, and W196A$_{ox}$ structures. Visible residues in the β-hairpin and the regulatory 509-560 C-loop are shown in red, magenta, and salmon, respectively, for WT$_{ox}$, WT CTC, and W196A$_{ox}$ structures. Missing fragments of the C-loop (P545-D559, K518-G557 and A511-D559 in WT$_{ox}$ chain A, WT CTC chain C, and W196A$_{ox}$ chain A structures, respectively) are indicated as dashed lines. Detail of the W196A$_{ox}$ NADH$_A$ binding site overlaid with (b) WT$_{ox}$ and (c) WT CTC. Detail of the W196A$_{ox}$ NADH$_B$ binding site overlaid with (d) WT$_{ox}$ and (e) WT CTC. Side chains for relevant residues are shown as CPK colored sticks with C atoms in salmon for W196A$_{ox}$ and in light grey for WT$_{ox}$ and WT CTC structures. NAD($^+$/H)$_A$ and NADH$_B$ in the WT CTC structure are shown as CPK colored sticks with its C atoms in blue.

hAIF$_{\Delta 1-101}$ variants (UniProtKB O95831) were obtained by site-directed mutagenesis from Mutagenex® and then subcloned into the pET28a expression vector with a cleavable N-terminal His$_6$-tag similar to that reported for the WT protein [10]. The cDNAs encoding for human CypA (UniProtKB P62937), CHCHD4 (UniProtKB Q8N4Q1), and Histone H2AX (UniProtKB P16104) were synthetized with a cleavable N-terminal His$_6$-tag (CACCAT) and codon optimized for *Escherichia coli* expression by GenScript®. The coding sequences were subcloned into the pET28a expression vector between two restriction sites: NdeI-NotI for CypA and CHCHD4 and NcoI-NdeI for H2AX. The resulting constructs were used to transform the *E. coli* C41 (DE3) strain for heterologous protein expression. Proteins were expressed and purified as described in the supplementary materials.

2.2. Molecular Weight Determination by Size Exclusion Chromatography.
The hAIF$_{\Delta 1-101}$ variants, either in the presence or absence of a 10-fold excess of NADH, were loaded onto a HiPrep 26/60 Sephacryl™S-200 High Resolution (*GE Healthcare*, Chicago, IL) column attached to a fast pressure liquid chromatographic system (*GE Healthcare*, Chicago, IL). Protein elution was performed in 50 mM phosphate buffer, 150 mM NaCl, pH 7.4, at a flow rate of 0.5 mL/min. The column was previously calibrated with the GE Healthcare LMW calibration kit (6 proteins in the 6400-160000 Da range). The obtained chromatograms were fitted to a set of Gaussian functions.

2.3. Stabilization of Cross-Linked Protein Oligomers and Electrophoretic Analysis.
Reaction mixtures containing 4 μM of the hAIF$_{\Delta 1-101}$ variants in 10 mM phosphate, pH 7.4 were incubated with a 100-fold excess of the homobifunctional-bis[sulfosuccinimidyl]-suberate (BS^3) (Pierce) cross-linker at room temperature in the absence or presence of a 10-fold excess of NADH. Reactions were stopped by the addition of the denaturing bromophenol blue sample buffer and heated 5 min at 95°C. Sample mixtures were then resolved by 12% SDS-PAGE.

2.4. Spectroscopic Characterization.
UV-visible spectra were recorded in a Cary 100 Bio spectrophotometer (*Agilent*, Santa Clara, CA). Protein concentrations were determined using the molar absorption coefficients of each variant, which were estimated by protein denaturation with 3 M guanidinium chloride in 10 mM phosphate, pH 7.4, followed by quantification of the released FAD. The extinction coefficients for WT, W196A, W196L, and W196Y hAIF$_{\Delta 1-101ox}$ were $\varepsilon_{451nm} = 13.7$ M^{-1} cm^{-1} [10], $\varepsilon_{451nm} = 13.35$ M^{-1} cm^{-1}, $\varepsilon_{451nm} = 13.92$ M^{-1} cm^{-1}, and $\varepsilon_{452nm} = 14.01$ M^{-1} cm^{-1} respectively. Circular dichroism (CD) spectra were recorded in a thermostated Chirascan (*Applied Photophysics Ltd.*, Surrey, UK). Far-UV CD spectra were acquired using 1 μM protein in a 0.1 cm pathlength cuvette, while near-UV/Vis CD spectra were recorded using 20 μM protein in a 1 cm pathlength cuvette. Fluorescence spectra were recorded in a thermostated Cary Eclipse Fluorescence spectrophotometer (*Agilent*, Santa Clara, CA) using 2 μM protein in a 1 cm pathlength cuvette. Flavin fluorescence emission spectra were acquired in the 480-600 nm range upon excitation at 450 nm. Fluorescence emission spectra of aromatic residues were collected from 300 to 550 nm upon excitation at 280 nm. CD and fluorescence spectra were recorded in the absence and presence of a 100-fold excess of NADH at 10°C (folded state) and 90°C (thermally denatured state).

2.5. Thermal Denaturation Assays.

Thermal denaturation curves were followed by changes in the FAD fluorescence emission upon its release from the protein by sample excitation at 450 nm. Curves were monitored from 10 °C to 90 °C with scan rates of 1°C/min, both in the absence and presence of a 100-fold excess of NADH. The curves for each variant were roughly normalized to values between 0 and 1 and globally fitted to a two-step process describing a single transition unfolding equilibrium (native (N)↔unfolded (U)) by using the following equation [23]:

$$S_{\text{obs}} = \frac{S_N + m_N T + (S_U + m_U T)e^{-(\Delta G/RT)}}{1 + e^{-(\Delta G/RT)}}, \qquad (1)$$

in which S_{obs} is the measured protein signal at a given temperature (T). S_N and S_U are intercept at 0 K with the y-axis of the linear extrapolation for the native and unfolded pre- and posttransition regions, respectively, while m_N and m_U are the corresponding slopes. The stabilization Gibbs energy depends on temperature according to $\Delta G = \Delta H(1 - 1/T_m) + \Delta C_P(T - T_m - T \ln(T/T_m))$, where ΔH is the unfolding enthalpy, T_m is the midtransition temperature, ΔC_P is the unfolding heat capacity change, and R is the ideal gas constant.

2.6. Kinetics Measurements.

The steady-state diaphorase activity of hAIF$_{\Delta 1\text{-}101}$ variants was measured in air saturated 50 mM potassium phosphate, pH 8.0, using NADH as the substrate donor and 95 μM dichlorophenolindophenol (DCPIP, $\Delta \varepsilon_{620\text{nm}} = 21 \text{ mM}^{-1} \text{ cm}^{-1}$) as acceptor [10]. When saturation profiles on the pyridine nucleotide concentration were observed, kinetic constants were estimated by fitting initial reaction rates at different coenzyme concentrations to the Michaelis-Menten equation:

$$\frac{v}{e} = \frac{k_{\text{cat}}[\text{NADH}]}{K_m^{\text{NADH}} + [\text{NADH}]},$$

$$\frac{v}{e} = \frac{k_{\text{cat}}/K_m^{\text{NADH}}[\text{NADH}]}{1 + (k_{\text{cat}}/K_m^{\text{NADH}}[\text{NADH}]/k_{\text{cat}})}, \qquad (2)$$

where v stands for the initial velocity, e is the enzyme concentration, K_m^{NADH} is the Michaelis constant for the enzyme-NADH complex, k_{cat} is the turnover number of the enzyme, and $k_{\text{cat}}/K_m^{\text{NADH}}$ is the enzyme catalytic efficiency.

The reactivity of the CTC towards molecular oxygen was monitored by full reduction of hAIF$_{\Delta 1\text{-}101}$ samples with NADH (1.5-fold the concentration of the protein) in 50 mM phosphate buffer, pH 7.4, and following their reoxidation in a Cary 100 spectrophotometer (*Agilent*, Santa Clara, CA). Absorption spectra were recorded at 25 °C until full oxidation of the flavin cofactor was achieved. For each time, the percent remaining of CTC versus reoxidation by molecular oxygen was estimated as $\Delta A_t/\Delta A_{\text{max}}$, where ΔA_{max} is the difference between the minimum and the maximum absorbance at 700 nm, and ΔA_t is the difference of each value at 700nm minus the minimum absorbance at 700 nm. The CTC half-life is the time at which 50% of CTC still remains.

A SX18.MV stopped-flow spectrophotometer (*Applied Photophysics Ltd.*, Surrey, UK), interfaced with the ProData-SX software and a photodiode array detector, was used to investigate the fast kinetic reduction of the hAIF variants by the NADH coenzyme. Samples of ~10 μM hAIF$_{\Delta 1\text{-}101\text{ox}}$ were mixed with increasing concentrations of NADH (0.03-10 mM) under aerobic conditions in 50 mM potassium phosphate, pH 7.4, at 25 °C. The enzyme and NADH concentrations are the final ones obtained after mixing equal volumes of substrate and enzyme. Observed rate constants for the hydride transfer (HT) event (k_{obs}) were calculated by global analysis and numerical integration methods (simultaneously using all spectral data in the 400-800 nm region along time evolution). A single-step model (A→B) best fitted to describe the overall reaction at all NADH concentrations assayed. Averaged k_{obs} values at each NADH concentration were then fitted to the equation that describes the formation of an enzyme:substrate complex prior to the HT event:

$$k_{\text{obs}} = \frac{k_{\text{HT}}\text{NADH}}{K_d^{\text{NADH}} + \text{NADH}} + k_{\text{rev}}, \qquad (3)$$

where k_{HT} is the limiting rate constant for HT from the pyridine nucleotide coenzyme to the FAD cofactor of hAIF, K_d^{NADH} is the dissociation constant of the transient hAIF$_{\Delta 1\text{-}101\text{ox}}$:NADH complex, and k_{rev} is the reaction constant for a potential overall reverse process.

Stopped-flow spectrophotometry was also used to evaluate the rate constants of CTC formation when mixing photoreduced hAIF$_{\Delta 1\text{-}101}$ (hAIF$_{\Delta 1\text{-}101\text{phrd}}$) with increasing concentrations of NAD$^+$ (0.125-5 mM) under anaerobic conditions. hAIF$_{\Delta 1\text{-}101\text{phrd}}$ samples were obtained by photoreduction in the presence of 5 μM methyl viologen, 3 μM 5-deazariboflavin, and 20 mM EDTA. The assays were performed at 25 °C in 50 mM potassium phosphate, pH 7.4, under anaerobic conditions (obtained by several cycles of vacuum application and bubbling with O$_2$ free argon). Data were global fitted to a single step model (A→B), and k_{obs} were determined at the different NAD$^+$ concentrations assayed. These values were then fitted to the equation that describes the formation of a transient hAIF$_{\Delta 1\text{-}101\text{phrd}}$:NAD$^+$ complex prior to the CTC stabilization:

$$k_{\text{obs}} = \frac{k_{\text{CTC}}[\text{NAD}^+]}{K_d^{\text{NAD+}} + [\text{NAD}^+]}, \qquad (4)$$

in which k_{CTC} is the limiting rate constant for the rearrangement of the encounter complex to form the CTC, and $K_d^{\text{NAD+}}$ is the dissociation constant for the mentioned transient encounter complex.

2.7. Isothermal Titration Calorimetry (ITC).

ITC assays were carried out using an Auto-iTC200 (*MicroCal, Malvern-Panalytical*, Malvern, UK) thermostated at 25 °C. Typically, 10-20 μM protein partner and dsDNA samples—prepared as described below—were used to titrate ~10 μM hAIF$_{\Delta 1\text{-}101}$ variants. All solutions were degassed at 15°C for 1 min before each assay. A sequence of 2 μL injections of titrant solution

every 150 s was programmed, and the stirring speed was set to 750 rpm. The association constant (K_a), the enthalpy of binding (ΔH), and the binding stoichiometry (N) were estimated through nonlinear least-squares regression of the experimental data employing a single-ligand binding site model implemented in Origin 7.0 (*OriginLab*, Northampton, MA). The dissociation constant (K_d), the free energy change (ΔG), and the entropy change (ΔS) were obtained from basic thermodynamic relationships.

Since hAIF binds DNA unspecifically, a 0.5 mM dsDNA sample was prepared from 1 mM solutions of HPLC-purified forward and a reverse complementary 15-bp oligonucleotides (5′- GGT TAG TTA TGC GCG -3′; randomly designed) synthetized by Integrated DNA Technologies. The pair of oligonucleotides was mixed at an equimolar ratio and annealed by heating 1 min at 99°C and performing a 3 h temperature scanning from 95 to 25°C, decreasing 1°C each 3 min. 0.5 mM dsDNA stock solutions were obtained.

2.8. Generation of Structural Models. Models containing the missing C-loop residues (546–558 and 518-559, respectively, for crystal structures of WT hAIF$_{\Delta 1-101ox}$ and hAIF$_{\Delta 1-101rd}$:NAD$^+$ states), as well as W196A, W196L, and W196Y mutations, were built using as templates, the coordinates of WT hAIF$_{\Delta 1-101ox}$ (PDB 4BV6) and hAIF$_{\Delta 1-101rd}$:NAD$^+$ (PDB 4BUR) and the Swiss-Model server [7, 10, 24]. Routines for minimization and molecular dynamics (MD) simulations followed previous reported protocols [7] and are summarized in the supplementary materials. Improvements include using a time step of 2 fs and performing five replicas of 10 ns MD production for each model structure.

2.9. Data Analysis. Data were fit and shown using SigmaPlot (*Systat. Software Inc. Richmond*, CA, USA), Origin 7.0 (*OriginLab Corporation*, Northampton, MA), and Pro-K (*Applied Photophysics Ltd.*, Surrey, UK). VMD [25] and PyMol [26] were used to analyze and visualize structural data, as well as to produce structural figures.

3. Results and Discussion

3.1. Mutations at W196 Residue Hardly Impacts the Overall hAIF$_{\Delta 1-101}$ Core Conformational Properties in Oxidized and NADH-Reduced States. The three W196 variants here studied were purified to homogeneity as holoproteins after their expression in *E.coli* as described previously for the WT protein [10]. Their UV-visible absorption spectra showed the characteristic bands I and II of the flavin at 451 and 380 nm, respectively, a shoulder at 476 nm, and A_{280}/A_{451} ratio ≈11, indicating that, similarly to the WT protein, the cofactor was in the oxidized state and correctly incorporated to the protein (Figure S2A). Only W196A showed a distorted shape for band II and lower A_{451}/A_{380} ratio reflecting some differences in the environment of its flavin ring.

The W196 variants also had similar far-UV CD spectra to the WT protein, with minima at ~222 and ~208 nm indicative of high α-helix content (Figure S2B). Reduction of the FAD cofactor by NADH produced the decrease in relative intensity of minima at 208 nm for all mutants (Figure S2C),

as previously reported for the WT protein [7]. This suggests similar overall conformations in the CTCs. The near-UV/Vis CD spectra of the variants showed the WT characteristic maxima (~300 nm and ~365 nm) and minima (~453 and ~477 nm) (Figure S2D). Finally, changes observed upon incubation with NADH were also consistent with FAD reduction (lack of near-UV CD signal at 300 nm and in the 350-500 nm range) and CTC stabilization (new minima at ~405 nm and broad bands at ~600 nm) in all variants (Figure S2E) [7].

Since the crystal structure is only available for W196A$_{ox}$, we built structural models containing the W196 mutations, as well as the missed C-loop residues in the WT X-ray structures, to further evaluate the impact of mutations on the conformation of hAIF$_{\Delta 1-101ox}$ and its CTC [7, 10]. Models for oxidized variants, including W196A$_{ox}$, were built using the WT$_{ox}$ crystal structure as a template to better evaluate the effect of each mutation on native structures, thus preventing the other variant's models from being "forced" to behave as W196A$_{ox}$. After 10 ns MD relaxation, only small fluctuations within each simulated system were detected for averaged values of energy, radius of gyration, RMSD, and solvent accessible surface (SAS) of ligands, as well as for the main interactions coupling the FAD cofactor and NADH coenzyme to the protein (Figures S3A and S4). These observations contrast with those obtained when similarly evaluating the pathogenic deletion of residue R201 situated together with W196 in the β-hairpin and also contributing to C-loop linking [7]. This clinical ΔR201 variant rapidly breaks the network linking the FAD cofactor, the β-hairpin itself, the active site residues, the central β-strand, and the C-loop during the MD production [7]. Altogether, experimental and modelling evidences indicate that substitutions at W196 retain the WT hAIF$_{\Delta 1-101}$ architecture at the active site and the protein core, in both the oxidized and CTC states. In agreement, W196A$_{ox}$ was even able to crystallize [11].

3.2. W196 Side Chain Modulates the Monomer-Dimer Equilibrium in hAIF$_{\Delta 1-101}$. Gel filtration chromatography was used to study the impact of mutations on the ability of hAIF$_{\Delta 1-101}$ to undergo NADH-linked dimerization. While, similarly to the WT$_{ox}$ protein (Figure 2(a)) [10], the W196Y$_{ox}$ mutant eluted as a monomer of apparent molecular weight (appMW) ~45-58 kDa (Figure 2(b)), the W196L$_{ox}$ and W196A$_{ox}$ variants eluted as considerably broad peaks with lower exclusion volumes. Peak deconvolution suggested two populations with appMW of 63 and 115 kDa for W196L$_{ox}$ and 75 and 138 kDa for W196A$_{ox}$ (Figures 2(c) and 2(d), respectively), indicating less compact monomeric conformations and/or a quick monomer-dimer exchange. Upon incubation with NADH, the W196Y and W196L variants eluted mainly as a new peak of lower exclusion volume (~145-155 kDa) (Figures 2(b) and 2(c)) that was previously related to the CTC dimer in the WT protein (Figure 2(a)). Finally, the elution peak for W196A in the presence of NADH, when compared to W196A$_{ox}$, also gets narrower and slightly displaced towards the WT CTC dimer elution volume (Figure 2(d)).
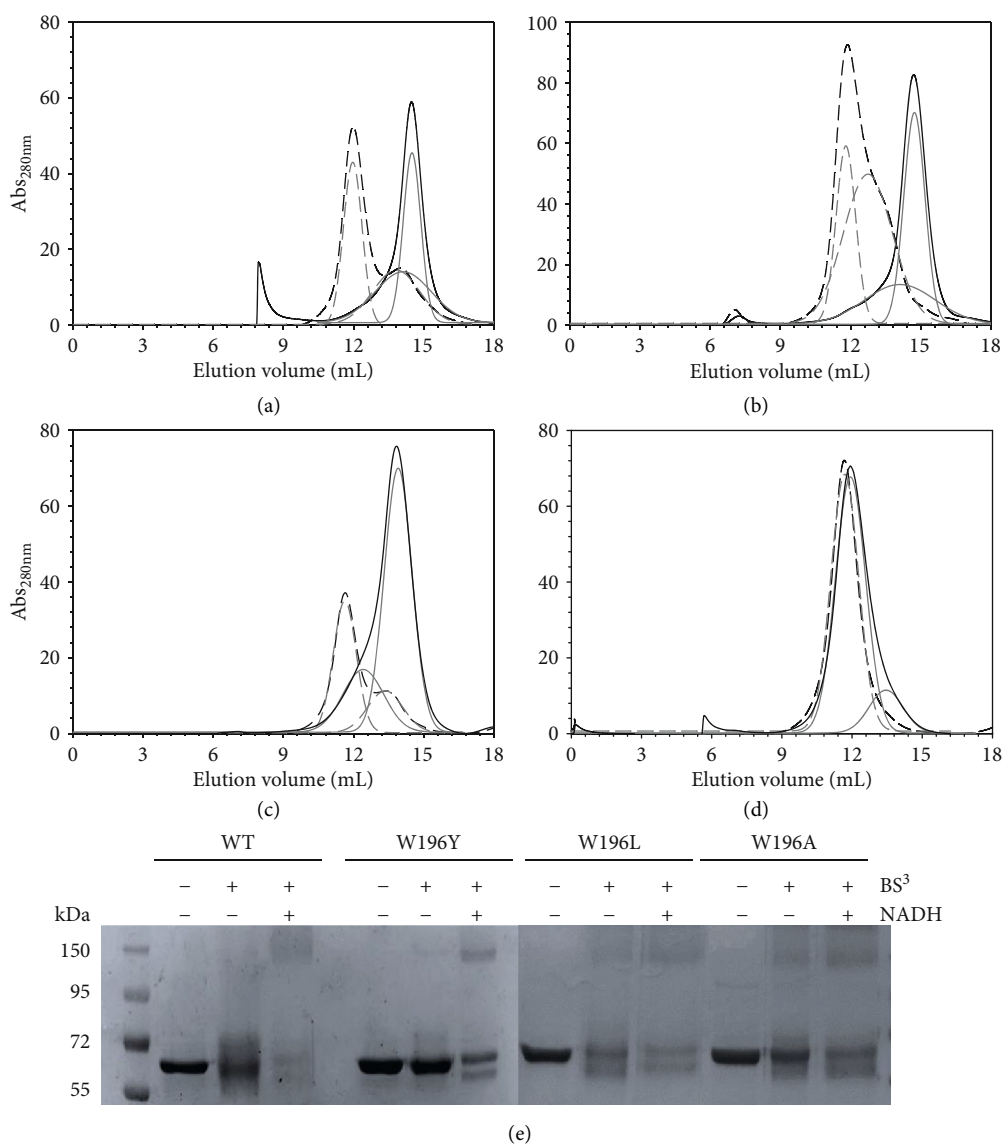
FIGURE 2: Effect of W196 replacement on the hAIF$_{\Delta1-101}$ ability to stabilize dimers. Elution profile of (a) WT, (b) W196Y, (c) W196L, and (d) W196A on a Sephadex S-200 column at 6°C. The assays were performed in absence and presence of a 10-fold excess of NADH, and profiles are, respectively, shown in black continuous and dashed lines. The respective different populations assigned by Gaussian analysis are depicted in grey lines. (e) Chemical cross-linking of hAIF$_{\Delta1-101}$ samples (~3 μM proteins) with a 100-fold excess of the BS^3 cross-linker in the absence and presence of NADH (300 μM). After 45 minutes of incubation, the reactions were stopped by the addition of bromophenol sample buffer and resolved by 12% SDS-PAGE.

Chemical cross-linking with BS^3—able to covalently conjugate hAIF dimers but not monomers—followed by assessment of species by SDS-PAGE (Figure 2(e)), was then used to evaluate whether the observed chromatographic changes might relate to W196 mutations influencing the compactness of protein conformation and/or the CTC dimer lifetime. Upon incubation with BS^3, all oxidized mutants exhibited the band of ~55 kDa corresponding to the hAIF$_{\Delta1-101ox}$ monomer, although it was in general more diffuse than in the cross-linker absence. When variants were preincubated with both NADH and BS^3, an additional broad band of ~170 kDa was detected. In WT hAIF$_{\Delta1-101}$, this band is related to the protein ability to undergo dimerization in the CTC state upon NADH binding and flavin reduction [10].

Noticeably, this band, indicative of dimer stabilization, was also observed for W196A$_{ox}$ (in the absence of the coenzyme), in agreement with the exclusion chromatography data obtained for this variant (Figure 2(d)) and with its reported dimeric crystal structure [11]. These data confirm that all W196 variants are able to dimerize upon NADH reduction, but also show that the mutations modulate the CTC dimer stability. They also suggest conformational changes that favor the displacement of the monomer-dimer equilibrium towards the dimer in the oxidized state, particularly in W196A$_{ox}$.

3.3. W196 Highly Contributes to Modulate the Low Efficiency of hAIF$_{\Delta1-101}$ as NADH Oxidase. Under physiological

TABLE 1: Steady-state and pre-steady-state kinetic parameters of WT $hAIF_{\Delta1\text{-}101}$ and its W196 variants.

hAIF	Steady-state				Pre-steady-sate				
	k_{cat} (s^{-1})	K_m^{NADH} (μM)	k_{cat}/K_m^{NADH} $(s^{-1}mM^{-1})$	k_{HT} (s^{-1})	K_d^{NADH} (μM)	k_{HT}/K_d^{NADH} $(s^{-1}mM^{-1})$	k_{CTC}^{1} (s^{-1})	K_d^{NAD+} (μM)	k_{CTC}/K_d^{NAD+} $(s^{-1}mM^{-1})$
WT	0.9 ± 0.1	495 ± 170	1.9 ± 0.9	1.5 ± 0.1	4090 ± 300	0.4 ± 0.1	45 ± 2	2080 ± 250	22 ± 3
W196Y	2.7 ± 0.1	505 ± 35	5.3 ± 0.6	12 ± 1	2870 ± 320	4.0 ± 0.8	16 ± 1	183 ± 27	87 ± 14
W196L	2.8 ± 0.1	187 ± 18	15 ± 1.9	36 ± 1	1725 ± 210	21 ± 3	29 ± 2	433 ± 11	67 ± 18
W196A	4.3 ± 0.2	25 ± 4	172 ± 35	126 ± 1	1070 ± 40	117 ± 5.3	30 ± 1	394 ± 50	76 ± 10

Assays were performed at 25°C in 50 mM potassium phosphate, pH 7.4 ($n = 3$, mean ± SD). [1]Kinetic parameters for CTC formations were obtained with $hAIF_{\Delta1\text{-}101phrd}$ variants.

conditions, hAIF exhibits a NADH oxidase activity that can be *in vitro* monitored using the steady-state DCPIP-dependent diaphorase reaction. When evaluated in this way, all W196 variants showed higher turnover rates than the WT protein (~3-fold increase for W196Y and W196L and ~5-fold for W196A) (Table 1). Regarding K_m^{NADH}, the W196Y variant value was similar to that for the WT, while the W196L and W196A variants showed a significant decrease (~3- and 10-fold, respectively). Thus, W196Y, W196L, and W196A variants were ~3, ~8, and~45 times more efficient oxidizing NADH than the WT protein. Nonetheless, despite these W196 variants are more efficient as oxidoreductases than WT $hAIF_{\Delta1-101}$, they were unable to oxidize NADH when using molecular oxygen as electron acceptor, analogously to the WT protein [10]. In the light of these results, we studied the impact of the W196 mutations on the HT reaction from NADH to the FAD cofactor of $hAIF_{\Delta1-101}$ by using stopped-flow transient kinetics. The kinetic traces recorded for all variants at different NADH concentrations indicated an essentially irreversible two-electron reduction of the FAD cofactor and the concomitant formation of a long wavelength broad band related to the stabilization of the $hAIF_{\Delta1-101rd}$:NAD$^+$ CTC species (Figure 3 and S5). The intensity of this CTC band (area in the 510−800 nm region minus that of the free protein) for W196A and W196Y variants was in the range of that observed for the WT [10], suggesting similar percentage of CTC stabilization. However, the lower intensity of W196L CTC band (~76%) indicates either different charge distribution between coenzyme and FAD rings in the CTC (suggestive of different CTC geometry) or reduction of the amount of the CTC stabilized. In all cases, global analyses of the spectral range time evolutions best fitted to a one-step model (A→B). Thus, the observed processes appeared including the fast formation of the transient $hAIF_{\Delta1-101}$:NADH reactive complex followed by the HT reaction and the CTC formation (Scheme 1). As a consequence, the conformational switches in β-hairpin and C-loop induce protein dimerization in W196 variants, with the potential exception of W196A that presumably might be mostly a dimer with the C-loop already released in the oxidized state [11]. The k_{obs} values obtained showed hyperbolic dependence on NADH concentration for all variants, allowing k_{HT} and K_d^{NADH} determination upon fitting to the equation (4) (Figure 3(e) and Table 1). All variants showed faster HT rate constants and higher affinity for the

NADH substrate than the WT protein (up to ~29- and 5-fold, respectively, for W196A). Consequently, W196Y, W196L, and W196A were ~12-, ~24-, and up to ~153-fold more efficient than the WT enzyme as hydride acceptors from NADH. Noticeably, and, contrary to that described for the WT protein, all these W196 variants showed k_{HT} values higher than their turnover rates, suggesting that for them, the HT reaction is not the limiting step during catalysis. Therefore, the W196 side chain highly contributes to modulate the properties of $hAIF_{\Delta1-101}$ as a nonefficient NADH oxidase.

Structurally, W196 does not form part of the protein redox active site itself. However, W196 side chain stacks to P488 at the edge of the central β-strand, contributing to situate the β-hairpin and the C-loop forming a cavity at the bottom of which sits W483—a residue that flanks the pyrimidine ring of FAD—(Figure 1(b)). W196A mutation increases W483 solvent accessibility and C-loop and β-hairpin flexibility, favoring their displacement from the WT_{ox} positions (Figures 1(c)–1(e) and 4). Noticeably, we observed the β-hairpin displacement from P488 as well as the central β-strand retraction from the beginning of our $W196A_{ox}$ model MD trajectories (starting from WT_{ox} structure) (Figure 5(a)). However, the Y196 and L196 side chains contribute to maintain β-hairpin position in the $W196Y_{ox}$ and $W196L_{ox}$ trajectories, and retraction of the central β-strand is hardly deduced for $W196L_{ox}$ (Figure 5(a)). Trajectories also show a larger increase in the SAS of the β-hairpin of $W196A_{ox}$ relative to the other two variants and the WT (Figure S3B). Thus, MD simulations predict an increase in distances between W483 and atomic positions at the active site of the oxidized variants (Figure S4A). Such changes in W483 solvent accessibility and active site compression must impact substrate affinity and coupling into a competent complex for HT, as well as the FAD midpoint reduction potential and/or electronic distribution—as was previously reported for the murine W196A variant (70 mV higher redox potential than those for the WT protein)—[9]. In agreement, kinetic parameters show W196A as the variant differing more from the WT behavior regarding efficiency for both HT and NADH binding, followed—by far—by W196L and being the aromatic substitution the one producing a milder effect. Dynamics of active site in CTCs show higher flexibility regarding oxidized state (Figure S4A-B), but WT CTC keeps its characteristic
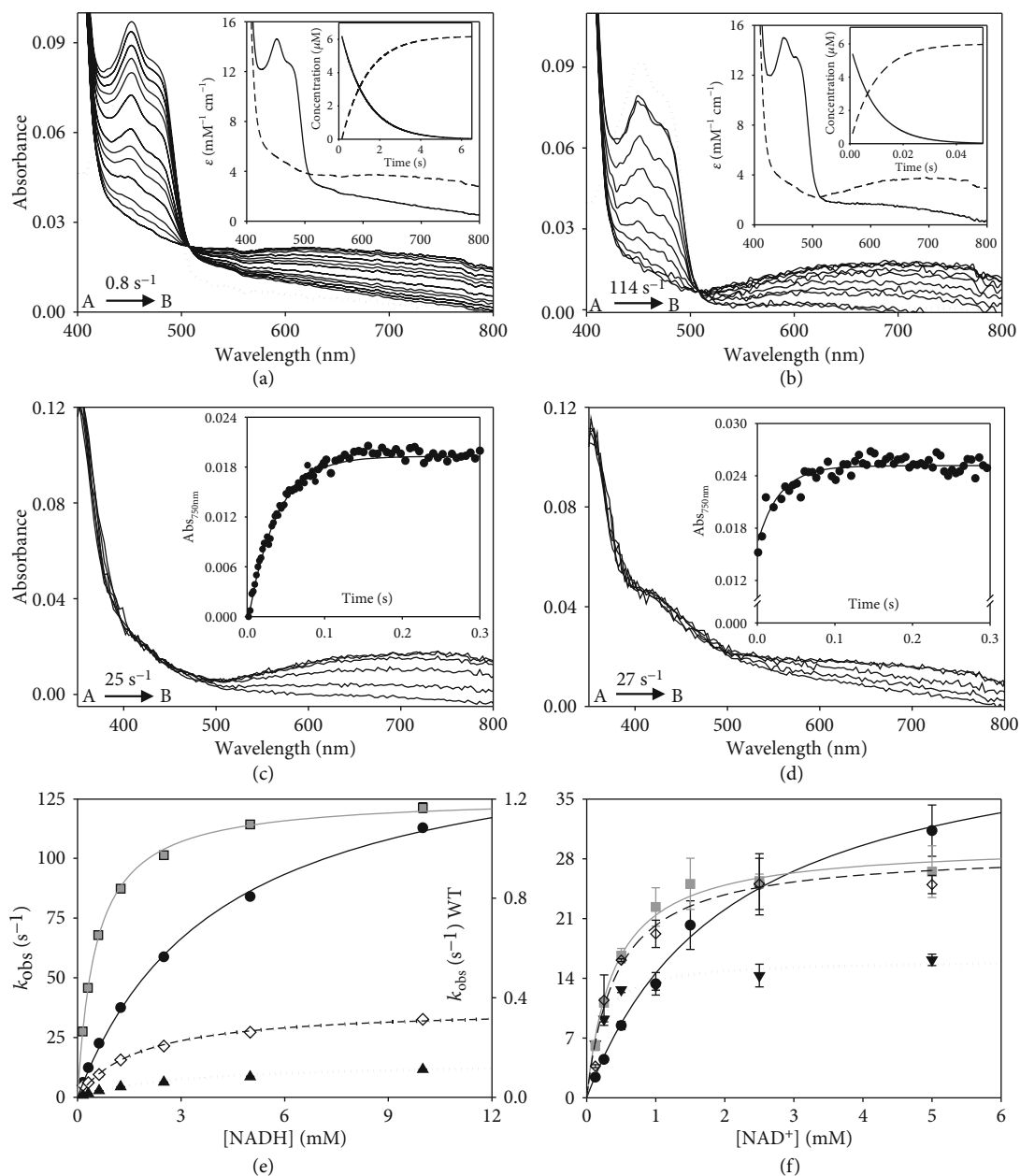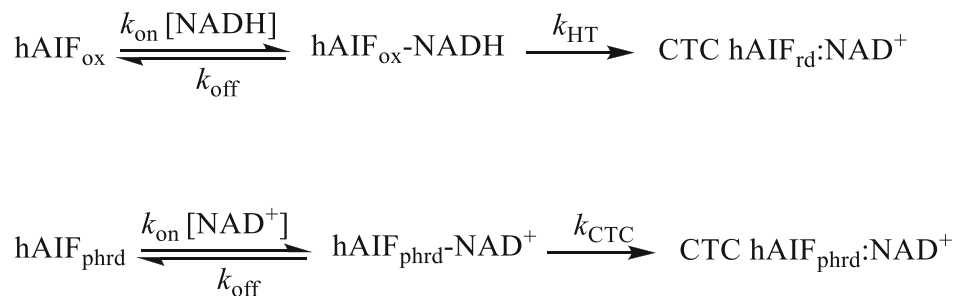
FIGURE 3: Kinetic characterization of W196 hAIF$_{\Delta1-101}$ variants. Spectral evolution of the reduction of (a) WT (~10 μM) and (b) W196A variant (~ 10 μM) when mixed with NADH (2 and 5 mM for WT and W196A, respectively). Spectra for the reduction of WT$_{ox}$ are shown at 0.15, 1.05, 2.1, 4.2, 6, 10.05, 12.45, 20.1, 30, 40.05, and 50.1 s after mixing and those for W196A at 0.005, 0.05, 0.1, 0.15, 0.2, 0.25, 0.3, 0.45, 0.5, and 0.55 s. Dotted lines correspond to the spectra of oxidized enzymes before mixing with the coenzyme. The corresponding insets show the absorbance spectra for the intermediate species obtained by fitting the spectral evolution to a single step model (A→B) and the evolution of the concentration of each species. Kinetics of CTC formation upon mixing of the hAIF$_{\Delta1-101phrd}$ forms of (c) WT and (d) its W196A variant with NAD$^+$ (5 mM) under anaerobic conditions. Spectral evolution for CTC formation of WT at 0.001, 0.005, 0.01, 0.015, 0.02, 0.07, 0.1, 0.15, 0.2, 0.33, 0.4, and 0.5 s after mixing and those for W196A at 0.001, 0.002, 0.005, 0.006, 0.007, 0.008, 0.009, 0.01, 0.03, 0.05, 0.07, 0.09, 0.1, 0.3, and 0.5 s. The corresponding insets show the absorption evolution at 750 nm (black circle) and the fits (continuous line) at this wavelength after globally fitting evolution at a single step model (A→B). (e) Dependence of the observed rate constants for flavin reduction for the WT (black circle), W196Y (black triangle), W196L (black diamond), and W196A (grey square) reactions on the NADH concentration. Lines represent the fits of experimental data to equation (3). (f) Dependence of observed rate constants for CTC formation when using WT (black circle), W196Y (black triangle), W196L (black diamond), and W196A (grey square) hAIF$_{\Delta1-101phrd}$ on the NAD$^+$ concentration. Lines represent the fit of experimental data to equation (4). Assays were performed in a stopped-flow spectrophotometer in 50 mM potassium phosphate, pH 7.4, and at 25°C (n = 3, mean ± SD).

$$\text{hAIF}_{ox} \xrightarrow[k_{off}]{k_{on}\,[\text{NADH}]} \text{hAIF}_{ox}\text{-NADH} \xrightarrow{k_{HT}} \text{CTC hAIF}_{rd}\text{:NAD}^+$$

$$\text{hAIF}_{phrd} \xrightarrow[k_{off}]{k_{on}\,[\text{NAD}^+]} \text{hAIF}_{phrd}\text{-NAD}^+ \xrightarrow{k_{CTC}} \text{CTC hAIF}_{phrd}\text{:NAD}^+$$

SCHEME 1.

parallel ionic pair through stacking of the NAD^+ nicotinamide and $FADH^-$ isolloxazine reacting rings (Figure S4D). In such arrangement, the angle formed between the C4n hydride donor of the nicotinamide of the coenzyme, the hydride to be transferred and the N5 acceptor atom of the FAD isolloxazine ring (C4n-hydride-N5) appears far from collinearity, involving a large free energy penalty for geometric deformations and partial loss of the π stacking interaction to achieve the transition state [27, 28]. Therefore, despite the C4n-N5 distance being compatible with HT, the hydride shift can be quite inefficient. This seems to be the situation for HT in WT, showing inefficient k_{cat} and k_{HT} values for NADH oxidation. Noticeably, MD simulations for the W196 CTC variants suggest the distortion of the $FADH^-$:NAD^+ pair and the pulling apart of C4n and N5 reacting atoms (Figure S4C). This effect is observed in W196A and W196L CTCs and to a lower extent in W196Y CTC, in agreement with improvement in their k_{HT} parameters. Therefore, the size and aromaticity of the side chain of W196 in hAIF$_{\Delta 1-101}$ are key to fix the β-hairpin position and, despite not forming part of the active site itself, set the active site geometry to make it a nonefficient NADH oxidase.

3.4. W196 Contributes to Stabilize the CTC State.

Changes above detected in K_m^{NADH} and K_d^{NADH} envisage an important impact of mutations at W196 on the association/dissociation equilibria of NADH and NAD^+ to hAIF$_{\Delta 1-101}$. Therefore, we proceeded to evaluate transient rate constants for CTC formation as well as stability of the CTCs once formed. To determine rate constants for CTC formation, we mixed hAIF$_{\Delta 1-101phrd}$ samples with different concentrations of NAD^+ in the stopped-flow equipment (Figures 3(c) and 3(d), and Figure S5). For all W196 variants, kinetic traces showed CTC formation following an essentially irreversible two-species process with k_{obs} values showing hyperbolic dependence on NAD^+ concentration (Figure 3(f)). This allows to determine K_d^{NAD+} as well as the limiting kinetic constant related to the establishment of the nicotinamide:isolloxazine electronic exchange within the CTC species (k_{CTC}) (Table 1, Scheme 1). Mutations at W196 produce a strong impact in K_d^{NAD+}, whose value decreases ~5-fold in the Leu and Ala variants and up to ~11-fold in the Tyr one. This indicates stronger affinity for NAD^+ in the case of the reduced mutants regarding the WT counterpart. On the contrary, the introduced mutations slightly decrease k_{CTC} values

(up to less than 3-fold for W196Y). Therefore, W196 replacement induces stronger affinity of hAIF$_{\Delta 1-101phrd}$ for NAD^+ relative to the oxidized state, but hardly influences the kinetic evolution of the initial transient interacting complex to achieve the final CTC conformation. These data indicate that replacements at W196 kinetically favor CTC formation by increasing the hAIF$_{\Delta 1-101phrd}$ affinity for NAD^+. Noticeably, comparing K_d^{NADH} and K_d^{NAD+} values (Table 1), all W196 variants increase the thermodynamic preference for the binding of NAD^+ over that for NADH regarding the WT. This agrees with the high impact of mutations on k_{HT} becoming considerably milder in k_{cat} values, where release of the NAD^+ product will limit the overall oxidoreductase activity.

We then evaluated the mutational effect on reactivity towards O_2 for the CTC formed upon NADH oxidation. As shown in Figure 6(a), the W196A CTC was highly stable versus reoxidation by O_2, similarly to the WT CTC, (half-lives of 62 and 72 min, respectively), while CTC lifetimes were slightly shorter for W196Y and W196L (half-lives of 42 and 32 min, respectively). Therefore, Tyr and Leu replacements favor O_2 access to the FAD cofactor in the CTC. Altogether, these observations point to W196 and the β-hairpin conformation also contributing to the strength of NADH/NAD^+ binding to the hAIF active site.

3.5. W196 Mutations Reduce Thermostability of hAIF$_{\Delta 1-101ox}$, but Not of the CTCs.

Fluorescence emission curves reflecting FAD release upon protein thermal denaturation were then obtained to evaluate the effect of W196 substitution on FAD binding and hAIF$_{\Delta 1-101}$ stability (Figure 6(b) and Table 2). All W196$_{ox}$ variants were less stable than WT$_{ox}$, with T_m^{FAD} dramatically decreasing between ~8 and ~11 °C. Formation of the WT CTC upon NADH mixing has an even more negative impact in WT hAIF$_{\Delta 1-101}$ stability, decreasing T_m^{FAD} for the CTC ($T_{m\,CTC}^{FAD}$) by ~13 °C relative to T_m^{FAD} [7]. This destabilizing effect was related to release of the regulatory C-loop in the hAIF$_{\Delta 1-101}$ apoptotic domain promoting looser tertiary structure contacts at the active site fostering cofactor dissociation [7]. Interestingly, all reduced CTC variants showed similar $T_{m\,CTC}^{FAD}$ to the WT CTC. This reflects that CTC formation induces a considerably lower destabilizing effect in W196L and W196Y relative to their oxidized states than in the WT case ($T_{m\,CTC}^{FAD}$ ~2 and ~6 °C lower than their T_m^{FAD}, respectively), while no destabilization is produced at all for W196A. These data suggest that the decrease in
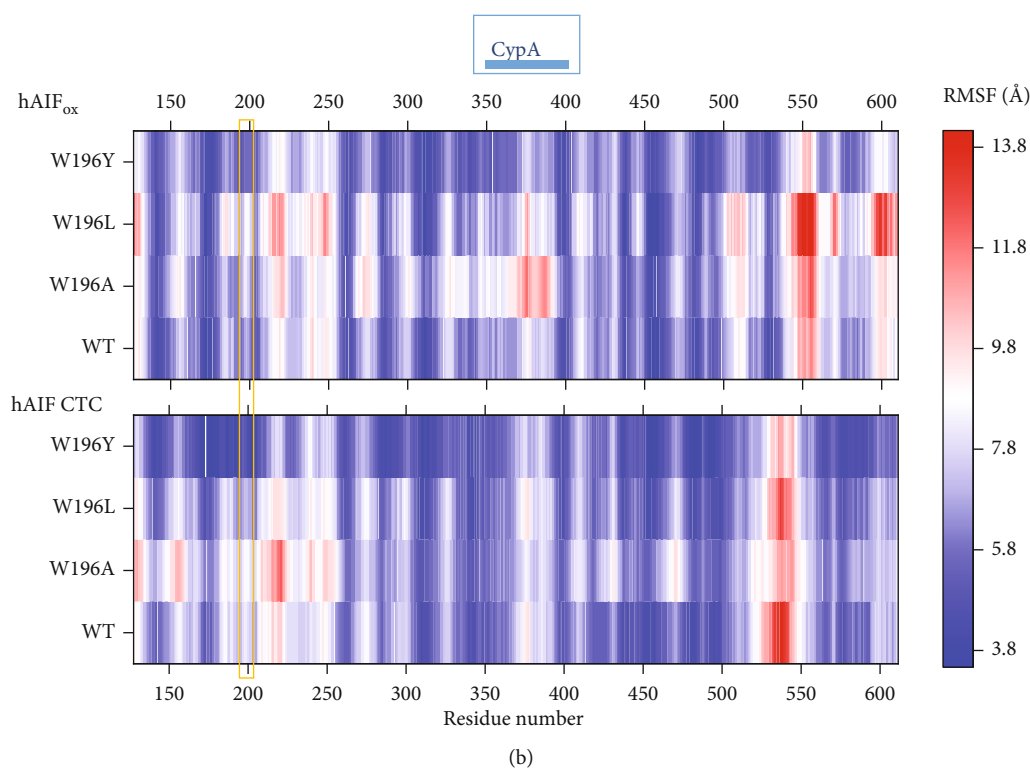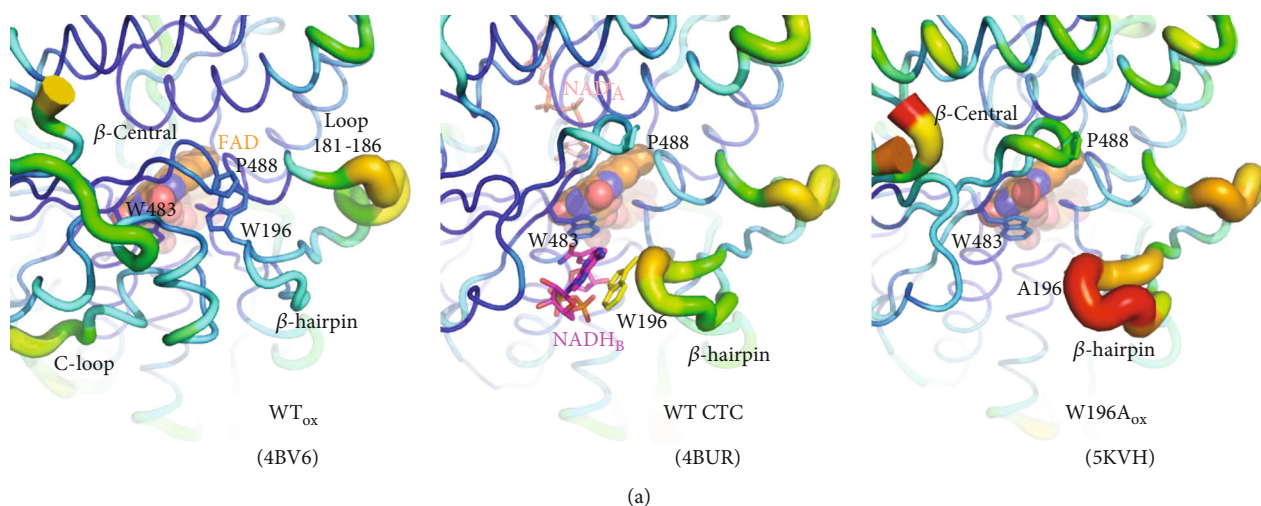
(a)

(b)

FIGURE 4: Impact of mutations on hAIF$_{\Delta1-101}$ flexibility. (a) B-factor putty representation of crystal structures of WT hAIF$_{\Delta1-101ox}$ (4BV6), WT CTC (4BUR), and W196A hAIF$_{\Delta1-101ox}$ (5KVH) focusing in the environment of the β-hairpin containing residue 196 and the central β-strand. Orange to red colors and a wider tube indicate regions with higher B-factors, whereas shades of blue and a narrower tube indicate regions with lower B-factors. The FAD cofactor is shown as sphere representation with carbons in orange, while, when present, the NAD^+_A and NADH$_B$ are shown as sticks with carbons in salmon and pink, respectively. (b) Heat map representation of the average Cα root mean square fluctuation (RMSF) of five replicates for 10 ns MD simulations of the different W196 variants in both the hAIF$_{\Delta1-101ox}$ and CTC states. The region corresponding to the β-hairpin is highlighted with an orange square and that predicted for interaction of CypA is indicated on the top of the panel.

compactness of the hAIF$_{\Delta1-101ox}$ active site depends on W196 mutation. In agreement, structural predictions indicate that W196A$_{ox}$ has a larger propensity for β-hairpin release, increasing of β-hairpin SAS as well as conformational rearrangement of the central β-strand and the loop connecting it to the His-rich helix (Figure 5 and Figure S3B). Thus, W196A$_{ox}$ backbone dynamics at these regions envisages a behavior more similar to the CTC than

to WT$_{ox}$, while an intermediate situation appears for W196L$_{ox}$ and W196Y$_{ox}$ (Figures 5(c) and 5(d)). On this side, the very low impact of mutations on T^{FAD}_{mCTC} agrees with conformational rearrangements already produced upon CTC formation, having the W196 side chain less relevance in contributing to the active site compactness. Finally, since, according to the WT CTC crystal structure, the W196 side chain contributes to stack the adenine
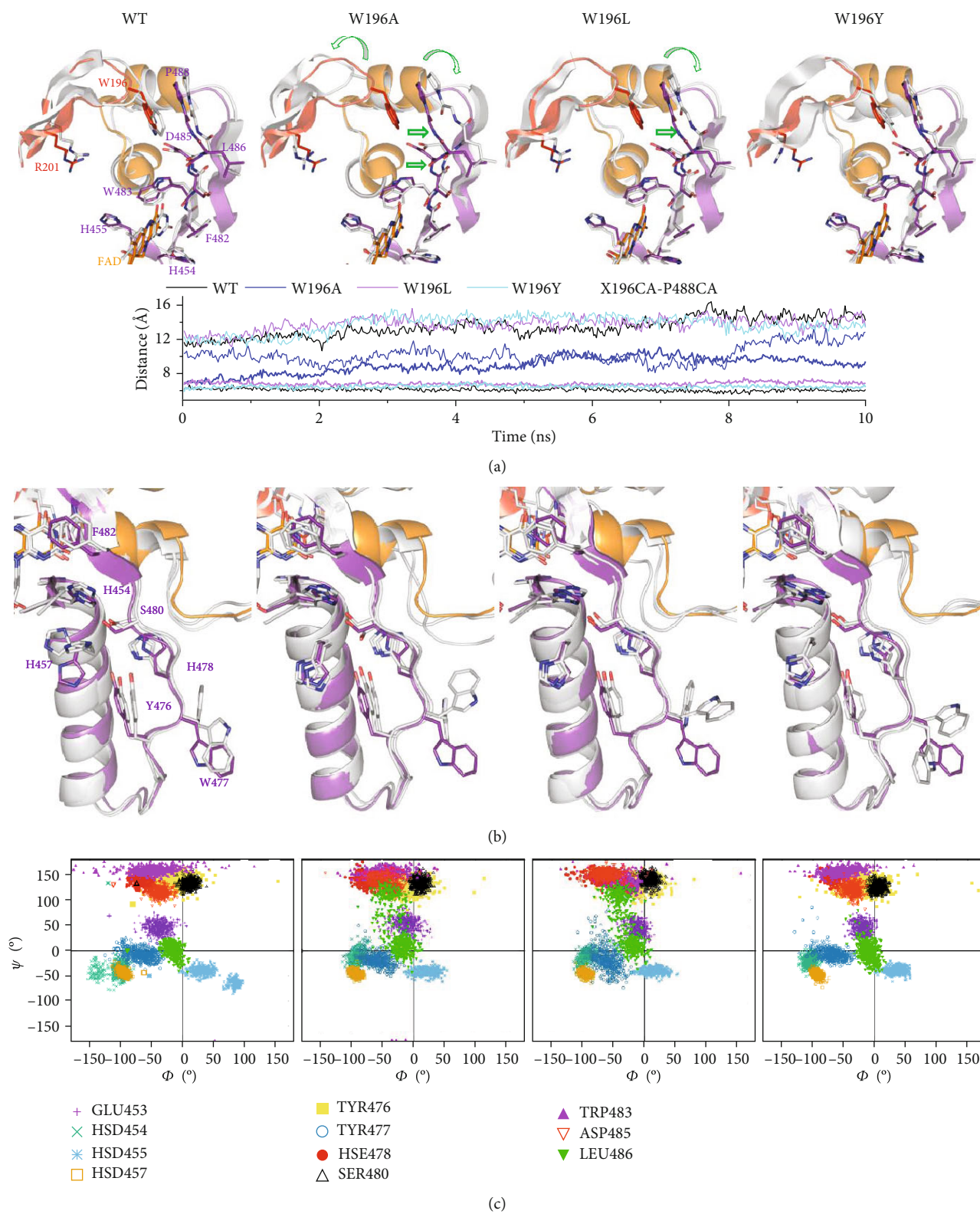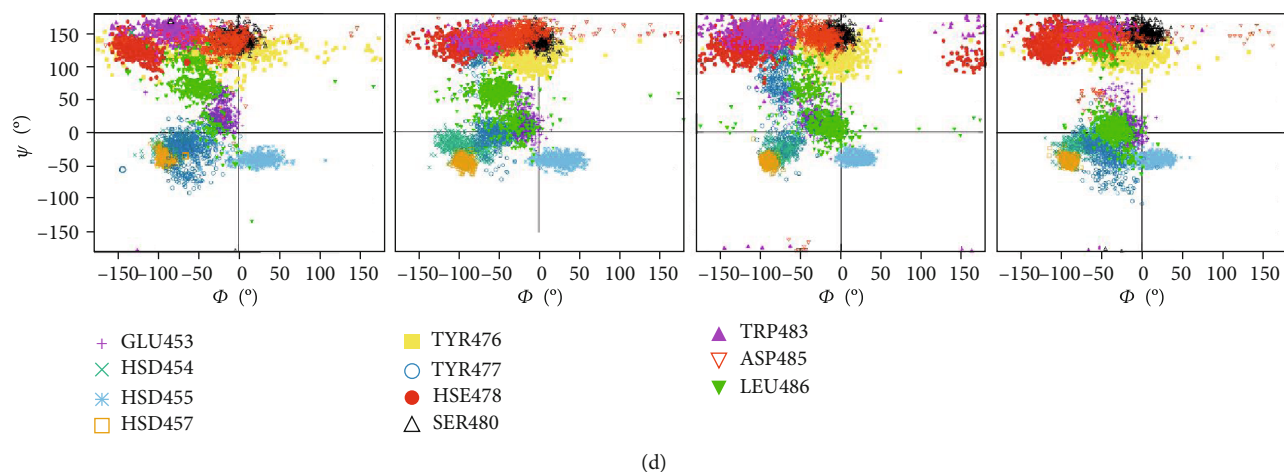
(a)

(b)

(c)

Figure 5: Continued.

(d)

FIGURE 5: Impact of W196 $hAIF_{\Delta 1-101}$ mutations on the dynamics of the β-hairpin and its environment. Representative conformations of the (a) β-hairpin and the central β-strand and the (b) His-rich helix and the loop connecting it to the central β-strand in final MD structures of selected replicates for each $W196_{ox}$ variant. MD final replicates are shown in grey in each panel. All panels compare to the crystallographic WT_{ox} structure (4BV6) that shows the β-hairpin in red, the C-loop in orange, and the rest of the protein in purple. Open green arrows indicate relevant displacements of structural elements relative to the crystallographic WT_{ox} structure. The lower panel in (a) shows the time evolution of the distances between Cαs of the residue at position 196 in the β-hairpin and P488 in the β-sheet. For each variant, data show averaged values for the 5 MD replicates run for each model in the $hAIF_{\Delta 1-101ox}$ (bold lines) and CTC (line) states. Ramachandran plots of the distribution of key main chain Φ/ψ conformational along the MD of selected replicates for each (c) oxidized and (d) reduced W196 variant.

moiety of $NADH_B$ (Figure 1(e)), such lack of effect is suggestive of $NADH_B$ binding being considerably weaker than that of $NADH_A$. This is clearly supported by the larger SAS for $NADH_B$ over $NADH_A$ in the MD simulations, which is in addition independent of the W196 variant considered (Figure S3A). Therefore, these thermal stability analyses suggest that mutations at W196 decrease the compactness of $hAIF_{\Delta 1-101ox}$. Noticeably, some of the pathogenic mutations located at β-hairpin, such as ΔR201, or involved in interaction between the β-hairpin and the regulatory C-loop, such as F210S/L, are reported to also show diminished compactness and/or stability [7, 29, 30].

3.6. W196 Contributes to Modulate the Conformation of the Interaction Surfaces of $hAIF_{\Delta 1-101}$ with Its Physiological Partners. AIF plays a key role in cell death and life through its interaction with nucleotides, but also with DNA and a broad number of proteins. We selected some representative ligands to evaluate the mutational effect of W196 on the hAIF interaction network: CHCHD4 as a mitochondrial partner key in OXPHOS and energy homeostasis, as well as the nuclease CypA and DNA as nuclear partners for chromatinolysis and PCD. We determined the binding parameters that describe the formation of binary complexes using ITC (Table 3, Figure 7 and S7). Due to the observed W196L tendency to denature during ITC assays, these studies were restricted to WT, W196A, and W196Y variants. For all ligands, the binding isotherms adequately fitted to a model of a single binding site with K_d in the micromolar range.

A number of evidences place CHCHD4 in the pathway linking hAIF to the biogenesis of mitochondrial complexes by facilitating the mitochondrial import of CHCHD4 and its proper localization in IMS [12]. Nonetheless, heat

exchange was not observed when titrating WT_{ox} and $W196Y_{ox}$ with CHCHD4, resulting in binding thermogram characteristic of noninteracting systems (not shown). In contrast, the titration of $W196A_{ox}$ with CHCHD4 revealed a strong binding of CHCHD4 to $W196A_{ox}$ ($K_d\sim$0.4 μM). Binding was entropically driven with the enthalpic contribution being unfavorable (Figure 7(c) and S8A) and suggesting that nonspecific forces contribute to this interaction. When we analyzed the interaction of all CTC variants—obtained by preincubation with NADH—with CHCHD4 (Figure 7 and S8A), binding was detected, in agreement with previous studies that described such interaction as NADH dependent [13]. The WT CTC:CHCHD4 interaction was driven by a large favorable enthalpic contribution indicative of specific binding, while the entropic contribution was unfavorable. This suggests a structurally more organized complex than its separated protein components. W196Y CTC and W196A CTC showed a thermodynamic profile similar to that of WT CTC, but the mutations decreased the magnitude of the favorable enthalpic contribution to the binding and made the entropic term considerably less and slightly more unfavorable, respectively. Regarding CHCHD4 affinity, no significant effect was produced by the alanine substitution in both redox states relative to WT CTC, but the W196Y CTC significantly decreased it ($K_d\sim$10-fold higher). Structurally, $W196A_{ox}$ in solution appears to be mainly a dimer with a disordered C-loop [11], sharing these features with WT CTC. Thus, our data might support an essential role of the arrangement of either the dimer conformation or the site exposed by C-loop displacement or even the C-loop itself in the interaction with CHCHD4. Such observations agree with deletion mutants and pathogenic point mutations at the NADH domain of hAIF that compromise NADH oxidase activity
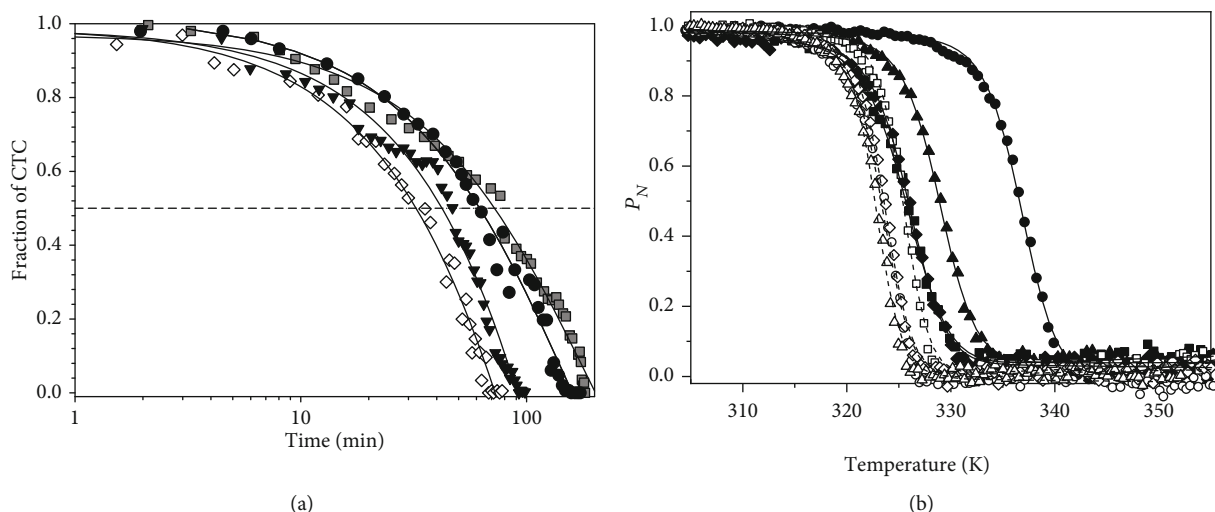
(a)

(b)

FIGURE 6: Effect of W196 replacements on the CTC half-life and the thermal stability of hAIF$_{\Delta1-101}$. (a) Reactivity of the CTC towards O$_2$ in W196 hAIF$_{\Delta1-101}$ variants. hAIF$_{\Delta1-101\text{rd}}$:NAD$^+$ CTC decay was monitored at 750 nm and 25°C in air saturated 50 mM potassium phosphate at pH 7.4. CTC hAIF$_{\Delta1-101\text{rd}}$:NAD$^+$ samples were obtained by mixing hAIF$_{\Delta1-101\text{ox}}$ variants with NADH (0.7-fold the enzyme concentration). The traces for WT (black circle), W196Y (black triangle), W196L (black diamond), and W196A (grey square) hAIF$_{\Delta1-101}$ are shown normalized from 1 to 0 as fraction of CTC remaining along the time. The solid line represents the fit of the traces to a single-exponential decay process to determine CTC half-life. (b) The thermal stability for flavin release (T_m^{FAD}) of hAIF$_{\Delta1-101}$ variants. Curves for FAD thermal release in oxidized variants (closed symbols) and its CTC state (open symbols), as monitored by increase in FAD fluorescence emission upon protein denaturation. The WT, W196A, W196L, and W196Y hAIF$_{\Delta1-101}$ are in black circle, black square, black diamond, and black triangle, respectively. The curves are roughly normalized to the change in fluorescence signal of the FAD bound fraction (P_N, from 1 to 0), with their fits to a two-transition unfolding model (continuous and dashed lines for oxidized and reduced states, respectively). Decrease in FAD bound fraction was experimentally followed by the increase in its fluorescence upon release from the holoprotein along a 20 to 85°C temperature ramp. Data were obtained in 50 mM potassium phosphate at pH 7.4 and at a final ionic strength of 150 mM. Protein concentration was ~2 μM. The CTC forms were obtained by premixing hAIF$_{\Delta1-101\text{ox}}$ and NADH at a 1:100 ratio.

TABLE 2: Thermal stability for flavin release of WT and W196 hAIF$_{\Delta1-101}$ variants in oxidized and CTC states.

| hAIF | hAIF$_{\Delta1-101\text{ox}}$ | | | CTC hAIF$_{\Delta1-101\text{rd}}$:NAD$^+$ | | | |
	T_m^{FAD} (K)	ΔH (kcal/mol)	ΔT_m^{FAD} (K)	$T_{m\text{CTC}}^{\text{FAD}}$ (K)	ΔH (kcal/mol)	$\Delta T_{m\text{CTC}}^{\text{FAD}}$ (K)	$T_{m\text{CTC}}^{\text{FAD}} - T_m^{\text{FAD}}$ (K)
WT	337 ± 1	128 ± 3	–	324 ± 1	150 ± 4	–	−13 ± 2
W196Y	329 ± 1	123 ± 3	−8 ± 2	323 ± 1	167 ± 4	−1 ± 2	−6 ± 2
W196L	326 ± 1	118 ± 3	−11 ± 2	324 ± 1	159 ± 4	0	−2 ± 2
W196A	326 ± 1	103 ± 3	−11 ± 2	326 ± 1	170 ± 4	2 ± 2	0

Values obtained by fitting fluorescence thermal denaturation curves to a two-state unfolding model. Data obtained in 50 mM potassium phosphate, pH 7.4, at a final ionic strength of 150 mM, from 283.15 to 363.15 K. Protein concentrations was ~2 μM, and NADH concentration was in 100-fold excess ($n = 3$, mean ± SD).

and CTC structural rearrangements, consequently affecting CHCHD4 binding and resulting in mitochondriopathy phenotypes [13, 31]. However, the W196A$_{\text{ox}}$ enthalpic/entropic thermodynamic binding profile for CHCHD4 indicates nonspecific interactions, while those for CTCs suggest specific organized interactions (Figure S8, Table 3). A defined interacting region for CHCHD4 has not been identified yet in hAIF, suggesting a relevant role for its entire ternary organization. On the contrary, CHCHD4 binds through a short N-terminal 27-amino-acid-long fragment, and its redox state appears irrelevant for the interaction. Moreover, this N-terminus is unstructured when CHCHD4 is free [32], but appears to get a defined and organized structure

when interacting with the CTC [13]. This agrees with our data that clearly indicates a specific CHCHD4 binding to WT CTC. On the contrary, the thermodynamic parameters here reported for CHCHD4 binding to W196A$_{\text{ox}}$ suggest that, despite the conformational changes produced by the mutation, CHCHD4 recognition is allowed and the complex formed will be far from the specific interaction presumably produced with WT CTC. Therefore, structural NADH-dependent changes in AIF must play a key role in the binding of CHCHD4. This is further supported by the Tyr and Leu replacements in W196 also having a strong impact in the specificity and organization of this interaction. Altogether, these observations suggest that (i)

TABLE 3: Thermodynamic parameters for the binary interaction of $hAIF_{\Delta 1-101}$ variants with CHCHD4, CypA, and DNA.

$hAIF_{\Delta 1-101}$ form	Titrating ligand	K_d (μM)	ΔH (kcal/mol)	ΔG (kcal/mol)	$- T\Delta S$ (kcal/mol)
WT_{ox} and $W196Y_{ox}$	CHCHD4		No detected binding		
$W196A_{ox}$	CHCHD4	0.4	9.6	-8.4	-18.0
WT CTC	CHCHD4	0.2	-20.1	-8.7	11.4
W196Y CTC	CHCHD4	2.1	-8.2	-7.5	0.7
W196A CTC	CHCHD4	0.5	-5.9	-8.3	14.2
WT_{ox}	CypA	2.7	-24.5	-7.3	17.2
$W196Y_{ox}$	CypA	1.0	17.0	-7.9	-24.9
$W196A_{ox}$	CypA	1.8	27.3	-7.6	-34.9
WT_{ox}	dsDNA	1.6	4.8	-7.6	-12.4
$W196Y_{ox}$	dsDNA	6.9	19.2	-6.8	-26.0
$W196A_{ox}$	dsDNA	5.8	15.0	-6.9	-22.0

Values obtained from ITC assays at 25°C in 50 mM potassium phosphate, pH 7.4. n is the calculated biding stoichiometry. The thermodynamic parameters were calculated by $K_d = (K_a)^{-1}$, $\Delta G = RT.\ln K_d$, and $-T\Delta S = \Delta G - \Delta H$. Errors considered in the measured parameters (±20% in K_d and ±0.3 kcal/mol in ΔH and $-T\Delta S$) were taken larger than the standard deviation between replicates and the numerical error after the fitting analysis.

the competent interaction of hAIF with CHCHD4 relies on the adequate CTC architecture to favor the assembly of potentially disordered regions from both proteins to achieve a specific conformation. (ii) W196 contributes to provide such CTC architecture, by potentially regulating the proper β-hairpin configuration that is key for the structural transition of hAIF and its role in mitochondrial homeostasis. In agreement, a nonproductive interaction between hAIF and CHCHD4 has been suggested for the clinical mutation F210L that results in abnormal assembly of mitochondrial complexes I and III [30].

Parameters for the titration of WT_{ox} with CypA indicated the enthalpically driven formation of a binary complex with unfavorable entropic binding contribution (Table 3, Figures S7A and S8B). This agrees with the large number of electrostatic contacts reported for the CypA interaction with the AIF synthetic peptide (370-394) [33–35], as well as with the complex adopting a large complementarity of the two proteins. Noticeably, the enthalpic contribution to the CypA binding turned into unfavorable for $W196Y_{ox}$ and $W196A_{ox}$ (Table 3, Figures S7B-C and S8B). However, this is compensated by a change in the sign of the binding entropic contribution that became highly favorable and made the mutational effect being insignificant regarding overall affinity (enthalpy-entropy compensation). Nevertheless, the mutational switch in thermodynamic contributions to the hAIF:CypA interaction suggests specificity decrease and production of nonnative-like conformations. This is interesting, because W196 and the β-hairpin do not share the protein surface with the AIF NADH domain where the 370-394 β-strand (binding spot for CypA) is situated (Figures S8E and S9). Nonetheless, replacements at W196 have important effects in $hAIF_{\Delta 1-101ox}$ stability (Table 2), as well as in the conformation of the C-loop, the central β-strand, and the dimerization interface located far away from W196. Therefore, conformational changes occurring in the β-hairpin might be also transmitted to the CypA binding site identified in

hAIF. These conformational changes on one side might hinder charge contacts of the 370-394 β-strand to CypA, while on the other they might favor CypA binding to hAIF by C-loop structural transition towards a more organized and favorable conformation as indicated by the entropy becoming favorable. In agreement, reduction of the flexibility of a stapled hAIF (370-394) peptide analogue constructed to stabilize its β-strand organization as in hAIF considerably improved its affinity for CypA [35]. Therefore, the higher specificity of WT_{ox} for CypA versus the $W196_{ox}$ variants might derive from its increased conformational rigidity favoring a lock-and-key mechanism of recognition, while increasing protein flexibility turns into an unspecific interaction.

Finally, positive charges clustered along the AIF surface are likely to contribute to DNA binding, but a clear sequence specificity is not expected since AIF recognizes DNA and RNA, as well as a large panel of ribonucleoproteins [36]. Our thermograms for WT_{ox} titration with dsDNA further confirm such lack of specificity, since they show an entropically driven binding with an unfavorable enthalpy contributing to the interaction (Figures S7D and S8C, Table 3). W196A and W196Y mutations hardly impair the $hAIF_{\Delta 1-101ox}$ affinity for DNA in binary complexes (K_d values~4-fold higher than WT). However, although thermodynamic patterns resembled the WT ones, the entropic and enthalpic binding contributions for W196A and W196Y variants were more favorable and less unfavorable, respectively (Figures S7E-F and S8C, Table 3). Structurally, binding of DNA to $hAIF_{ox}$ is proposed to occur through the nucleotide strand wrapping around a positively charged protein crown. This crown appears considerably modulated in shape as well as in accessibility when comparing crystallographic WT_{ox} to $W196A_{ox}$ structure as well as in MD models for all variants (Figure S9), in agreement with the modulation observed in experimental binding parameters.

Altogether, these results show that the W196 side chain influences the enthalpic and entropic contributions to the
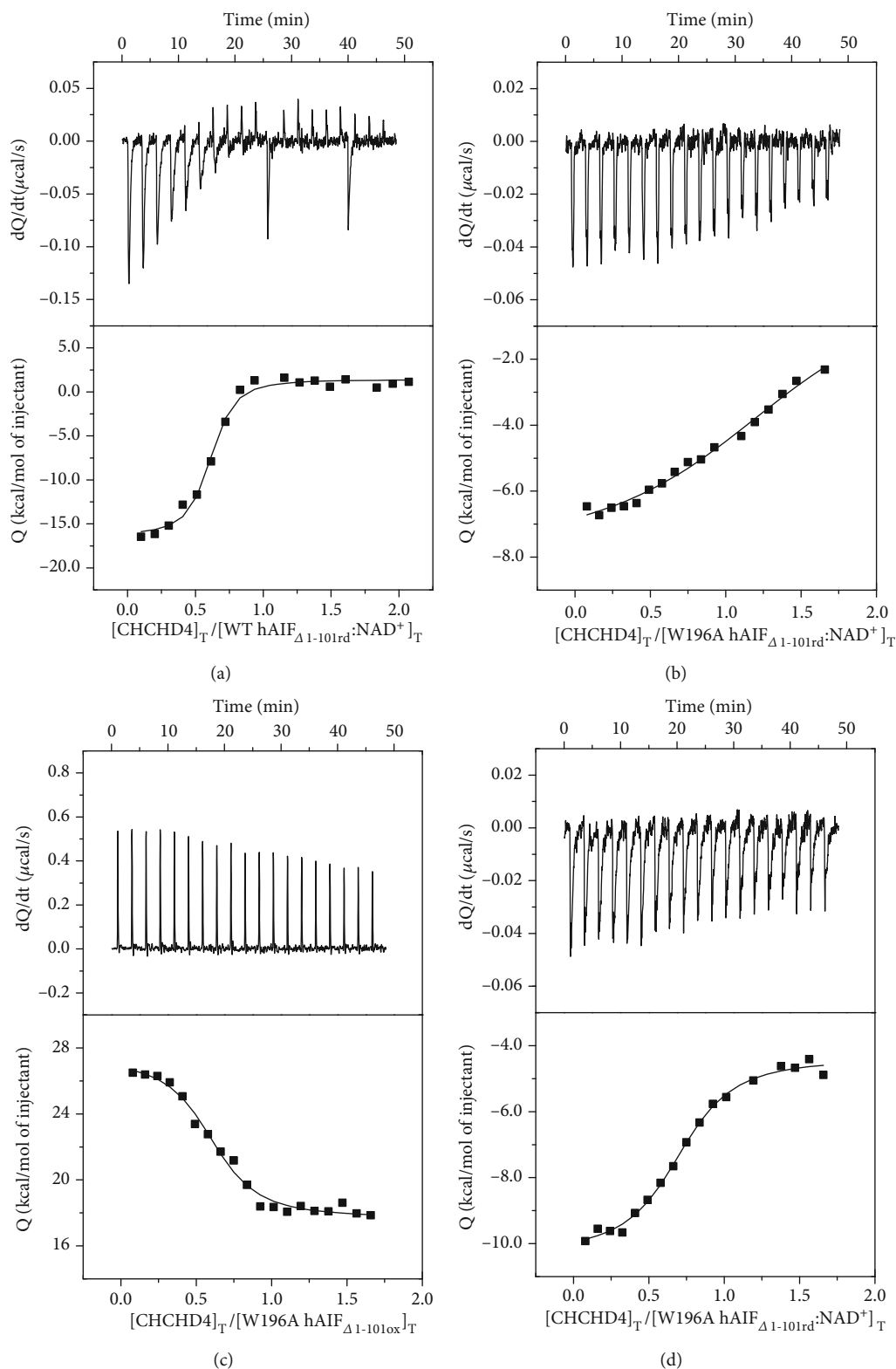
FIGURE 7: Effect of the W196 replacement in the binding of CHCHD4 to hAIF$_{\Delta 1-101}$. Calorimetric titrations of (a) WT CTC, (b) W196Y CTC, (c) W196A$_{ox}$, and (d) W196A CTC with CHCHD4. The upper plots show the thermograms (thermal power as a function of time), whereas the lower plots show the binding isotherm (normalized heats as a function of the CHCHD4/hAIF molar ratio). Measurements were carried out in 50 mM potassium phosphate, pH 7.4, at 25°C. The CTC forms were obtained by premixing hAIF$_{\Delta 1-101ox}$ and NADH at a 1 : 100 ratio. The binding parameters were estimated through nonlinear least-squares regression applying a single-ligand binding model (continuous lines in binding isotherms).

free energy of hAIF binding in binary complexes with CHCHD4, CypA, and DNA. Whereas, its replacement has in general a negative impact on the enthalpic binding contribution, while improves the entropic one (with the only exception of W196A CTC:CHCHD4 complex). Therefore, W196 contributes to stabilize the conformation of the interaction surfaces of hAIF with CHCHD4, CypA, and DNA.

3.7. W196 Contributes to Control the hAIF Conformational Landscape to Adapt to Its Physiological Roles. AIF is a moonlight protein with functions in the mitochondria, cytosol, and nucleus, where it appears to behave as a redox sensor of $NAD(H/^+)$ cellular levels [9–11]. The cellular redox state ($NAD^+/NADH$ ratio) may modulate the AIF conformational landscape regarding both overall protein conformation and quaternary organization, which in turn seems to be critical for establishing its biomolecular interaction network. The regulatory C-loop in AIF is a predicted internally disordered region that tends to adopt an organized conformation in the protein oxidized state (Figure 1, Figure S8 and S9), but that is released upon NADH-dependent protein reduction, CTC formation, and protein dimerization. The structural properties of $W196A_{ox}$ suggested that the W196 side chain and the β-hairpin coupling to the C-loop are key to modulate the structural transition of hAIF in a cellular context.

In healthy mitochondria, hAIF is present in a monomer-dimer equilibrium—regulated by the cytoplasmic NADH pools—that modulates its participation in respiratory complex assembly by physical interactions with CHCHD4 [10, 12–14]. This AIF switching may be critical for maintaining mitochondrial homeostasis along changes in $NAD^+/NADH$ ratios in response to diet, diseases such as neurodegenerative disorders, and other processes associated to NAD-consuming enzymes—particularly PARP-1 whose activity is increased during aging due to DNA damage accumulation—[37, 38]. In response to NAD^+ depletion by hyperstimulation of PARP-1, hAIF is released from the mitochondria to the cytosol, allowing its translocation to the nucleus and promoting parthanatos cell death. PARP-1 binding to AIF has been proved to mediate its release from IM by likely inducing conformational changes in the protein [39]. Curiously, the expression levels of AIF were found to be gradually decreased during development and growth in spiral ganglion neurons involved in auditory neuropathy spectrum disorder, a disease caused by point mutations in hAIF, while increased in the aging-related cell dysfunctions where the hAIF role as apoptosis inducer might be more important [40]. To investigate the different potential roles of AIF during development and aging and their regulatory mechanisms, future studies will be required.

In the last years, a significant number of rare mitochondrial diseases caused by more than 20 point mutations in the *AIFM1* gene have been identified. Some mutations in the cell death domain give rise to phenotypes with progressive disorders from childhood, as the Cowchock syndrome. On their side, mutations affecting the hAIF reductase properties decrease the content of respiratory complexes and produce cell respiration deficiencies, while some of them

prevent in addition the correct folding of the protein by decreasing its conformational stability. In this later case, the search of molecular chaperones represents an alternative therapeutic strategy yet poorly explored [7, 31, 41–44]. These mutations produce serious mitochondrial encephalopathies, in many cases with severe processes of neurodegeneration and early death. Noticeably, all characterized pathogenic hAIF mutants show a substantially decrease in CTC lifetime, suggesting that its stability is crucial for mitochondrial homeostasis and human health [18, 45]. Further molecular and cellular studies will be required to determine the impact of these pathogenic mutations on the hAIF intracellular processing and interaction with its physiological partners, as well as their link to their multiple clinical neurodegenerative phenotypes.

4. Conclusions

This report provides insights into the role in hAIF of W196 and β-hairpin motif in the molecular basis of its cellular activities. Our mutational study shows that, contrary to the pathogenic ΔR201 mutation—another residue located in the β-hairpin and involved in the interaction with the regulatory C-loop—, changes at W196 residue hardly impact the overall conformational folding of hAIF in oxidized and NADH-reduced states. Nonetheless, W196 is key to stabilize β-hairpin motif conformation by contacts that are substantially diminished and impaired in all characterized W196 variants. Moreover, the W196 and the β-hairpin motif conformation strongly modulate the redox-linked monomer-dimer structural transition in hAIF. The size and aromaticity of the side chain of W196 is key to (i) maintain the proper β-hairpin position that stabilizes and retains the regulatory C-loop in the protein score of oxidized hAIF, favoring protein compactness and stability; (ii) configure the NADH active site making hAIF inefficient for NADH oxidation and trigger the C-loop release to the solvent in the reduced state: critical factors for CTC stability and mitochondrial homeostasis; and (iii) define the interaction surfaces with CHCHD4, CypA, and DNA, by modulating the enthalpic and entropic contributions to the free energy of binding. These features contribute to modulate hAIF monomer-dimer equilibrium in a cellular context, which might be relevant for its proper function as a redox sensor of $NAD(H/^+)$ levels and for its interaction network.

Abbreviations

^{app}MW:	Apparent molecular weight
BS^3:	Homobifunctional-bis[sulfosuccinimidyl]-suberate
CHCHD4:	Coiled-coil-helix-coiled-coil-helix domain containing 4
CTC:	Charge transfer complex
CD:	Circular dichroism
CypA:	Cyclophilin A
DCPIP:	Dichlorophenolindophenol
FAD:	Flavin adenine dinucleotide
hAIF:	Human apoptosis-inducing factor

hAIF$_{ox}$:	Oxidized hAIF
hAIF$_{rd}$:	Reduced hAIF
hAIF$_{phrd}$:	Photoreduced hAIF
IMS:	Intermembrane space
NADH:	Reduced nicotinamide adenine dinucleotide
NAD$^+$:	Oxidized nicotinamide adenine dinucleotide
OXPHOS:	Oxidative phosphorylation
PARP-1:	Poly(ADP-ribose) polymerase-1
ROS:	Reactive oxygen species
SAS:	Solvent accessible surface.

Data Availability

All data are contained within the manuscript and the supplementary materials.

Conflicts of Interest

The authors declare that they have no conflicts of interest.

Acknowledgments

Supplementary Materials

The file contains the following: (i) the protocol for production and purification of proteins and for MD simulations and (ii) Figures S1-S9. (*Supplementary Materials*)

References

[1] S. A. Susin, H. K. Lorenzo, N. Zamzami et al., "Molecular characterization of mitochondrial apoptosis-inducing factor," *Nature*, vol. 397, no. 6718, pp. 441–446, 1999.

[2] H. K. Lorenzo, S. A. Susin, J. Penninger, and G. Kroemer, "Apoptosis inducing factor (AIF): a phylogenetically old, caspase-independent effector of cell death," *Cell Death and Differentiation*, vol. 6, no. 6, pp. 516–524, 1999.

[3] L. Delavallée, N. Mathiah, L. Cabon et al., "Mitochondrial AIF loss causes metabolic reprogramming, caspase-independent cell death blockade, embryonic lethality, and perinatal hydrocephalus," *Molecular Metabolism*, vol. 40, article 101027, 2020.

[4] H. Otera, S. Ohsakaya, Z.-I. Nagaura, N. Ishihara, and K. Mihara, "Export of mitochondrial AIF in response to proapoptotic stimuli depends on processing at the intermembrane space," *The EMBO Journal*, vol. 24, no. 7, pp. 1375–1386, 2005.

[5] H. Ye, C. Cande, N. C. Stephanou et al., "DNA binding is required for the apoptogenic action of apoptosis inducing factor," *Nature Structural Biology*, vol. 9, no. 9, pp. 680–684, 2002.

[6] M. J. Mate, M. Ortiz-Lombardia, B. Boitel et al., "The crystal structure of the mouse apoptosis-inducing factor AIF," *Nature Structural Biology*, vol. 9, no. 6, pp. 442–446, 2002.

[7] R. Villanueva, S. Romero-Tamayo, R. Laplaza et al., "Redox- and ligand binding-dependent conformational ensembles in the human apoptosis-inducing factor regulate its pro-life and cell death functions," *Antioxidants & Redox Signaling*, vol. 30, no. 18, pp. 2013–2029, 2019.

[8] I. Y. Churbanova and I. F. Sevrioukova, "Redox-dependent changes in molecular properties of mitochondrial apoptosis-inducing factor," *The Journal of Biological Chemistry*, vol. 283, no. 9, pp. 5622–5631, 2008.

[9] I. F. Sevrioukova, "Redox-linked conformational dynamics in apoptosis-inducing factor," *Journal of Molecular Biology*, vol. 390, no. 5, pp. 924–938, 2009.

[10] P. Ferreira, R. Villanueva, M. Martínez-Júlvez et al., "Structural insights into the coenzyme mediated monomer-dimer transition of the pro-apoptotic apoptosis inducing factor," *Biochemistry*, vol. 53, no. 25, pp. 4204–4215, 2014.

[11] C. A. Brosey, C. Ho, W. Z. Long et al., "Defining NADH-driven allostery regulating apoptosis-inducing factor," *Structure*, vol. 24, no. 12, pp. 2067–2079, 2016.

[12] N. Modjtahedi, E. Hangen, P. Gonin, and G. Kroemer, "Metabolic epistasis among apoptosis-inducing factor and the mitochondrial import factor CHCHD4," *Cell Cycle*, vol. 14, no. 17, pp. 2743–2747, 2015.

[13] E. Hangen, O. Féraud, S. Lachkar et al., "Interaction between AIF and CHCHD4 regulates respiratory chain biogenesis," *Molecular Cell*, vol. 58, no. 6, pp. 1001–1014, 2015.

[14] N. Modjtahedi, K. Tokatlidis, P. Dessen, and G. Kroemer, "Mitochondrial proteins containing coiled-coil-helix-coiled-coil-helix (CHCH) domains in health and disease," *Trends in Biochemical Sciences*, vol. 41, no. 3, pp. 245–260, 2016.

[15] E. Hangen, K. Blomgren, P. Benit, G. Kroemer, and N. Modjtahedi, "Life with or without AIF," *Trends in Biochemical Sciences*, vol. 35, no. 5, pp. 278–287, 2010.

[16] J. A. Klein, C. M. Longo-Guess, M. P. Rossmann et al., "The harlequin mouse mutation downregulates apoptosis-inducing factor," *Nature*, vol. 419, no. 6905, pp. 367–374, 2002.

[17] V. El Ghouzzi, Z. Csaba, P. Olivier et al., "Apoptosis-inducing factor deficiency induces early mitochondrial degeneration in brain followed by progressive multifocal neuropathology," *Journal of Neuropathology and Experimental Neurology*, vol. 66, no. 9, pp. 838–847, 2007.

[18] I. F. Sevrioukova, "Structure/function relations in *AIFM1* variants associated with neurodegenerative disorders," *Journal of Molecular Biology*, vol. 428, no. 18, pp. 3650–3665, 2016.

[19] C. C. Alano, P. Garnier, W. Ying, Y. Higashi, T. M. Kauppinen, and R. A. Swanson, "NAD$^+$ depletion is necessary and sufficient for poly(ADP-ribose) polymerase-1-mediated neuronal death," *The Journal of Neuroscience*, vol. 30, no. 8, pp. 2967–2978, 2010.

[20] S. A. Susin, H. K. Lorenzo, N. Zamzami et al., "Mitochondrial release of caspase-2 and -9 during the apoptotic process," *The Journal of Experimental Medicine*, vol. 189, no. 2, pp. 381–394, 1999.

[21] C. Cande, N. Vahsen, I. Kouranti et al., "AIF and cyclophilin A cooperate in apoptosis-associated chromatinolysis," *Oncogene*, vol. 23, no. 8, pp. 1514–1521, 2004.

[22] C. Artus, H. Boujrad, A. Bouharrour et al., "AIF promotes chromatinolysis and caspase-independent programmed necrosis by interacting with histone H2AX," *The EMBO Journal*, vol. 29, no. 9, pp. 1585–1599, 2010.

[23] J. Sancho, "The stability of 2-state, 3-state and more-state proteins from simple spectroscopic techniques... plus the structure of the equilibrium intermediates at the same time," *Archives of Biochemistry and Biophysics*, vol. 531, no. 1-2, pp. 4–13, 2013.

[24] M. Biasini, S. Bienert, A. Waterhouse et al., "SWISS-MODEL: modelling protein tertiary and quaternary structure using evolutionary information," *Nucleic Acids Research*, vol. 42, no. W1, pp. W252–W258, 2014.

[25] W. Humphrey, A. Dalke, and K. Schulten, "VMD: visual molecular dynamics," *Journal of Molecular Graphics*, vol. 14, no. 33-38, pp. 27–38, 1996.

[26] W. L. Delano, "PyMOL: an open-source molecular graphics tool," *CCP4 Newsletter on Protein Crystallography*, vol. 40, pp. 82–92, 2002.

[27] I. Lans, J. R. Peregrina, M. Medina, M. Garcia-Viloca, A. Gonzaalez-Lafont, and J. M. Lluch, "Mechanism of the Hydride Transfer between *Anabaena* Tyr303Ser FNR$_{rd}$/FNR$_{ox}$ and NADP$^+$/H. A Combined Pre-Steady-State Kinetic/Ensemble-Averaged Transition-State Theory with Multidimensional Tunneling Study," *The Journal of Physical Chemistry B*, vol. 114, no. 9, pp. 3368–3379, 2010.

[28] I. Lans, M. Medina, E. Rosta et al., "Theoretical study of the mechanism of the hydride transfer between ferredoxin-NADP$^+$ reductase and NADP$^+$: the role of Tyr303," *Journal of the American Chemical Society*, vol. 134, no. 50, pp. 20544–20553, 2012.

[29] P. Sancho, A. Sánchez-Monteagudo, A. Collado et al., "A newly distal hereditary motor neuropathy caused by a rare *AIFM1* mutation," *Neurogenetics*, vol. 18, no. 4, pp. 245–250, 2017.

[30] B. Hu, M. Wang, R. Castoro et al., "A novel missense mutation in *AIFM1* results in axonal polyneuropathy and misassembly of OXPHOS complexes," *European Journal of Neurology*, vol. 24, no. 12, pp. 1499–1506, 2017.

[31] I. Berger, Z. Ben-Neriah, T. Dor-Wolman et al., "Early prenatal ventriculomegaly due to an AIFM1 mutation identified by linkage analysis and whole exome sequencing," *Molecular Genetics and Metabolism*, vol. 104, no. 4, pp. 517–520, 2011.

[32] L. Banci, I. Bertini, C. Cefaro et al., "MIA40 is an oxidoreductase that catalyzes oxidative protein folding in mitochondria," *Nature Structural & Molecular Biology*, vol. 16, no. 2, pp. 198–206, 2009.

[33] B. Farina, G. Di Sorbo, A. Chambery et al., "Structural and biochemical insights of CypA and AIF interaction," *Scientific Reports*, vol. 7, no. 1, 2017.

[34] B. Farina, M. Sturlese, F. Mascanzoni et al., "Binding mode of AIF(370-394) peptide to CypA: insights from NMR, label-free and molecular docking studies," *The Biochemical Journal*, vol. 475, no. 14, pp. 2377–2393, 2018.

[35] A. Monti, M. Sturlese, A. Caporale et al., "Design, synthesis, structural analysis and biochemical studies of stapled AIF(370-394) analogues as ligand of CypA129717," *Biochimica et Biophysica Acta - General Subjects*, vol. 1864, no. 12, 2020.

[36] N. Vahsen, C. Cande, P. Dupaigne et al., "Physical interaction of apoptosis-inducing factor with DNA and RNA," *Oncogene*, vol. 25, no. 12, pp. 1763–1774, 2006.

[37] E. Verdin, "NAD$^+$ in aging, metabolism, and neurodegeneration," *Science*, vol. 350, no. 6265, pp. 1208–1213, 2015.

[38] S. Lautrup, D. A. Sinclair, M. P. Mattson, and E. F. Fang, "NAD$^+$ in brain aging and neurodegenerative disorders," *Cell Metabolism*, vol. 30, no. 4, pp. 630–655, 2019.

[39] Y. Wang, N. S. Kim, J. F. Haince et al., "Poly(ADP-ribose) (PAR) binding to apoptosis-inducing factor is critical for PAR polymerase-1-dependent cell death (parthanatos)," *Science Signaling*, vol. 4, no. 167, p. ra20, 2011.

[40] L. Zong, J. Zhao, W. Wu, J. Wang, D. Huang, and M. Liu, "AIF knockdown induce apoptosis and mitochondrial dysfunction in cochlear spiral ganglion neurons in vitro," *Molecular Medicine Reports*, vol. 21, no. 4, pp. 1910–1920, 2020.

[41] D. Diodato, G. Tasca, D. Verrigni et al., "A novel *AIFM1* mutation expands the phenotype to an infantile motor neuron disease," *European Journal of Human Genetics*, vol. 24, no. 3, pp. 463–466, 2016.

[42] A. Ardissone, G. Piscosquito, A. Legati et al., "A slowly progressive mitochondrial encephalomyopathy widens the spectrum of *AIFM1* disorders," *Neurology*, vol. 84, no. 21, pp. 2193–2195, 2015.

[43] L. Sorrentino, F. Cossu, M. Milani, A. Aliverti, and E. Mastrangelo, "Structural bases of the altered catalytic properties of a pathogenic variant of apoptosis inducing factor," *Biochemical and Biophysical Research Communications*, vol. 490, no. 3, pp. 1011–1017, 2017.

[44] G. Heimer, E. Eyal, X. Zhu et al., "Mutations in *AIFM1* cause an X-linked childhood cerebellar ataxia partially responsive to riboflavin," *European Journal of Paediatric Neurology*, vol. 22, no. 1, pp. 93–101, 2018.

[45] C. Rinaldi, C. Grunseich, I. F. Sevrioukova et al., "Cowchock syndrome is associated with a mutation in apoptosis-inducing factor," *American Journal of Human Genetics*, vol. 91, no. 6, pp. 1095–1102, 2012.